

# Catalytic Applications of Nickel and Copper Complexes Stabilised by Large Ring N-Heterocyclic Carbenes

Hall, Jonathan

*Award date:*
2021

*Awarding institution:*
University of Bath

# Catalytic Applications of Nickel and Copper Complexes Stabilised by Large Ring N-Heterocyclic Carbenes


## Jonathan Wei Leong Hall


A thesis submitted in partial fulfilment of the requirements for the degree of

**Doctor of Philosophy**



University of Bath

Department of Chemistry


December 2020



Signed…… Date……

# Contents

# Acknowledgements

The first person I would like to thank is Professor Mike Whittlesey. I wouldn't have been able to do this without his guidance and support. From my undergraduate degree and throughout my PhD he has always had his door open to help. I appreciate the opportunity he gave me to work in his lab and I will go forward with the invaluable skills he has taught me. Maybe now I can actually slack off and go to Butlins….

I would similarly like to thank the many group members I have worked with. The amazing postdocs Drs Sara Sabater, Maia Espinal, Fedor Miloserdov and Anne-frederique Percharman. The PhD students (Dr) Mat Cybulski, (Dr) Will Blackaby and Connie Isaac. Their companionship in and out of the lab have carried me through my PhD and I am grateful for their support over these four years.

I would also like to thank members of the chemistry department who have helped and collaborated with my work as well as being lovely people to talk to; Dr Mary Mahon for the help with X-ray Diffraction and chats about animals, Dr John Lowe for all the NMR spectroscopy help and baked goods, Dr Vera Krewald for the computational work, Dr Matthew Jones for the help with gas chromatography, Dr Shaun Reeksting for the help with mass spectrometry and Professor Frank Marken for the help with the cyclic voltammetry.

The help I received was not just limited to being at Bath, and so I would like to thank those collaborators and people I have worked with during my PhD from further afield. From those at Cardiff University: Professor Damien Murphy, Dr Andrea Foli and especially Dr Emma Richards for their support and expertise in the field of EPR. Dr Louis Luk for being a great supervisor and friend. As well as Dr Louis Morrill, Thomas Williams, Dr Yuhsuan Tsai and Dr Alexander Nodling. In addition, I would like to thank those at the University of Ghent; Professor Catherine Cazin, Dr Fady Nahra, Sofie Vanden Broeck, the rest of the Cazin and Nolan groups for their support during my time on secondment there.

Finally, I would like to thank my family, friends and Elizabeth for their endless love, patience and support during my time here in Bath.

# Abstract

This thesis reports the effect of ring expansion of N-heterocyclic carbenes (NHCs) on complexes of copper and nickel in synthesis and catalysis. Chapters 2, 3 and 4 describe the influence of ring expansion on linear two-coordinate Cu complexes of the form (carbene)CuX, whereas chapter 5 focuses on a low coordinate Ni(I) species, Ni(6-Mes)($PPh_3$)Br (**5.1**), which has been stabilised by a ring-expanded NHC (RE-NHC).

Chapter 2 expands upon previous work describing the semihydrogenation of 1-phenyl-1-propyne by (6-Mes)Cu$O^tBu$ (**2.1**). A series of (RE-NHC)Cu$O^tBu$ complexes, synthesised through the protonolysis of (RE-NHC)CuMes with $^t$BuOH, were then compared to **2.1** for the semihydrogenation of alkynes. Complex **2.1** was found to give the best results and upon optimisation of the conditions, proved active at 0.5 mol%. The hydroboration of alkynes was also investigated with (RE-NHC)Cu$O^tBu$ species, and with a preliminary mechanistic study undertaken.

Chapter 3 reports the synthesis of six new examples of (carbene)CuF species (all structurally characterised) which were employed in the catalytic allylation of octanal. The bulky (ITr)CuF complex (**3.3**) was found to afford the best catalytic activity. Mechanistic experiments point to the involvement of Cu silicates.

Chapter 4 details the synthesis of (RE-NHC)CuX (X = Cl, Br and I) *via a* cuprate intermediate that avoided having to use a free carbene. A range of (RE-NHC)CuX complexes were synthesised employing this method, although increasing ring size, steric bulk or employment of a heavier halide resulted in more forcing conditions. The (RE-NHC)CuX complexes were also employed in the [3+2] cycloaddition of alkynes and azides. (6-Mes)CuF (**3.2**) and (6-Mes)CuI (**4.3**) were found to be the most active precursors, although variation of NHC ring size gave no clear trend.

Chapter 5 provides a mechanistic study of the catalytic hydrodehalogenation of aryl halides involving the low coordinate Ni(I) complex Ni(6-Mes)($PPh_3$)Br (**5.1**). Initial stoichiometric investigations with Ar-Br revealed formation of two Ni(II) species, Ni(6-Mes)($PPh_3$)$Br_2$ (**5.7**) and Ni(6-Mes)($PPh_3$)(Ar)Br through a bimolecular oxidation, and formation of a series of Ni(I) alkoxide complexes with NaOR. The resulting complexes were characterised and spectroscopically studied, with EPR studies employed for Ni-OR. A complicated mechanism was revealed involving two cycles, one involving a postulated Ni(II)/Ni(0) cycle and the other a Ni(I) cycle.

# Abbreviations

**Analytical**

| | |
|---|---|
| $\%V_{bur}$ | Percentage buried volume |
| *A* | Superhyperfine coupling constant |
| APCI | Atmospheric pressure chemical ionization |
| BDE | Bond Dissociation Energy |
| br | Broad |
| Calcd | Calculated |
| COSY | Correlation spectroscopy |
| CREF | Carbene relative energy of formation |
| CV | Cyclic voltammetry |
| d | Doublet |
| DEPT | Distortionless Enhancement by Polarization Transfer |
| DFT | Density functional theory |
| DOSY | Diffusion-ordered NMR spectroscopy |
| EI | Electron ionisation |
| EPR | Electron paramagnetic resonance |
| ESI-MS | Electrospray ionisation mass spectrometry |
| FID | Flame ionization detector |
| *g* | *g* factor in EPR |
| $g_e$ | Free electron spin *g* value |
| HEP | Huynh's electronic parameter |
| HOMO | Highest occupied molecular orbital |
| HMBC | Heteronuclear multiple bond correlation |
| HPLC | High performance liquid chromatography |
| HRMS | High resolution mass spectrometry |
| HSQC | Heteronuclear single quantum coherence |
| $^{i}$ *(e.g. $^{i}$PrOH)* | *Ipso-* |
| $^{n}J_{XR}$ | Exchange coupling constant, n = number of bonds, X coupling to R |
| $K_a$ | Acid dissociation constant |
| LUMO | Lowest unoccupied molecular orbital |
| m | Multiplet |
| MO | Molecular orbital |
| MS | Mass spectrometry |
| $^{n}J_{XY}$ | Coupling constant of X to Y across n bonds |
| NMR | Nuclear magnetic resonance |
| p$K_a$ | $-\log_{10}$ of the acid dissociation constant ($K_a$) |
| q | Quartet |
| quin | Quintet |
| s | Singlet |
| sept | Septet |
| t | Triplet |
| t | Time |
| TOF | Turnover frequency |
| TEP | Tolman electronic parameter |

**Units**

| | |
|---|---|
| μL | Microlitre |
| Å | Angström |
| $e^-$ | Electron |
| g | Gram |
| h | Hour |
| Hz | Hertz |
| K | Kelvin |
| kcal | Kilocalorie |
| m/z | Mass to charge ratio |
| mT | Millitesla |
| ppm | Part per million |
| s | Second |
| T | Tesla |
| V | Volt |

**Chemical**

| | |
|---|---|
| *μ*- | Bridging |
| 5-Bn | 1,3-bis(benzyl)imidazolin-2-ylidene |
| 6-Bn | 1,3-bis(benzyl)-3,4,5,6-tetrahydropyrimid-2-ylidene |
| 6-Et | 1,3-bis(ethyl)-3,4,5,6-tetrahydropyrimid-2-ylidene |
| 6-$^i$Pr | 1,3-bis(isopropyl)-3,4,5,6-tetrahydropyrimid-2-ylidene |
| 6-Dipp | 1,3-bis(2,6-diisopropylphenyl)-3,4,5,6-tetrahydropyrimid-2-ylidene |
| [6-DippH]$^+$ | 1,3-bis(2,6-diisopropylphenyl)-3,4,5,6-tetrahydropyrimidinium |
| 6-Mes | 1,3-bis(2,4,6-trimethylphenyl)-3,4,5,6-tetrahydropyrimid-2-ylidene |
| [6-MesH]$^+$ | 1,3-bis(2,4,6-trimethylphenyl)-3,4,5,6-tetrahydropyrimidinium |
| 6-MesDAC | 1,3-bis(2,4,6-trimethylphenyl)-4,6-diketo-5,5-dimethylpyrimidin-2-ylidene |
| 6-*o*-anis | 1,3-bis(2-methoxyphenyl)-3,4,5,6-tetrahydropyrimid-2-ylidene |
| 6-*o*-Tolyl | 1,3-bis(2-methylphenyl)-3,4,5,6-tetrahydropyrimid-2-ylidene |
| 6-Xylyl | 1,3-bis(2,6-dimethylphenyl)-3,4,5,6-tetrahydropyrimid-2-ylidene |
| [6-XylylH]$^+$ | 1,3-bis(2,6-dimethylphenyl)-3,4,5,6-tetrahydropyrimidinium |
| 7-Bn | 1,3-bis(benzyl)-4,5,6,7-tetrahydro-[1,3]-diazepin- 2-ylidene |
| 7-Cy | 1,3-bis(cyclohexyl)-4,5,6,7-tetrahydro-[1,3]-diazepin- 2-ylidene |
| 7-Dipp | 1,3-bis(2,6-diisopropylphenyl)-4,5,6,7-tetrahydro-[1,3]-diazepin-2-ylidene |
| [7-DippH]$^+$ | 1,3-bis(2,6-diisopropylphenyl)-4,5,6,7-tetrahydro-[1,3]-diazepinium |
| 7-Mes | 1,3-bis(2,4,6-trimethylphenyl)-4,5,6,7-tetrahydro-[1,3]-diazepin-2-ylidene |
| [7-MesH]$^+$ | 1,3-bis(2,4,6-trimethylphenyl)-4,5,6,7-tetrahydro-[1,3]-diazepinium |
| 7-neoPent | 1,3-bis(neopentyl)-4,5,6,7-tetrahydro-[1,3]-diazepin-2-ylidene |
| [7-neoPentH]$^+$ | 1,3-bis(neopentyl)-4,5,6,7-tetrahydro-[1,3]-diazepinium |
| 7-*o*-Tolyl | 1,3-bis(2-methylphenyl)-4,5,6,7-tetrahydro-[1,3]-diazepin-2-ylidene |

| | |
|---|---|
| 7-$^{t}$Bu | 1,3-bis(*tert*-butyl)-4,5,6,7-tetrahydro-[1,3]-diazepin-2- ylidene |
| 7-Xylyl | 1,3-bis(2,6-dimethylphenyl)-4,5,6,7-tetrahydro-[1,3]-diazepin-2-ylidene |
| [7-XylylH]$^{+}$ | 1,3-bis(2,6-dimethylphenyl)-4,5,6,7-tetrahydro-[1,3]-diazepinium |
| 8-*o*-Tolyl | 1,3-bis(2-methylphenyl)-1,3-diazocane-2-ylidene |
| 8-Dipp | 1,3-bis(2,6-diisopropylphenyl)-1,3-diazocane-2-ylidene |
| 8-Mes | 1,3-bis(2,4,6-trimethylphenyl)-1,3-diazocane-2-ylidene |
| [8-MesH]$^{+}$ | 1,3-bis(2,4,6-trimethylphenyl)-1,3-diazocinium |
| 8-Xylyl | 1,3-bis(2,6-dimethylphenyl)-1,3-diazocane-2-ylidene |
| 9-Mes | 1,3-bis(2,4,6-trimethylphenyl)-4,9-tetrahydro-5,7-dibenzo-[1,3]-diazonin-2-ylidene |
| 9-Dietph | 1,3-bis(2,6-diethylphenyl)-4,9-tetrahydro-5,7-dibenzo-[1,3]-diazonin-2-ylidene |
| 9-Dipp | 1,3-bis(2,6-diisopropylphenyl)-4,9-tetrahydro-5,7-dibenzo-[1,3]-diazonin-2-ylidene |
| 10-Mes | 5,7-bis(2,4,6-trimethylphenyl)-4,8-tetrahydro-2,9-dibenzo-[1,5,7]-oxadiazecin-2-ylidene |
| 10-Dipp | 5,7-bis(2,6-diisopropylphenyl)-4,8-tetrahydro-2,9-dibenzo-[1,5,7]-oxadiazecin-2-ylidene |
| Ad | 1-adamantyl |
| BAC | bis-(diisopropylamino)cyclopropenylidene |
| $BAr^{F}_{4}$ | Tetrakis(3,5-bis(trifluoromethyl)phenyl)borate |
| -BPin | 4,4,5,5-tetramethyl-1,3,2-dioxaborolan-2-yl |
| CAAC | Cyclic(alkyl)(amino)carbene |
| $^{Cl}$IPr | 1,3-bis(2,6-diisopropylphenyl)-4,5-dichloroimidazol-2-ylidene |
| COD | Cycloocta-1,5-diene |
| Cp | Cyclopentadienyl |
| Cp* | 1,2,3,4,5-pentamethylcyclopentadienyl |
| CPME | Cyclopentyl methyl ether |
| Cy | Cyclohexyl |
| Dietph | 2,6-diethylphenyl |
| DME | Dimethoxyethane |
| (*E*)- | Trans geometry |
| HBPin | Pinacolborane |
| IAd | 1,3-diadamantylimidazol-2-ylidene |
| $^{i}Pr_{2}$-bimy | 1,3-diisopropylbenzimidazolin-2-ylidene |
| ICy | 1,3-dicyclohexylimidazol-2-ylidene |
| $IMe_{4}$ | 1,3,4,5-tetramethylimidazol-2-ylidene |
| IMes | 1,3-bis(2,4,6-trimethylphenyl)imidazol-2-ylidene |
| IPr | 1,3-bis(2,6-diisopropylphenyl)imidazol-2-ylidene |
| IPr* | 1,3-bis(2,6-dibenzhydryl-4-methylphenyl)imidazol-2-ylidene |
| $^{i}Pr_{2}$Im | 1,3-bis(isopropyl)imidazol-2-ylidene |
| ($^{iPr}$PCP) | 2,6-bis(diisopropylphosphinomethyl)phenyl |
| I$^{t}$Bu | 1,3-di-*tert*-butylimidazol-2-ylidene |
| ITr | 1,3-ditritylimidazol-2-ylidene |
| ITrDipp | 1-trityl-3-(2,6-diisopropylphenyl)imidazol-2-ylidene |
| KHMDS | Potassium bis(trimethylsilyl)amide |
| L | Ligand |
| LDA | Lithium diisopropylamide |
| M | Metal |

| | |
|---|---|
| $(MeO)_3SiCH_2CH=CH_2$ | Trimethoxyallylsilane |
| Mes | 2,4,6-trimethylphenyl |
| $^{Menthyl}$CAAC | 1-[(2,6-Diisopropyl)phenyl]-3-(1-isopropyl-3-methylcyclohexyl)-5,5-dimethyl-2-pyrrolidinylidene |
| Naph-8-Mes | 2,4-Dimesityl-4,5-dihydro-1H-naphtho[1,8-ef][1,3]diazocane-2-ylidene |
| NBS | N-Bromosuccinimide |
| $^{n}$Bu | Normal butyl |
| NHC | N-Heterocyclic carbene |
| $[NHCH]^+$ | Imidazolium |
| $HNPh_2$ | Diphenylamine |
| Pent | Pentane |
| PMHS | Polymethylhydrosiloxane |
| PTFE | Polytetrafluoroethylene |
| *p*TsOH | *para*-Toluenesulfonic acid |
| R | Aryl or alkyl group |
| RE-NHC | Ring-expanded N-heterocyclic carbene |
| SICy | 1,3-bis(cyclohexyl)imidazolin-2-ylidene |
| SIMes | 1,3-bis(2,4,6-trimethylphenyl)imidazolin-2-ylidene |
| SIPr | 1,3-bis(2,6-diisopropylphenyl)imidazolin-2-ylidene |
| $^{t}$Bu | *tert*-butyl |
| TEMPO | (2,2,6,6-Tetramethylpiperidin-1-yl)oxyl |
| TMS | trimethylsilyl |
| X | Halide (unless otherwise specified) |
| (*Z*)- | Cis geometry |
| $\kappa^n$- | K binding mode of a ligand with n atoms (denticity) |
| $\eta^n$- | η binding mode of a ligand with n atoms (hapticity) |

# Chapter 1

# Chapter 1 – Introduction

## 1.1 – Carbenes

Carbenes are highly reactive neutral compounds containing a divalent carbon atom with six electrons in the valence shell. Carbenes can possess either a triplet or singlet ground state, which is determined by the relative energies of the HOMO and LUMO. If the gap between them is large, a singlet ground state is expected. One way to manipulate which state exists is through changing the geometry around the carbenic carbon so it formally does not change hybridisation. For example, if we consider a linear geometry with a divalent carbon, *sp* hybridisation would be expected. This means four of the electrons are used in bonding and the remaining two will occupy two degenerate *p* orbitals ($p_x$ and $p_y$), giving a triplet ground state. By bending the structure around the carbenic carbon, the hybridisation will become closer to an $sp^2$ hybridised carbon in which the degeneracy between the $p_x$ and $p_y$ orbitals is lost. As a result, the $p_x$ orbital will become more *sp* like. The $p_x$ and $p_y$ orbitals for the purpose of the rest of the chapter will be referred to $\sigma$ and $p_\pi$ respectively. Generally, the $\sigma$ orbital is lower in energy than $p_\pi$ leading to this orbital being occupied by both non-bonding electrons, resulting in a singlet ground state (Figure 1.1).[1]

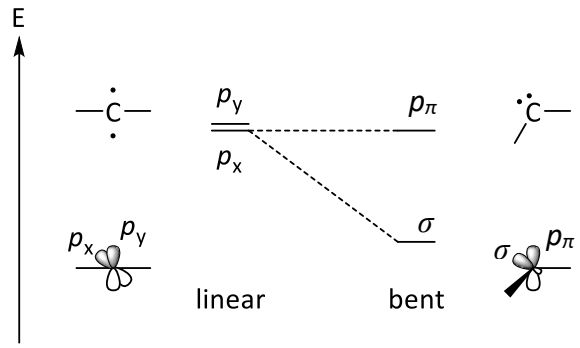


Figure 1.1 – The effect of geometry on orbitals in a carbenic carbon.[1] (Left) Triplet carbene with degenerate $p_x$ and $p_y$ orbitals. (Right) Singlet carbene with a $sp^2$ like hybridised carbon centre containing $\sigma$ and $p_\pi$ orbitals.

## 1.2 – N-Heterocyclic Carbenes

N-heterocyclic carbenes (NHCs) are singlet carbenes based on heterocycles containing four or more ring atoms and at least one nitrogen atom. The most common NHC is based on the parent forms of imidazoline or imidazolidine, where the carbenic carbon is situated in the C2 position in-between two nitrogen atoms (Figure 1.2).


Figure 1.2 – Nomenclature and numbering of two examples of NHCs following the Hantzsch-Widman system.[2]

The more electronegative substituents on the carbenic carbon atom enhance the *s* character of the $\sigma$ orbital, increasing its stability and ultimately the gap between it and the $p_\pi$ orbital (inductive effect). In addition, the presence of π-donating substituents on either side of the carbenic carbon, increases the energy of the $p_\pi$ orbital (mesomeric effect). These, with aid of the constrained geometry, stabilise the singlet ground state (Figure 1.3).

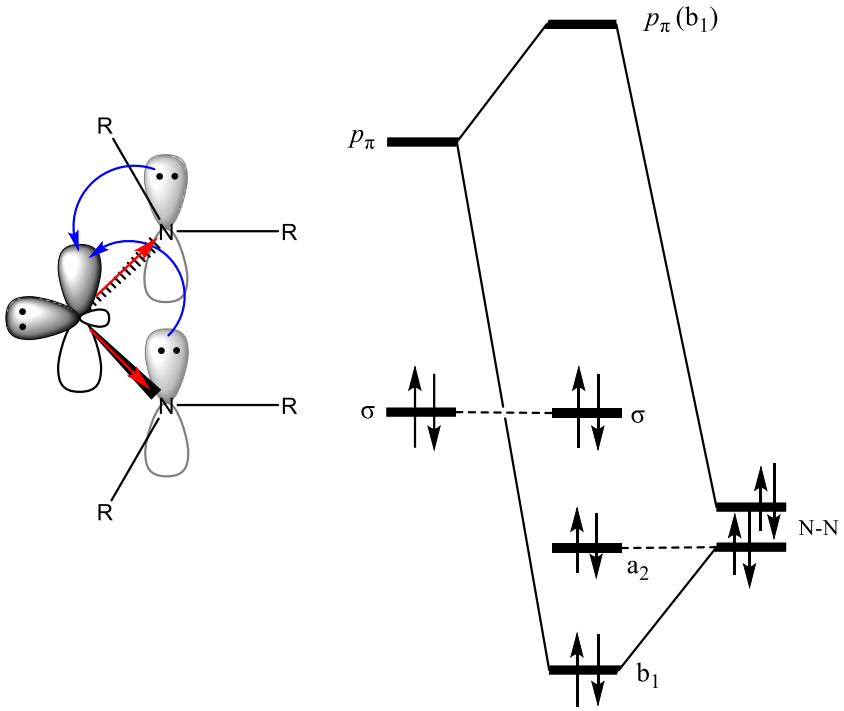


Figure 1.3 – (Left) Electronic features of NHCs. Red arrows showing inductive and blue showing mesomeric. (Right) Partial molecular orbital diagram of an NHC, showing the interaction between the $p_\pi$ non-bonding orbital of the carbene and the *p* orbitals of the two nitrogen atoms.

The level of saturation at the backbone position of the ring is subtle but important. NHC's with unsaturated backbones have a degree of aromaticity, which has been linked to aiding the isolation of the carbenes (Figure 1.4).[2] For example, carbene **A** in Figure 1.4 could be isolated, whereas only the dimer (**B**) of the saturated analogue proved stable.[3,4] The aromaticity of the carbene ring is generally thought to increase the inductive effect from the carbene substituents, which prevents

the dimerization.[2] Arduengo demonstrated having larger N-substituents such as mesityl could prevent dimerization and allow isolation of an imidazolidine-2-ylidene species such as **D**.[5]

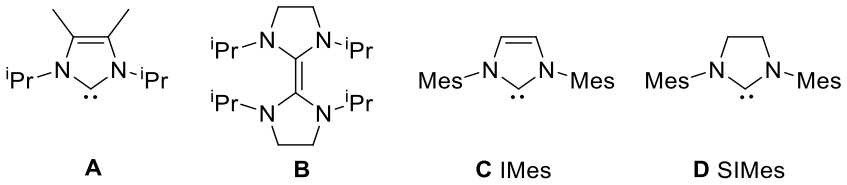


Figure 1.4 – **A** 1,3-di(isopropyl)-4,5-dimethylimidazol-2-ylidene.[3] **B** the dimer of 1,3-di(isopropyl)-imidazolidin-2-ylidene.[4] **C** IMes.[5] **D** SIMes.[5]

## 1.3 – Ring-expanded NHCs

Approaches to modifying NHCs commonly take the form of changing the N-substituents or saturation of the backbone. Exploration into other types of alterations has recently diversified this area.[6] One such approach is the expansion of the heterocyclic ring to contain more than 5 atoms, resulting in what are commonly referred to as ring-expanded NHCs (RE-NHCs) or expanded-ring NHCs (ER-NHCs). By increasing the ring size, a twofold effect occurs. The endo NCN angle increases, which results in a decrease in *s* character of the σ-orbital, making it more directional and nucleophilic at a cost of reducing the HOMO/LUMO gap.[7] The exo NCN angle decreases, bringing the N-substituents closer to atoms coordinated to, for example a metal atom coordinated to the carbenic carbon, increasing steric impact.[2]

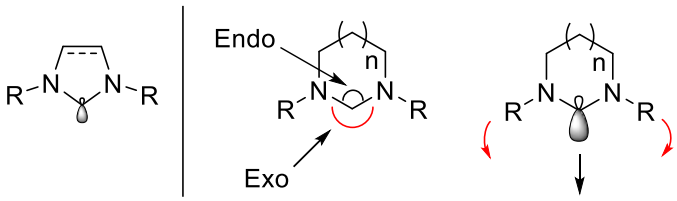


Figure 1.5 – (Left) 5-membered NHC. (Right) Effect of increasing the ring size on the NHC. Black arrow indicates the elongation of the more *p* like *σ*-orbital. Red arrows indicate the increased steric impact of the R groups.

## 1.4 – History of RE-NHCs

The first reported RE-NHC metal complex was by Iwasaki et al. in 1996.[8] The authors demonstrated Pd and Pt carbene pincer complexes could be synthesised in one step *via* the oxidative addition of a tetraazathiapentalene framework to a zero-valent Pd/Pt precursor (Scheme 1.1). Later work applied this methodology to form a Rh(III) species, although application to Cu(I) yielded no results.[9]

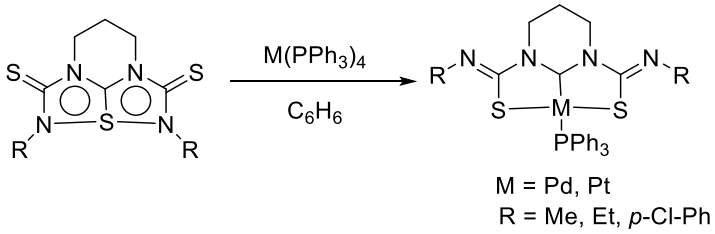


Scheme 1.1 – Synthesis of RE-NHC pincer complexes by Iwasaki.[8]

The isolation of the first free six-membered carbene was described by Alder in 1999 (Scheme 1.2).[10] Deprotonation of [6-$^{i}$PrH]$BF_4$ by sodium bis(trimethylsilyl)amide at -78 °C afforded 6-$^{i}$Pr with a 40% yield. This was stable in solution at room temperature and no dimerization was observed, in contrast to its 5-membered analogue shown in Figure 1.4.[4]

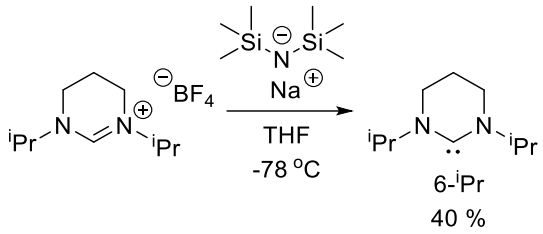


Scheme 1.2 – Synthesis of the first isolated 6-membered NHC, 6-$^{i}$Pr.[10]

Isolation of a larger ringed carbene was not achieved until 2007 by Cavell.[11] The 7-membered RE-NHCs 7-Cy (**1.ii**) and bicyclic **1.iv** were isolated through the use of strong bases (Scheme 1.3). Traditional deprotonation methods commonly used for the 5-membered NHCs such as KH or KO$^{t}$Bu were found to be unsuitable for the preparation of **1.ii** and **1.iv** from the corresponding salts **1.i** and **1.iii**.[2] In the case of KO$^{t}$Bu, the *tert*-butoxide adducts **1.v** and **1.vi** were formed, which were found be unreactive in attempted complexation to $[Ir(COD)Cl]_2$. For **1.i**, KHMDS was shown to be suitable although, **1.iii** required LDA, reflecting the relative basicity of the two salts. In contrast to **1.ii**, **1.iv** was found to have poor stability, and deprotonation to generate the carbene *in-situ* allowed subsequent complexation to metal centres.

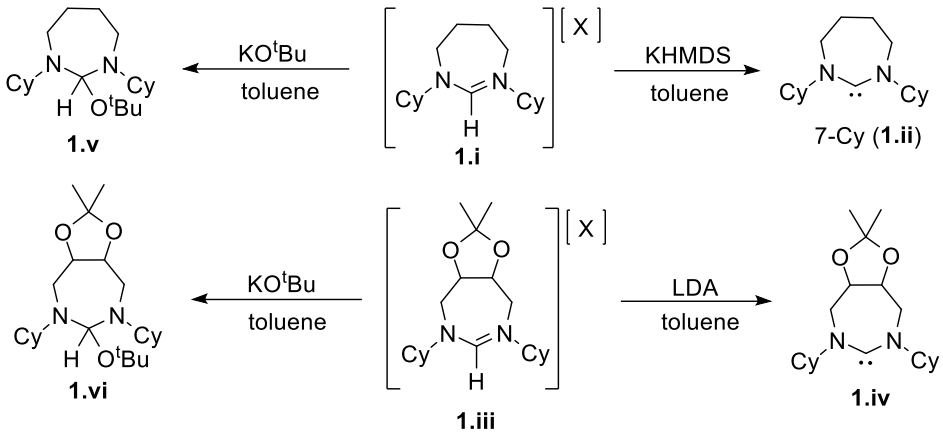


Scheme 1.3 – Isolation of free 7-membered carbenes.[11]

Later work by Cavell reported the first 8-membered NHCs, which could be isolated as the free carbenes in reasonable yields upon deprotonation of the corresponding azolium bromide salts with KHMDS (Scheme 1.4). Complexation of the 8-membered rings to metals proved difficult in comparison to the 6- and 7- membered derivatives. Attempts to synthesise (8-Dipp)AgBr proved unsuccessful, while attempts to complex the 8-membered carbenes to $[Rh(COD)Cl]_2$ only worked with the least sterically imposing 8-membered ring, 8-*o*-tolyl, to yield (8-*o*-tolyl)Rh(COD)Cl (**1.x**).

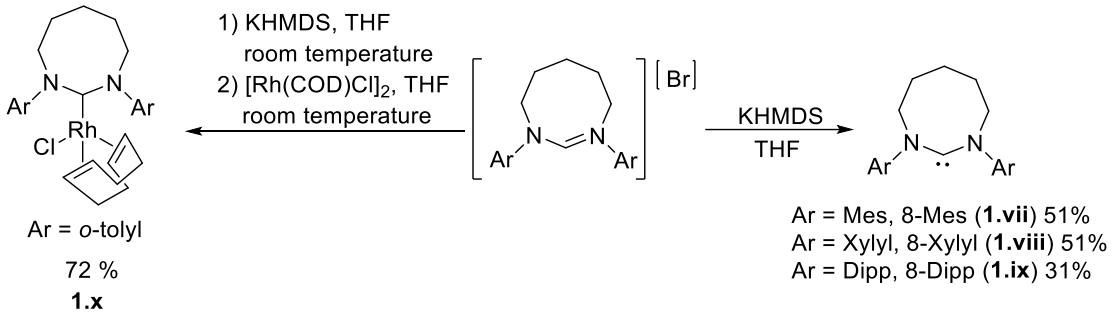


Scheme 1.4 – Synthesis of free 8-membered NHCs and Rh coordination chemistry by Cavell.[12]

In light of unsuccessful attempts to isolate the first examples of 9- and 10-membered ring free NHCs, Hashmi complexed the *in-situ* deprotonated RE-NHC salts to $AuCl(SMe_2)$ to yield an array of (RE-NHC)AuCl complexes (including **1.xi** and **1.xii**) for further study (Figure 1.6).[13] The NCN angle of both **1.xi** (117.2°) and **1.xii** (119.5°) were found to be smaller than that of their amidinium salts, while also smaller than the NCN angle of (7-Dipp)AuCl (121.2°).[14] The authors believed this was due to the torsion angle (α°) between the planes (*vide infra*) being large for **1.xi** (α = 48.2°) and **1.xii** (α = 52.4°), which reduces the NCN angle. The Au complexes were subsequently tested in the cycloisomerization of propargylamides (Figure 1.6). The least bulky (9-Mes)AuBr was found to provide the highest yield.

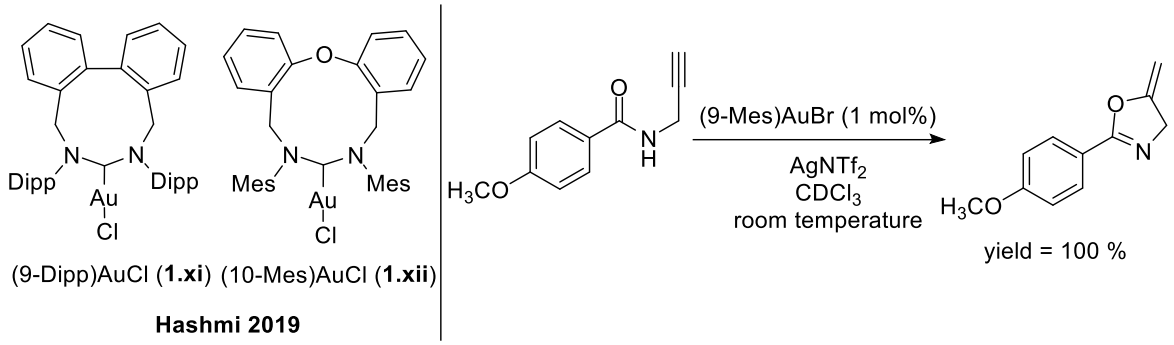


Figure 1.6 – (Left) (9-Dipp)AuCl (**1.xi**) and (10-Dipp)AuCl (**1.xii**). (Right) Catalytic conditions employed for the cycloisomerization of a propargylamide substrate.

## 1.5 – Synthesis of RE-NHCs

During the synthesis of the first free six-membered RE-NHC, Alder described the synthesis of [(6-$^{i}$Pr)H]$BF_4$ in a convenient one pot synthesis from the corresponding diamide with azeotropic removal of EtOH (Scheme 1.5a).[10] While the authors did not delve into further detail, this approach provided the basis for further development by Buchmeiser (Scheme 1.5b).[15]

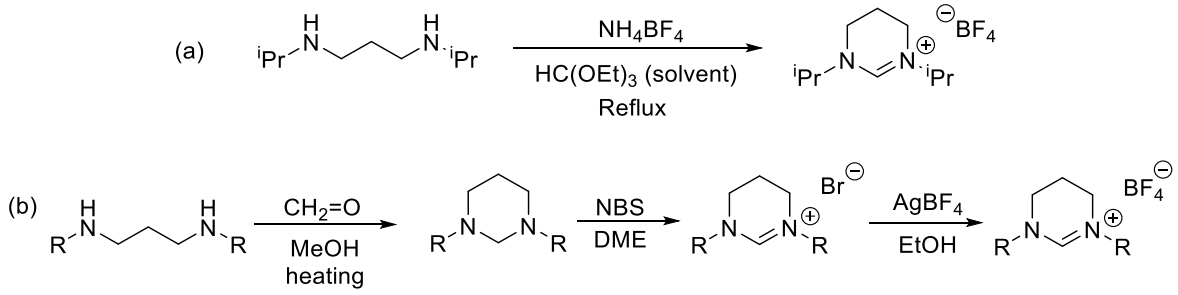


Scheme 1.5 – (a) Synthetic route Alder employed to synthesise [(6-$^{i}$Pr)H]$BF_4$.[10] (b) Buchmeiser's method to RE-NHC salts.[15]

Cavell developed an alternative (and facile) two step synthesis to RE-NHC salts containing aryl N-substituents, which could be scaled up to multiple grams (Scheme 1.6a).[7] In this method, the RE-NHC salts are formed from the formamidine, which is then subsequently ring closed *via* reaction with a dihaloalkane. Customisation of the RE-NHC salts can be achieved by choice of the initial amine, which can lead to mixed substitutions of the formamidine,[16] and on ring size in the subsequent step depending on chain length of the dihaloalkyl substrate.[11,12] Later work by Cavell extended the approach to the preparation of RE-NHC salts with N-alkyl substituents (Scheme 1.6b).[17]

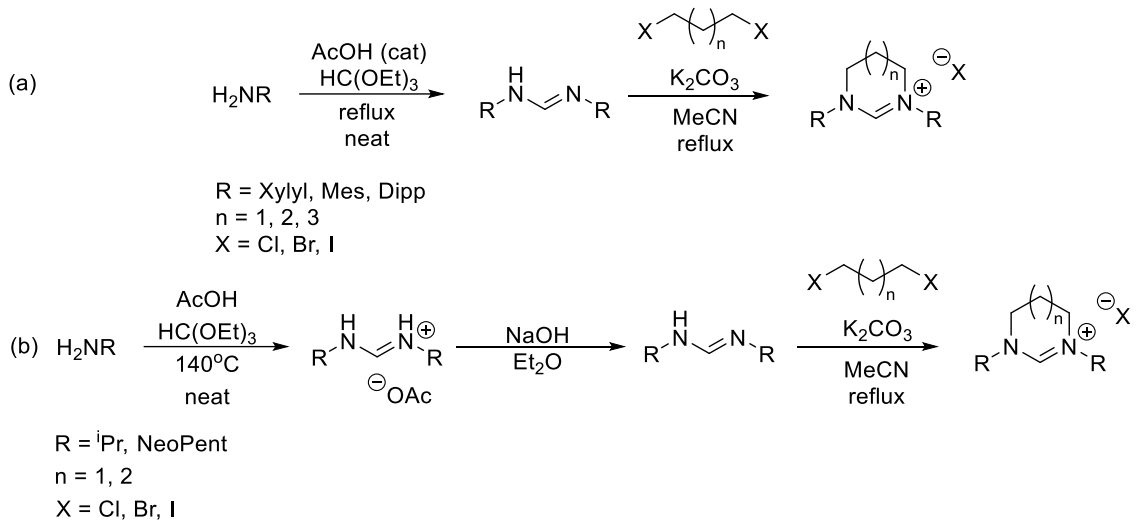


Scheme 1.6 – a) Synthesis of N-aryl substituted RE-NHC salts,[7] and b) Synthesis of N-alkyl substituted RE-NHC salts.[17]

## 1.6 – Properties of RE-NHCs

One of the reasons for increasing the ring size in the NHCs is to influence the extent of σ-donation to a coordinated metal centre. However, there have been disputes as to which method is suitable for assessing this property. For example, Tolman's electronic parameter, which was commonly used to assess phosphines, was found to give contradictory results depending on choice of solvent and the metal system employed (Ni, Rh or Ir).[2] One important spectrochemical feature of a carbene is its $^{13}C_{carbene}$ chemical shift, which is diagnostic and usually resides highly downfield of other signals (> 200 ppm) (Figure 1.7).

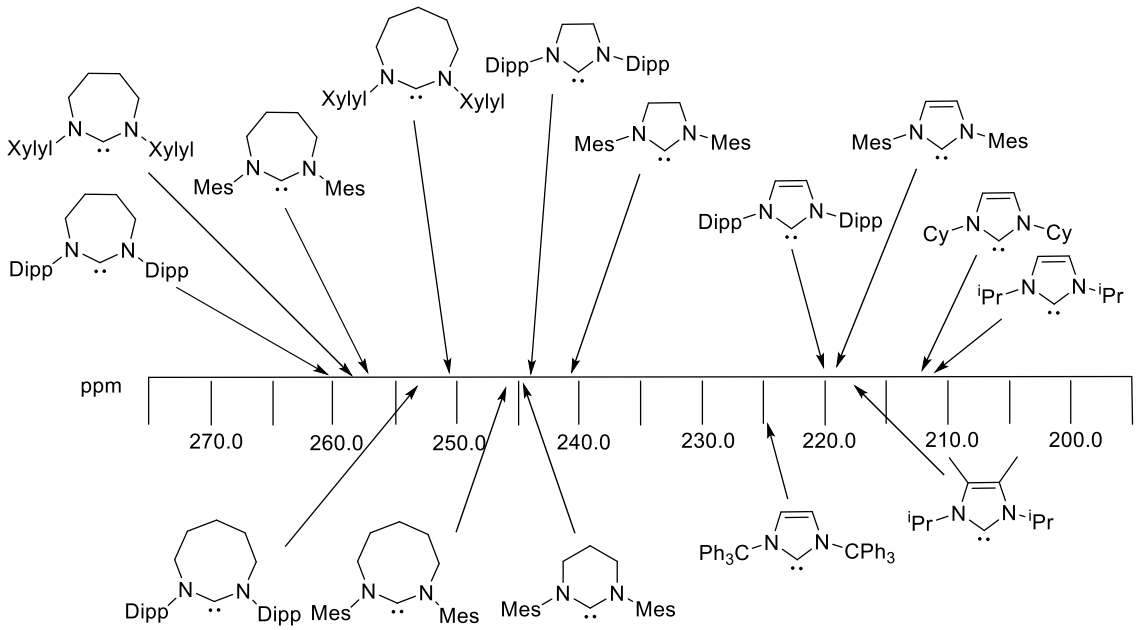


Figure 1.7 – $^{13}C$ NMR chemical shifts (in $C_6D_6$) of RE-NHCs and some selected 5-membered ring NHCs.[11,12,18–20]

When an NHC is bound to a metal centre, the effect of the ligand trans to the NHC was found to strongly influence the $^{13}C_{carbene}$ chemical shift.[21,22] Realising this, Huynh developed a method to assess the σ-donating ability of an NHC by complexing it to a (NHC)Pd species, $[PdBr_2(^iPr_2\text{-bimy})]_2$, to provide a standardised method for comparison (Figure 1.8). While this method is suitable for smaller NHCs, when applied to RE-NHCs, it was found to have its limitations. Firstly, when RE-NHCs were complexed as $PdBr_2(^iPr_2\text{-bimy})$(RE-NHC), the larger steric bulk associated with RE-NHCs (*vide infra*) led to elongated Pd-C distances which pushed the $^{13}C_{carbene}$ shift more upfield than expected. Comparison of the ring sizes containing flexible benzyl N-substituents gave in order of increasing downfield shift, 5-Bn < 6-Bn < 8-Bn < 7-Bn, which was more expected, although 8-Bn, which has the widest NCN angle, proved to not follow this trend due to its flexible backbone (*vide infra*).

When changing to a linear Au(I) species $[Au(^iPr_2\text{-bimy})$(RE-NHC)]X to overcome such problems, an anisotropic effect arising from the proximity of the N-substituents to the metal led to unexpected results.[23] Further development of an experimental method to assess donation in RE-NHCs is still being developed.

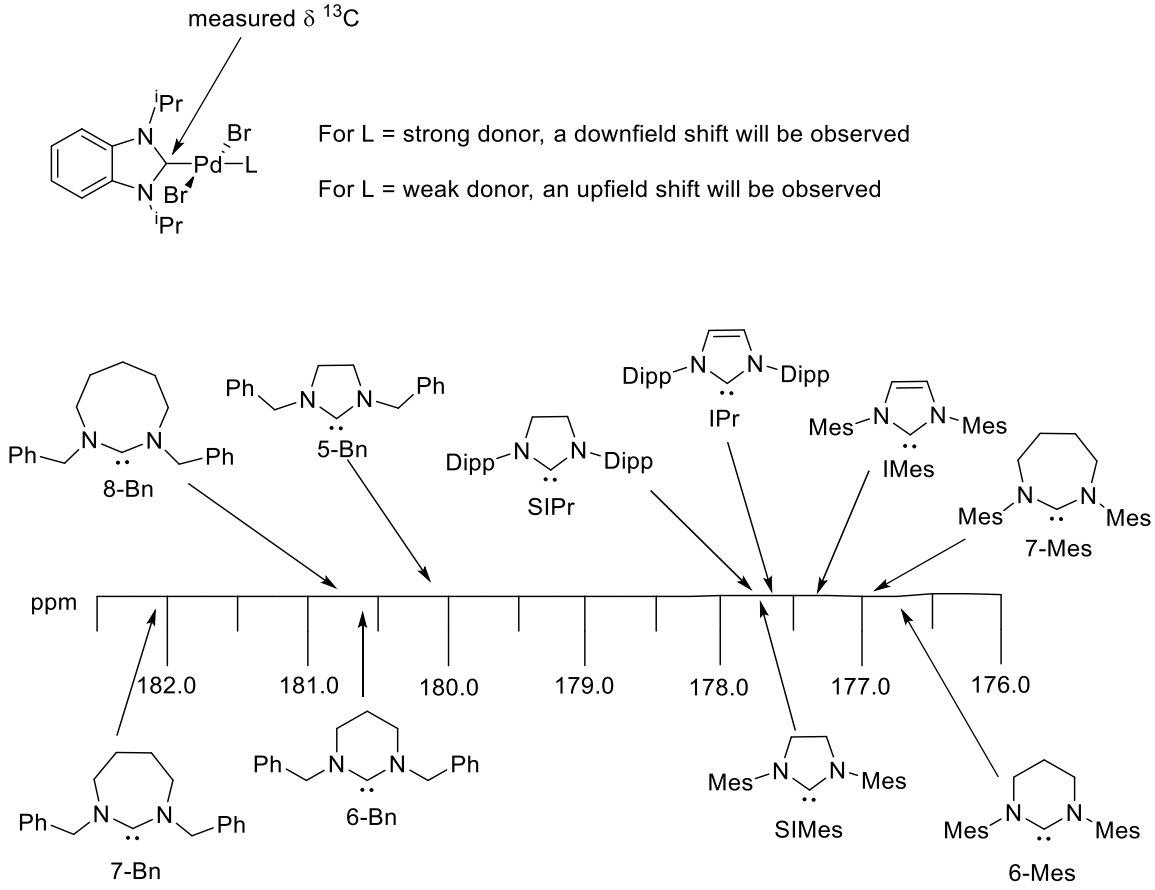


Figure 1.8 – Huynh Electronic Parameter (HEP) of selected NHCs complexed to $PdBr_2(^iPr_2\text{-bimy})$.[2,23]

A computational approach by Ramsden and Oziminski has been developed in the last 5 years in which they assess the relative energy of formation of carbenes (CREF), from their salt precursors.[24,25] The metric (Figure 1.9) is based solely on the σ-donating properties of the carbene, excluding steric and π considerations.[24,25] RE-NHCs are yet to be assessed, but this method could provide a good indication of σ-donating properties without being influenced by other parameters.

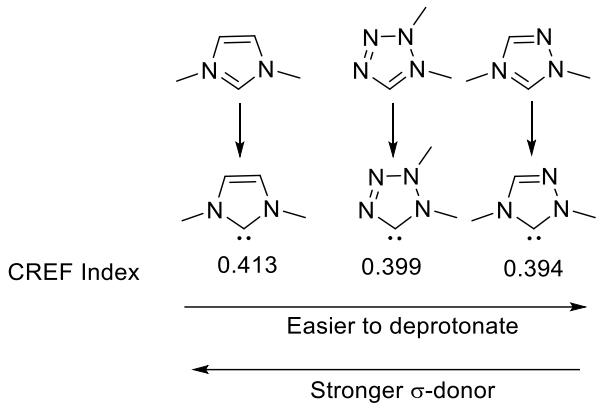


Figure 1.9 – CREF index by Ramsden and Oziminski.[24,25] In CREF units, 0.01 CREF unit = 6.2 kcal mol$^{-1}$.

As a final example, Nolan and co-workers compared C-H *J*-couplings in salt precursors to determine σ-donor strength (Figure 1.10).[26] The magnitude of the $J_{CH}$ coupling is linked to the hybridisation of the carbon centre, where those with a larger coupling have more *s* orbital character on the σ orbital, thus being a weaker donor. Comparison of salts using $^{1}H/^{13}C$ NMR spectroscopy provided an easily accessible method without needing to form M-carbene complexes. While the authors showed that concentration and counter anion effects have little influence, it will become apparent in Chapter 4 that subtle influences might arise from alterations of solvent and counter anion.

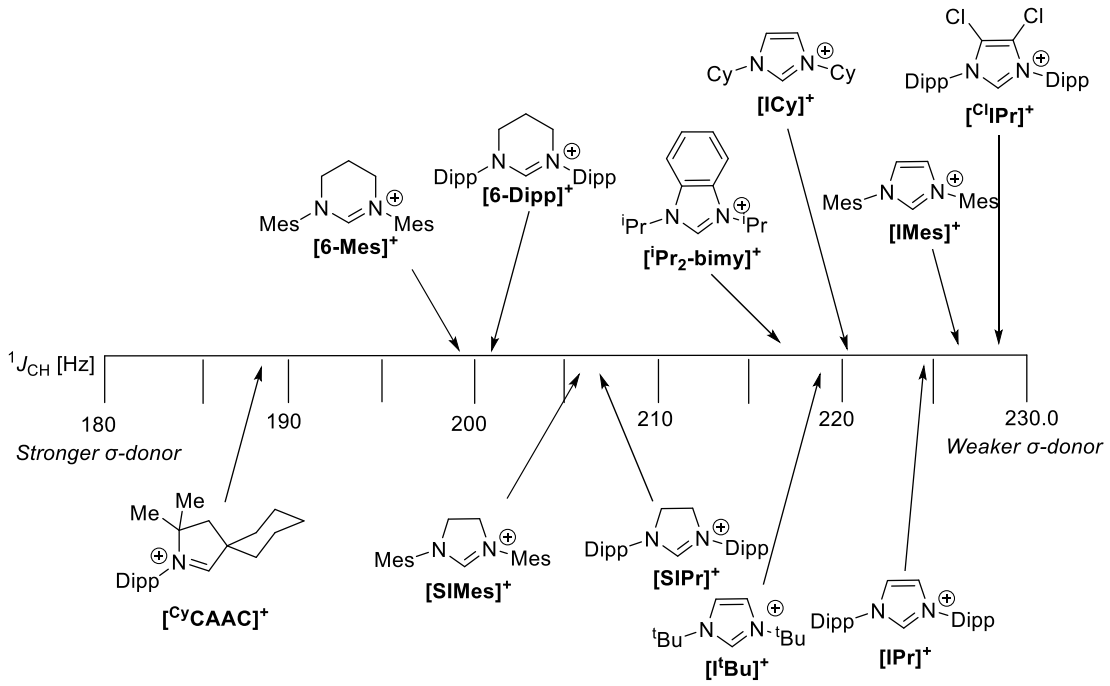


Figure 1.10 - σ-Donor ability of NHC precursors based on Nolan's unified $^{1}J_{CH}$ scale.

It is also worth mentioning minor studies of the π-acceptor properties of carbenes have been investigated by methods involving complexation of the carbene to Pt,[27] P [28] and Se.[29] π-acceptor properties has been considered to play a minor, almost negligible effect, on catalysis, although there are exceptions where this influence was shown to be important.[30]

## 1.7 – Steric Bulk

Compared to phosphines, which have spatial arrangements of a cone, NHCs are described as having spatial arrangements like an umbrella[31] this led to difficulty assessing the steric bulk of NHCs through Tolman's cone angle (Figure 1.11a). Nolan and Clavier proposed an alternative method called percentage buried volume (%$V_{Bur}$).[32–35] The method visualises a sphere around the metal centre of a set radius and calculates the percentage occupancy of this sphere to give %$V_{Bur}$ (Figure 1.11b). In addition to a value, a steric map is also provided highlighting features on an NHC which impacts more on steric bulk through a topological map. Overall, this parameter works efficiently on complexes with less congested M centres such as two coordinate Au(I) or Cu(I) complexes. However, with congested centres, unrepresentative arrangements of the NHC might influence results. In addition, since this method is based on crystal structure data, it may not represent the solution based steric bulk of an NHC.[36,37]

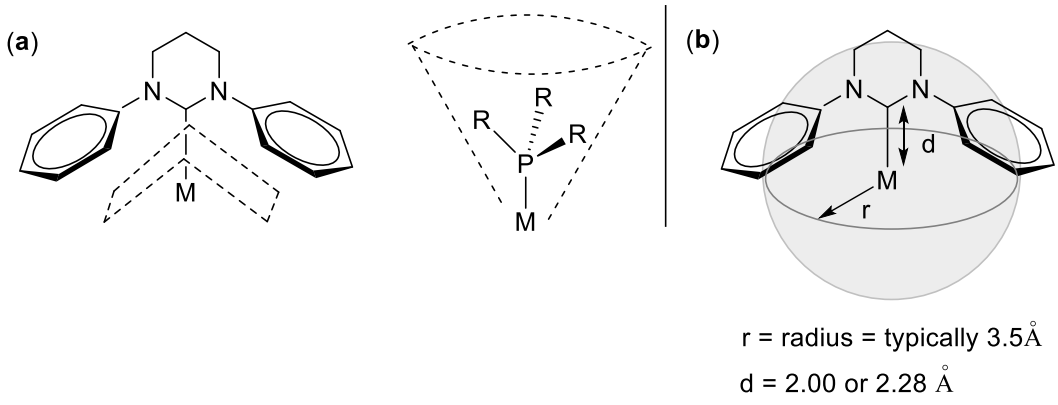


Figure 1.11 – (a) Umbrella spatial arrangement of NHCs vs cone spatial arrangement of phosphines. (b) Percentage buried volume (%$V_{Bur}$).[32–35]

In general, RE-NHCs are found to be far bulkier than their 5-membered ring counterparts, aside from a few exceptions, such as ITr (Figure 1.12).[13,19] One feature of RE-NHCs which influences their steric presence on the metal centre is twisting of the ring (measured by the torsion angle (α°)) and its puckering (Figure 1.13).[38] This feature can lead to less predictable steric and electronic properties of the RE-NHC as the NCN angle is influenced by these changes. One approach to overcome this issue with RE-NHCs is by adding a rigid backbone to reduce flexibility.[37]

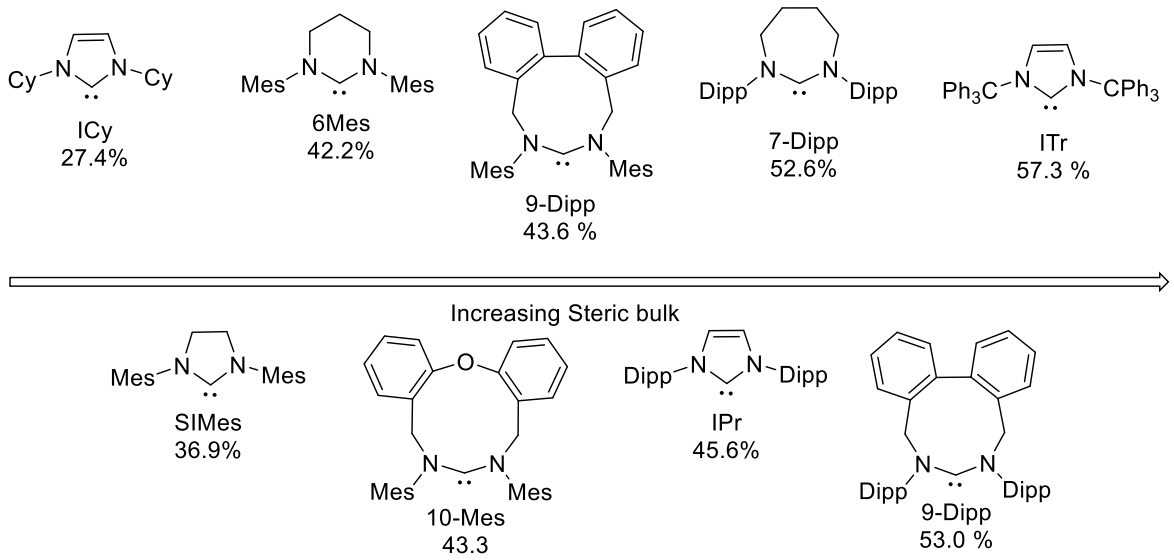


Figure 1.12 – $\%V_{Bur}$ values of NHCs in their (NHC)AuCl complexes.[13,19,33]

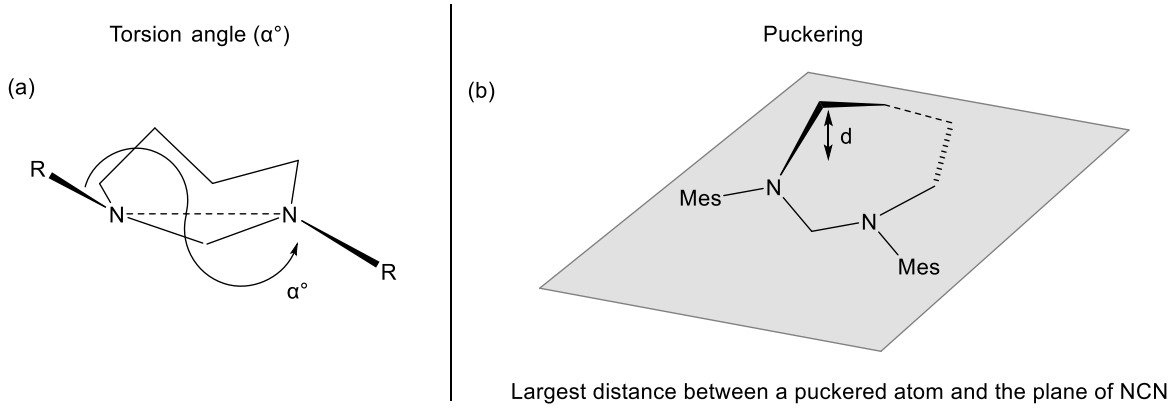


Figure 1.13 – (a) Torsion angle (α°) described by Cavell.[7] (b) Illustration of ring puckering.[38]

## 1.8 – Metal Complexes of RE-NHCs in Catalysis

RE-NHCs have been employed as ligands for a wide array of metals in catalysis including: Fe,[39–41] Ni,[16,42] Cu,[43,44] Zn,[45] Ga,[46] Rh,[47] Pd,[48–52] In,[46] Ir,[53] Pt[54] and Au.[13,55–57] The free carbenes have also been employed as catalysts.[45,58,59] A few examples will be discussed below.

The first comparative study utilising RE-NHCs was by Dunsford and Cavell in 2011 on the Pd(0) catalysed Mizoroki-Heck coupling of 4-bromoacetophenone with n-butyl acrylate (Scheme 1.7).[60] A range of 6- and 7- membered ring (RE-NHC)Pd(0) precursors, along with an (IMes)Pd(0) precursor, were synthesised and tested (Scheme 1.7). The study revealed a significant increase in activity upon expansion of the NHC ring, in the order IMes < 6-Mes < 7-Mes, with a fivefold increase in TOF between the 6-Mes and 7-Mes cases. Comparison of N-substituent effects showed the activity between 6-Mes, 6-Xylyl and 6-*o*-Tolyl to be comparable. The (6-*o*-anis)Pd(0) precursor was found to be the most reactive of the 6-membered RE-NHCs, with the authors

suggesting the *ortho*-methoxy group helped stabilise intermediates in the catalytic cycle. Comparison of the 7-membered NHCs revealed a different order of reactivity, 7-Mes > 7-Xylyl > 7-*o*-tolyl.

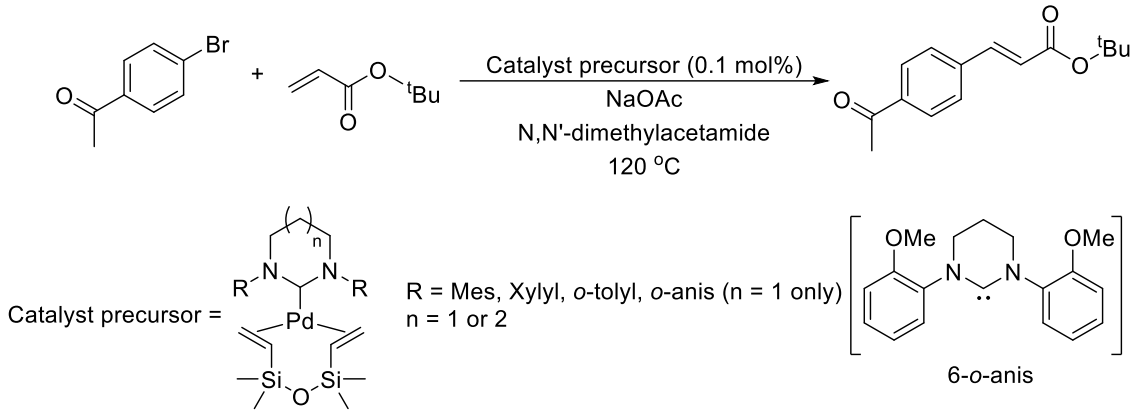


Scheme 1.7 – (RE-NHC)Pd(0) catalysed Mizoroki-Heck coupling.[60]

Nechaev demonstrated a "goldilocks" effect of 5-, 6- and 7-membered NHCs in the (RE-NHC)Pd catalysed Suzuki-Miyaura cross coupling of 3-chloropyridine with 4-tolylboronic acid (Table 1.1).[48] The catalyst screen revealed the N-Dipp substituted NHCs gave higher yields compared to their mesityl analogues. However, 7-Dipp was detrimental to catalysis, seemingly because it was too bulky. Huynh and co-workers demonstrated a similar trend with RE-NHCs in their structure-activity relationship (SAR) of iron catalysed Kumada coupling, where a balance of ring size and N-substituent sterics were found to be required to bring about the best results.[39]

Table 1.1 - Catalyst screen for Suzuki-Miyaura coupling of 3-chloropyridine and 4-tolylboronic acid by Nechaev.

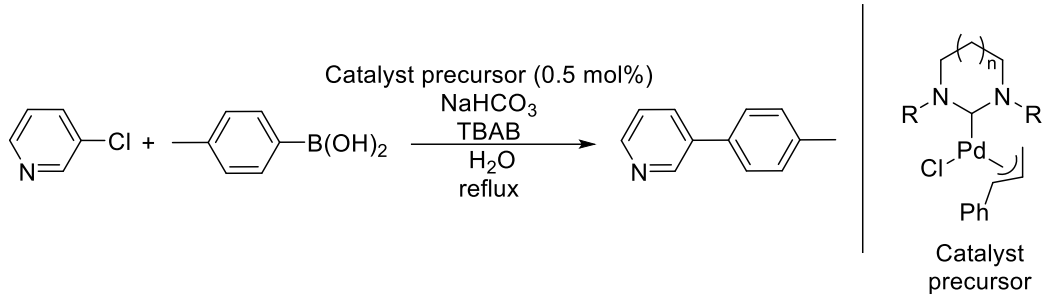


| Entry | NHC | Isolated Yield (%) |
|---|---|---|
| 1 | SIMes | 3 |
| 2 | 6-Mes | 33 |
| 3 | 7-Mes | 15 |
| 4 | SIPr | 84 |
| 5 | 6-Dipp | 86 |
| 6 | 7-Dipp | 25 |

Huynh and co-workers also demonstrated that increased steric bulk associated with ring expansion can be less detrimental in their Au catalysed hydroamination of alkynes.[56] The most active systems, (RE-NHC)AuBr, varied in the order 6-Mes < 7-Mes < 8-Mes (Scheme 1.8). However, other species in the study revealed poorer activity, which the authors attributed to the increased steric bulk around the Au centre and strong Au-C bonds providing harder access to vacant sites (Scheme 1.8).

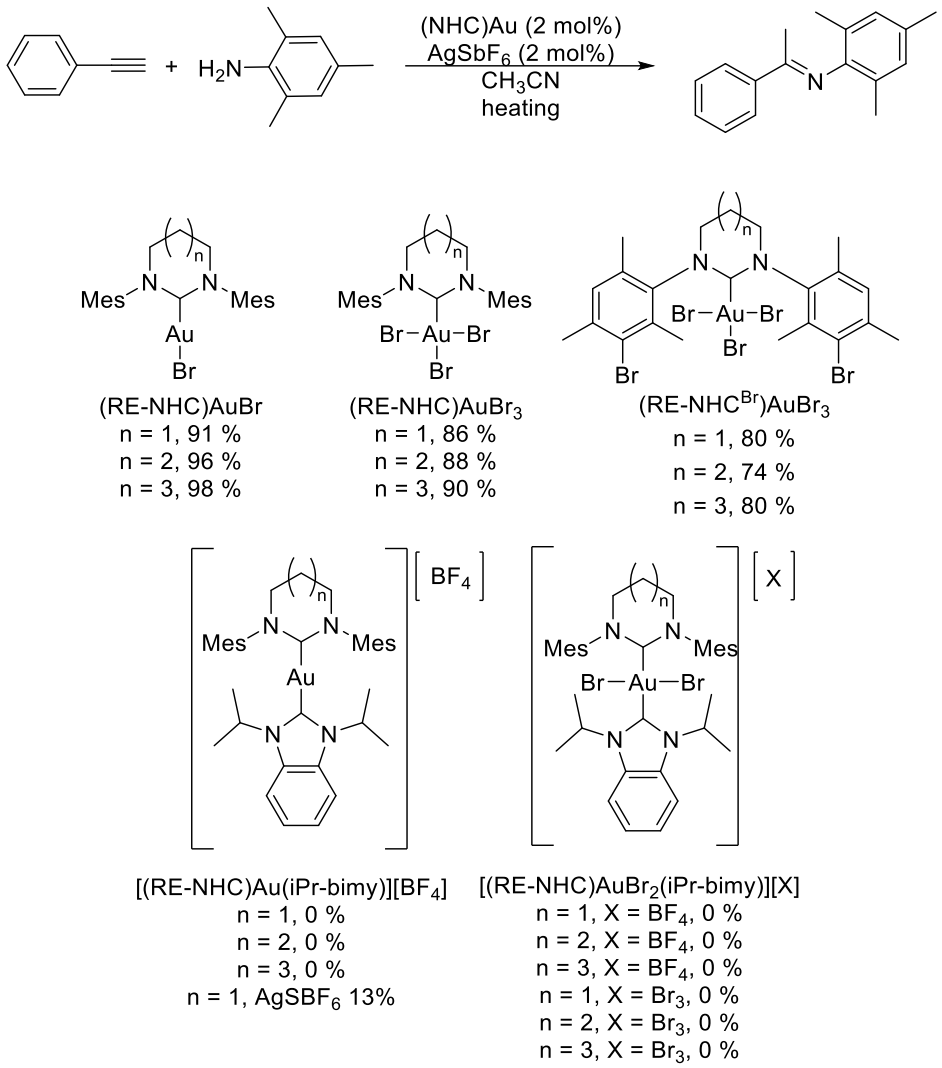


Scheme 1.8 – Gold systems tested by Huynh in the hydroamination of phenylacetylene.[56]

## 1.9 – (RE-NHC)Cu Complexes

In recent years, studies of (RE-NHC)Cu complexes focussed on Cu reduction chemistry and Cu catalysed alkyne-azide cycloadditions (CuAAC). A summary of the (RE-NHC)CuX complexes are shown in Figure 1.14.[i] The first example in the literature in 2005 targeted heteroleptic (RE-NHC)CuX complexes immobilized on a support to provide a recoverable catalyst for the cyanosilylation of carbonyls.[61] Synthesis of **1.xiii**, **1.xiv** and **1.xv** will be discussed in Chapter 4. Both **1.xiv** and **1.xv** displayed good catalytic reactivity with TONs of *ca.* 40,000 for an array of substrates. However, the authors were unable to determine the reactive Cu component of **1.xv**.

[i] Complexes assigned with numbers other than **1** are discussed in later chapters and will follow those numberings to maintain the same designation throughout the thesis.

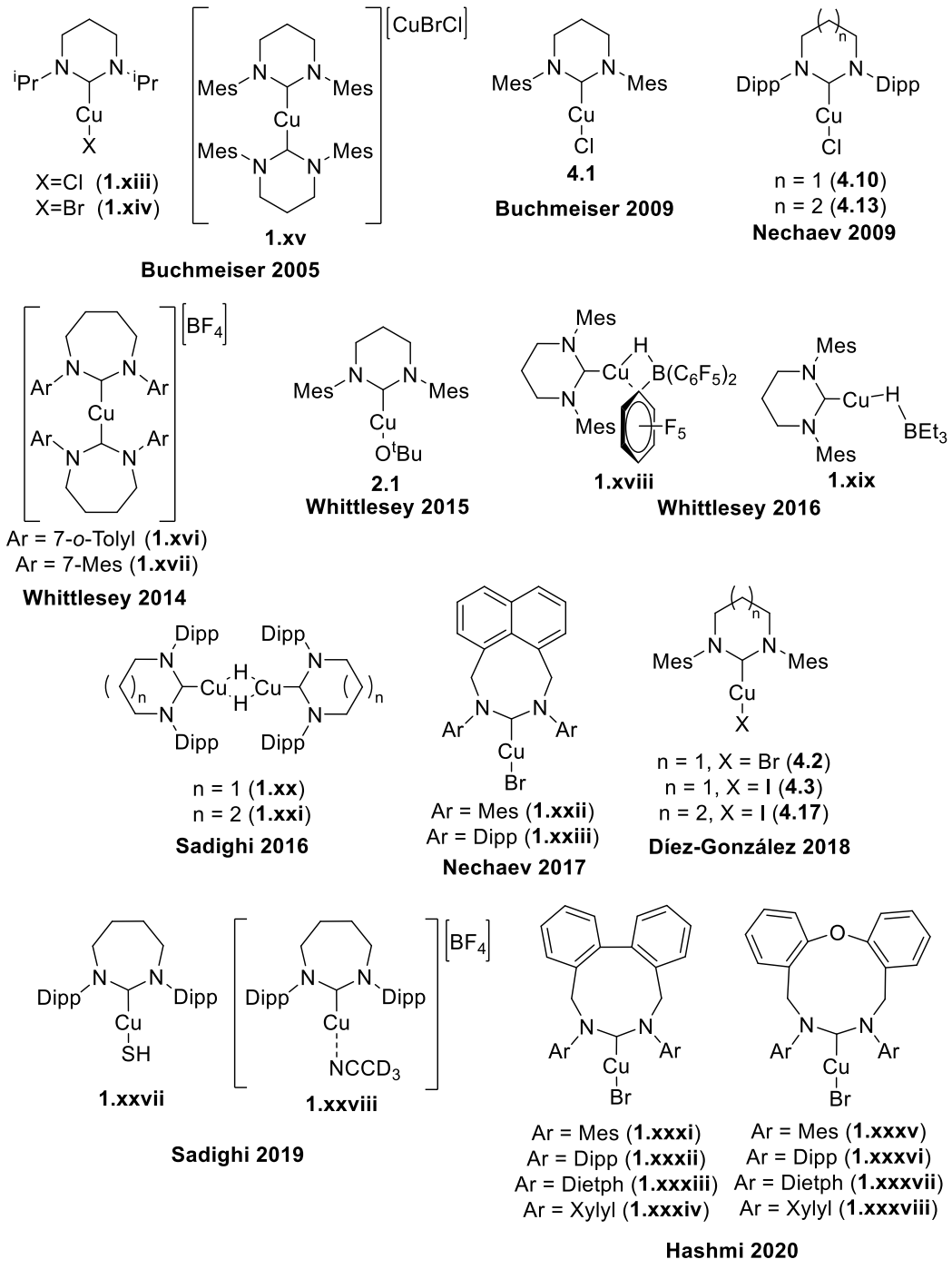


Figure 1.14 – (RE-NHC)Cu complexes in the literature.[44,61–69]

Whittlesey and co-workers demonstrated that the homoleptic [(RE-NHC)$_2$Cu][BF$_4$] complexes, **1.xvi** and **1.xvii**, were active in CuAAC reactions down to 0.5 mol % loadings under neat conditions or on-water. However, only a limited range of substrates were tolerated during this study.[64] Nechaev demonstrated the synthesis of (RE-NHC)CuBr upon transmetallation from (RE-NHC)AgBr precursors.[63,67] Comparison of the different NHC ring sizes revealed comparable activity for (6-Mes)CuBr (**4.2**) and (Naph-8-Mes)CuBr (**1.xxii**), both of which were greater than (SIMes)CuBr, (7-Mes)CuBr and the corresponding Dipp analogues (Table 1.2). **1.xxii** was shown

to be tolerant to a wide array of alkyne and azide substrates, providing high yields (>90%) at a 1 mol % loading.

Table 1.2 – CuAAC catalyst screen by Nechaev.[67]

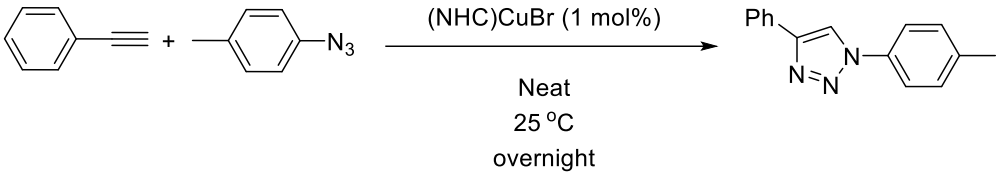


| Entry | (NHC)CuBr | Yield (%) |
|---|---|---|
| 1 | (SIMes)CuBr | 90 |
| 2 | (6-Mes)CuBr | >99 |
| 3 | (7-Mes)CuBr | 33 |
| 4 | (Napth-8-Mes)CuBr | >99 |
| 5 | (SIPr)CuBr | 4 |
| 6 | (6-Dipp)CuBr | 5 |
| 7 | (7-Dipp)CuBr | 1 |
| 8 | (Napth-8-Dipp)CuBr | 2 |

Sadighi and co-workers utilised RE-NHCs for the isolation of reactive (NHC)Cu species.[66,70] Most recently the group have moved towards understanding the activity of CuS clusters with $NO^+$ in biological systems by utilising $[(7\text{-Dipp})CuS]_2$ (**1.xxv**), $[(7\text{-Dipp})Cu\}_2(\mu\text{-S})]$ (**1.xxvi**) and (7-Dipp)CuSH (**1.xxvii**) (Scheme 1.9).[68] In the presence of $NO^+$, all were found to yield a low coordinate $[(7\text{-Dipp})Cu][BF_4]$ species (Scheme 1.10) stabilised by $CD_3CN$ (**1.xxviii**). Using fluorobenzene instead of $CD_3CN$ led to interaction of the $BF_4$ anion with $[(7\text{-Dipp})Cu]^+$, which was observed by a broadening and upfield shift of the $BF_4^-$ signal by $^{19}F$ NMR spectroscopy (Scheme 1.10b). Subsequent reaction with $PPh_3$ led to the $BF_4^-$ peak sharpening and shifting downfield, as a result of the formation of $[(7\text{-Dipp})Cu(PPh_3)][BF_4]$ (**1.xxx**).

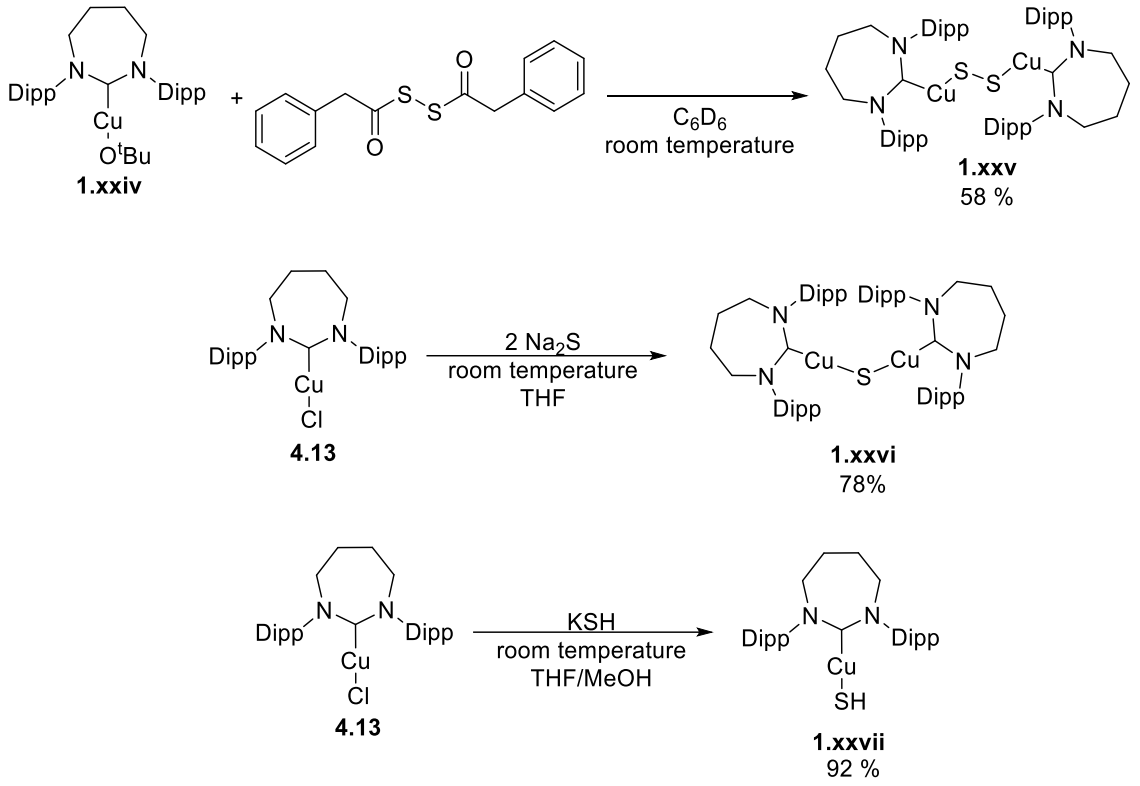


Scheme 1.9 – Synthesis of (7-Dipp)Cu(I) sulfides **1.xxv** and **1.xxvi**, and thiolate **1.xxvii**.[68]

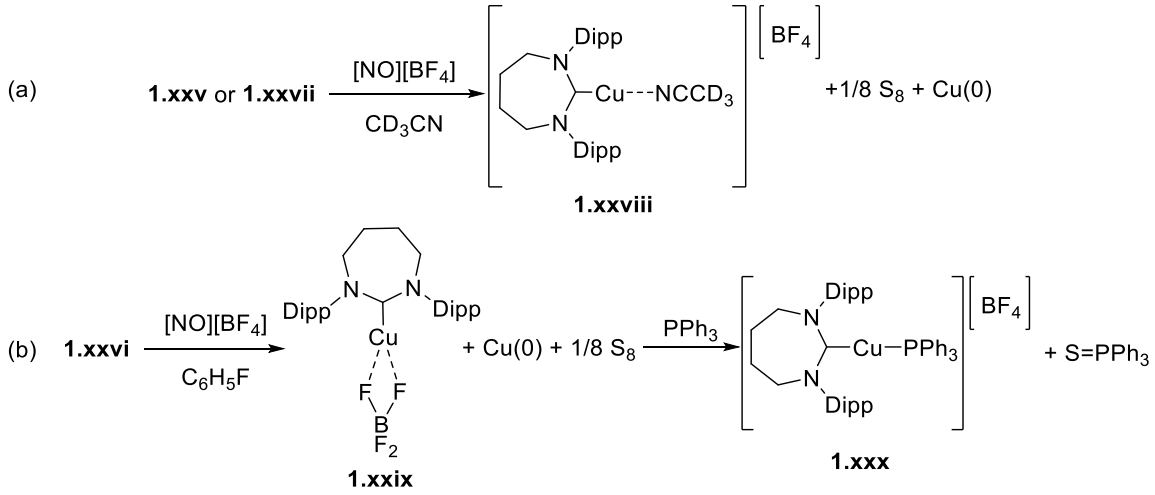


Scheme 1.10 – Formation of the low-coordinate [(7-Dipp)Cu]$^+$ cation.[68]

In addition to their 9- and 10- membered RE-NHC Au complexes,[13] Hashmi provided more examples with Ag(I) and Cu(I).[69] The Cu complexes (Figure 1.14) could be synthesised in good yield *via* the free carbene or *via* transmetallation from the corresponding AgBr reagents. However, with the less bulky N-Xylyl substituent, attempts to form **1.xxxiv** and **1.xxxviii** led to traces of three-coordinate [(RE-NHC)$_2$CuBr] being observed. The authors postulated an equilibrium *via* a Br bridging species (observed by mass spectrometry) which lies towards (RE-NHC)CuBr (Scheme 1.11).

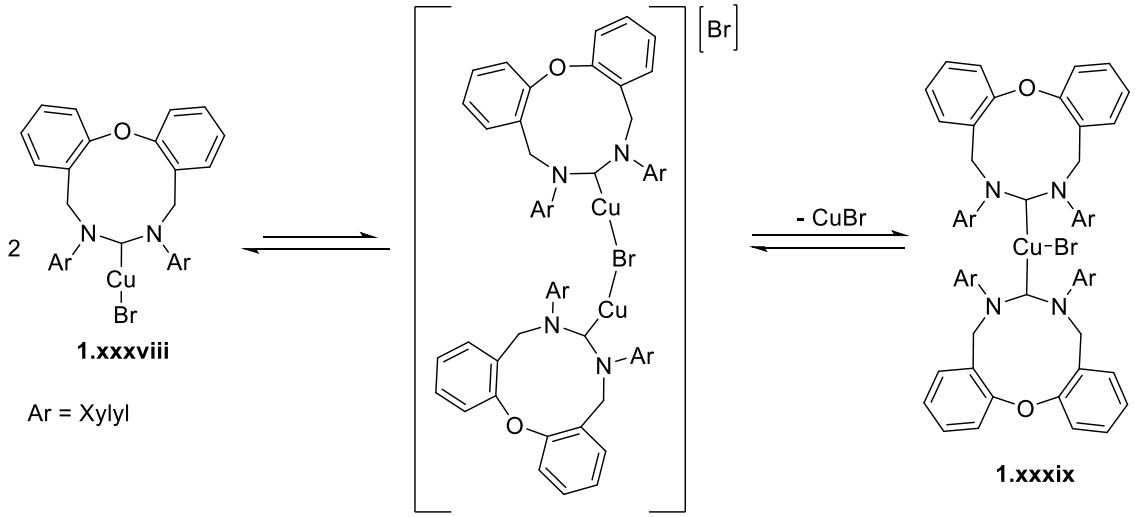


Scheme 1.11 – Postulated equilibrium of (10-Xylyl)CuBr (**1.xxxviii**) with [{(10-Xylyl)Cu}$_2$Br] (**1.xxxix**).[69]

(9-Dipp)CuBr (**1.xxxii**) was subsequently tested in the catalytic synthesis of oxazoline **1.xl.** The presence of $AgBF_4$ proved important for catalytic activity (Scheme 1.12), as neither **1.xxxii** nor $AgBF_4$ alone catalysed the reaction. The authors postulated reactivity to be analogous to that of (9-Dipp)AuBr, where a cationic $[(9\text{-Dipp})Au]^+$ species was the active species.

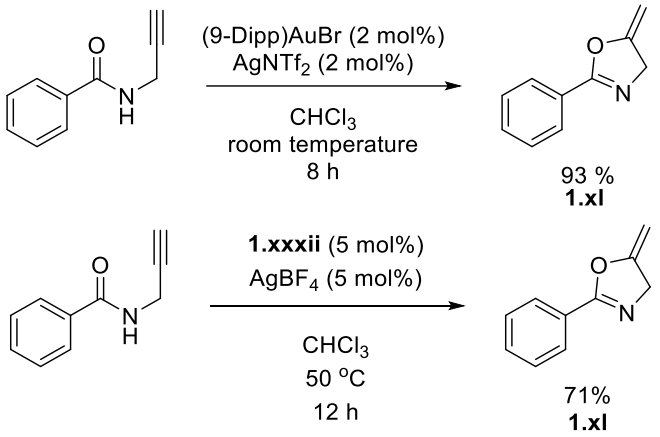


Scheme 1.12 – Au or Cu catalysed synthesis of oxazoline **1.xl**.[69]

## 1.10 – Low-coordinate Complexes and Catalysis

With increased steric bulk/protection and donation of electron density, NHCs have been shown to aid the isolation of intermediates on a catalytic cycle, as well as allow access to highly active, low coordinate organometallic species.[71] In some cases, the low coordinate nature of an organometallic species has resulted in novel activity, such as C-H activation of the N-substituent[72–74] or activation of silicon grease.[75,76]

### 1.10.1 – Low Coordinate Ni Species with NHCs

The employment of NHCs was found to provide facile access into (NHC)Ni(I) chemistry. During studies to prepare Ni(II) complexes of the type Ni(NHC)(allyl)Cl, Sigman and co-workers isolated a rare low coordinate Ni(I) dimer, $[(IPr)Ni(\mu\text{-}Cl)]_2$ (**1.xli**), amongst a mixture of other Ni species.[77] The subsequent comproportionation of $Ni(COD)_2$ and $Ni(DME)Cl_2$ in the presence of free IPr or SIPr led to **1.xli** as well as $[(SIPr)Ni(\mu\text{-}Cl)]_2$ (**1.xlii**) in reasonable yields (Scheme 1.13). Diamagnetic $^1H$ NMR spectra of **1.xli** and **1.xlii** were consistent with presence of a Ni-Ni bond.

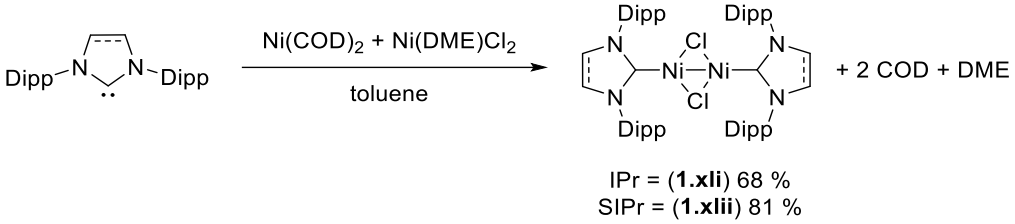


Scheme 1.13 – Synthesis of $[(IPr)Ni(\mu\text{-}Cl)]_2$ (**1.xli**) and $[(SIPr)Ni(\mu\text{-}Cl)]_2$ (**1.xlii**).

Matsubara later demonstrated that addition of $PPh_3$ to **1.xli** formed the low coordinate Ni(I) complex $Ni(IPr)(PPh_3)Cl$ (**1.xliii**) in a reversible manner (Scheme 1.14a).[78] Likewise the addition of IPr to **1.xli** to yield **1.xliv** was also found to be reversible.[78,79] Halide abstraction took place in chloroform to afford the corresponding Ni(II) dichloride species (Scheme 1.14b and c). In a later publication, Matsubara also demonstrated the ability to form two-coordinate Ni(I) species through the reaction of **1.xli** with $HNPh_2$ in the presence of base (Scheme 1.14d).[80]

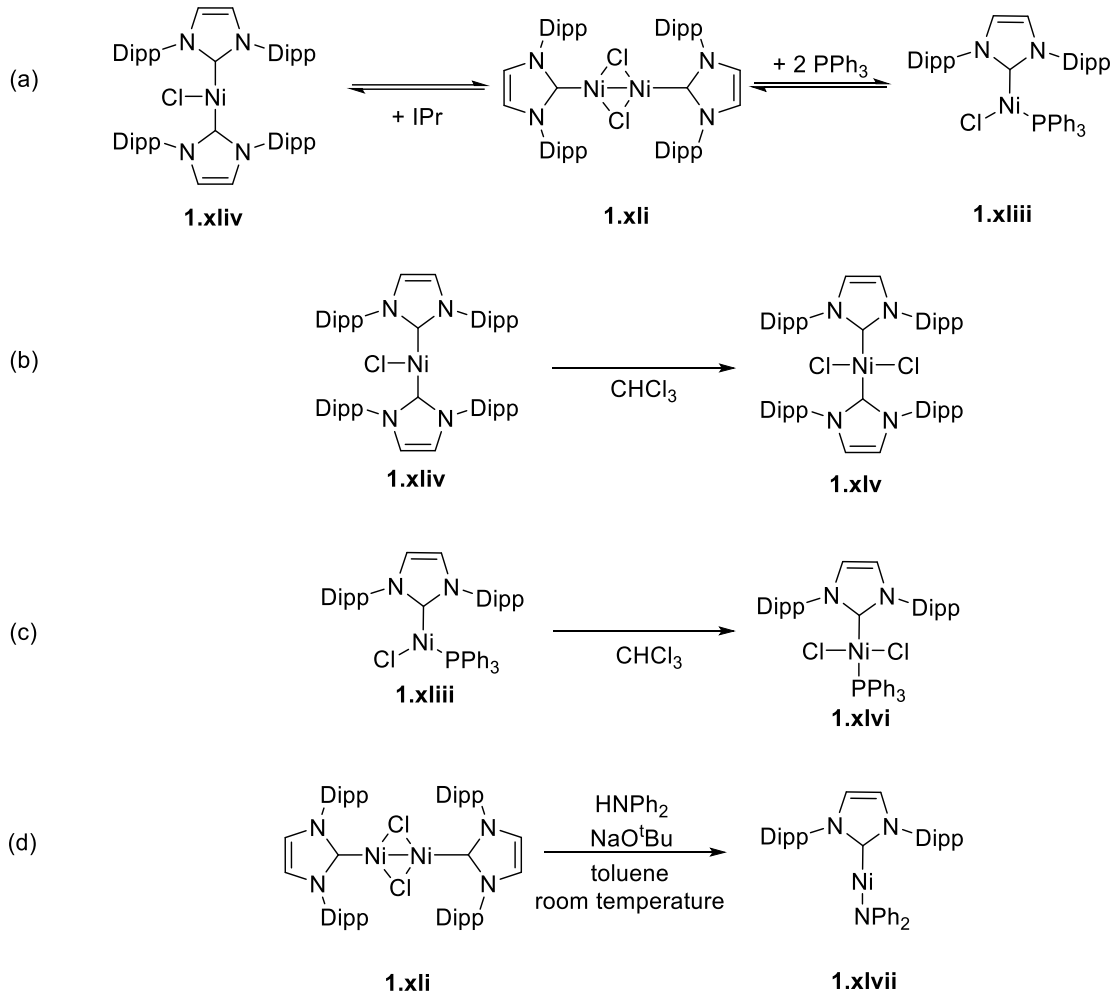


Scheme 1.14 – (a) Formation of complex **1.xli**, **1.xliii** and **1.xliv** observed by Matsubara.[78] (b)/(c) Halide abstraction observed with **1.xlv** and **1.xlvi** and $CHCl_3$. (d) Formation of the two coordinate Ni(I) complex **1.xlvii**.[80]

## 1.10.2 – Low Coordinate Ni Species with RE-NHCs

There are only a few examples of RE-NHC Ni complexes in the literature (Figure 1.15), the first of which was described by Whittlesey and co-workers in 2010.[73]

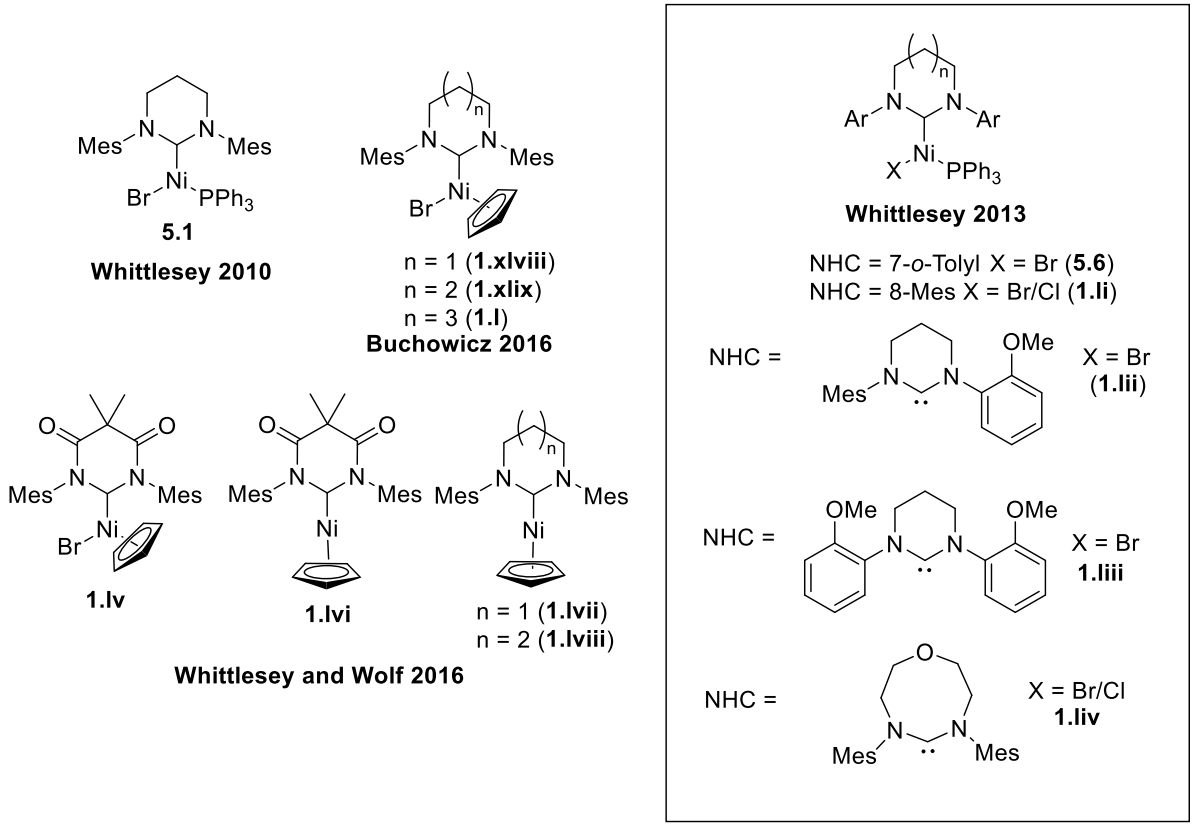


Figure 1.15 – RE-NHC Ni complexes in the literature.[42,73,81,82]

Following a similar method to that used by Sigman, comproportionation of a 1:1 mixture of $Ni(PPh_3)_2Br_2$ and $Ni(COD)_2$ in the presence of 6-Mes was used to yield the three coordinate Ni(I) species, Ni(6-Mes)($PPh_3$)Br (**5.1**) (Scheme 1.15).[73]

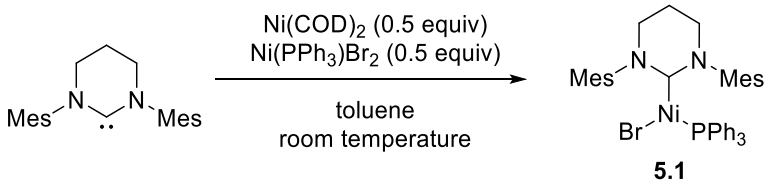


Scheme 1.15 – Synthesis of Ni(6-Mes)($PPh_3$)Br.[73]

Unlike Matsubara's three-coordinate species **1.xliii**, **5.1** was found to exist solely as a monomer in solution, with no evidence for a mono-dimer equilibrium. As discussed below, **5.1** has been studied extensively. A wider range of RE-NHCs were used to synthesise three coordinate Ni(I) analogues **1.li** – **1.liv** and **5.6** using the same methodology (Figure 1.15).[16] EPR studies of the

complexes, including **5.1**, revealed them all to have a rhombic g profile, although the different NHC ligands had a subtle effect on the SOMO of the complexes, as reflected in the corresponding g tensors. A preliminary study of the activity of **1.li** – **1.liv**, **5.1** and **5.6** in Kumada-Tamao-Corriu coupling of aryl halides and aryl Grignard reagents revealed **5.1** to be the most reactive. Blackaby demonstrated it was possible to use very bulky N-alkyl substituted RE-NHCs to form **1.lix** – **1.lxii** (Scheme 1.16), although less sterically demanding alkyl groups led to four-coordinate Ni(II) complexes, such as Ni(6-Et)($PPh_3$)$Br_2$ (**1.lxiii**) and Ni(6-$^{i}$Pr)($PPh_3$)$Br_2$ (**1.lxiv**).

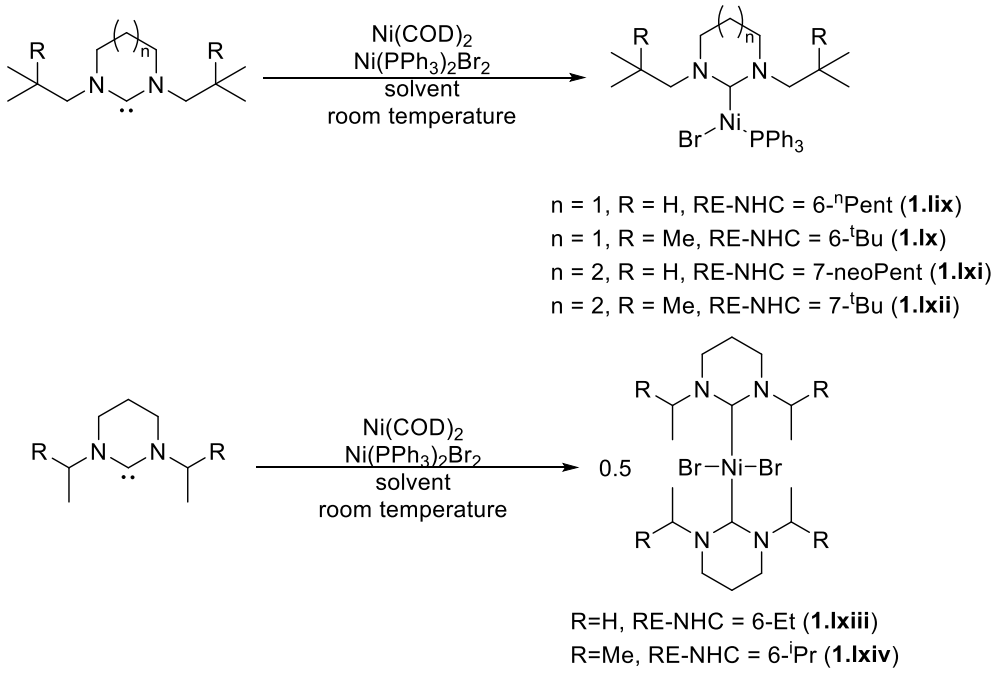


Scheme 1.16 – Attempted synthesis of alkyl analogues of **5.1** by Blackaby.[83]

In 2016, Buchowicz utilised 6-, 7- and 8-Mes as ligands to isolate Ni(II) half sandwich complexes for use in Kumada-Tamao-Corriu coupling, with the 6-Mes containing **1.xlviii** yielding the best result.[42]

Following work by Hazari and co-workers on linear CpNi(NHC) systems,[84] Whittlesey and Wolf demonstrated linear Ni(I) species could be isolated with the bulky 6-MesDAC, 6-Mes and 7-Mes ligands upon reduction of the three coordinate CpNi(NHC)Br precursors (such as **1.lv**) to yield **1.lvi** – **1.lviii** with $KC_8$.[81]

As noted above within the research group, the stoichiometric reactivity of **5.1** has received considerable attention (Scheme 1.17). Addition of 1 equivalent of 6-Mes was found to yield the two-coordinate Ni(I) salt [Ni(6-Mes)$_2$][Br] **1.lxv**.[85] The 13 electron Ni(I) centre was found to be stable to air for several minutes, in contrast to **5.1**, which reacted instantly with $O_2$ to yield the dimeric Ni(II) complexes **1.lxvi** and **1.lxvii**.[72] **1.lxv** was found to exhibit single-molecule magnet (SMM) properties, the first example of a mononuclear Ni complex to show such behaviour. It

was found that addition of $KC_8$ could reduce **1.lxv** to the highly air-sensitive Ni(0) complex, Ni(6-Mes)$_2$ (**1.lxviii**). Further homoleptic, as well as heteroleptic analogues of **1.lxv** containing an array of RE-NHCs were synthesised and discussed further by Blackaby.[83] Efforts were also focused on forming two-coordinate Ni(I) complexes from **5.1** in a similar manner to the previously described bromide abstraction.[86] Of note were the dimers {Ni(6-Mes)}$_2$($\mu$-$BH_4$)$_2$ (**1.lxix**) and [{Ni(6-Mes)}$_2$($\mu$-Br)][$BAr^F{}_4$] (**1.lxx**). **1.lxix** was observed to remain dimeric in solution based on the diamagnetic $^1$H NMR spectrum, whereas EPR spectroscopy showed that **1.lxx** dissociated to give two Ni(I) species, one of which was identified as **5.1**.

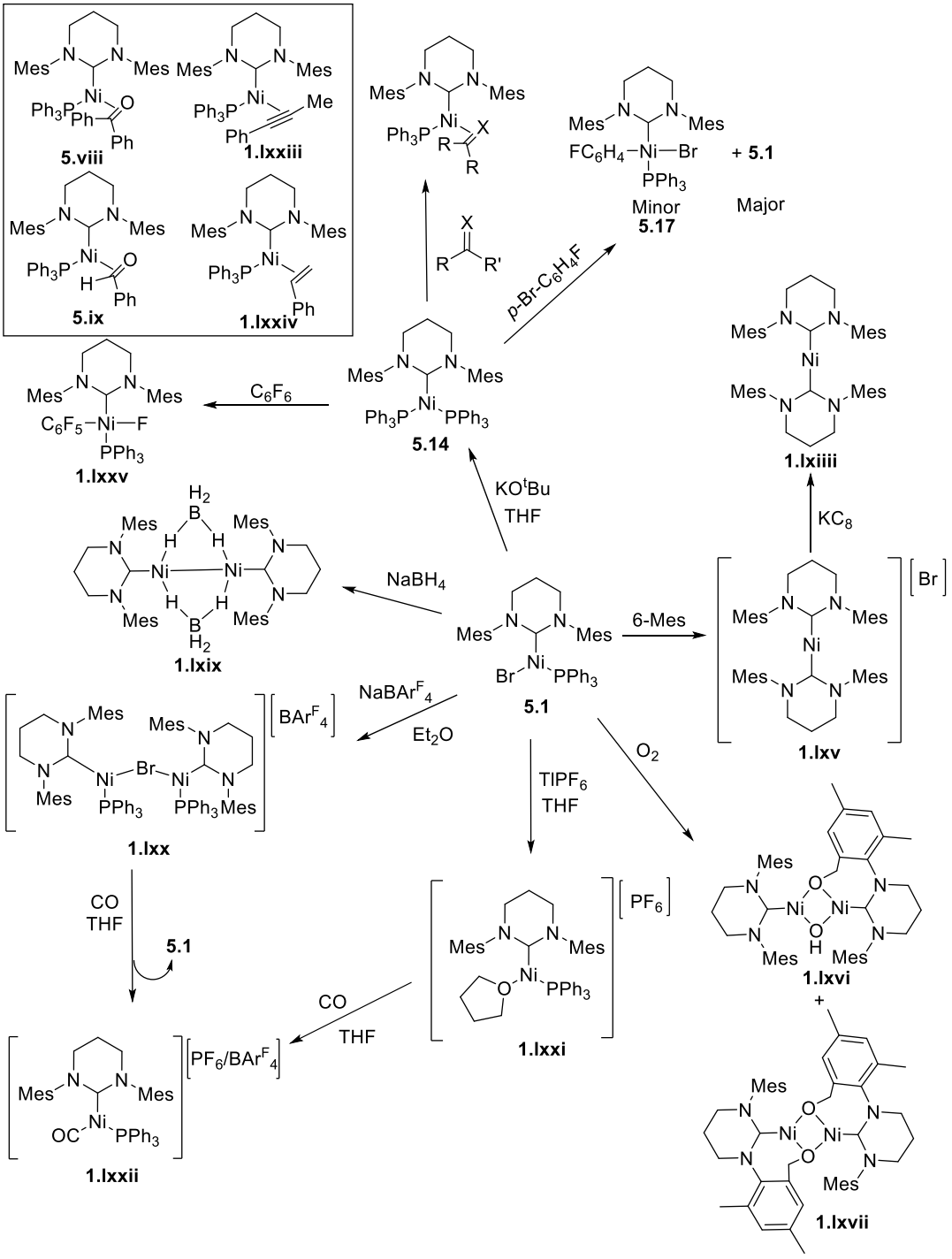


Scheme 1.17 – (RE-NHC)Ni species observed by the Whittlesey group starting from complex **5.1**.

The reaction of **5.1** with KO$^t$Bu led to the formation of Ni(6-Mes)(PPh$_3$)$_2$ (**5.14**) in low yields. While **5.14** was not the initial product (see Chapter 5), it led to an interesting array of coordination chemistry with unsaturated substrates (e.g. **1.lxxiii**, **1.lxxiv**, **5.viii** and **5.ix**), as well as bond activiation products (e.g. **1.lxxv**, **5.17**) Similar oxidation products to **5.1** were observed by Louie with Ni(IMes$_2$) (**1.lxxvi**), the formation of benzene being suggestive of a radical pathway (Scheme

1.18a).[87] In contrast, complexes with smaller NHCs, such as $Ni_2(^iPr_2Im)_4(COD)$ (**1.lxxx**), demonstrated the formation of four-coordinate species (Scheme 1.18b).[88]

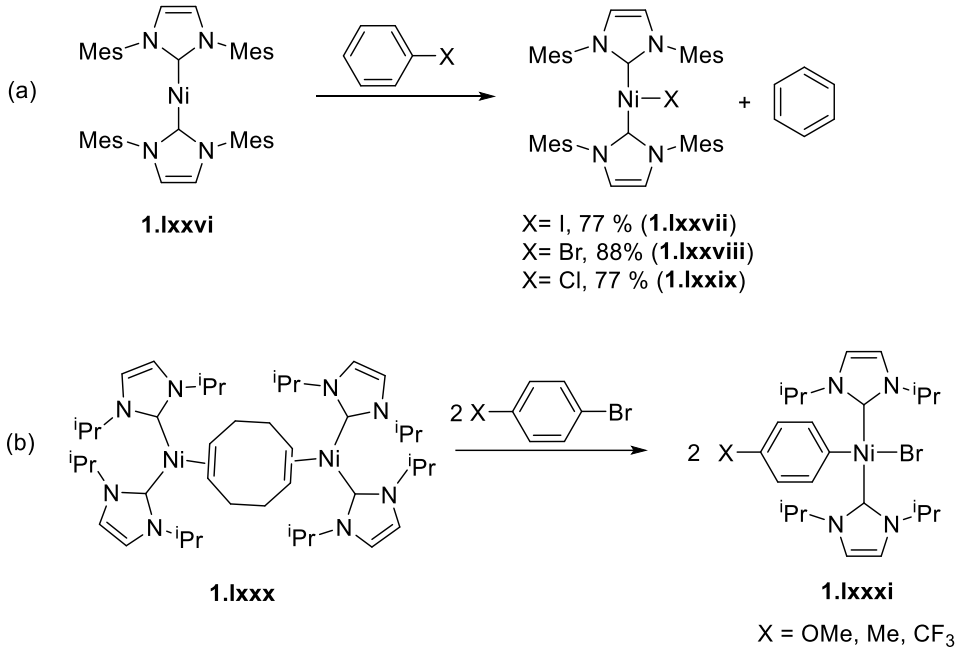


Scheme 1.18 – (a) Oxidation of **1.lxxvi** in the presence of aryl halide observed by Louie.[87] (b) Oxidation of **1.lxxx** observed by Radius.[88]

## 1.11 – Thesis Aims

This thesis will be structured around the catalytic applications of RE-NHCs as ligands for Cu and Ni. Chapter 2 reports the synthesis of (RE-NHC)CuO$^t$Bu complexes and their application in both the semihydrogenation and hydroboration of alkynes. Chapter 3 reveals new examples of (carbene)CuF complexes, along with investigation of their involvement in catalytic aldehyde allylation. Chapter 4 discusses the synthesis of (RE-NHC)CuX complexes (X = Cl, Br and I) though a cuprate methodology.

As shown in Scheme 1.17, Ni(6-Mes)$PPh_3$Br (**5.1**) has been widely studied within the group, but with only limited mechanistic studies of the catalysis it can mediate. Thus, the final results chapter of the thesis (Chapter 5) builds upon a preliminary report from 2010 on the catalytic hydrodehalogenation of aryl halides.[73] A mechanistic study of this reaction is described resulting from the isolation of rare Ni(I)-alkoxide complexes.

## 1.12 – References for Chapter 1


1 D. Bourissou, O. Guerret, F. P. Gabbaï and G. Bertrand, *Chem. Rev.*, 2000, **100**, 39–92.

2 H. V. Huynh, *The Organometallic Chemistry of N-Heterocyclic Carbenes*, Wiley, Singapore, 1st edn., 2017.

3 R. W. Alder, P. R. Allen and S. J. Williams, *J. Chem. Soc. Chem. Commun.*, 1995, 1267–1268.

4 M. K. Denk, A. Thadani, K. Hatano and A. J. Lough, *Angew. Chem. Int. Ed.*, 1997, **36**, 2607–2609.

5 A. J. Arduengo, F. Davidson, H. V. R. Dias, J. R. Goerlich, D. Khasnis, W. J. Marshall and T. K. Prakasha, *J. Am. Chem. Soc.*, 1997, **119**, 12742–12749.

6 D. Munz, *Organometallics*, 2018, **37**, 275–289.

7 M. Iglesias, L. Male, M. B. Hursthouse, A. Dervisi, I. A. Fallis, J. C. Knight, A. Stasch, L. Ooi, S. Coles, D. J. Beetstra and K. J. Cavell, *Organometallics*, 2008, **27**, 3279–3289.

8 M. Yasui, S. Yoshida, S. Kakuma, S. Shimamoto, N. Matsumura and F. Iwasaki, *Bull. Chem. Soc. Jpn*, 1996, **69**, 2739–2747.

9 F. Iwasaki, M. Yasui, S. Yoshida, H. Nishiyama, S. Shimamoto and N. Matsumura, *Bull. Chem. Soc. Jpn*, 1996, **69**, 2759–2770.

10 R. W. Alder, M. E. Blake, C. Bortolotti, S. Bufali, C. P. Butts, E. Linehan, J. M. Oliva, A. G. Orpen and M. Quayle, *Chem. Commun.*, 1999, 241–242.

11 M. Iglesias, D. J. Beetstra, A. Stasch, P. N. Horton, M. B. Hursthouse, S. J. Coles, K. J. Cavell, A. Dervisi and I. A. Fallis, *Organometallics*, 2007, **26**, 4800–4809.

12 W. Y. Lu, K. J. Cavell, J. S. Wixey and B. Kariuki, *Organometallics*, 2011, **30**, 5649–5655.

13 A. Cervantes-Reyes, F. Rominger, M. Rudolph and A. S. K. Hashmi, *Chem. Eur. J.*, 2019, **25**, 11745–11757.

14 J. J. Dunsford, K. J. Cavell and B. M. Kariuki, *Organometallics*, 2012, **31**, 4118–4121.

15 M. Mayr, K. Wurst, K. H. Ongania and M. R. Buchmeiser, *Chem. Eur. J.*, 2004, **10**, 1256–1266.

16 M. J. Page, W. Y. Lu, R. C. Poulten, E. Carter, A. G. Algarra, B. M. Kariuki, S. A.

Macgregor, M. F. Mahon, K. J. Cavell, D. M. Murphy and M. K. Whittlesey, *Chem. Eur. J.*, 2013, **19**, 2158–2167.

17 J. J. Dunsford, D. S. Tromp, K. J. Cavell, C. J. Elsevier and B. M. Kariuki, *Dalton. Trans.*, 2013, **42**, 7318–7329.

18 S. J. Ryan, S. D. Schimler, D. C. Bland and M. S. Sanford, *Org. Lett.*, 2015, **17**, 1866–1869.

19 M. M. D. Roy, P. A. Lummis, M. J. Ferguson, R. McDonald and E. Rivard, *Chem. Eur. J.*, 2017, **23**, 11249–11252.

20 N. Ortega, C. Richter and F. Glorius, *Org. Lett.*, 2013, **15**, 1776–1779.

21 M. V Baker, P. J. Barnard, S. K. Brayshaw, J. L. Hickey, B. W. Skelton and A. H. White, 2005, **8**, 37–43.

22 D. J. Cardin, B. Çetinkaya, E. Çetinkaya, M. F. Lappert, L. J. Manojlović-Muir and K. W. Muir, *J. Organomet. Chem.*, 1972, **44**, C59–C62.

23 A. Kumar, D. Yuan and H. V. Huynh, *Inorg. Chem.*, 2019, **58**, 7545–7553.

24 C. A. Ramsden and W. P. Oziminski, *J. Org. Chem.*, 2016, **81**, 10295–10301.

25 C. A. Ramsden and W. P. Oziminski, *J. Org. Chem.*, 2017, **82**, 12485–12491.

26 G. Meng, L. Kakalis, S. P. Nolan and M. Szostak, *Tetrahedron Lett.*, 2019, **60**, 378–381.

27 S. Fantasia, J. L. Petersen, H. Jacobsen, L. Cavallo and S. P. Nolan, *Organometallics*, 2007, **26**, 5880–5889.

28 O. Back, M. Henry-Ellinger, C. D. Martin, D. Martin and G. Bertrand, *Angew. Chem.*, 2013, **125**, 3011–3015.

29 A. Liske, K. Verlinden, H. Buhl, K. Schaper and C. Ganter, *Organometallics*, 2013, **32**, 5269–5272.

30 M. Alcarazo, T. Stork, A. Anoop, W. Thiel and A. Fürstner, *Angew. Chem. Int. Ed.*, 2010, **49**, 2542–2546.

31 T. Dröge and F. Glorius, *Angew. Chem. Int. Ed.*, 2010, **49**, 6940–6952.

32 J. Jover and J. Cirera, *Dalton. Trans.*, 2019, **48**, 15036–15048.

33 H. Clavier and S. P. Nolan, *Chem. Commun.*, 2010, **46**, 841–861.

34 L. Falivene, R. Credendino, A. Poater, A. Petta, L. Serra, R. Oliva, V. Scarano and L.

Cavallo, *Organometallics*, 2016, **35**, 2286–2293.

35 L. Falivene, Z. Cao, A. Petta, L. Serra, A. Poater, R. Oliva, V. Scarano and L. Cavallo, *Nat. Chem.*, 2019, **11**, 872–879.

36 G. Altenhoff, R. Goddard, C. W. Lehmann and F. Glorius, *Angew. Chem. Int. Ed.*, 2003, **42**, 3690–3693.

37 K. R. Sampford, J. L. Carden, E. B. Kidner, A. Berry, K. J. Cavell, D. M. Murphy, B. M. Kariuki and P. D. Newman, *Dalton. Trans.*, 2019, **48**, 1850–1858.

38 R. C. Poulten, PhD Thesis, University of Bath, 2015.

39 Q. Teng, W. Wu, H. A. Duong and H. V. Huynh, *Chem. Commun.*, 2018, **54**, 6044–6047.

40 J. Cheng, Q. Chen, X. Leng, S. Ye and L. Deng, *Inorg. Chem.*, 2019, **58**, 13129–13141.

41 H. Z. Kaplan, B. Li and J. A. Byers, *Organometallics*, 2012, **31**, 7343–7350.

42 Ł. Banach, P. A. Guńka and W. Buchowicz, *Dalton. Trans.*, 2016, **45**, 8688–8692.

43 J. Li and L. Xu, *Tetrahedron*, 2015, **71**, 2858–2862.

44 F. Sebest, J. J. Dunsford, M. Adams, J. Pivot, P. D. Newman and S. Díez-González, *ChemCatChem*, 2018, **10**, 2041–2045.

45 L. R. Collins, L. A. Moffat, M. F. Mahon, M. D. Jones and M. K. Whittlesey, *Polyhedron*, 2016, **103**, 121–125.

46 M. Cybularczyk-Cecotka, A. M. Dabrowska, P. A. Guńka and P. Horeglad, *Inorganics*, 2018, **6**, 1–16.

47 A. Binobaid, K. J. Cavell, M. S. Nechaev and B. M. Kariuki, *Aust. J. Chem.*, 2011, **64**, 1141–1147.

48 E. L. Kolychev, A. F. Asachenko, P. B. Dzhevakov, A. A. Bush, V. V. Shuntikov, V. N. Khrustalev and M. S. Nechaev, *Dalton. Trans.*, 2013, **42**, 6859–6866.

49 U. Siemeling, C. Färber, C. Bruhn, S. Fürmeier, T. Schulz, M. Kurlemann and S. Tripp, *Eur. J. Inorg. Chem.*, 2012, 1413–1422.

50 E. Ö. Karaca, N. Gürbüz, I. Özdemir, H. Doucet, O. Şahin, O. Büyükgüngör and B. Çetinkaya, *Organometallics*, 2015, **34**, 2487–2493.

51 M. J. Spallek, D. Riedel, F. Rominger, A. S. K. Hashmi and O. Trapp, *Organometallics*, 2012, **31**, 1127–1132.

52 E. Ö. Karaca, M. Akkoç, M. Nawaz Tahir, C. Arıcı, F. İmik, N. Gürbüz, S. Yaşar and İ. Özdemir, *Tetrahedron Lett.*, 2017, **58**, 3529–3532.

53 A. Binobaid, M. Iglesias, D. Beetstra, A. Dervisi, I. Fallis and K. J. Cavell, *Eur. J. Inorg. Chem.*, 2010, 5426–5431.

54 S. A. Rzhevskiy, M. A. Topchiy, K. A. Lyssenko, A. N. Philippova, M. A. Belaya, A. A. Ageshina, M. V. Bermeshev, M. S. Nechaev and A. F. Asachenko, *J. Organomet. Chem.*, 2020, **912**, 121140.

55 O. S. Morozov, A. V. Lunchev, A. A. Bush, A. A. Tukov, A. F. Asachenko, V. N. Khrustalev, S. S. Zalesskiy, V. P. Ananikov and M. S. Nechaev, *Chem. Eur. J.*, 2014, **20**, 6162–6170.

56 A. Kumar, C. Singh, H. Tinnermann and H. V. Huynh, *Organometallics*, 2020, **39**, 172–181.

57 N. Phillips, T. Dodson, R. Tirfoin, J. I. Bates and S. Aldridge, *Chem. Eur. J.*, 2014, **20**, 16721–16731.

58 W. J. M. Blackaby, S. E. Neale, C. J. Isaac, S. Sabater, S. A. Macgregor and M. K. Whittlesey, *ChemCatChem*, 2019, **11**, 1893–1897.

59 J. Li, B. Zhou, Y. Jiang and X. Liu, *Catalysts*, 2018, **8**, 1–9.

60 J. J. Dunsford and K. J. Cavell, *Dalton. Trans.*, 2011, **40**, 9131–9135.

61 B. Bantu, D. Wang, K. Wurst and M. R. Buchmeiser, *Tetrahedron*, 2005, **61**, 12145–12152.

62 G. M. Pawar, B. Bantu, J. Weckesser, S. Blechert, K. Wurst and M. R. Buchmeiser, *Dalton. Trans.*, 2009, 9043–9051.

63 E. L. Kolychev, I. A. Portnyagin, V. V Shuntikov, V. N. Khrustalev and M. S. Nechaev, *J. Organomet. Chem.*, 2009, **694**, 2454–2462.

64 L. R. Collins, T. M. Rookes, M. F. Mahon, I. M. Riddlestone and M. K. Whittlesey, *Organometallics*, 2014, **33**, 5882–5887.

65 L. R. Collins, I. M. Riddlestone, M. F. Mahon and M. K. Whittlesey, *Chem. Eur. J.*, 2015, **21**, 14075–14084.

66 A. J. Jordan, C. M. Wyss, J. Bacsa and J. P. Sadighi, *Organometallics*, 2016, **35**, 613–616.

67 G. A. Chesnokov, M. A. Topchiy, P. B. Dzhevakov, P. S. Gribanov, A. A. Tukov, V. N.

Khrustalev, A. F. Asachenko and M. S. Nechaev, *Dalton. Trans.*, 2017, **46**, 4331–4345.

68 A. J. Jordan, R. K. Walde, K. M. Schultz, J. Bacsa and J. P. Sadighi, *Inorg. Chem.*, 2019, **58**, 9592–9596.

69 A. Cervantes-Reyes, F. Rominger and A. S. K. Hashmi, *Chem. Eur. J.*, 2020, **26**, 5530–5540.

70 N. P. Mankad, D. S. Laitar and J. P. Sadighi, *Organometallics*, 2004, **23**, 3369–3371.

71 L. J. Taylor and D. L. Kays, *Dalton. Trans.*, 2019, **48**, 12365–12381.

72 R. C. Poulten, I. López, A. Llobet, M. F. Mahon and M. K. Whittlesey, *Inorg. Chem.*, 2014, **53**, 7160–7169.

73 C. J. E. Davies, M. J. Page, C. E. Ellul, M. F. Mahon and M. K. Whittlesey, *Chem. Commun.*, 2010, **46**, 5151–5153.

74 N. Phillips, J. Rowles, M. J. Kelly, I. Riddlestone, N. H. Rees, A. Dervisi, I. A. Fallis and S. Aldridge, *Organometallics*, 2012, **31**, 8075–8078.

75 S. Caddick, F. G. N. Cloke, P. B. Hitchcock and A. K. de K. Lewis, *Angew. Chem.*, 2004, **116**, 5948–5951.

76 L. C. Pop and M. Saito, *Coord. Chem. Rev.*, 2016, **314**, 64–70.

77 B. R. Dible, M. S. Sigman and A. M. Arif, *Inorg. Chem.*, 2005, **44**, 3774–3776.

78 S. Nagao, T. Matsumoto, Y. Koga and K. Matsubara, *Chem. Lett.*, 2011, **40**, 1036–1038.

79 K. Matsubara, K. Ueno and Y. Shibata, *Organometallics*, 2006, **25**, 3422–3427.

80 T. Inatomi, Y. Fukahori, Y. Yamada, R. Ishikawa, S. Kanegawa, Y. Koga and K. Matsubara, *Catal. Sci. Technol.*, 2019, **9**, 1784–1793.

81 S. Pelties, E. Carter, A. Folli, M. F. Mahon, D. M. Murphy, M. K. Whittlesey and R. Wolf, *Inorg. Chem.*, 2016, **55**, 11006–11017.

82 Y. Jiang, C. Gendy and R. Roesler, *Organometallics*, 2018, **37**, 1123–1132.

83 W. J. M. Blackaby, PhD Thesis, University of Bath, 2020.

84 J. Wu, A. Nova, D. Balcells, G. W. Brudvig, W. Dai, L. M. Guard, N. Hazari, P. H. Lin, R. Pokhrel and M. K. Takase, *Chem. Eur. J.*, 2014, **20**, 5327–5337.

85 R. C. Poulten, M. J. Page, A. G. Algarra, J. J. Le Roy, I. López, E. Carter, A. Llobet, S. A. Macgregor, M. F. Mahon, D. M. Murphy, M. Murugesu and M. K. Whittlesey, *J. Am.*

*Chem. Soc.*, 2013, **135**, 13640–13643.

86 W. J. M. Blackaby, S. Sabater, R. C. Poulten, M. J. Page, A. Folli, V. Krewald, M. F. Mahon, D. M. Murphy, E. Richards and M. K. Whittlesey, *Dalton. Trans.*, 2018, **47**, 769–782.

87 K. Zhang, M. Conda-Sheridan, S. R. Cooke and J. Louie, *Organometallics*, 2011, **30**, 2546–2552.

88 T. Zell, P. Fischer, D. Schmidt and U. Radius, *Organometallics*, 2012, **31**, 5065–5073.

# Chapter 2

# Chapter 2 – (RE-NHC)CuO$^t$Bu Complexes for the Semihydrogenation and Hydroboration of Alkynes.

Some of the work in this chapter has been published in:[1]

J. W. Hall, D. M. L. Unson, P. Brunel, L. R. Collins, M. K. Cybulski, M. F. Mahon and M. K. Whittlesey, *Organometallics*, 2018, **37**, 3102–3110.

The purpose of this chapter is to develop the reactivity of (6-Mes)CuO$^t$Bu (**2.1**) initiated by Collins for the semihydrogenation of alkynes.[2] The synthesis and reactivity of other (NHC)CuO$^t$Bu complexes will also be tested as a comparison. The complexes will subsequently be tested in the catalytic hydroboration of alkynes, along with preliminary mechanistic investigations.

## 2.1 – Semihydrogenation of Alkynes by (NHC)Cu Systems

Compared to the other coinage metals, (NHC)Cu species were initially less studied despite being reported early on by Arduengo in 1993.[3] It was not until 2001, when Woodward demonstrated (NHC)Cu-catalysed conjugate additions of enones and $ZnEt_2$, that (NHC)Cu catalysis developed.[4] Since then there have been many publications and reviews involving (NHC)Cu systems.[5–8] A popular catalytic use of (NHC)Cu is in reduction reactions involving the putative formation of a (NHC)CuH species. While Stryker's hydride $[HCu(PPh_3)]_6$ has been known since the 1970's,[9] isolation of the first (NHC)CuH species was not described until 2004 by Sadighi and co-workers in the form of $[(IPr)CuH]_2$ (**2.i**).[10] The bulky carbene IPr allowed for spectroscopic characterisation of **2.i** at low temperatures (-40 $^oC$), however, it was short lived at room temperature. Employing ring-expanded carbenes as ligands, Sadighi demonstrate it was possible to isolate $[(6\text{-Dipp})CuH]_2$ (**2.iii**) and $[(7\text{-Dipp})CuH]_2$ (**2.iv**) which were stable at room temperature in solution for days.[11] Both **2.i** and **2.iv** were shown to undergo the selective insertion of unsaturated substrates (Scheme 2.1).

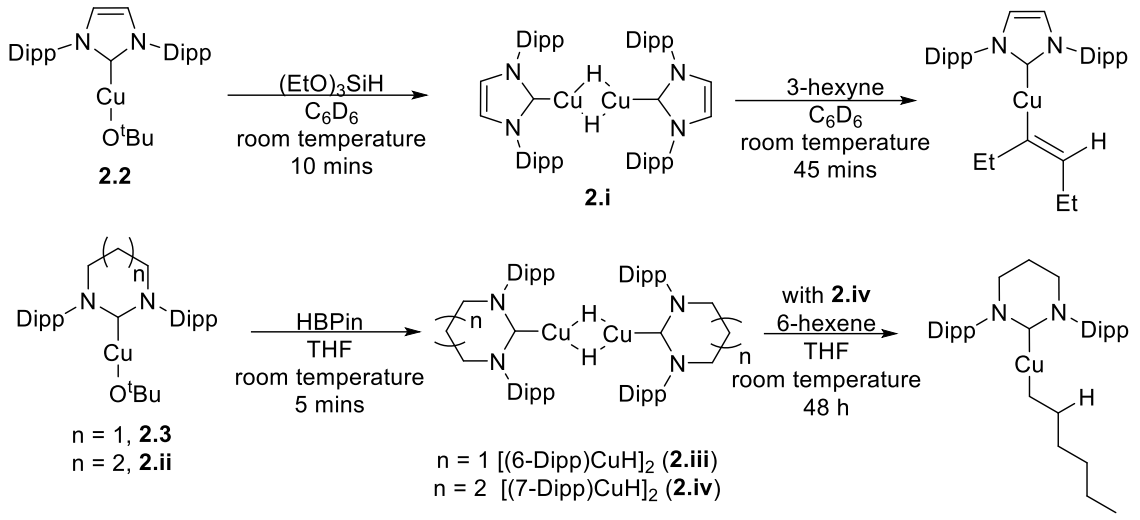


Scheme 2.1 – (NHC)CuH species [(IPr)CuH]$_2$ (**2.i**), [(6-Dipp)CuH]$_2$ (**2.iii**) and [(7-Dipp)CuH]$_2$ (**2.iv**) observed by Sadighi.[11]

Despite Sadighi demonstrating alkyne insertion in 2004, catalytic development of this did not occur until 2012.[12] Previously Lindlar's catalyst was known to be the most efficient system to semihydrogenate alkynes, however, it lacked *E*/*Z* selectivity and was known to over-reduce products into their respective alkanes, especially with internal alkynes.[13] To overcome this, Tsuji employed Cu(OAc)$_2$ with the chelating diphosphine CF$_3$Ar-Xan in the presence of silane (to generate the hydride) and HO$^t$Bu (as a proton source), to selectively semihydrogenate a wide array of internal alkynes to the respective (*Z*)-alkenes (Scheme 2.2). However, the CF$_3$Ar-Xan system lacked the ability to convert terminal alkynes. The same group demonstrated ($^{Cl}$IPr)CuCl could overcome this issue, while also maintaining the high selectivity towards internal alkynes.

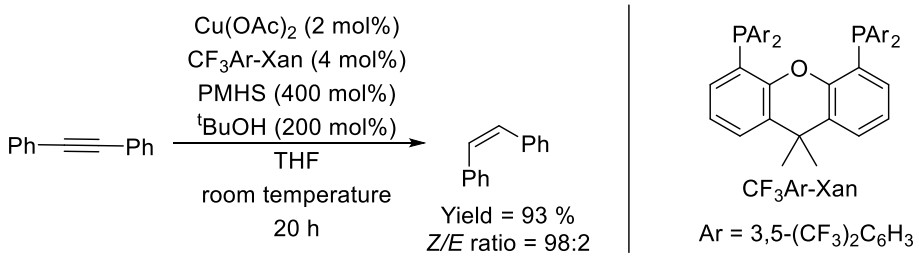


Scheme 2.2 – An example of conditions used by Tsuji in the semihydrogenation of diphenylacetylene.[12]

A catalytic cycle for the semihydrogenation of alkynes was proposed for the ($^{Cl}$IPr)CuCl system (Scheme 2.3).[12] Salt metathesis with NaO$^t$Bu leads to ($^{Cl}$IPr)CuO$^t$Bu, which then undergoes σ-bond metathesis with the silane to generate the putative ($^{Cl}$IPr)CuH species (step A). Regioselective insertion of the alkyne gives a ($^{Cl}$IPr)Cu(alkenyl) species (step B), which upon protonolysis by $^t$BuOH, eliminates the desired (*Z*)-alkene and regenerates ($^{Cl}$IPr)CuO$^t$Bu (step C).

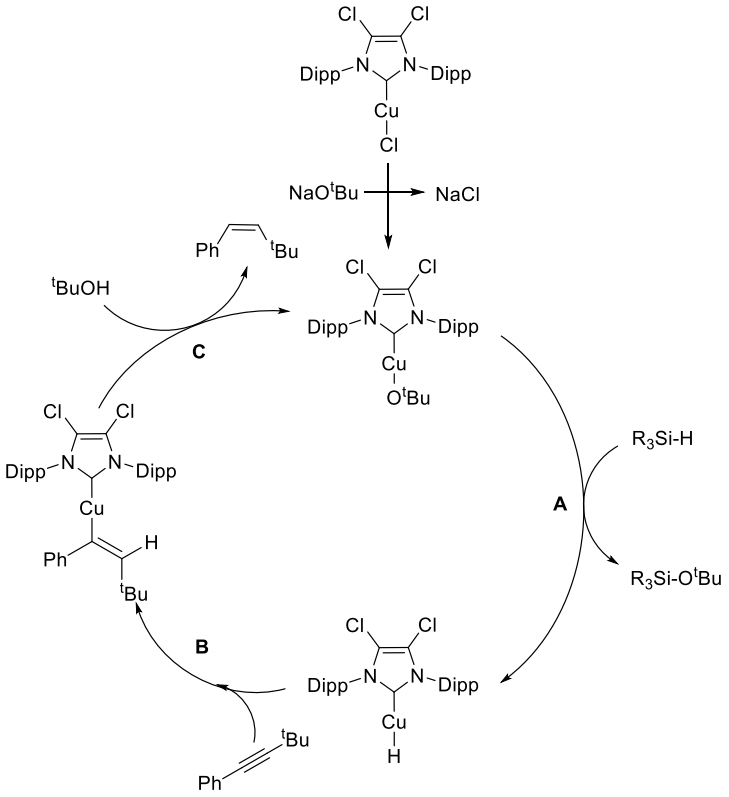


Scheme 2.3 – Mechanistic cycle for the semihydrogenation of internal alkynes proposed by Tsuji.[12]

Since then, there have been multiple examples of alkyne semihydrogenation with (NHC)Cu systems. Teichert reported a system based upon an NHC with a tethered alkoxide group, which can activate hydrogen as its hydride and proton source under forcing conditions (Scheme 2.4a).[14] Following this, Sawamura proved milder pressures of $H_2$ could be used to achieve similar activity in (SIMes)CuCl, albeit at elevated temperature (Scheme 2.4b).[15] As an alternative to $H_2$, Teichert demonstrated the use of $H_3N{\cdot}BH_3$ in a later report, however this required slow addition of $H_3N{\cdot}BH_3$ to prevent $H_2$ formation (Scheme 2.4c).[16] Lalic demonstrated low loadings of 0.5 mol% of (IPr)CuO$^t$Bu (**2.2**) could still afford high yields and high selectivity when using poly(methylhydrosiloxane) (PMHS) as the source of hydride (Scheme 2.4d).[17] Finally, Liu established it was possible to incorporate $B_2(Pin)_2$ to utilise alcohol as a proton and hydride source without the formation of hydroboration products (Scheme 2.4e).[18] In all cases the ability to semihydrogenate internal alkynes selectively was confirmed, however, terminal alkynes were shown to be difficult to convert.

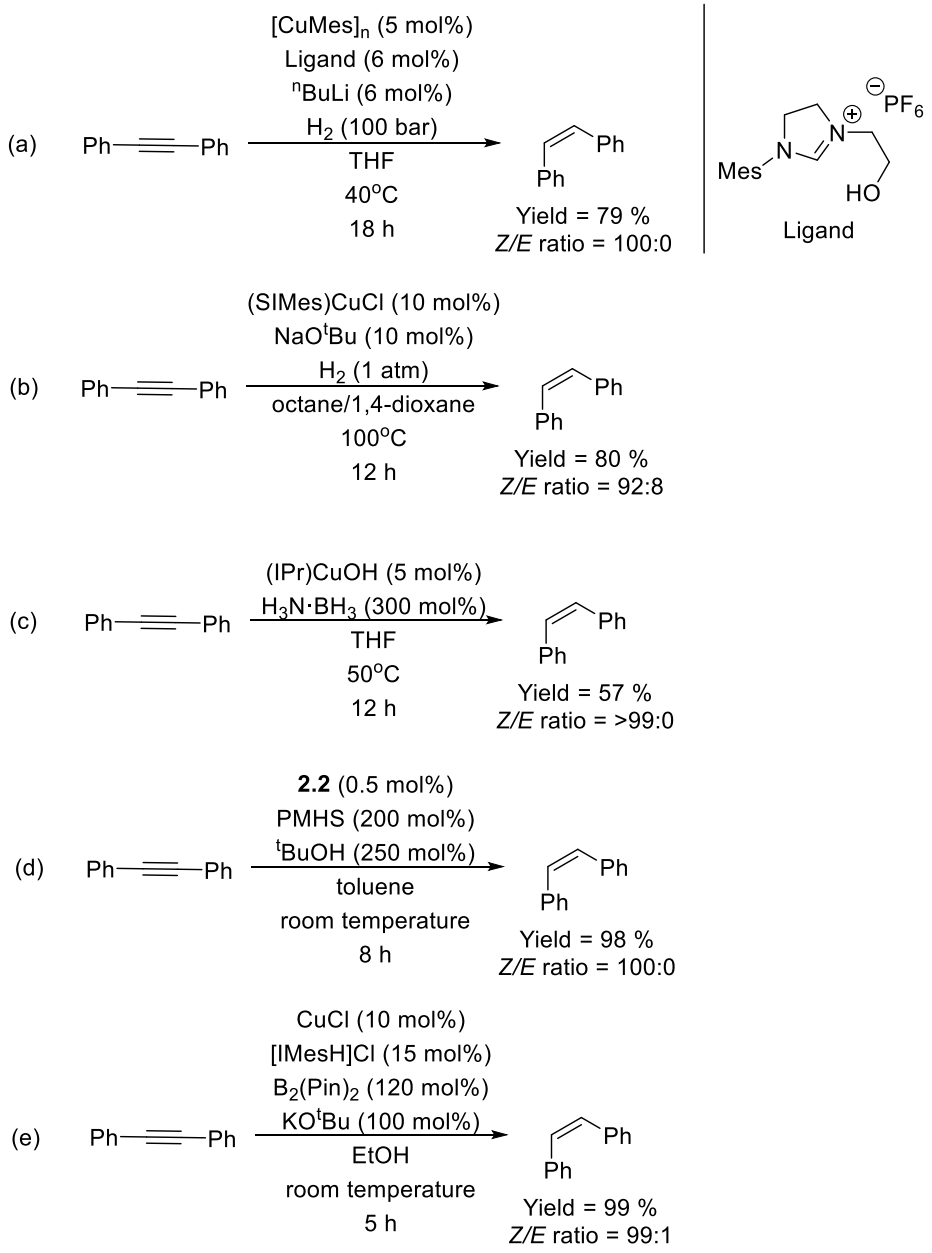


Scheme 2.4 – Examples of semihydrogenation of diphenylacetylene in the literature.

During an investigation into the semihydrogenation of terminal alkynes, Lalic identified three potential side reactions which limited reactivity (Scheme 2.5). Firstly, if a less sterically demanding carbene ligand, such as ICy is employed, the formation of $H_2$ is preferred over the semihydrogenation reaction (Scheme 2.5a). The second side reaction involved formation of an alkynyl, (IPr)CuC≡CPh, rather than alkenyl complex, as a result of the slow reactivity of **2.2** and $Et_3SiH$ (Scheme 2.5b). It was found by changing to a more reactive silane (PMHS), the formation of **2.ii** was encouraged, suppressing the formation of (IPr)CuC≡CPh. Finally, more acidic alcohols such as EtOH and $^{i}$PrOH generated hydrogen in a side reaction with **2.ii**, a reaction that was suppressed upon turning to $^{t}$BuOH.

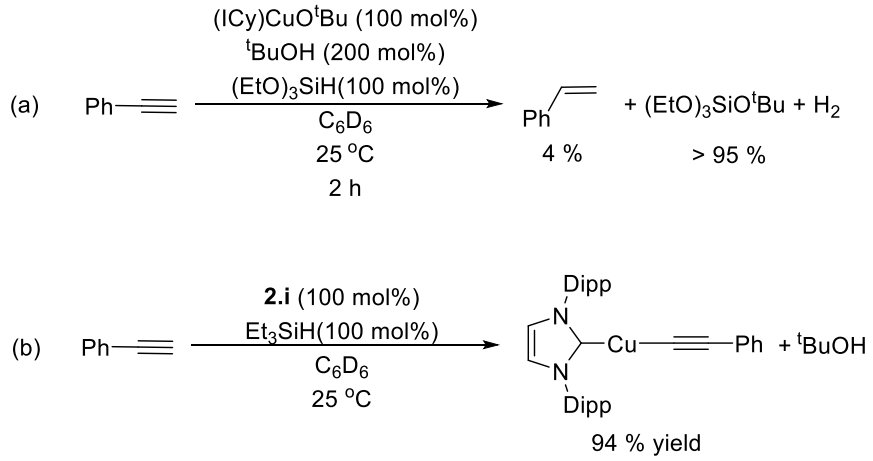


Scheme 2.5 – Side reactions observed by Lalic.[17]

## 2.2 –Results and Discussion

The purpose of this chapter is to expand on work by Collins et al. by optimising catalytic conditions and testing an array of (RE-NHC)CuO$^t$Bu complexes for the semihydrogenation of alkynes.[2,19] Collins demonstrated it was possible to semihydrogenate 1-phenyl-1-propyne exclusively to the (*Z*)-alkene after 13 days with the complex (6-Mes)CuO$^t$Bu (**2.1**) (Scheme 2.6). Elevating the temperature reduced the reaction time to 17 h to achieve the same yield, although to the detriment of the *Z*/*E* ratio (96:4). Thus, we wanted to investigate how this reactivity was influenced by the ring expansion of the NHC, the N-substituent and the conditions employed.

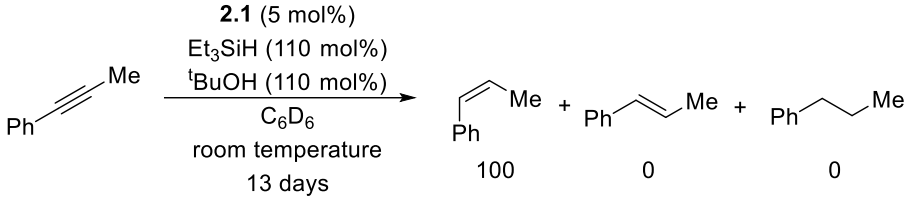


Scheme 2.6 – Semihydrogenation of 1-phenyl-1-propyne by Collins.[2]

2.2.1 – Optimisation of Conditions.

Initial investigation looked to employ conditions by Lalic,[17] where PMHS was used as the hydride source. In comparison to $Et_3SiH$, PMHS accelerated the reaction and a high yield was observed after 1 hour (96 %) with retention of the high selectivity (Table 2.1, entry 1). Reducing the catalyst loading of **2.1** to 1 mol% also provided high activity (85%) after 1 h (entry 2). When other sources of hydride were tested (entries 3, 4, 5 and 6), PMHS was found to be the highest yielding after 2 h. The amine borane $Me_2NH{\cdot}BH_3$ gave a poor yield, although a rapid evolution of $H_2$ was observed within minutes of addition (detected by $^1$H NMR spectroscopy) (entry 8). The addition of HBPin gave full conversion of the alkyne, however no formation of the alkene or alkane

products were observed (entry 9). Instead, it was found to yield the α-hydroboration product (*Z*)-4,4,5,5-tetramethyl-2-(1-phenylprop-1-en-1-yl)-1,3,2-dioxaborolane (**2.vi**) (94 % yield).

Table 2.1 – Results for the testing of other hydride sources for the semihydrogenation of 1-phenyl-1-propyne.[a]

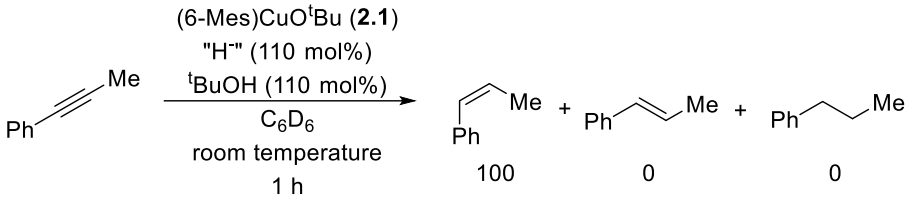


| Entry | Loading of **2.1** (mol %) | "H$^-$" source | Yield (%)[b] | Selectivity (*E*/*Z*/Alkane) |
|---|---|---|---|---|
| 1 | 5 | PMHS | 96 | 0:100:0 |
| 2 | 1 | PMHS | 85 | 0:100:0 |
| 3[c] | 1 | $Me_2EtSiH$ | Traces | 0:100:0 |
| 4[c] | 1 | $PhMe_2SiH$ | 5 | 0:100:0 |
| 5[c] | 1 | $Ph_2MeSiH$ | 1 | 0:100:0 |
| 6[c] | 1 | $Ph_3SiH$ | 2 | 0:100:0 |
| 7[c] | 5 | $Ph_3SiH$ | 57 | 0:100:0 |
| 8 | 5 | $Me_2NH{\cdot}BH_3$ | Traces | - |
| 9 | 5 | HBPin | 0[d] | - |
| 10 | - | PMHS | 0 | - |

[a]1-phenyl-1-propyne (0.22 mmol), "H$^-$" (110 mol%), $^t$BuOH (110 mol%) and **2.1** in $C_6D_6$ at room temperature for 1 h. [b]Determined by $^1$H NMR spectroscopy using 1,3,5-$(MeO)_3C_6H_3$ as an internal standard. [c]Reaction time 2 h. [d]Full conversion observed.

The formation of α-hydroboration product was not completely unexpected. Cazin and co-workers reported it was possible to form such products starting from the alkyne, *in-situ* generated (NHC)CuOH and HBPin (Scheme 2.7).[20]

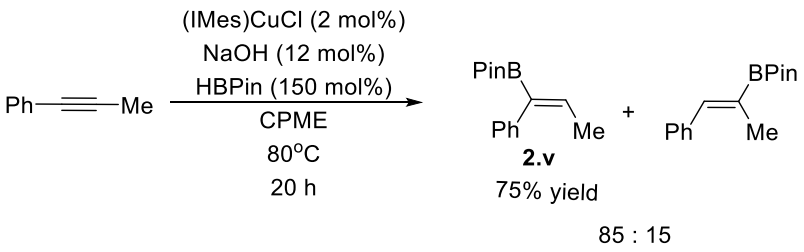


Scheme 2.7 – Conditions used by Cazin for the α-hydroboration of alkynes.

The formation of the α-hydroboration product under the semihydrogenation conditions (Table 2.1, entry 9) suggests the HBPin intercepts the Cu-alkenyl intermediate before $^{t}$BuOH, preventing the semihydrogenation product (Scheme 2.8).

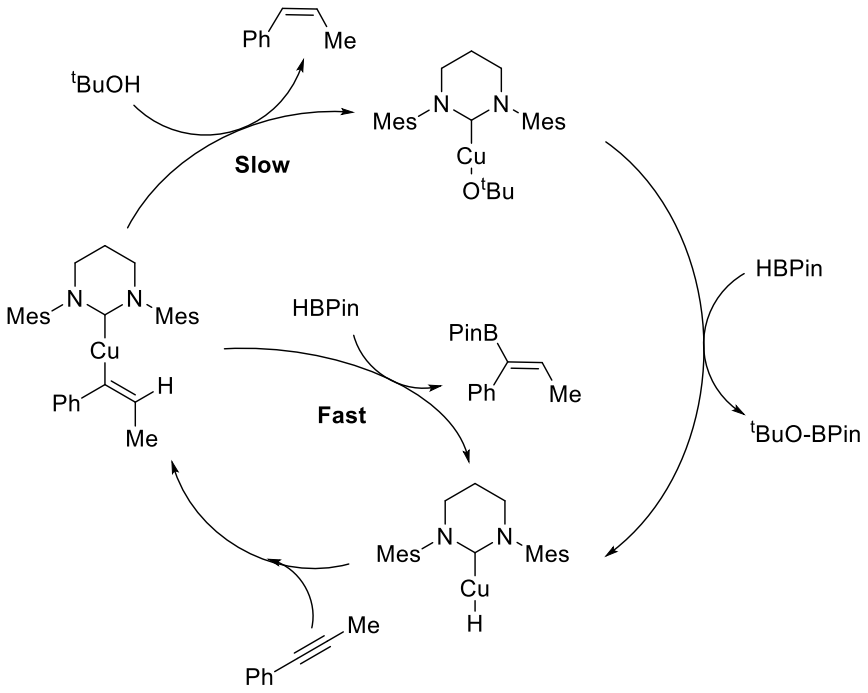


Scheme 2.8 – Proposed mechanism for the activity observed by in Entry 9 Table 2.1.

## 2.3 – Synthesis of (RE-NHC)CuO$^{t}$Bu Complexes

To investigate the semihydrogenation of alkynes as a function of NHC ring size and N-substitution, three new complexes were synthesised, (7-Mes)CuO$^{t}$Bu (**2.4**), (6-*o*-Tol)CuO$^{t}$Bu (**2.5**) and (6-Xylyl)CuO$^{t}$Bu (**2.6**), using a similar route to **2.1** (Scheme 2.9).[2,19] The known complexes (IPr)CuO$^{t}$Bu (**2.2**),[10] (6-Dipp)CuO$^{t}$Bu (**2.3**)[11] and (SIMes)CuO$^{t}$Bu (**2.7**)[21] were also synthesised *via* this route for comparison. Complexes **2.2 – 2.7** were isolated in yields ranging from 17 – 93%.[ii]

[ii] The (NHC)Cu(Mes) precursors are reported in the experimental section, with crystal structures and corresponding data shown in the appendices.

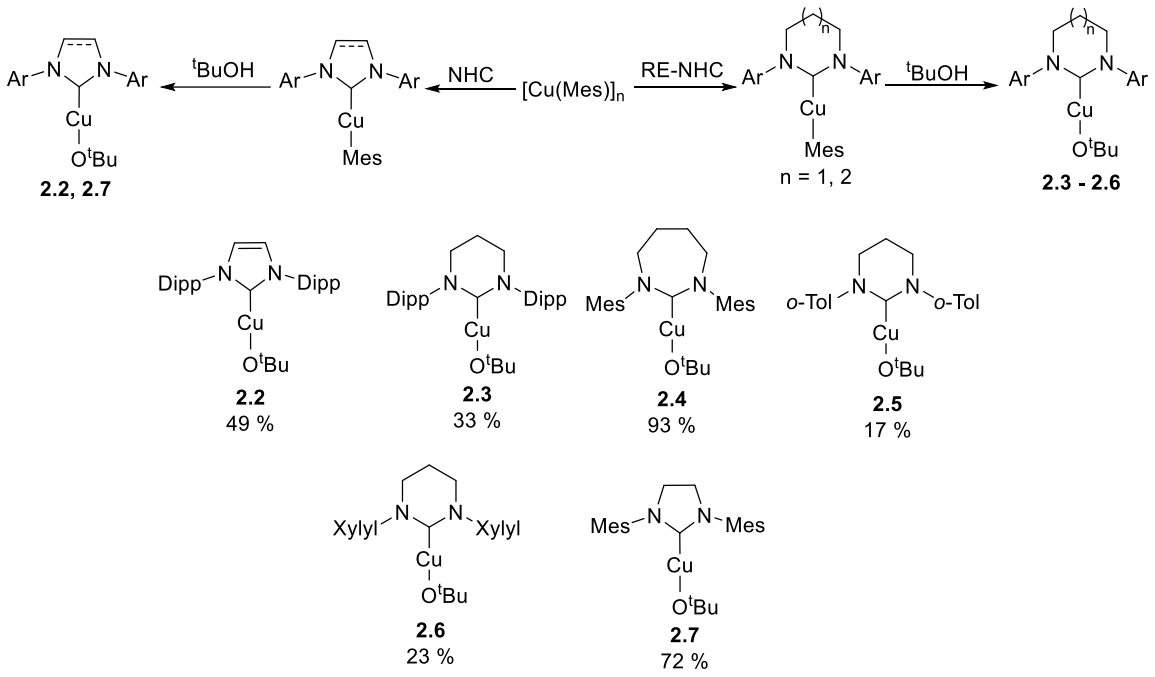


Scheme 2.9 – Synthesis of (NHC)CuO$^t$Bu complexes.

X-ray quality crystals of **2.3**, **2.4** and **2.5** were grown from hexane layered benzene solutions of the complexes while **2.7** was grown from pentane layered toluene at -30 °C. Attempts to crystallise **2.6** failed. The structures of **2.3**, **2.4**, **2.5** and **2.7** are shown in Figure 2.1. Metrics are summarised in Table 2.2. The four complexes exhibited Cu-O bond lengths between 1.788(2) - 1.809(3) Å. The distances in **2.3**, **2.4** and **2.5** were comparable to the value of 1.8104(13) Å reported for **2.1**[2] and **2.2**,[10] whereas **2.7** demonstrated the shortest Cu-O bond length of 1.788(2) Å. Compared to **2.1**, complexes **2.3**, **2.4** and **2.5** showed no significant differences regardless of N-substituent or expansion to larger 7-membered (NHC)Cu system (in the case of **2.4**). The (RE-NHC)CuO$^t$Bu complexes **2.3**, **2.4** and **2.5** showed elongation of the Cu-$C_{carbene}$ bond length compared to the 5-membered NHC complexes **2.2** and **2.6**, as well as **2.1**. As expected, the N-C-N angle increases with ring size with the largest being **2.4** (119.51(13)°) and smallest being **2.2** (104.2(15)°). The difference in NCN angle between the 5- and 6-membered rings were found to be larger than that in the 6- and 7-membered systems which is suggested to be due to the twisting within the larger ring. This trend is also reflected in the $\%V_{Bur}$ values (Table 2.2). Comparing N-C-N angle to the size of the N-substituent within the 6-membered rings shows **2.3** has the smallest angle of 116.8(3)°, which is potentially as a result of steric congestion around the Cu centre.

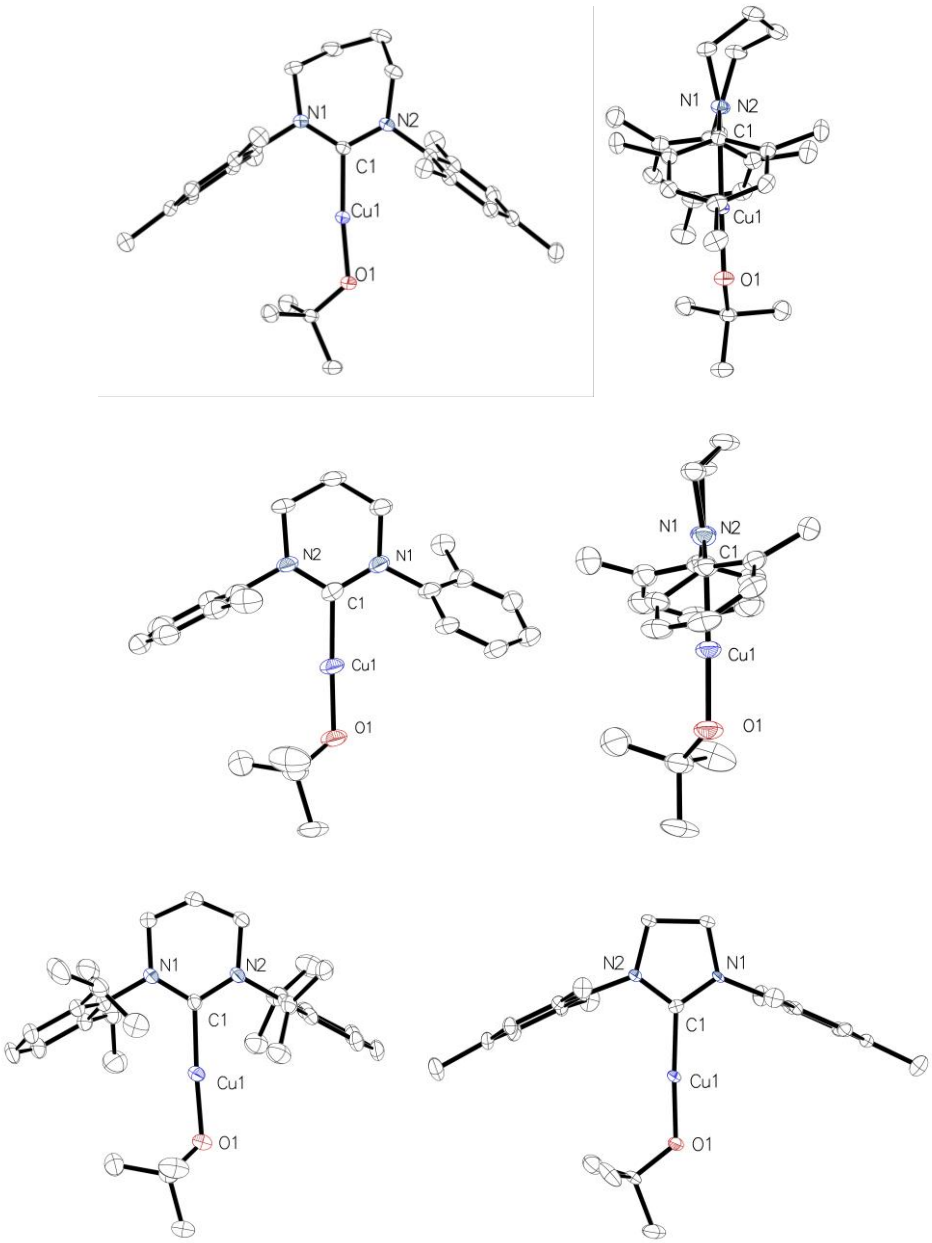


Figure 2.1 – Molecular structures of (left to right, top to bottom) **2.4** and an alternative view of **2.4** for aiding visualisation of the structure and twisting in the backbone, **2.5** and an alternative view of **2.5** for aiding visualisation of the structure, **2.3** and **2.7**. In all cases, ellipsoids are shown at 30% probability and hydrogen atoms have been omitted for clarity. In **2.3**, the structure of the molecule based on Cu1 in the asymmetric unit is shown. In **2.7** toluene was omitted for clarity.

Table 2.2 – Structural comparison of distances (Å) and angles (°) in (carbene)CuO$^t$Bu complexes **2.1** – **2.7** (excluding **2.6**).

| | **2.1**[2] | **2.2**[10] | **2.3** | **2.4** | **2.5** | **2.7** |
|---|---|---|---|---|---|---|
| **Cu-O** | 1.8016(15) | 1.8104(13) | 1.808(2) | 1.8032(10) | 1.809(3) | 1.788(2) |
| **Cu-$C_{carbene}$** | 1.874(2) | 1.8641(18) | 1.885(3) | 1.8818(14) | 1.881(5) | 1.844(3) |
| **$C_{carbene}$-Cu-O** | 175.31(8) | 179.05(7) | 176.74(12) | 174.44(5) | 177.7(2) | 176.09(12) |
| **N-$C_{carbene}$-N** | 117.65(18) | 103.42(15) | 116.8(3) | 119.51(13) | 117.3(4) | 107.8(3) |
| **%$V_{Bur}$**[a] | 44.0 | 44.6 | 52.0 | 45.4 | 38.1 | 38.2 |

[a]Values calculated at an M-$C_{carbene}$ distance of 2.0 Å. Parameters used: Bondi radii scaled by 1.17, a 3.5 Å sphere radius, 0.1 exhaustiveness, and exclusion of hydrogens.[22]

## 2.4 – Semihydrogenation of Internal Alkynes

Entries 1, 4 and 7 in Table 2.3 compare the catalytic activity of (NHC)CuO$^t$Bu for the semihydrogenation of 1-phenyl-1-propyne as a function of ring size. Activity was found to decrease from 6-Mes > SIMes > 7-Mes. This trend was further highlighted in entries 8 – 10 where a lower loading of the complexes was used (2 mol%). The N-substituent was found to decrease yield in the order Mes > Xylyl > *o*-Tolyl > Dipp (entries 1, 3, 5 – 6), suggesting this reaction is sensitive to the (NHC)CuO$^t$Bu complex having N-substituents either too small or too large. It was found that changing the alcohol enhanced the reactivity of **2.3** ($^i$PrOH entry 11 and EtOH entry 12). Activity could be increased for $^i$PrOH using prolonged reaction times (72 % after 48 h), however this was not observed for EtOH, most likely due to a competing reaction with (NHC)CuH to give $H_2$.[17] In all cases, selectivity towards the (*Z*)-isomer was retained with no observation of the (*E*)-isomer or further reduction of alkenes into alkanes.

Table 2.3 – Catalytic semihydrogenation of 1-phenyl-1-propyne by complexes **2.1** – **2.7**.[a]

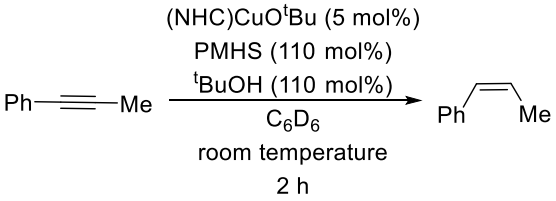


| Entry | Complex | Yield[b] |
|---|---|---|
| 1 | **2.1** | 94 |
| 2 | **2.2** | 33 |
| 3 | **2.3** | Trace |
| 4 | **2.4** | 82 |
| 5 | **2.5** | 22 |
| 6 | **2.6** | 87 |
| 7 | **2.7** | 85 |
| 8[c] | **2.1** | 86 |
| 9[c] | **2.4** | 66 |
| 10[c] | **2.7** | 76 |
| 11[c,d] | **2.3** | 52[f] |
| 12[c,e] | **2.3** | 31 |

[a]1-phenyl-1-propyne (0.22 mmol), PMHS (110 mol%), $^t$BuOH (110 mol%), Cu precursor (5 mol%) in $C_6D_6$ at room temperature for 2 h. [b]Determined by $^1$H NMR spectroscopy using 1,3,5-$(MeO)_3C_6H_3$ as an internal standard and an average of 2 runs. [c]2 mol%. [d] $^i$PrOH (110 mol%) replacing $^t$BuOH. [e] EtOH (110 mol%) replacing $^t$BuOH. [f]Yield after 48 h was 73%.

To further investigate the effect of the NHCs, **2.1, 2.2** and **2.4** – **2.7** were used in the semihydrogenation of diphenylacetylene. Comparing reactivity as a function of ring size, revealed a decrease in the order SIMes >> 6-Mes > 7-Mes (entries 1,3 and 6). This can be partly attributed to the precipitation of a yellow solid during the catalytic runs with **2.1** and **2.4**, which in the case of **2.1** was isolated and shown to be the insertion product, (6-Mes)Cu(C(Ph)=C(H)Ph) (**2.8**). In the cases of the other (NHC)CuO$^t$Bu complexes, no precipitation was observed, consistent with their good activity.

Table 2.4 – Semihydrogenation of diphenylacetylene by **2.2 – 2.4**, **2.6** and **2.7**.[a]

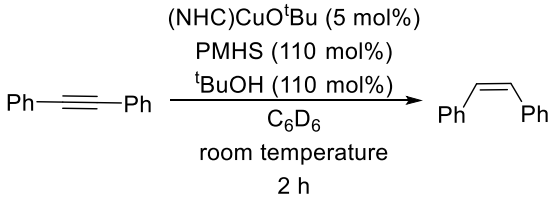


| Entry | Complex | Yield[b] |
|---|---|---|
| 1 | **2.1** | 29 |
| 2 | **2.2** | 30 |
| 3 | **2.4** | 27 |
| 4 | **2.5** | 45 |
| 5 | **2.6** | 77 |
| 6 | **2.7** | 99 |

[a] Diphenylacetylene (0.22 mmol), PMHS (110 mol%), $^t$BuOH (110 mol%), Cu precursor (5 mol%) in $C_6D_6$ at room temperature for 2 h. [b]Determined by $^1$H NMR spectroscopy using 1,3,5-$(MeO)_3C_6H_3$ as an internal standard and an average of 2 runs.

## 2.4.1 – Synthesis and Characterisation of (6-Mes)Cu(C(Ph)=C(H)Ph) (**2.8**)

An alternative approach to synthesising (6-Mes)Cu(C(Ph)=C(H)Ph) (**2.8**) was one employed by Collins for the analogue (6-Mes)Cu(C(Ph)=C(H)Me) (**2.vi**).[2] Thus, in the presence of two equivalents of $Et_3SiH$, **2.1** was stirred with a stoichiometric amount of diphenylacetylene for 48 hours at room temperature to yield **2.8** (57 %) (Scheme 2.10).[2,11] Isolation of the complex proved to be facile as a result of precipitation from $C_6H_6$. This also supports the drop in yield observed in the catalysis (Table 2.4).

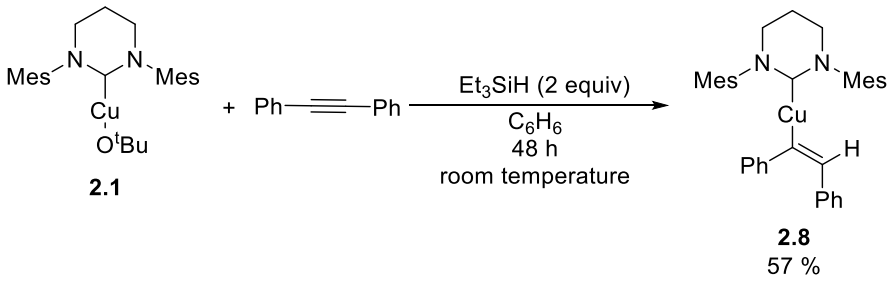


Scheme 2.10 – Synthesis of **2.8** following a procedure by Collins.[2]

By $^{1}$H NMR spectroscopy, the 6-Mes environment was symmetrical with two set of methyl resonances, one corresponding to the *para* methyl and the other to the *ortho* in a 1:2 ratio respectively. The alkenyl proton was found at 5.65 ppm.[2,10,23] X-Ray quality crystals were obtained from layering a concentrated solution of **2.8** in THF with hexane at room temperature. The structure consists of one 6-Mes and alkenyl moiety bound to Cu in a near linear geometry (177.97°) (Figure 2.2). The Cu-$C_{alkenyl}$ bond was observed to be shorter than that in **2.vi** (1.899(2) vs 1.919(2) Å respectively), but within the range observed for other (NHC)Cu-alkenyl complexes (e.g. in (IPr)Cu(C(Et)=C(Et)H) Cu-$C_{carbene}$ (1.897(3) Å)[10]; (SIPr)Cu(C(H)=C(H)$C_3H_6$Ph) Cu-$C_{carbene}$ (1.9063(18) Å)).[23] The alkenyl moiety sits at 31.0° to the NCN plane, a value comparable to that in **2.vi** (30.1°).

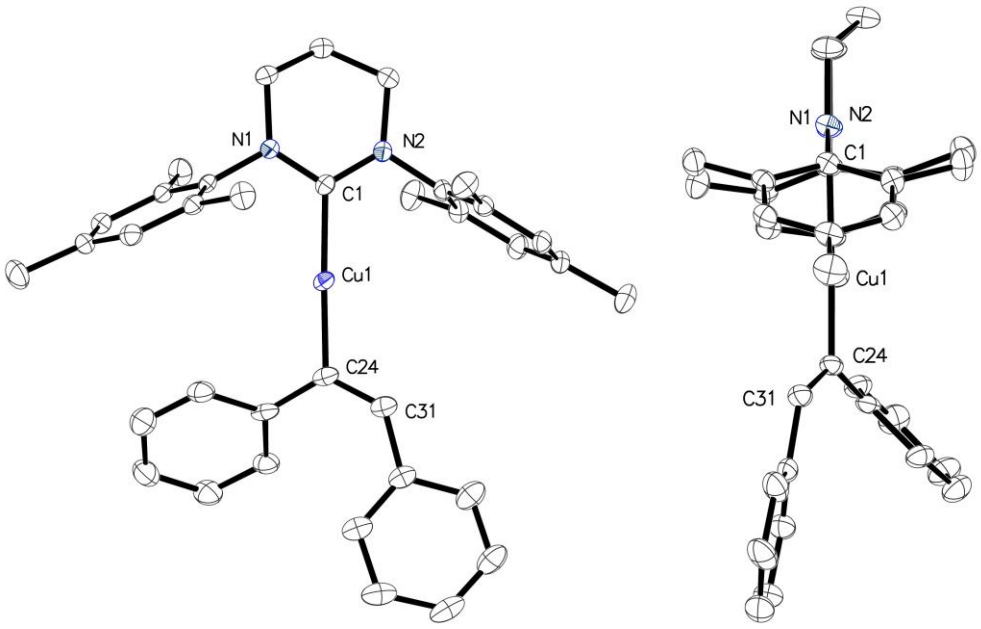


Figure 2.2 – Molecular structure of **2.8** from two views. Ellipsoids at 30 % probability. Hydrogens omitted for clarity. Selected bond lengths (Å) and angles (°). Cu1-C1 1.917(2), Cu1-C24 1.899(2), C24-C31 1.365(4), C1-Cu1-C24 177.97(11).

## 2.5 – Semihydrogenation of Terminal Alkynes

The semihydrogenation of terminal alkynes was also examined with **2.1 – 2.4** and **2.6**. Unlike the internal substrates, the terminal alkynes were known to have catalytic limitations (see above).[17] Fortunately, the catalysts in this study demonstrated reasonable levels of activity for the semihydrogenation of both phenylacetylene and 1-hexyne (Table 2.5). In the case of the former, the highest yield was observed to be 60% across all the catalysts. High yields were obtainable with 1-hexyne with all the complexes, aside from **2.3**, in which a black precipitate forms during the reaction, suggestive of decomposition. The higher pKa of 1-hexyne vs phenylacetylene (25[24]

and 21[25] respectively) suggests the more acidic terminal proton might be a factor limiting the semihydrogenation of phenylacetylene by a competing reaction.[17]

Table 2.5 – Semihydrogenation of terminal alkynes by **2.1 – 2.4** and **2.6**.[a]

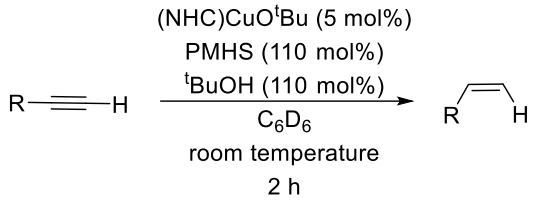


| Entry | Complex | R = | Yield[b] |
|---|---|---|---|
| 1 | **2.1** | Ph | 60 |
| 2 | **2.2** | Ph | 54 |
| 3 | **2.3** | Ph | 38 |
| 4 | **2.4** | Ph | 59 |
| 5 | **2.6** | Ph | 59 |
| 6 | **2.1** | $C_4H_9$ | 82 |
| 7 | **2.2** | $C_4H_9$ | 88 |
| 8 | **2.3** | $C_4H_9$ | 5 |
| 9 | **2.4** | $C_4H_9$ | 90 |
| 10 | **2.6** | $C_4H_9$ | 90 |

[a] Alkyne (0.22 mmol), PMHS (110 mol%), $^t$BuOH (110 mol%), Cu precursor (5 mol%) in $C_6D_6$ at room temperature for 2 h. [b]Determined by $^1$H NMR spectroscopy using 1,3,5-$(MeO)_3C_6H_3$ as an internal standard and an average of 2 runs.

## 2.6 – Further Reactivity of 2.1

Considering the reasonable activity of **2.1**, the substrate scope was expanded. Changing the stoichiometry of PMHS and $^{t}$BuOH to two equivalents relative to the alkyne allowed for 0.5 mol% loadings of **2.1** to provide high yields of (*Z*)-1-phenyl-1-propene after 24 h (Scheme 2.11, entry 1). As a result of this, dilution of **2.1** resulted in no precipitation of **2.8** during the semihydrogenation of diphenylacetylene leading to a good yield (Scheme 2.11, entry 2). This supports the reduced reactivity in Table 2.4 (entry 1) as a result of the poor solubility of the Cu-alkenyl intermediate **2.8**. Lower activity was found with the bulkier $SiMe_3$ group (entry 4). The effect of steric bulk was apparent in entries 5-7, where the *ortho* -Me containing substrate gave a significantly lower yield after 3 h (entry 7). A low tolerance to a carbonyl containing moiety (not observed by Lalic[17]) led to the reduction of equivalents used for the transformation in entry 9. Internal aliphatic alkynes were also shown to be suitable under these conditions with reasonable yields, however these were lower than compared to the literature.[17]

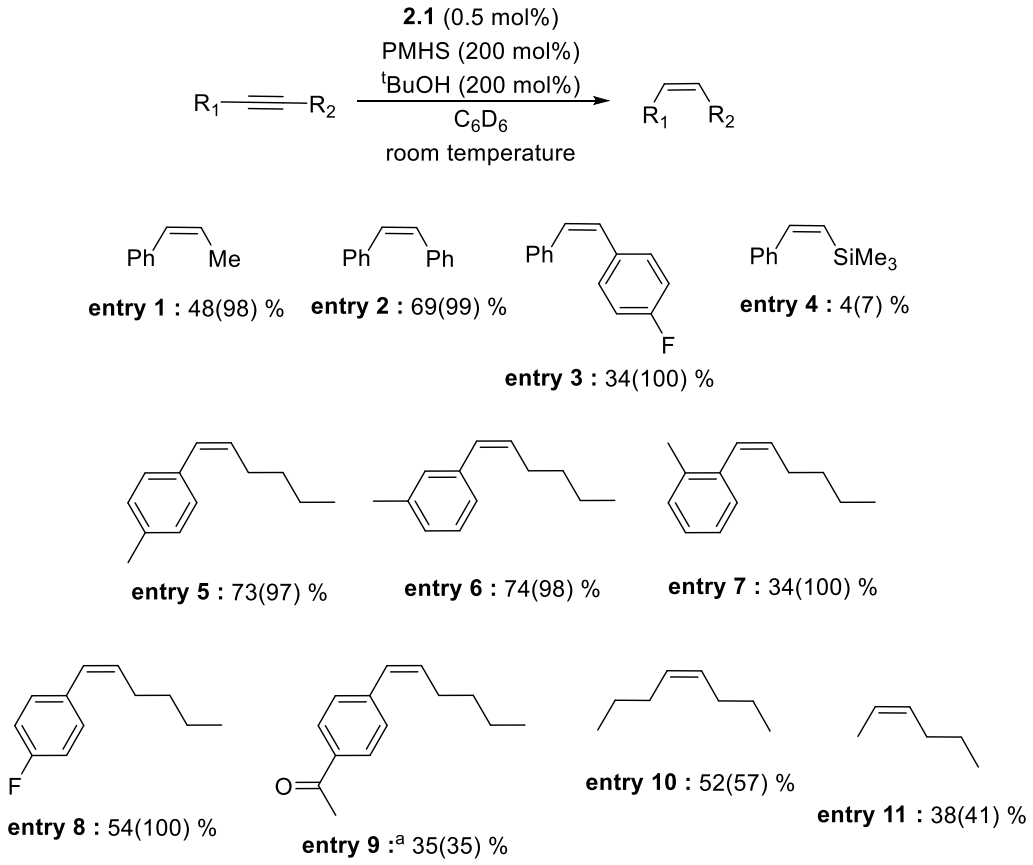


Scheme 2.11 – Substrate scope for the semihydrogenation with **2.1**. Conditions: alkyne (0.22 mmol), **2.1** (0.5 mol%), PMHS (200 mol%), $^{t}$BuOH (200 mol%), $C_6D_6$, room temperature. Product yields determined by $^{1}$H NMR spectroscopy using 1,3,5-$(MeO)_3C_6H_3$ as an internal

standard. Yields shown after 3 h and in parentheses 24 h. [a]PMHS (110 mol%) and [t]BuOH (110 mol%) were used.

## 2.7 – Hydroboration of Alkynes by (NHC)Cu Systems

The hydroboration of 1-phenyl-1-propyne by **2.1** (Table 2.1, entry 9), led to a wider investigation of the RE-NHC systems. Hydroboration of an alkyne/alkene most commonly shows anti-Markovnikov selectivity where the boryl group is attached to the least hindered carbon during the reduction of the unsaturated bond. Substrates containing unsymmetrical internal alkynes are traditionally difficult to transform selectively compared to terminal alkynes,[26] although this can be overcome in the presence of a suitable catalyst. For example, Fujihara demonstrated selective hydroboration of unsymmetrical internal alkynes with a Cu-catalysed system, where the choice of X-BPin (X= H, BPin) and ligand was found to influence the selectivity (Scheme 2.12).[27] The effect of ligand on selectivity was further highlighted by Cazin, who showed that an increased steric bulk of the NHC was detrimental to catalysis (IMes > IPr > IPr*, Table 2.6).[20]

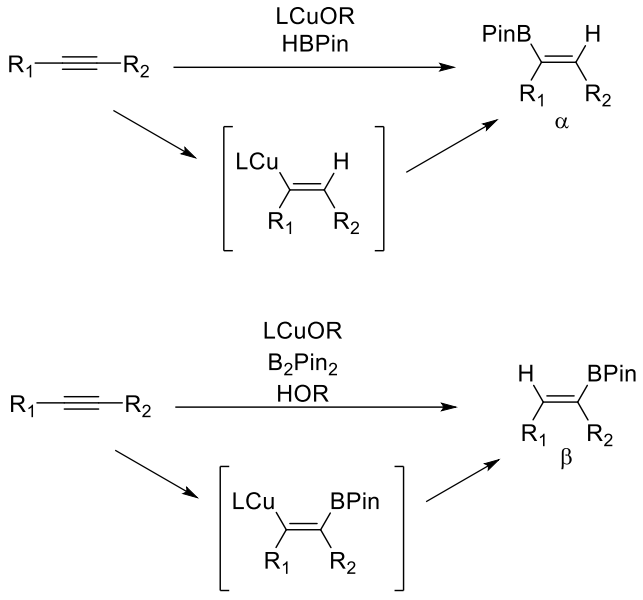


Scheme 2.12 – Cu catalysed hydroboration of unsymmetrical internal alkynes by Fujihara.[27]

Table 2.6 – NHC screen by Cazin for the hydroboration of 1-phenyl-1-butyne.[a]

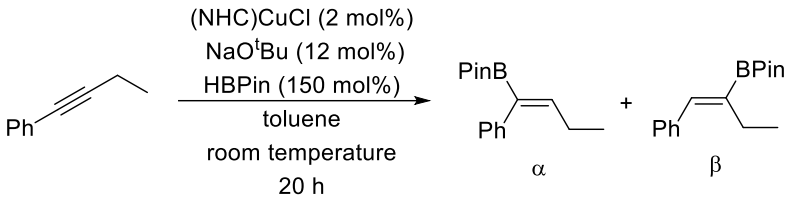


| Entry | NHC | Conversion | Selectivity (α:β) |
|---|---|---|---|
| 1 | IMes | 63 | 95:5 |
| 2 | IPr | 99 | 87:13 |
| 3 | IPr* | 99 | 75:25 |
| 4[b] | IMes | 98 | 93:7 |

[a]Alkyne (0.5 mmol), HBPin (0.75 mmol), NaO$^t$Bu (12 mol%), (NHC)CuCl (2 mol%), toluene, room temperature, 20 h. [b] 80ºC

## 2.8 – Effect of RE-NHC on the Hydroboration of 1-phenyl-1-propyne

At 1 mol% loading of **2.1**, a high yield and selectivity for the hydroboration of 1-phenyl-1-propyne was obtained after 1 h (97 %, α:β = 96:4) (Scheme 2.13).

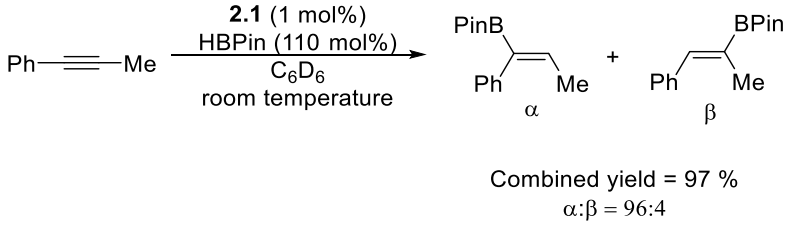


Scheme 2.13 – Conditions used for the hydroboration of 1-phenyl-1-propyne catalysed by **2.1**.

Reducing the loading to 0.2 mol% gave a modest yield (59 %) of the α-product and retention of selectivity (Table 2.7, entry 1). At 0.2 mol% loadings of **2.2** and **2.4 - 2.7**, it was found that increasing the NHC ring size vastly improves reactivity in the order 7-Mes > 6-Mes > SIMes (entries 1, 4 and 6), with no change to selectivity. A decrease in selectivity was exhibited by the Dipp containing complexes **2.2** and **2.3** with ratios of 63:37 and 78:22 respectively, suggesting the N-substituents influence the selectivity of the reaction (entries 4 and 6). In contrast to HBPin, HBCat gave no reaction.

Table 2.7 – (NHC)CuO$^t$Bu catalysed hydroboration of 1-phenyl-1-propyne with HBPin.[a]

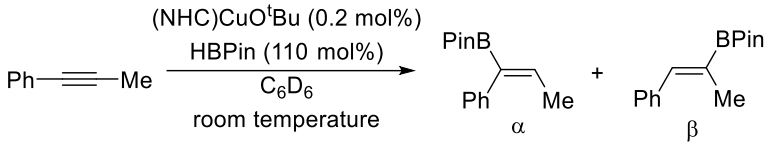


| Entry | Complex | Yield[b] | Selectivity (α:β)[b] |
|---|---|---|---|
| 1 | **2.1** | 59 | 96:4 |
| 2 | **2.2** | 21 | 78:22 |
| 3 | **2.3** | 44 | 63:37 |
| 4 | **2.4** | 85 | 96:4 |
| 5 | **2.5** | 2 | - |
| 6 | **2.7** | 13 | 96:4 |
| 7 | **2.1**[c] | 0 | - |

[a]Alkyne (0.51 mmol), HBPin (110 mol%), (NHC)CuO$^t$Bu (0.2 mol%), $C_6D_6$ (0.5 mL), room temperature, 3 h and inert atmosphere. Average of 2 runs. Yield refers to overall yield of α/β products. [b]Determined by GC using 1,3,5-$(MeO)_3C_6H_3$ as an internal standard. [c] HBCat used.

## 2.9 – Preliminary Study into the Effect of Substrate on the Hydroboration of Alkynes by 2.1

**2.1** was employed on a small-scale scope of internal alkynes (Scheme 2.14). In the case of the bulky $SiMe_3$ containing substrate, an overall yield of only 16% was observed, along with a 70:30 selectivity for of α/β (entry 2). Cazin, saw no loss of selectivity for this substrate with (NHC)CuOH suggesting the presence of the RE-NHC causes loss of selectivity and reactivity.[20] When 1-fluoro-4-(phenylethynyl)benzene was employed, selectivity and yield were diminished, showing the subtle changes imparted by the alkyne substituent.

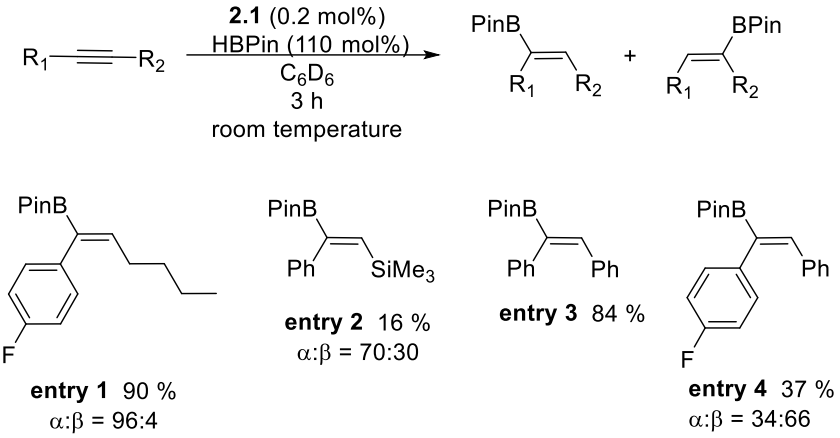


Scheme 2.14 – Substrate scope for the hydroboration with **2.1**. Products shown are the α-hydroboration products. Conditions: Alkyne (0.51 mmol), HBPin (110 mol%), **2.1** (0.2 mol%), $C_6D_6$ (0.5 mL), room temperature, 3 h and inert atmosphere. Average of 2 runs. Yield refers to overall yield of α/β products. Determined by $^1H$ NMR spectroscopy using 1,3,5-$(MeO)_3C_6H_3$ as an internal standard.

## 2.10 – Preliminary Mechanistic Study

Tsuji proposed a cupration pathway for the α-hydroboration of alkynes which involves the formation of a Cu-alkenyl species (Scheme 2.15)[27] upon syn insertion of the alkyne into the Cu-H bond, followed by reaction with HBPin to regenerate the hydride and yield the α-hydroboration product.

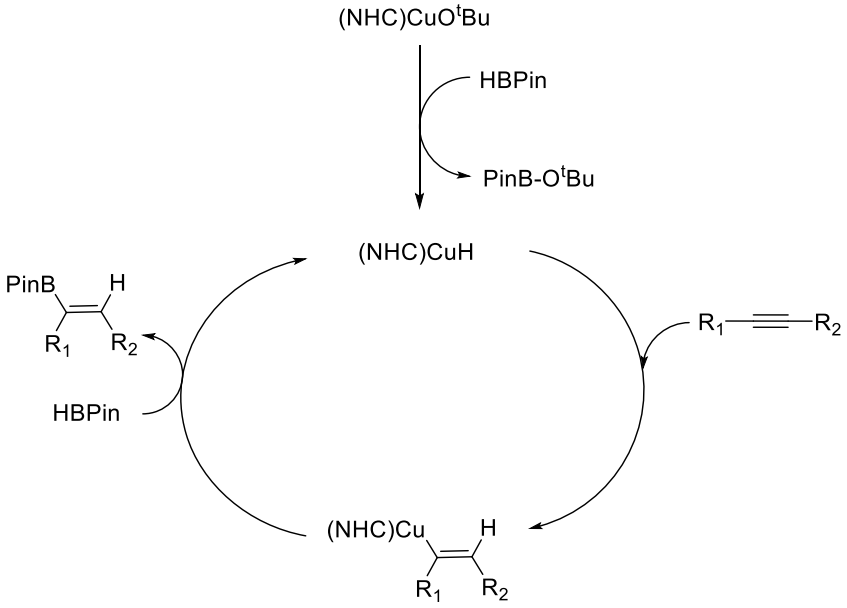


Scheme 2.15 – Proposed mechanistic pathway for the α-hydroboration of alkynes.

A computational study by Li supported Tsuji's proposal, while also revealing the rate limiting step to be the insertion of the alkyne into the Cu-H bond.[28] The model computational system which employed 1,3-dimethylimidazol-2-ylidene (IMe) and 1-phenyl-1-butyne, also showed the pathway leading to the β-product to be less energetically favourable by *ca.* 3 kcal/mol (Scheme 2.16).

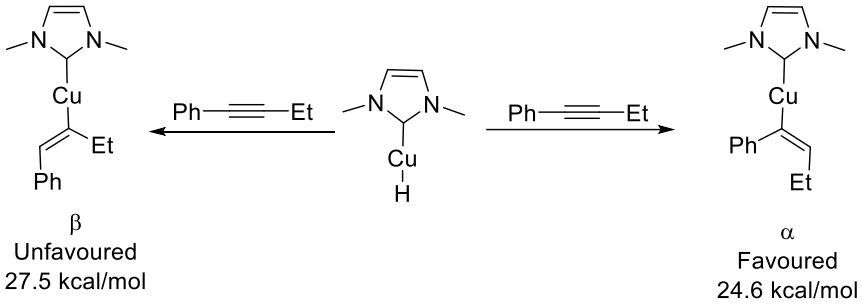


Scheme 2.16 – Rate limiting step calculated by Li.[28]

A room temperature stoichiometric reaction of **2.1** and HBPin in $C_6D_6$ resulted in the rapid formation of a bright yellow solution, which quickly dulled leaving (6-Mes)Cu(6-MesH) (**2.vii**) (identified $^1$H NMR spectroscopy) and a black precipitate. Complex **2.vii** was observed by Collins as a decomposition product of the (6-Mes)CuH dimer (**2.viii**) (Scheme 2.17), suggesting formation of **2.viii** in our system.[2] Repeating the experiment at 222 K revealed the formation **2.viii** and the elimination of $^t$BuO-BPin by $^1$H NMR spectroscopy (Figure 2.3).

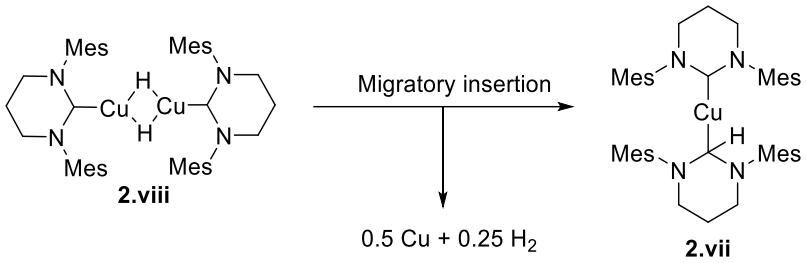


Scheme 2.17 – Migratory insertion observed by Collins.[2]

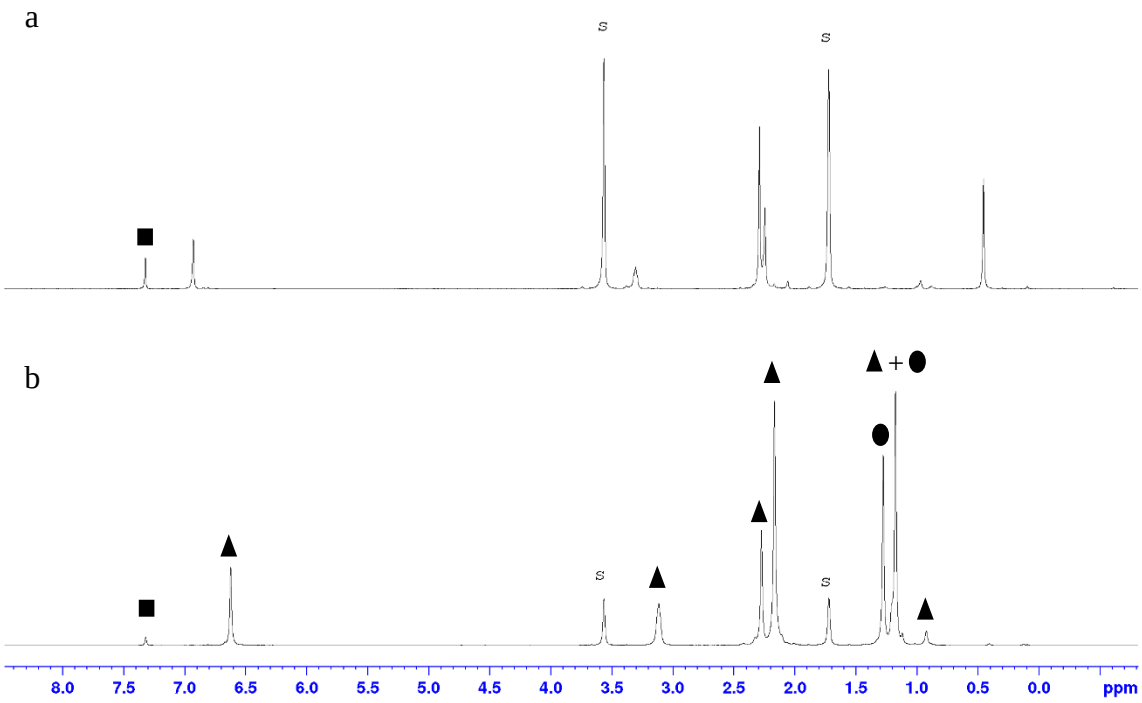


Figure 2.3 – $^{1}$H NMR spectra (400 MHz) of a) (6-Mes)CuO$^{t}$Bu (**2.1**) in $d_8$-THF at 222 K, and b) **2.1** + HBPin (1 equiv) (2 mins before being cooled to 222 K). S denotes $d_7$-THF. ▲(6-Mes)CuH (**2.viii**)[2], ● $^{t}$BuO-B(Pin), ■ Residual $C_6H_6$

Having shown the formation of **2.viii** from **2.1** and HBPin, the reaction of **2.vi** and HBPin was investigated by low temperature $^{1}$H NMR spectroscopy (Figure 2.4). Upon the addition of HBPin the formation of **2.viii** was observed along with only (*Z*)-4,4,5,5-tetramethyl-2-(1-phenylprop-1-en-1-yl)-1,3,2-dioxaborolane (**2.v**).[iii] No intermediates were seen, suggesting the transformation of **2.vi** to **2.viii** was extremely facile.

[iii] None of the β-product was observed by $^{1}$H NMR spectroscopy or GC-MS

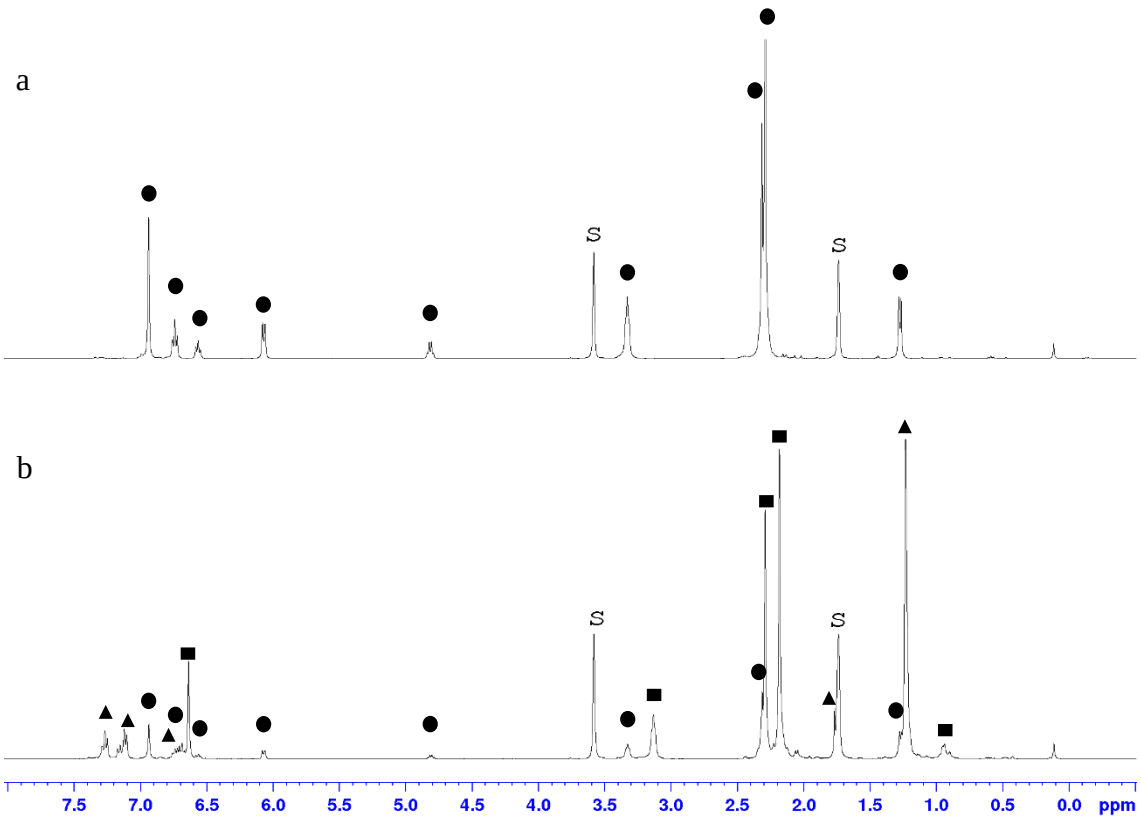


Figure 2.4 – $^{1}$H NMR spectra (400 MHz) of a) (6-Mes)Cu(C(Ph)=C(H)Me) (**2.vi**) in $d_8$-THF at 222 K, and b) **2.vi** + HBPin (1 equiv) (2 mins before cooled to 222 K). S denotes $d_7$-THF. ▲ **2.v**, ● **2.vi**, ■ **2.viii**.

## 2.11 – Conclusions

In conclusion, different (RE-NHC)CuO$^{t}$Bu complexes were utilised for the semihydrogenation and hydroboration of alkynes, where the steric effects of ring expansion and N-subsitiution were shown to influence catalytic activity. For semihydrogenation, a "goldilocks" effect was observed with (6-Mes)CuO$^{t}$Bu (**2.1**) being the most reactive. However, in the case of hydroboration, increasing the ring size to the larger 7-Mes carbene improved reactivity without hindering selectivity, warranting further investigation in the future. Mechanistic studies of α-hydroboration revealed the formation of (6-Mes)CuH upon addition of HBPin to **2.1**. Addition of HBPin to (6-Mes)Cu(C(Ph)=C(H)Me) (**2.vi**) revealed the formation of the α-hydroboration product and regeneration of (6-Mes)CuH, completing the cycle (Scheme 2.18). With only the α-hydroboration product formed, it suggested selectivity is determined by the insertion of the alkyne into Cu-H.

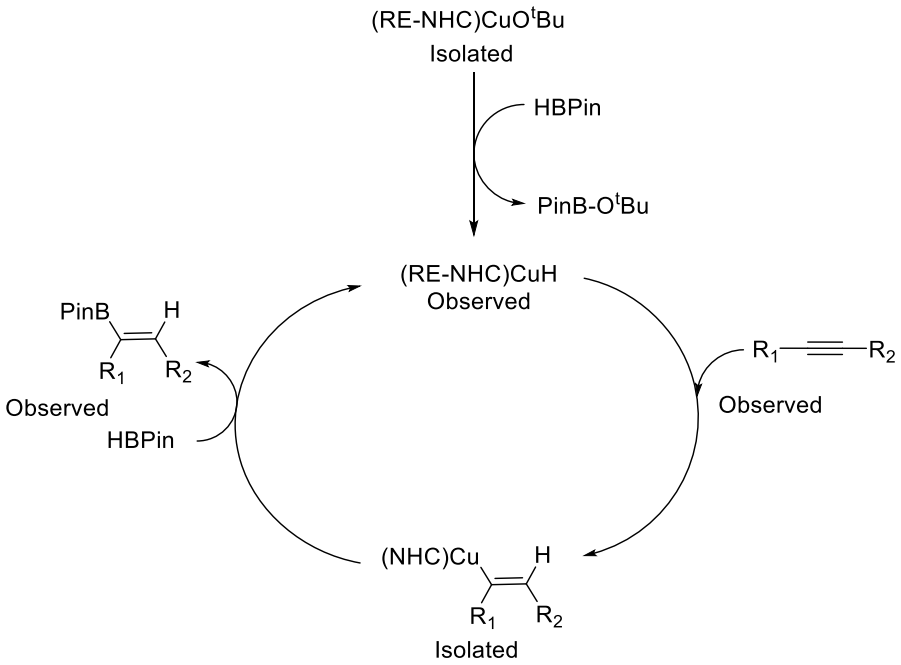


Scheme 2.18 – Updated mechanism for hydroboration of alkynes by (RE-NHC)Cu.

## 2.12 – References for Chapter 2


1 J. W. Hall, D. M. L. Unson, P. Brunel, L. R. Collins, M. K. Cybulski, M. F. Mahon and M. K. Whittlesey, *Organometallics*, 2018, **37**, 3102–3110.

2 L. R. Collins, PhD Thesis, University of Bath, 2016.

3 A. J. Arduengo, H. V. R. Dias, J. C. Calabrese and F. Davidson, *Organometallics*, 1993, **12**, 3405–3409.

4 P. K. Fraser and S. Woodward, *Tetrahedron Lett.*, 2001, **42**, 2747–2749.

5 F. Lazreg, F. Nahra and C. S. J. Cazin, *Coord. Chem. Rev.*, 2015, **293**–**294**, 48–79.

6 A. A. Danopoulos, T. Simler and P. Braunstein, *Chem. Rev.*, 2019, **119**, 3730–3961.

7 A. J. Jordan, G. Lalic and J. P. Sadighi, *Chem. Rev.*, 2016, **116**, 8318–8372.

8 J. C. Y. Lin, R. T. W. Huang, C. S. Lee, A. Bhattacharyya, W. S. Hwang and I. J. B. Lin, *Chem. Rev.*, 2009, **109**, 3561–3598.

9 J. F. Daeuble, C. McGettigan and J. M. Stryker, *Tetrahedron Lett.*, 1990, **31**, 2397–2400.

10 N. P. Mankad, D. S. Laitar and J. P. Sadighi, *Organometallics*, 2004, **23**, 3369–3371.

11 A. J. Jordan, C. M. Wyss, J. Bacsa and J. P. Sadighi, *Organometallics*, 2016, **35**, 613–616.

12 K. Semba, T. Fujihara, T. Xu, J. Terao and Y. Tsuji, *Adv. Synth. Catal.*, 2012, **354**, 1542–1550.

13 C. Oger, L. Balas, T. Durand and J. M. Galano, *Chem. Rev.*, 2013, **113**, 1313–1350.

14 F. Pape, N. O. Thiel and J. F. Teichert, *Chem. Eur. J.*, 2015, **21**, 15934–15938.

15 T. Wakamatsu, K. Nagao, H. Ohmiya and M. Sawamura, *Organometallics*, 2016, **35**, 1354–1357.

16 E. Korytiaková, N. O. Thiel, F. Pape and J. F. Teichert, *Chem. Commun.*, 2017, **53**, 732–735.

17 A. M. Whittaker and G. Lalic, *Org. Lett.*, 2013, **15**, 1112–1115.

18 H. Bao, B. Zhou, H. Jin and Y. Liu, *J. Org. Chem.*, 2019, **84**, 3579–3589.

19 L. R. Collins, I. M. Riddlestone, M. F. Mahon and M. K. Whittlesey, *Chem. Eur. J.*, 2015, **21**, 14075–14084.

20 Y. D. Bidal, F. Lazreg and C. S. J. Cazin, *ACS Catal.*, 2014, **4**, 1564–1569.

21 G. G. Dubinina, J. Ogikubo and D. A. Vicic, *Organometallics*, 2008, **27**, 6233–6235.

22 L. Falivene, Z. Cao, A. Petta, L. Serra, A. Poater, R. Oliva, V. Scarano and L. Cavallo, *Nat. Chem.*, 2019, **11**, 872–879.

23 A. M. Suess, M. R. Uehling, W. Kaminsky and G. Lalic, *J. Am. Chem. Soc.*, 2015, **137**, 7747–7753.

24 W. H. Brown, C. S. Foote, B. L. Iverson and E. V. Anslyn, *Organic Chemistry*, Wadsworth Publishing Co Inc, Belmont, CA, United States, 5th edn., 2008.

25 R. E. Dessy, Y. Okuzumi and A. Chen, *J. Am. Chem. Soc.*, 1962, **84**, 2899–2904.

26 C. E. Tucker, J. Davidson and P. Knochel, *J. Org. Chem.*, 1992, **57**, 3482–3485.

27 K. Semba, T. Fujihara, J. Terao and Y. Tsuji, *Chem. Eur. J.*, 2012, **18**, 4179–4184.

28 Y. Li, *J. Phys. Org. Chem.*, 2017, **30**, 1–8.

# Chapter 3

# Chapter 3 – (Carbene)CuF Complexes for the Catalytic Allylation of Aldehydes

Some of the work in this chapter has been published in:[1]

J. W. Hall, F. Seeberger, M. F. Mahon and M. K. Whittlesey, *Organometallics*, 2020, **39**, 227–233.

The purpose of this chapter is to discuss the synthesis and reactivity of (NHC)CuF complexes. A selection of these complexes will be subsequently used in the catalytic allylation of octanal, along with mechanistic investigations.

## 3.1 – Literature Examples of (NHC)CuF Complexes

### 3.1.1 – Synthesis and Applications of (NHC)CuF

The use of (NHC)CuX catalyst precursors (where X = Cl, Br and I) has been at the forefront of early advances of (NHC)Cu chemistry, allowing many structural comparisons in catalysis between the NHCs in these systems.[2–4] The (NHC)CuF class of complexes have remained rare and comparison of these to their heavier halide congeners and other (carbene)CuF species is limited.[5,6] Due to the hard/soft mismatch of the Cu-F bond,[7] which can render it labile and reactive, unique reactivity for Cu has been recently discovered aiding interest in this area.[6,8–10] That being said, there are only a few characterised examples in the literature, all containing 5-membered NHCs (Figure 3.1).[3,5,8,10–12]

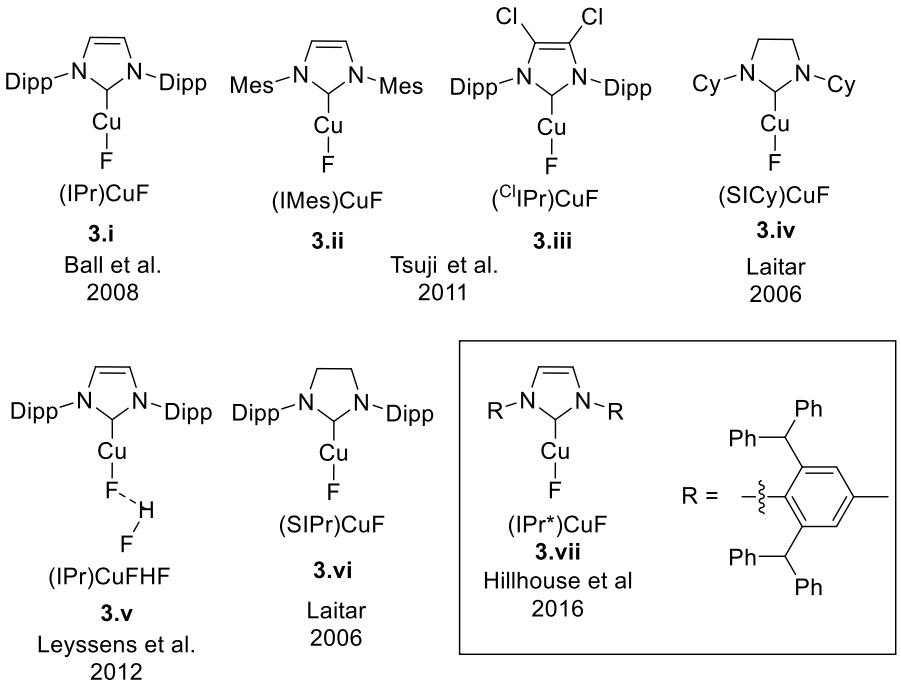


Figure 3.1 – (NHC)CuF complexes in literature.[5,8,11–15]

A common approach to the synthesis of (NHC)CuF complexes is *via* the reaction of $Et_3N{\cdot}3HF$ with a (NHC)CuOR precursor (Scheme 3.1).[5,8,11] The stoichiometry is important as excess $Et_3N{\cdot}3HF$ can lead to the formation of bifluoride complexes instead, such as (IPr)CuFHF (**3.v**).[13,16] The by-products of the reaction, ROH and $NEt_3$, can make spectroscopic comparisons and isolation difficult due to unwanted hydrogen bonding to the resulting (NHC)CuF complex.[11,13,17]

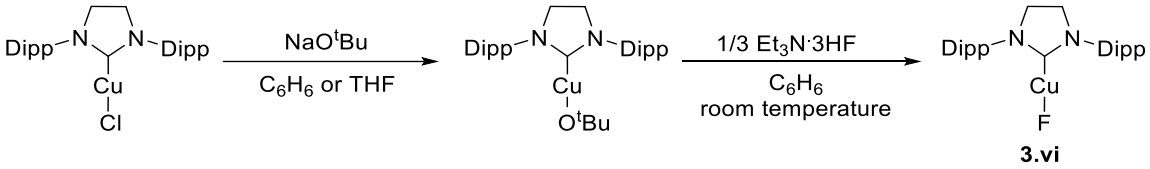


Scheme 3.1 – Laitar's synthesis of (SIPr)CuF.[11]

In one approach to overcome such issues, Sadighi employed the use of benzoyl fluoride for the synthesis of **3.vi** (Scheme 3.2).[18] The resulting *tert*-butyl benzoate by-product provided no issues in the synthesis of the CuF product as a high yield was obtained (86%). Both Laitar and Lalic employed the use of a non-polar solvent ($C_6H_6$ or toluene), which caused the precipitation of the desired Cu-F products from solution during the reaction, allowing for clean and facile work up.

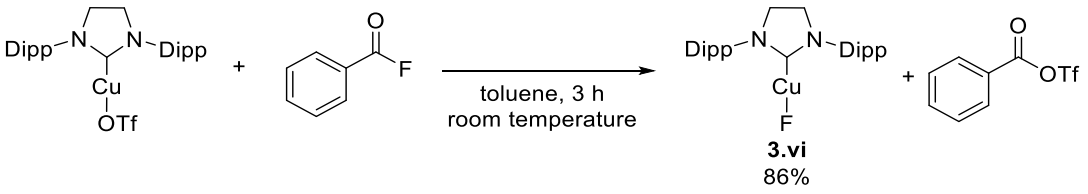


Scheme 3.2 – Wyss's method for synthesising (SIPr)CuF (**3.vi**) with benzoyl fluoride.[18]

An alternative route employing a metal fluoride salt was presented by Lalic in 2014.[10] The solubility of the metal fluoride salts was found to be the limitation of this method. An extensive solvent screen found 1,4-dioxane, an aprotic solvent, to be suitable, yielding **3.i** in good yields (88 %) (Scheme 3.3). Later work by Lalic also revealed CsF as a suitable alternative to KF.[19]

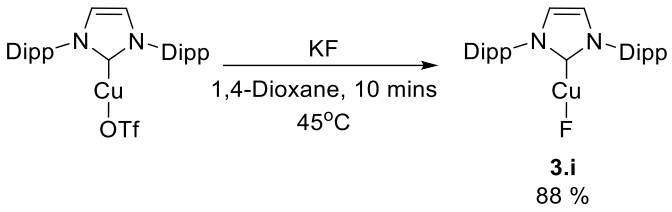


Scheme 3.3 – Lalic's synthesis of (IPr)CuF.[10]

## 3.1.2 – Catalysis with (NHC)CuF

The presence of a fluoride moiety in (NHC)CuF compared to (NHC)CuX (X= Cl, Br, I) can provide a more direct route into catalytic cycles without the need for other reagents. Thus Tsuji found that starting with (IMes)CuF (**3.ii**) to get to a putative (IMes)CuH species for alkyne hydrocarboxylation, resulted in higher reactivity and selectivity over a route employing the *in-situ* formation of (IMes)CuO$^t$Bu, followed by reaction with an organosilane to generate '(IMes)CuH' (Scheme 3.4).[20]

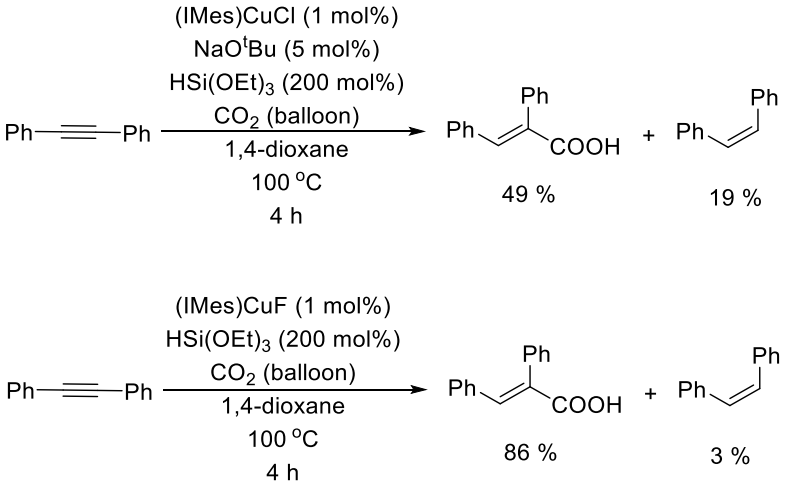


Scheme 3.4 – Catalytic conditions utilised by Tsuji.[5]

(NHC)CuF precursors have also been shown to react with organosilicon compounds not just as a route to (NHC)CuH products. With a large BDE (*ca.*150 kcal $mol^{-1}$),[21] Si-F bond formation is typically used as a driving force in reactions. This can allow for organosilicon reagents which typically have high BDEs themselves (Si-C *ca.* 80 kcal $mol^{-1}$),[22] to be used as reagents in catalysis. Ball demonstrated this in the isolation and characterisation of a rare (NHC)Cu-allyl complex (Scheme 3.5a), which proved valuable for catalytic applications (Scheme 3.5b).[8]

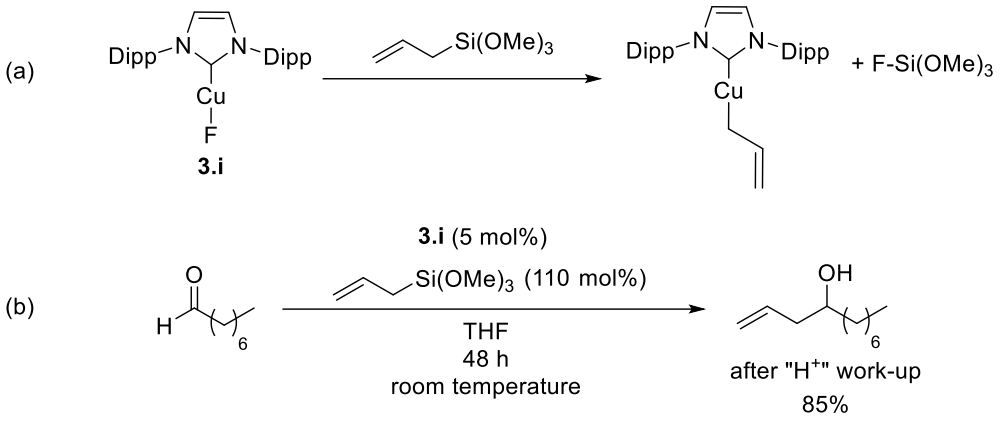


Scheme 3.5 – (NHC)Cu(allyl) formation and reactivity.[8]

In a later study by Ball, it was found that addition of (*n*-octyl)$SiF_3$ allowed aldehydes to be allylated with a wider range of silane substrates (Scheme 3.6).[23] The (*n*-octyl)$SiF_3$ was proposed to aid the C-C bond forming step, although exactly how was not made clear.

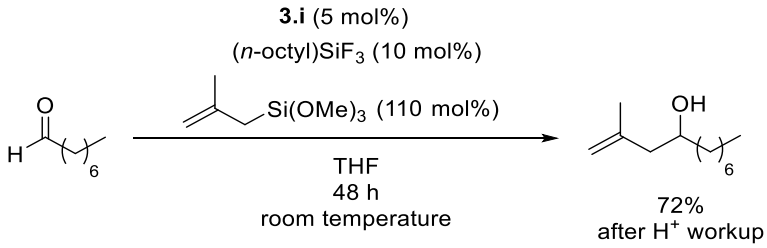


Scheme 3.6 – Catalytic allylation of aldehydes in the presence of (*n*-octyl)$SiF_3$.[23]

Lalic demonstrated it was possible to fluorinate alkyl triflates with *in-situ* generated **3.i** (Scheme 3.7).[10] *In-situ* generation of alkyl triflates themselves meant that alcohols could be used as the initial substrates in the reaction. While reactivity was limited to alkyl triflates, Sanford demonstrated it was possible to radiofluorinate aryl halides bearing directing groups such as pyridines. At this stage the reaction is stoichiometric and requires forcing conditions (Scheme 3.8).[9]

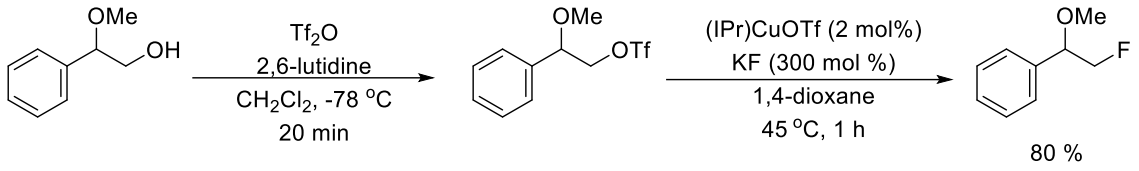


Scheme 3.7 - Catalytic activity demonstrated by Lalic.[10]

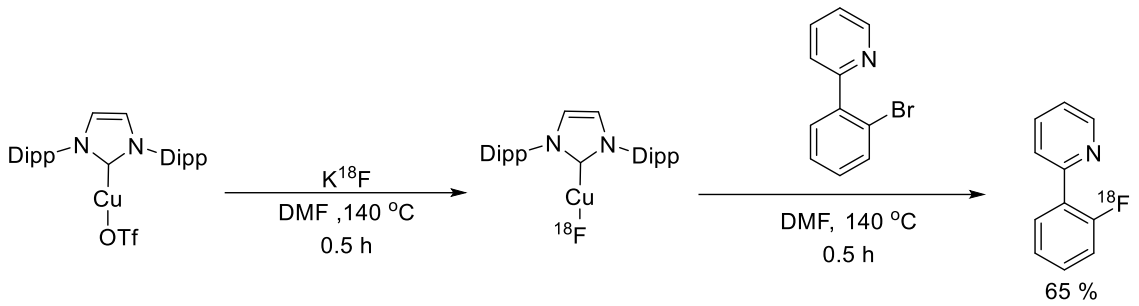


Scheme 3.8 – Radiofluorination of aryl halides demonstrated by Sanford.[9]

## 3.2 – Results and Discussion

(NHC)CuF complexes have been shown to provide alternative catalytic routes which avoid a common (NHC)CuH intermediate.[24] Instead with the ability to cleave traditionally difficult bonds such as Si-C and even C-X bonds (X = I, Br, OTf),[9,10] the field is open to new transformations. Our aim was to expand the diversity of the carbene ligands in (NHC)CuF complexes to aid developments in this area. In addition, we wanted to probe the mechanism by which catalytic allylation occurs (shown in Scheme 3.5b), particularly to establish the ease with which the (NHC)CuF species is regenerated in the catalytic cycle.

## 3.3 – Synthesis of (carbene)CuF

The synthesis of an array of (RE-NHC)CuO$^t$Bu complexes was demonstrated in chapter 2. We envisaged utilisation of (RE-NHC)CuO$^t$Bu would provide the easiest route to synthesise (RE-NHC)CuF following the procedure by Laitar.[11] Employing (7-Mes)CuO$^t$Bu (**2.2**) as our starting complex, the addition of 0.3 equivalents of $Et_3N{\cdot}3HF$ (0.9 equiv of HF) led to almost immediate precipitation (< 5 min) of a white solid in $C_6H_6$ (Scheme 3.9). The use of < 1 equivalents of "HF" to **2.2** is important as this reduces the potential formation of bifluoride or other unwanted species.[25] Upon dissolving the precipitate in $CD_2Cl_2$, $^{19}F\{^1H\}$ NMR spectroscopy revealed a low frequency signal at -246 ppm, which by comparison to the reported (NHC)CuF species (Figure 3.1), [5,8,11–15] is indicative of formation of (7-Mes)CuF (**3.1**).

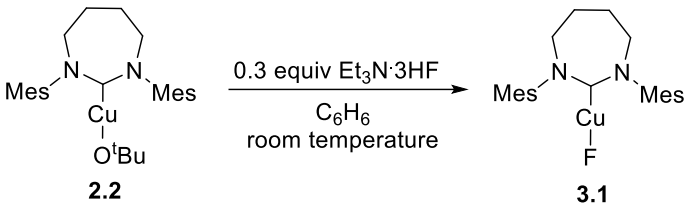


Scheme 3.9 – Initial synthesis of **3.1**.

In addition to **3.1**, $^{19}F\{^1H\}$ NMR spectroscopy (Figure 3.2a), showed the presence of a minor impurity at *ca.* -50 ppm, which required numerous washes with $C_6H_6$ to remove. Believing this arose from having $^t$BuOH present, (7-Mes)CuMes was chosen an alternative precursor.[iv] Protonation with $Et_3N{\cdot}3HF$ would give mesitylene, removing the possibility of hydrogen bonding with the resulting (NHC)CuF species. Figure 3.2b shows this approach gave clean **3.1**.

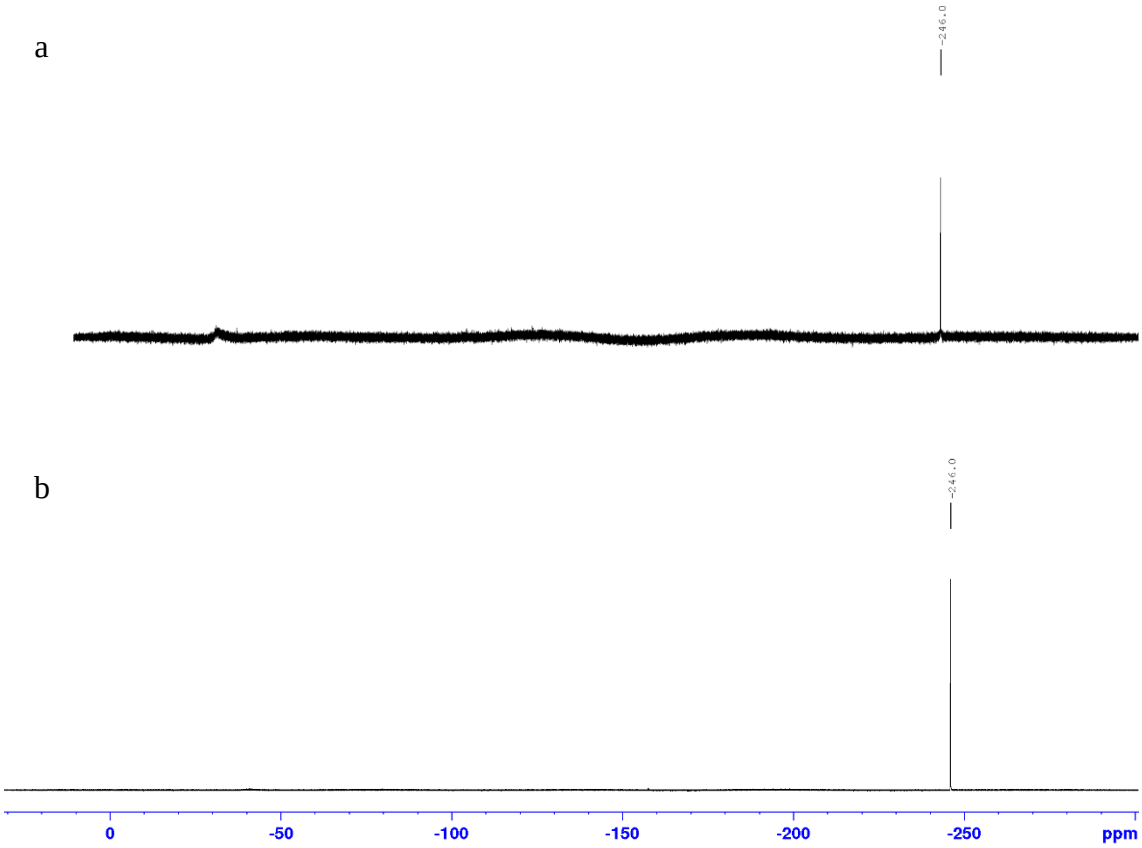


Figure 3.2 – $^{19}F$ NMR spectra (470 MHz, $CD_2Cl_2$, 298 K) of **3.1**. (a) from the reaction of (7-Mes)CuO$^t$Bu (**2.2**) and $Et_3N{\cdot}3HF$, (b) from the reaction of (7-Mes)CuMes and $Et_3N{\cdot}3HF$.

Employing this method, an array of (carbene)CuF species were synthesised (Scheme 3.10), including complexes featuring a bulky NHC (ITr), a diamido carbene (DAC) and cyclic alkyl amino carbene (CAAC). Isolated yields ranged from 42 to 82 %. Benzene proved suitable for

[iv] Experimental details for (carbene)CuMes complexes can be found in chapter 6. Crystallographic details are given in the appendix.

most of the reactions as this allowed precipitation of the final products during the reaction. In the case of the unsymmetrical carbene complex (ITrDipp)CuF (**3.4**), the addition of $Et_2O$ was required to precipitate **3.4** from solution. ($^{Menthyl}$CAAC)CuF (**3.5**) was synthesised in $Et_2O$ as the precursor ($^{Menthyl}$CAAC)CuMes was soluble in most solvents, allowing for clean precipitation of **3.5** during the reaction.

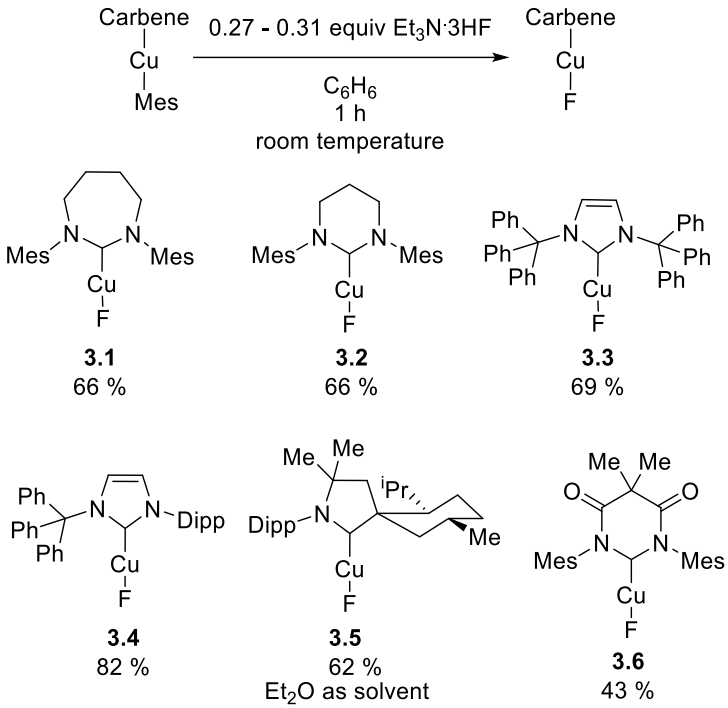


Scheme 3.10 – (Carbene)CuF species (together with yields) isolated in this study.

## 3.4 – Characterisation of (carbene)CuF Complexes

The six complexes **3.1** – **3.6** were all soluble in chlorinated solvents and revealed similar upfield shifts in the $^{19}F\{^1H\}$ NMR spectra around -240 ppm in $CD_2Cl_2$ and -250 ppm in $CDCl_3$ (Figure 3.3). All the peaks were sharp, aside from those belonging to **3.6**, which may be due to additional binding interactions of the fluoride ligand. By $^{13}C$ NMR spectroscopy, a doublet resonance was observed for the C2 (carbenic) carbon for complexes **3.1**, **3.3** and **3.4** with $^2J_{CF}$ splittings of 32 – 36 Hz. The doublet splitting confirms the monomeric nature of these species in solution. The C2 carbon signal in **3.2** could only be characterised by $^1H$-$^{13}C$ HMBC measurements, while **3.6** showed no observable C2 peak. In the case of **3.5**, only a broad resonance was observed.

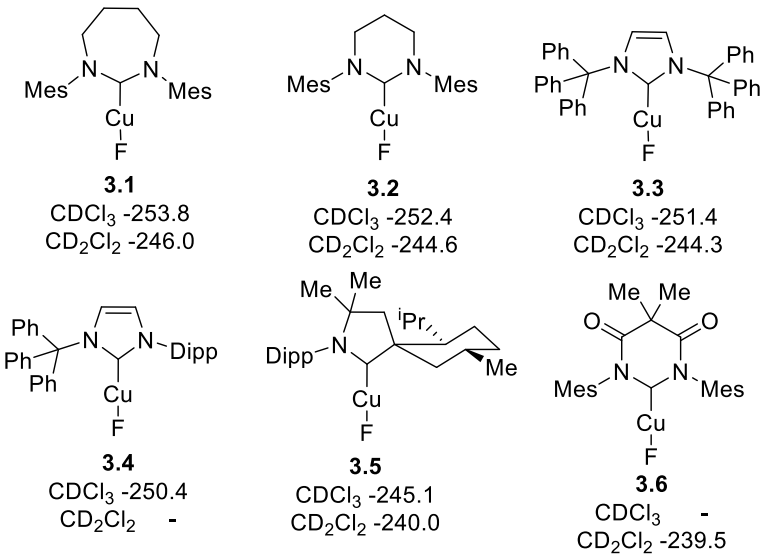


Figure 3.3 – $^{19}$F NMR shifts of complexes **3.1** – **3.6** (ppm).

X-ray quality crystals of **3.1** – **3.5** were grown from hexane layered $CH_2Cl_2$ solutions of the complexes (Figure 3.4 and Table 3.1). Numerous attempts to crystallise the diamido carbene derivative **3.6** failed. Complexes **3.1** – **3.5** showed Cu-F bond lengths between 1.7865(10) – 1.816(2) Å, which were consistent with values in the literature.[11] Hydrogen bonding interactions were seen in all the complexes, as illustrated in Figure 3.5. As commented by Laitar, the different nature of these interactions (i.e 1 – 3 hydrogen bonds) can limit meaningful comparison of Cu-F distances.[11] In the case of **3.3**, hydrogen bonding to $CH_2Cl_2$ was observed, rather than the NHC backbone C-H bonds (Figure 3.5). The steric bulk of the ITr moiety (%$V_{Bur}$ of 62.5 %, Table 3.1), could explain this.[26] **3.4** is also bulky, however the asymmetric nature of the ligand potentially allows closer packing of another molecule. Interestingly **3.4** only showed one hydrogen bonding interaction, yielding the shortest hydrogen bond distance in this series (2.0149(10) Å).[v]

[v] Values can be found in the description of Figure 3.5.

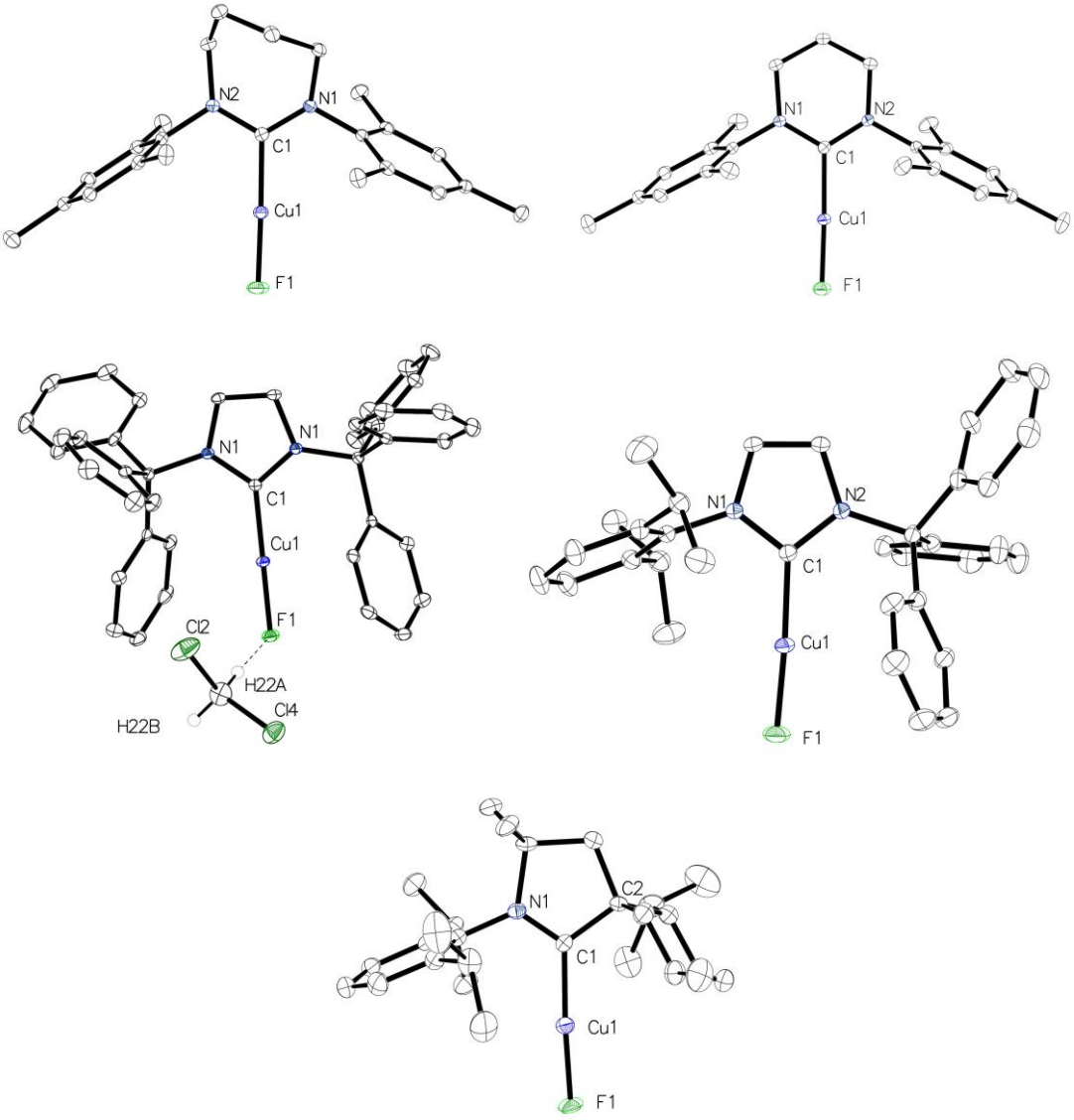


Figure 3.4 – Molecular structures of (left to right, top to bottom) **3.1** – **3.5**. In all cases, ellipsoids are shown at 30% probability and hydrogen atoms have been omitted for clarity. In **3.2** and **3.5**, the structure of the molecule based on Cu1 in the asymmetric unit is shown. In **3.3** a hydrogen bonded $CH_2Cl_2$ molecule was shown, F1-H22A 2.1539(8) Å.

Table 3.1 – Structural comparison of distances (Å) and angles (°) in (carbene)CuF complexes **3.1** – **3.5**.

| | **3.1** | **3.2** | **3.3** | **3.4** | **3.5** |
|---|---|---|---|---|---|
| **Cu - F** | 1.7940(11) | 1.8037(10) | 1.816(2) | 1.7865(10) | 1.808(4) |
| **Cu - $C_{carbene}$** | 1.8647(18) | 1.8737(15) | 1.877(4) | 1.8525(13) | 1.865(5) |
| **$C_{carbene}$ - Cu - F** | 177.29(7) | 174.30(6) | 180[vi] | 176.34(6) | 176.58(18) |
| **$\%V_{Bur}$[a]** | 45.0 | 42.7 | 62.5 | 54.6 | 51.9 |

[a]Value calculated at an M-$C_{carbene}$ distance of 2.0 Å. Parameters used: Bondi radii scaled by 1.17, 3.5 Å sphere radius, 0.1 exhaustiveness, and exclusion of hydrogens.[27]

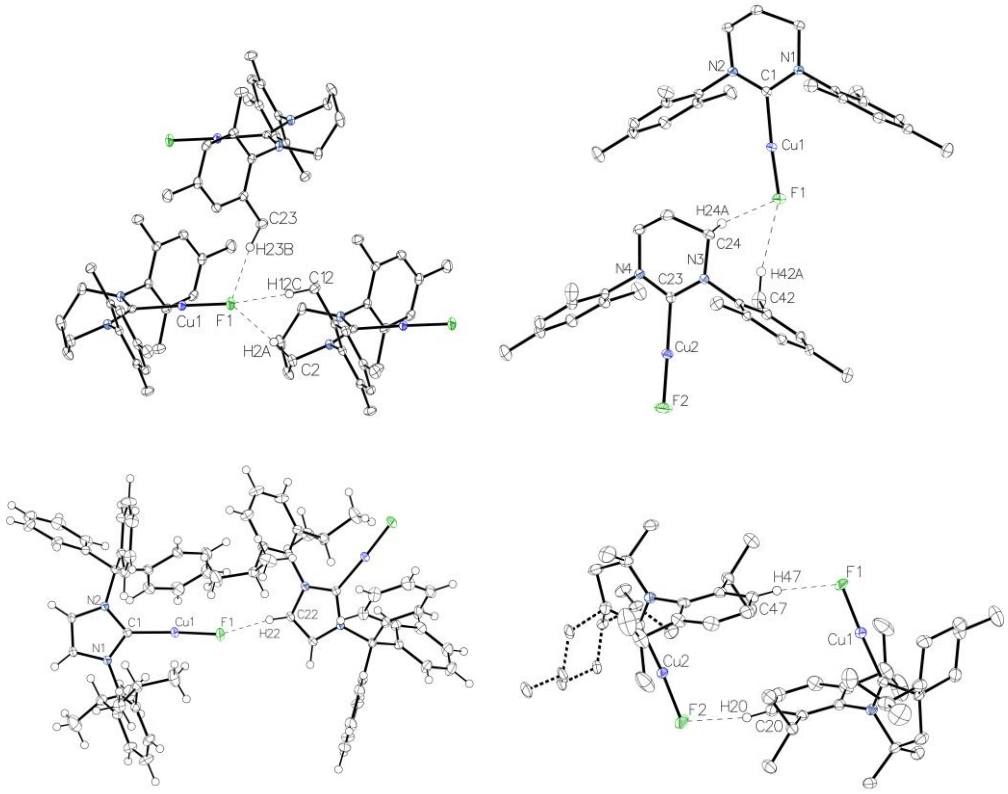


Figure 3.5 – Hydrogen bonding interactions in (left to right, top to bottom): **3.1**, F1-H23B (2.5430(12) Å), F1-H2A (2.3012(11) Å), F1-H12C (2.3457 (12) Å); **3.2**, F1-H24A (2.3782(12) Å), F1-H42A (2.5465(11) Å); **3.4**, F1-H22 (2.0149(10) Å); **3.5**, F1-H47 2.386(4) Å, F2-H20 2.370(4) Å (dotted bonds were also shown for one moiety of the cyclohexyl ring of **3.5** as this was shown to be disordered in 75:25 ratio).

[vi] C-Cu-F are coincident with a crystallographic 2-fold rotation axis.

## 3.5 – (Carbene)CuF Catalysed Allylation of Octanal

A preliminary catalytic study on the allylation of octanal was investigated using complexes **3.1** – **3.5**.[vii] Similar conditions to those used by Ball were employed with $C_6D_6$ used as a solvent to allow *in-situ* NMR monitoring.[8] Employing **3.2**, loadings of 5, 2 and 1 mol% were tested over 24 h (Table 3.2, entries 1 - 6). At 5 mol % (entry 1), 99% conversion of octanal was found within 1 h (*c.f.* 99% conversion after 48 h with **3.i**).[8] 1 mol % of **3.2** resulted in a significant reduction in conversion even after 2 h (entry 5), although full conversion could be achieved over 24 h (entry 6). In $d_8$-THF, conversion with 1 mol% of **3.2**, remained low even after 24 h. The presence of black precipitate in the reaction vessel suggested decomposition of the copper species.

Table 3.2 – Initial studies of **3.2** in the catalytic allylation of octanal.[a]

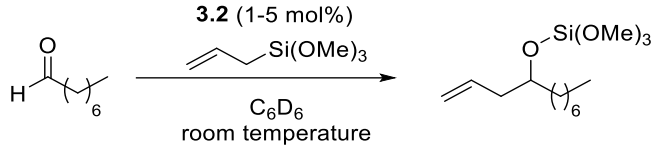


| Entry | Loading (mol %) | Time (h) | Conversion |
|---|---|---|---|
| 1 | 5 | 1 | 99 |
| 2 | 2 | 1 | 68 |
| 3 | 2 | 2 | 95 |
| 4 | 1 | 1 | 34 |
| 5 | 1 | 2 | 40 |
| 6 | 1 | 24 | 99 |
| 7[b] | 1 | 24 | 26 |

[a]Octanal (1 mmol), allyltrimethoxysilane (110 mol%) in $C_6D_6$ (1 mL) at 25 °C. Monitored by $^1$H NMR spectroscopy using 1,3,5-$C_6H_3(OMe)_3$ as an internal standard. [b]$d_8$-THF as solvent.

The other (carbene)CuF complexes **3.1**, **3.3**, **3.4**, and **3.5** were examined (Table 3.3), under scaled up conditions to allow for isolation of the 1-undecen-4-ol after acidic work up. **3.3**, containing the bulky carbene ITr, was found to yield the best result with 77 % conversion after 4 h (Entry 3). The CAAC containing complex, **3.5**, showed the poorest conversion, at 45 % over 24 h. Both **3.4** and **3.5** showed significant discrepancies between conversion of octanal and percentage isolated yield of 1-undecen-4-ol suggesting that other processes are occurring. During catalysis with **3.4**

[vii] Complex **3.6** was made post study and not tested catalytically.

and **3.5**, a black precipitate and brown plating was observed suggesting instability of catalytic intermediates during the catalytic run.

Table 3.3 – Catalytic allylation of octanal.[a]

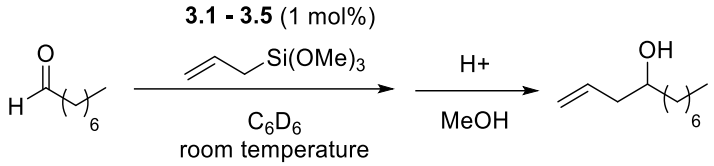


| Entry | Precursor | Conversion of Octanal (%)[b] | Isolated Yield of 1-Undecen-4-ol (%)[c] |
|---|---|---|---|
| 1 | **3.1** | 28 (68) | 58 |
| 2 | **3.2** | 39 (79) | 64 |
| 3 | **3.3** | 77 (99) | 78 |
| 4 | **3.4** | 28 (95) | 26 |
| 5 | **3.5** | 20 (45) | 7 |
| 6 | - | 0 (0) | 0 |

[a]Octanal (3 mmol), allyltrimethoxysilane (110 mol%), (carbene)CuF (1 mol%) in $C_6D_6$ (1 mL) at 25 °C. [b]Conversion after 4 h (in parentheses, 24 h) measured by $^1$H NMR spectroscopy using 1,3,5-$C_6H_3(OMe)_3$ as an internal standard and as an average of two runs. [c]Isolated yield of 1-undecen-4-ol after 24 h following work up with *p*TsOH in MeOH as an average of two runs.

## 3.6 – Synthesis and Characterisation of (ITr)Cu($CH_2CHCH_2$) (3.7)

As shown in Scheme 3.5a, Ball reported the conversion of **3.i** to an allyl complex, which they proposed to be a species of relevance to the catalytic cycle.[8] Using **3.3** we performed a stoichiometric reaction with allyltrimethoxysilane. A rapid colour change from colourless to bright yellow was observed and by $^1$H NMR spectroscopy ($d_8$-toluene), a new quintet (5.8 ppm, $^3J_{HH}$ = 11 Hz, 1H) and doublet (2.4 ppm, $^3J_{HH}$ = 11 Hz, 4H) were found (alongside signals between 7.5 – 6.4 ppm corresponding to the ITr ligand) indicative of (ITr)Cu($CH_2CHCH_2$) (**3.7**, Scheme 3.11). The observation of a quintet and doublet suggest rapid interchange between $\eta^1$- and $\eta^3$-allyl coordination modes, as seen for (IPr)Cu($CH_2CHCH_2$).[8] The fluxionality in **3.7** was retained in $d_8$-THF even down to 199 K (Figure 3.6).

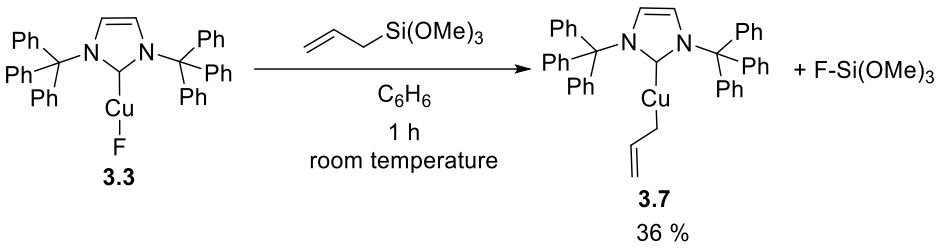


Scheme 3.11 – Synthesis of (ITr)Cu($CH_2CHCH_2$) (**3.7**)

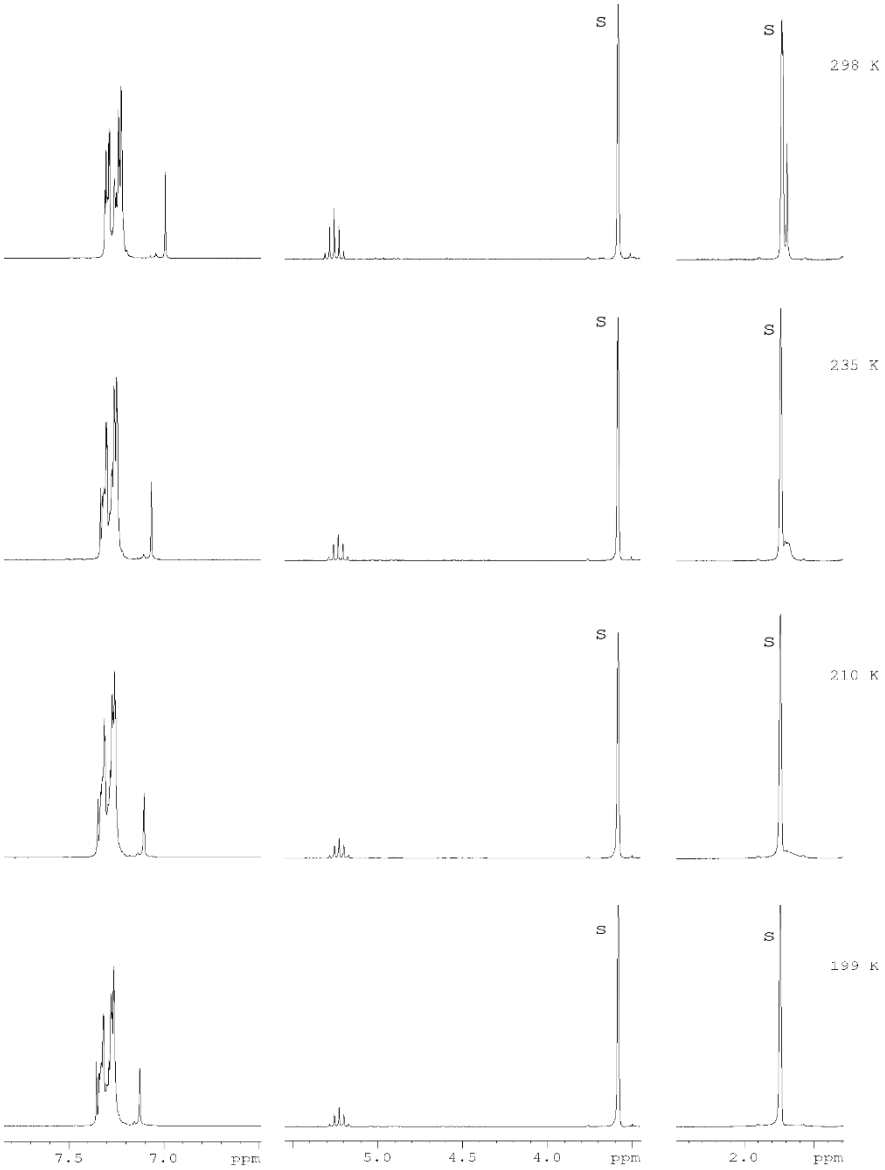


Figure 3.6 – Variable temperature $^1$H NMR spectra (400 MHz) of ITrCu($CH_2CHCH_2$) (**3.7**) in $d_8$-THF.

**3.7**, which was isolated as a colourless solid in 36 % yield, proved to be stable for over a week in solution at room temperature. It was soluble in $Et_2O$, allowing X-ray quality crystals to be isolated upon laying a concentrated $Et_2O$ solution of the complex with pentane at -30 °C. The structure

consists of one ITr and one $\eta^1$- bound allyl ligand coordinated to Cu in a linear geometry (Figure 3.7). The Cu - $C_{carbene}$ bond length (1.9099(18) Å) is within the range observed for the IPr bound examples of allyl complexes by Ball ((IPr)Cu($CH_2CHCH_2$) 1.8926(18) Å and (IPr)Cu($CH_2C(CH_3)CH_2$) 1.902(2) Å).[23] No significant differences were seen in Cu-$C_{allyl}$ distance nor in the Cu-C-C-C dihedral angle.

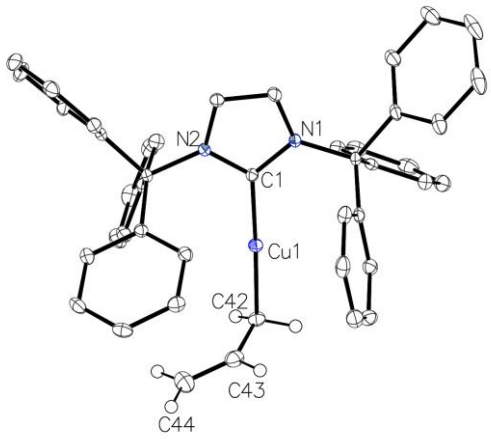


Figure 3.7 – Molecular structure of (ITr)Cu($CH_2CHCH_2$) (**3.7**). Hydrogen atoms, with the exceptions of those in the allyl ligand, have been omitted for clarity. Ellipsoids are represented at 30% probability. Selected bond lengths (Å) and angles (°): Cu1-C1 1.9099(18), Cu1-C42 1.9587(19), C42-C43 1.446(3), C43-C44 1.316(3), C1-Cu1-C42 175.03(9), Cu1-C42-C43 107.23(14), C42-C43-C44 128.5(2), Cu1-C42-C43-C44 103.657.

## 3.7 – Attempted Synthesis of (6-Mes)Cu($CH_2CHCH_2$)

Attempts were made to synthesise the 6-Mes analogue of **3.7**. Upon mixing a suspension of **3.2** and allyltrimethoxysilane in $C_6D_6$, a dull yellow suspension was generated, although this proceeded to give a black precipitate, which increased in quantity over time. At early times, the $^1$H NMR spectrum showed a quintet and doublet with similar chemical shifts to those of **3.7**. By $^{19}F\{^1H\}$ NMR spectroscopy, two signals were present; one at -156 ppm (corresponding to $(MeO)_3SiF$)[28] and another at -142 ppm (*vide infra*). There was no residual **3.2** remaining, based on the absence of a Cu-F resonance, although as the reaction afforded a suspension this could reflect any remaining **3.2** simply not being in solution.

During the formation of **3.7** only $(MeO)_3SiF$ was observed by $^{19}F\{^1H\}$ NMR spectroscopy; however, if an additional equivalent of allyltrimethoxysilane was added to the reaction, a signal at -142 ppm was observed. This showed $^{29}$Si satellites ($^1J_{F\text{-}Si}$ = 146 Hz), suggesting that it is a fluorosilane species which arises from the reaction of allyltrimethoxysilane with $(MeO)_3SiF$. The

reaction shown in Scheme 3.12 affords a $^{19}F$ signal at a similar chemical shift with a similar magnitude of $^{1}J_{F\text{-}Si}$ suggesting that the product we see is a silicate.

The appearance of this species in the case of **3.2** implies that the reaction of allyltrimethoxysilane with $(MeO)_3SiF$ is presumably faster than that of allyltrimethoxysilane and **3.2**, which is most likely due to the poor solubility of **3.2** in $C_6D_6$. Literature on fluorosilicates in organometallic reactions are rare but there are a few examples suggesting their involvement in catalysis (one example shown in Scheme 3.12).[16,28–30]

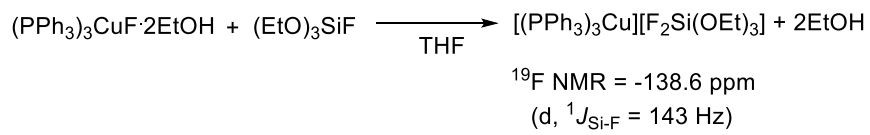


Scheme 3.12 – Fluorosilicate formation observed by Shibasaki.[28]

## 3.8 – Further Studies of the Allylation of Octanal

In contrast to the excellent activity of **3.3** (Table 3.3, entry 3), **3.7** gave not only poor conversion of octanal (Table 3.4, entry 1), but failed to generate the desired product. The difference in the two catalytic runs is the presence of a fluorine containing moiety suggesting that the lack of such a species is detrimental to catalysis. As mentioned previously, Ball used an additive of trifluorooctylsilane to improve catalysis.[23] Upon addition of $(EtO)_3SiF$ (1 mol%) (the closest commercially available species to $(MeO)_3SiF$), conversion was greatly increased for **3.7** to 90 % after 24 h (Table 3.3, entry 2), a similar result to **3.3** (Table 3.3, entry 3).

The involvement of a Cu-alkoxide intermediate in the catalytic cycle was also investigated. Due to issues in forming (ITr)CuO$^t$Bu,[viii] (6-Mes)CuO$^t$Bu (**2.1**) was employed as a representative alkoxide. **2.1** was found to be poor for the allylation reaction (35% conversion observed after 24 h). As with **3.7**, percentage conversion failed to agree with the amount of isolated product. Addition of $(EtO)_3SiF$ increased conversion (58% after 24 h) and the desired product was observed (Table 3.4, entry 4). By itself, $(EtO)_3SiF$ (5 mol%), gave no conversion, proving that Cu is essential for the reaction (Table 3.4, entry 5).

[viii] (ITr)CuMes and $^t$BuOH did not yield the desired alkoxide and very little conversion was seen, which we assume is due to the steric bulk of the NHC. The smaller alkoxide complex, (ITr)CuO$^i$Pr, could be synthesised but was not used for this study (see appendix 7.6).

Table 3.4 – Catalytic allylation of octanal.[a]

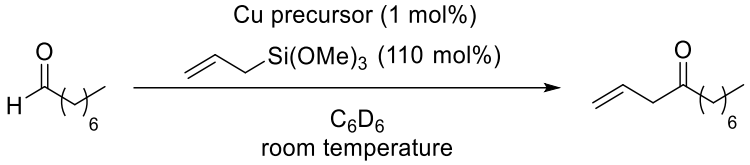


| Entry | Precursor | Conversion of Octanal (%)[b] |
|---|---|---|
| 1 | **3.7** | 13(25)[c] |
| 2 | **3.7** + $(EtO)_3SiF$[d] | 61(90) |
| 3 | **2.1** | 22(35)[c] |
| 4 | **2.1** + $(EtO)_3SiF$[d] | 30(58) |
| 5 | $(EtO)_3SiF$[e] | 0(0) |

[a]Octanal (1 mmol), allyltrimethoxysilane (110 mol%), (carbene)CuF (1 mol%) in $C_6D_6$ (1 mL) at 25 °C. [b]Conversion after 4 h (in parentheses, 24 h) measured by $^1H$ NMR spectroscopy using 1,3,5-$C_6H_3(OMe)_3$ as an internal standard and as an average of two runs. [c]The conversion of aldehyde was not accompanied by formation of product. [d]$(EtO)_3SiF$ (1 mol%). [e]5 mol%.

## 3.9 – Investigations of the Catalytic Cycle

A proposed catalytic cycle based upon these results is shown in Scheme 3.13. Starting from (carbene)CuF, the reaction with allylsilane takes place to give (carbene)Cu(allyl), eliminating $(MeO)_3SiF$ (Scheme 3.13, step **A**). Octanal insertion into the (carbene)Cu(allyl) species would then afford (carbene)CuOR (step **B**). Re-insertion of $(MeO)_3SiF$ into the cycle in step **C** then leads to the elimination of the desired product, reforming the (carbene)CuF species.

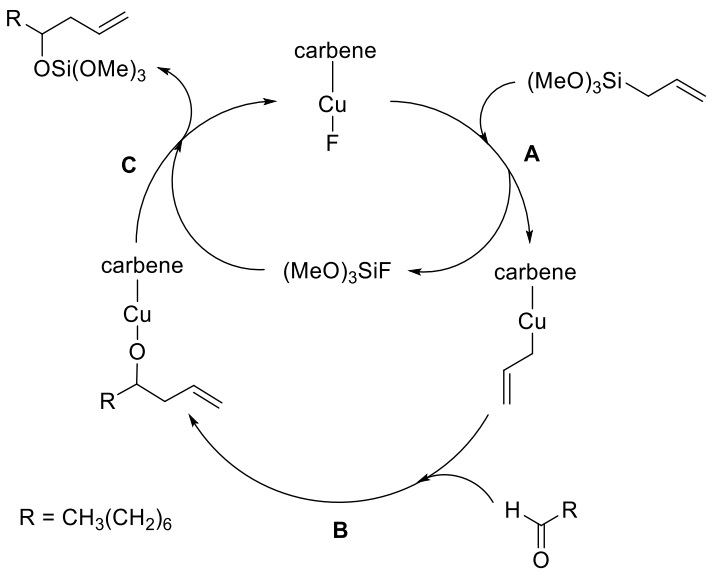


Scheme 3.13 – Postulated catalytic cycle for aldehyde allylation.

To rule out step **A** involving reaction with octanal rather than allysilane, **3.3** was mixed with 1 equivalent of the former. In both $C_6D_6$ and $CD_2Cl_2$, there was no reaction by both $^1H$ and $^{19}F\{^1H\}$ NMR spectroscopy after 1 h. Increasing the equivalents of octanal to ten, did reveal a change to the $^{19}F\{^1H\}$ NMR spectrum although only after leaving overnight. The Cu-F resonance of **3.3** broadened and a minor sharp peak of unknown origin appeared at -139 ppm (Figure 3.8). As **3.3** reacts rapidly with allyltrimethoxysilane, this does appear to be the most likely first step of the catalytic cycle.

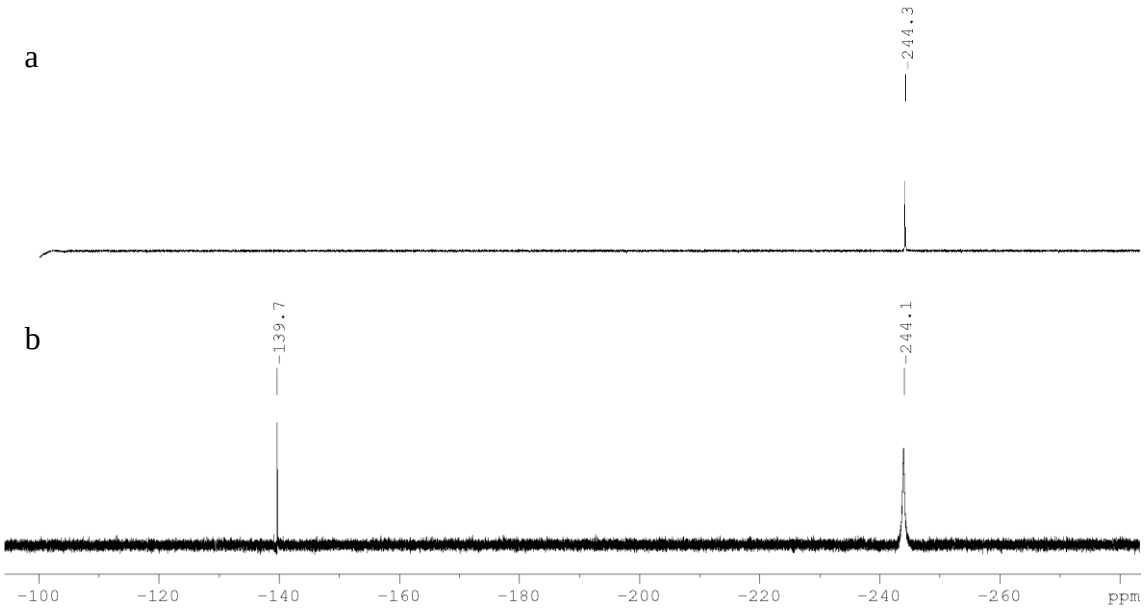


Figure 3.8 – $^{19}F\{^1H\}$ NMR (470 MHz) spectra of a) **3.3** + octanal (1 equivalent) in $CD_2Cl_2$ after 1 h and b) after 20 h with 1 equivalent of octanal.

Step **B** involves the insertion of octanal into a (carbene)Cu(allyl) species. Upon addition of octanal (1 equivalent) to **3.**7 in $C_6D_6$, a rapid colour change from yellow to colourless took place. By $^1H$ NMR spectroscopy, both octanal and **3.7** had been consumed to generate a set of broad resonances, presumed to arise from the copper alkoxide species suggested by Ball.[8]

There is most conjecture around step **C**. Ball suggested the role of $(EtO)_3SiF$ in the catalytic cycle was to help the C-C bond forming step, but they did not delve further into the potential intermediates involved.[23] Shibasaki suggested $(EtO)_3SiF$ aided their reactions through the formation of silicates, which were believed to be active intermediates in their cycle (Scheme 3.12).[28,30] This was supported by a later report by Leyssens, who used calculations to probe the interaction of $Ph_3SiF$ with **3.i**.[16] The study postulated two silicate complexes could form, a van der Waals complex or a tight ion pair, which could be differentiated by the $^{19}F$ NMR data (Figure 3.9).

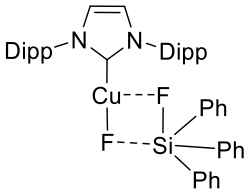


van der Waals complex
$^{19}F$ NMR$_{calc}$ = -228.0 ppm, -191.2 ppm
($^1J_{Si-F}$ = 273.2 Hz)

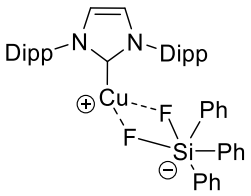


Tight ion pair
$^{19}F$ NMR$_{calc}$ = -167.5 ppm, -102.6 ppm
(dd, $^1J_{Si-F}$ = 242.3, 218.6 Hz)

$^{19}F$ NMR$_{observed}$ = -157.0 ppm ($^1J_{Si-F}$ = 181.2 Hz),
-139.6 ppm ($^1J_{Si-F}$ = 146.5 ppm)

Figure 3.9 – Calculated and experimental $^{19}F$ NMR shifts of the silicate species by Leyssens.[16,28,31]

To probe the role of $(EtO)_3SiF$ in our case, a series of reactions were carried out with **2.1**. The addition of 1 equivalent of allyltrimethoxysilane to a $C_6D_6$ solution of **2.1** resulted in partial conversion (40%) to (6-Mes)Cu(allyl) over *ca.* 2 h. Addition of 1 equivalent of $(EtO)_3SiF$ to this solution led to > 80% conversion of **2.1** into (6-Mes)Cu(allyl) after 2 h (Scheme 3.14). As noted in section 3.2.5, this was seen to decompose in solution. By $^{19}F\{^1H\}$ NMR spectroscopy, there was no indication of **3.2** forming, but instead there was a resonance at -138 ppm, suggestive of silicate formation.

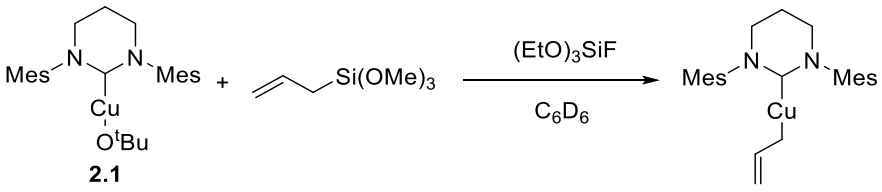


Scheme 3.14 – Addition of allyltrimethoxysilane and $(EtO)_3SiF$ to **2.1**.

Mixing differing amounts of $(EtO)_3SiF$ (1/2/3 equivalents) with a $C_6D_6$ solution of **2.1** led in all cases, to formation of a precipitate after < 30 mins. X-Ray suitable crystals were isolated through layering a concentrated $CH_2Cl_2$ solution of the precipitate with pentane at 298 K and shown to be $[\{(6\text{-Mes})Cu\}_2(\mu\text{-OEt})][SiF_5]$ (**3.8**) (Figure 3.10).

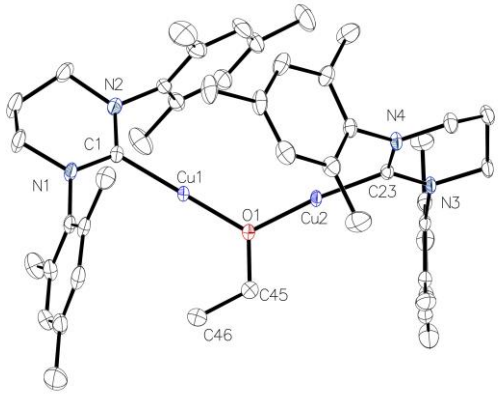


Figure 3.10 – Molecular structure of the cation in $[\{(6\text{-Mes})Cu\}_2(\mu\text{-OEt})][SiF_5]$ (**3.8**). Ellipsoids shown at 30% probability. Hydrogen atoms are removed for clarity.

The $^1H$ NMR spectrum of **3.8** in $CD_2Cl_2$ revealed one carbene environment along with a broad set of peaks for the ethyl group at 2.37 ppm (2H) and 0.07 ppm (3H). Cooling to 235 K, resolved the broad peaks into a triplet and quartet (Figure 3.11). By $^{19}F$ NMR spectroscopy a single peak at -139.6 ppm ($^1J_{F\text{-}Si}$ =147 Hz) was observed, in accordance with literature values for the $[SiF_5]^-$ anion.[32–35] The mechanism of the formation of **3.8** is unknown, but it is unlikely to be a simple reaction due to its formation under differing stoichiometries of **2.1** and $(EtO)_3SiF$.

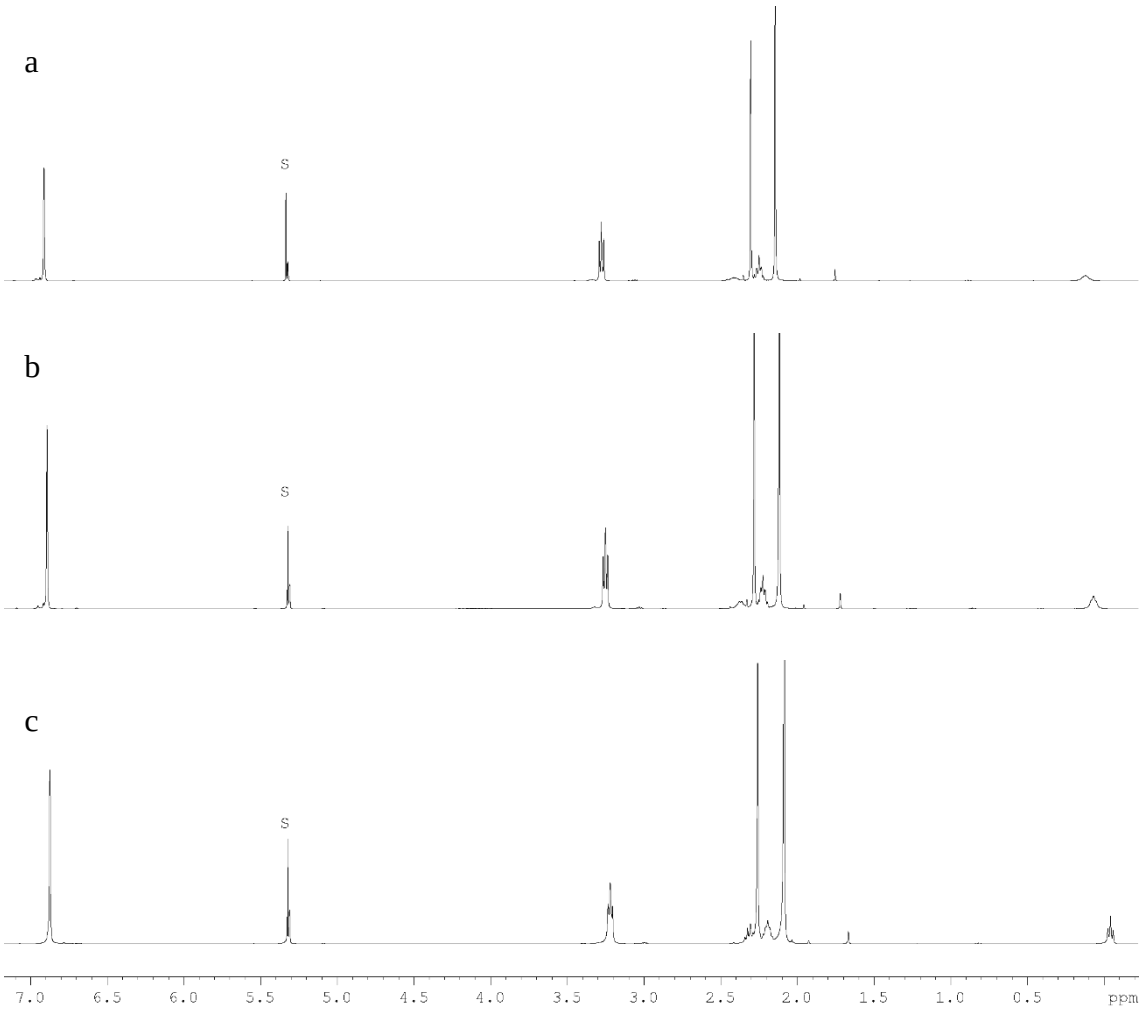


Figure 3.11 – Variable temperature $^{1}H$ NMR spectra (400 MHz) of complex **3.8** in $CD_2Cl_2$ at a) 298 K, b) 273 K and c) 235 K.

Complex **3.8** was also the product of the reaction of (6-Mes)CuF (**3.2**) with $(EtO)_3SiF$, and could be generated in very high yield (81%) when the reagents were combined in a 1:3 ratio. $[SiF_5]^-$ formation appears to be a very favourable process and it was postulated that it could take place through the series of steps shown in Scheme 3.15.

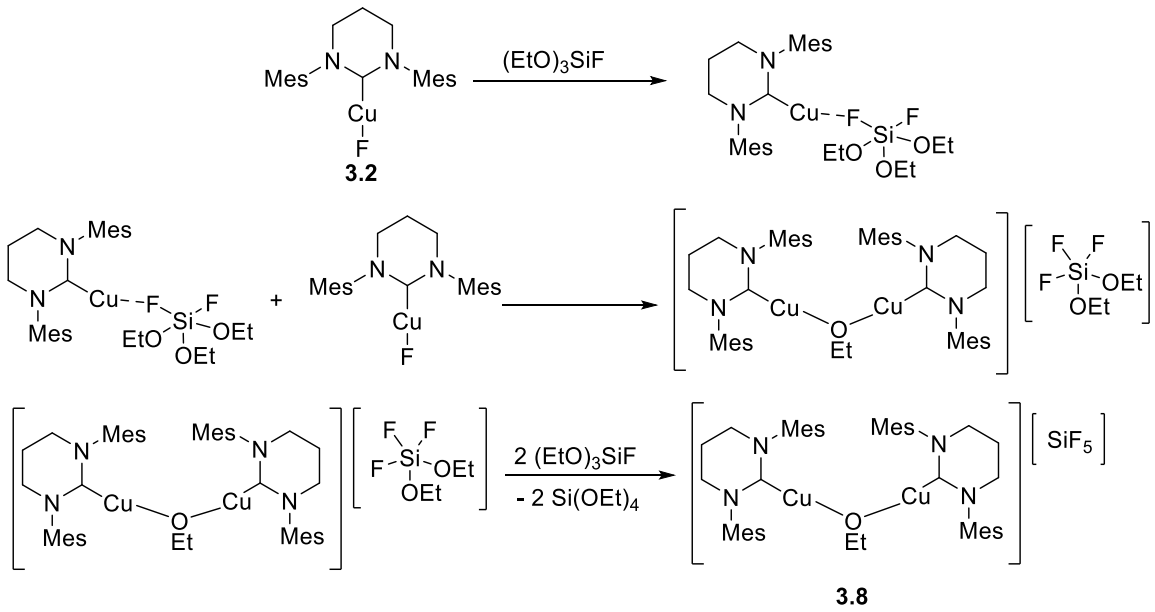


Scheme 3.15 - Proposed mechanism for the formation of **3.8**

Both ITr complex **3.3** and CAAC complex **3.5** reacted in a similar way with $(EtO)_3SiF$ to give $[\{(ITr)Cu\}_2(\mu\text{-}OEt)][SiF_5]$ (**3.9**) and $[\{(^{Menthyl}CAAC)Cu\}_2(\mu\text{-}OEt)][SiF_5]$ (**3.10**) (Scheme 3.16). X-ray quality crystals of both complexes were obtained from $CH_2Cl_2$/pentane (Figure 3.12 and Figure 3.13). Table 5 summarises selected bond lengths and angles in **3.8** – **3.10**, along with $[\{(IPr)Cu\}_2(\mu\text{-}OH)]^+$.[36] The structures of **3.8** – **3.10** comprise of a $[SiF_5]^-$ anion and a cationic species containing two [(NHC)Cu] moieties bound together by a bridging ethoxy group. The Cu1···Cu2 separations in **3.8** – **3.10** range from 3.2563(6) – 3.5374(6) Å, which is greater than twice the van der Waals radius for Cu (1.4 Å),[37] suggesting there are no Cu-Cu interactions. Comparing the Cu-O bond distances, **3.8** – **3.10** show elongation compared to $[\{(IPr)Cu\}_2(\mu\text{-}OH)]^+$,[36] with the longest being **3.9** (1.873(2) and 1.875(2) Å). For both **3.8** and **3.9**, the Cu-O bond distances were shown to be longer than their neutral counterparts **2.1** (1.8016(15) Å) and (ITr)CuO$^i$Pr (1.8080(15) Å) respectively. The Cu-$C_{carbene}$ bond lengths of **3.8** – **3.10** were found to be longer than those of $[\{(IPr)Cu\}_2(\mu\text{-}OH)]$ with the longest belonging to **3.9**. In comparison to the cations $[(6\text{-}Mes)_2Cu]^+$ and $[(IPr)Cu(P^tBu_3)]^+$ and neutral **2.1** and (ITr)CuO$^i$Pr, **3.8** and **3.9** show values in-between. The Cu-O-Cu angle for **3.8** and **3.10** was smaller than that of $[\{(IPr)Cu\}_2(\mu\text{-}OH)]^+$, with **3.9** containing the largest angle (141.36(24)°).

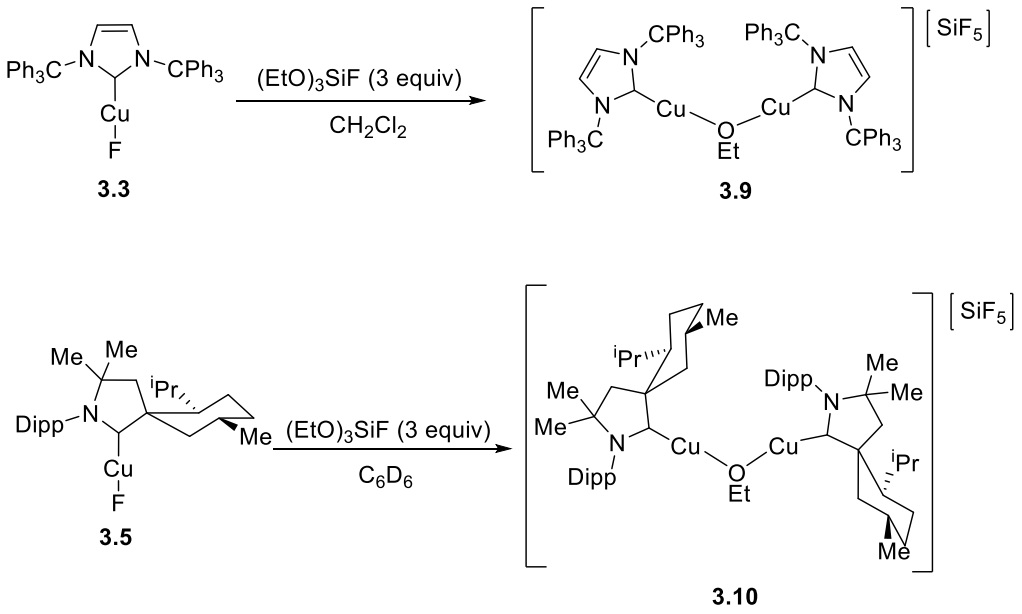


Scheme 3.16 – Formation of **3.9** and **3.10.**

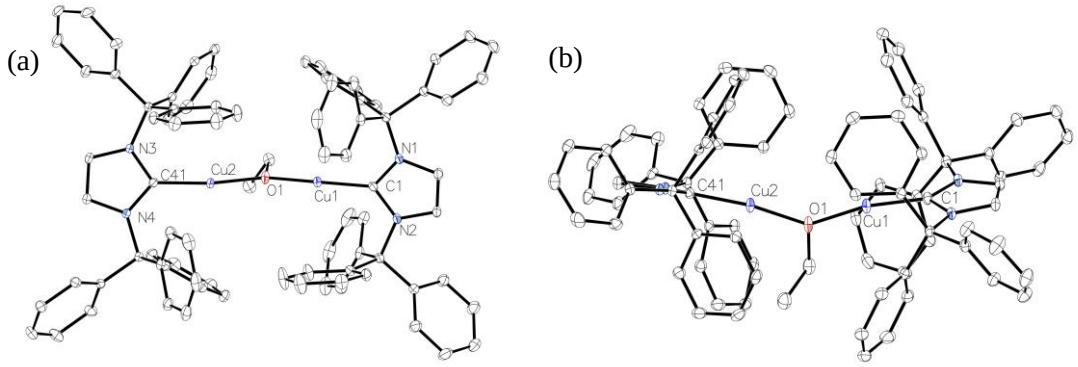


Figure 3.12 – (a) Molecular structure of the cation in $[\{(ITr)Cu\}_2(\mu\text{-}OEt)][SiF_5]$ (**3.9**). Ellipsoids shown at 30% probability. Hydrogen atoms and $[SiF_5]$ anion are removed for clarity. (b) An alternative view for aiding visualisation of the structure.

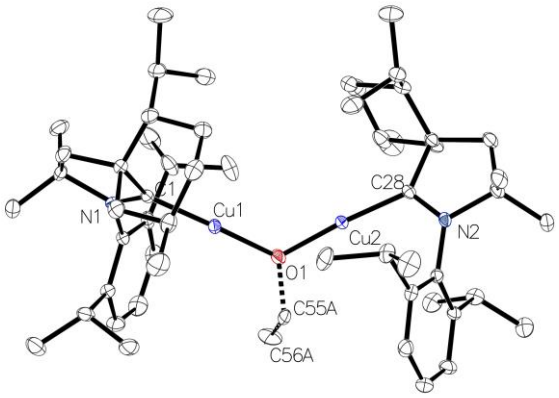


Figure 3.13 – Molecular structure of the cation [{($^{Menthyl}$CAAC)Cu}$_2$(μ-OEt)][$SiF_5$] (**3.10**). Ellipsoids shown at 30% probability. Hydrogen atoms, $CH_2Cl_2$ and [$SiF_5$] anion are removed for clarity. Dashed line indicates disorder of the OEt group.

Table 3.5 – Selected bond lengths (Å) and angles (°) in **3.8** – **3.10**.

| Complex | Cu-O | Cu-$C_{carbene}$ | Cu···Cu | Cu-O-Cu |
|---|---|---|---|---|
| **3.8** | 1.8477(16), 1.8531(16) | 1.88692(4), 1.88641(4) | 3.2563(6) | 123.27(9) |
| **3.9** | 1.873(2), 1.875 (2) | 1.889(3), 1.887(3) | 3.5374(6) | 141.36(24) |
| **3.10** | 1.850(3), 1.836(3) | 1.873(4), 1.877(4) | 3.2761(6), 3.208 | 125.38(19), 121.7(2) |
| [{(IPr)Cu}$_2$(μ-OH)][$BF_4$][36] | 1.8403(11), 1.8411(11) | 1.8713(13), 1.8695(13) | 3.3077(3) | 127.87(8) |
| **2.1** | 1.8016(15) | 1.874(2) | - | - |
| (ITr)CuO$^i$Pr | 1.8080(15) | 1.8747(18) | - | - |
| [(6-Mes)$_2$Cu][$CuCl_2$] | - | 1.910(5) | - | - |
| [(IPr)CuP$^t$Bu][$BF_4$][38] | - | 1.918(5) | - | - |

Re-dissolution of both crystalline **3.9** and **3.10** suggested the compounds were unstable in solution. In the case of **3.9**, $^{13}$C NMR spectroscopy indicated the presence of three ITr containing species. Two $^{19}$F containing species were apparent in a 1:1 ratio, with signals at -139.7 ppm ($^1J_{F\text{-}Si}$ = 145 Hz) and -156.2 ppm ($^1J_{F\text{-}Si}$ = 182 Hz). These values are very similar to what was observed experimentally by Leyssens (Figure 3.9).[16] Two resonances were also observed in the $^{19}$F spectrum of dissolved **3.10**, at -139.7 ppm ($^1J_{F\text{-}Si}$ = 146 Hz) and 157.04 ($^1J_{F\text{-}Si}$ = 183 Hz)

respectively. As shown in Figure 3.14, a trace (*ca.* 1%) of the species corresponding to the low frequency $^{19}F$ signal was present upon redissolving a crystalline sample of **3.8**.

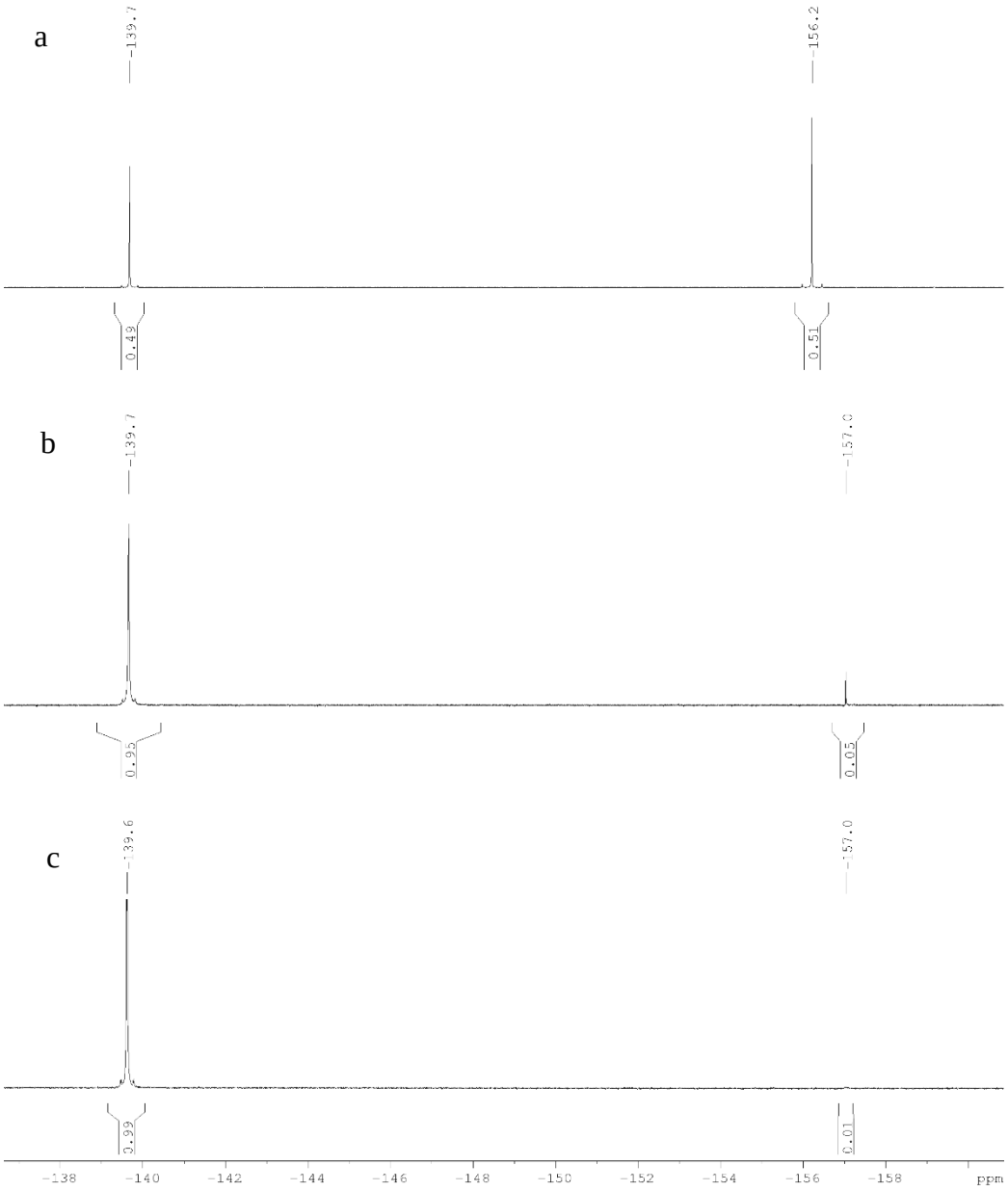


Figure 3.14 – $^{19}F\{^{1}H\}$ NMR spectra (470 MHz) of redissolved crystalline samples of a) **3.9**, b) **3.10**, c) **3.8** in $CD_2Cl_2$.

Although the solution behaviour of **3.9** and **3.10** remains to be elucidated, the presence of three ITr containing species and two fluorine containing species for the former could be explained by an equilibrium of **3.9**, the neutral (ITr)CuOEt and $[SiF_5]^-$ stabilised cation (Scheme 3.17). In support of this, Sadighi has reported that $[\{(NHC)Cu\}_2(\mu\text{-}F)][BF_4]$ (NHC = IPr, SIPr) dissociate in solution to (NHC)CuF and solvent stabilised $[(NHC)Cu]^+$.[12] Furthermore, it is known that ITr is bulky enough to stabilize the mononuclear Ag cation, $[(ITr)Ag]^+$.[39]

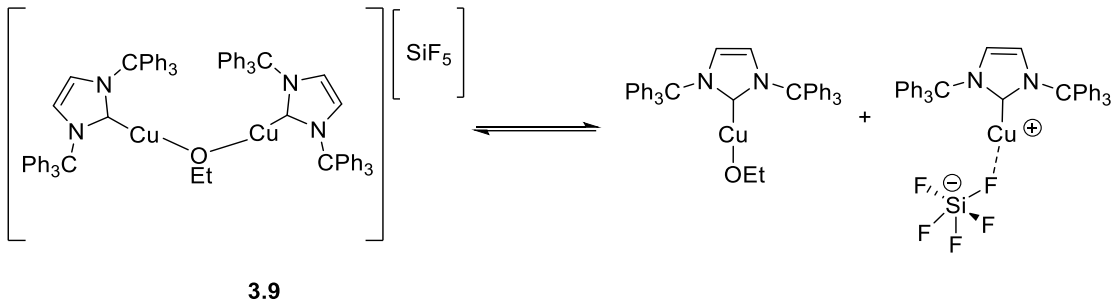

**3.9**

Scheme 3.17 – Proposed solution equilibrium behaviour of **3.9**.

## 3.10 – Potential for Catalysis with [{(carbene)Cu}$_2$(μ-OEt)][SiF$_5$]

Mixed valence (carbene)Cu bridging dimers have been identified recently as active intermediates in copper catalysed reactions (Scheme 3.18).[40-42] Lalic uncovered such Cu species in a mechanistic study of alkyne hydroalkylation.[42] The formation of [{(IPr)Cu}$_2$(μ-H)][OTf] (**3.vii**) was observed to be faster than the reaction of "(IPr)CuH" species with alkyltriflates (Scheme 3.18). **3.vii** was found not to react with alkyltriflate suggesting there is no dissociation into more reactive monomeric units such as (IPr)CuH.

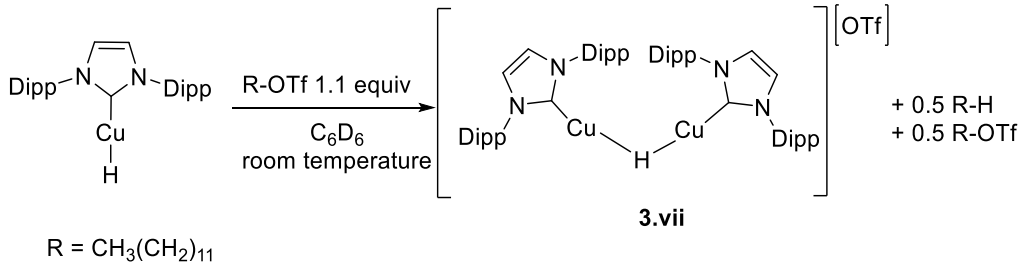

**3.vii**

R = $CH_3(CH_2)_{11}$

Scheme 3.18 – Formation of **3.vii** observed by Lalic.[42]

When **3.8** was tested in the allylation of octanal, mixed and irreproducible results ranging from full conversion to no conversion were observed. Further work and optimisation are required to test these complexes effectively.

## 3.11 – Conclusions

In conclusion, a new approach to synthesise (carbene)CuF complexes was demonstrated through the reaction of (carbene)CuMes and $NEt_3 \cdot 3HF$. Six new (carbene)CuF complexes were synthesised bearing ring-expanded 6- and 7-membered ring carbenes, extremely bulky 5-membered ringed NHCs, diamido carbenes and CAACs. In the allylation of octanal, these were demonstrated to have variable activity, with ITr complex **3.3** being the most reactive. As a result of mechanistic investigations, (ITr)Cu($CH_2CHCH_2$) complex (**3.7**) was isolated and characterised. In the absence of $(EtO)_3SiF$, it displayed poor catalytic activity, but upon the

addition of $(EtO)_3SiF$, the reactivity of **3.7** was comparable to that of **3.3**. One role of $(EtO)_3SiF$ appears to encourage silicate formation. With **2.1** and **3.2**, in the presence of $(EtO)_3SiF$, $[\{(6\text{-Mes})Cu\}_2(\mu\text{-OEt})][SiF_5]$ was isolated, while the analogues, $[\{(ITr)Cu\}_2(\mu\text{-OEt})][SiF_5]$ and $[\{(^{Menthyl}CAAC)Cu\}_2(\mu\text{-OEt})][SiF_5]$ were formed from **3.3** and **3.5** respectively. These rare dimeric cationic species show complex solution behaviour that requires further investigation to establish if they are relevant to catalysis. As a final thought, an updated postulated mechanism to that shown in Scheme 3.13 would not involve the reformation of Cu-F. Instead, it is suggested the role of Cu-F is to help access a cationic Cu pathway alongside providing means to access anionic $[SiF_n]^-$.

## 3.12 –References for Chapter 3


1 J. W. Hall, F. Seeberger, M. F. Mahon and M. K. Whittlesey, *Organometallics*, 2020, **39**, 227–233.

2 M. Trose, F. Nahra and C. S. J. Cazin, *Coord. Chem. Rev.*, 2018, **355**, 380–403.

3 A. A. Danopoulos, T. Simler and P. Braunstein, *Chem. Rev.*, 2019, **119**, 3730–3961.

4 F. Lazreg, F. Nahra and C. S. J. Cazin, *Coord. Chem. Rev.*, 2015, **293**–**294**, 48–79.

5 T. Fujihara, T. Xu, K. Semba, J. Terao and Y. Tsuji, *Angew. Chem. Int. Ed.*, 2011, **50**, 523–527.

6 M. R. Uehling, A. M. Suess and G. Lalic, *J. Am. Chem. Soc.*, 2015, **137**, 1424–1427.

7 R. G. Pearson, *J. Am. Chem. Soc.*, 1963, **85**, 3533–3539.

8 J. R. Herron and Z. T. Ball, *J. Am. Chem. Soc.*, 2008, **130**, 16486–16487.

9 L. S. Sharninghausen, A. F. Brooks, W. P. Winton, K. J. Makaravage, P. J. H. Scott and M. S. Sanford, *J. Am. Chem. Soc.*, 2020, **142**, 7362–7367.

10 H. Dang, M. Mailig and G. Lalic, *Angew. Chem. Int. Ed.*, 2014, **53**, 6473–6476.

11 D. S. Laitar, PhD Thesis, Massachusetts Institue of Technology, 2006.

12 C. M. Wyss, B. K. Tate, J. Bacsa, M. Wieliczko and J. P. Sadighi, *Polyhedron*, 2014, **84**, 87–95.

13 T. Vergote, F. Nahra, A. Welle, M. Luhmer, J. Wouters, N. Mager, O. Riant and T. Leyssens, *Chem. Eur. J.*, 2012, **18**, 793–798.

14 J. Zhai, A. S. Filatov, G. L. Hillhouse and M. D. Hopkins, *Chem. Sci.*, 2016, **7**, 589–595.

15 J. R. Herron, V. Russo, E. J. Valente and Z. T. Ball, *Chem. Eur. J.*, 2009, **15**, 8713–8716.

16 T. Vergote, F. Nahra, D. Peeters, O. Riant and T. Leyssens, *J. Organomet. Chem.*, 2013, **730**, 95–103.

17 D. J. Gulliver, W. Levason and M. Webster, *Inorg. Chim. Acta*, 1981, **52**, 153–159.

18 C. M. Wyss, B. K. Tate, J. Bacsa, T. G. Gray and J. P. Sadighi, *Angew. Chem. Int. Ed.*, 2013, **52**, 12920–12923.

19 A. M. Suess, M. R. Uehling, W. Kaminsky and G. Lalic, *J. Am. Chem. Soc.*, 2015, **137**, 1424-1427.

20 K. Semba, T. Fujihara, J. Terao and Y. Tsuji, *Chem. Eur. J.*, 2012, **18**, 4179–4184.

21 R. Walsh, *Acc. Chem. Res*, 1981, **14**, 246–252.

22 Sahar, A. Bari, M. Irfan, Z. Zara, B. Eliasson, K. Ayub and J. Iqbal, *J. Mol. Struct.*, 2017, **1143**, 8–19.

23 V. Russo, J. R. Herron and Z. T. Ball, *Org. Lett.*, 2010, **12**, 220–223.

24 A. J. Jordan, G. Lalic and J. P. Sadighi, *Chem. Rev.*, 2016, **116**, 8318–8372.

25 T. Vergote, F. Nahra, A. Welle, M. Luhmer, J. Wouters, N. Mager, O. Riant and T. Leyssens, *Chem. Eur. J.*, 2012, **18**, 793–798.

26 M. M. D. Roy, P. A. Lummis, M. J. Ferguson, R. McDonald and E. Rivard, *Chem. Eur. J.*, 2017, **23**, 11249–11252.

27 L. Falivene, Z. Cao, A. Petta, L. Serra, A. Poater, R. Oliva, V. Scarano and L. Cavallo, *Nat. Chem.*, 2019, **11**, 872–879.

28 K. Oisaki, Y. Suto, M. Kanai and M. Shibasaki, *J. Am. Chem. Soc.*, 2003, **125**, 5644–5645.

29 S. Yamasaki, K. Fujii, R. Wada, M. Kanai and M. Shibasaki, *J. Am. Chem. Soc.*, 2002, **124**, 6536–6537.

30 K. Oisaki, D. Zhao, M. Kanai and M. Shibasaki, *J. Am. Chem. Soc.*, 2006, **128**, 7164–7165.

31 Y. Kim, M. Kim and F. P. Gabbai, *Org. Lett.*, 2010, **12**, 600–602.

32 A. C. Cooper, J. C. Bollinger, J. C. Huffman and K. G. Caulton, *New J. Chem.*, 1998, **22**, 473–480.

33 F. Olbrich and R. J. Lagow, *Z. Anorg. Allg. Chem.*, 1995, **621**, 1929–1932.

34 H. Baumgarth, G. Meier, T. Braun and B. Braun-Cula, *Eur. J. Inorg. Chem*, 2016, 4565–4572.

35 B. Alič, M. Tramšek, A. Kokalj and G. Tavčar, *Inorg. Chem.*, 2017, **56**, 10070–10077.

36 H. Ibrahim, R. Guillot, F. Cisnetti and A. Gautier, *Chem. Commun.*, 2014, **50**, 7154–7156.

37 A. Bondi, *J. Phys. Chem.*, 1964, **68**, 441–451.

38 F. Lazreg, A. M. Z. Slawin and C. S. J. Cazin, *Organometallics*, 2012, **31**, 7969–7975.

39 M. M. D. Roy, M. J. Ferguson, R. McDonald and E. Rivard, *Chem. Commun.*, 2018, **54**, 483–486.

40 L. Jin, D. R. Tolentino, M. Melaimi and G. Bertrand, *Sci. Adv.*, 2015, **1**, e1500304.

41 E. A. Romero, R. Jazzar and G. Bertand, *Chem. Sci.*, 2017, **8**, 165-168.

42 A. M. Suess, M. R. Uehling, W. Kaminsky and G. Lalic, *J. Am. Chem. Soc.*, 2015, **137**, 7747-7753.

# Chapter 4

# Chapter 4 – Synthesis of (NHC)CuX (where X= Cl, Br and I)

The purpose of this chapter is to discuss methods used to synthesise (NHC)CuX complexes and demonstrate new methods to produce (RE-NHC)CuX instead of employing the traditional free carbene route. A selection of these complexes would then be subsequently used to investigate catalytic activity in the [3+2] cycloaddition of alkynes and azides as a function of NHC ring size and halide.

## 4.1 – Literature Routes to Synthesise (NHC)CuX

### 4.1.1 – Synthesis of (NHC)CuX by Free Carbene

The use of a free carbene is the most utilised approach to synthesise (NHC)CuX complexes (when X = Cl, Br and I) (Scheme 4.1). This can be easily done using CuCl, CuBr and CuI as these substrates are widely accessible, contrary to CuF.

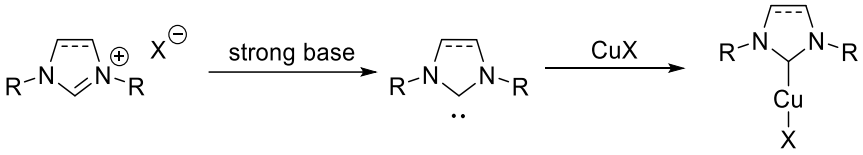


Scheme 4.1 – Synthesis of (NHC)CuX through a free carbene.

The [NHCH]X salts can either be deprotonated *in-situ* or used as an isolated reagent. This method has been used for many different examples, but the drawbacks to this approach are that they require inert conditions and a strong base.[1,2] Nolan et al. reported the synthesis of multiple examples from imidazolium/imidazolinium salts utilising this method.[3] In one example, employing NaO$^t$Bu, CuBr and [IPrH]Cl, high yields of (IPr)CuBr could be achieved (80 %). However, when trying to synthesise (IPr)CuI, even with excess CuI, a significant amount of a $[(IPr)_2Cu]^+$ species was observed. Changes to the base and conditions rectified this and generally this approach worked well for other [NHCH]Cl salts. Despite this, for [IMesH]Cl and [SIMesH]Cl homoleptic complexes were found to be unavoidable when attempting to prepare (NHC)CuI derivatives.

In the case of the RE-NHC 6-Mes, the formation of the homoleptic species $[(6\text{-Mes})_2Cu]^+$ was also observed, but not just for CuI. First reported by Buchmeiser, the *in-situ* formation of 6-Mes from NaO$^t$Bu and [6-MesH]Br in the presence of CuCl, led to the formation of the homoleptic Cu complex $[(6\text{-Mes})_2Cu][CuCl_2]$ (**4.i**) (Scheme 4.2).[4] In the same study it was found [6-$^i$PrH]X under similar conditions could form (6-$^i$Pr)CuX (X = Cl and Br). The reasons for this difference

was unknown as the authors initially thought the 6-Mes carbene would be able to form the heteroleptic complex due to 6-Mes being a bulkier ligand compared to 6-$^{i}$Pr.

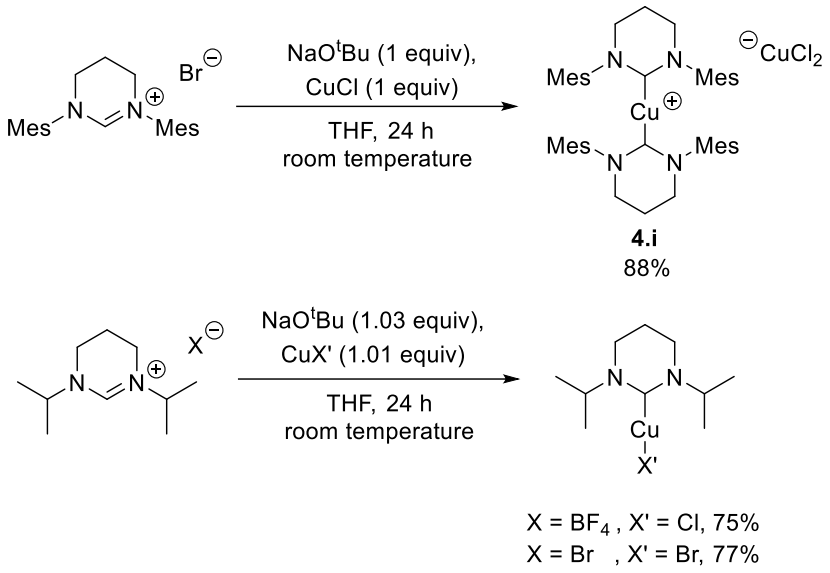


Scheme 4.2 – Unexpected synthesis of **4.i** and synthesis of (6-$^{i}$Pr)CuX (X = Cl, Br) reported by Buchmeiser.[4]

The unwanted formation of the homoleptic species [(6-Mes)$_2$Cu][CuX$_2$] was not just limited to the synthesis of (6-Mes)CuCl (**4.1**), but also to (6-Mes)CuBr (**4.2**) and (6-Mes)CuI (**4.3**). Díez-González reported a similar homoleptic by-product can form during their attempt to synthesise **4.2** (Scheme 4.3).[5] Complex **4.ii** was observed in a 1:4 ratio with **4.2**. Interestingly, there was no indication of such a product during their synthesis of **4.3**. With bulkier NHCs (7-Mes and 6-Dipp), no homoleptic by-products were observed upon forming the corresponding (NHC)CuI complexes.

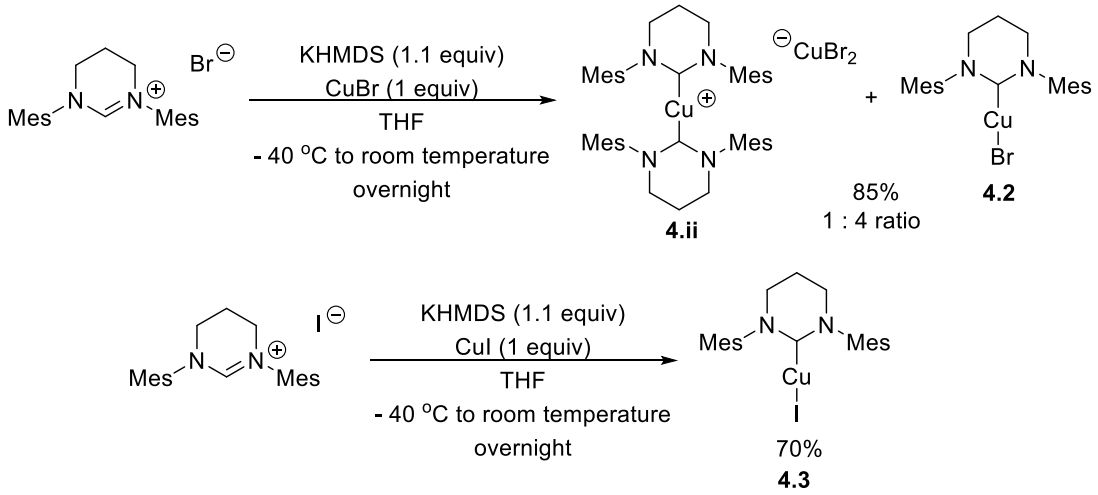


Scheme 4.3 – Hetero- and homoleptic complex formation observed by Díez-González.[5]

Contrary to this, Collins reported the formation of minor amounts of **4.iii** during preliminary work to cross couple (6-Mes)$CuC_6F_5$ with 3,5-bis(trifluoromethyl)iodobenzene (Scheme 4.4).[6] Upon separate synthesis of **4.3** *via* the free carbene, it was observed that addition of equimolar 6-Mes to CuI at room temperature led to the formation of **4.iii** with no indication of **4.3** (Scheme 4.5). It was postulated that after the initial formation of **4.3**, partial rearrangement of this complex gives **4.iii**. In the case of Scheme 4.4 vs Scheme 4.5, it would be expected the elevated temperature would promote this process. However, the opposite seems to be true, leading to the theory that use of a free carbene or CuI in this synthesis seems to promote this rearrangement. What is also interesting is the difference in reactivity seen by Díez-González (Scheme 4.3) vs Collins (Scheme 4.5). The former employs the use of an *in-situ* method to generate the carbene while the latter employs isolated carbene in the synthesis. It is hard to explain this difference, although the 6-Mes:CuI ratio might be a factor. The low temperature used by Díez-González to deprotonate [6-MesH]Br could result in a lower concentration of free carbene in solution compared to the 1:1 mixture used by Collins.

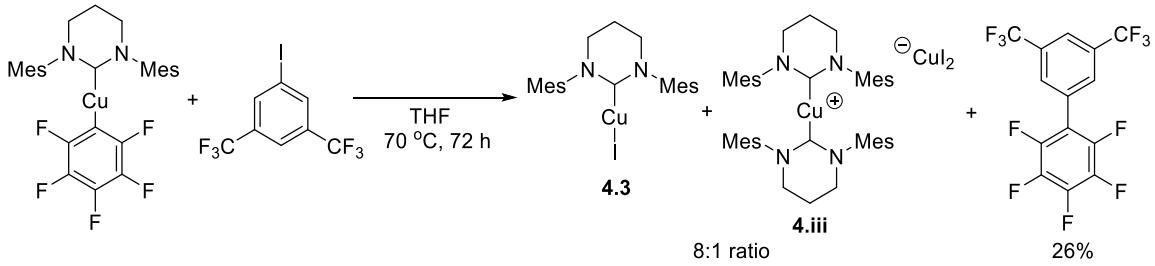


Scheme 4.4 – Preliminary cross-coupling study by Collins.[6]

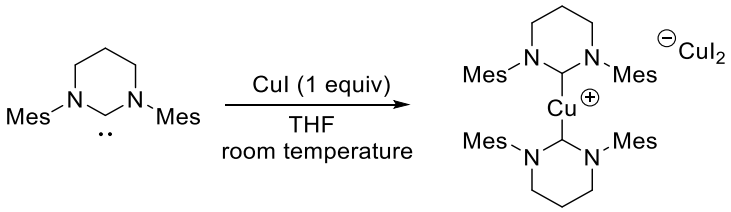


Scheme 4.5 – Reaction of 6-Mes with CuI demonstrated by Collins.[6]

## 4.1.2 – Synthesis of (NHC)Cu-X by Transmetallation Method

As previously mentioned, (NHC)CuX complexes have recently been used as transmetallating agents. Indeed, some (NHC)CuX complexes require the use of this method for their synthesis, notably for more sensitive NHC ligands such as those containing ester groups[7] and those that are difficult to access via deprotonation.[8] In the case of RE-NHC examples, Nechaev first demonstrated it was possible to transmetallate a (RE-NHC)AgX complex with CuBr. Starting

from [6-DippH]Br in the presence of $Ag_2O$, the salt was deprotonated at room temperature and complexed to silver to yield **4.iv** in reasonable yields (Scheme 4.6). The silver complex was then exposed to CuBr in the dark to give (6-Dipp)CuBr (**4.4**). During transmetallation there were no unwanted side products aside from the formation of AgBr. This method is useful, however, the loss of AgBr is not atom economic.

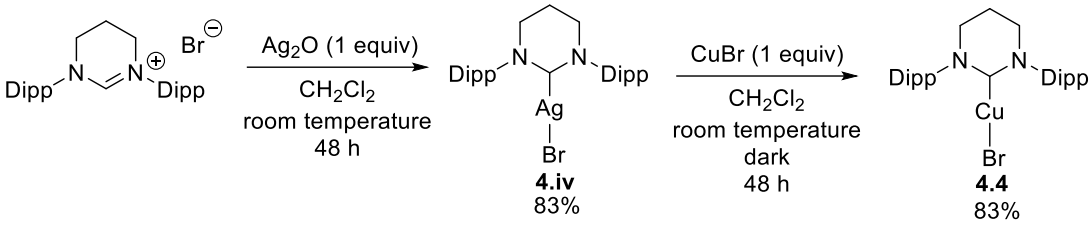


Scheme 4.6 – Nechaev's synthesis of (6-Dipp)CuBr.[9]

## 4.1.3 – Synthesis of (NHC)CuX with $Cu_2O$

The first isolated (NHC)CuX complex was synthesised using $Cu_2O$ and a carbene salt by Danopoulos and co-workers (Scheme 4.7).[10] The reaction provided clean formation of **4.v** with elimination of $H_2O$. Later Douthwaite also reported synthesis of their mixed valent Cu systems using $Cu_2O$, although it was found that the choice of solvent was paramount to the successful synthesis.[11]

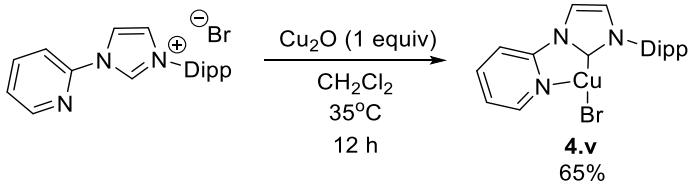


Scheme 4.7 – Earliest example of (NHC)CuX preparation via $Cu_2O$.[10]

The importance of solvent choice was further exemplified by Cazin.[12] Using six similar 5-membered NHCs, Cazin demonstrated there was disparity of reactivity in $CH_2Cl_2$ which could not be rationalised on the basis of steric or electronic effects (Table 4.1). Changing to toluene allowed for the use of elevated temperature and gave more uniform and higher conversions and yields across the board. Remarkably, it was also demonstrated this reaction could proceed in $H_2O$. However, water is not inert in all cases and results in urea formation in the case of the cyclohexyl substituted imidazolinium precursor.

Table 4.1– Results shown by Cazin during their study.

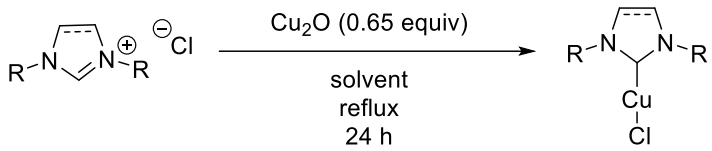


| Solvent | [NHCH]Cl, conversion (yield) | | | | | |
|---|---|---|---|---|---|---|
| | [IMesH]Cl | [SIMesH]Cl | [IPrH]Cl | [SIPrH]Cl | [ICyH]Cl | [SICyH]Cl |
| $CH_2Cl_2$ | 100 [a] | 14 [b] | < 5 [b] | 93 [a] | 47 [b] | - [b] |
| Toluene | 100(86) | 100(71) | 88(78) | 99(86) | 88(70) | 55(-) |
| $H_2O$ | 100(96) | 100(99) | 96(94) | 78(72) | 0(0) | 7(-) |

[a] Room temperature. [b]40 °C.

Navarro and Landers demonstrated that microwave heating could cut reaction times down to minutes without compromising yields (Table 4.2),[13] by taking advantage of the higher possible temperatures due to this method. This approach has also been applied to CAACs, abnormal carbenes and BACs.[14]

Table 4.2 – Microwave conditions for (NHC)CuCl synthesis.[13]

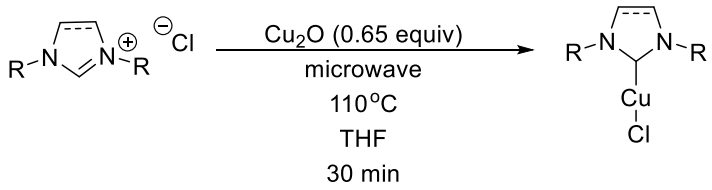


| Entry | [NHCH]Cl | Yield |
|---|---|---|
| 1 | IMes | 84 |
| 2 | SIMes | 73 |
| 3 | IPr | 98 |
| 4 | SIPr | 95 |

## 4.1.4 – Synthesis of (NHC)CuX with $K_2CO_3$ – Cuprate Method

Another versatile method to synthesise (NHC)CuX involves the use of a copper source that allows carbene formation from [NHCH]Cl with much weaker bases than NaO$^t$Bu and KHMDS (Scheme 4.2 and Scheme 4.3). First reported by Jiang in 2012,[15] it was shown in the presence of either CuCl or CuCl·2$H_2O$ that $K_2CO_3$ could activate [IPrH]Cl to give (IPr)CuCl (**4.v**) (Scheme 4.8).

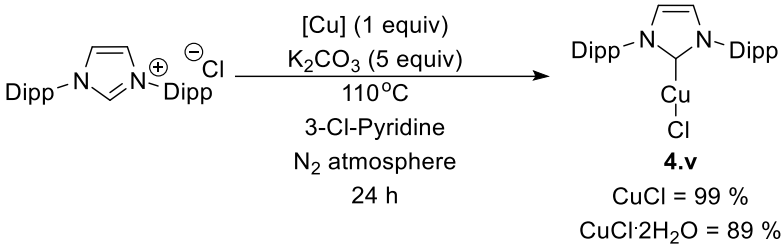


Scheme 4.8 – Synthesis of **4.v** using CuCl and $K_2CO_3$ reported by Jiang.[15]

Following from this and from an improved preparation of (NHC)AuX,[16,17] Cazin demonstrated that more facile conditions (milder temperature, lower $K_2CO_3$ loading and temperature), than previously seen in Scheme 4.8, could be employed upon the use of reagent grade acetone instead of 3-Cl-pyridine as the solvent (Scheme 4.9).[18] A wide array of imidazolium/imidazolinium salts were readily converted using these conditions including those with alkyl N-substituents, such as [I$^t$BuH]Cl. Mechanistic investigations by Cazin confirmed the presence of a cuprate species as an intermediate in their synthesis (Scheme 4.10), similar to what was observed for Au.[16] Subsequent addition of base to [IPrH][$CuCl_2$] (**4.vi**) yielded the desired complex **4.v** at elevated temperature (60 °C). In all cases, there was no observation of homoleptic complexes.

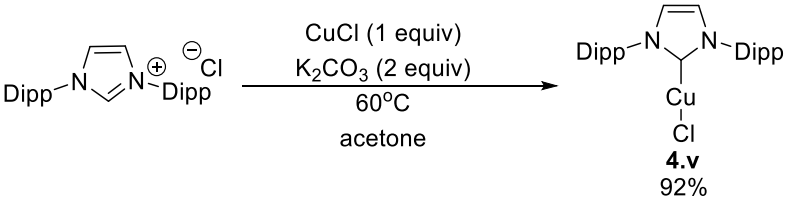


Scheme 4.9 – Conditions used by Cazin to synthesise complex **4.v**.

It was also demonstrated that changing CuCl to CuBr or CuI allowed the synthesis of (IPr)CuBr and (IPr)CuI, without any trace of **4.v**. Gram scale synthesis was possible for **4.v** and for the corresponding Br and I analogues in <15 h with 3 equivalents of base.

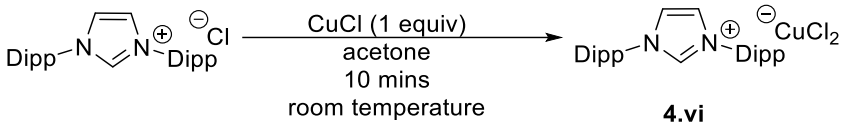


**4.vi**

Scheme 4.10 – Synthesis of [IPrH][$CuCl_2$](**4.vi**)

It is also important to mention the effect of mixed cuprate halide species (analogues of **4.vi**) which were also observed during this study. In a similar manner to Scheme 4.10, [IPrH][CuBrI] was made through the corresponding [IPrH]Br and CuI reagents. Upon the addition of base, only (IPr)CuI was observed. This was postulated to be linked to (i) the trans effect (I > Br > Cl) where the iodide exerts a greater trans labilisation of the bromide in the cuprate to yield the iodide complex and (ii) salt formation, which would be favoured in the order KCl > KBr > KI based upon lattice enthalpies. The exact role of the base and metal in the mechanism have yet to be determined as the base alone is not strong enough to deprotonate the C2 proton. It has been speculated that the role of the metal is to generate the "-ate" complex which enables the proton to be removed by a weak base. However, experimental pKa determinations by Nolan suggest the [NHCH]X and corresponding "ate" complex have the same pKa (in $CH_3CN$/water) ruling out a deprotonation.[19] The authors suggest the mechanism might involve a concerted metalation deprotonation (CMD) pathway.[19]

## 4.2 – Results and Discussion – Synthesis of (RE-NHC)CuX (X= Cl, Br and I)

From the synthetic procedures previously described, the only methods used to synthesise RE-(NHC)CuX complexes are through the free carbene route or by transmetallation.[4–6,20,21] The two less common methods, $Cu_2O$ and cuprate methods, have yet to be tested on RE-NHCs to determine efficiency and selectivity. This chapter will predominantly focus on the cuprate method, with some discussion on using $Cu_2O$.

### 4.2.1 – Resin Exchange [NHCH]$BF_4$ to [NHCH]Cl

To replicate conditions used by Cazin and Navarro (Table 4.2 and Scheme 4.9) formation of [RE-NHCH]Cl salts were required.[13,18] While the Br and I salts would be easier to start from as these are initially synthesised prior to anion exchange (Scheme 4.11), this would limit us to only (RE-NHC)CuBr and -I complexes.

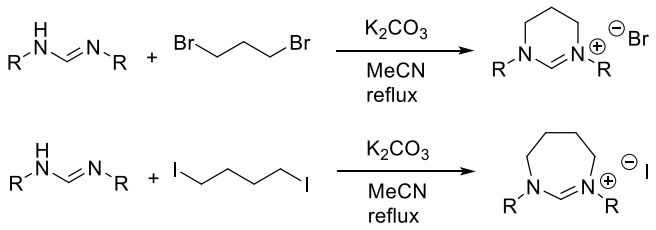


Scheme 4.11 – Generic scheme for the ring closing step of [RE-NHCH]X synthesis.

[NHCH]$BF_4$ was chosen as the starting salt, as exchange could be successfully monitored through the disappearance of the $BF_4$ signal by $^{19}F$ NMR spectroscopy. A variety of 6 and 7-membered [RE-NHCH]$BF_4$ salts (along with [8-MesH]$BF_4$) were subjected to anion exchange (Scheme 4.12). In all cases, aside from [6-DippH]Cl and [7-DippH]Cl, the chloride salts were extremely hygroscopic, which necessitated the pre-drying of the resin prior to use to ensure isolation of the [NHCH]Cl salts in good yield (78-99%).

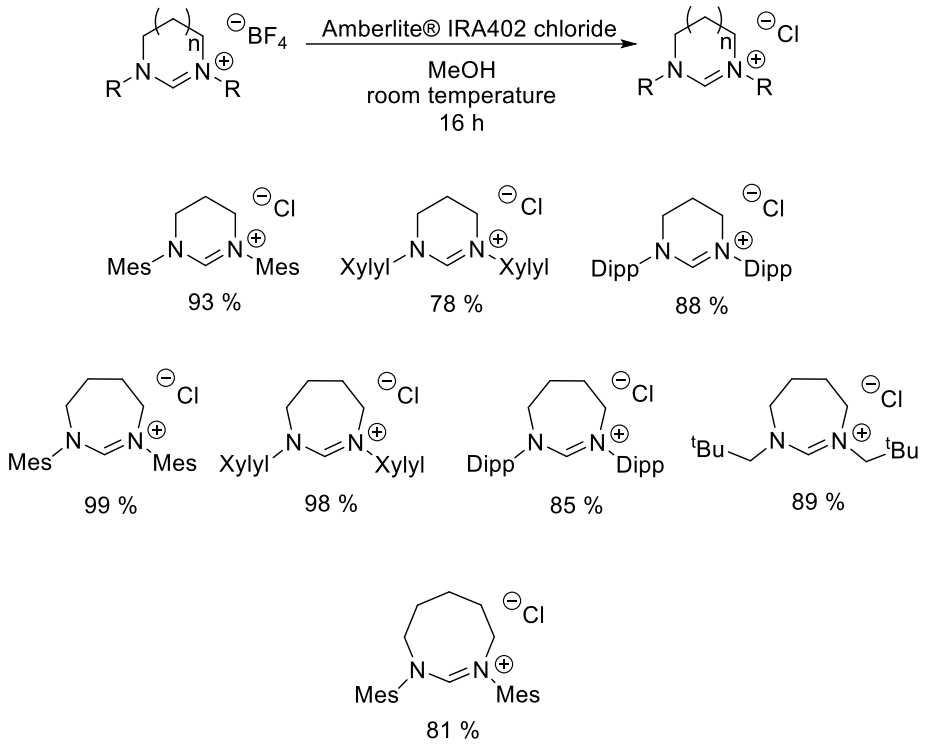


Scheme 4.12 – Anion exchange of [RE-NHCH]$BF_4$ to afford [RE-NHCH]Cl.

## 4.2.2 – $Cu_2O$ Method

First examining the Navarro method, [6-MesH]Cl was chosen for our model salt.[13] Two solvent systems were employed in which to test this method, as summarised in Scheme 4.13. Although water is produced in this reaction, inert conditions were used due to the hygroscopic nature of the [RE-NHCH]Cl salts.

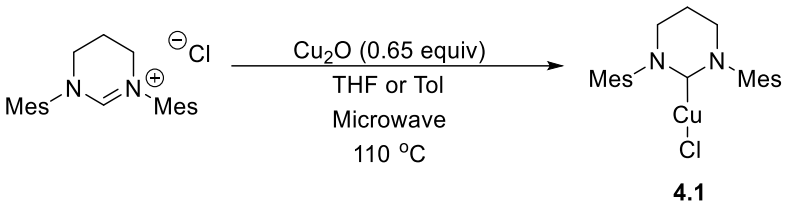


**4.1**

Scheme 4.13 – Conditions used to test $Cu_2O$ method.

Heating [6-MesH]Cl in THF at 110 °C for 0.5 h led to only a 20 % conversion of starting material into **4.1** by $^1$H NMR spectroscopy. Very little conversion was seen after a longer period of time (1 h). Interestingly, in toluene the conversion was higher (52%), but the yield of **4.1** was lowered (38%) by the presence of additional products. $^1$H NMR spectroscopy revealed 10 % of [6-$Mes_2Cu]^+$ salt was present along with another unidentified species (≈ 4%) (Figure 4.1).

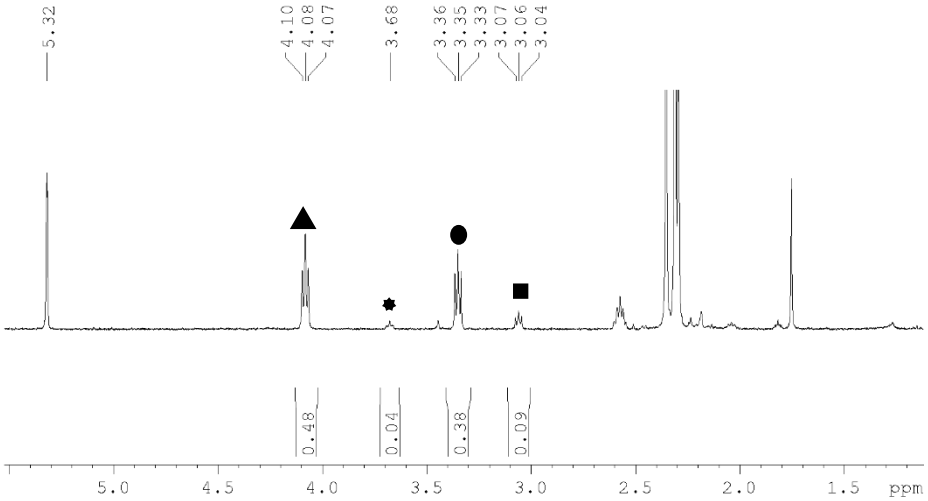


Figure 4.1 – $^1$H NMR spectrum (400 MHz, 298 K, $CD_2Cl_2$) of the reaction shown in Scheme 4.13 with toluene as the solvent after 0.5 h. The highlighted peaks represent different carbene environments. ▲ = [6-MesH]Cl, * = unknown species, ● = **4.1** and ■ = $[(6\text{-Mes})_2Cu]^+$ salt.

Other RE-NHC salts also gave low yields of Cu products with this method. [6-DippH]Br, [7-DippH]Cl and [7-DippH]I were screened at 110 °C and also 140 °C for 0.5 h to examine if elevated temperature can push the reaction further. In the case of [6-DippH]Br, no reactivity was seen at 110 °C (Table 4.3, entry 1) and only a minor amount of conversion was seen at 140 °C (Table 4.3, entry 2). [7-DippH]Cl also showed insignificant conversion at 110 °C (Table 4.3, entry

3), however elevating the temperature to 140 °C revealed nearly complete conversion after 0.5 h (Table 4.3, entry 4). Despite this only 45 % of the desired (7-Dipp)CuCl (**4.8**) was formed; the remainder was an unidentified product which could not be isolated. [7-DippH]I showed no conversion at 110 °C and 140 °C after 0.5 h (Table 4.3, entries 5 and 6). For the purpose of this study, although the chloride salts showed good conversions, this route was not pursued because of the formation of **4.i** seen in the case of [6-MesH]Cl, an additional unidentified product in the case of [7-DippH]Cl and the lack of reactivity when using the heavier halide salts.

Table 4.3 – Results using Navarro method.

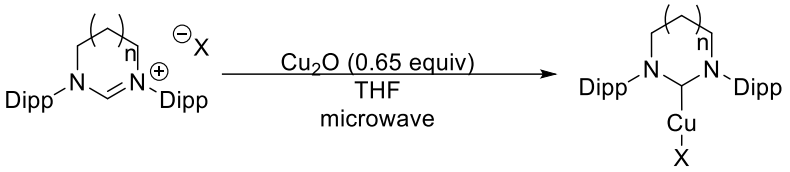


| Entry | [RE-NHCH]X | Temperature (°C) | Isolated Yield (%)[b] |
|---|---|---|---|
| 1 | [6-DippH]Br | 110 | - |
| 2 | | 140 | 5 |
| 3 | [7-DippH]Cl | 110 | 3 |
| 4 | | 140 | 45 |
| 5 | [7-DippH]I | 110 | -[a] |
| 6 | | 140 | -[a] |

[a]Another unknown product was also observed.

## 4.2.3 – Cuprate Method

Having found that the $Cu_2O$ method still produces a $[(6\text{-Mes})_2Cu]^+$ salt in the case of [6-MesH]Cl, our approach changed to the cuprate method. Again, inert conditions were used initially due to the hygroscopic nature of the [RE-NHCH]Cl salts. Mixing both [6-MesH]Cl and CuCl in dried acetone at room temperature led to the formation of [6-MesH][$CuCl_2$] (**4.4**) which could be isolated cleanly as a white powder. [6-XylylH][$CuCl_2$] (**4.5**), [7-MesH][$CuCl_2$] (**4.6**), [7-XylylH][$CuCl_2$] (**4.7**) and [7-neoPentH][$CuCl_2$] (**4.8**) (Scheme 4.14) were formed in the same manner. Yields were generally high, aside from **4.5** and **4.7**, which both contain the Xylyl N-substituent. The poorer yields of **4.5** and **4.7** were attributed to the partial solubility of the [RE-NHCH]Cl salts in acetone. Crystalline **4.5** could not be obtained, but all other complexes were isolated upon slow diffusion of pentane into concentrated $CH_2Cl_2$ solutions of the Cu complexes.

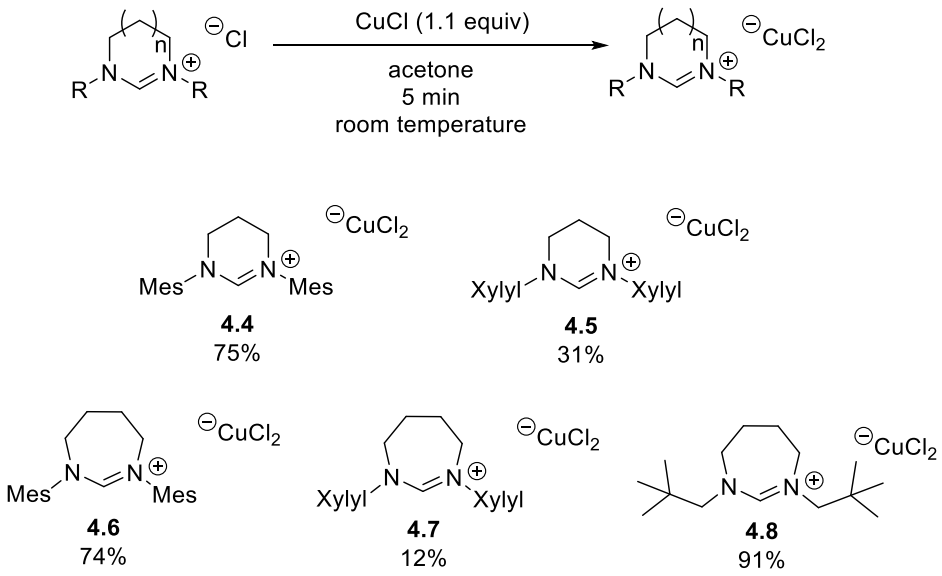


Scheme 4.14 – Synthesis of RE-NHC cuprate complexes.

By $^{1}$H NMR spectroscopy the most noticeable change was the downfield shift in the C2 proton upon changing the counter anion from $BF_4^-$ to $Br^-$ to $Cl^-$ to $[CuCl_2]^-$ (Figure 4.2). Anion effects are rarely investigated, however in a recent study, Huynh demonstrated this effect is important on NHC salts and are more predominant in organic solvents.[22] This can determine the acidity of the C2 proton which can be used for *in-situ* methods of catalyst formation. Huynh demonstrated the shift of the C2 proton relates to the electronegativity and hydrogen bonding ability of the anion. The more downfield the shift, the more electronegative and the greater the hydrogen bonding ability of the anion. This is reflected in our C2 proton signals by $^{1}$H NMR spectroscopy (Figure 4.2), suggesting the $[CuCl_2]$ anion is more hydrogen bond accepting compared to the monoatomic halides. This could then make the C2 proton more acidic and more easily activated by the weaker base. While critical assessment in this study of RE-NHCs cannot be done due to differing concentrations in the NMR solutions (partly because of the presence of water resulting from the hygroscopic nature of the salts), the general trend observed by Huynh is also seen in our case.

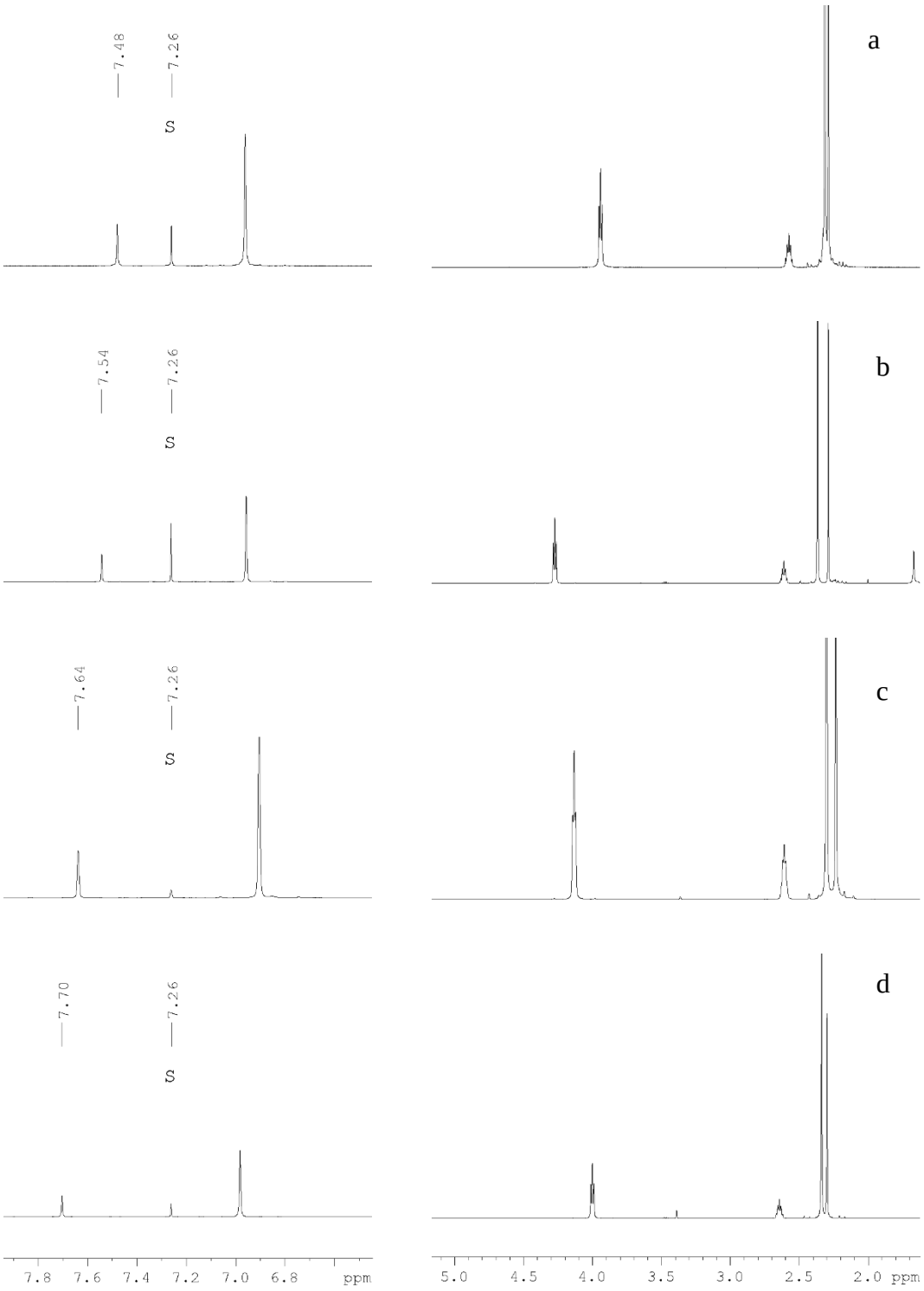


Figure 4.2 – $^{1}$H NMR spectra (500 MHz, 298K, $CDCl_3$) of a) [6-MesH]$BF_4$, b) [6-MesH]Br, c) [6-MesH]Cl, d) [6-MesH][$CuCl_2$]. S denotes the signal for $CHCl_3$.

Table 4.4 summarises the $^{1}$H NMR shifts of the C2 proton for complexes **4.4** – **4.8** in $CDCl_3$ compared to their chloride salts. In all cases apart from **4.8**, a downfield shift is observed. The RE-NHCs show a smaller shift in comparison to the literature examples [ICyH]Cl and [IPrH]Cl (entries 6 and 7). Interestingly the final shifts for the C2 proton in [RE-NHCH][$CuCl_2$] complexes

were around 7.38 – 7.85 ppm where the imidazolium analogues were found to be between 10.00 – 10.29 ppm. In addition, examples of the mixed cuprates [IPrH][CuBrI] and [IPrH][CuBrI] are shown (entries 8 and 9) and demonstrate increased upfield shifts in ppm as the halides get heavier. $^{13}$C NMR spectroscopy reveals minor downfield shifts for **4.4 – 4.7** (*ca.* 0.7 ppm), although again an upfield shift (2.1 ppm) was observed for **4.8**.

Table 4.4 – Shifts of [NHCH]X vs [NHCH][$CuX_2$] in $CDCl_3$.

| Entry | [NHCH]X | [NHCH][$CuCl_2$] | [NHCH]X C2 shift (ppm) | | [NHCH][$CuX_2$] C2 shift (ppm) | |
|---|---|---|---|---|---|---|
| | | | $^1$H | $^{13}$C | $^1$H | $^{13}$C |
| 1 | [6-MesH]Cl | **4.4** | 7.64 | 153.8 | 7.70 | 154.4 |
| 2 | [6-XylylH]Cl | **4.5** | 7.65 | 153.5 | 7.80 | 154.2 |
| 3 | [7-MesH]Cl | **4.6** | 7.22 | 158.0 | 7.38 | 158.7 |
| 4 | [7-XylylH]Cl | **4.7** | 7.27 | 157.8 | 7.43 | 158.5 |
| 5 | [7-neoPentH]Cl | **4.8** | 9.37 | 162.7 | 7.85 | 160.6 |
| 6 | [ICyH]Cl | [ICyH][$CuCl_2$] | 8.96[23] | 132.8 | 10.29 [18] | - |
| 7 | [IPrH]Cl | [IPrH][$CuCl_2$] (**4.vi**) | 11.25 ($CD_2Cl_2$)[24] | 145.5 | 10.00 ($CD_2Cl_2$)[18] | 145.3 |
| 8 | [IPrH]I | [IPrH][CuClI] | 11.25 ($CD_2Cl_2$)[24] | 145.5 | 9.10 ($CD_2Cl_2$)[18] | 145.3 |
| 9 | [IPrH]Br | [IPrH][CuBrI] | 11.2 ($CD_2Cl_2$)[25] | 145.5 | 8.87 ($CD_2Cl_2$)[18] | 145.3 |

The X-ray crystal structures of complexes **4.4**, **4.6**, **4.7** and **4.8** are shown in Figure 4.3. Table 4.5 summarises the bond distances of the hydrogen bonded C1 proton to a single Cl moiety of $CuCl_2$. Each displays a distance around 2.5 Å showing similar distances to that of the literature examples.[18] Complex **4.8** displays a larger distance of 2.7 Å. Complex **4.8** exhibits additional hydrogen bonding interactions with Cl1 to the proton of C6 with a distance of 2.85 Å. In all cases hydrogen bonding was also seen to the backbone protons of the ring from the Cl2 moiety of $CuCl_2$. The C1-H1···Cl1 angles were found to be between 150.6 – 177.7°. Those with NHCs with no para substitution on the aryl group, **4.7** and [IPrH][$CuCl_2$], displayed an angle closer to 180°. **4.8** showed an angle of 157.3° which is most likely due to the additional hydrogen bonds.

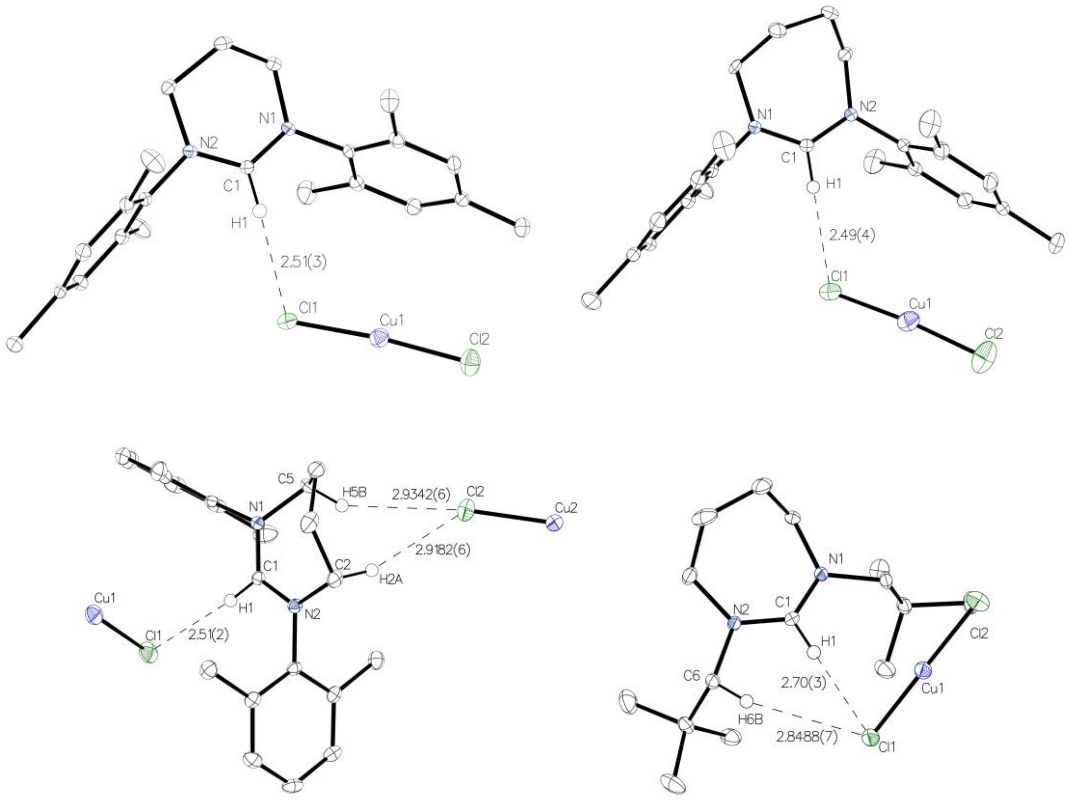


Figure 4.3 – From top left to bottom right: **4.4**, **4.6**, **4.7** and **4.8.** In all cases, aside from **4.7**, Cl hydrogen bonding to the backbone of the ring was observed but omitted for clarity. Hydrogens except those involved in hydrogen bonding were also omitted for clarity. Lengths are summarised in Table 4.5.

Table 4.5 – Comparison of H1 to Cl distances of complexes **4.4**, **4.6**, **4.7** and **4.8**. Literature examples are also included as a comparison. [a][ICyH][$CuCl_2$] showed no interaction of this type.

| Complex | Hydrogen bond length (H1···Cl1) (Å) | Angle C1-H1···Cl1 (°) |
|---|---|---|
| **4.4** | 2.51(3) | 163(2) |
| **4.6** | 2.49(4) | 167(3) |
| **4.7** | 2.51(2) | 172.6(16) |
| **4.8** | 2.70(3) | 158(2) |
| **[IPrH][$CuCl_2$]**[18] | 2.49 | 178 |
| **[SIMesH][$CuCl_2$]**[18] | 2.63 | 157 |
| **[IMesH][$CuCl_2$]**[18] | 2.45 | 151 |
| **[ICyH][$CuCl_2$]**[18] | -[a] | - |

With the identification of the [RE-NHCH][$CuCl_2$] species, conditions were investigated to synthesise (RE-NHC)CuX (Table 4.6). Mixing [6-MesH]Cl with CuCl and 2 equivalents of $K_2CO_3$ for 24 h at room temperature only yielded **4.4** by $^1$H NMR spectroscopy, suggesting more forcing conditions are needed (entry 1). Upon increasing the temperature to 60 °C a new species was present by $^1$H NMR spectroscopy after 5 h (entry 2). Isolation of this new species identified it as complex **4.1**. As the yield was poor, the number of equivalents of $K_2CO_3$ was increased to three, resulting now in a modest yield (entry 3). Increasing the reaction time to 20 h improved the yield further to 61% (entry 4). Promisingly **4.1** could be isolated cleanly following slight modification to the generic work up from Cazin, which involves the filtration of the reaction mixture through a slurry of silica (dried from $H_2O$ under vacuum) in $CH_2Cl_2$. Isolation using this method removes both residual starting material and any residual cuprate intermediate leaving only the desired copper complex. It is also worth mentioning here there was no indication of complex **4.i** being formed at the elevated temperature or elongated times.

Table 4.6 – Initial screening conditions using conventional heating.

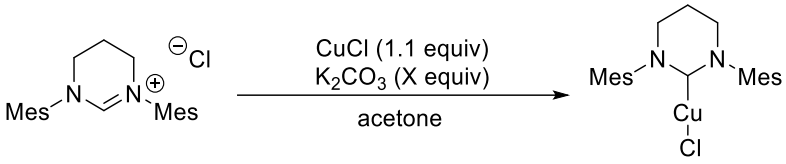


**4.1**

| Entry | Temperature (°C) | $K_2CO_3$ equivalents | Time (h) | Isolated Yield (%)[a] |
|---|---|---|---|---|
| 1 | 25 | 2 | 24 | - |
| 2 | 60 | 2 | 5 | 24 |
| 3 | 60 | 3 | 5 | 47 |
| 4 | 60 | 3 | 20 | 61 |

## 4.2.4 – Cuprate Method with Microwave Heating

An alternative method to reduce reaction times at elevated temperatures was demonstrated by Narvarro through the use of microwave heating.[13] The incorporation of this into the cuprate method could help increase yield by providing more efficient heating and higher obtainable temperatures. Initially, changing to microwave heating at 60 °C allowed for a shorter reaction time (2 h) to achieve a similar yield to that of the conventional method after 5 h (entry 1, Table 4.7 vs entry 3, Table 4.6). At 70 °C, a yield of 40% was achieved, which was attainable in half of the time at 80 °C (entry 2 vs entry 3, Table 4.7). Further increasing the temperature to 120 °C introduced new carbene environments into the $^1$H NMR spectra. No product was now seen, suggesting decomposition of **4.1**. Entry 3 provided the best results with balance of time and so this temperature was taken forwards for further optimisation.

Table 4.7 – Conditions investigated with microwave heating. [a]

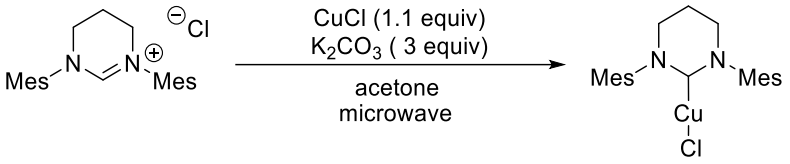


**4.1**

| Entry | Temperature (°C) | Time (h) | Isolated Yield (%) |
|---|---|---|---|
| 1 | 60 | 2 | 52 |
| 2 | 70 | 1 | 40 |
| 3 | 80 | 0.5 | 47 |
| 4 | 120 | 0.5 | - |

By increasing the number of equivalents of CuCl (1.1 to 1.2 equivalents) and reaction time (0.5 h to 1.5 h) the yield of **4.1** was significantly improved to > 90% based on $^1$H NMR measurements (entry 1, Table 4.8). *In-situ* $^1$H NMR spectroscopy revealed the presence of only **4.4** and **4.1** with no trace of **4.i**. These conditions were then employed with other [RE-NHCH]Cl salts and $^1$H NMR monitoring used to optimise reaction times. Overall, it was found that increasing the ring size (entries 1,4 and 7) led to longer reaction times for >90% NMR yields. The reaction times were generally acceptable for the different NHC salts, however [7-DippH]Cl proved to be low yielding even after 2.5 h (entry 6). Entries 1–3 compare the conversion of 6-membered salts. Increasing the bulk of the N-substituents decreased yield (after 1.5 h) in the order Xylyl > Mes > Dipp. Less of a pattern was found for the 7-membered ring systems (entries 4–6). The yield of (7-Xylyl)CuCl (**4.12**) was low as once it precipitated from solution, it was only partially soluble upon redissolving in $CH_2Cl_2$ and acetone making it difficult to work with, with high loss of yield upon workup with silica. Entry 7 showed a significantly lower isolated yield of (8-Mes)CuCl (**4.14**) compared to the NMR yield as a result of loss during silica filtration. The 7-membered alkyl complex (7-neoPent)CuCl (**4.15**) proved difficult to synthesise through this method. After 0.5 h at 70 or 80 °C, the cuprate **4.8** was identified by $^1$H NMR spectroscopy as the major product rather than the desired **4.15**. By changing the solvent from acetone to $CH_2Cl_2$, **4.15** could be formed in low yield (19 %), but no increase was seen under extended times.

Table 4.8 – Microwave route to (RE-NHC)CuCl complexes.

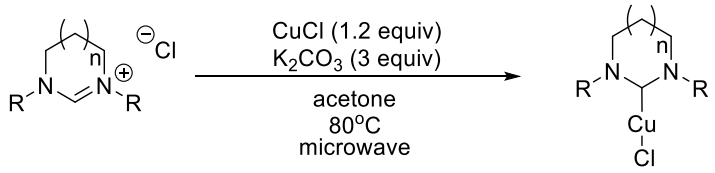


| Entry | [RE-NHCH]X | Time (h) | Product | Yield (%)[a] |
|---|---|---|---|---|
| 1 | [6-MesH]Cl | 1.5 | (6-Mes)CuCl (**4.1**) | 94 (82) |
| 2 | [6-XylylH]Cl | 1.5 | (6-Xylyl)CuCl (**4.9**) | 99 (98) |
| 3 | [6-DippH]Cl | 1.5 | (6-Dipp)CuCl (**4.10**) | 88 (73) |
| 4 | [7-MesH]Cl | 2.5 | (7-Mes)CuCl (**4.11**) | 94 (77) |
| 5 | [7-XylylH]Cl | 2.5 | (7-Xylyl)CuCl (**4.12**) | 95 (58) |
| 6 | [7-DippH]Cl | 2.5 | (7-Dipp)CuCl (**4.13**) | 54 (50) |
| 7 | [8-MesH]Cl | 6 | (8-Mes)CuCl (**4.14**) | 95 (36) |
| 8 | [7-neoPentH]Cl | 2.5 | (7-neoPent)CuCl (**4.15**) | 19 (19) |

[a] $^1$H NMR yield, isolated yield in parenthesis.

## 4.2.5 – Synthesis of (RE-NHC)CuX (X = Br, I)

It was also important to trial the other [RE-NHCH]X salts (X = Br or I) under these conditions as this would most likely be the preferred avenue to synthesising (RE-NHC)CuX (X = Br or I) complexes. This route would be more direct, removing the need for anion exchange on [RE-NHCH]X before reaction. Table 8 reports these results, [6-MesH]Br and [6-DippH]Br provided reasonable yields when reacted with CuCl after 2.5 h (entries 1 and 2). In neither case were the chloride analogues **4.1** and **4.10** observed by $^1$H NMR spectroscopy. The 7-membered analogues, [7-MesH]I and [7-DippH]I, proved to be problematic to use with this method as yields were low and isolation was difficult (entries 3 and 4). In both cases, upon any work-up, a bright yellow precipitate formed. The precipitate was found to be insoluble in $CH_2Cl_2$, $CHCl_3$, $C_6H_6$ and THF, even at elevated temperatures and so remains uncharacterised. (7-Dipp)CuI (**4.18**) proved impossible to isolate and attempts to extract with $CH_2Cl_2$ or $C_6H_6$ from this yellow precipitate failed. The occurrence of the yellow precipitate has not been reported by other groups during their synthesis of **4.18** suggesting it most likely arises from the incomplete reaction in the cuprate system. Unfortunately, no further conversion was seen after extending the time of the reaction. This precipitate was also seen during the work-up of (6-Mes)CuI (**4.3**, entry 5), however it proved to be less detrimental.

Table 4.9 – Conversions and yields of (RE-NHC)CuX (X= Br, I) complexes.

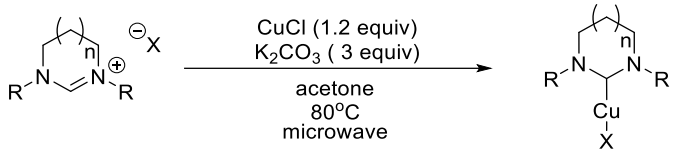


| Entry | [RE-NHCH]X | Time (h) | Product | Yield (%)[a] |
|---|---|---|---|---|
| 1 | [6-MesH]Br | 2.5 | (6-Mes)CuBr (**4.2**) | 85 (77) |
| 2 | [6-DippH]Br | 2.5 | (6-Dipp)CuBr (**4.16**) | 90 (89) |
| 3 | [7-MesH]I | 6 | (7-Mes)CuI (**4.17**) | 40 (18) |
| 4 | [7-DippH]I | 6 | (7-Dipp)CuI (**4.18**) | 48 (-) |
| 5[b] | [6-MesH]Br | 2.5 | (6-Mes)CuI (**4.3**) | 63 (37) |
| 6[b] | [6-MesH]Cl | 6 | (6-Mes)CuI (**4.3**) | 67 (54) |

[a] $^1$H NMR yield, isolated yields in parentheses. [b]CuI used instead of CuCl.

## 4.2.6 – Large Scale Synthesis of (RE-NHC)CuX (X = Cl, Br and I)

As demonstrated above, attempts to find a more general method proved difficult and as a result, individual conditions were used to obtain the best yields during the scale up reactions. Scale up to gram scale of **4.1** proved to be relatively straightforward with just the need to double the reaction time to achieve full conversion and high yield (entry 1, Table 4.10). An extended reaction time of 10 h was required for **4.11** to obtain a high NMR yield (entry 2). This was also required for the formation of **4.2** and **4.3** (entries 3 and 4 respectively). While these times are atypical for microwave chemistry, both reactions proved to be clean.[26] As with the rest of the entries in Table 4.10, the isolated yields drop significantly, largely due to the air sensitive techniques employed during work up. One of the biggest issues was scraping the solid from the ampoules after removing the solvent *in vacuo*, where a loss of >100 mg was usually seen.

Table 4.10 – Large scale synthesis of (RE-NHC)CuX.

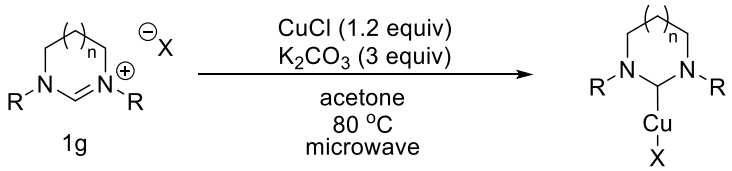


| Entry | RE-NHC·HX | Time (h) | Product | Yield (%)[a] |
|---|---|---|---|---|
| 1 | [6-MesHC]l | 2 | (6-Mes)CuCl (**4.1**) | 98 (78) |
| 2 | [7-MesH]Cl | 10 | (7-Mes)CuCl (**4.11**) | 98 (64) |
| 3 | [6-MesH]Br | 4 | (6-Mes)CuBr (**4.2**) | 90 (82) |
| 4[b] | [6-MesH]Br | 20 | (6-Mes)CuI (**4.3**) | 84 (64) |

[a] $^1$H NMR yield, isolated yields in parentheses. [b]CuI was used instead of CuCl.

## 4.2.7 – Characterisation of (RE-NHC)CuX

X-ray quality crystals of all the complexes could be obtained upon layering concentrated $CH_2Cl_2$ solutions of the (NHC)CuX complex with pentane at room temperature. Attempts to grow X-ray quality crystals of **4.15** proved unsuccessful. Figure 4.4 and Table 4.11 summarise selected bond lengths and angles of these structures.

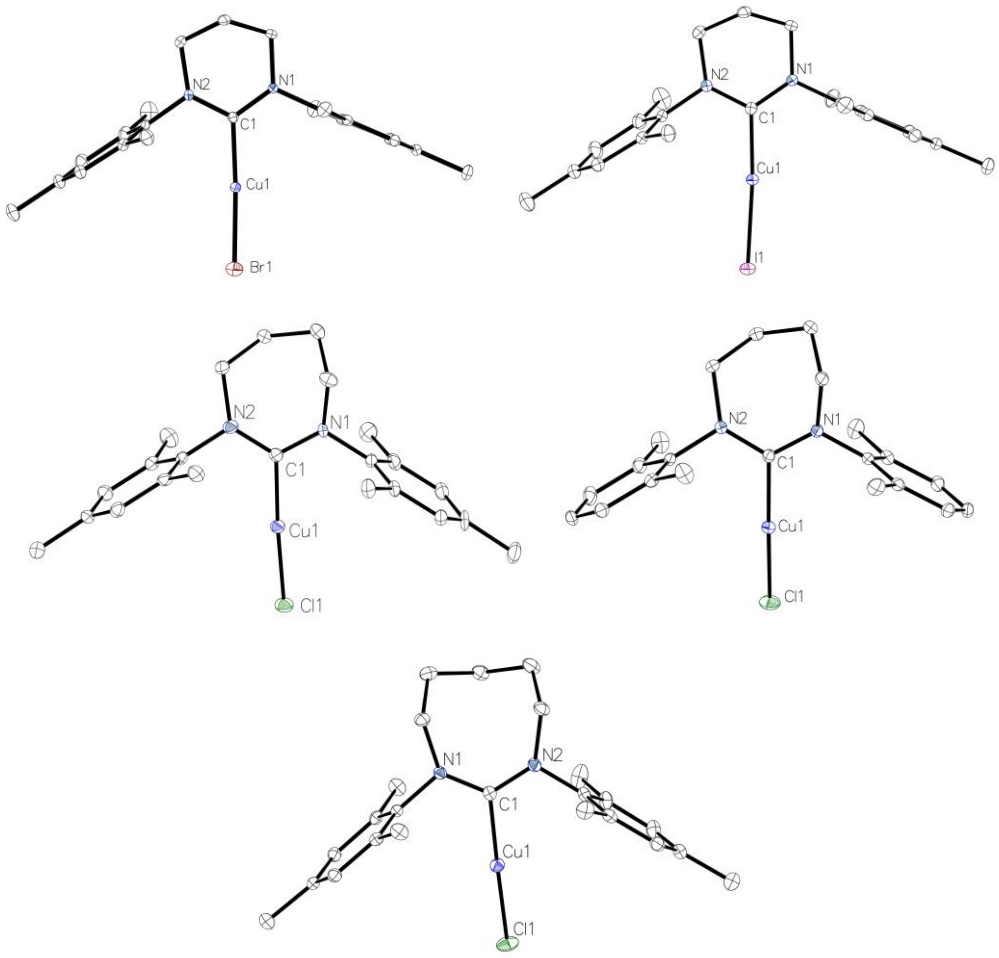


Figure 4.4 – Molecular structures (from top left to bottom left) of **4.2**, **4.3**, **4.11**, **4.12** and **4.14**. Hydrogens omitted for clarity.

Table 4.11– Selected bond lengths (Å) and angles (°) in (RE-NHC)CuX complexes.

| Entry | Compound | Cu-C | Cu-X | C-Cu-X |
|---|---|---|---|---|
| 1 | (6-Mes)CuBr (**4.2**) | 1.891(4) | 2.2072(7) | 175.54(13) |
| 2 | (6-Mes)CuI (**4.3**) | 1.907(3) | 2.3906(4) | 175.12(8) |
| 3 | (6-Xylyl)CuCl (**4.9**) | 1.8928(18) | 2.1028(5) | 175.39(5) |
| 4 | (7-Mes)CuCl (**4.11**) | 1.898(6) | 2.1156(18) | 176.3(2) |
| 5 | (7-Xylyl)CuCl (**4.12**) | 1.900(2) | 2.1138(7) | 173.69(9) |
| 6 | (8-Mes)CuCl (**4.14**) | 1.9109(18) | 2.1249(5) | 177.23(5) |
| 7 | (6-Mes)CuF (**3.2**) | 1.8737(15) | 1.8037(10) | 174.30(6) |
| 8 | (6-Mes)CuCl (**4.1**)[21] | 1.892(3) | 2.1011(9) | 176.20(9) |
| 9 | (7-Mes)CuF (**3.1**) | 1.8647(18) | 1.7940(11) | 177.29(7) |

Comparing structures **4.1**, **4.2**, **4.3** and **3.2** revealed the expected increase in Cu-X bond length from Cu-F (**3.2**) being the shortest at 1.8037(10) Å to Cu-I (**4.3**) at 2.3906(4) Å. Likewise, the C-Cu bond is the shortest bond in **3.2** and longest in **4.3**. This trend was also observed between **3.1** and **4.11**. As we increase ring size (**4.1** < **4.11** < **4.14**), there was very little change in C-Cu and Cu-X bond lengths despite having increased σ-donation from the larger-membered NHC rings. As illustrated in Figure 4.5, one factor which could influence this is the twisting/puckering of the larger rings (largest distance between puckered atom and mean plane of the carbene ring **4.1** = 0.349 Å, **4.11** = 0.566 Å, **4.14** = 0.775 Å), which could disrupt the electronics of the ring system affecting σ-donor strength. In fact, **4.14** showed slight elongation of C1-Cu bond which may indicate instability in the complex.[20,27]

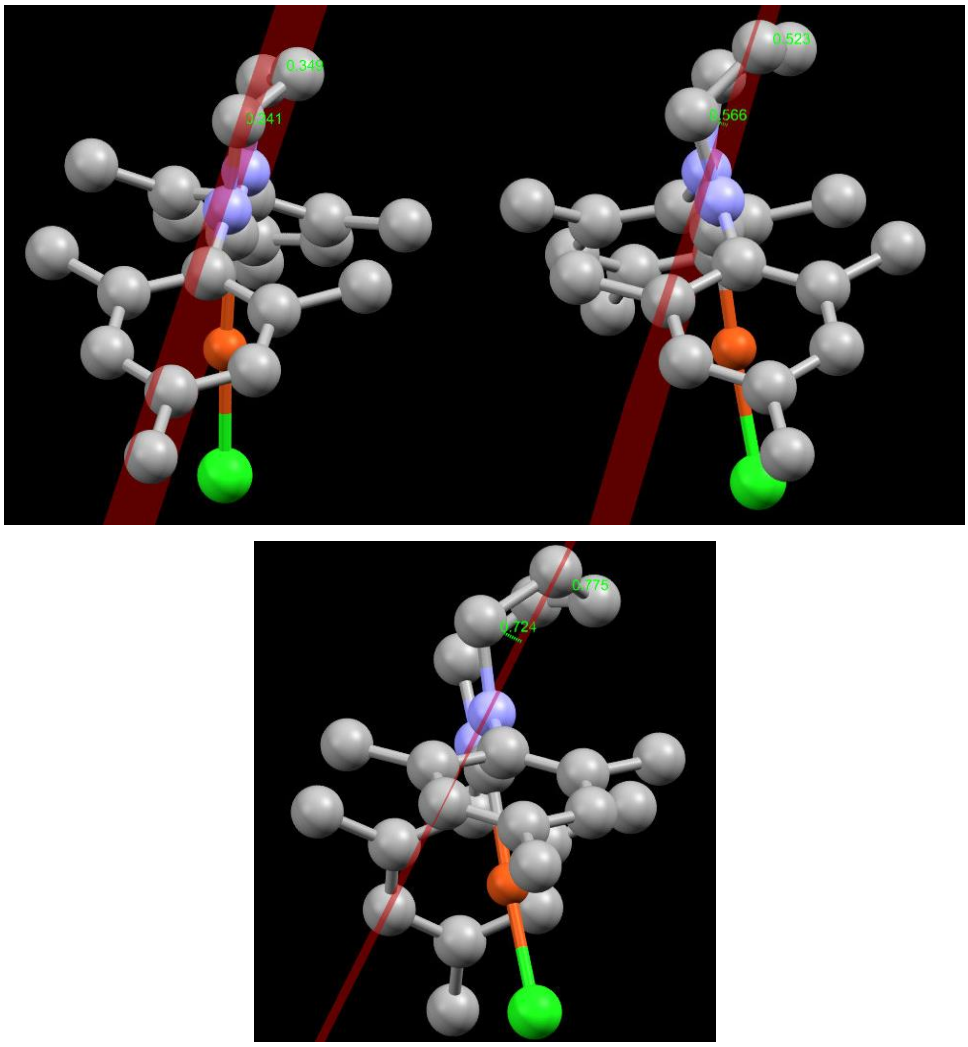


Figure 4.5 – Largest distance between puckered atom and mean plane of the carbene ring from left to right **4.1**, **4.11** and **4.14**.

### 4.2.8 – Discussion of the Synthesis of (RE-NHC)CuX

The chapter has demonstrated (RE-NHC)CuX complexes can be synthesised under milder conditions using the cuprate method rather than the free carbene method. In addition, there was no indications of homoleptic complex formation, which is a common occurrence with the latter method. However, elevated temperatures and extended times are required to achieve moderate conversions for the larger rings and heavier halides compared to the literature five-membered analogues.[18] Microwave heating helped achieve those conditions but changes to the solvent and base should be considered in future work in an effort to further improve yields. A comparison of [NHC·H][$CuX_2$] to [RE-NHC][$CuCl_2$] suggests that the resulting small downfield NMR shift of the C2-H resonance upon forming the RE-NHC cuprate complex is not sufficient enough to achieve facile reactivity. With the five-membered analogues having C2 proton signals around 9-10 ppm (compared to 7 – 7.5 ppm residual signals of the ring expanded systems) (Table 4.4), these are perhaps sufficiently acidic enough to activate with $K_2CO_3$. Within the literature examples (Table 4.4), as the halide becomes heavier and less electronegative, the C2 proton shift is more upfield, but still above 8 ppm, which could reflect the more forcing conditions required to synthesise **4.2** and **4.3** compared to **4.1**. In Nolan's report investigating the mechanism of this process, they calculated bulkier NHCs required a higher energy to break the C2-H bond when complexed to base and $MX_2^-$ fragment. Potentially this is reciprocated in the RE-NHC systems with the larger halides adding to this effect.

## 4.3 – [3+2] Cycloaddition of Azides with (RE-NHC)CuX

Cu complexes are commonly employed as catalysts of the [3+2] cycloaddition of azides with alkynes to yield 1,4-disubstituted-1,2,3-triazoles as single products.[28,29] With the employment of NHCs as ligands, highly active catalyst systems have been developed.[30] This ligand class has also aided the isolation of intermediates in this system to aid further the mechanistic understanding of the catalytic cycle.[31–34] The newly synthesised (RE-NHC)CuCl species, as well as (6-Mes)CuF (**3.2**), provided the opportunity for further understanding in this area by looking at catalytic performance as a function of ring size and halide.

### 4.3.1 – Importance of [3+2] Cycloaddition Conditions

To begin investigations, a similar method to that used by Cazin was employed. Where independent reactions were carried out and quenched at set times to yield an overall conversion plot based on GC-MS analysis.[14] Three different systems were investigated as shown in Scheme 4.15.

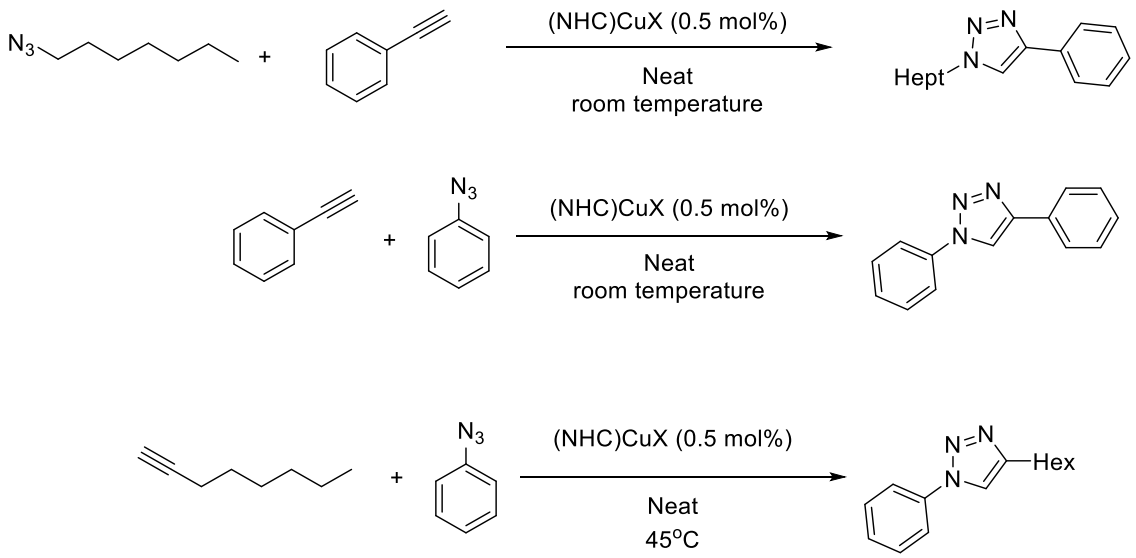


Scheme 4.15 – Reactions used to test the reactivity of the catalysts.

The temperature was closely monitored during course of the reactions, and for those at room temperature, an increase from 20 to 25 °C was observed throughout each run. The influence of temperature was noticeable and those runs which were above this range were re-run within the appropriate temperature range (see Figure 4.6 for an example).

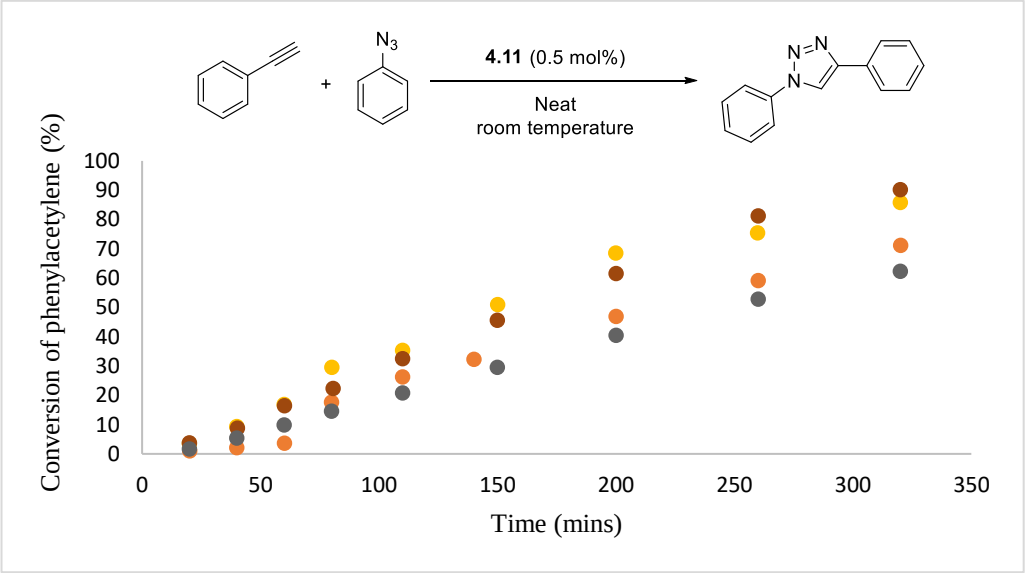


Figure 4.6 – Kinetic profiles of [3+2] cycloaddition of azidoheptane and phenylacetylene. Yellow and brown 26 – 32 °C temperature range recorded. Orange and grey 20 – 25 °C temperature range recorded. Each point represents an independent run quenched at that time.

Discrepancies were also observed between batches of azide and alkyne. To reduce this issue and provide reproducible results within this study, the batches were combined, and all the catalytic runs were from the same bulk batch of substrates. The substrates could contain contaminants of

trace amounts of water and air which could be influencing results. Given this has not been reported literature when "neat" conditions are used, further studies were undertaken.[5,18]

The catalytic system was exposed to a range of conditions as displayed in Figure 4.7. The addition of pure $O_2$ was found to be detrimental to this reaction, but when air is added, this effect is reduced. Exposure to dry air gave a similar result to compressed air from the atmosphere, supporting $O_2$ as being unfavourable for the reaction. Interestingly, exposure of the reaction to 10 µL of deionised water (DI) (*ca*. 50 mol%) enhanced the conversion, but this seems to be a limited effect as increasing the amount of water 10-fold (500 mol %) gave only a slight improvement in conversion. Water is commonly used as a solvent for the [3+2] cycloadditions which could help disperse the catalyst, but in this case of quite hydrophobic reagents, suggestion of on-water reactivity could be considered.[35,36]

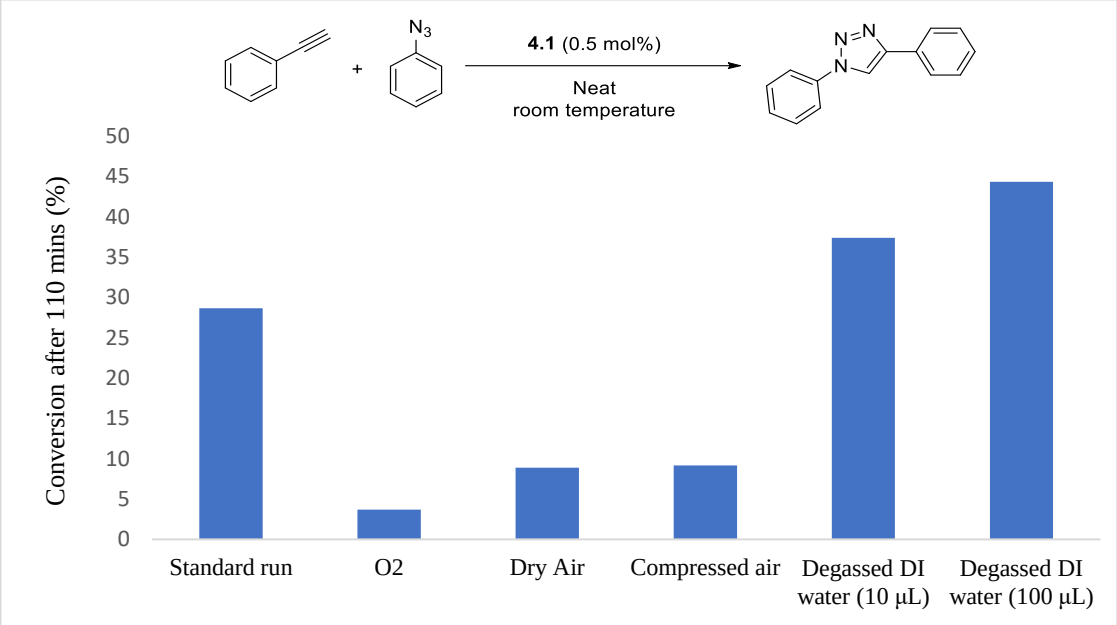


Figure 4.7 – Conversion after 110 mins for the [3+2] cycloaddition of phenylacetylene and phenylazide catalysed by **4.1** in the presence of additives. Addition of substrates occurred after 10 mins of the catalytic run. Average of 2 runs.

## 4.3.2 – Catalyst Screening – Effect of Halide in (RE-NHC)CuX

Previous work investigating the effect of halide, carried out by Nolan in 2010, identified that reactivity in (NHC)CuX catalysed [3+2] cycloadditions of terminal alkynes follows the order I > Br > Cl, suggesting that a more easily displaced halide ligand could promote activity, perhaps by facilitating formation of an (NHC)Cu(alkynyl) intermediate.[3] This was proposed to then react with the azide to form a (NHC)Cu(triazolide), which upon protonation by the alkyne, gave the

cycloaddition product (Scheme 4.16). This cycle was supported by later observations by Cazin and Straub.[33,34,37]

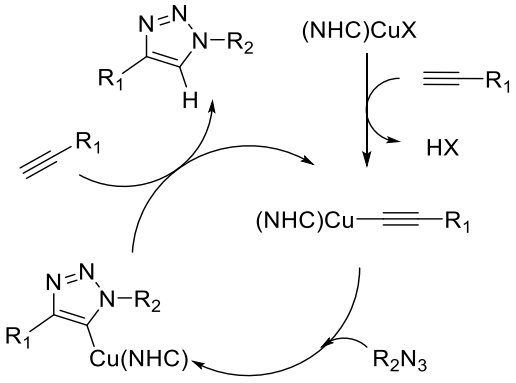


Scheme 4.16 – Generic catalytic scheme proposed by Nolan.[3]

Contrary to this, the order of reactivity of (NHC)CuX changed when alkyl N-substituted carbenes ICy and I$^t$Bu were employed. Nolan suggested this was due to the poorer stability of the (NHC)CuX complex under the catalytic conditions, with the NHC providing an alternative ligand to the halide for displacement. Chen and co-workers noticed that their reactivity is not based upon the lability of the halide, but rather its trans effect on the NHC.[31] The basis for this observation was from the reaction of their (NHC)CuCl complex with phenylacetylene, which failed to give the corresponding (NHC)Cu(alkynyl), but rather an imidazolium salt with an (alkynyl)CuX counter anion (Scheme 4.17).

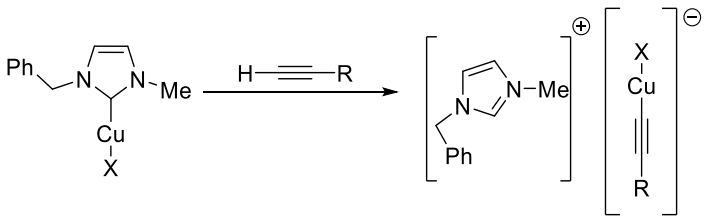


Scheme 4.17 – Reactivity observed by Chen.[31]

Later work by Folkin and Bertrand, established a parallel dinuclear mechanism for the [3+2] cycloaddition species through kinetic studies and the isolation of key intermediates.[32,38] However, in terms of initial activation both of the previous examples (Nolan and Chen) are still plausible (Scheme 4.18).[32,38–40]

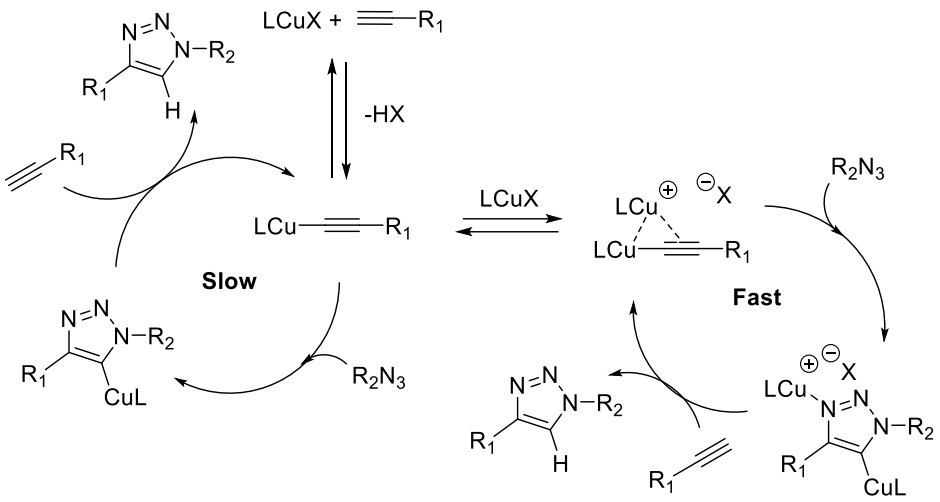


Scheme 4.18 – Dinuclear mechanism of [3+2] cycloaddition proposed by Bertrand.[38]

To compare the halides in the (RE-NHC)CuX system, (6-Mes)CuX was chosen as the comparison scaffold by using complexes **4.1**, **4.2**, **4.3** and **3.2**. The results from the reaction of azidoheptane and phenylacetylene are shown in graph A of Figure 4.8. The order of activity as a function of halide (I ≈ F > Br > Cl) revealed similar results to what was observed by Nolan.[3] Changing to an aromatic azide (phenylazide) did not affect the trend in reactivity (graph B, Figure 4.8). However, at elevated temperatures, the [3+2] cycloaddition of 1-octyne and phenylazide revealed **3.2** to be most reactive (graph C, Figure 4.8). This could be an effect of temperature causing **3.2** to destabilise and become more reactive; however, upon addition of 1-octyne to **3.2** at room temperature a bright yellow solution was observed suggesting some form of interaction. The results shown do not conclusively support Chen's proposal of the trans effect since **3.2** should be the least reactive if it were true. However, it cannot be discounted as two different initiation pathways could be present, hence why we see **3.2** and **4.3** being the most reactive across this series. The reactivity of **3.2** warrants further investigation alongside **4.3**.

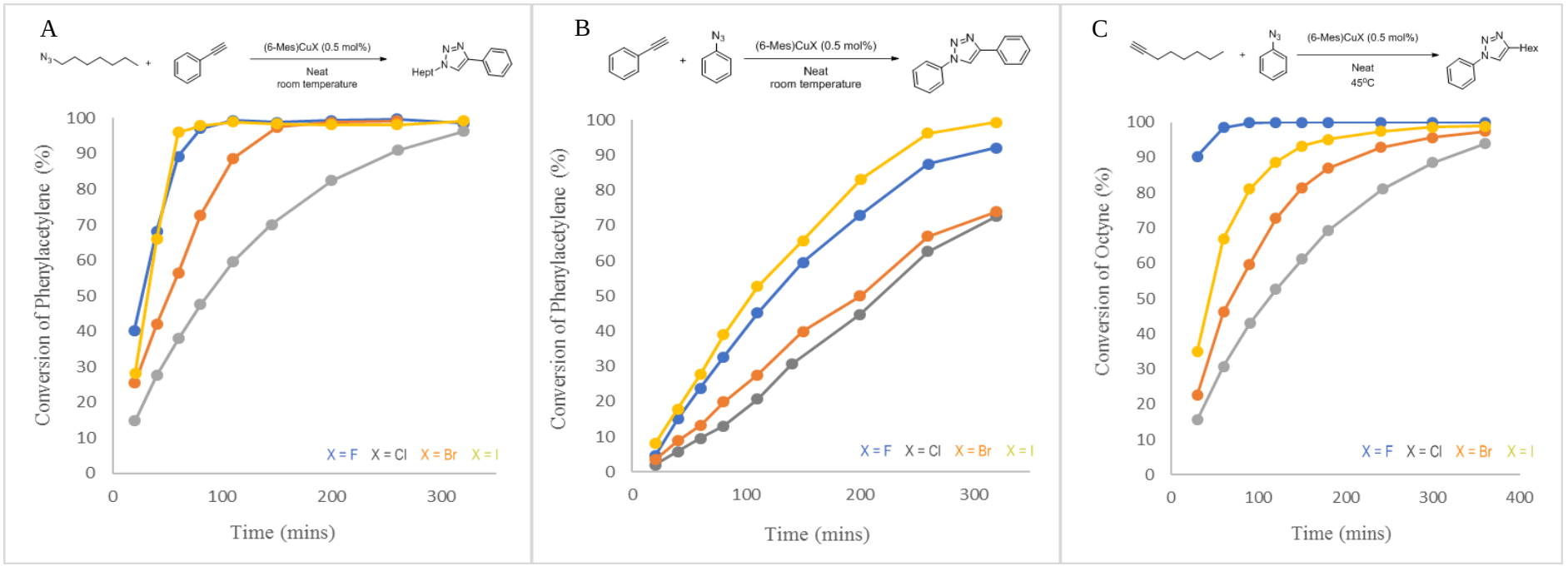


Figure 4.8 – Kinetic profiles of [3+2] cycloaddition of (A) azidoheptane and phenylacetylene. Reaction conditions: Catalyst (0.5 mol%), azidoheptane (1.0 mmol), phenylacetylene (100 mol%), solvent free, room temperature, B) azidobenzene and phenylacetylene. Reaction conditions: Catalyst (0.5 mol%), azidobenzene (1.0 mmol), phenylacetylene (100 mol%), solvent free, room temperature and C) azidobenzene and 1-octyne. Reaction conditions: Catalyst (0.5 mol%), azidobenzene (1.0 mmol), 1-octyne (100 mol%), solvent free, 45 °C. Lines are visual aids and not curve fits. Each point represents an average of at least two independent reactions quenched at that time. Blue: (6-Mes)CuF (**3.2**), Grey : (6-Mes)CuCl (**4.1**), Orange : (6-Mes)CuBr (**4.2**), Yellow : (6-Mes)CuI (**4.2**).

## 4.3.3 – Effect of NHC Ring Size on the [3+2] Cycloadditions

Díez-González utilised RE-NHCs in their catalytic study and found high activity when **4.3** was employed at 100 ppm.[5] Upon comparison of ring size, it was found the reactivity followed the order 6-Mes > SIMes > 7-Mes. However, only (NHC)CuX (X = Br and I) complexes were investigated. In addition, like with SIPr,[41] 7-Dipp was found to be poorly yielding suggesting increased bulk on the N-substituent to be detrimental to catalysis. (SIMes)CuCl (**4.vi**)[ix], (6-Mes)CuCl (**4.2**) and (7-Mes)CuCl (**4.11**) were employed and the results are shown in Figure 4.9. Generally, the reactions showed no distinctive trends versus ring size of the NHC. For azidoheptane and phenylacetylene, the order was **4.2** ≈ **4.11** > **4.vi** (graph A, Figure 4.9), while with an aromatic azide (phenylazide), the order was **4.vi** > **4.2** ≈ **4.11** (graph B, Figure 4.9). Moving to 1-octyne and phenylazide gave the order **4.vi** > **4.11** > **4.2** (graph C, Figure 4.9). Without a clearer understanding of the mechanism, it is not possible to comment further on the different trends seen for different alkyne/azide combinations.

[ix] **4.vi** was kindly donated by the Cazin group.

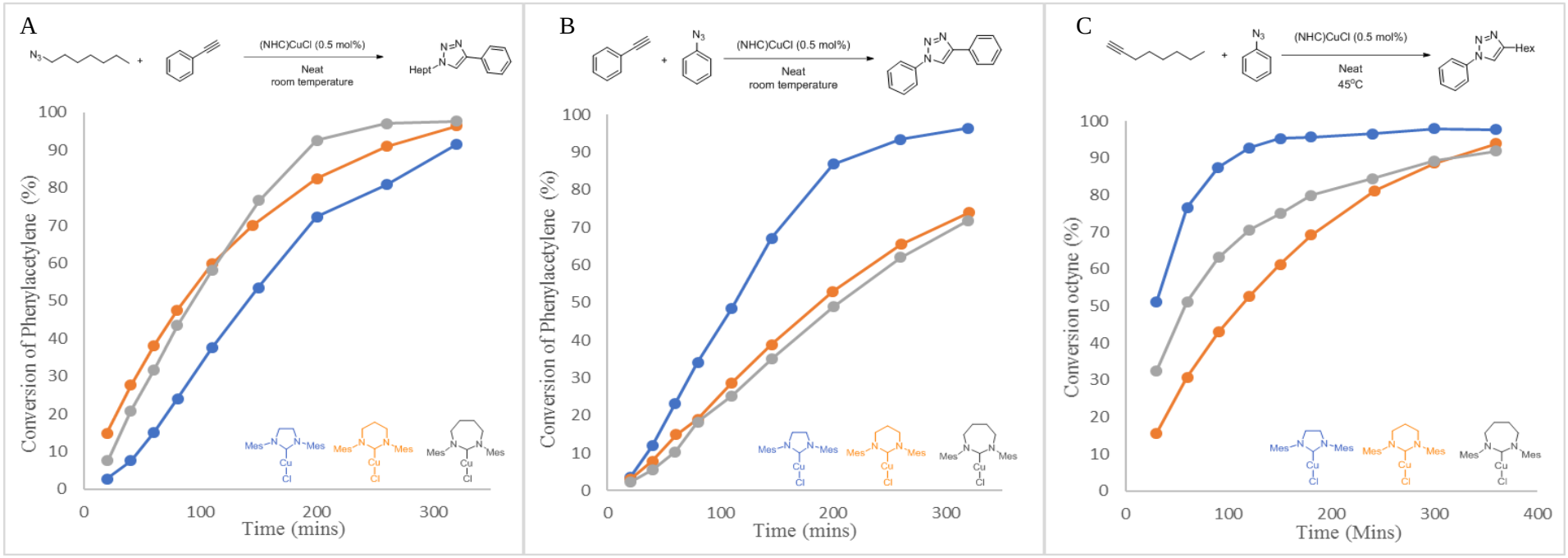


Figure 4.9 – Kinetic profiles of [3+2] cycloaddition of A) azidoheptane and phenylacetylene. Reaction conditions: Catalyst (0.5 mol%), azidoheptane (1.0 mmol), phenylacetylene (100 mol%), solvent free, room temperature, B) phenylazide and phenylacetylene. Reaction conditions: Catalyst (0.5 mol%), phenylazide (1.0 mmol), 1-octyne (100 mol%), solvent free, room temperature and C) azidobenzene and 1-octyne. Reaction conditions: Catalyst (0.5 mol%), azidobenzene (1.0 mmol), 1-octyne (100 mol%), solvent free, 45 °C. Lines are visual aids and not curve fits. Each point represents an average of at least two independent reactions quenched at that time. Blue : (SIMes)CuCl (**4.vi**), Orange : (6-Mes)CuCl (**4.1**), Grey : (7-Mes)CuCl (**4.11**).

## 4.4 – Conclusions

This chapter has described the utilisation and modification of the cuprate method for synthesising (RE-NHC)CuX complexes in reasonable yields on both 100 mg and 1 g scale for all of X =Cl, Br and I. The cuprate intermediates of selected RE-NHCs were also synthesised and characterised. X-ray diffraction revealed hydrogen bonding interactions between the C2 proton and $CuCl_2$ anion which was believed to be important for the mechanism. To improve the synthesis conditions, a stronger base could be employed, however this may deter away from a mild base approach originally set out with the cuprate work. (6-Mes)CuX (X = F, Cl, Br, I) were tested in the catalytic [3+2] cycloaddition of alkynes and azides. (6-Mes)CuF (**3.2**) and (6-Mes)CuI (**4.3**) were found to be highly reactive in reactions run at room temperature, while in the case of 1-octyne and phenylazide performed at 45 °C, **3.2** showed the highest activity. There was no clear trend in reactivity as a function of ring size as the order changed between substrates, suggesting the reactivity is dependent on the particular system being catalysed. While the catalytic runs utilised "neat" conditions, it was found a small amount of water (10 uL) could accelerate the catalysis and so these results could have been influenced by use of in-house prepared reagents which could contain traces of water. However, the potential of **3.2** and **4.3** have been demonstrated, warranting further study.

## 4.5 – References for Chapter 4


1 A. J. Jordan, C. M. Wyss, J. Bacsa and J. P. Sadighi, *Organometallics*, 2016, **35**, 613–616.

2 J. Al Thagfi and G. G. Lavoie, *Organometallics*, 2012, **31**, 7351–7358.

3 S. Díez-González, E. C. Escudero-Adán, J. Benet-Buchholz, E. D. Stevens, A. M. Z. Slawin and S. P. Nolan, *Dalton. Trans.*, 2010, **39**, 7595–7606.

4 B. Bantu, D. Wang, K. Wurst and M. R. Buchmeiser, *Tetrahedron*, 2005, **61**, 12145–12152.

5 F. Sebest, J. J. Dunsford, M. Adams, J. Pivot, P. D. Newman and S. Díez-González, *ChemCatChem*, 2018, **10**, 2041–2045.

6 L. R. Collins, PhD Thesis, University of Bath, 2016.

7 M. Pellei, V. Gandin, M. Marinelli, C. Marzano, M. Yousufuddin, H. V. R. Dias and C. Santini, *Inorg. Chem.*, 2012, **51**, 9873–9882.

8 M. Delgado-Rebollo, C. García-Morales, C. Maya, A. Prieto, A. M. Echavarren and P. J. Pérez, *J. Organomet. Chem.*, 2019, **898**, 120856.

9 E. L. Kolychev, I. A. Portnyagin, V. V Shuntikov, V. N. Khrustalev and M. S. Nechaev, *J. Organomet. Chem.*, 2009, **694**, 2454–2462.

10 A. A. D. Tulloch, A. A. Danopoulos, S. Kleinhenz, M. E. Light, M. B. Hursthouse and G. Eastham, *Organometallics*, 2001, **20**, 2027–2031.

11 S. Simonovic, A. C. Whitwood, W. Clegg, R. W. Harrington, M. B. Hursthouse, L. Male and R. E. Douthwaite, *Eur. J. Inorg. Chem*, 2009, 1786–1795.

12 C. A. Citadelle, E. Le Nouy, F. Bisaro, A. M. Z. Slawin and C. S. J. Cazin, *Dalton. Trans.*, 2010, **39**, 4489–4491.

13 B. Landers and O. Navarro, *Eur. J. Inorg. Chem*, 2012, 2980–2982.

14 Y. D. Bidal, M. Lesieur, M. Melaimi, F. Nahra, D. B. Cordes, K. S. A. Arachchige, A. M. Z. Slawin, G. Bertrand and C. S. J. Cazin, *Adv. Synth. Catal.*, 2015, **357**, 3155–3161.

15 S. Zhu, R. Liang and H. Jiang, *Tetrahedron*, 2012, **68**, 7949–7955.

16 A. Collado, A. Gómez-Suárez, A. R. Martin, A. M. Z. Slawin and S. P. Nolan, *Chem. Commun.*, 2013, **49**, 5541–5543.

17 R. Visbal, A. Laguna and M. C. Gimeno, *Chem. Commun.*, 2013, **49**, 5642–5644.

18 O. Santoro, A. Collado, A. M. Z. Slawin, S. P. Nolan and C. S. J. Cazin, *Chem. Commun.*, 2013, **49**, 10483–10485.

19 N. V. Tzouras, F. Nahra, L. Falivene, L. Cavallo, M. Saab, K. Van Hecke, A. Collado, C. J. Collett, A. D. Smith, C. S. J. Cazin and S. P. Nolan, *Chem. Eur. J.*, 2020, **26**, 4515–4519.

20 K. Sampford, PhD Thesis, Cardiff University, 2013.

21 G. M. Pawar, B. Bantu, J. Weckesser, S. Blechert, K. Wurst and M. R. Buchmeiser, *Dalton. Trans.*, 2009, 9043–9051.

22 H. V. Huynh, T. T. Lam and H. T. T. Luong, *RSC Adv.*, 2018, **8**, 34960–34966.

23 W. J. Kerr, R. J. Mudd and J. A. Brown, *Chem. Eur. J.*, 2016, **22**, 4738–4742.

24 B. C. Liu, N. Ge, Y. Q. Zhai, T. Zhang, Y. S. Ding and Y. Z. Zheng, *Chem. Commun.*, 2019, **55**, 9355–9358.

25 A. C. Filippou, O. Chernov and G. Schnakenburg, *Angew. Chem. Int. Ed.*, 2009, **48**, 5687–5690.

26 A. Beillard, X. Bantreil, T. X. Métro, J. Martinez and F. Lamaty, *Chem. Rev.*, 2019, **119**, 7529–7609.

27 R. C. Poulten, PhD Thesis, University of Bath, 2015.

28 E. Haldón, M. C. Nicasio and P. J. Pérez, *Org. Biomol. Chem.*, 2015, **13**, 9528–9550.

29 S. Neumann, M. Biewend, S. Rana and W. H. Binder, *Macromol. Rapid Commun.*, 2020, **41**, 1900359.

30 F. Lazreg, F. Nahra and C. S. J. Cazin, *Coord. Chem. Rev.*, 2015, **293**–**294**, 48–79.

31 Y. C. Lin, Y. J. Chen, T. Y. Shih, Y. H. Chen, Y. C. Lai, M. Y. Chiang, G. C. Senadi, H. Y. Chen and H. Y. Chen, *Organometallics*, 2019, **38**, 223–230.

32 B. T. Worrell, J. A. Malik and V. V. Fokin, *Science*, 2013, **340**, 457–461.

33 C. Nolte, P. Mayer and B. F. Straub, *Angew. Chem. Int. Ed.*, 2007, **46**, 2101–2103.

34 A. Makarem, R. Berg, F. Rominger and B. F. Straub, *Angew. Chem. Int. Ed.*, 2015, **54**, 7431–7435.

35 R. N. Butler and A. G. Coyne, *Org. Biomol. Chem.*, 2016, **14**, 9945–9960.

36 L. R. Collins, T. M. Rookes, M. F. Mahon, I. M. Riddlestone and M. K. Whittlesey, *Organometallics*, 2014, **33**, 5882–5887.

37 F. Lazreg, A. M. Z. Slawin and C. S. J. Cazin, *Organometallics*, 2012, **31**, 7969–7975.

38 L. Jin, D. R. Tolentino, M. Melaimi and G. Bertrand, *Sci. Adv.*, 2015, **1**, e1500304.

39 V. O. Rodionov, V. V. Fokin and M. G. Finn, *Angew. Chem. Int. Ed.*, 2005, **44**, 2210–2215.

40 R. Berg, J. Straub, E. Schreiner, S. Mader, F. Rominger and B. F. Straub, *Adv. Synth. Catal.*, 2012, **354**, 3445–3450.

41 S. Díez-González, E. D. Stevens and S. P. Nolan, *Chem. Commun.*, 2008, 4747–4749.

# Chapter 5

# Chapter 5 – Low Coordinate Nickel Complexes for the Hydrodehalogenation of Aryl and Alkyl Halides

## 5.1 – Introduction

### 5.1.1 – Preface for Hydrodehalogenation

Hydrodehalogenation (HDH) of organic halides is a well-studied process which can be catalysed by many different metals such as Li, Al, Cr and Pd.[1] Trends relating to the ease of HDH on organic halides have been well-established allowing for selective HDH with different systems. Generally, it has been found the ease of HDH of organic halides follows the bond dissociation energy of the carbon-halogen bond, with C-I being the easiest and C-F being the hardest to transform.[1] In addition, it has also been found that cleavage of the C-X bond is favoured in the following order; aliphatic < aromatic < vinylic < allylic < benzylic.[1] Depending on the mechanism of HDH, the reactivity order of substitution on aliphatic halides can change. For example, an $S_N1$ mechanism would favour tertiary C-X bonds over primary. HDH is well reviewed[1] and so the focus of the rest of section 5.1 will be on modern examples of homogeneous Ni catalysis and systems which contain Ni and/or NHCs.

### 5.1.2 – Nickel Hydrodehalogenation

The first dedicated piece of work employing an NHC ligand in Ni catalysed HDH was by Fort and co-workers in 2001.[2] The system involved the use of what was presumed to be a Ni(0) catalyst formed *in-situ* from $Ni(acac)_2$, [IMesH]Cl and NaH in the presence of $^{i}$PrOH (Figure 5.1).

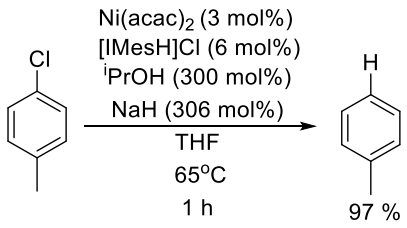


Figure 5.1 – Conditions used by Fort.[2]

Under the conditions shown in Figure 5.1, a range of aryl chlorides could be hydrodehalogenated. It was generally found that steric factors strongly influenced yields, as demonstrated by the yields for 2-chlorotoluene (82 %) vs 4-chlorotoluene (97 %). When the substrate was electron poor, such as chlorobenzotrifluoride, $CF_3$ substitution at the *meta* position reduced the reaction time to 25 mins compared to the *ortho* and *para* derivatives which required 1 h. It was also found the strongly activating 2-chloropyridine and 2-chloroquinoline gave the $S_NAr$ products 2-

isopropoxypyridine and 2-isopropoxyquinoline in modest yields (49 and 46 % respectively) instead of the desired hydrodehalogenated products.

Fort found the base to be another important feature of the reaction. Li and K salts were found to be less suitable than Na salts in the reaction. Moreover, β-hydrogen elimination from the alcohol/alkoxide was crucial for the reaction to occur. This was demonstrated by (i) the lack of reactivity when $^{t}$BuOH/NaH was used and (ii) incorporation of deuterium into the product when *in-situ* $d_7$-NaO$^{i}$Pr was employed during catalysis. The mechanism shown in Scheme 5.1 was proposed. This includes common reaction steps such as oxidative addition and reductive elimination, as well as a key step in the formation of a Ni-H species *via* β-hydride elimination.

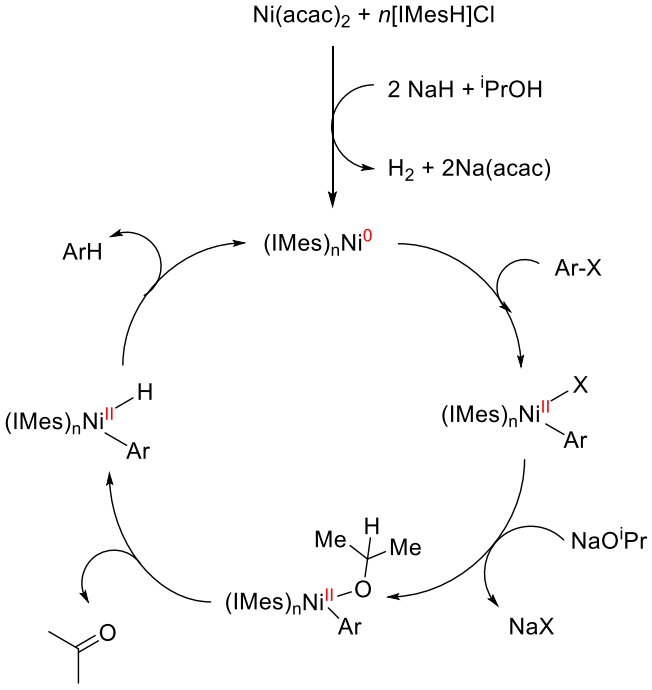


Scheme 5.1 – Proposed catalytic cycle by Fort.[2]

In a later publication by the same group, the efficient defluorination of aryl fluorides was established upon decreasing the ratio of carbene to Ni precursor (Scheme 5.2).[3] It was suggested a more reactive low coordinate Ni species was formed *in-situ* increasing catalytic activity. Other ligands which are bidentate and tridentate shut down reactivity, providing support for this hypothesis.

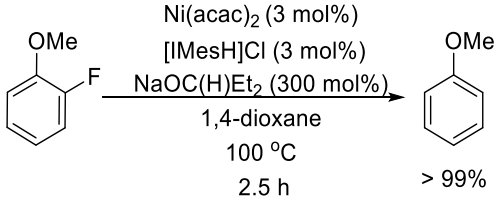


Scheme 5.2 – Conditions used in Fort's HDH of fluoroaryls.[4]

The importance of reducing a Ni(II) precursor was also supported by Nolan.[5] Employing a half sandwich CpNi(NHC)X system for HDH, they observed poor yields (Table 5.1) compared to Fort's work, even at elevated temperatures. The authors suggested the poor catalytic activity might reflect an unwillingness of the Ni(II) precursors to undergo facile reduction to a Ni(0) species.

Table 5.1 – Catalytic results from a study by Nolan.[5]

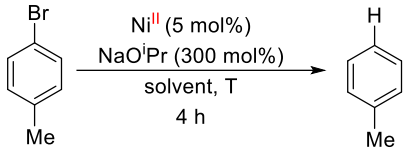


| | Conversion (%)[a] | | | |
|---|---|---|---|---|
| Solvent, T (°C) | CpNi(IPr)Cl | CpNi(SIPr)Cl | CpNi(IMes)Cl | CpNi(SIMes)Cl |
| THF, 65 | 24 | 29 | 40 | 37 |
| *p*-dioxane, 105 | 30 | 31 | 40 | 23 |

[a]Conversions : average of two runs by GCMS

Gade employed a Ni(I) complex with a tridentate pincer ligand (**5.i**) for HDH (Scheme 5.3a),[6] which was observed to be actively involved in the catalytic cycle. Mechanistic studies found the addition of 1-chloro-4-fluorobezene to **5.i** led to the bimolecular oxidation of **5.i** affording the two Ni(II) species, **5.ii** and **5.iii** (Scheme 5.3a). Matsubara also observed a similar oxidation reaction when $Ni(COD)_2$ was mixed with IPr and 4-chlorotoluene, however this led to the dimeric Ni(I) complex **5.iv** (Scheme 5.3b).[7]

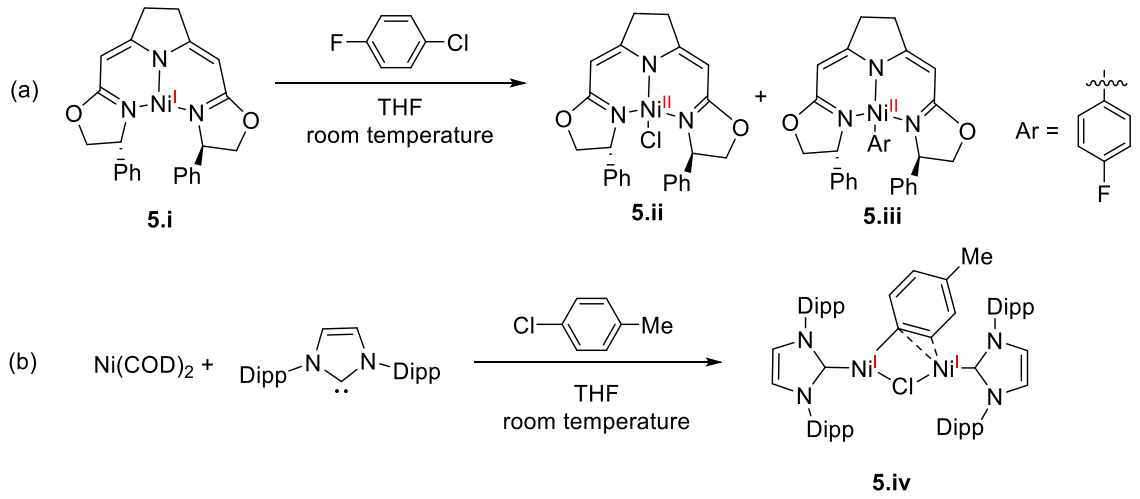


Scheme 5.3 – (a) Gade's bimolecular oxidation reaction of aryl halides at independent Ni(I) centres.[6] (b) Matsubara's oxidation to yield a dimeric Ni(I) complex.[8]

When employed in HDH, complex **5.ii** was found to be just as reactive as **5.i**, although **5.iii** was found to be inert in the system. During catalytic runs with 1-chloro-4-fluorobezene, **5.iii** was shown to accumulate as the reaction proceeded. This was found not to be the case when digeminal alkyl chloride substrates were used, such as 2,2-dichloro-1,2,3,4-tetrahydronaphthalene. DFT calculations suggested this difference in reactivity was due to the aryl radical of 1-chloro-4-fluorobenzene forming a more stable Ni(III) intermediate **5.v** with complex **5.ii**, allowing subsequent reaction with additional **5.i** to give **5.ii** and **5.iii**. The aryl radical was still proposed to be able to disperse to continue the reaction alongside this side reaction due to the low concentration of Ni in the system (Scheme 5.4). Contrary to this, the alkyl radical was calculated to have little difference in energy upon coordinating to **5.ii**, thus allowing it to disperse in the reaction mixture for reaction with the hydride.

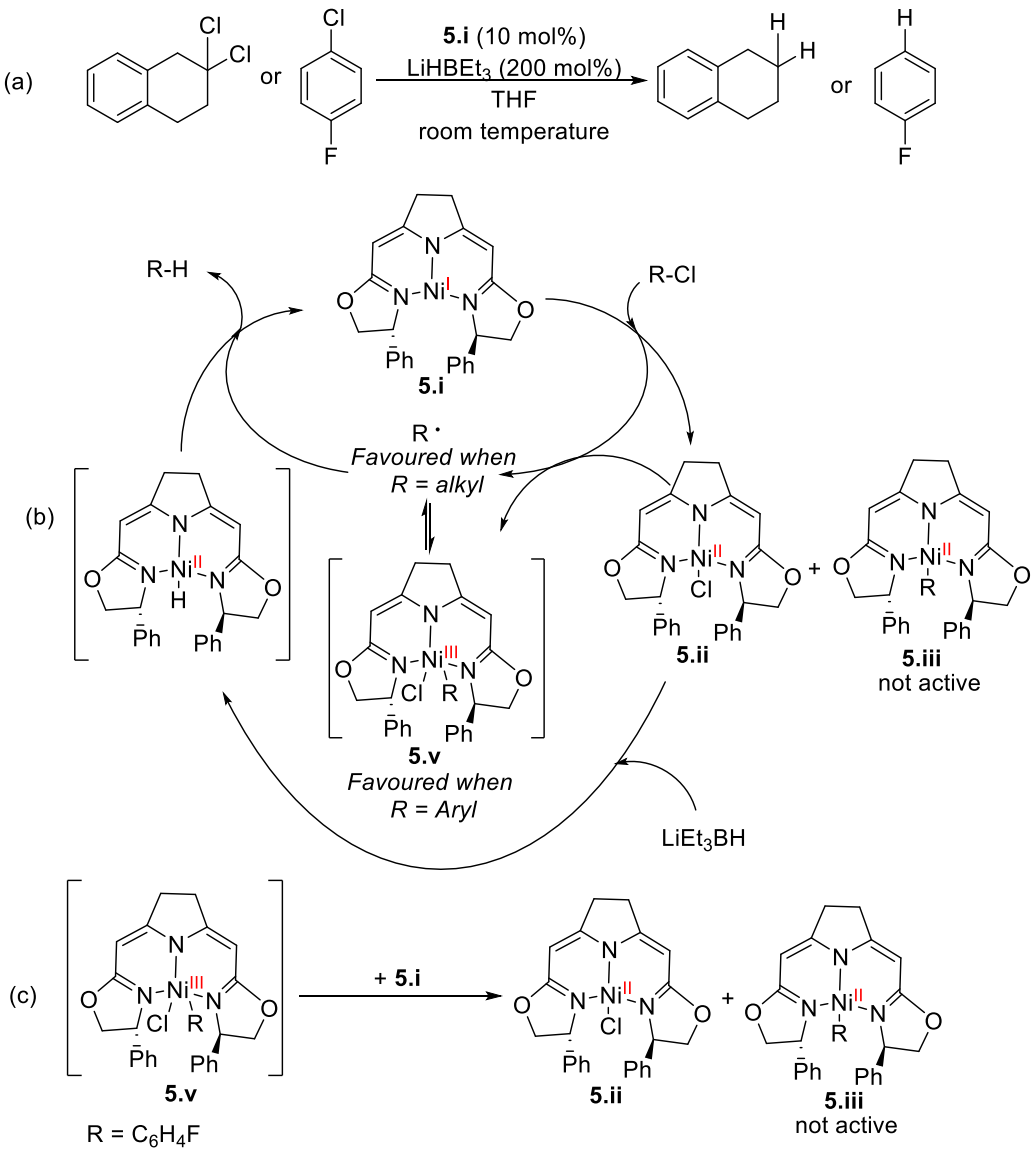


Scheme 5.4 – a) Gade's catalytic conditions. b) Proposed cycle. c) Additional postulated reactivity of **5.v**.[6]

Fenske identified an isolated Ni(II) hydride species that was capable of the HDH of alkyl halides and aryl halides.[9] Starting from complex **5.vi** with $(EtO)_3SiH$ and $NaO^tBu$ in stoichiometric amounts, they were able to isolate the Ni(II) hydride species **5.vii**, which was stable in solution for 2 h (Scheme 5.5).

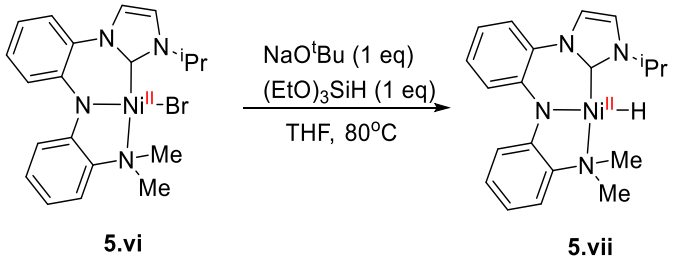


Scheme 5.5 – Synthesis of a Ni-H species by Fenske.[9]

Using complex **5.vii** in the presence of excess $(EtO)_3SiH$, $NaO^tBu$ and n-octyl bromide they demonstrated catalytic HDH (Scheme 5.6). This was extended to aryl bromides and chlorides, apart from more electron rich substrates such as 4-bromoanisole or 2-bromoaniline, which were found not to react. They also demonstrated that complex **5.vi** gave similar catalytic yields to **5.vii** in the HDH of *n*-octyl bromide, leading them to propose that both **5.vi** and **5.vii** are on the same catalytic cycle. A stoichiometric reaction of **5.vii** and ethyl bromide led to the formation of complex **5.vi**, further supporting this. Addition of TEMPO to a catalytic run led to complete shutdown of catalysis, leading to the conclusion that radicals are involved in the mechanism. However, it is unclear whether TEMPO is reacting with a Ni(I) radical or organic radical to shut down the catalysis. These results are reflected in their proposed catalytic cycle shown in Scheme 5.7.

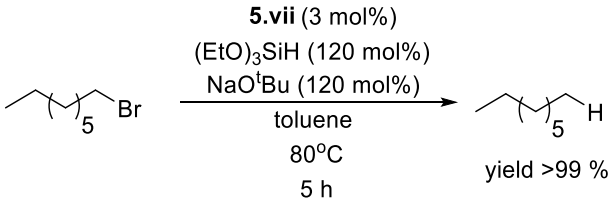


Scheme 5.6 – Catalytic conditions for the HDH of *n*-octyl bromide used by Fenske.[9]

Starting from **5.vi**, they propose the formation of complex **5.vii** *via* a Ni(II) alkoxide intermediate. The Ni(II) hydride undergoes initiation to form a Ni(I) intermediate and H radical. The H radical then reacts with the alkyl halide forming the desired dehalogenated alkyl species and a halide radical, which is trapped by the low-coordinate Ni(I) intermediate to reform complex **5.vi** and complete the cycle. The nature of the hydride interaction with alkyl halide is only supported by their TEMPO observation, however the formation of **5.vii** from **5.vi** provides insight into how a hydride intermediate can be involved in HDH.

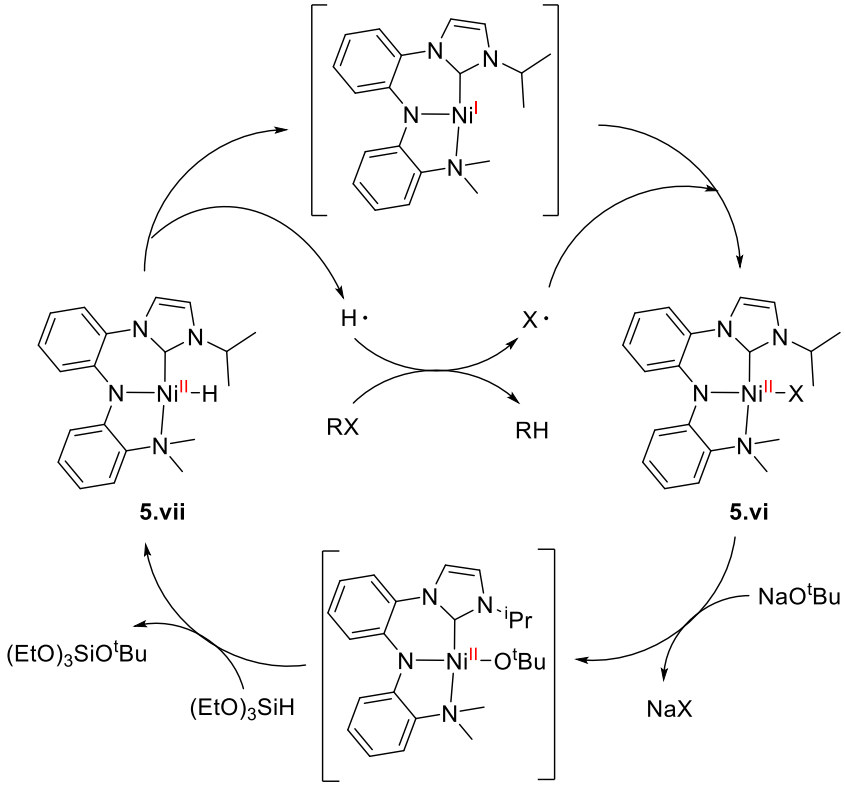


Scheme 5.7 – Mechanistic proposal for HDH based upon complexes **5.vi** and **5.vii**.[9]

The examples above show that the nature of the ligands can play a significant role in varying the precise pathway of Ni catalysed HDH. However, two common features arise from these studies, namely the importance of a β-hydride/hydride source and the occurrence of a Ni-H species.

## 5.2 – Hydrodehalogenation Catalysed by Ni(RE-NHC)(PPh$_3$)Br Complexes

### 5.2.1 – Optimisation

Initial attempts could not reproduce exactly the results from the original 2010 report by our group (Scheme 5.8).[10] In order to achieve the reported full conversion after 30 mins, $^i$PrOH was needed, which was not included in the original conditions. A comparison of the old to the new conditions are shown in Scheme 5.8. The addition of $^i$PrOH was found to enhance the reactivity of the system allowing for a lower loading of NaO$^i$Pr to be used. It is also worth noting a new side product was also identified during the reaction whilst optimising the HDH of 1-bromo-4-fluorobenzene, which was determined to be 4-FC$_6$H$_4$O$^i$Pr (**5.13**). This will be discussed later in the chapter.

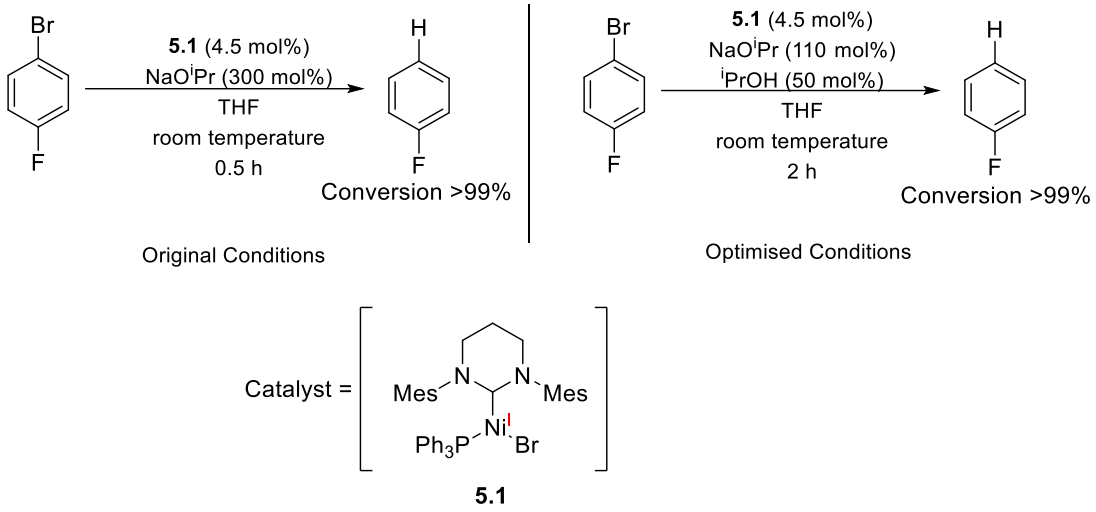


Scheme 5.8 – A comparison of original reported conditions to the optimised conditions for this study.[10]

Catalytic runs containing $d_1$-$^i$PrOD (in both 50 mol% and 200 mol%) were also run to examine if deuterium incorporation into the final HDH product occurred (Scheme 5.9). In both cases no deuterium incorporation was detected in the $C_6H_5F$ by mass spectrometry, suggesting the hydride is either from the other protons on the alkoxide/alcohol moiety or from another source.

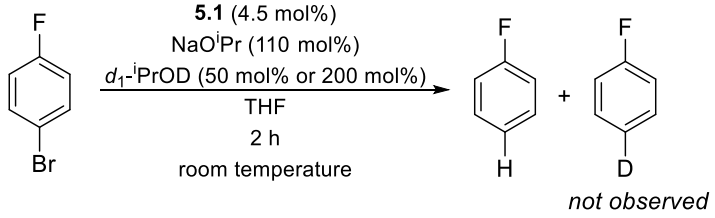


Scheme 5.9 – Catalytic run with **5.1** and $d_1$-$^i$PrOD rather than $^i$PrOH.

## 5.2.2 – Catalyst and Substrate Screening

Once the optimised conditions were established, the effect of NHC ring size on activity was first investigated. Ni(6-Xylyl)($PPh_3$)Br (**5.2**),[11] Ni(6-*o*-Tolyl)($PPh_3$)Br (**5.3**),[12] Ni(7-Mes)($PPh_3$)Br (**5.4**),[13] Ni(7-Xylyl)($PPh_3$)Br (**5.5**)[11] and Ni(7-*o*-Tolyl)($PPh_3$)Br (**5.6**),[12] alongside Ni(6-Mes)($PPh_3$)Br (**5.1**), were examined for their catalytic efficiency in HDH (Table 5.2). In general, the activities were found to be related to the level of substitution on the N-substituent, with the more substituted mesityl being more reactive than the least substituted *o*-tolyl, although **5.1** and **5.2** exhibited similar activity (entries 1 and 2). It was also found the Ni complexes containing 6-membered ring NHCs were better than their 7-membered ring analogues. Given these results and the high level of study on complex **5.1** in previous publications in the group, **5.1** was used as our catalyst precursor for the rest of this work.[10,12,14]

Table 5.2 – Results of Ni(RE-NHC)($PPh_3$)Br catalysed HDH of 4-bromotoluene as a function of N-substituents and ring size.[a]

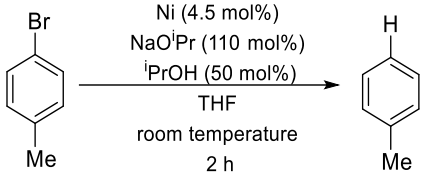


| Entry | Catalyst | Yield (%)[b] |
|---|---|---|
| 1 | Ni(6-Mes)($PPh_3$)Br (**5.1**) | 95 |
| 2 | Ni(6-Xylyl)($PPh_3$)Br (**5.2**) | 99 |
| 3 | Ni(6-*o*-Tolyl)($PPh_3$)Br (**5.3**) | 26 |
| 4 | Ni(7-Mes)($PPh_3$)Br (**5.4**) | 60 |
| 5 | Ni(7-Xylyl)($PPh_3$)Br (**5.5**) | 43 |
| 6 | Ni(7-*o*-Tolyl)($PPh_3$)Br (**5.6**) | 16 |

[a]Reaction conditions: 0.134 mmol 4-bromotoluene, 4.5 mol% Ni precursor, 110 mol% NaO$^i$Pr, 50 mol% $^i$PrOH in THF (1 mL). [b]Yields determined by GC-MS relative to an internal standard of dodecane and reported as an average of two runs after 2 hours.

The HDH of a range of aryl halide substrates, as well as two alkyl halides, was screened (Table 5.3). As previously reported,[10] chloro substrates required more time (24 h) and an elevated temperature (50 °C) to react compared to bromo substrates. Entries 1–3 show that yields of the bromofluorobenzene HDH product fluorobenzene increased as the site of Br substitution changed from *meta* > *ortho* > *para* in the initial 0.5 h of the reaction, although after the allocated reaction time (2 h), this changed to *meta* ≈ *para* > *ortho*.[x] The initial high conversion of the *meta* substrate could be considered a result of electronics over sterics. In entries 4–6, where bromotoluene was employed, similar conversions were initially seen, although, after 2 h, the result *para* > *meta* > *ortho* might reflect some steric involvement. Both influences were seen by Fort and co-workers with chlorosubstrates.[2] The electron rich 4-bromoanisole (entry 7) showed lower activity compared to other aryl bromides. The electron poor 4-bromobenzotrifluoride showed a lack of conversion to α,α,α-trifluorotoluene beyond 31 % after 30 mins. By $^{19}$F NMR spectroscopy full conversion of 4-bromobenzotrifluoride was seen, however, upon closer inspection, another product was present, which we believe to be 4-isopropoxybenzotrifluoride, based upon GC-MS

[x] No substitution of the fluoride group was seen in this study.

characterisation. It is worth noting that a similar by-product, appeared to be formed with all the substrates, although not to the same extent as for 4-bromobenzotrifluoride. The difficulty of synthesising $^{i}PrOC_6H_4X$ compounds means their assignments and yields remain tentative. For the chlorofluorobenzene substrates (entries 9–11), *meta* substitution also gives a higher yield over a short period of time. Contrary to Fenske's work, both 1-bromodecane and 1-chlorodecane exhibited rapid conversion under milder conditions. As noted earlier, alkyl substrates are traditionally more difficult substrates to convert using HDH compared to aryl halides.[1,9]

Table 5.3 – Substrate screen using complex **5.1** for HDH.

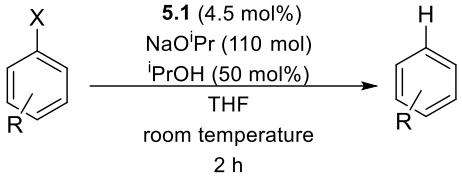


| Entry | Substrate | | Yield [%][b] |
|---|---|---|---|
| | R | X | |
| 1 | *p*-F | Br | 27 (88) |
| 2 | *m*-F | Br | 86 (87) |
| 3 | *o*-F | Br | 38 (71) |
| 4 | *p*-Me | Br | 36 (95) |
| 5 | *m*-Me | Br | 34 (88) |
| 6 | *o*-Me | Br | 40 (78) |
| 7 | *p*-OMe | Br | 22 (73) |
| 8 | *p*-$CF_3$ | Br | 31 (31) |
| 9[c] | *p*-F | Cl | 69[d] |
| 10[c] | *m*-F | Cl | 88[d] |
| 11[c] | *o*-F | Cl | 72[d] |
| 12[c] | *p*-Me | Cl | 52[d] |
| 13 | 1-bromodecane | | 93[e] |
| 14[c] | 1-chlorodecane | | (82) |

[a]Reaction conditions: 0.134 mmol aryl halide/alkyl halide, 4.5 mol% complex **5.1**, 110 mol% NaO$^{i}$Pr, 50 mol% $^{i}$PrOH in THF (1 mL) at room temperature. [b]Yield determined by GC-MS relative to an internal standard of dodecane and reported as an average of two runs after 0.5 h and, in parentheses, 2 hours. [c] 50°C. [d]After 24 h. [e]After 5 mins.

## 5.3 – Mechanistic Investigations - Overview

Mechanistic investigations of Ni(6-Mes)($PPh_3$)Br (**5.1**) mediated HDH, revealed a series of interconnected steps. In order to make the results digestible, the final proposed cycle is presented first (Scheme 5.10). The separate components leading to this final cycle will be discussed individually in the following sections. For clarity, the cycle is split into two halves. The cycle containing blue labelled pathways represent the "Ni(I) alkoxide route" and the cycle containing the pink labelled pathways represents the "Ni(II) route". The next section of this chapter will focus on the "Ni(I) alkoxide route" (section 5.4), followed by consideration of the "Ni(II) route" (section 5.5) and ending with a discussion linking the two sections together. All the compounds involved are listed in Figure 5.2, as well as in appendix 7.5). The purpose of this listing is to allow fluid communication of the results without having to label them differently as some complexes would have not been identified in the text at that point.

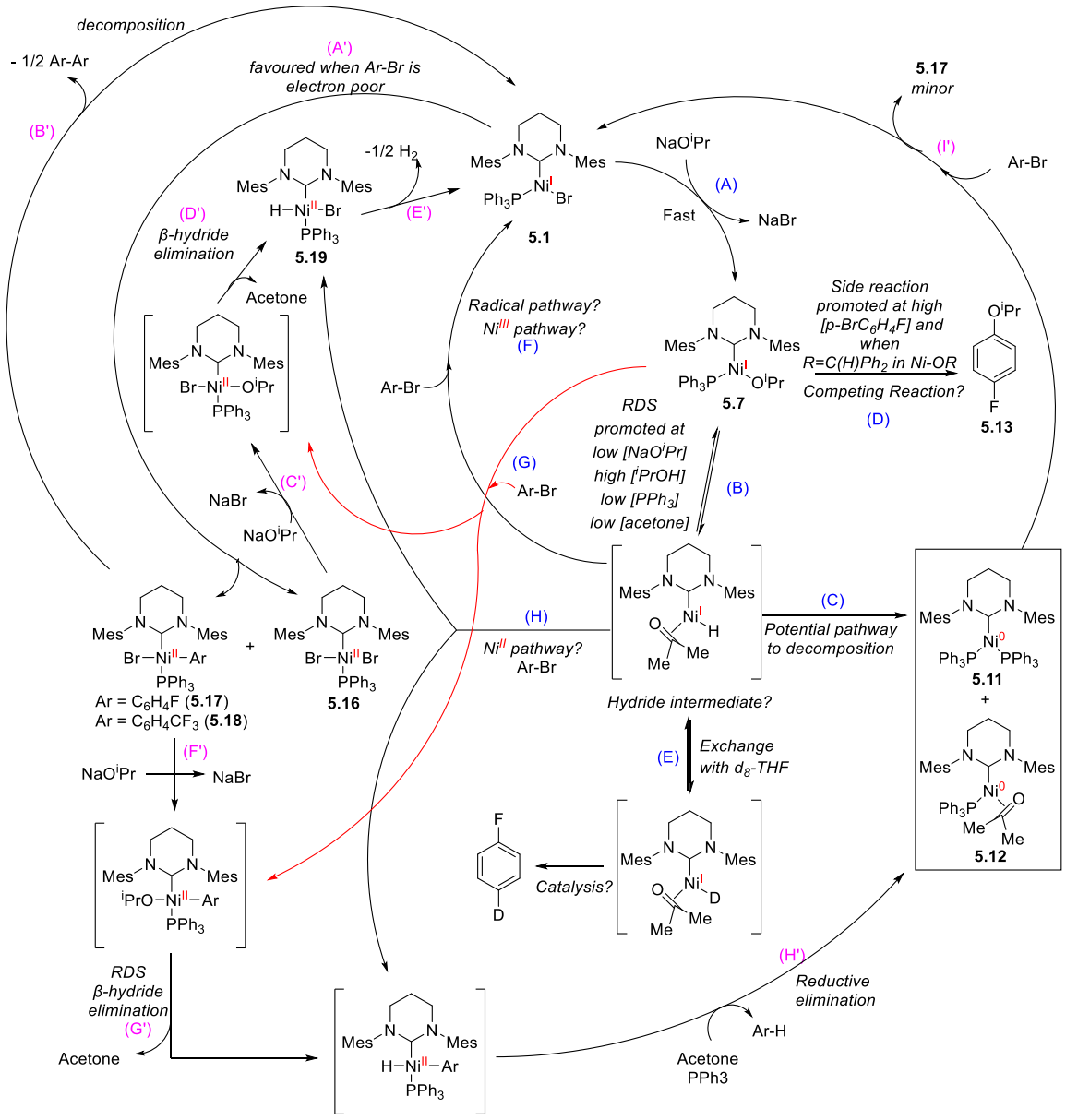


Scheme 5.10 – Proposed final scheme for Ni(RE-NHC)($PPh_3$)Br mediated HDH. Complexes in brackets represent postulated intermediates. Red arrows are only to distinguish a separate pathway for clarity.

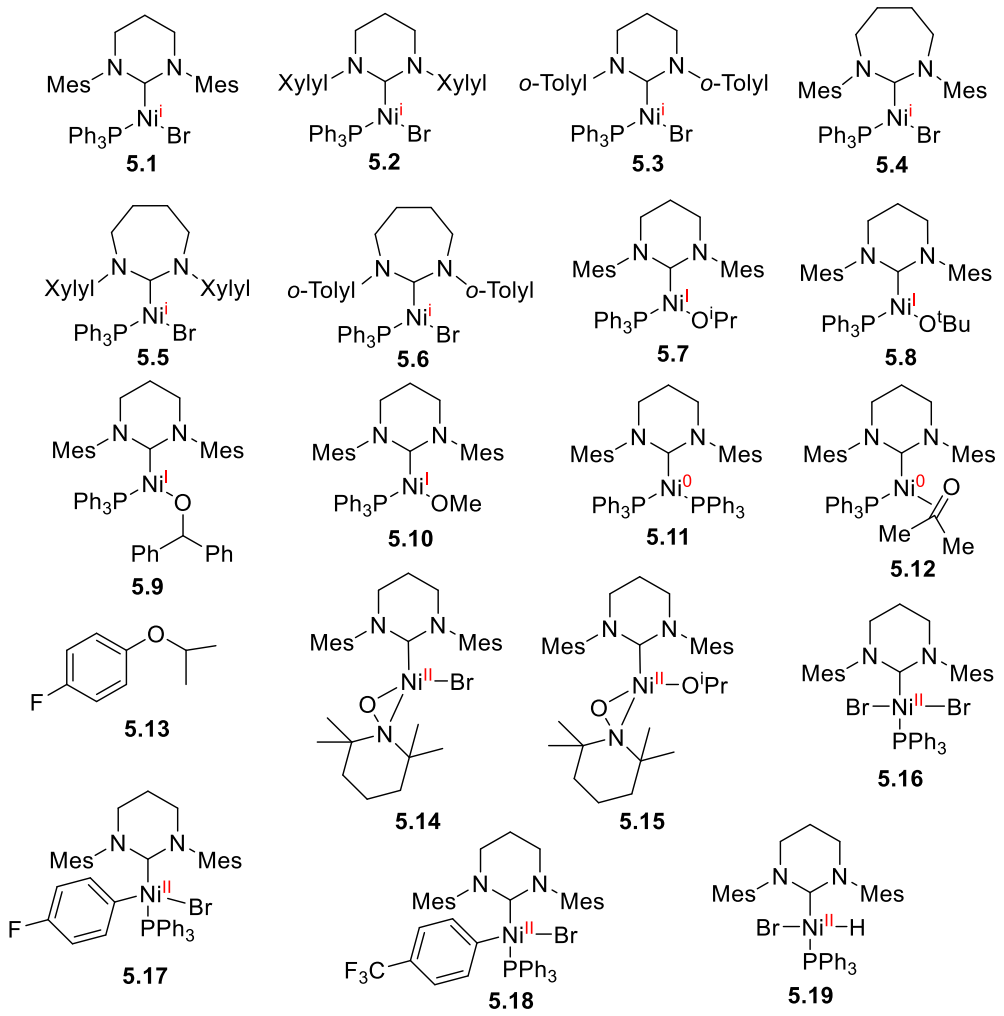


Figure 5.2 – Complexes in chapter 5.

## 5.4 – Ni(I) Alkoxide Cycle

### 5.4.1 – Overview

Our starting hypothesis was the two possible reactions suggested by Fort and Fenske (section 5.1). The first step of the reaction from **5.1** could either go *via* a salt metathesis with NaO$^i$Pr (Step A, Scheme 5.11) or by reaction with Ar-X (Step A', Scheme 5.11).[xi] Interaction with Ar-X could be in the form of a classical oxidative addition to yield a Ni(III) intermediate,[15] or in the form of a bimolecular oxidation to two independent Ni(I) centres yielding two Ni(II) complexes.[8,16] The former (Step A) and subsequent reactivity will be discussed as part of the Ni(I) alkoxide cycle, before we discuss Step A' as part of the Ni(II) cycle (section 5.5).

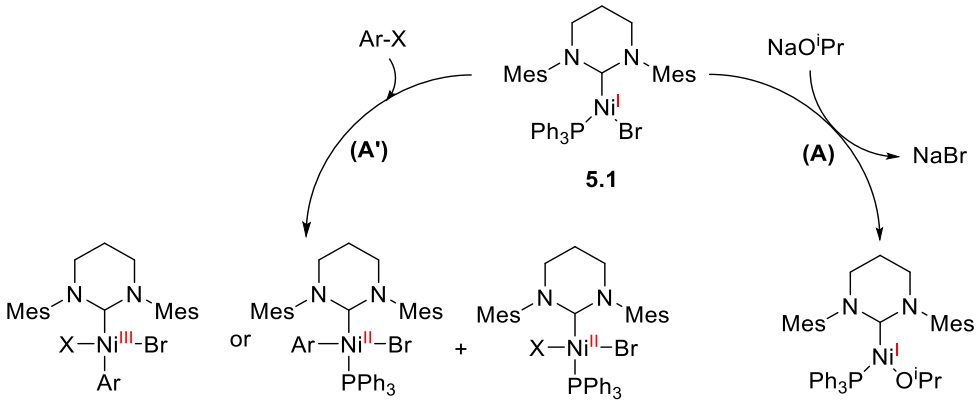


Scheme 5.11 – Potential reactions of **5.1**.

### 5.4.2 – Stoichiometric Reaction of **5.1** with NaO$^i$Pr

Addition of NaO$^i$Pr (1 equivalent) to yellow solution of **5.1** in THF led to the almost instant appearance of a deep orange solution. By $^1$H NMR spectroscopy, a new paramagnetic species was present and only minor amounts of complex **5.1** remained. Upon layering this solution with pentane at -30 °C, orange crystals (suitable for single crystal X-ray diffraction) of Ni(6-Mes)(PPh$_3$)O$^i$Pr (**5.7**) (Scheme 5.12 and Figure 5.3). Further discussion of the NMR spectroscopy and X-ray characterisation is given in section 5.4.3.

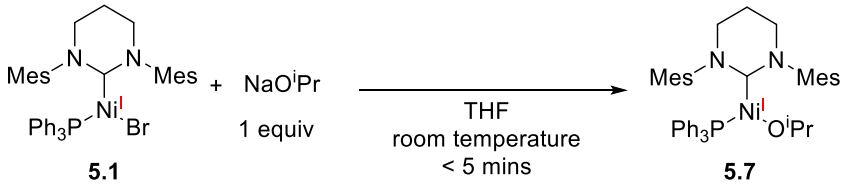


Scheme 5.12 – Formation of **5.7** from the reaction of **5.1** and NaO$^i$Pr.

[xi] Due to the fast reacting nature of alkyl-halides the rest of this study will focus on aryl halides.

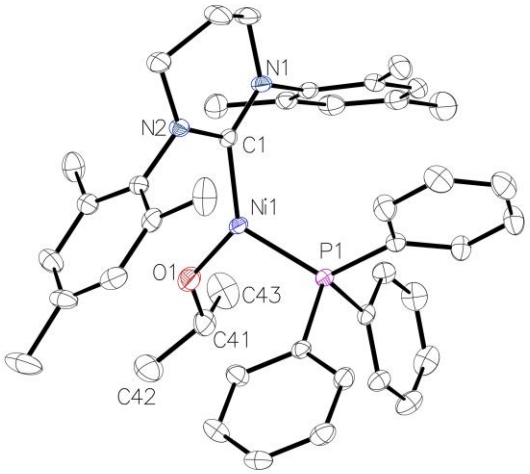


Figure 5.3 – Molecular structure of **5.7**. Hydrogen atoms have been omitted for clarity. Ellipsoids are represented at 30% probability.

To obtain cleaner compound, (with less residual **5.1**) an alternative route to **5.7** was used, employing the *in-situ* formation of KO$^{i}$Pr from KH and $^{i}$PrOH. Upon addition of $^{i}$PrOH to a suspension of **5.1** and KH in $Et_2O$, the solution went deep orange, consistent with the formation of complex **5.7**. There was no reaction of complex **5.1** with KH alone in $Et_2O$/THF or $C_6H_6$ prior to the addition of $^{i}$PrOH. Complex **5.7** was found to have poor stability in solution once extracted away from the reaction mixture (*vide infra*) and so low temperature was employed during the reaction (Scheme 5.13) which also involved rapid removal of solvent once extracted to maximise yield (56%). This compound proved to be extremely sensitive to air in THF, $C_6H_6$ and $Et_2O$ solutions, turning from orange to colourless. In addition, when exposed to air in the solid state, it rapidly turned from orange to a deep brown. X-Ray suitable crystals can also be grown from a concentrated solution of complex **5.7** in $Et_2O$ layered with pentane at -30°C. $Et_2O$ was found to be a more suitable solvent as it allows easy separation from salts and **5.1**, both of which were insoluble in $Et_2O$.

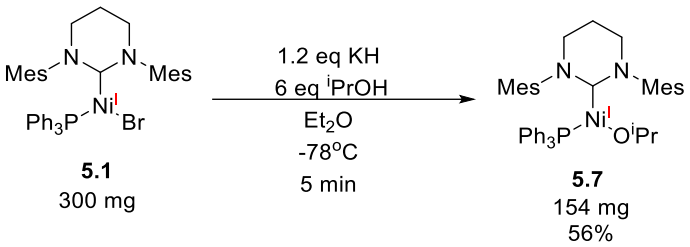


Scheme 5.13 – Optimised synthesis of complex **5.7**.

## 5.4.3 – Characterisation of **5.7** and Synthesis and Characterisation of its Analogues

Using a similar synthetic procedure to Scheme 5.13, three other alkoxides derivatives were prepared: Ni(6-Mes)($PPh_3$)O$^t$Bu (**5.8**), Ni(6-Mes)($PPh_3$)OC(H)$Ph_2$ (**5.9**) and Ni(6-Mes)($PPh_3$)OMe (**5.10**) (Figure 5.4). Like **5.7**, all were yellow/orange in solution. Complexes **5.7** – **5.10** all displayed paramagnetic $^1$H NMR spectra with signals in the range δ 31.7 to -17.5 ppm, similar to **5.1**.[10] Both $^{13}$C and $^{31}$P NMR spectra revealed no visible signals and the room temperature solution magnetic moments of **5.7** – **5.10** ranged from 1.82 – 2.08 μB in THF (Evans method), suggesting a S = ½ ground state. X-ray suitable crystals were grown using similar conditions to complex **5.7**.

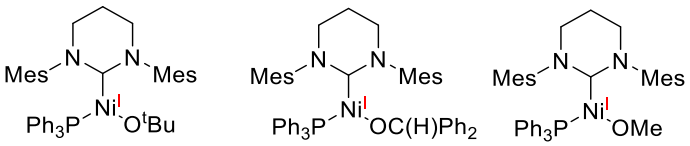


**5.8** **5.9** **5.10**

Figure 5.4 – Three coordinate Ni alkoxide analogues of complex **5.7**.

X-ray diffraction studies revealed similar distorted trigonal planar geometries for all four complexes (Figure 5.5), whose selected angles and bond lengths are summarised in Table 5.4. The widest angle for all the alkoxide complexes is the $C_{NHC}$-Ni-O angle, which ranged from 131.23(9) - 135.20(8)°. Ni-$C_{NHC}$ bond lengths range from 1.9155(19) – 1.928(2) Å which is similar to other three coordinate NHC-Ni(I) complexes.[17] Between the alkoxides the only notable differences were in **5.7**, with both a shorter Ni-$C_{NHC}$ bond length and wider $C_{NHC}$-Ni-O angle. There are few examples of (NHC)Ni-OR complexes in the literature which do not exist in the form of a metallacycle,[18,19] and one example of a $Ni^I$(NHC)OR complex in the form of the low coordinate $Ni^I$(IPr)(O(2,6-$^t$Bu$_2$-4-tolyl)). The Ni-O bond lengths of this Ni(I) complex were found to be 1.778(2) Å and 1.7612(19) Å,[xii] which is significantly shorter by comparison to **5.7** – **5.10**. The Ni-NHC bond distance was also found to be shorter in this complex compared to **5.7** – **5.10**. While not directly comparable, complexes **5.7 – 5.10** were found to have slightly shorter Ni-O distances to the 4 coordinate ($^{iPr}$PCP)$Ni^{II}$-OR reported by Cámpora, with their ($^{iPr}$PCP)$Ni^{II}$-O$^i$Pr complex also exhibiting the shortest Ni-O bond of the monomeric species (1.852(9) Å).[20]

[xii] Two molecules were found in the unit cell, with a third containing a hydride.

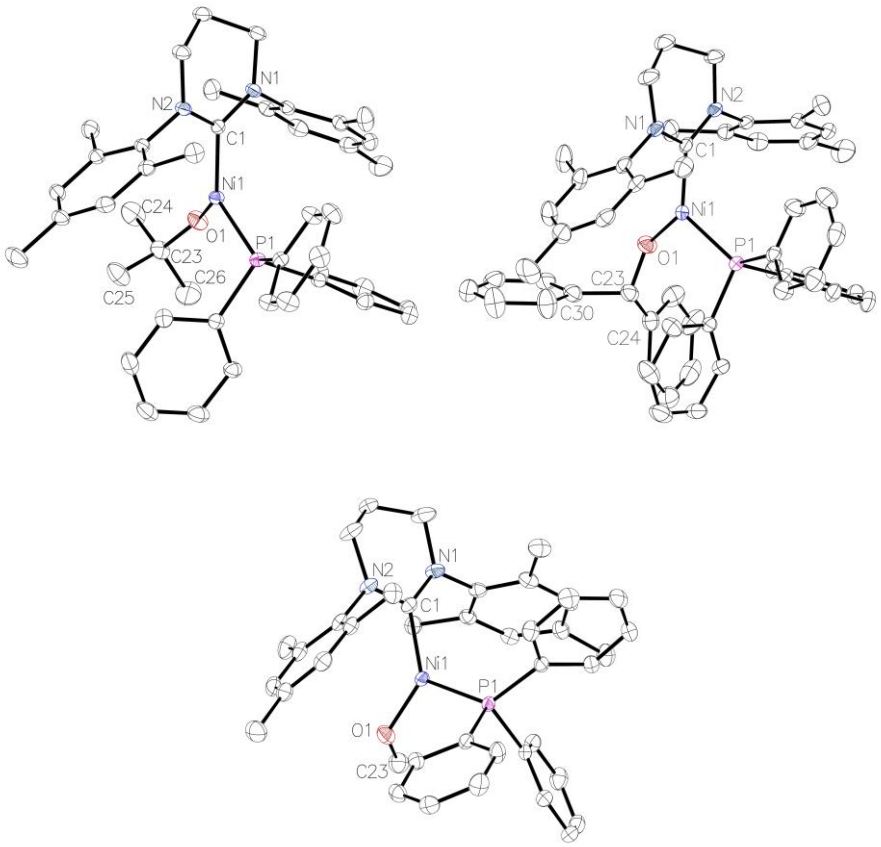


Figure 5.5 – Molecular structures of (from left to right, top to bottom) **5.8**, **5.9** and **5.10**. Thermal ellipsoids shown at 30% probability. Hydrogen atoms omitted for clarity.

Table 5.4 – Selected bond lengths and angles for compounds **5.7**, **5.8**, **5.9** and **5.10**, along with **5.1** for comparison.

| Compound | Ni-$C_{NHC}$ (Å) | Ni-P (Å) | Ni-O (Å) | $C_{NHC}$-Ni-P (°) | $C_{NHC}$-Ni-O (°) | P-Ni-O (°) |
|---|---|---|---|---|---|---|
| **5.7** | 1.9155(19) | 2.1749(6) | 1.8487(17) | 113.60(6) | 135.20(8) | 110.92(5) |
| **5.8** | 1.9262(14) | 2.1883(4) | 1.8220(11) | 114.11(4) | 132.01(6) | 113.05(4) |
| **5.9** | 1.928(2) | 2.1898(7) | 1.848(2) | 117.51(7) | 131.23(9) | 111.26(7) |
| **5.10** | 1.9243(17) | 2.1941(5) | 1.8427(14) | 111.53(5) | 132.26(7) | 116.00(5) |
| **5.1** | 1.942(2) | 2.2188(6) | (Ni-Br) 2.3331(3) | 117.01(6) | ($C_{NHC}$-Ni-Br) 133.46(6) | (P-Ni-Br) 109.531(19) |

EPR spectra of the new Ni-alkoxide species were also measured to provide further characterisation. Spectra of the new alkoxide complexes **5.7 – 5.10** are shown in Figure 5.6. The EPR measurements were carried out at 140 K by Dr Emma Richards, Prof Damien Murphy and

Dr Andrea Foli at Cardiff University. The *g* tensor components which have been simulated are shown in Table 5.5.

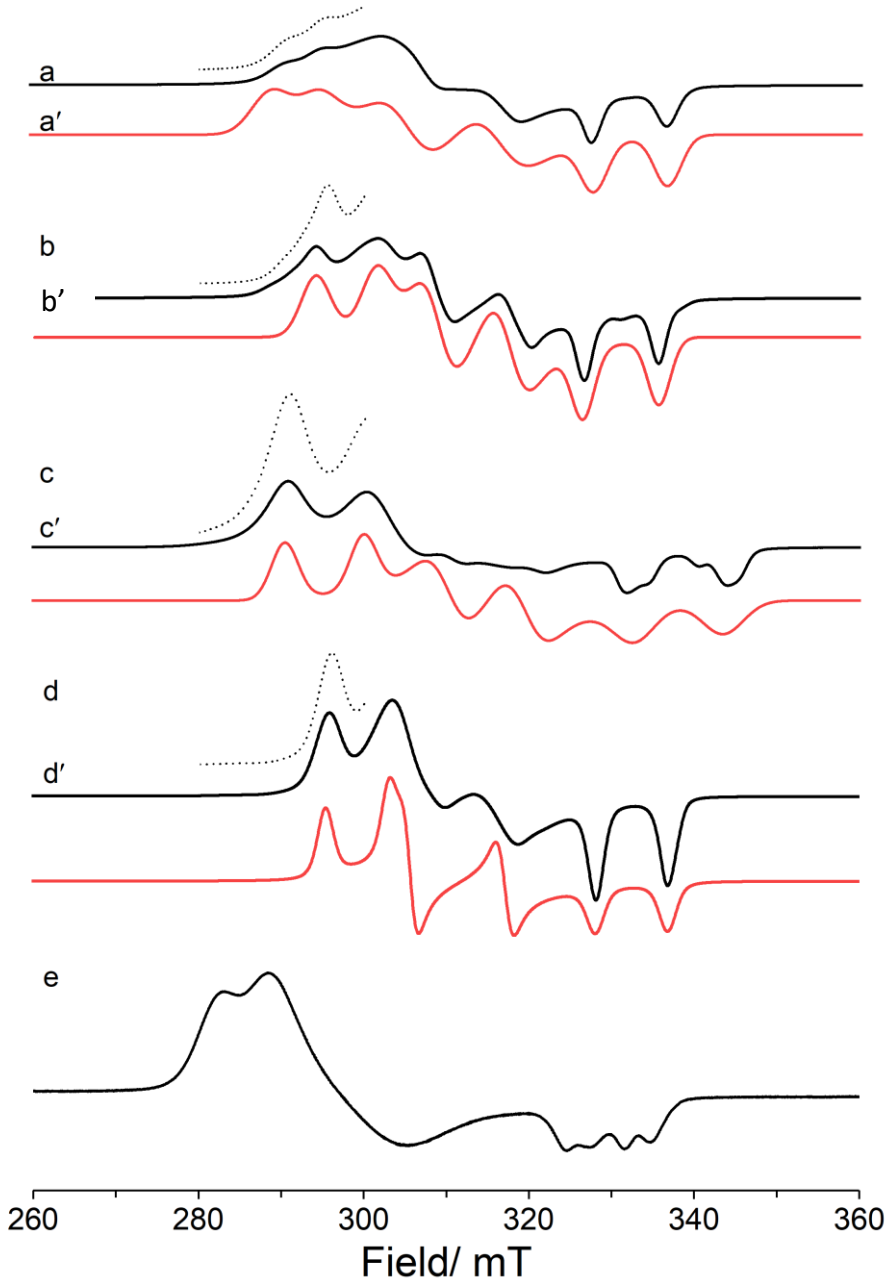


Figure 5.6 – CW X-band EPR spectra (140 K). a) **5.7** b) **5.8** c) **5.9** d) **5.10**. The red spectra in each represents the simulated data. e) Spectrum of **5.1** for comparison. Dotted lines are expansions of the black lined spectra for clarity.

Table 5.5 – Spin Hamiltonian parameters for complexes **5.7 – 5.10**. Complex **5.1** is also included as a comparison.

| Complex | $g_1$ | $g_2$ | $g_3$ | $g_3 - g_2$ | $g_2 - g_1$ | ${}^{P}A_1$ / *MHz* | ${}^{P}A_2$ / *MHz* | ${}^{P}A_3$ / *MHz* |
|---|---|---|---|---|---|---|---|---|
| **5.7** | 2.045 | 2.16 | 2.272 | 0.112 | 0.115 | 210 | 250 | 230 |
| **5.8** | 2.039 | 2.185 | 2.27 | 0.085 | 0.146 | 220 | 235 | 270 |
| **5.9** | 2.039 | 2.157 | 2.28 | 0.123 | 0.118 | 230 | 230 | 270 |
| **5.10** | 2.044 | 2.184 | 2.321 | 0.137 | 0.14 | 202 | 312 | 266 |
| **5.1** | 2.073 | 2.270 | 2.365 | 0.095 | 0.197 | 186 | 206 | 208 |

As with complex **5.1**,[14] the alkoxide complexes exhibit a rhombic nature and significantly broadened linewidths which arise from the large superhyperfine coupling with the $^{31}$P nucleus. It should be noted that the *g*-tensor is a descriptor of the electronic ground state of the complex, which in turn can be correlated with the geometry at the metal centre. As previously noted by Whittlesey and co-workers,[21] the fact that one component of the g-tensor ($g_1$) is close to the free spin value of $g_e$ (2.0023) indicates a considerable $3dz^2$ character in the SOMO. The shift from $g_e$ for the remaining two g-values results from the large spin-orbit coupling parameter for Ni ($\zeta Ni^+$ = 565 $cm^{-1}$). A complete description of the electronic ground state can be determined from Density Functional Theory calculations, which are currently ongoing. Furthermore, the magnitude of phosphorus hyperfine coupling is also an indication of the extent of electron delocalisation across the complex and ligand backbone. This was found to be greater for the Ni(I)-OR complexes in comparison to **5.1**. Ultimately, the electronic ground state and delocalisation of electron spin density may reflect in the resulting reactivity of the complex, due to variances of ligand lability and propensity for creating vacant coordination sites for incoming substrates. A more complete discussion of the EPR data is beyond the scope of this thesis.

To provide more information on the nature of the Ni complexes, cyclic voltammetry was employed to assess the redox potentials. Due to the poor stability of **5.7**, **5.8** and **5.10** in solution (see section 5.4.4) and the time required to run measurements, only complex **5.9** was used. **5.1** and **5.9** were compared by cyclic voltammetry at a 3 mm diameter glassy carbon electrode as 2 mM solutions in THF with $[N(^nBu)_4]PF_6$ electrolyte (20 mM). The results for **5.1** and **5.9** are shown below in Figure 5.7. Each compound demonstrated irreversible chemical oxidation and reductions. Complex **5.1** demonstrated an onset of oxidation at 0.0 V vs $FeCp^*_2{}^{+/0}$ and an onset of reduction at -2.2 V vs $FeCp^*_2{}^{+/0}$. The alkoxide containing **5.9** was found to be easier to oxidise with an onset of oxidation at -0.3 V (vs $FeCp^*_2{}^{+/0}$). An onset of reduction was also observed at -1.9 V (vs $FeCp^*_2{}^{+/0}$). The smaller difference between the onset of oxidation and reduction of

**5.9**, suggests the HOMO/LUMO gap is smaller than in **5.1**. This is also supported by the difference in colour between the two complexes (**5.1** yellow vs **5.9** yellow orange). Since **5.9** was found to be easier to oxidise than **5.1**, it suggests this complex is more likely to favour interaction with the aryl halide.

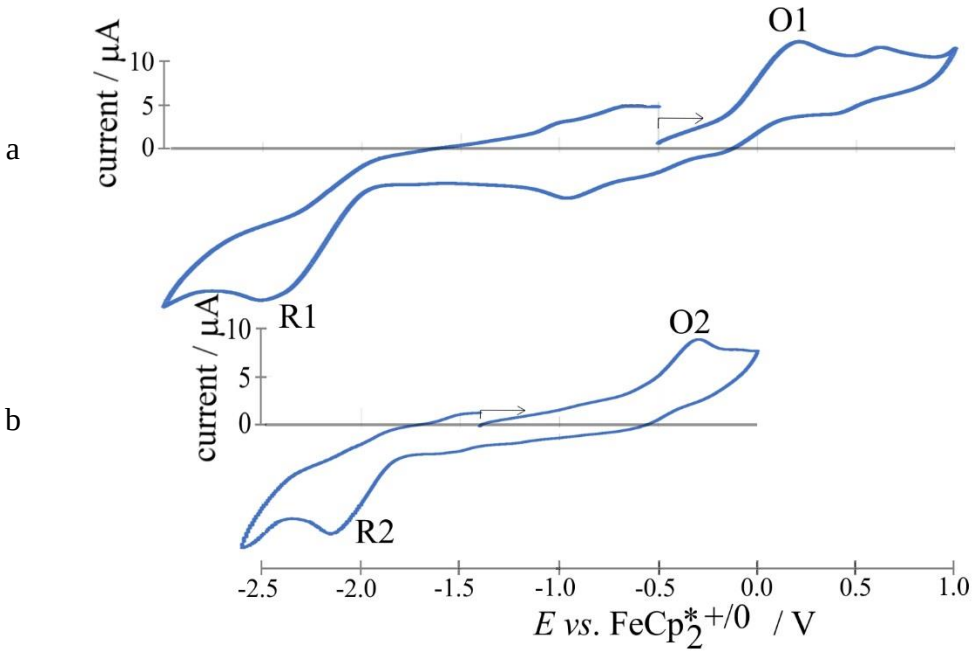


Figure 5.7 – Cyclic voltammograms of compounds a) **5.1** and b) **5.9** vs $FeCp^*_2{}^{+/0}$ in THF (scan rate 0.05 V $s^{-1}$, 2 mM). Arrows indicate scanning direction.

## 5.4.4 – Stability of **5.7 – 5.10**

While in solution (< 10 mins), **5.7** shows slow growth of three signals by $^{31}P$ NMR spectroscopy in both $d_8$-THF and $C_6D_6$. The $^{31}P\{^1H\}$ NMR signals resided at 16.8, 37.7 and 40.5 ppm. The two lowest frequency signals were assigned to be the Ni(0) complexes Ni(6-Mes)$(PPh_3)_2$ (**5.11**; 16.8 ppm) and Ni(6-Mes)$PPh_3$(O=C(H)$Me_2$) (**5.12**; 37.8 ppm) (Scheme 5.14). Complex **5.11** was previously reported and although complex **5.12** could not be isolated,[22] addition of acetone to **5.11** gave a $^{31}P\{^1H\}$ NMR signal suggestive of **5.12**. Analogues of **5.12** were also reported and have very similar shifts to the presumed acetone complex (Figure 5.8).[22]

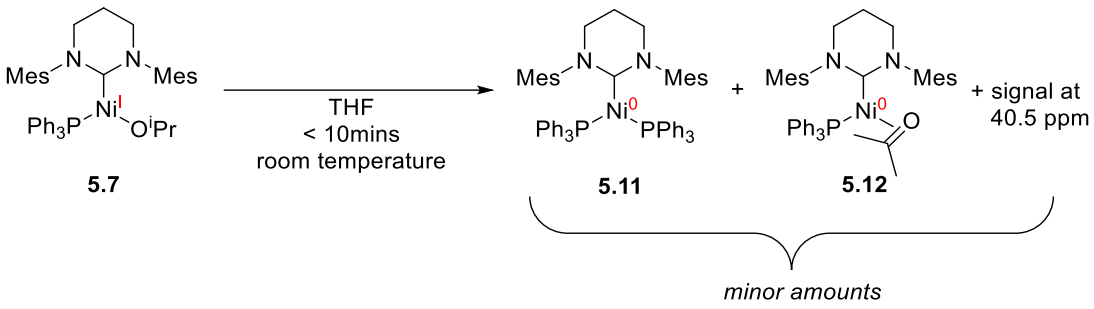


Scheme 5.14 - Decomposition of **5.7** in THF.

Within 1 hour, orange solutions of **5.7** darkened to a deep red. Paramagnetic signals were observable in the $^{1}$H NMR spectrum up to three days in solution, although in reduced amounts suggestive of **5.7** decomposing slowly. The growth of other unassignable signals was detected during this period making the spectrum unassignable and inconclusive to further analysis. By $^{31}$P{$^{1}$H} NMR spectroscopy, **5.11** and **5.12**, along with minor amounts of the species at 40.5 ppm, remained the only detectable signals over time. The nature of how we obtain complexes **5.11** and **5.12** in Scheme 5.14 is unknown. It could be linked to the unknown species seen at 40.5 ppm.

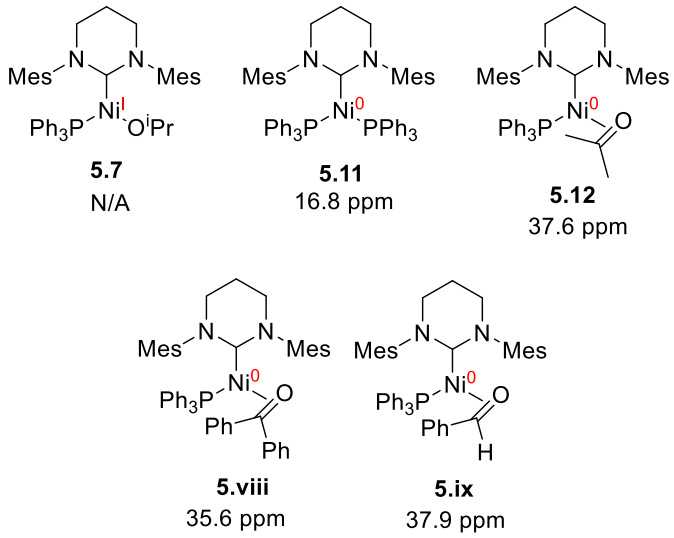


Figure 5.8 - $^{31}$P{$^{1}$H} chemical shifts of complexes **5.7**, **5.11**, **5.12**, **5.viii** and **5.ix**. Complexes **5.11**, **5.viii** and **5.ix** were reported previously.[22]

Like complex **5.7**, the other alkoxide complexes **5.8**, **5.9** and **5.10** showed decomposition in solution over time, but at differing rates (Figure 5.9). Complex **5.10** was the most unstable in solution; immediate darkening of orange $d_8$-THF solutions to red took place at room temperature. Complexes **5.8** and **5.9** only decomposed at elevated temperatures (50 °C) over 1 h and 16 h respectively. Milstein and Blum found that increasing the substitution of the -R group on their Ir(III)-OR complexes, decreased the rate of β-hydride elimination in the order Me > Et > $^{i}$Pr,[23] which could support the difference in decomposition rates between the alkoxide complexes if this

was *via* a hydride intermediate. Complexes **5.7** and **5.9** decomposed to form **5.11** as well as **5.12** (from **5.7**) or **5.viii** (from **5.9**). The decomposition of complex **5.9** gave almost quantitative formation of complex **5.viii**. For complexes **5.8** and **5.10**, decomposition gave NMR spectra that were inconclusive as to the exact nature of the products. Scheme 5.15 summarises the most pertinent findings to this point.

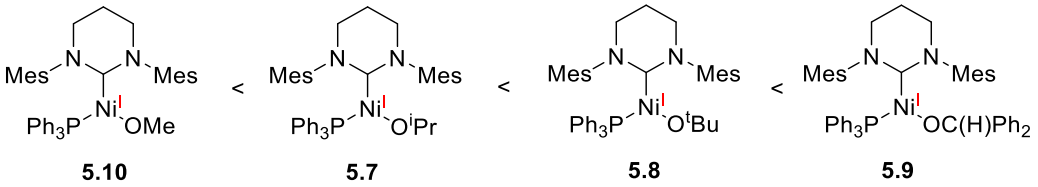


Figure 5.9 - Relative stabilities of alkoxides **5.7** – **5.10**. **5.10** being the least stable.

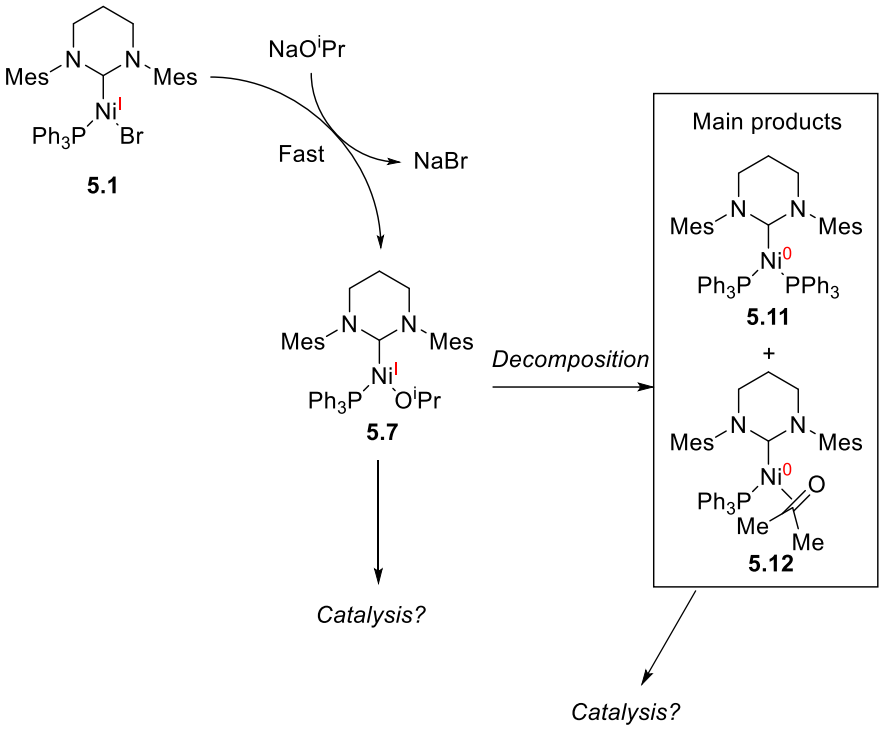


Scheme 5.15 – Synthesis and stability of Ni(I)-O$^i$Pr complex **5.7**.

## 5.4.5 – Reactions monitored by EPR spectroscopy.

The propagation of the HDH cycle was probed by EPR spectroscopy. 5:1 THF:toluene solutions of the reactions (*vide infra*) were prepared in an Ar-filled glovebox.[xiii] The samples were sealed and frozen upon removal from the box and X-band EPR spectra were then recorded at 140 K.

The EPR spectrum of **5.1** is shown in Figure 5.10a.[14] Figure 5.10b shows the spectrum following addition of 1-chloro-4-fluorobenzene where no change to the EPR spectrum was observed. In the presence of NaO$^{i}$Pr, the EPR spectrum was significantly different indicating a change to the Ni(I) centre, this was a result of the formation of **5.7** which was observed after <5 mins. The spectrum remained unchanged for at least 1.5 h (Figure 5.10c and d). The lack of further reactivity supports the need for higher temperature found for the HDH of chloro substrates (section 5.2.2). **5.1** was also exposed to 1-bromo-4-fluorobenzene in the presence of NaO$^{i}$Pr (Figure 5.11). Again after < 5 mins, the EPR spectrum revealed formation of **5.7** (Figure 5.11a), although after 4 h, a weak signal was observed suggestive of decomposition or a formation of diamagnetic species (Figure 5.11b).[xiv]

[xiii] Toluene was added to ensure the quality of the frozen polycrystalline glass to improve quality of the EPR spectra.

[xiv] At the time of this measurement being taken, there was no access to sealable J. Youngs EPR tubes, and so the possibility of reaction with $O_2$ cannot be rules out.

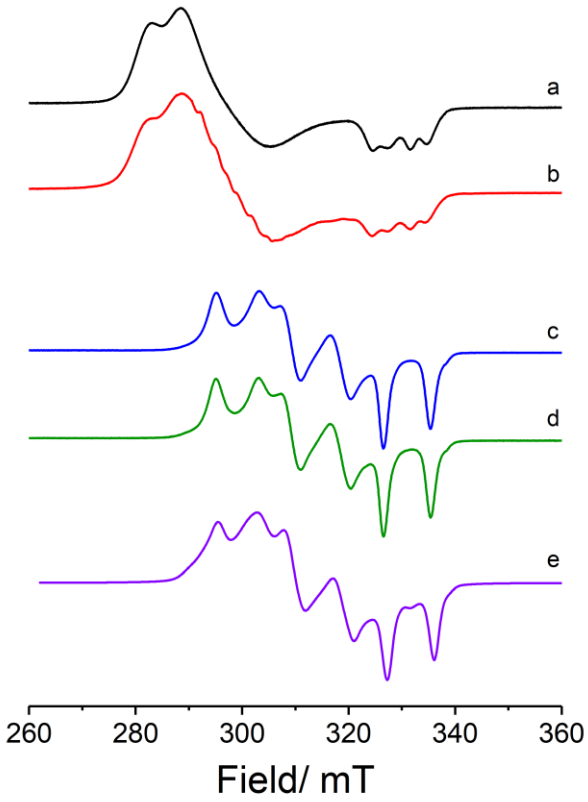


Figure 5.10 – CW X-band EPR spectra (140 K). a) **5.1**; b) **5.1** + 1-chloro-4-fluorobenzene, t = < 5 mins; c) **5.1** + 1-chloro-4-fluorobenzene + NaO$^{i}$Pr, t = < 5 mins; d) **5.1** + 1-chloro-4-fluorobenzene + NaO$^{i}$Pr after 1.5 h at room temperature; e) The spectrum of **5.7** for comparison.

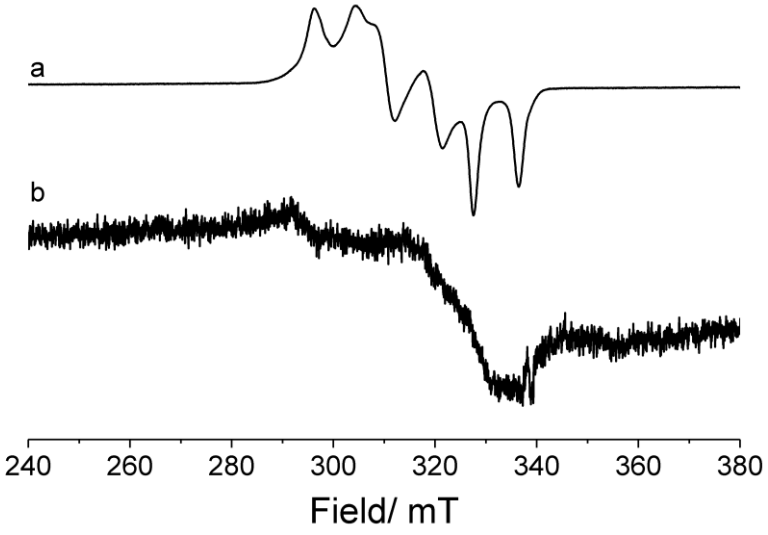


Figure 5.11 - CW X-band EPR spectra (140 K). a) complex **5.1** + 1-bromo-4-fluorobenzene + NaO$^{i}$Pr, t = < 5 mins; b) **5.1** + 1-bromo-4-fluorobenzene + NaO$^{i}$Pr, t = 4 h at room temperature.

EPR spectroscopy was also used to probe the reaction of **5.7** and 4-bromoanisole (Figure 5.12). The 140 K EPR spectra of a mixture of **5.7** and 4-bromoanisole reacted for <5 mins at room temperature (Figure 5.12b) shows the presence of **5.7** alongside traces of the Ni(I)-Br complex **5.1**. Upon sampling after 5 mins, the latter is now clearly the major component in solution (Figure 5.12c). Most importantly, **5.7** and **5.1** were the only detectable paramagnetic species.

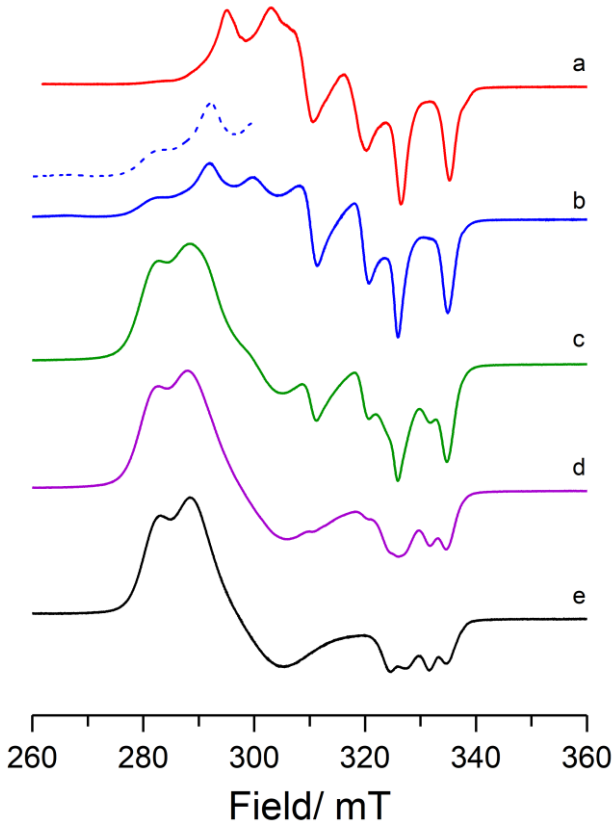


Figure 5.12 – CW X-band EPR spectra (140 K). a) **5.7**; b) **5.7** + 4-bromoanisole, t = < 5 min; c) t = 5 mins; d) t = 10 mins; e) spectra of **5.1** for comparison. Dotted line is present to help the clarity of the comparisons of spectra a-e.

To confirm catalytic turnover with **5.7**, a catalytic hydrodehalogenation reaction with 4-bromoanisole (Scheme 5.16) was then examined by EPR spectroscopy (Figure 5.13). A sample was taken from the mixture immediately as the reaction started and frozen (140 K) to give a spectrum at t = < 5 mins (Figure 5.13a). The spectrum shows a mixture of complexes **5.1** and **5.7** which converted completely to **5.1** over 2 hours at room temperature (Figure 5.13b).

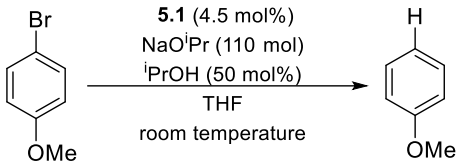


Scheme 5.16 – Catalytic conditions monitored by EPR spectroscopy.

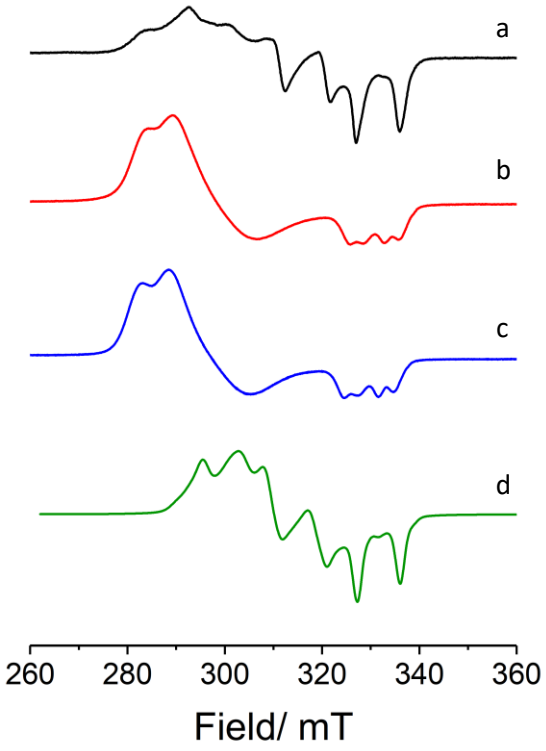


Figure 5.13 - CW X-band EPR spectra (140 K) from a mixture of **5.1** (4.5 mol %), 4-bromoanisole (0.134 mmol), NaO$^{i}$Pr (110 mol%) and $^{i}$PrOH (50 mol%) in THF (1 mL). Aliquots were taken from the mixture at the corresponding time point, mixed with THF/Tol (3:1) and frozen at 140K for EPR spectroscopy. a) t = <5 mins; b) t = 2 h; the spectra of **5.1** (c) and **5.7** (d) are provided for comparison.

The EPR experiments support the conclusion that **5.1** and **5.7** are catalytically relevant as they have been shown to exist in mixtures in both stoichiometric and catalytic systems. It has also identified **5.7** as a potential resting state, as transformations involving the formation of **5.7** show its presence without change or loss of signal until **5.1** is formed.

However, the experiments failed to identify any new intermediates. This could be due to (i) the concentration of such an intermediate could be very small (due to a short lifetime) thus the signal could be lost amongst the other signals, or (ii) the reaction proceeds *via* diamagnetic species which would be EPR silent (Scheme 5.17).

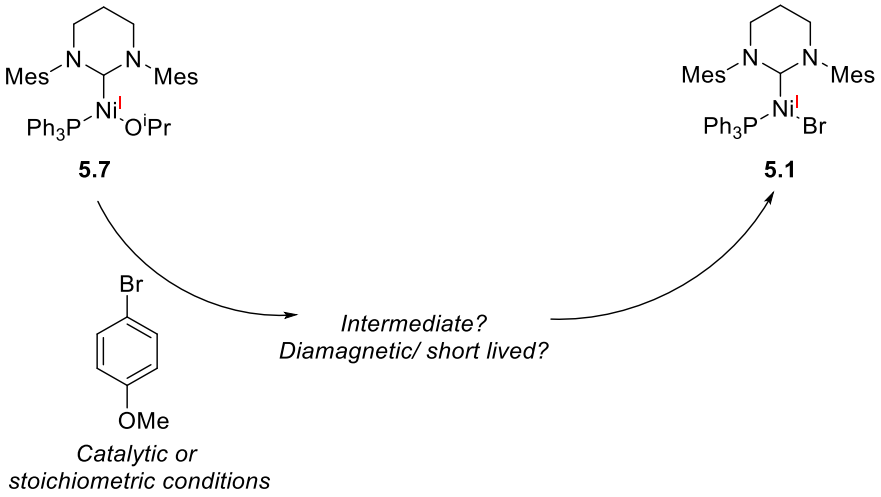


Scheme 5.17 – Postulated step based upon results in section 5.4.6.

## 5.4.6 –Kinetic Studies

To gain further insight into the reaction mechanism, kinetic studies were undertaken. A model system was used (Scheme 5.18) which made it possible to monitor the reaction by quantitative $^{19}F$ NMR spectroscopy using 1,4-difluorobenzene as an internal standard. Paramagnetism did not limit the data collection quality and to ensure accurate integration data, a d1 value of 25 seconds was used to make sure complete relaxation of $^{19}F$ signals took place.

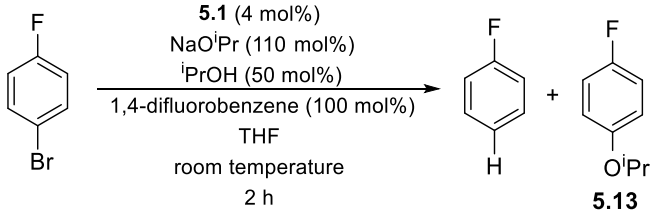


Scheme 5.18 - Initial model system for kinetic studies.

Figure 5.14 shows the rate at which [1-bromo-4-fluorobenzene] decreases is similar to that at which [$C_6H_5F$] grows. In addition to these species, 4-$FC_6H_4O^iPr$ (**5.13**) and an unknown Ni species (labelled Ni species **A**) is observed.[xv] Ni species **A** is present in a maximum of 1.5 % (ca. 38 % of the catalyst) and is consumed by the end of the reaction suggesting catalytic relevance. The organic product **5.13** slowly increases over time (but only to a maximum of 8 %) and then does not deplete suggesting it is not an intermediate on the reaction pathway. It is also worth noting catalytic runs using **5.13** as a substrate failed to yield any fluorobenzene, further confirming that it is not an intermediate on the catalytic cycle and instead a by-product.

[xv] This species is identified later in the chapter (section 5.5.7) and will be discussed then.

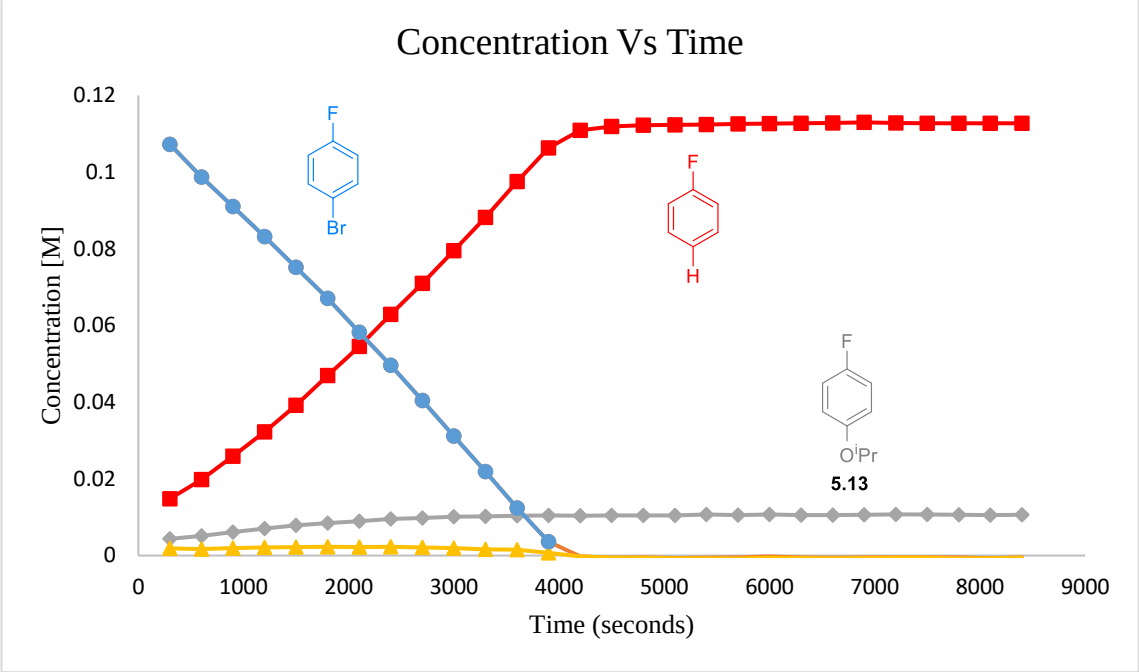


Figure 5.14 - Kinetic plot for Scheme 5.18. Blue = [1-bromo-4-fluorobenzene]; Red = [$C_6H_5F$]; Grey = [**5.13**]; Yellow = Ni species **A**.

A reaction in $d_8$-THF was performed to allow additional analysis by $^{1}H$, $^{19}F\{^{1}H\}$ and $^{31}P\{^{1}H\}$ NMR spectroscopy to identify any other intermediates and to potentially provide another way to monitor the reaction (Scheme 5.19).

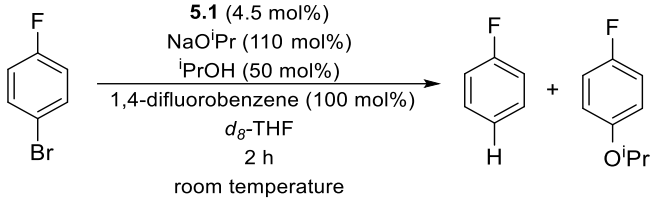


Scheme 5.19 – Conditions used for monitoring a catalytic run by $^{1}H$, $^{19}F\{^{1}H\}$, $^{31}P\{^{1}H\}$ NMR spectroscopy.

By $^{19}F\{^{1}H\}$ NMR spectroscopy: $C_6H_5F$ (-114.2 ppm), 1-bromo-4-fluorobenzene (-116.5 ppm), 1,4-difluorobenzene (-120.7 ppm), **5.13** (-125.6 ppm) and Ni species **A** (-128.5 ppm) were observed (Figure 5.15). The $C_6H_5F$ signal had an additional signal close lying which was later identified to be *p*-$d_1$-$C_6H_4FD$ by mass spectrometry. This was also supported by the differing intensities of the residual protio THF in $d_8$-THF by $^{1}H$ NMR spectroscopy, where the peak representing the C3-H and C4-H positions of THF had grown (Figure 5.16).[24] The signal at -128.5 ppm representing Ni species **A** was found to represent *ca.* 35% of the Ni species in solution as observed previously. The $^{31}P\{^{1}H\}$ NMR revealed two signals, one which was unassigned (23 ppm) and a broad signal at -5 ppm suggesting free $PPh_3$ was present. Considering the large

amount of species **A** in the $^{19}F\{^{1}H\}$ NMR spectrum, the signal at 25 ppm in the $^{31}P$ NMR is suggested to be linked to this.

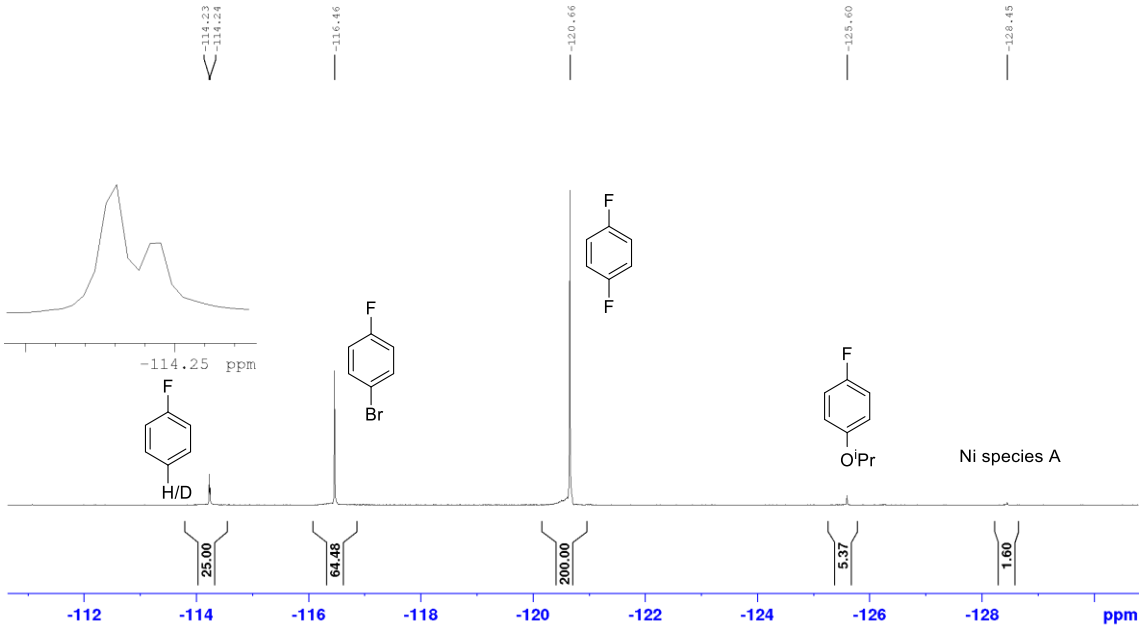


Figure 5.15 – $^{19}F\{^{1}H\}$ NMR spectrum (470 MHz) of a HDH catalytic run (Scheme 5.19) after 10 mins.

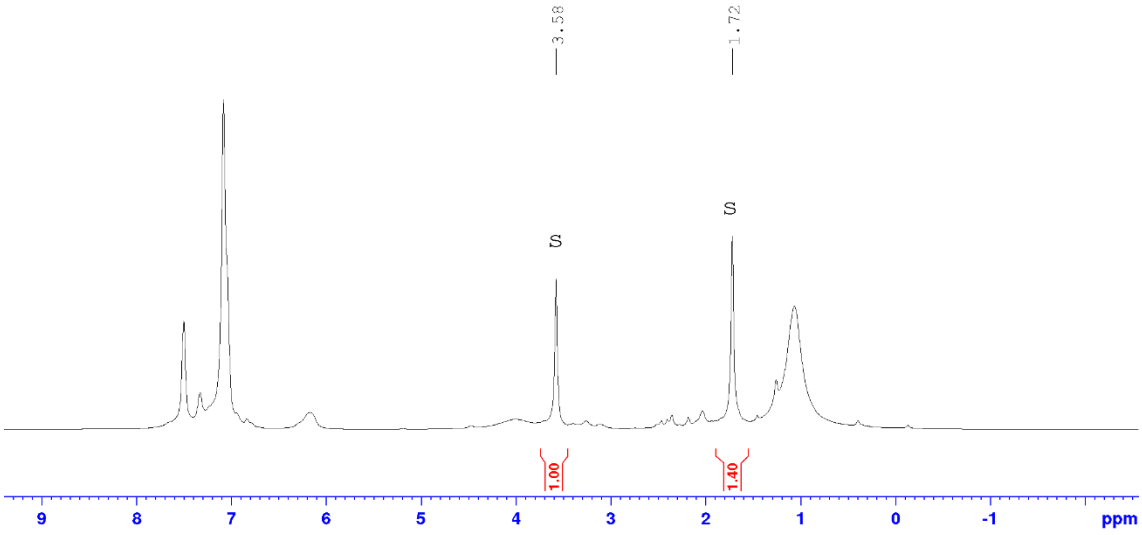


Figure 5.16 – Differing peak intensities of the residual protio THF in $d_8$-THF.

After 2 h there were very small amounts of **5.7** observable by $^{1}H$ NMR spectroscopy. By $^{19}F\{^{1}H\}$ NMR spectroscopy almost full conversion of 1-bromo-4-fluorobenzene was observed accompanied by the disappearance of Ni species **A**. In addition, the signals associated with $C_6H_5F$ and *p*-$d_1$-$C_6H_4FD$ were found to have grown in a similar ratio to what was observed at 10 mins (Figure 5.15 vs Figure 5.17).

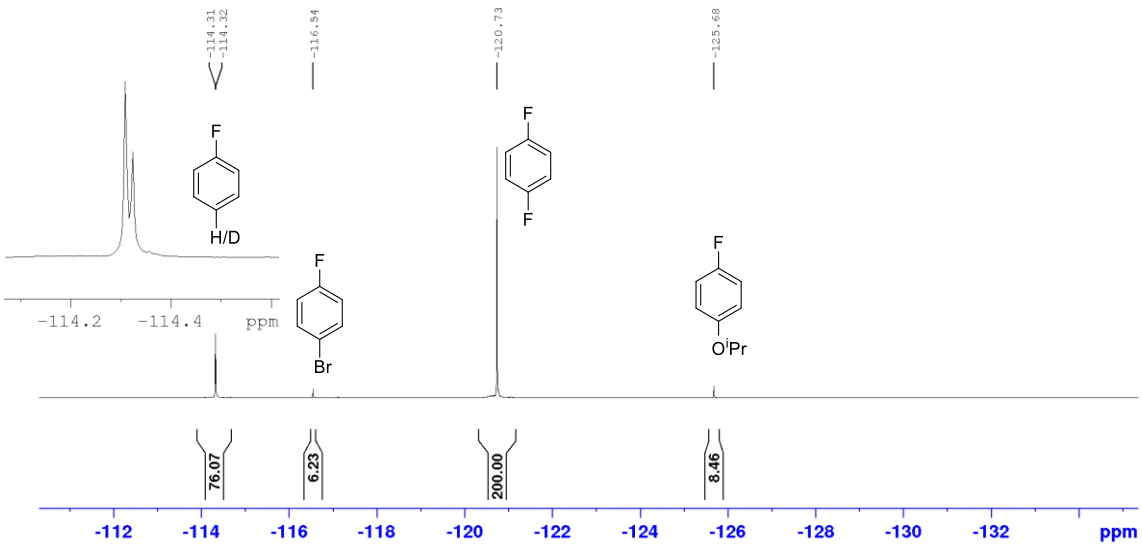


Figure 5.17 - $^{19}F\{^{1}H\}$ NMR spectrum (470 MHz) of a HDH catalytic run (Scheme 5.19) after 2 h.

Considering the deuterium incorporation when *d*$_8$-THF was utilised, the kinetic studies were carried out in protio THF. The order of reaction with respect to **5.1** was investigated by varying the concentration of **5.1** and keeping a constant stock solution of the substrates. The reaction was monitored over a 2 h period with data collected every 5 mins. Plots of [$C_6H_5F$] or [1-bromo-4-fluorobenzene] vs time were plotted to give the initial rates which are then plotted as initial rate vs [$C_6H_5F$] or [1-bromo-4-fluorobenzene] (Figure 5.18). This plot shows both the consumption of 1-bromo-4-fluorobenzene and formation of $C_6H_5F$ are linear, with a slight difference in gradient between them. The slightly higher rate of consumption can be attributed to the formation of the side product (**5.13**) in the background, that aids the loss the starting material (see Table 5.6 for values). The linear plot suggests the reaction is first order with respect to catalyst.[xvi]

[xvi] Replacing **5.1** with the Ni-O$^i$Pr precursor **5.7** also gave a linear plot 1$^{st}$ order plot but with a lower set of initial rates. Due to potential decomposition in solution (section 5.5.4), the concentration of stock solutions of **5.7** may not stay constant. For this reason, these results have not been included.

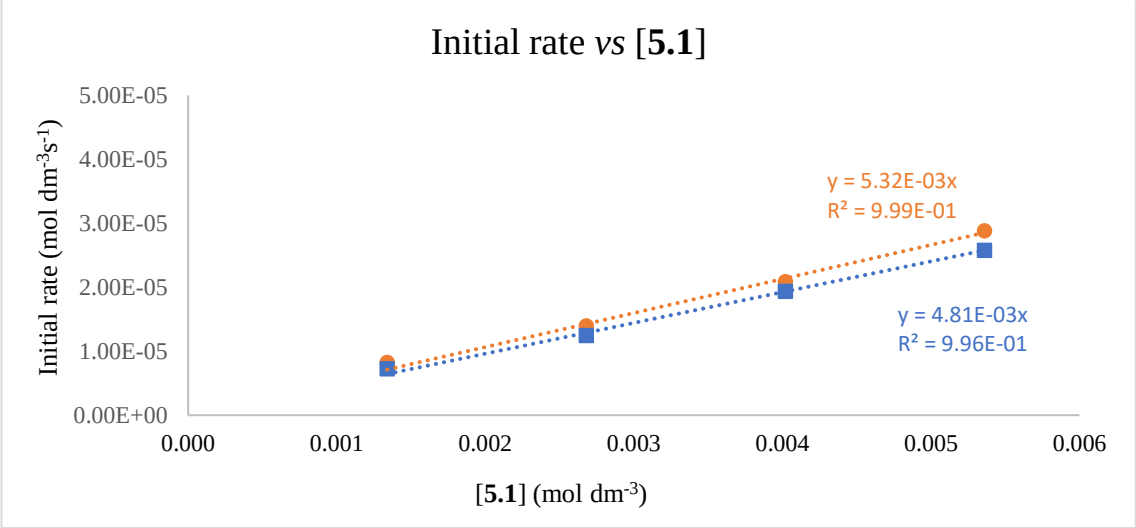


Figure 5.18 – Initial rate *vs* [**5.1**]. Orange = consumption of 1-bromo-4-fluorobenzene. Blue = formation of $C_6H_5F$.

The role of each of the other substrates was individually examined at different concentrations in order to probe their relevance to the rate determining step of the reaction. Figure 5.19 shows a plot of initial rate *vs* [1-bromo-4-fluorobenzene], which indicates a zero-order relationship. Again, a slight gradient is observed for the consumption of 1-bromo-4-fluorobenzene due to the formation of **5.13** (see Table 5.6, *vide infra*). The study was also repeated at 4 mol % [Ni] where little difference was seen in the rate supporting zeroth order (see appendix).

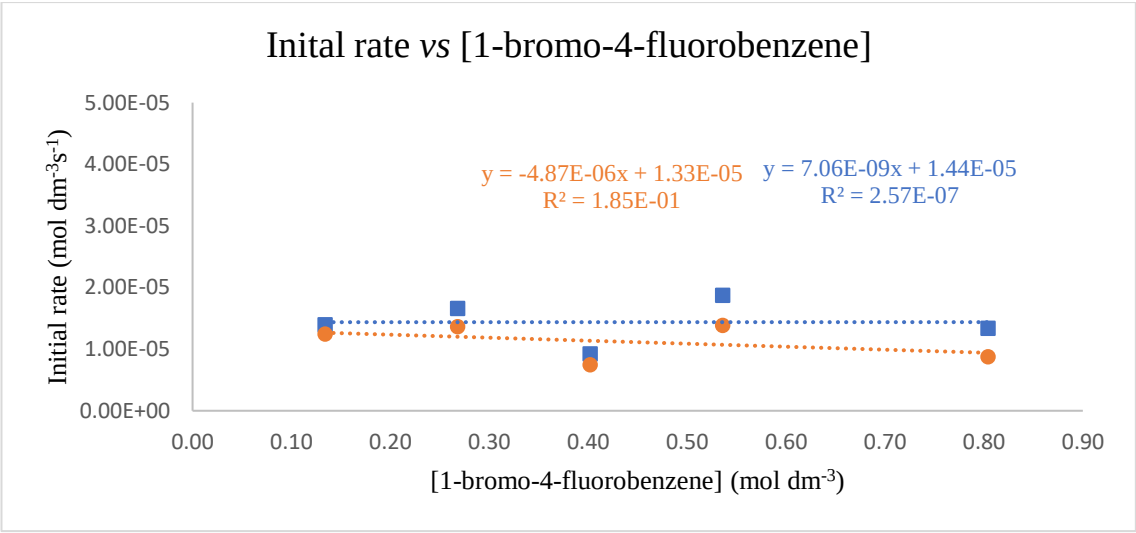


Figure 5.19 - Plot of initial rate *vs* [1-bromo-4-fluorobenzene]. Orange = consumption of 1-bromo-4-fluorobenzene, Blue = formation of $C_6H_5F$.

The plot shown in Figure 5.20 indicates inverse dependence on [NaO$^i$Pr] with a minor influence on rate at high [NaO$^i$Pr]. The slight decrease in gradient could be linked to the decreased formation of the by-product **5.13** as the [NaO$^i$Pr] increases (*vide infra*, Table 5.6), resulting in the

rate of consumption of 1-bromo-4-fluorobenzene at higher [NaO$^{i}$Pr] being slightly lower. However, this does not account for the reduced rate of $C_6H_5F$ formation which accompanies this.

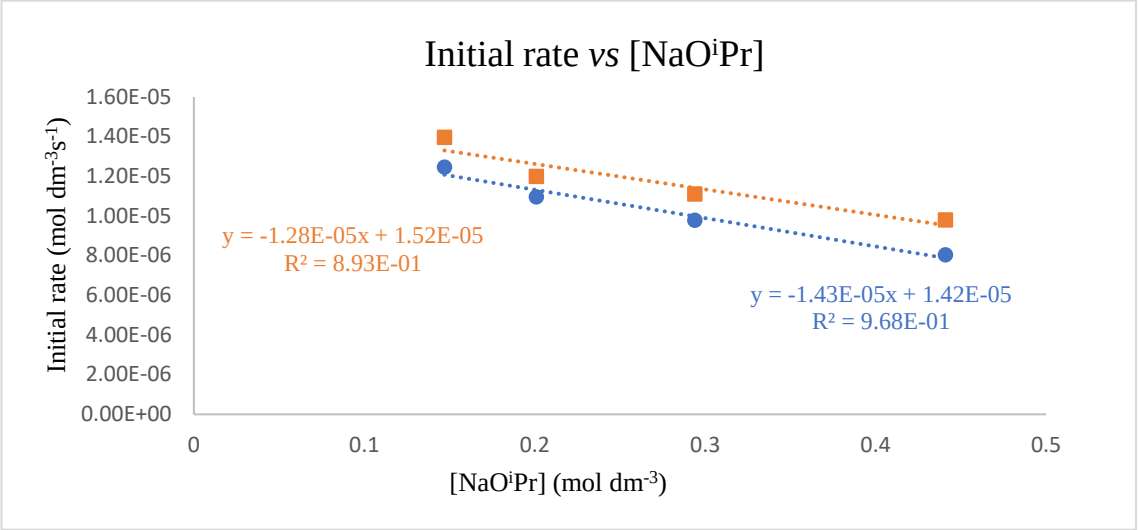


Figure 5.20 - Plot of initial rate *vs* [NaO$^{i}$Pr]. Orange = Consumption of 1-bromo-4-fluorobenzene. Blue = Formation of $C_6H_5F$.

The [$^{i}$PrOH] was found to be the most significant influence, aside from the catalyst, providing a 1$^{st}$ order plot when initial rate was plotted against [$^{i}$PrOH]. The two closely lying plots suggest that [$^{i}$PrOH] does not affect the formation of **5.13**.

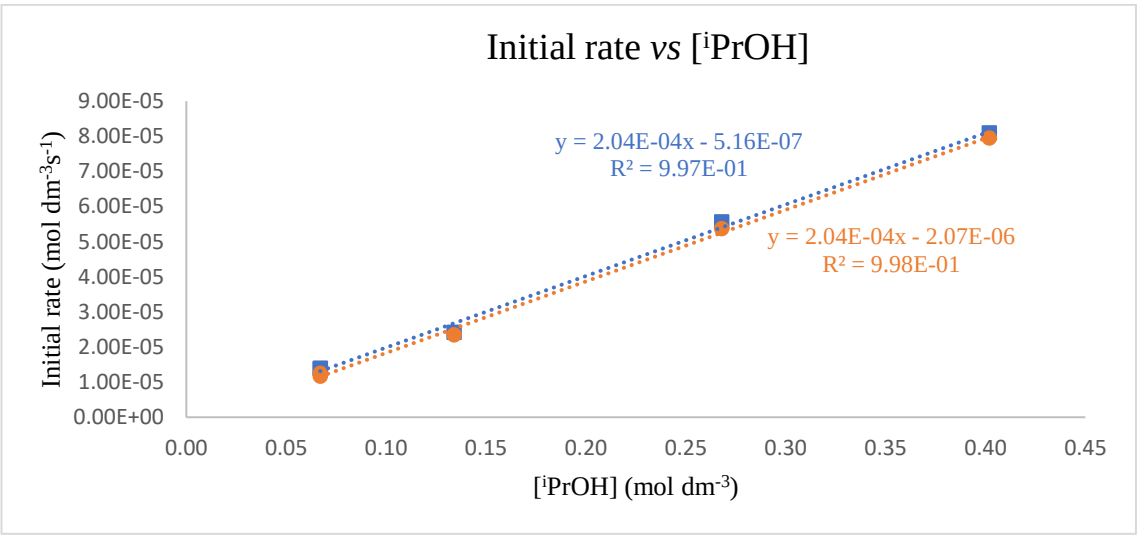


Figure 5.21 - Plot of initial rate *vs* [$^{i}$PrOH]. Orange = Consumption of 1-bromo-4-fluorobenzene. Blue = Formation of $C_6H_5F$.

As shown in section 5.4.4, generation and then degradation of **5.7** can lead to acetone formation which has the potential to interfere with the catalysis. Monitoring the initial rate of product formation and starting material consumption as a function of [acetone] revealed a decrease in

initial rate at high [acetone] (100 mol%, 200 mol % and 300 mol%), but an almost negligible influence at low [acetone] (Figure 5.22). While the change in rate is minor (*cf*. Figure 5.21), it suggests an inverse order dependence which could support a β-hydride elimination process (*vide infra*).

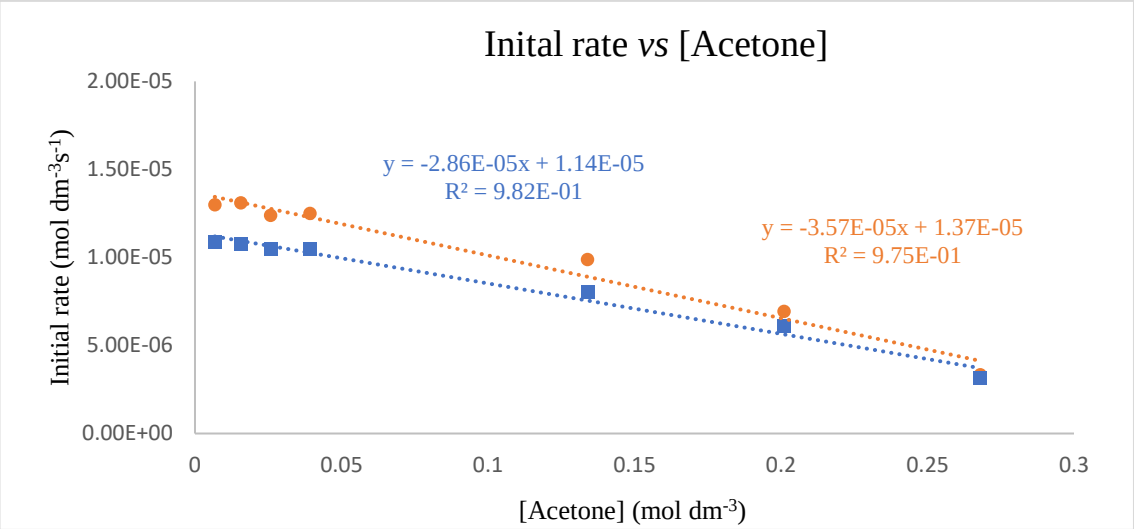


Figure 5.22 - Plot of initial rate vs [acetone]. Orange = Consumption of 1-bromo-4-fluorobenzene. Blue = Formation of $C_6H_5F$.

The final part of the kinetic study investigated the involvement of $PPh_3$ in the reaction. The initial rate vs [$PPh_3$] plot shows an inverse nonlinear curve (Figure 5.23). The non-linearity suggests a more complex role of $PPh_3$ beyond simple dissociation, which would be implied if this plot was linear.[25] Plotting the initial rate vs [$PPh_3$]$^{-1}$ revealed a positive non-zero intercept in the

consumption of 1-bromo-4-fluorobenzene, suggesting an alternative pathway may be present.[25] However, more points at higher [$PPh_3$] are required to confirm this.

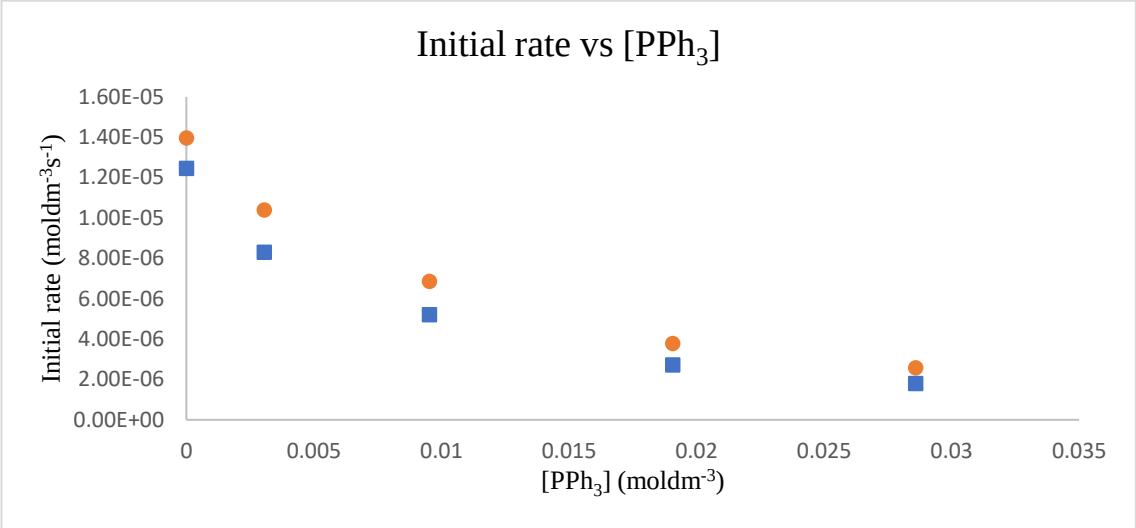


Figure 5.23 - Plot of initial rate vs [$PPh_3$] vs. Orange = Consumption of 1-bromo-4-fluorobenzene. Blue = Formation of $C_6H_5F$.

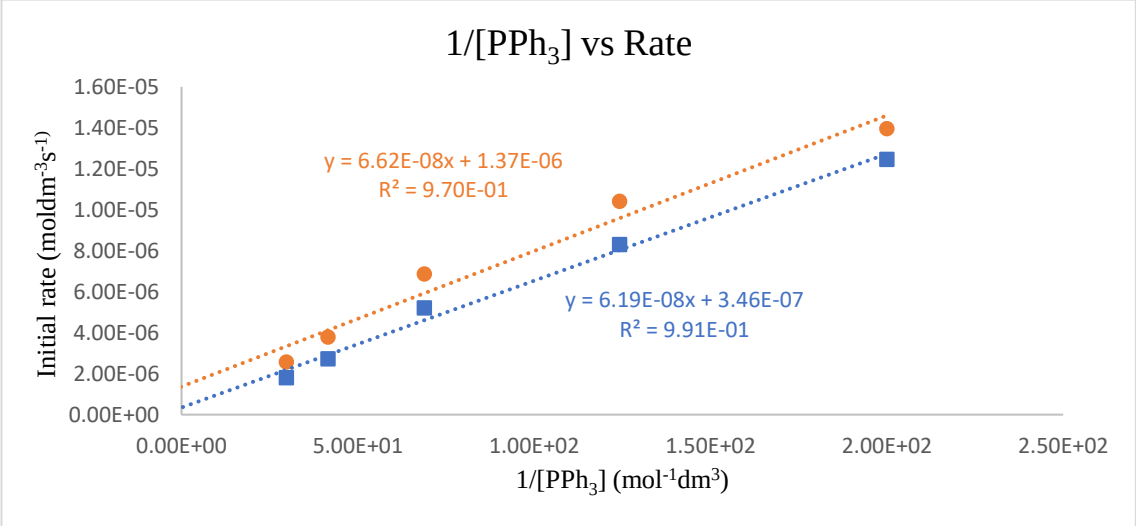


Figure 5.24 - Plot of 1/[PPh3] vs initial rate. Orange = Consumption of 1-bromo-4-fluorobenzene. Blue = Formation of $C_6H_5F$.

From the kinetic runs, additional data on the formation of **5.13** was obtained as summarised in Table 5.6. Notably upon increasing [1-bromo-4-fluorobenzene] which showed a zero order dependence with respect to the initial rate, the yield of **5.13** increased, which can account for the slight gradient of 1-bromo-4-fluorobenzene consumption in Figure 5.19 (Table 5.6, entries 1–4 and 8–10).

Table 5.6 – Yields of **5.13** from the different conditions applied to the kinetic runs.

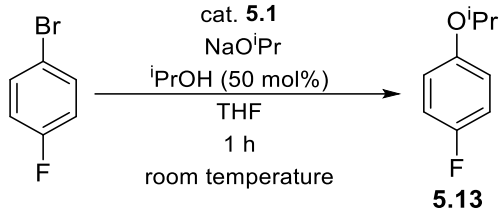

**5.13**

| Entry | Loading of NaO$^i$Pr (mol %) | Loading of **5.1** (mol %) | Loading of 1-bromo-4-fluorobenzene (mol %) | Loading of $PPh_3$ (mol %) | Loading of $^i$PrOH (mol %) | Yield of **5.13** (%) |
|---|---|---|---|---|---|---|
| 1 | 110 | 2 | 100 | 0 | 50 | 6 |
| 2 | 150 | 2 | 100 | 0 | 50 | 7 |
| 3 | 220 | 2 | 100 | 0 | 50 | 5 |
| 4 | 330 | 2 | 100 | 0 | 50 | 1 |
| 5 | 110 | 1 | 100 | 0 | 50 | 4 |
| 6 | 110 | 3 | 100 | 0 | 50 | 8 |
| 7 | 110 | 4 | 100 | 0 | 50 | 8 |
| 8 | 110 | 2 | 200 | 0 | 50 | 8 (12) |
| 9 | 110 | 2 | 300 | 0 | 50 | 9 (15) |
| 10 | 110 | 2 | 400 | 0 | 50 | 12 (17) |
| 11 | 110 | 2 | 100 | 2.3 | 50 | 5 |
| 12 | 110 | 2 | 100 | 7 | 50 | 4 |
| 13 | 110 | 2 | 100 | 21 | 50 | 2 |
| 14 | 110 | 2 | 100 | 0 | 100 | 5 |
| 15 | 110 | 2 | 100 | 0 | 200 | 4 |
| 16 | 110 | 2 | 100 | 0 | 300 | 4 |

Parentheses show results from experiments with 4 mol% of **5.1.**

In summary, the kinetic plots show that the rate determining step of the HDH reaction is influenced by **5.1** (1$^{st}$ order), NaO$^i$Pr (-1 order), $^i$PrOH (1$^{st}$ order) and acetone (-1 order). The plots also show that 1-bromo-4-fluorobenzene is not involved in this step (zero order), suggesting the RDS is after the formation of **5.7**, but before any interaction with the aryl halide. The inverse order associated with NaO$^i$Pr suggests higher [NaO$^i$Pr] prolongs the transformation of **5.7**, which could potentially be linked with its decomposition (this was observed to accelerate when **5.7** was isolated from the reaction solution, section 5.4.2). The inverse order associated with acetone suggests the potential formation of acetone *via* β-hydride elimination is reversible,[26] or the RDS

requires dissociation of acetone from Ni. The effect of $PPh_3$ suggests there is more than one process going on which involves $PPh_3$ in its rate determining step.[25] This requires further investigation beyond the scope of this study, however its ability to dissociate is considered further in section 5.4.7 along with a study of the role of $^{i}$PrOH (section 5.4.8). The formation of the organic by-product (**5.13**) is promoted by high [1-bromo-4-fluorobenzene] suggesting a side reaction with **5.7**. Based on the kinetic results, Scheme 5.20 shows propagation of the catalytic cycle starting from **5.7**. A proposed reason for the incorporation of deuterium is through the hydride exchange of Ni-H with $d_8$-THF to form Ni-D which was observed by Lu in their Ni(II) system.[27] The position of where the exchange is occurring is suggested to be on C3 and C4 positions,[24] suggesting this is not a radical process as this would favour the C2 and C5 positions.[28, 68]

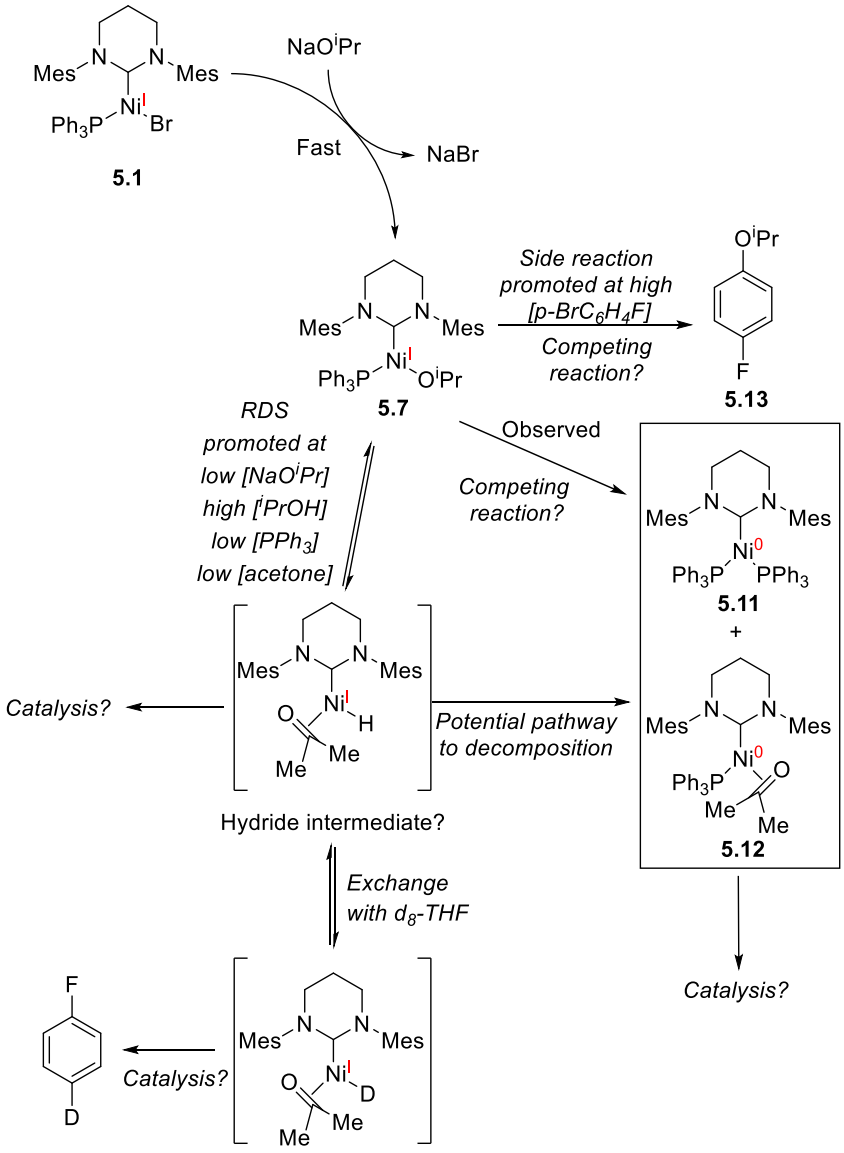


Scheme 5.20 – Updated postulated mechanism after section 5.4.6. Postulated intermediates are shown in square brackets.

## 5.4.7 – $PPh_3$ Dissociation

To examine $PPh_3$ dissociation, exchange reactions of both **5.1** and **5.7** were undertaken. Although both complexes **5.1** and **5.7** are both $^{31}P$ NMR "silent", EPR spectroscopy indicates the retention of $PPh_3$ in both complexes in frozen 140 K solutions by the appearance of $^{31}P$ superhyperfine couplings (section 5.4.3).[14] However, this does not exclude the possibility of dissociation in solution as suggested by the kinetic studies. To probe the possibility of $PPh_3$ loss, two equivalents of the phosphines shown in Figure 5.25 were added to $d_8$-THF solutions of **5.1**. $^{31}P\{^1H\}$ NMR spectroscopy revealed the broadening of the signals for these free phosphines, suggesting exchange is occurring. This was confirmed upon cooling the respective solutions to 223 K, which revealed a signal for free $PPh_3$ as well as sharpening of the signal for the other phosphines (see Figure 5.26 for example). Two equivalents of $PCy_3$ resulted in sharp signals in the $^{31}P\{^1H\}$ NMR spectrum at 298 K for both free $PCy_3$ and $PPh_3$ suggesting displacement had occurred with no further exchange, (as for **5.1** itself, the $PCy_3$ analogue of the complex gave no signal in the $^{31}P\{^1H\}$ NMR spectrum.[xvii] Contrary to this, addition of $PCy_3$ to complex **5.7** resulted in a broad $PCy_3$ signal in the $^{31}P\{^1H\}$ NMR spectrum at 298K.

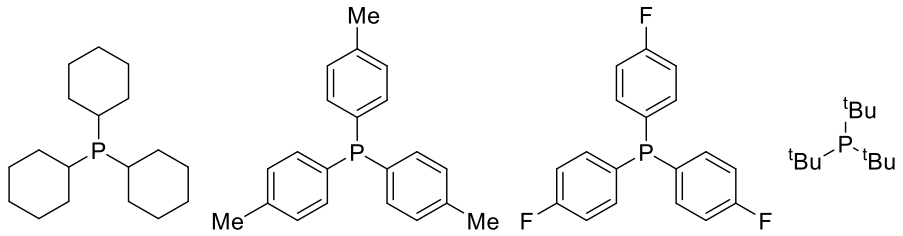


Figure 5.25 - Phosphines used in exchange experiments.

[xvii] Synthesis of Ni(6-Mes)($PCy_3$)Br was reported previously using one equivalent of $PCy_3$ with **5.1**.[11] However, the reaction was incomplete under these conditions and so an alternative route was employed for the synthesis.

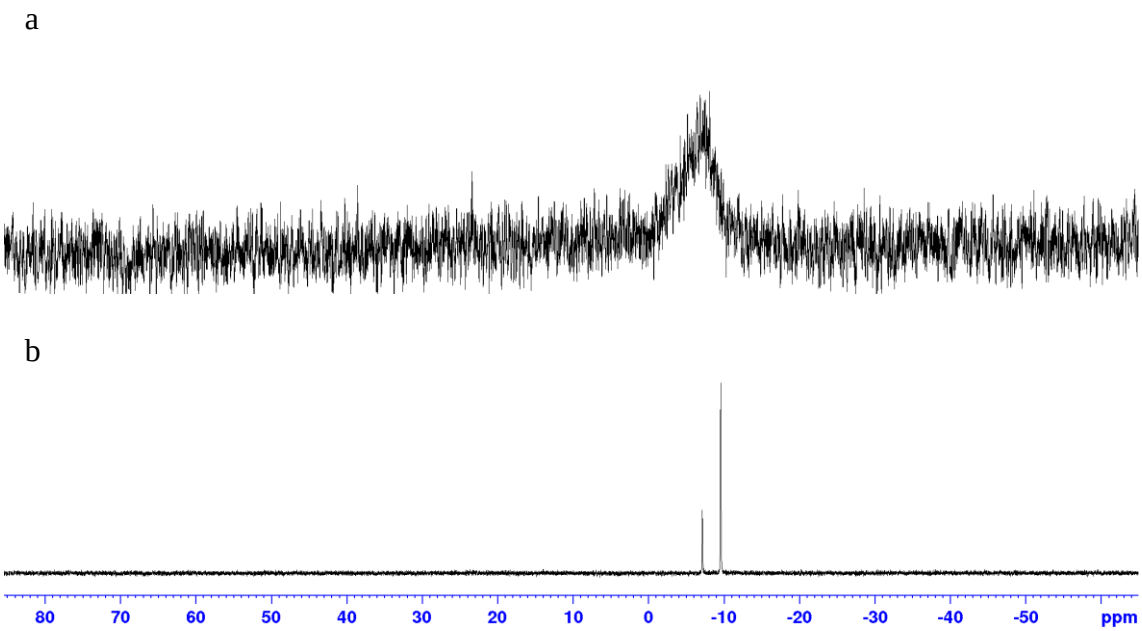


Figure 5.26 – $^{31}P\{^{1}H\}$ NMR spectra (162 MHz, $d_8$-THF) of **5.1** and two equivalents of P(*p*-tolyl)$_3$ at a) 298 K and b) 223 K.

The presence of two equivalents $PCy_3$ did not slow the decomposition of **5.7** to the Ni(0) species **5.11** and **5.12**, although addition of five equivalents of $PPh_3$ to **5.7** did result in slower decomposition, judged by the presence of paramagnetic peaks still being observable in the $^{1}H$ NMR spectrum after five days in solution (*cf.* complete loss of paramagnetic peaks occurs within three days without $PPh_3$).

Based on the addition of the other phosphines in Figure 5.25 to **5.1** and **5.7**, it is clear there is ligand exchange occurring, which supports the inverse order observed in section 5.6. The slowing of the degradation of **5.7** to **5.11** and **5.12** by addition of $PPh_3$ suggests the degradation is also linked to the dissociation of $PPh_3$ (Scheme 5.21). If the decomposition of **5.7** is *via* a Ni(I) hydride species, the previous observation could support this given that a vacant site is required for β-hydride elimination.

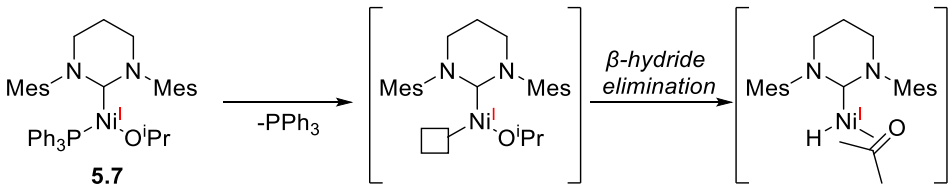


Scheme 5.21 – Postulated role of $PPh_3$ in the decomposition of **5.7**.

## 5.4.8 – Role of $^{i}$PrOH

As shown in section 5.4.6, [$^{i}$PrOH] impacted on the rate of HDH significantly. In attempt to identify its role in the system, stoichiometric reactions with Ni(6-Mes)($PPh_3$)OR precursors **5.7** and **5.8** were carried out. Exchange has been reported between M-OH complexes and free ROH;[29,30] M-OR and ROH exchange would therefore be expected. To probe this, **5.7** was exposed to 10 equivalents of $^{t}$BuOH. After 5 mins of shaking, the solution volatiles were vacuum transferred, and both the residue and filtrate examined by $^{1}$H NMR spectroscopy. A mixture of **5.7** and **5.8** was observed, along with $^{i}$PrOH (44%) (Scheme 5.22a). It was also found in smaller excess of $^{i}$PrOH, **5.8** was found to exchange to give **5.7** (Scheme 5.22b).

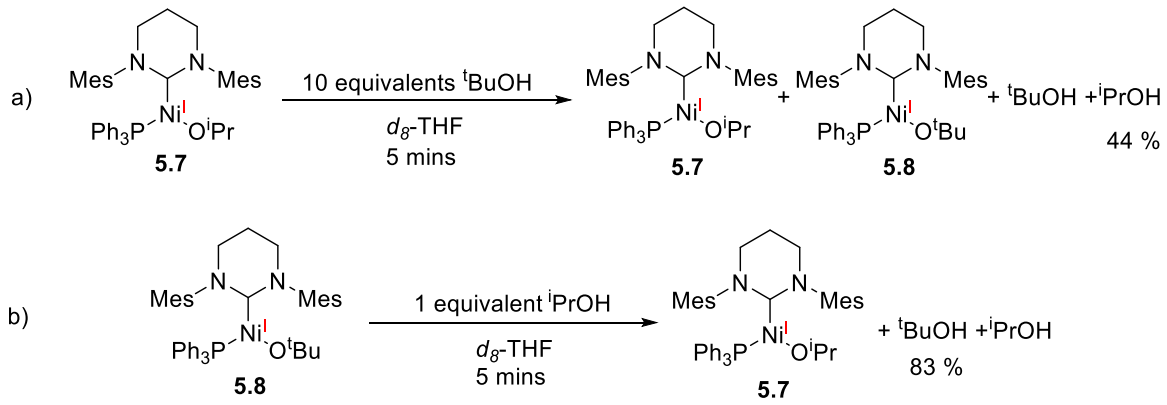


Scheme 5.22 – Exchange of alkoxides in Ni(I)OR species.

The alcohol exchange limits the potential reactions that can be carried out to determine the alcohols role. Thus, the precise involvement of alcohol remains unclear in this study, aside from having an accelerating effect on the reaction. Within the literature, there are examples of β-hydride elimination from metal-alkoxide complexes which are assisted by free alcohols.[31–34] Milstein proposed a β-hydride elimination process which occurs without a vacant coordination site on the metal centre, suggesting instead alcohol assisted dissociation of the alkoxide (Scheme 5.23).[31,32,33] This was established through retention of the trans hydride geometry in **5.xi**, instead of the hydride being generated *cis* as would occur in traditional β-hydride elimination from Ir-OMe group in **5.x** into a vacant site. The absence of $P(CD_3)_3$ incorporation during thermolysis of **5.x** ruled out dissociation of $PMe_3$ during the β-hydride elimination. A similar result was observed by Goldberg.[32] Bäckvall also proposed free alcohol assisted β-hydride elimination in a Ru system based upon the lack of CO dissociation by IR spectroscopy during β-hydride elimination.[33]

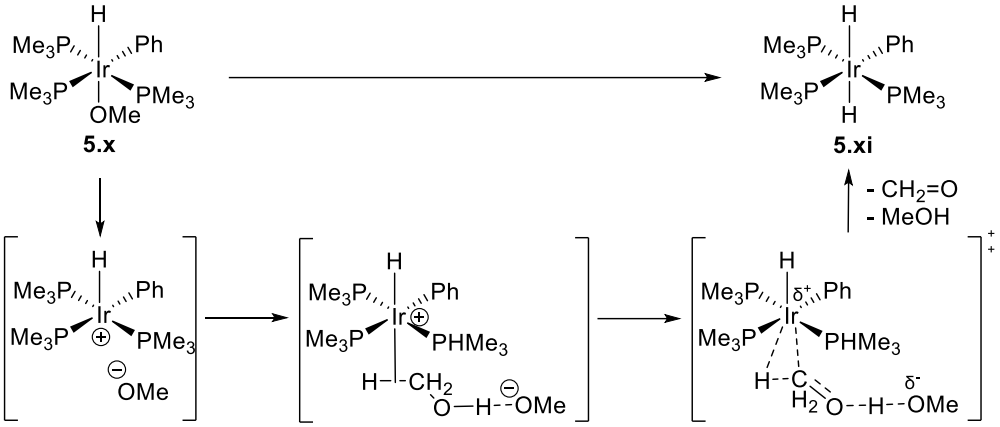


Scheme 5.23 – β-hydride elimination process which occurs without a vacant coordination site proposed by Milstein.[31]

## 5.4.9 – Reactivity of **5.7**

In the reaction of **5.7** with 4-bromoanisole (and also most likely 1-bromo-4-fluorobenzene), EPR spectroscopy showed only **5.7** and **5.1** (section 5.4.5). In an effort to look for possible diamagnetic intermediates, the stoichiometric reaction of **5.7** with different aryl halides was investigated.

A $d_8$-THF solution of **5.7** and 4-bromoanisole was prepared and placed into a pre-cooled NMR spectrometer. Starting from 235 K and gradually warming to room temperature resulted in no reaction until 272 K, at which point **5.1** was observed. There was no evidence for any other Ni containing species by $^1$H NMR.

When a room temperature reaction of 1-bromo-4-fluorobenzene with **5.7** in $d_8$-THF was followed by $^1$H, $^{19}$F{$^1$H} and $^{31}$P{$^1$H} NMR spectroscopy, **5.1**, $C_6H_5F$ and *p*-$d_1$-$C_6H_4FD$ (1:1 ratio of the two fluorobenzene isotopomers) were the major products of the reaction. Small amounts of **5.13** (9%) and Ni species **A** were formed (Scheme 5.24), in addition to a small amount of a hydride species, which as shown later, is Ni(6-Mes)($PPh_3$)(H)Br (**5.19**).[xviii]

[xviii] Further discussion on **5.19** will be in sections 5.5.5 and 5.5.6. Actual values of **5.19** to **5.1** are difficult to determine due to the paramagnetism of the $^1$H NMR spectrum along with the decay of **5.19** to **5.1**.

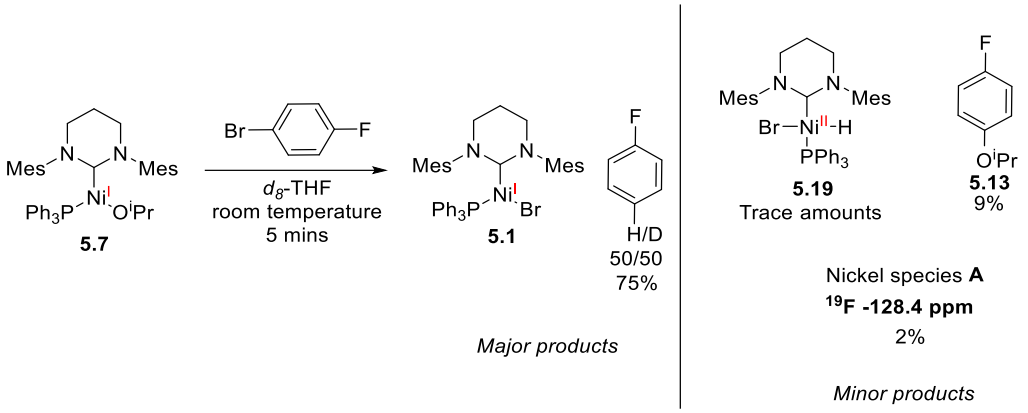


Scheme 5.24 – Stoichiometric reactions of **5.7** with 1-bromo-4-fluorobenzene in $d_8$-THF. Yields of organic products determined by $^{19}F$ NMR spectroscopy. **5.1** and **5.19** detected by $^{1}H$ NMR spectroscopy.

An analysis reaction of 4-bromobenzotrifluoride with **5.7** (now in $C_6D_6$), led to the immediate formation of **5.1** and $C_6H_5CF_3$ but with more significant amounts of both **5.19** (10% in relation to **5.1**) and 4-isopropoxybenzotrifluoride (5%) (Scheme 5.25a). $^{19}F\{^{1}H\}$ NMR spectroscopy a new species was observed at -60.9 ppm (accounting for 10% of the products) which is assigned as Ni(6-Mes)($PPh_3$)($C_6H_4CF_3$)Br (**5.18**).[xix]

Upon turning to 4-chlorobenzotrifluoride, Ni(6-Mes)($PPh_3$)Cl (**5.1a**)[xx] was generated, along with now less of 4-isopropoxybenzotrifluoride and only baseline amounts of **5.19** (Scheme 5.25b). Treatment of **5.7** with 4-fluorobenzotrifluoride gave only the Ni(0) decomposition products of the alkoxide complex, **5.11** and **5.12**.

[xix] **5.18** will be discussed later in section 5.5.1, however it is worth noting that the mechanism for the formation of such a species is unknown from this reaction and instead, it is suggested **5.18** is formed from excess 4-bromobenzotrifluoride and **5.1** (which is the major product from the initial reaction).
[xx] Ni(6-Mes)($PPh_3$)Cl synthesised and characterised within the group by Page and Poulten.[13]

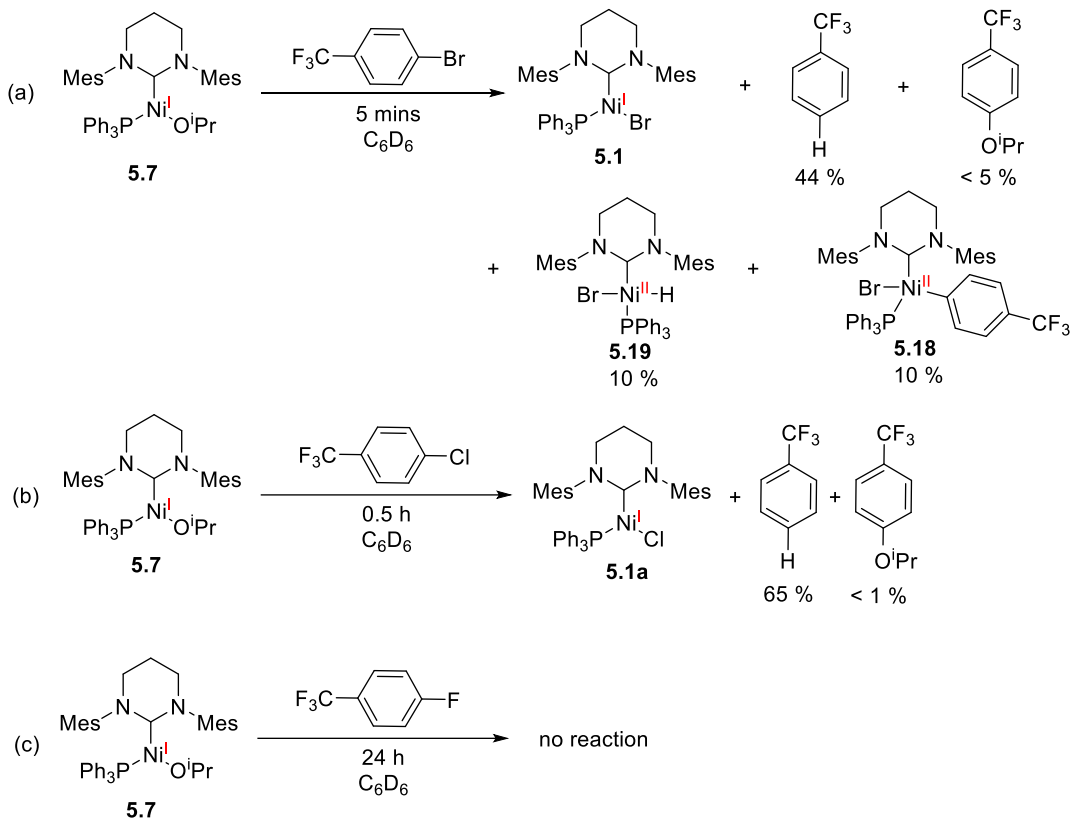


Scheme 5.25 – a) to c) Observed activity of **5.7** with *para*-halobenzotrifluorosubstrates.

In all the cases above, the major products are **5.1** and the dehalogenated aryl species. Minor amounts of the organic isopropoxy by-products (e.g. **5.13**) were observed. The steps leading to the formation of these by-products are unknown at this stage but will be discussed further in section 5.4.11. Similarly, discussion of the Ni species **A**, **5.18** and **5.19** will be held over to section 5.5.

## 5.4.10 – Reactivity of **5.9**

It was noted earlier that the Ni-$OCHPh_2$ complex **5.9** showed greater stability than the isopropoxide analogue **5.7**. To probe the influence of this greater stability, stoichiometric reactions of **5.9** with 4-bromoanisole and 1-bromo-4-fluorobenzene were carried out.

In the case of 4-bromoanisole, **5.9** reacted sluggishly in $d_8$-THF at room temperature. After ca. 30 mins, **5.9** was still observable in the $^{1}$H NMR spectra (Figure 5.27), along with **5.1** and **5.19**. In addition, the benzophenone complex **5.viii**, resulting from degradation of **5.9**, could be seen by $^{31}$P NMR spectroscopy (see section 5.4.4).

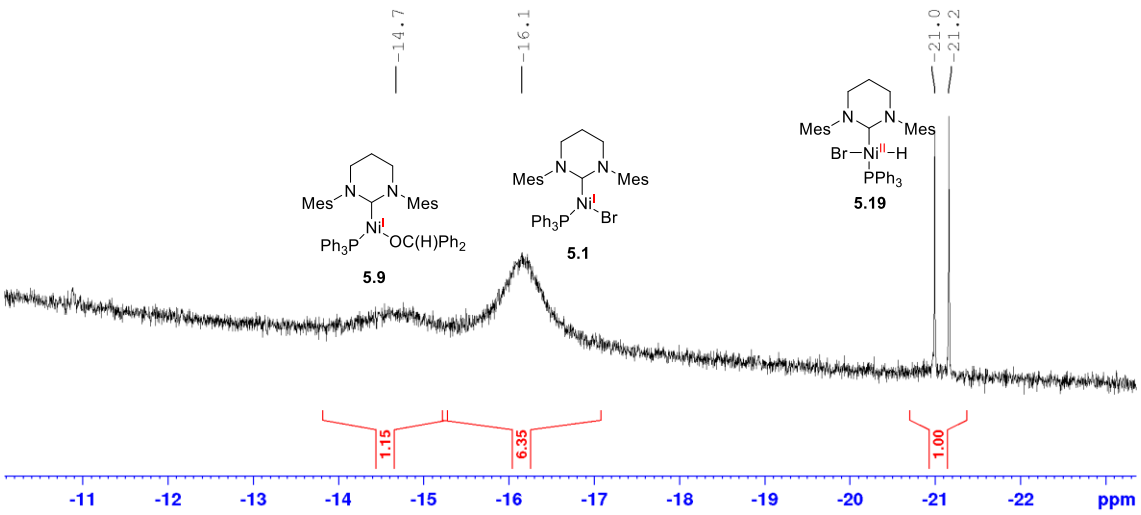


Figure 5.27 - $^{1}$H NMR spectrum (500 MHz) in $d_8$-THF of the reaction of **5.9** with 4-bromoanisole after 30 mins at room temperature.

A stoichiometric reaction of **5.9** with 1-bromo-4-fluorobenzene in $d_8$-THF also led to the slow formation of **5.1** and **5.19** in *ca.* a 5:1 ratio ($^{1}$H NMR integration) after 1 h. The $^{19}$F{$^{1}$H} NMR spectrum revealed equal amounts of $C_6H_5F$/*p*-$d_1$-$C_6H_4DF$ and 4-$FC_6H_4OC(H)Ph_2$ (identified by GC-MS), along with a signal lying at -128.9 ppm believed to be an analogue of Ni species **A.** This is labelled as Ni species **B** (Figure 5.28) and will be discussed later in the chapter (section 5.5.8). Inverse-gated $^{31}$P NMR spectroscopy revealed two major phosphorus environments of equal intensity, doublet at 26.9 ppm (**5.19**) and a singlet at 35.3 ppm (**5.viii**) along with a minor signal (22.9 ppm) (postulated to be Ni species **B**). The ratios of the Ni species are summarised in Scheme 5.26. Compared to **5.7**, the reaction of **5.9** with 1-bromo-4-fluorobenzene led to a larger observable amount of **5.19** (Scheme 5.26 vs Scheme 5.24).

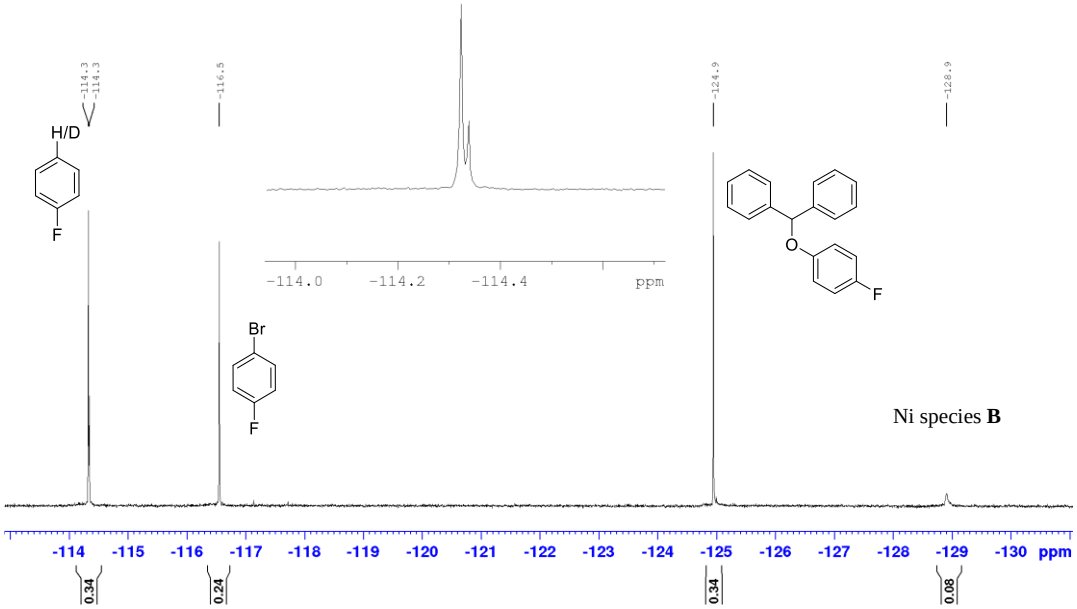


Figure 5.28 - $^{19}F$ NMR spectrum (470 MHz) of the reaction products of **5.9** with 1 equivalent of 1-bromo-4-fluorobenzene in $d_8$-THF.

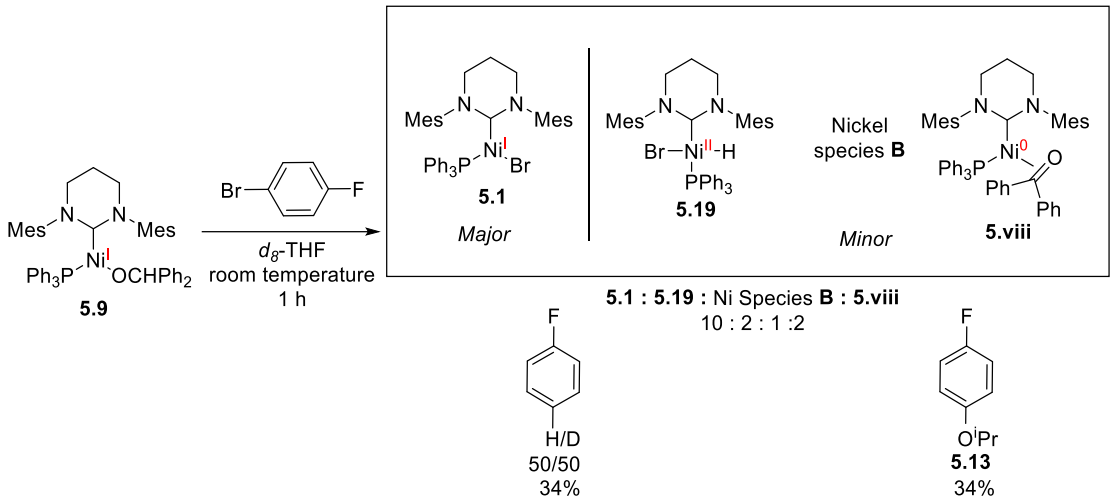


Scheme 5.26 – Reaction products of **5.9** with 1-bromo-4-fluorobenzene in $d_8$-THF. Yields of organic products determined by $^{19}F$ NMR spectroscopy. The ratio of **5.1** and **5.19** determined by $^{1}H$ and $^{31}P$ NMR spectroscopy.

Comparison of the reactivity of **5.7** and **5.9** (section 5.4.9 vs 5.4.10) with 1-bromo-4-fluorobenzene indicates that the more stable **5.9** generates greater amounts of 4-ROC$_6$H$_4$F and the Ni(II) species **5.19**. Moreover, more Ni species **B** is formed compared to Ni species **A**. It is postulated this side reaction occurs before the RDS. An updated mechanism is shown in Scheme 5.27.

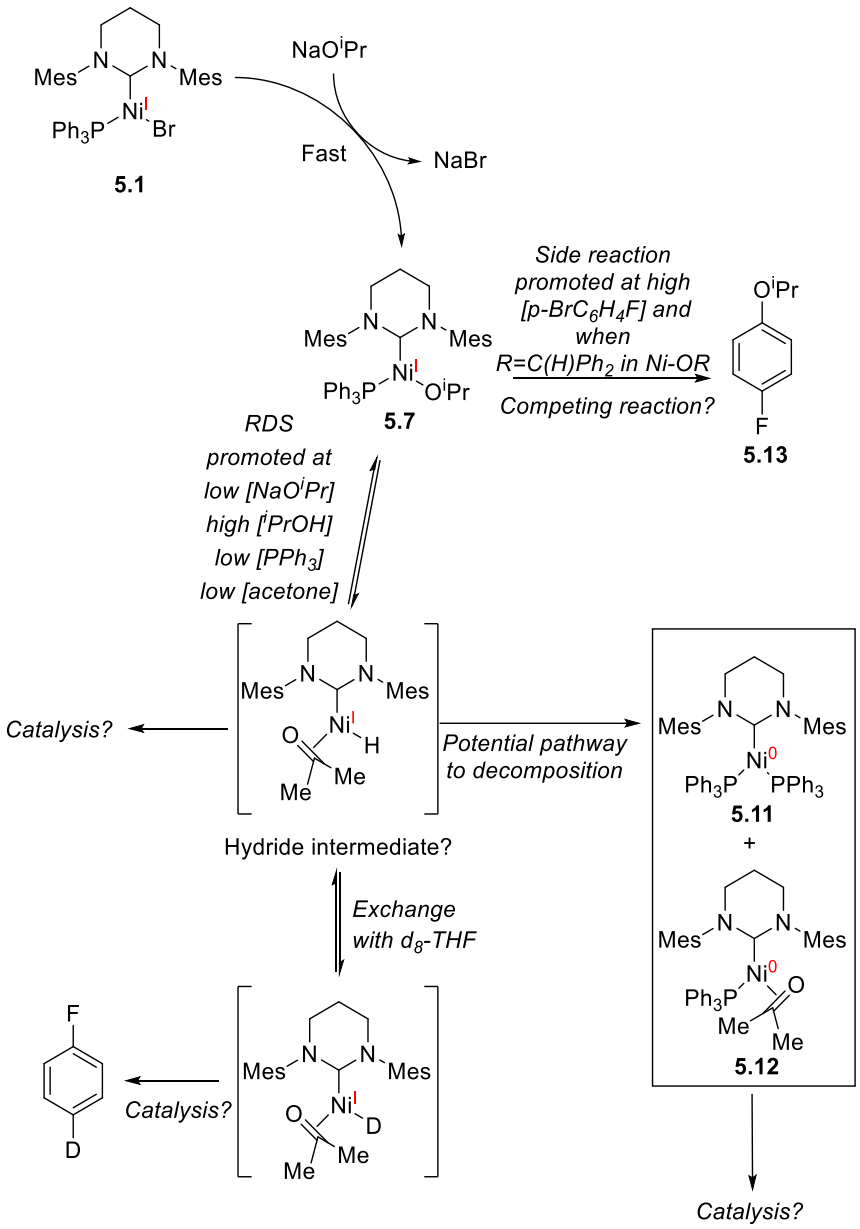


Scheme 5.27 – Updated postulated mechanism after section 5.4.40. Postulated intermediates are shown in square brackets.

## 5.4.11 – Role of the β-hydrogen in Catalytic HDH

The likely involvement of a β-hydride elimination step in Ni catalysed HDH was noted in the introduction from Fort's work. The results with the Ni(I)-OR systems described thus far are also consistent with the importance of such a step, most notably the kinetic dependence on [Ni-OR] prior to reaction with Ar-X and also the lack of deuterium incorporation when performing catalysis with NaO$^i$Pr and $^i$PrOD (section 5.2.1). Moreover, the formation of ketone complexes in the decomposition reaction of **5.7** and **5.9** is also suggestive of β-hydride elimination.

Direct evidence for a β-hydride elimination process came upon reaction of Ni(6-Mes)($PPh_3$)($d_7$-O$^i$Pr) (**5.7a**) with 4-bromanisole in $C_6D_6$, which led to the formation $d_1$-anisole (confirmed by GC-MS) (Scheme 5.28).

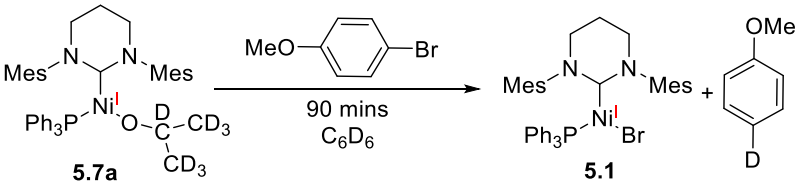


Scheme 5.28 - Observed products from the reaction of **5.7a** and 4-bromoanisole after 90 mins by $^1$H NMR spectroscopy.

To further probe the need for a β-hydrogen, the Ni(I)-O$^t$Bu complex **5.8** was exposed to a stoichiometric amount of 4-bromobenzotrifluoride. Although, the formation of **5.1** and 4-(*tert*-butoxy)benzotrifluoride[xxi] (20 % vs 80 % 4-bromobenzotrifluoride) were detected there was no formation of α,α,α-trifluorotoluene (Scheme 5.29).[xxii]

[xxi] Detected by GC-MS.

[xxii] The transformation of **5.8** to **5.1** was not restricted to just electron withdrawing groups on Ar-Br. EPR (spectrum below) showed the same process took place between **5.8** and 4-bromoanisole .

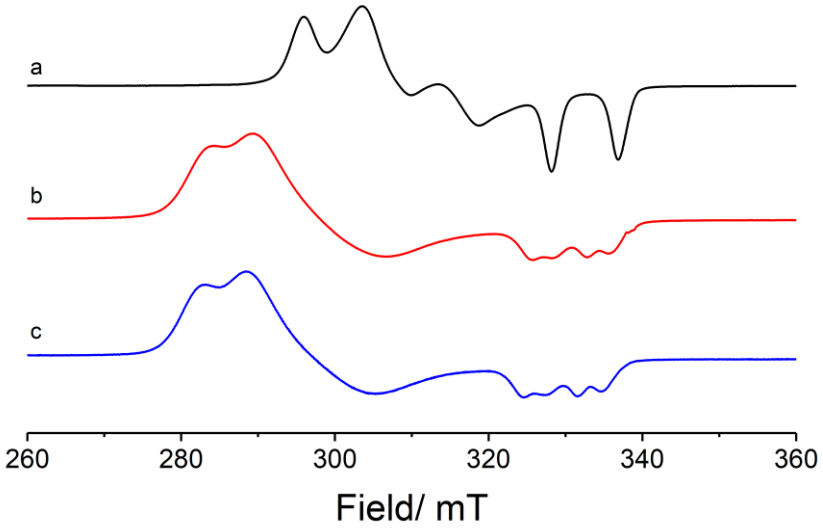


CW X-band EPR spectra (140 K) a) **5.8**, b) **5.8** + 4-bromoanisole t = <5 min, c) **5.1**.

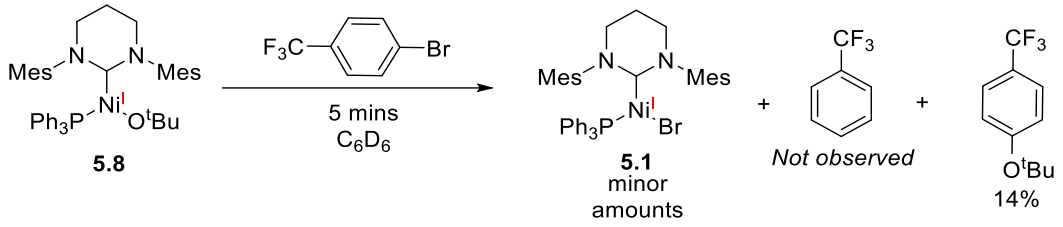


Scheme 5.29 – Reaction of **5.8** and 4-bromobenzotrifluoride.

Considering that both **5.1** and 4-(*tert*-butoxy)benzotrifluoride are formed, it seems likely that both result from the same interaction of **5.8** and 4-bromobenzotrifluoride. A possible route to explain this could involve reductive elimination from a Ni(III) intermediate (Scheme 5.30).

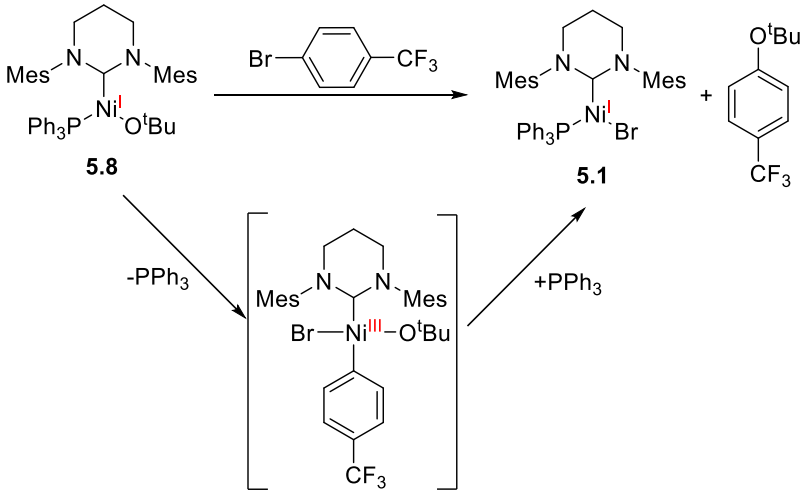


Scheme 5.30 – Postulated mechanism for the formation of **5.1** from the reaction of **5.8** and 4-bromobenzotrifluoride.

Although Ni mediated C-O reductive elimination is rare in the literature (contrary to Pd), it is typically limited to Ni(III) and Ni(IV) intermediates,[35–39] which could support the reactivity postulated in Scheme 5.30. However, examples of Ni(III) species with NHCs are limited with only a very recent example being postulated by Matsubara in the Buchwald-Hartwig amination of aryl bromides.[15]

## 5.4.12 – Initial Efforts to Generate Ni(I)-H

As β-hydride elimination from **5.7** would yield a Ni(I)-H species, the reaction of **5.7** with silanes was investigated, in line with the approach used by Fenske in Scheme 5.7.[9,40] Both $MePh_2SiH$ and $Ph_2SiH_2$, led immediately to formation of deep red solutions. However, there were no paramagnetic species formed based on the $^1H$ NMR spectra, but appearance of the Ni(0) bisphosphine complex **5.11** in the $^{31}P\{^1H\}$ NMR spectra was observed. In the case of $MePh_2SiH$, a black precipitate was formed which was not detected with $Ph_2SiH_2$. $Ph_2SiH_2$ gave instead a

second major species at 31.8 ppm in the $^{31}P\{^{1}H\}$ NMR spectrum. With both silanes, silyl ether by-products were detected in the $^{1}H$ NMR spectra suggesting that metathesis of Ni-O$^{i}$Pr does take place, but the lack of any identifiable Ni(I)-H species suggests, unsurprisingly, that they are not stable.

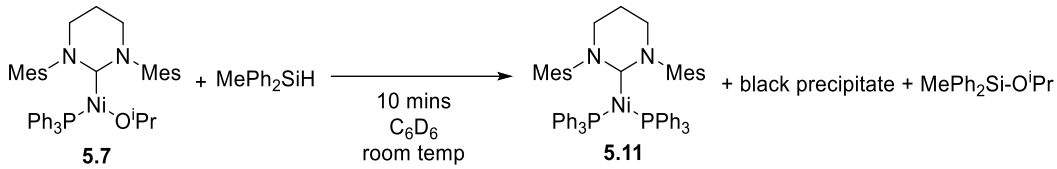


Scheme 5.31 - Reaction of complex **5.7** with $MePh_2SiH$.

## 5.4.13 – The Postulated Role of Radicals in Ni(I) Catalysed HDH

In the course of a report on the reactivity of $Ni^{I}$(Xantphos)X (X= Br, Ph) with aryl/alkyl bromides, Diao and co-workers summarised a range of pathways through which Ni(I) complexes could generate organic radicals (Scheme 5.32).[41] Given the potential involvement of radicals in the HDH system, both stoichiometric and catalytic reactions involving **5.1** and **5.7** were undertaken in the presence of radical traps.

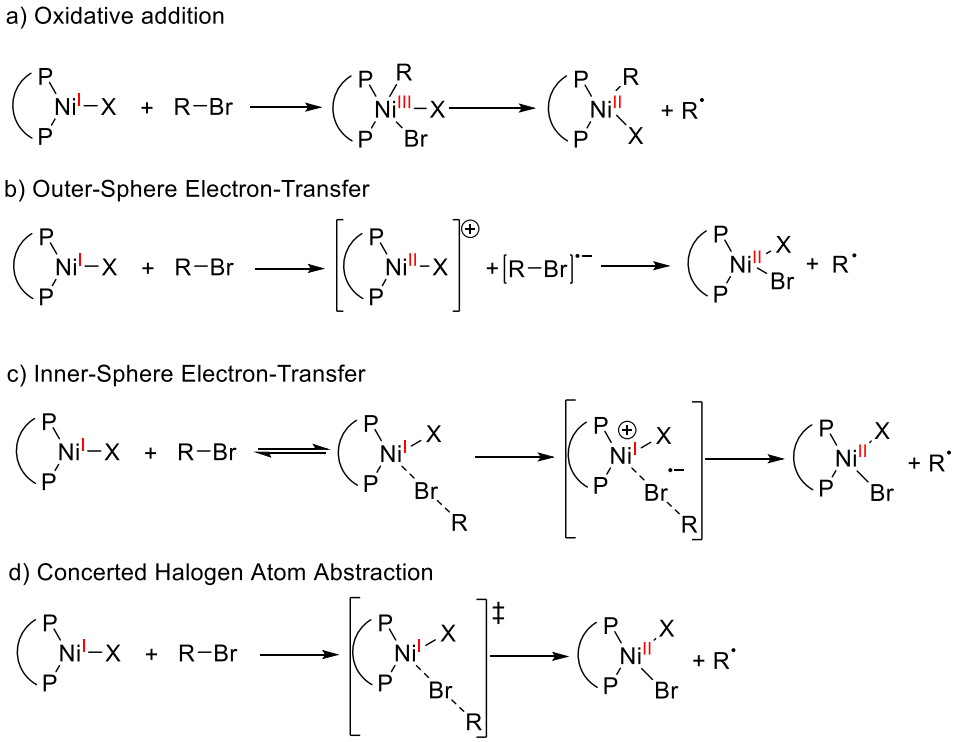


Scheme 5.32 – Pathway to radical formation described for the case of Ni(Xantphos)X (X = halide, R = aryl/alkyl).[41]

The addition of TEMPO to **5.1** immediately formed a deep red solution in $C_6D_6$ (Scheme 5.33). Layering the solution with pentane provided large deep red blocks suitable for X-ray crystallography of the Ni(II) TEMPO complex, Ni(6-Mes)($\kappa^2$-TEMPO)Br (**5.14**) (Figure 5.29, left). The Ni-O$^i$Pr analogue **5.15** was isolated upon addition of 1 equivalent of TEMPO to **5.7** accompanied by a similar colour change to deep red (Figure 5.29, right). The displacement of $PPh_3$ in both reactions is consistent with the phosphine exchange reactions in section 5.4.7.

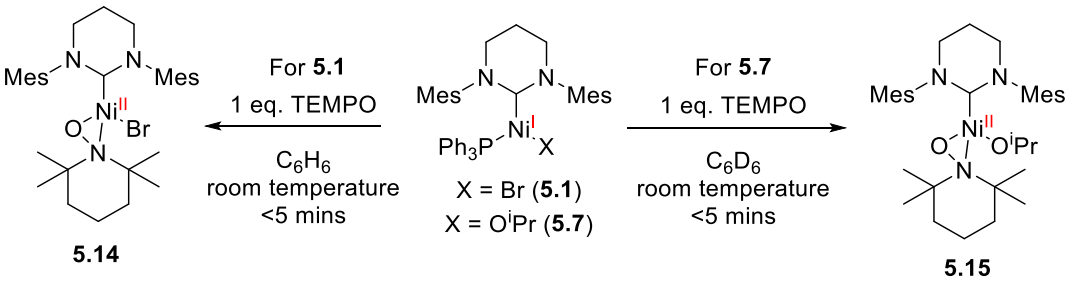


Scheme 5.33 – Reactions of **5.1** and **5.7** with TEMPO.

Both complexes showed distorted square planar arrangements with $\kappa^2$ binding of the TEMPO ligand similar to CpNi(IPr)($\kappa^2$-TEMPO).[42] **5.14** exhibited a significantly shorter Ni-N bond (1.924(2) Å) than either **5.15** or CpNi(IPr)($\kappa^2$-TEMPO) (1.963(3) and 1.9581(16) Å respectively). Of the Ni TEMPO complexes in the literature,[42–46] the alternative $\kappa^1$-O binding is rare and seems to be limited to coordinatively saturated species.[46,47]

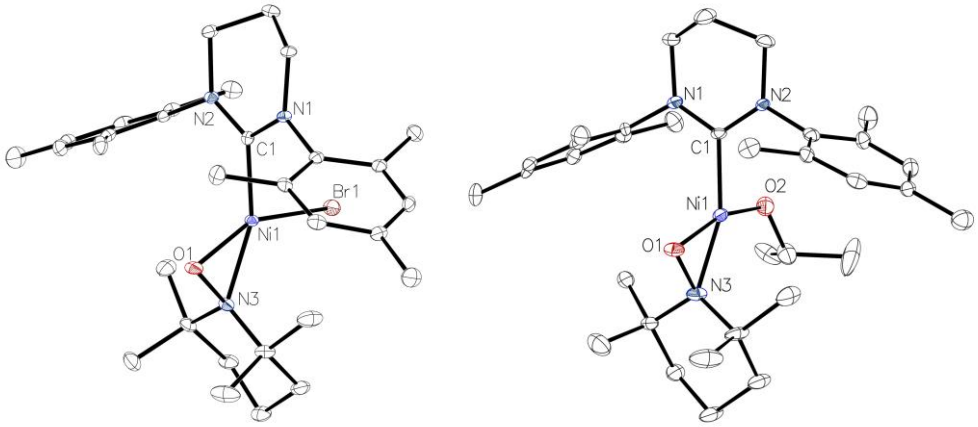


Figure 5.29 – Molecular structures of **5.14** (left) and **5.15** (right). Hydrogen atoms have been omitted for clarity. Ellipsoids are represented at 30% probability. Selected bond lengths (Å) and angles (°) for **5.14**: Ni1-C1 1.906(3), Ni1-O1 1.8363(17), Ni1-Br1 2.3289(4), Ni1-N3 1.924(2), C1-Ni1-O1 111.63(9), C1-Ni1-Br1 97.00(7). C1-Ni1-N3 154.98(9), Br1-Ni1-N3 108.01(6). For **5.15**: Ni1-C1 1.909(3), Ni1-O1 1.843(2), Ni1-O2 1.847(2), Ni1-N3 1.963(3), C1-Ni1-O1 108.26(11), C1-Ni1-O2 90.67(12), C1-Ni1-N3 151.07(12), O2-Ni1-N3 118.22(11).

The diamagnetic nature of **5.14** and **5.15** was confirmed by $^{1}$H NMR spectroscopy, although broad resonances were observed at room temperature (see appendix). Variable temperature NMR of **5.15** revealed sharpening of two broad peaks (2.9 – 2.0 ppm, see appendix) at 343 K to one single peak of an integral of 12H relating to the *ortho*-methyl substituents on the 6-Mes ligand.

When **5.14** was formed *in-situ* from **5.1** and two equivalents of TEMPO under catalytic conditions, no HDH reaction of the 1-bromo-4-fluorobenzene substrate was seen (Scheme 5.34).

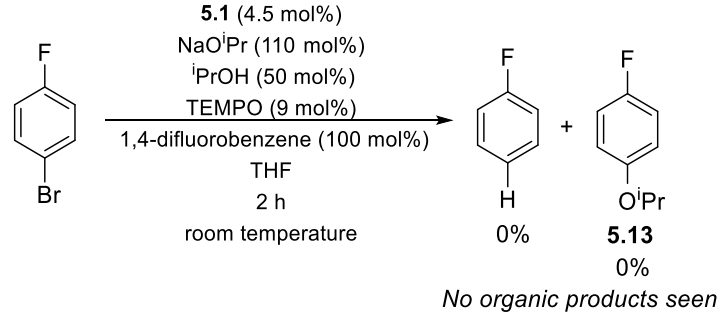


Scheme 5.34 – Catalytic run with 9 mol % TEMPO.

Bromomethylcyclopropane is a commonly employed radical clock. Reacting with a radical converts it into a cyclopropyl methyl radical, which upon hydrogen abstraction and rearrangement, yields 1-butene (Scheme 5.35a).[48] The formation of other products is also possible, including 1,7-octadiene (Scheme 5.35b),[41] 1-bromo-4-butene and methylcyclopropane (Scheme 5.35c).[49]

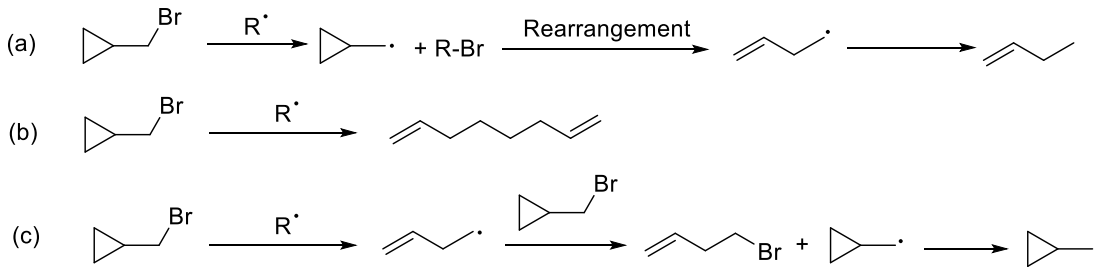


Scheme 5.35 – Reactivity of bromomethylcyclopropane with radicals.[41,48,49]

No reaction was observed between bromomethylcyclopropane and **5.1**, whereas with **5.7**, an instant change from orange to brown took place (Scheme 5.36). $^{1}$H NMR spectroscopy showed formation of **5.1** and Ni(6-Mes)($PPh_3$)(H)Br **5.19** in a 3:1 ratio, along with 1-butene, which was observed in a similar quantity to **5.1**. NMR analysis of the volatiles following vacuum transfer revealed formation of 1-butene and acetone alongside two other major products (one which contains an isopropoxy group and other which could not be identified) and a minor amount of 1,7-octadiene (1 : 2.5 ratio with 1-butene).

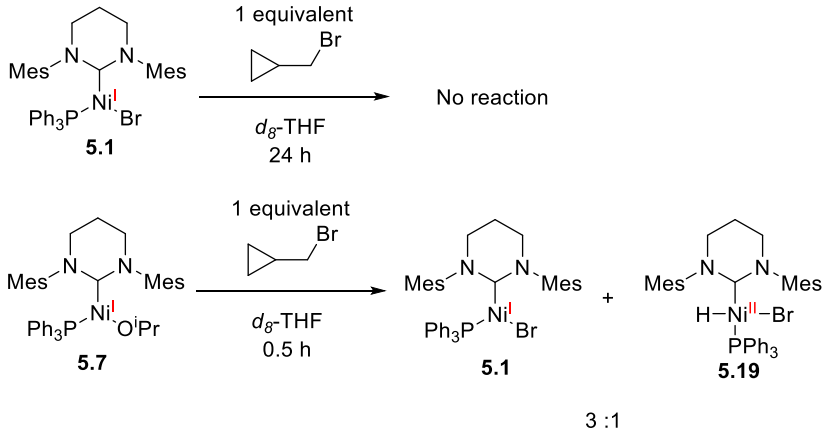


Scheme 5.36 - Reactivity of bromomethylcyclopropane with a) **5.1** and b) **5.7**.

**5.8** was also exposed to bromomethylcyclopropane where formation of **5.1** was observed after 10 mins. Most importantly there was no formation of **5.19** suggesting the formation of **5.1** is not linked to this species in this reaction.

Using bromomethylcyclopropane as a substrate for HDH catalysed by **5.1** resulted in the formation of 1-butene but only 3 turnovers worth (12 %). In all the reactions above it was hard to distinguish the presence of any methylcyclopropane.

6-Bromo-1-hexene is a similar reagent with more easily identifiable products. Radical interaction with this substrate leads to methylcyclopentane, whereas simple hydrodehalogenation would yield 1-hexene (Scheme 5.37).[50]

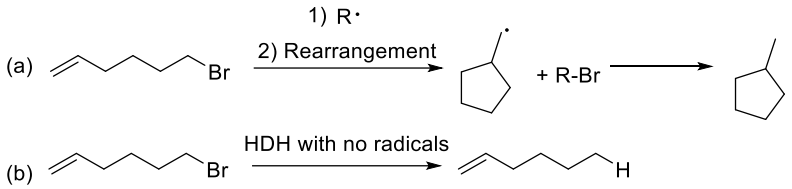


Scheme 5.37 – a) Reactivity of 6-bromo-1-hexene in the presence of a radical. b) Expected product from HDH if no radicals are involved.

Exposing **5.1** to this substrate resulted in no change after 2 hours in $d_8$-THF. In contrast, rapid reaction of a 1:1 mixture of **5.7** with 6-bromo-1-hexene ensued to give a 4:1 mixture of **5.1** and **5.19** after just 10 mins. In addition, 1-hexene and methylcyclopropane (3:2 ratio) were identified (by $^1$H NMR spectroscopy), together with minor other unidentifiable products.

Despite the single electron available in **5.1**, stoichiometric reactions of **5.1** with the different radical traps led to only an interaction with TEMPO. **5.7** reacts in the same way with TEMPO. As a result, addition of TEMPO to a typical catalytic run resulted in shutdown of the catalysis.

No conclusions can be made can be made from these results. Conclusions also cannot be drawn from the catalytic results as the presence radicals/radical traps might perturb activity.[51]

In the case of bromomethylcyclopropane and 6-bromo-1-hexene, reactions with **5.7** revealed radical activity. However, other products were observed suggesting this is not limited to just radical interactions. It is also important to consider the radical traps are alkyl containing substrates which are more susceptible to radical interactions over their aryl halide counterparts which could influence reactivity. Thus, the different radical traps neither confirm nor deny radical involvement in HDH, instead it suggests there is some radical character to this catalytic process.

### 5.4.14 – Summary of Section 5.4

A final scheme for section 5.4 is shown in Scheme 5.38. The study suggests while the Ni(I) species **5.1** and **5.7** are observed in the cycle, it is not limited to just Ni(I) species. Starting from **5.1** a rapid metathesis with $NaO^iPr$ is observed yielding the Ni(I) complex **5.7** (sections 5.4.2 and 5.4.3). **5.7** was found to decompose into **5.11** and **5.12** (section 5.5.4). Step B is proposed to be the rate determining step which is significantly affected by high concentrations of $^i$PrOH. This is supported by EPR and the kinetic results which also suggests **5.7** is a resting state in the catalytic cycle (sections 5.4.5, and 5.4.6). The RDS was also affected by [$PPh_3$] and [acetone] which suggests this step involves a β-hydride elimination reaction. It is also postulated that the decomposition of **5.7** proceeds through this route to yield **5.11** and **5.12** (step C). Step D, which is a side reaction, was shown to be influenced by [Ar-Br] and a bulkier alkoxide moiety on the Ni(I) species. This is postulated to be a *via* a Ni(III) intermediate based upon results in section 5.4.11. Step E is suggested to account for the observed deuterium incorporation (section 5.4.9). Steps F and G are still to be determined. From the radical studies (section 5.4.13), some radical features are observed in the catalytic cycle, however non-radical interactions were also detected. Unlike the aryl halides used in the rest of the study, the radical traps were alkyl halides which might infer different activity thus conclusions cannot be drawn. Two other possible interaction can also be considered. A Ni(III) intermediate which would reform **5.1**, or a bimolecular oxidation to form Ni(6-Mes)(Ar)H and Ni(6-Mes)(H)Br. As mentioned previously Ni(II) species have been observed and will be discussed in section 5.5.

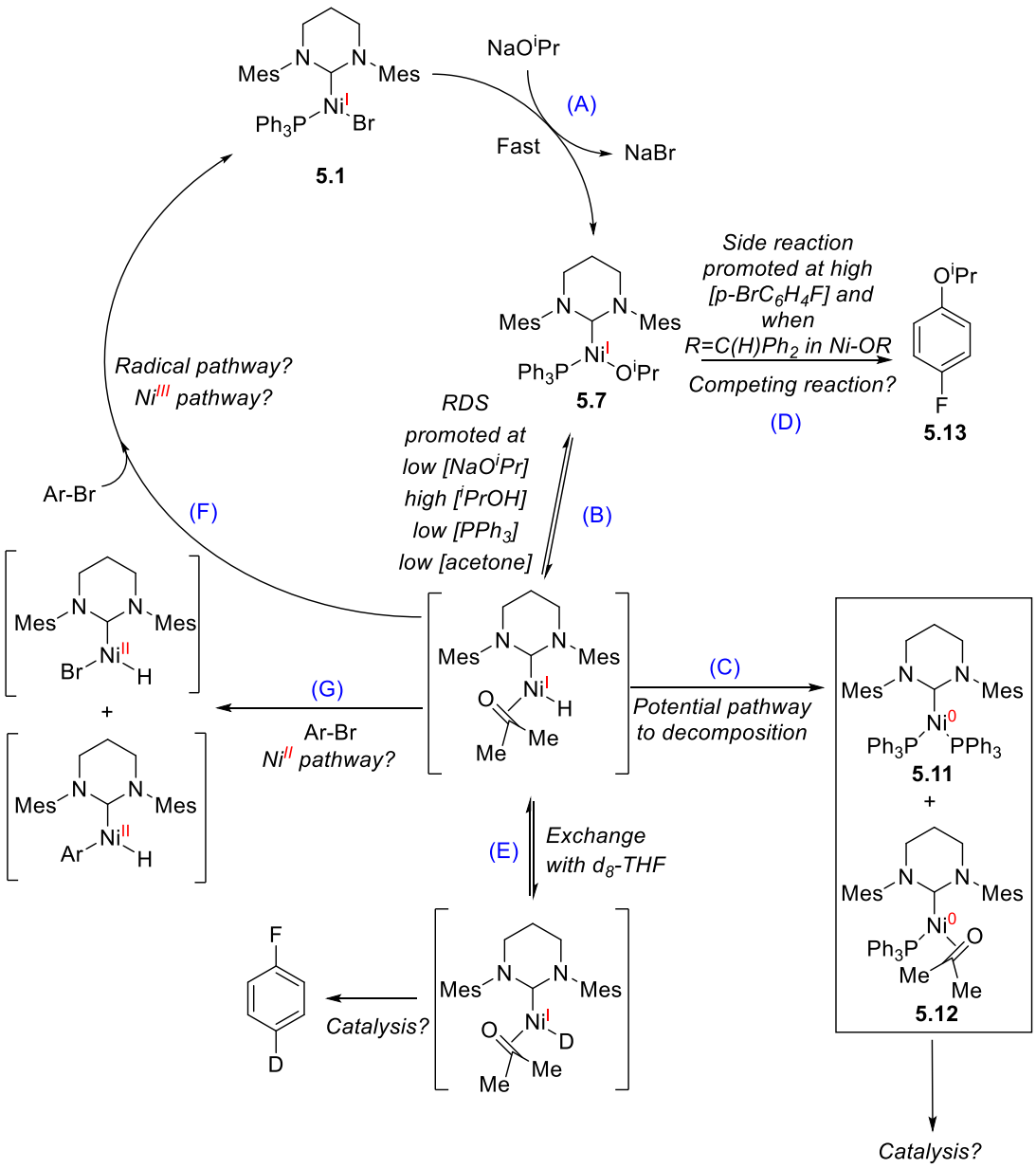


Scheme 5.38 – Postulated mechanism for the Ni(I) cycle.

## 5.5 – Ni(II) cycle

This section will focus on the second cycle of the overall scheme seen in Scheme 5.39. It will also discuss Ni species **A** which has been mentioned previously (sections 5.4.6, 5.4.9 and 5.4.10), along with comments on the formation of complex **5.19**.

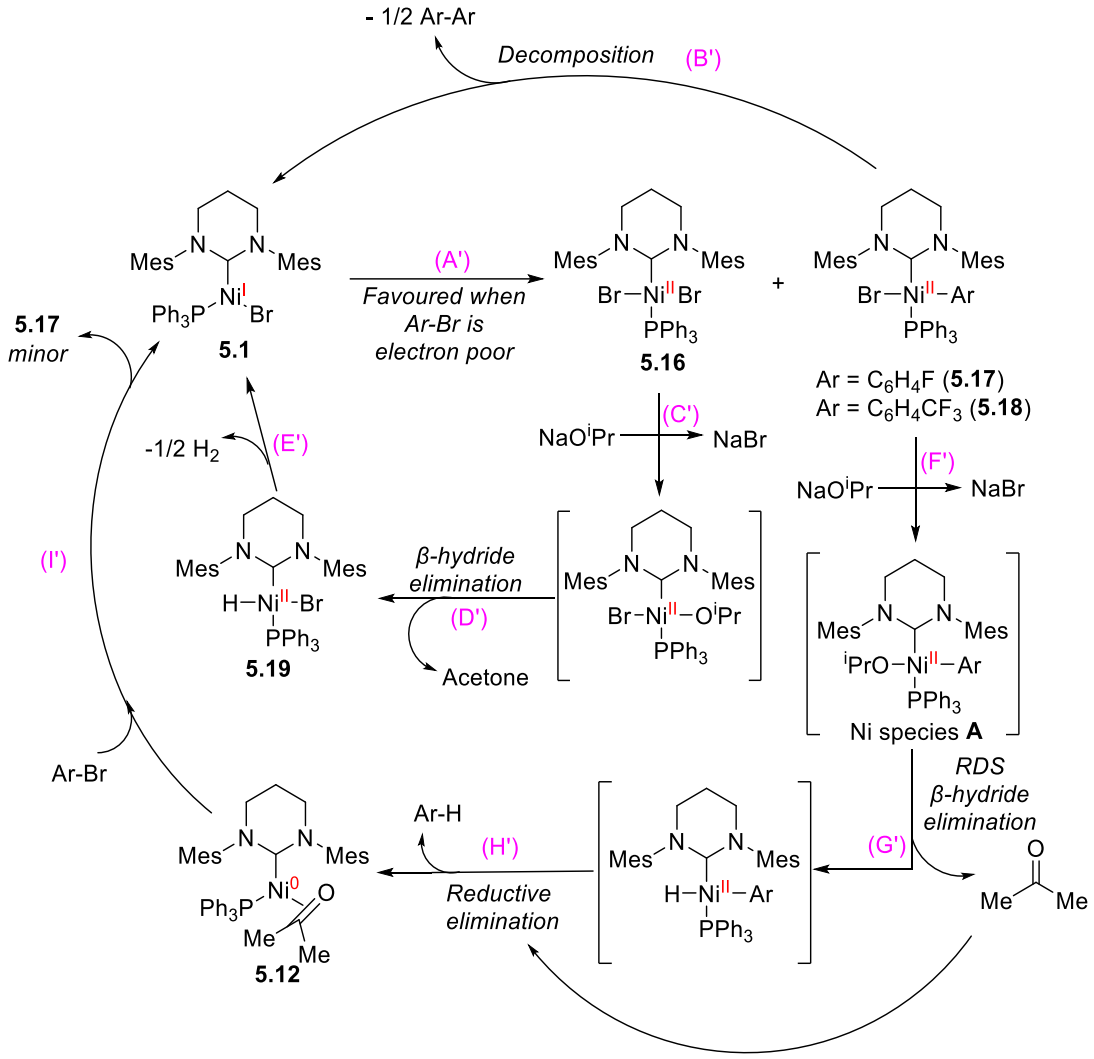


Scheme 5.39 - Postulated Ni(II) cycle for HDH. Postulated species are shown with square brackets.

## 5.5.1 – Stoichiometric Reaction of **5.1** with Ar-X

To begin investigations **5.1** was exposed to stoichiometric amounts of aryl halides with both electron donating and electron withdrawing substituents. In the case of the electron rich substrate, 4-bromoanisole, **5.1** displayed no interaction on a catalytic timescale (i.e. over 2 h at room temperature), but over 12 h the bright yellow solution changed to green. Attempts to identify reaction products failed and efforts to crystallise products yielded only a green/blue amorphous precipitate.

Treatment of complex **5.1** with an equimolar amount of 1-bromo-4-fluorobenzene revealed the rapid, but incomplete formation of two new diamagnetic Ni species over the course of 15 h (Scheme 5.40). Analysis utilising NMR spectroscopy and X-ray diffraction identified these Ni species as the Ni(II) complexes Ni(6-Mes)($PPh_3$)$Br_2$ (**5.16**) and Ni(6-Mes)($PPh_3$)($C_6H_4F$)Br (**5.17**). By $^{31}P$ NMR spectroscopy, **5.16** and **5.17** resonated at δ 16.8 (broad peak) and 25.7 ppm respectively. In the $^{19}F\{^1H\}$ NMR spectrum, **5.17** appeared at -128.8 ppm. Layering the reaction mixture with pentane yielded large yellow blocks of residual **5.1** and purple blocks of **5.16** (suitable for X-ray crystallography), but no crystals of **5.17** could be generated. Complex **5.17** has been previously reported by the Whittlesey group as one of a number of products from the reaction of Ni(6-Mes)($PPh_3$)$_2$ (**5.11**) with 1-bromo-4-fluorobenzene but was only characterised *in-situ* by NMR spectroscopy.[22]

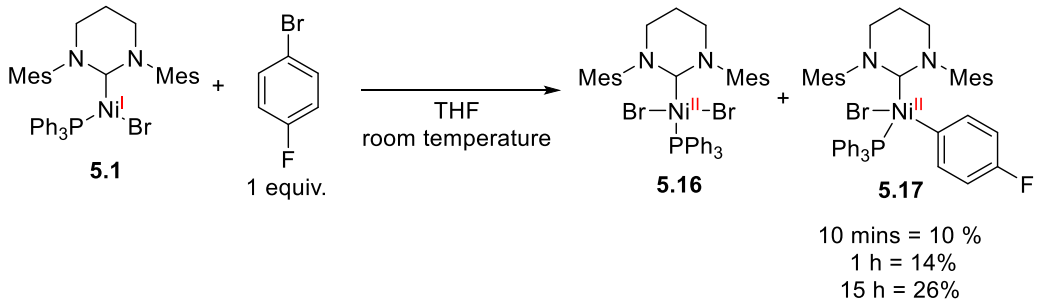


Scheme 5.40 – Reaction of complex **5.1** with equimolar 1-bromo-4-fluorobenzene. The yield of complex **5.17** was quantified by $^{19}F\{^1H\}$ NMR spectroscopy.

As a mixture of complexes **5.16** and **5.17** was formed in Scheme 5.40, **5.16** was synthesized independently as a single product from Ni($PPh_3$)$_2Br_2$ and 6-Mes (Scheme 5.41a). Attempts to form complex **5.17** from Ni(COD)$_2$, 6-Mes, $PPh_3$ and 1-bromo-4-fluorobenzene failed to give clean product. Instead, a mixture of species including complex **5.17** was formed (Scheme 5.41b). A

mixture of products was also reported previously upon addition of 1-bromo-4-fluorobenzene to Ni(6-Mes)($PPh_3$)$_2$ (**5.11**).[22]

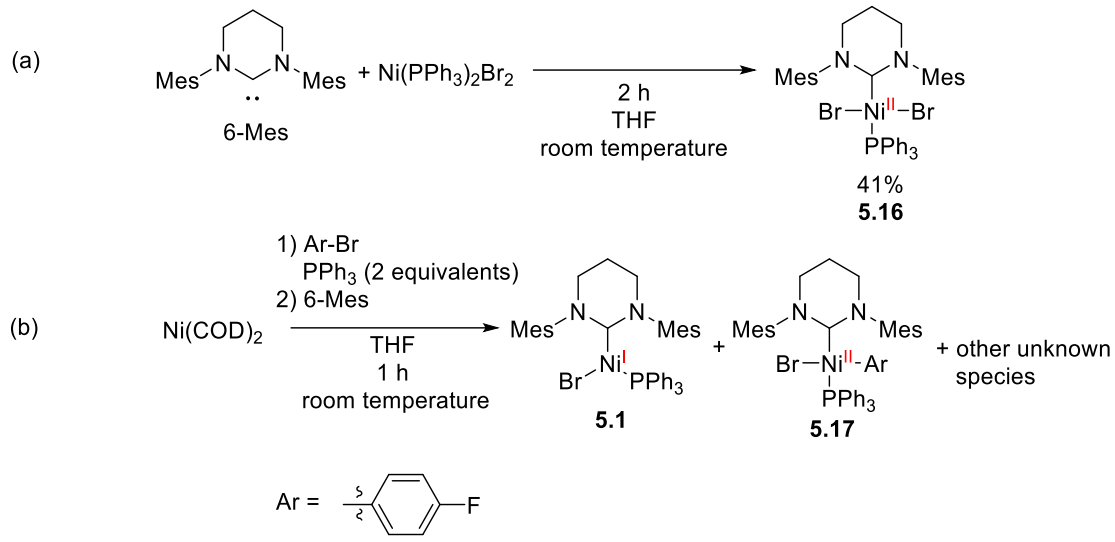


Scheme 5.41 – (a) Synthesis of complex **5.16**, and (b) Attempt to prepare complex **5.17**.

Increasing the number of equivalents of 1-bromo-4-fluorobenzene to 10 in the presence of **5.1**, increased the conversion of complex **5.1** into complexes **5.16** and **5.17** to 80% in 10 mins. Excess 1-bromo-3-fluorobenzene, which also showed fast reactivity in HDH (Table 5.3, entry 2), likewise reacted with **5.1** to give 94% conversion after 10 mins of **5.16** and the corresponding aryl bromide analogue of complex **5.17**. Thus, while incorporation of the F- substituent at either the 3- or 4- position results in rapid stoichiometric reactions with **5.1**, the different behaviour of the two substrates at early times of the catalytic HDH (Table 5.3, entries 1 and 2) imply that this is not related to biomolecular addition of the aryl bromides.

With a more electron withdrawing substrate, 4-bromobenzotrifluoride, an immediate colour change from yellow to brown was observed in a 1:1 reaction with **5.1** in THF. $^{31}P\{^1H\}$ NMR spectroscopy showed the formation of two species; **5.16** (15.1 ppm) and a product at 24.6 ppm assigned as Ni(6-Mes)($PPh_3$)($C_6H_4CF_3$)Br (**5.18**). By $^{19}F\{^1H\}$ NMR spectroscopy, 25% of **5.18** was formed within 20 mins, followed by a slow increase to 30% over 3.5 hours (Scheme 5.42a). Increasing the ratio of 4-bromobenzotrifluoride to 4:1 led to more **5.18** (43% within 15 mins) (Scheme 5.42b). There was no reaction of **5.1** with 4-chlorobenzotrifluoride.

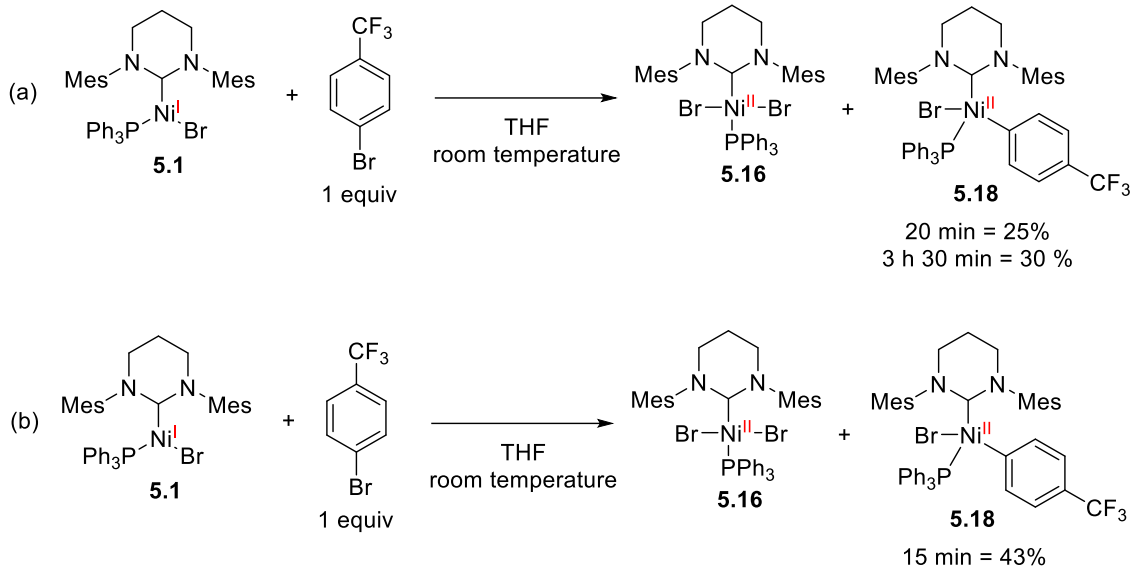


Scheme 5.42 – Product distribution in the reactions of complex **5.1** with 4-bromobenzotrifluoride in a) a 1:1 ratio and b) 4:1 ratio. The yield of complex **5.18** was quantified by $^{19}F\{^{1}H\}$ NMR spectroscopy.

**5.18** could only be crystallised with **5.16**, however crystals were picked out individually to provide characterisation (section 5.5.2 and 5.5.3). In all cases, no further reactivity nor formation of other organic products beyond **5.16** and **5.17**/**5.18** were seen over longer times (20 h).

To summarise, depending on the nature of the aryl halide the extent of the oxidation of **5.1** is affected. Those which contain electron withdrawing substrates demonstrate the ability to oxidise **5.1** with 4-bromobenzotrifluoride demonstrating a faster conversion after a shorter amount of time. A summary scheme is shown in Scheme 5.43.

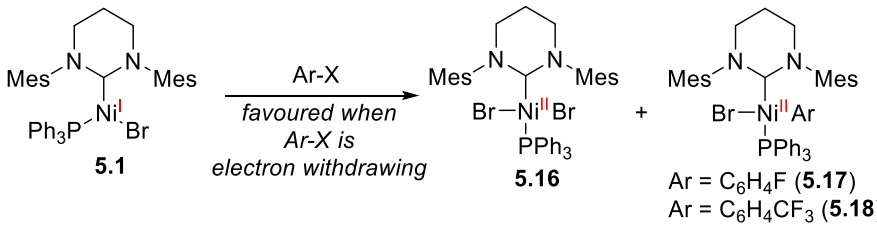


Scheme 5.43 – Scheme summarising results in section 5.5.1.

## 5.5.2 – Structural Characterisation of **5.16** and **5.18**

The X-ray structures of **5.16** and **5.18** displayed distorted square planar geometries with trans NHC-Ni-$PPh_3$ arrangements (Figure 5.30 and Figure 5.31). Notably, the $C_{NHC}$-Ni distance in **5.16** (1.9402(14) Å) is elongated upon comparison to the few other mixed NHC-Ni-$PPh_3$ complexes reported in the literature.[12,52–54] The nearest value is in Ni(IPr)($PPh_3$)$Br_2$ (1.922(5) Å reported by Zhang)[52], with the others ranging from 1.905(3) – 1.912(4) Å. The more strongly σ-donating RE-NHC ligand might be expected to yield a shorter Ni-C bond, as seen in Ni(7-*o*-tolyl)($PPh_3$)$Br_2$ ($C_{NHC}$-Ni = 1.911(5) Å),[12] the postulated difference with **5.16** is potentially due to the highly congested space around the Ni centre resulting from the bulk of the N-mesityl groups.

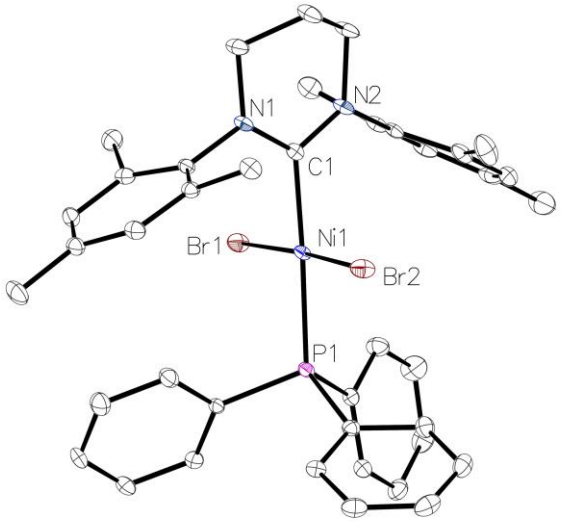


Figure 5.30 – Molecular structure of **5.16**. Hydrogen atoms have been omitted for clarity. Ellipsoids are represented at 30% probability. Selected bond lengths (Å) and angles (°): Ni1-C1 1.9402(14), Ni1-Br1 2.3026(2), Ni1-Br2 2.2997(2), Ni1-P1 2.2586(4), C1-Ni1-Br1 91.87(4), C1-Ni1-Br2 90.73(4), C1-Ni1-P1 177.24(4).

Examples of Ni(NHC)($PR_3$)(Aryl)X complexes with N-aryl substituted carbenes are scarce. Thus, the closest comparison is the phosphite complex, Ni(SIMes)($P(OPh)_3$)($C_6H_4CN$)Cl, recently described by Dorta and Stewart *via* an oxidative addition of the aryl chloride to Ni(SIMes)($P(OPh)_3$)$_2$.[55] The metrics are not that different to those in **5.18**. It is worth commenting that efforts to bring about oxidative addition to $Ni^0(NHC)_2$ precursors (NHC = IPr, IMes) instead gave three coordinate $Ni^I(NHC)_2X$ products,[56,57] whereas those with less sterically demanding NHCs, were found to undergo traditional oxidative addition.[58,59]

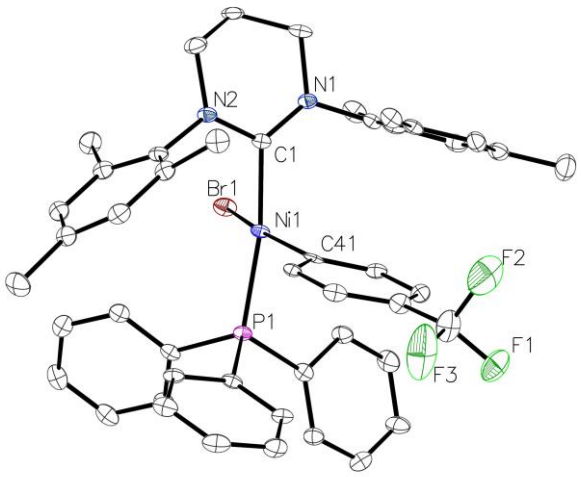


Figure 5.31 – Molecular structure of **5.18**. Hydrogen atoms have been omitted for clarity. Ellipsoids are represented at 30% probability. Selected bond lengths (Å) and angles (°): Ni1-C1 1.952(6), Ni1-Br1 2.3840(10), Ni1-C41 1.926(6), Ni1-P1 2.2236(17), C1-Ni1-Br1 90.60(18), C1-Ni1-C41 95.4(2), C1-Ni1-P1 169.69(4).

Cyclic voltammetry of the Ni(II) complex **5.16** showed no oxidation wave, however, after an initial onset of reduction at -1.3 V vs $FeCp^*_2{}^{+/0}$, similar onsets were seen in comparison to **5.1** (onset of reduction -2.3 vs $FeCp^*_2{}^{+/0}$ and an onset of oxidation at 0.0 V vs $FeCp^*_2{}^{+/0}$) (see section 5.4.3) suggesting a similar species is formed to **5.1** (if not **5.1**) which results in the same products and features.

## 5.5.3 – Solution Behaviour and Stability of **5.16** and **5.18**

As noted previously, the $^{31}P\{^{1}H\}$ NMR spectrum of **5.16** is broad, as clearly apparent from a spectrum shown in Figure 5.32 of **5.16** and **5.18** generated upon addition of 4-bromobenzotrifluoride to **5.1**.

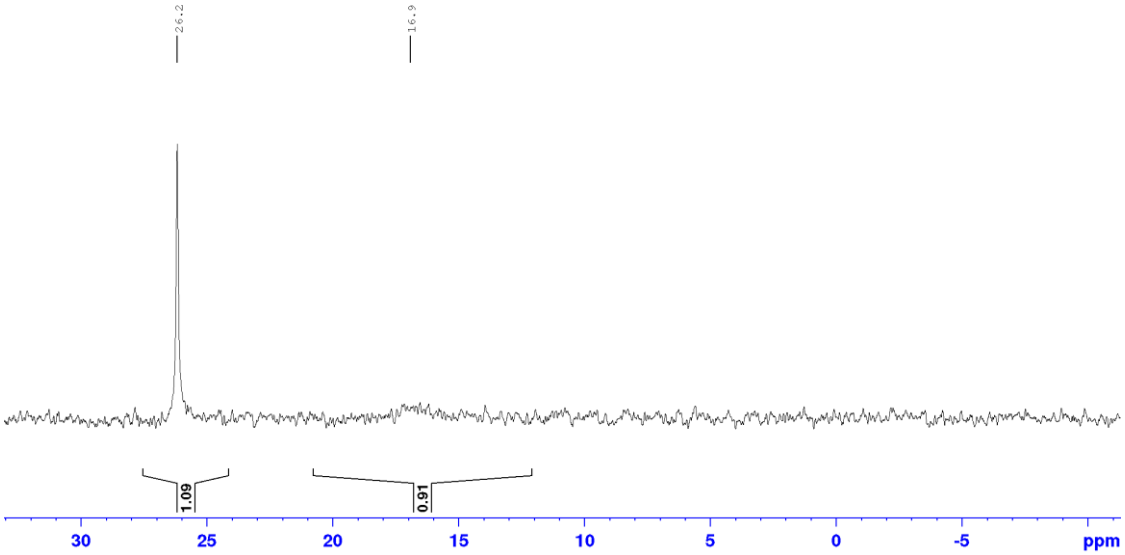


Figure 5.32 – Inverse-gated $^{31}P$ NMR spectrum (202 MHz, $d_8$-THF) of **5.16** and **5.18** from a reaction of **5.1** and 4-bromobenzotrifluoride highlighting the broadness of the resonance for **5.16**.[xxiii]

Figure 5.363 shows that upon cooling a redissolved sample of isolated **5.16**, the broad $^{31}P$ NMR resonance sharpened. The broadness that is observed for **5.16** contrasts to data for other Ni(NHC)($PR_3$)$X_2$ complexes, which are all reported to exhibit sharp $^{31}P$ signals at room temperature; Ni(IPr)($PPh_3$)$Br_2$,[52,53] Ni(I$^t$Bu)($PPh_3$)$X_2$ (X = Cl, Br),[52] Ni(IPr*)($PPh_3$)$Br_2$[60] and Ni(IPr)($PCy_3$)$Cl_2$.[54]

[xxiii] Slight shifts of the signal of **5.16** by $^{31}P$ NMR spectroscopy are observed when formed *in-situ* compared to the signal of redissolved, isolated complex (*vide-infra*).

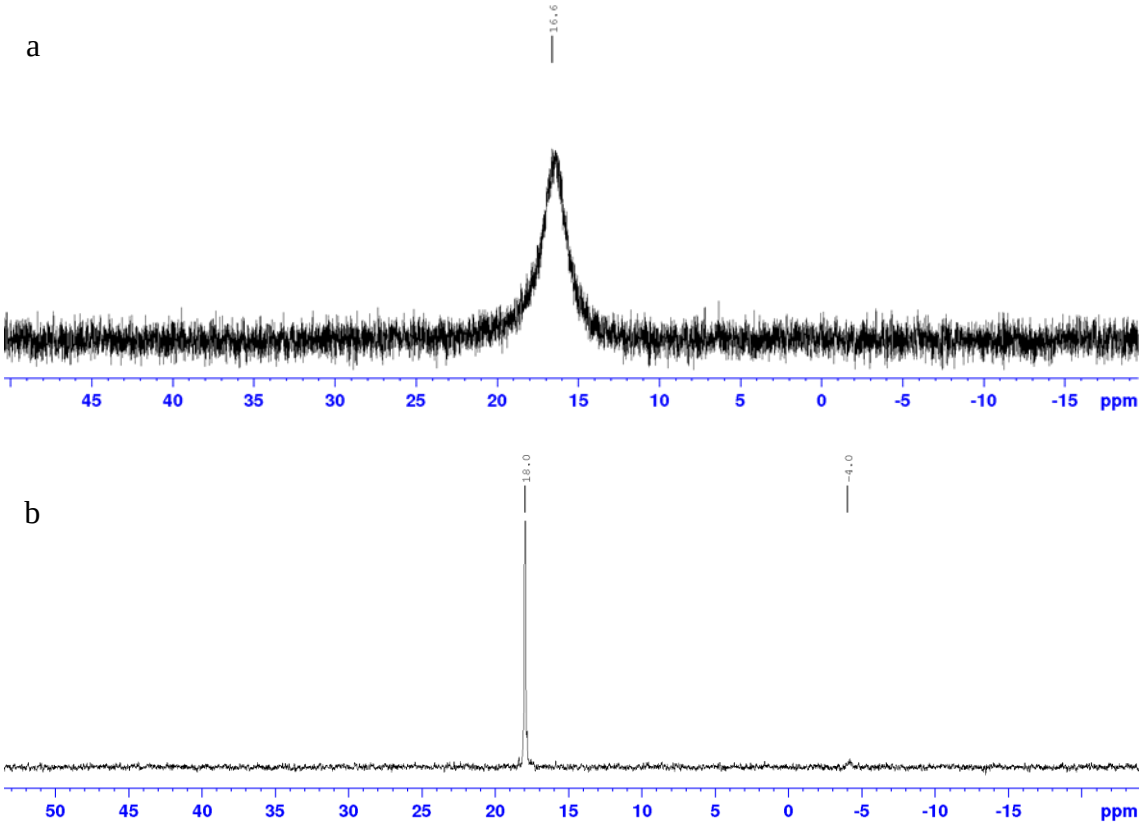


Figure 5.33 – (a) $^{31}$P NMR spectrum of **5.16** (202 MHz, $d_8$-THF) at a) 298 K and (b) 235 K (162 MHz, $d_8$-THF).

The room temperature $^{1}$H NMR spectrum of crystalline complex **5.16** revealed broad peaks between δ 8.0 – 1.0 ppm in a range of solvents ($CD_2Cl_2$, $C_6D_6$ and $d_8$-THF). Lowering the temperature to 235 K resulted signals of the 6-Mes ligand on being resolved in both the $^{1}$H (Figure 5.34) and $^{13}$C NMR spectra (see appendix 7.1.2).

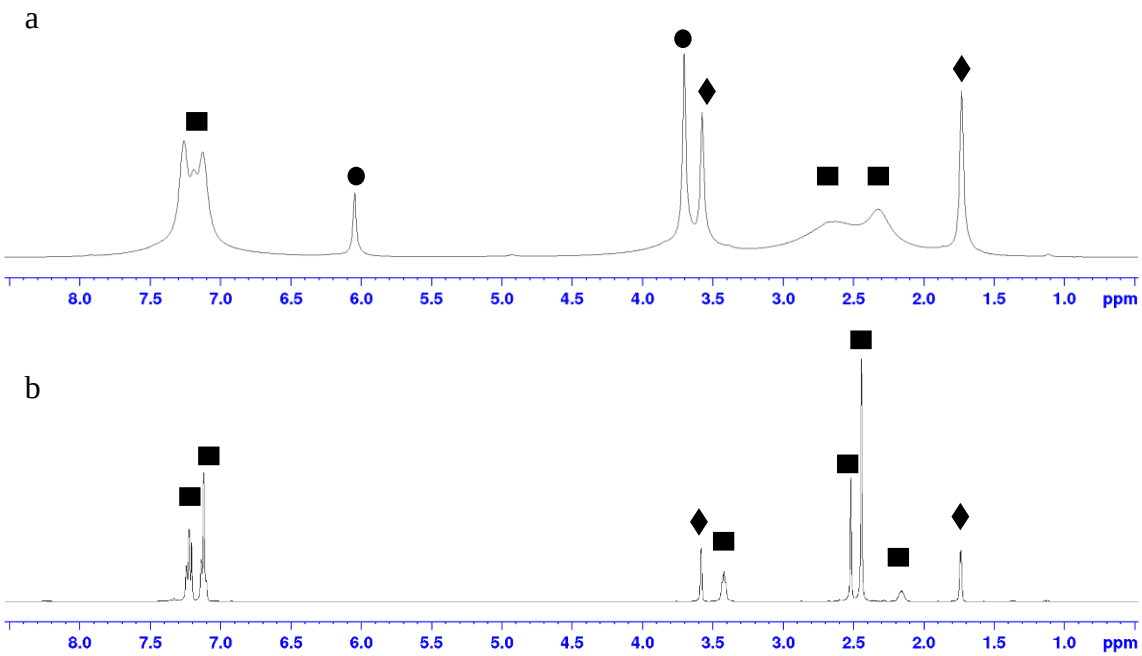


Figure 5.34 - $^{1}$H NMR spectra (400 MHz) of (a) **5.16** (■) + 1,3,5-trimethoxybenzene (●) at 298 K and (b) of **5.16** at 235 K in $d_8$-THF. ♦ $d_7$-THF

In contrast, the aryl halide complex **5.18** showed sharp $^{1}$H, $^{13}$C, $^{19}$F and $^{31}$P NMR signals at room temperature. However, over *ca*. 20 h in solution, **5.18** began to decompose with signals for 4,4'-bis(trifluoromethyl)biphenyl and **5.1** apparent from a combination of $^{1}$H and $^{19}$F NMR spectra (Scheme 5.44). The disappearance of **5.18** was slow, the compound still being observable by NMR spectroscopy after 8 days in solution at room temperature. In contrast, **5.16** was perfectly stable in solution over weeks and could be stored in air.

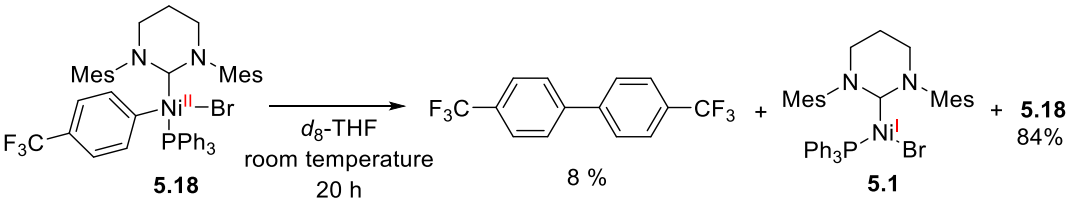


Scheme 5.44 – Decomposition of **5.18**.

## 5.5.4 – Stoichiometric reactivity of **5.16** with Ar-X and NaOR

To investigate any possible role for **5.16** in the catalytic HDH, it was subjected to a series of stoichiometric reactions. No reaction was observed when **5.16** was exposed to 1 equivalent of 1-bromo-4-fluorobenzene (Scheme 5.45a), whereas, treatment with an equimolar amount of NaO$^{i}$Pr resulted in an immediate colour change from deep purple to red. A $^{1}$H NMR spectrum recorded after 10 mins showed the major product to be the hydride complex **5.19** mentioned previously in section 5.4.9 and 5.4.10 (Scheme 5.45). Minor amounts of **5.1** and a second hydride containing species (doublet signal at -27 ppm) were also formed.

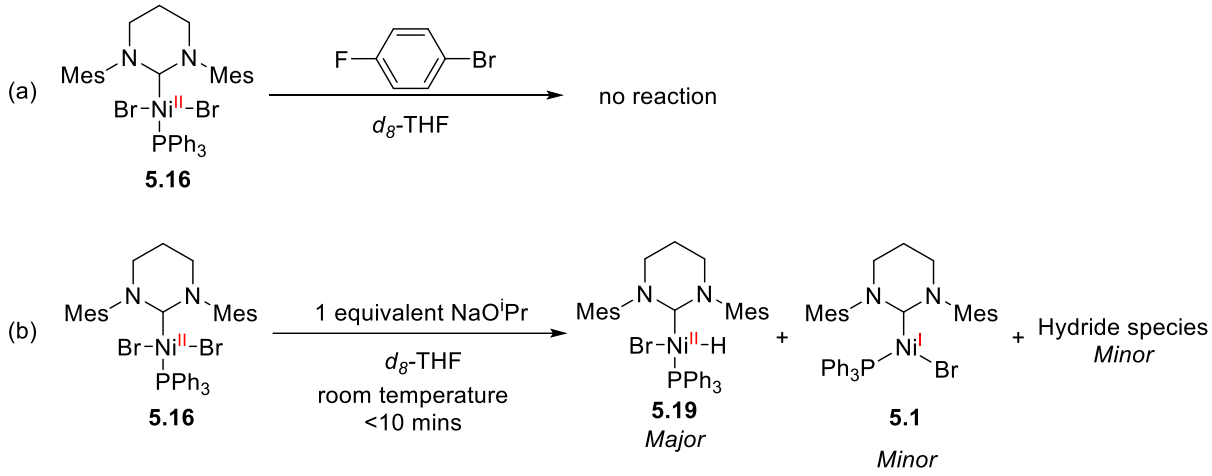


Scheme 5.45 – Stoichiometric reactions of **5.16** with (a) 1-bromo-4-fluorobenzene and (b) NaO$^{i}$Pr.

Complex **5.19** is drawn as the trans H-Ni-Br isomer on the basis of the hydride signal at -21 ppm showing a doublet coupling of $^{2}J_{HP}$ = 84 Hz. The magnitude of the $^{2}J_{HP}$ coupling it suggests the hydride is *cis*- to a phosphine.[61–67] Three signals in the alkyl region were also observed integrating to 6H each with respect to a 1H Ni-H resonance, each representing the methyl groups on the *N*-mesityl substituents in an asymmetric environment.

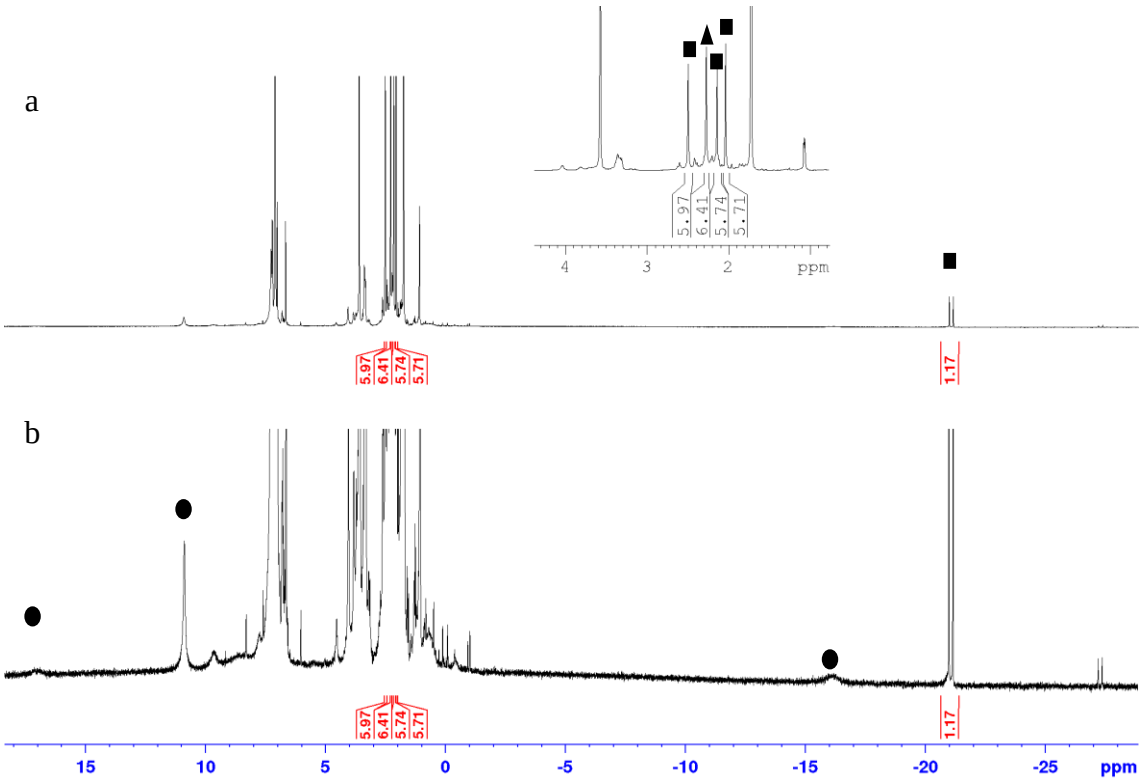


Figure 5.35 - $^{1}$H NMR spectra (500 MHz, $d_8$-THF, 298K) a) **5.16** + 1 equivalent of NaO$^{i}$Pr after 10 mins of reaction time. b) Magnified version of spectrum a. ■ = Hydride species, ● = **5.1**, ▲ = acetone, S = $d_7$-THF.

By $^{31}$P NMR spectroscopy, **5.19** appeared at 27 ppm with a doublet coupling of 84 Hz; decoupling experiments confirmed its relation to the signal at -21 ppm in the $^{1}$H NMR spectrum. The $^{13}$C NMR spectrum of the crude mixture containing **5.19** failed to show the expected doublet NCN resonance of **5.19**.

Scheme 5.46 summarises the findings from the reactions of **5.1** with electron withdrawing aryl halides followed by the reactivity of **5.16** with NaO$^{i}$Pr.

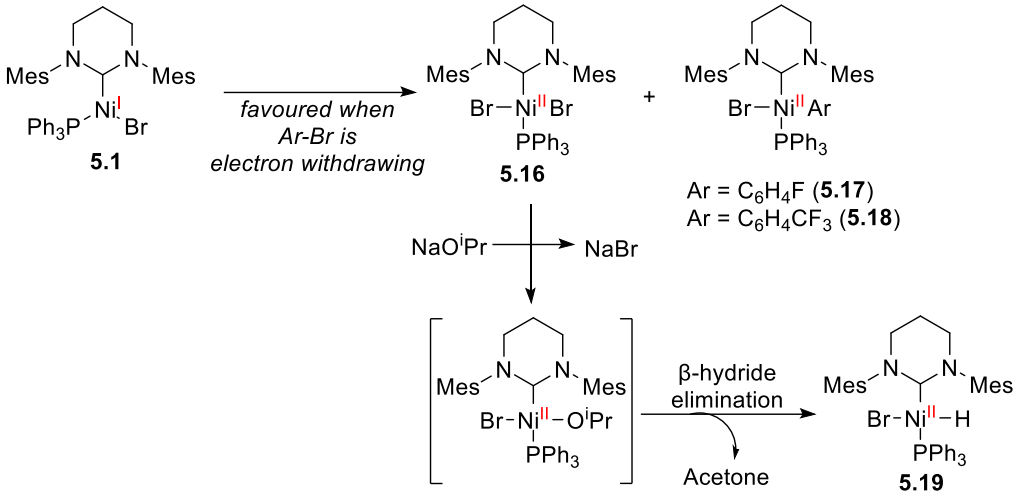


Scheme 5.46 - Updated postulated mechanism after section 5.5.5. Postulated intermediates are shown in square brackets.

## 5.5.5 – Attempts to Synthesise **5.19**

Although **5.19** was the major product in from the reaction of **5.16** and NaO$^{i}$Pr, it could not be isolated (Scheme 5.45). Thus, alternative routes to **5.19** were pursued. **5.16** failed to react with either NaH or KH in $d_8$-THF (Scheme 5.47a) and although LiHBEt$_3$ did give **5.19** (Scheme 5.47b), there was still contamination with minor amounts of complex **5.1**. Upon leaving the NMR scale reaction overnight, the concentration of **5.1** increased.

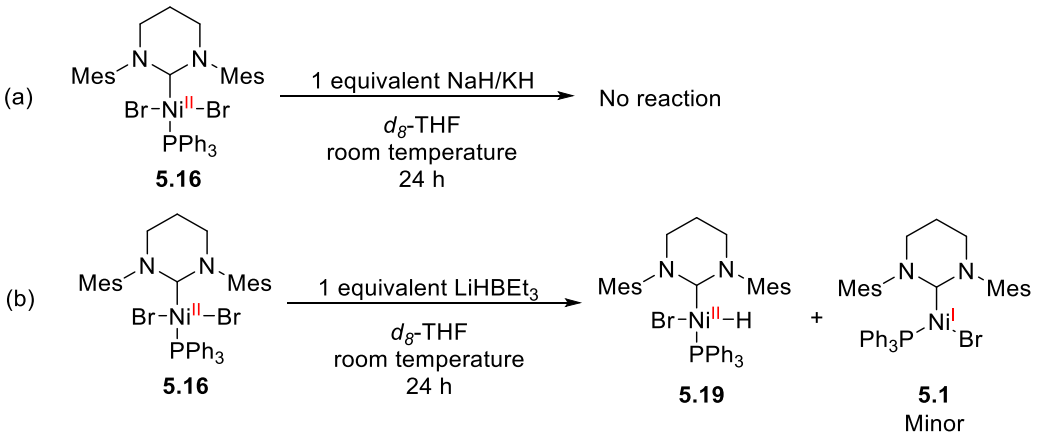


Scheme 5.47 – Attempted syntheses of **5.19**.

A possible pathway to account for the conversion of **5.19** to **5.1** would involve a bimolecular loss of hydrogen (Scheme 5.48), and indeed, free $H_2$ was observed (by $^1$H NMR spectroscopy) in a larger scale reaction of **5.16** and LiHBEt$_3$ (Figure 5.36).

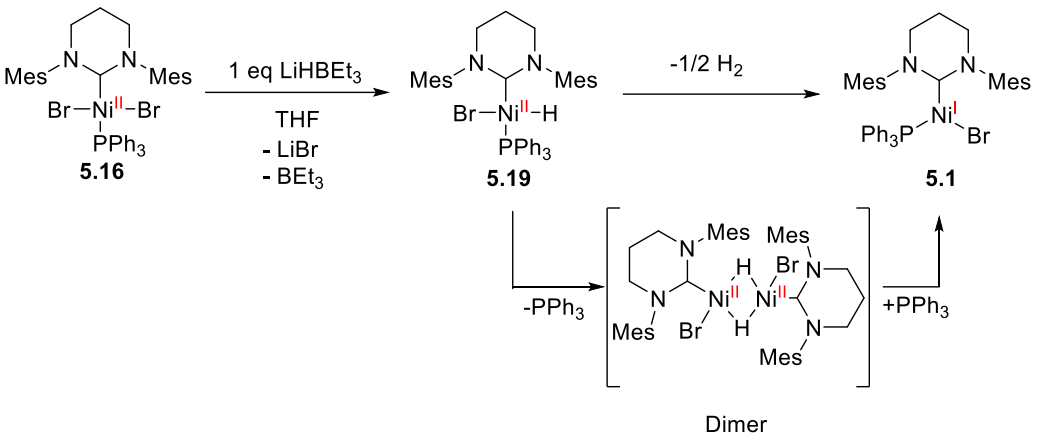


Scheme 5.48 – Postulated mechanism for the formation of **5.1** from **5.19**.

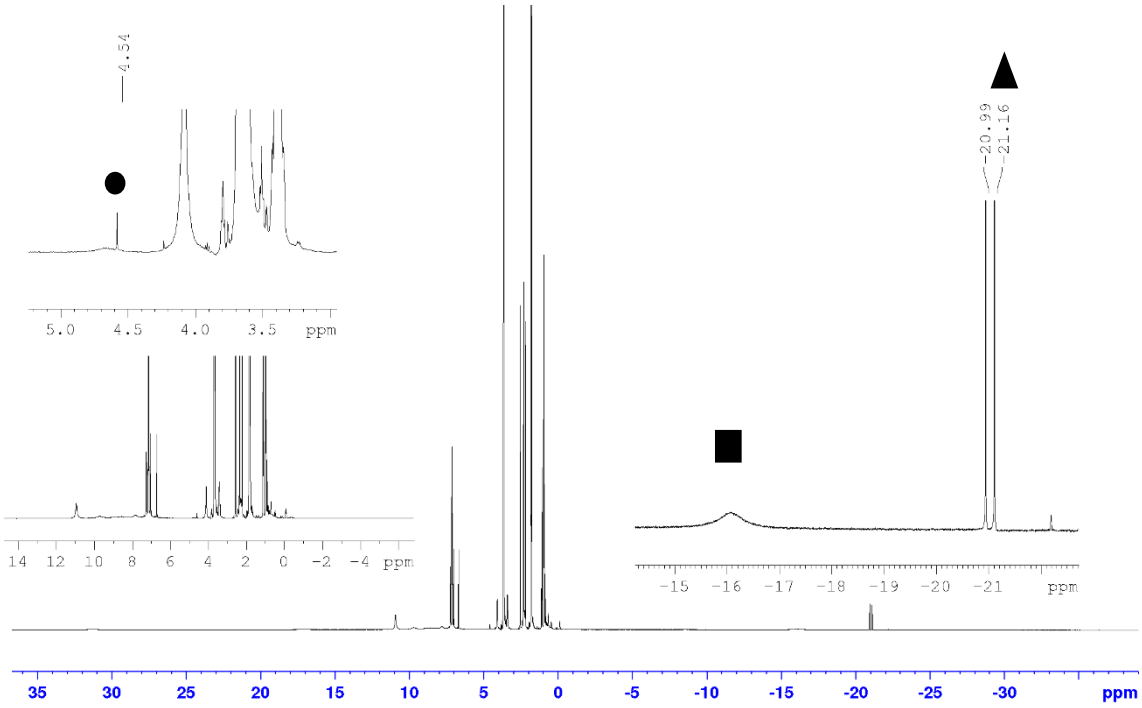


Figure 5.36 – $^{1}$H NMR (500 MHz) spectrum showing the crude presence of $H_2$ in a crude reaction mixture of **5.16** with equimolar $LiHBEt_3$ (2 M solution in THF) in $d_8$-THF. ● $H_2$, ■ **5.1** and ▲ **5.19**.

## 5.5.6 – *In-situ* reactivity of **5.19**

With the isolation of **5.19** impossible because of its slow degradation to **5.1**, efforts were turned to probing its *in-situ* reactivity. Addition of 1 equivalent of 1-bromo-4-fluorobenzene to **5.19** (generated *in-situ* from **5.16** and 1 equivalent of $NaO^{i}Pr$), led to small amounts of $C_6H_5F$ and *p*-$d_1$-$C_6H_4FD$ (< 8 % in total) by $^{19}F\{^{1}H\}$ NMR spectroscopy after 30 mins. $^{1}$H NMR spectroscopy revealed that **5.19** was mainly unaltered, suggesting that **5.19** does not react readily with 1-bromo-4-fluorobenzene.

Adding two equivalents of NaO$^i$Pr to **5.16** led to the formation of **5.19**, but now along with **5.7** (Scheme 5.49), presumably *via* the reaction of the degradation product **5.1** with excess NaO$^i$Pr. Subsequent addition of 1-bromo-4-fluorobenzene led to a greater conversion to $C_6H_5F$, but due to reaction with the Ni-O$^i$Pr complex.

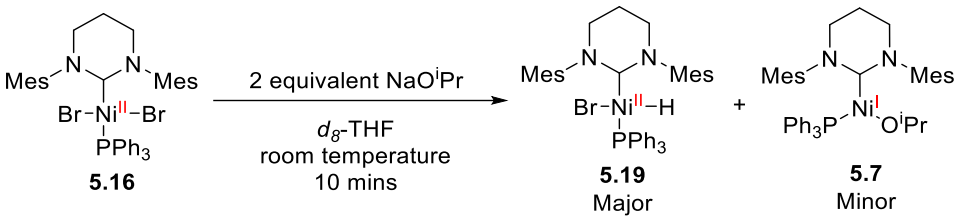


Scheme 5.49 - Reaction of **5.16**

## 5.5.7 – Ni Species **A**

Earlier in the chapter, mentions of a Ni species **A** were seen in both stoichiometric and catalytic reactions (Scheme 5.50).

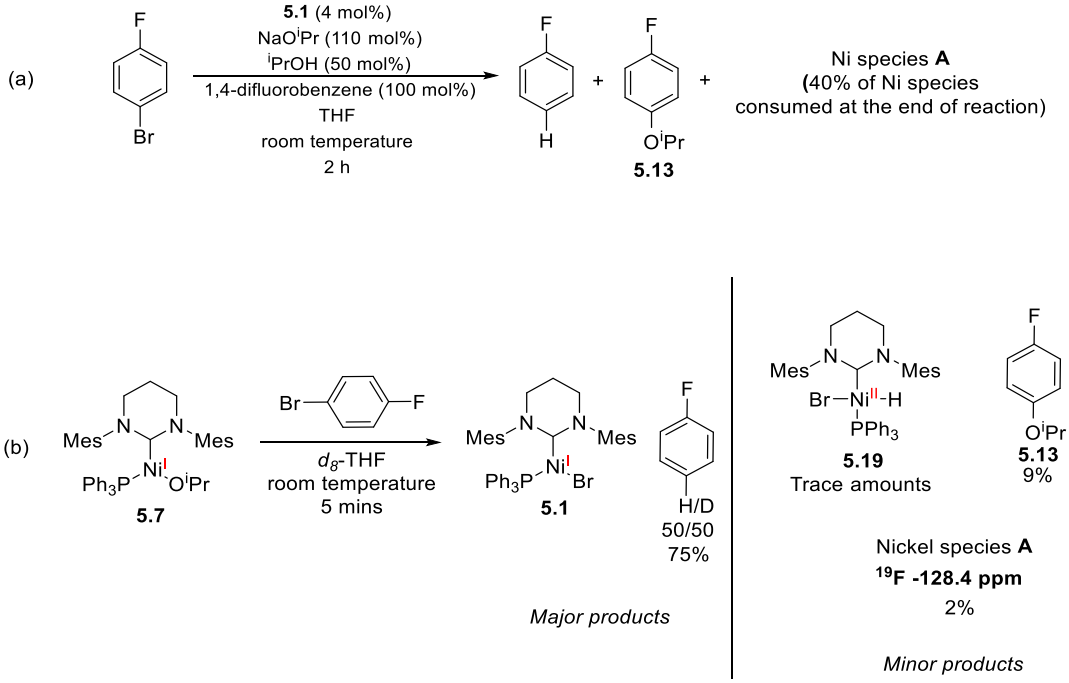


Scheme 5.50 – A summary of the previous reactions forming Ni species **A**. a) Kinetic HDH resulting in Ni species **A**. b) Stoichiometric reaction of **5.7** and 1-bromo-4-fluorobenzene resulting in Ni species **A**.

The $^{19}$F NMR signal of Ni species **A** is found at -128.4 ppm. The similarity of this chemical shift to that of **5.17** (-128.8 ppm) led to the initial postulation that Ni species **A** was **5.17**. However, when the *in-situ* formed mixture of **5.16** and **5.17** was exposed to 1 equivalent NaO$^i$Pr, $^{19}$F NMR spectroscopy revealed two closely lying peaks at -128.4 and -128.8 ppm (**5.17**) after 15 mins

(Figure 5.37a), together with $C_6H_5F$ (-114.2 ppm) and 1-bromo-4-fluorobenzene (-116.4 ppm). Overnight, the $^{19}F$ NMR spectrum revealed loss of the signal at -128.4 ppm, consumption of 1-bromo-4-fluorobenzene, together with increased amounts of $C_6H_5F$, and appearance of a new product identified as 4,4'-difluorobiphenyl (-117.1 ppm). An analogue of the new biaryl species (4,4'-bis(trifluoromethyl)biphenyl) was identified upon decomposition of the Ni(II) species **5.18** suggesting this is happening in this case with **5.17** (section 5.5.3).

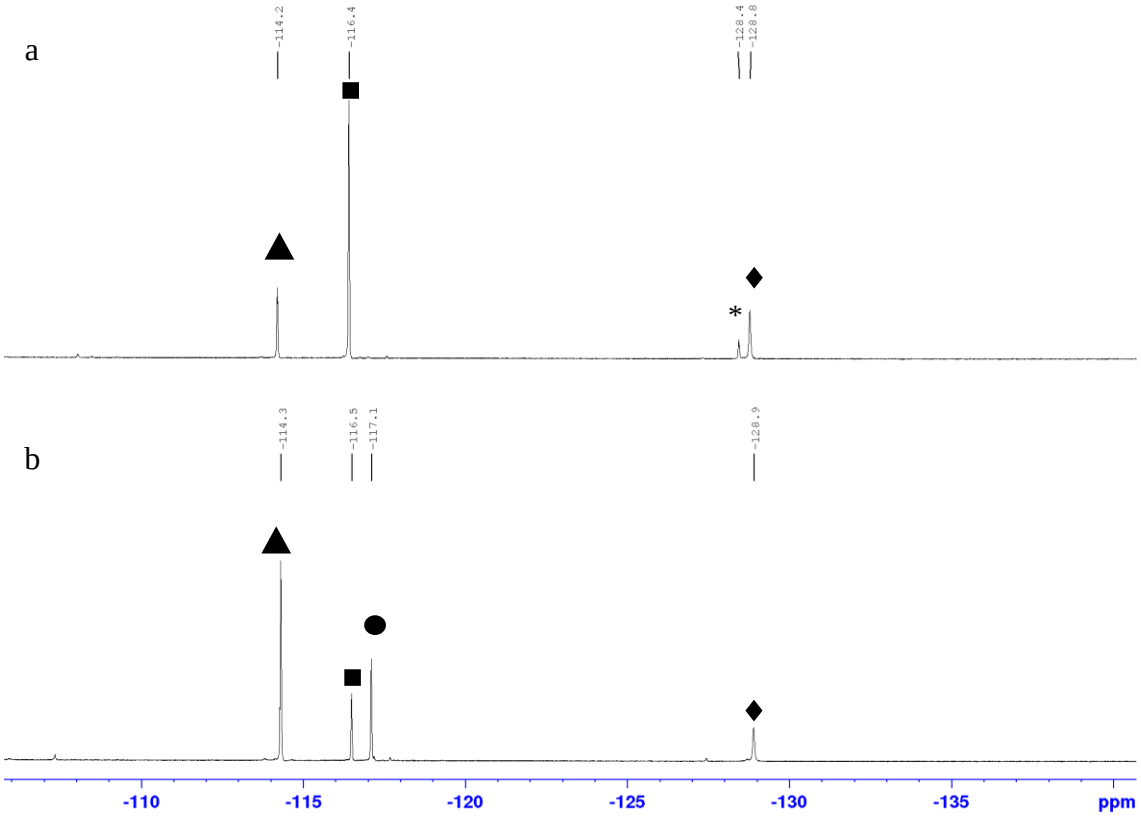


Figure 5.37 - $^{19}F$ NMR (470 MHz, $d_8$-THF) spectra of, a) **5.1** + 1 equivalent of 1-bromo-4-fluorobenzene left for 5 h followed by the addition of 1 equivalent of NaO$^i$Pr, spectrum acquired after 15 mins at room temperature. b) After leaving overnight. ■ 1-bromo-4-fluorobenzene, ▲ $C_6H_5F$/ *p*-$d_1$-$C_6H_4FD$, ● 4,4'-difluorobiphenyl, ♦ **5.8**, ***** Unknown species.

To help identify this unknown species at -128.4 ppm the isolated Ni(6-Mes)($PPh_3$)($C_6H_4CF_3$)Br (**5.18**), was exposed to NaO$^i$Pr on a small-scale experiment with its crystals. Upon addition of NaO$^i$Pr, the solution changed from pale yellow to orange. By $^1H$ NMR spectroscopy, after 5 minutes complete consumption of **5.18** was observed accompanied by the formation of a new set of carbene resonances as a major species. **5.19** and **5.1** were detected as minor products and could be assigned as products from the reaction of NaO$^i$Pr with contaminants of **5.16** (seen previously in section 5.5.4). It is worth noting no hydride peaks (aside from **5.19**) were observed.

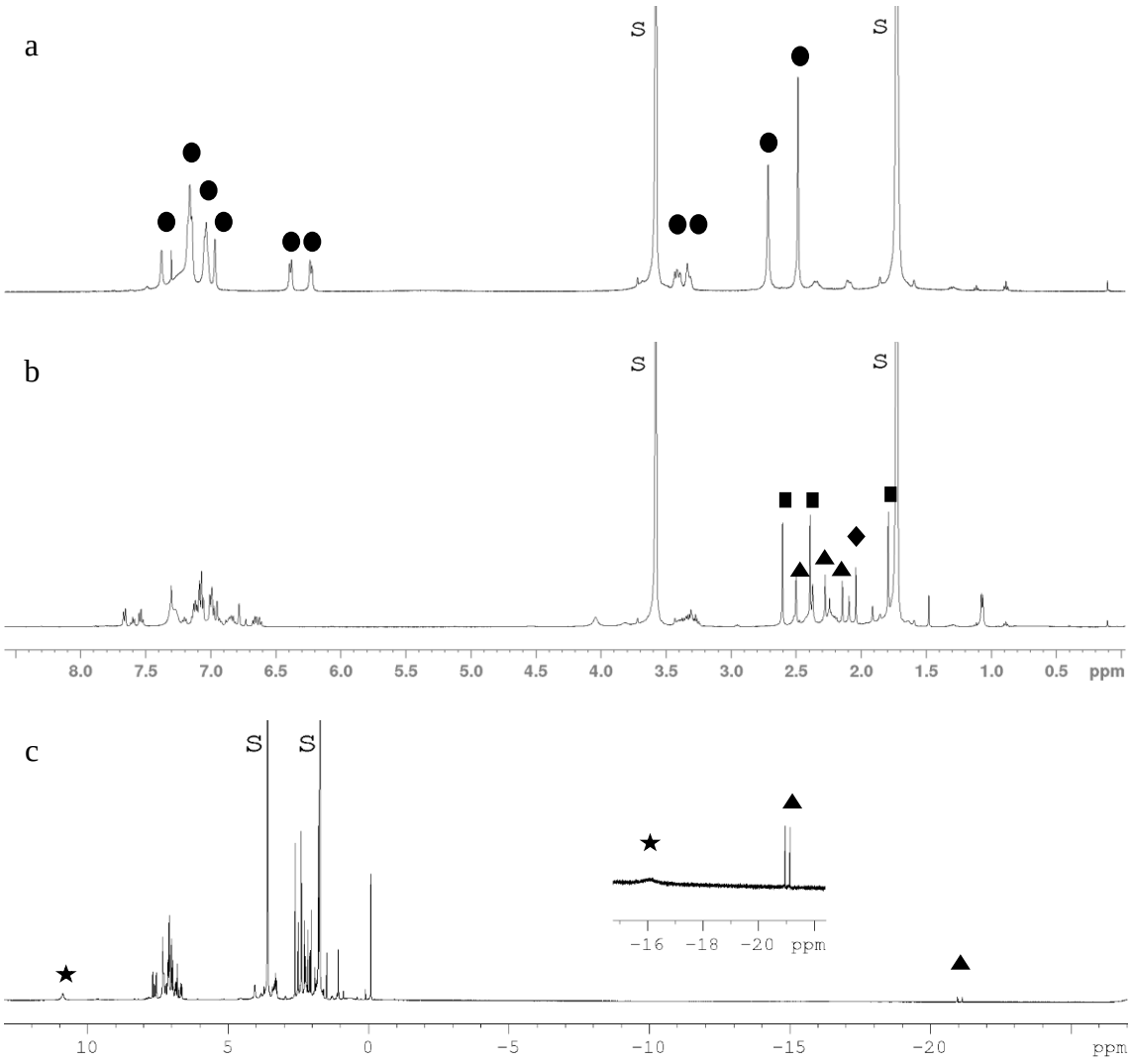


Figure 5.38 – $^{1}$H NMR (500 MHz) spectra a) **5.9** (●). b) **5.9** + 1 equivalent NaO$^{i}$Pr, 5 mins. c) Full width of spectrum b showing **5.1** (*) and **5.19** (▲). ■ denotes a new species which is unidentified but postulated to be linked to a signal 62.3 ppm by $^{19}$F{$^{1}$H} NMR spectroscopy. S denotes *d*$_{7}$-THF.

By $^{19}$F{$^{1}$H} NMR spectroscopy the formation of α,α,α-trifluorotoluene (-63.5 ppm) and an unidentified signal was observed (-62.3 ppm) (Figure 5.39), the latter was postulated to be linked with the major species in the $^{1}$H NMR spectrum (Figure 5.38). The signal at -62.3 ppm was shown to diminish overnight with the growth of α,α,α-trifluorotoluene (Figure 5.39b and c). Considering the reaction conditions, this new species is postulated to be Ni(6-Mes)($PPh_3$)($C_6H_4CF_3$)O$^{i}$Pr. Its degradation in solution is suggested to result from a β-hydride elimination and subsequent reductive elimination to provide α,α,α-trifluorotoluene. This is supported by the observed presence of **5.12** by $^{31}$P NMR spectroscopy. In light of what was observed above, it suggests Ni species **A** (-128.4 ppm by $^{19}$F NMR spectroscopy) is Ni(6-Mes)($PPh_3$)($C_6H_4F$)O$^{i}$Pr. A summary of these findings is shown in Scheme 5.51.

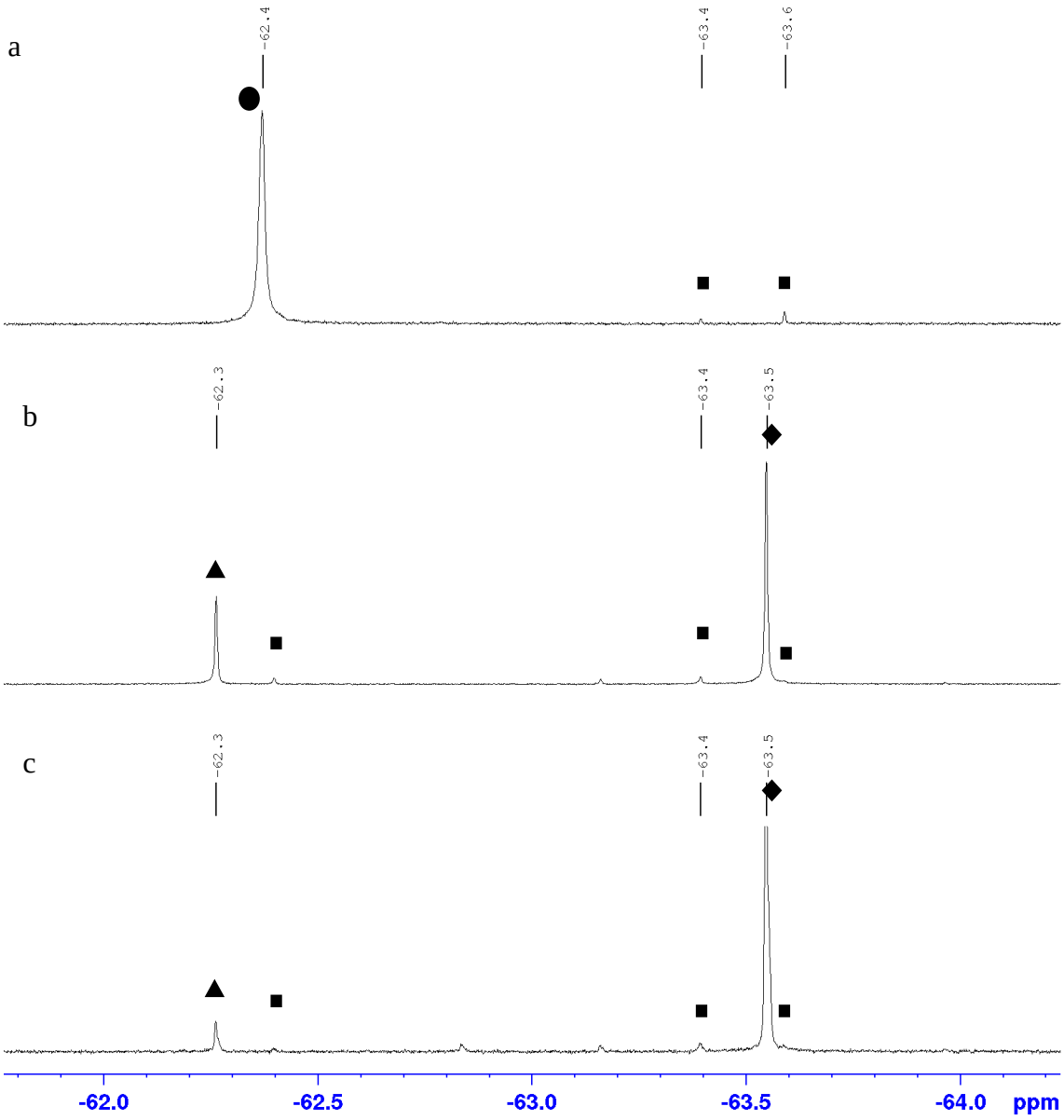


Figure 5.39 – $^{19}F\{^{1}H\}$ NMR (500 MHz) spectra a) **5.9** (●) with minor impurities (denoted as ■). b) **5.9** + 1 equivalents $NaO^{i}Pr$, 5 mins. Unidentified species (▲). c) Spectrum b left overnight at room temperature. (♦) α,α,α-trifluorotoluene.

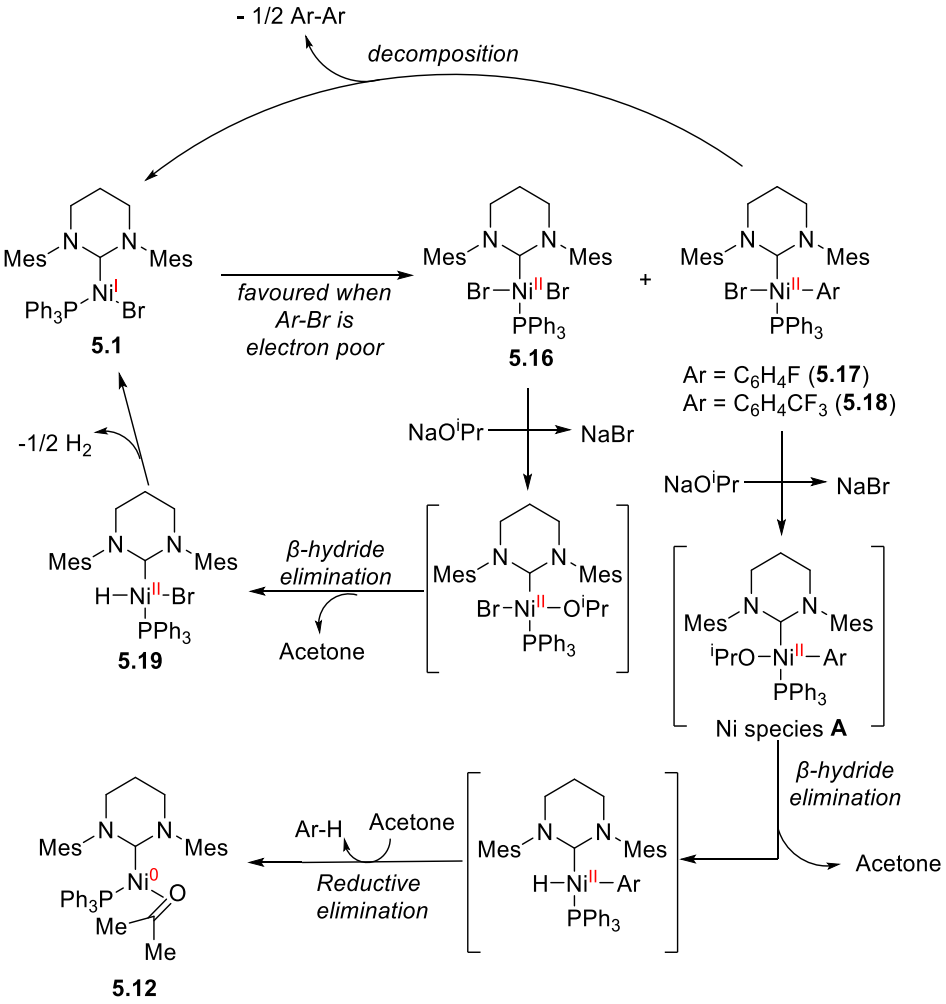


Scheme 5.51 – Updated postulated mechanism after section 5.5.7. Postulated intermediates are shown in square brackets.

It is worth considering the formation of Ni species **A** from the reaction of **5.7** and 1-bromo-4-fluorobenzene (section 5.4.9). A biomolecular oxidation of **5.7** with Ar-X would yield Ni(6-Mes)($PPh_3$)($O^iPr$)X and Ni(6-Mes)($PPh_3$)(Ar)$O^iPr$ (Scheme 5.52). The former species is postulated to result in **5.19**, where the latter is suggested to yield the desired dehalogenated product. Considering the quantity of **5.19** observed from the reaction of **5.7** and 1-bromo-4-fluorobenzene it suggests this reaction is a side reaction.

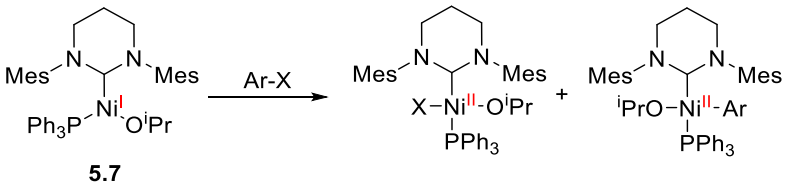


Scheme 5.52 – Postulated mechanism for the observation of Ni species **A**.

Another subtle feature this section has highlighted is the lack of $^{i}PrOC_6H_4X$ formation (X = F, $CF_3$). The most likely species to yield the organic by-product would be the Ni(II) species in the form of Ni(6-Mes)($PPh_3$)(Ar)O$^{i}$Pr (Ar = $C_6H_4F$, $C_6H_4CF_3$), however neither species formed such products. This further supports the postulation of a Ni(III) intermediate is involved to form this product (section 5.4.11).

## 5.5.8 – Ni Species **B**

As mentioned previously in section 5.4.10, reaction of **5.9** and 1-bromo-4-fluorobenzene (redrawn in Scheme 5.53) led to the formation of a species that was referred to as Ni species **B**.

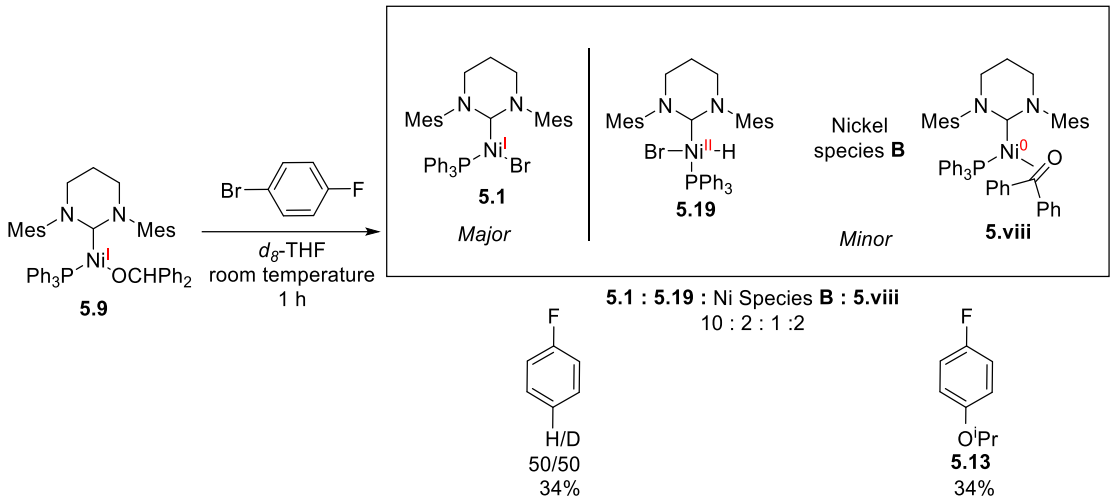


Scheme 5.53 – Products formed from the stoichiometric reaction of **5.9** and 1-bromo-4-fluorobenzene. The ratio of Ni species determined from $^{1}H$, $^{19}F\{^{1}H\}$ and $^{31}P$ NMR spectroscopy.

If we consider it an analogue of Ni species **A**, then in light of the results in section 5.5.7, it can be postulated as Ni(6-Mes)($PPh_3$)($C_6H_5F$)$OCHPh_2$. A larger amount of Ni species **B** was observed upon stoichiometric reaction of **5.9** with 1-bromo-4-fluorobenzene compared to that of Ni species **A** resulting from **5.7** and 1-bromo-4-fluorobenzene.

As with Ni species **A** if this results from a bimolecular oxidation then this would result in Ni(6-Mes)($PPh_3$)($OCHPh_2$)Br and Ni(6-Mes)($PPh_3$)($C_6H_4F$)$OCHPh_2$ (Scheme 5.54). The former would undergo β-hydride elimination to yield **5.19**. The latter through a β-hydride elimination and reductive elimination could account for the observation of **5.viii**. However, despite Ni species **B** being more predominant than Ni species **A** in this reaction, the major product is still **5.1** supporting the biomolecular oxidation of Ni(I)-OR as a side reaction under stoichiometric conditions.

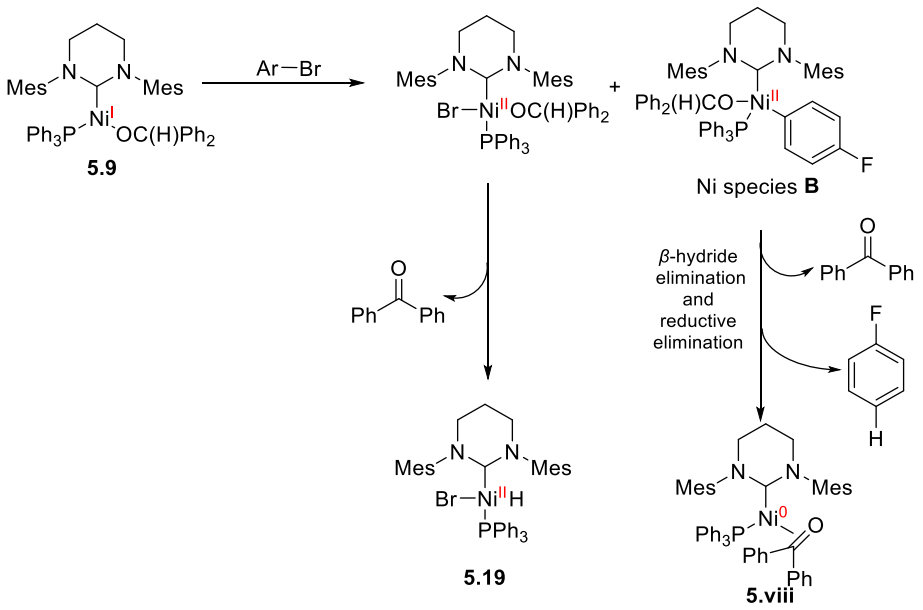


Scheme 5.54 – Postulated reactivity of **5.9**.

## 5.5.9 – Potential roles for Ni(0) species in HDH

The roles of two other Ni species in catalysis need to be considered; the Ni(0) complex Ni(6-Mes)($PPh_3$)$_2$ (**5.11**) and Ni(6-Mes)($PPh_3$)(O=C($CH_3$)$_2$) (**5.12**). **5.12** could not be isolated, however was observed in section 5.4.4 as a decomposition product (alongside **5.11**) from **5.7**. **5.12** was also observed as a final product from **5.18** with NaO$^i$Pr (section 5.5.7). Sabater demonstrated **5.12** could be formed *in-situ* from **5.11** and acetone which suggests these two complexes can be products of each other depending on the conditions.[22] A key reaction for these Ni(0) species is their reactivity to Ar-X. Sabater demonstrated in the presence of 1.3 equivalents of 1-bromo-4-fluorobenzene **5.11** would be oxidised to a mixture of **5.1** (major) and **5.17** (minor) (Scheme 5.55b).[22]

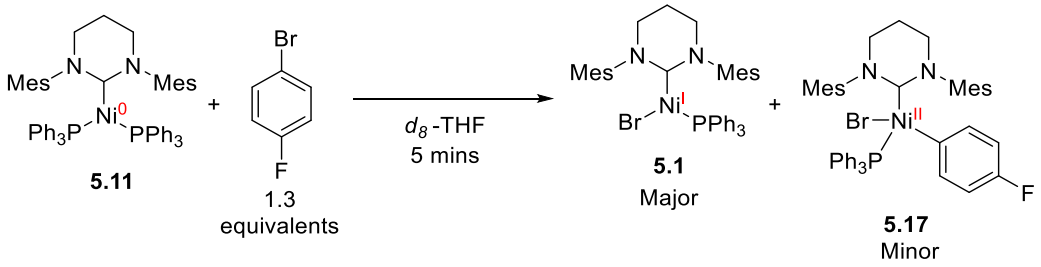


Scheme 5.55 – Reactivity of **5.11**.

To probe **5.11** reactivity further, a 1:1 reaction with **5.16** was carried out where the formation of **5.1** was observed by $^1$H NMR spectroscopy after 0.5 h (Scheme 5.56). Extended times led to the $^1$H NMR spectrum becoming more paramagnetic. By $^{31}$P{$^1$H} NMR no free $PPh_3$ was observed, however a broad baseline peak was observed suggesting interchange of $PPh_3$ with a Ni species

(section 5.4.7). If both **5.11** and **5.16** are present during catalysis it does provide an alternative pathway back to **5.1**. The Ni(0) complex **5.12** may also undergo a similar reaction with **5.16**, potentially resulting in a more favourable interaction**.**

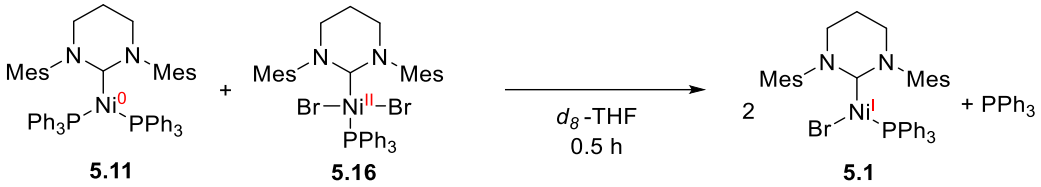


Scheme 5.56 – Observed reactivity from a stoichiometric reaction of **5.11** and **5.16** in $d_8$-THF.

## 5.5.10 – Catalytic testing of **5.7**, **5.9**, **5.11** and **5.16**

The complexes obtained previously were tested under catalytic conditions to determine if they are catalytically active for HDH of 1-bromo-4-fluorobenzene (Table 5.7). **5.7** gave comparable yields to **5.1** of both $C_6H_5F$ and the by-product **5.13** (entries 1 vs 2). Both the bulkier Ni(I) alkoxide **5.9** as well as the Ni(0) complex **5.11** proved less active (entries 3 and 4). Interestingly the Ni(II) complex **5.16** gave the highest yield of HDH product with only minimal formation of **5.13** (entry 5). An experiment which involved the premixing of **5.1** with 1-bromo-4-fluorobenzene to form **5.16** and **5.17** *in-situ* before the addition of $NaO^iPr$ (to start the catalysis) was also run, where comparable results to entries 1 and 2 were obtained.

Table 5.7 - Results of HDH with different Ni precursors.[a]

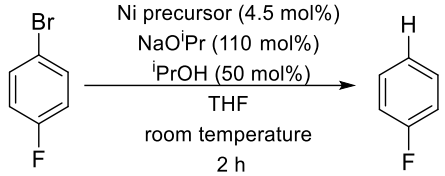


| Entry | Catalyst precursor | Yield of $C_6H_5F$ (%) | Yield of 4-$FC_6H_4O^iPr$ (**5.13**) (%) |
|---|---|---|---|
| 1 | Ni(6-Mes)($PPh_3$)Br (**5.1**) | 88 | 7 |
| 2 | Ni(6-Mes)($PPh_3$)O$^i$Pr (**5.7**) | 90 | 6 |
| 3 | Ni(6-Mes)($PPh_3$)$OCHPh_2$ (**5.9**) | 41 | 7 |
| 4 | Ni(6-Mes)($PPh_3$)$_2$ (**5.11**) | 40 | 1 |
| 5 | Ni(6-Mes)($PPh_3$)$Br_2$ (**5.16**) | 94 | 1 |
| 6 | Ni(6-Mes)($PPh_3$)Br (**5.1**)[c] | 84 | 5 |

[a]Reaction conditions: 0.134 mmol 1-bromo-4-fluorobenzene, 4.5 mol% Ni precursor, 110 mol% NaO$^i$Pr, 50 mol% $^i$PrOH in THF (1 mL). Yields determined by $^{19}F\{^1H\}$ NMR spectroscopy relative to an internal standard of 1,4-difluorobenzene (100 mol%) and reported as an average of two runs after 2 hours. [c]**5.1** and 1-bromo-4-fluorobenzene premixed for 2 h before addition of NaO$^i$Pr to start the catalysis.

As expected, **5.7** demonstrated similar yields to **5.1**, suggesting both species can access the same catalytic cycle. The bulkier Ni(I) alkoxide, **5.9**, demonstrated a loss of activity compared to **5.1** and **5.7** which suggests after the initial turn over, the resulting Ni species in the system are not as active, as the catalytic conditions utilise NaO$^i$Pr which would ultimately form a cycle with **5.1** and **5.7**. The Ni(0) complex **5.11** was shown to b**e** catalytically active, however only at half the capacity compared to **5.1** suggesting this is not a major species on the cycle.

The role of **5.16** is perplexing. From the stoichiometric experiments in section 5.5.4, the formation of **5.1** can be achieved *via* reaction of **5.16** with NaO$^i$Pr. If this was the case then similar activity and by-products are to be expected to entry 1 and 2 (Table 5.7), however this is not the case.

## 5.5.11 – Summary of Section 5.5

A final mechanism summarising section 5.5 is shown in Scheme 5.57. In the presence of electron withdrawing groups on Ar-Br, **5.1** undergoes a bimolecular oxidation (step A') to yield Ni(6-Mes)($PPh_3$)$Br_2$ (**5.16**) and Ni(6-Mes)($PPh_3$)(Ar)Br (**5.17** or **5.18**). **5.17**/**5.18** were observed to slowly decompose in solution back to **5.1** with the elimination of Ar-Ar (section 5.5.3) (step B'). It is worth noting during the catalytic HDH, that no such species is observed. Step C' is the reaction of **5.16** with $NaO^iPr$ which has been postulated to form Ni(6-Mes)($PPh_3$)($O^iPr$)Br (section 5.5.4) this rapidly forms Ni(6-Mes)($PPh_3$)(H)Br (**5.19**) which is observed (step D'). **5.19** was found to reduce in solution to **5.1** (step E') and showed no interaction with Ar-Br (section 5.5.5). **5.17**/**5.18** both reacted with $NaO^iPr$, leading to a new species postulated to be Ni(6-Mes)($PPh_3$)(Ar)$O^iPr$ (step F') (section 5.5.7). These species were found to be consumed over time to give the desired dehalogenated product *via* β-hydride elimination and reductive elimination (steps G' and H'). The resulting Ni species was found to be **5.12**. Step I' would be the reformation of **5.1** through the reaction of **5.12** and Ar-X with minor amounts of Ni(6-Mes)($PPh_3$)(Ar)Br.

During the kinetic studies, **5.17** and/or Ni(6-Mes)($PPh_3$)($C_6H_4F$)$O^iPr$ was observed in a large amount (38% mol% of Ni species).[xxiv] This suggests Ni species **A** is a resting state in this cycle.

[xxiv] This was difficult to identify since the catalytic runs were in protio THF resulting in slightly broader $^{19}F$ signals making distinction of the two species **5.17** and Ni(6-Mes)($PPh_3$)($C_6H_4F$)$O^iPr$ difficult.

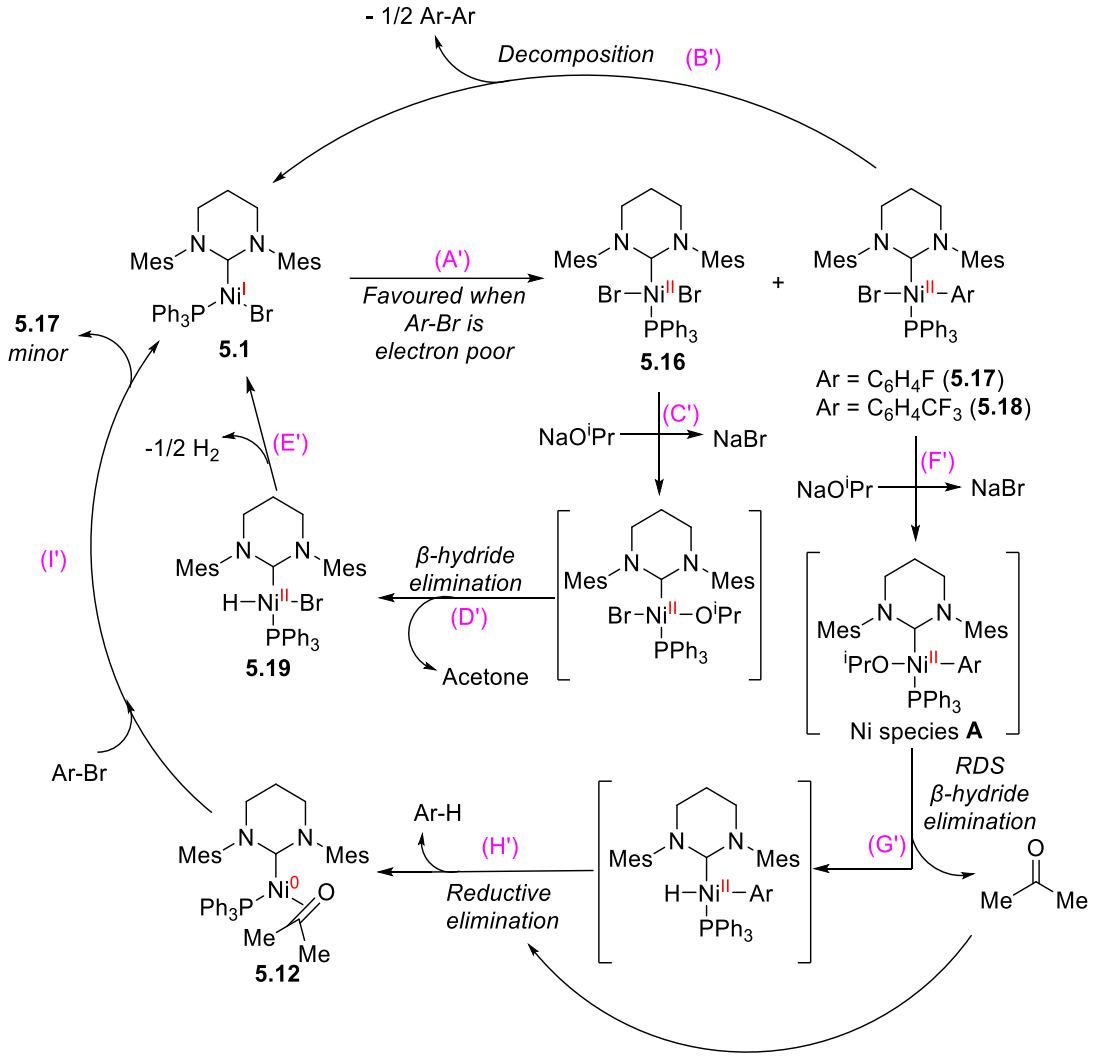


Scheme 5.57 – Postulated mechanism for the Ni(II) cycle.

## 5.6 – Conclusions and Future Work

Combining the two mechanisms from section 5.4.14 and 5.5.11 results in the overall proposed pathway for the HDH reaction shown in Scheme 5.58. While the initial direction of the cycle could potentially be dictated by the aryl halide, there are some steps which can potentially provide access to the other cycle without forming **5.1**. For example, **5.7** in the presence of 1 equivalent of 1-bromo-4-fluorobenzene yielded minor amounts of **5.19** and Ni(6-Mes)($PPh_3$)(Ar)O$^i$Pr (section 5.4.10). Under catalytic conditions this pathway may be promoted which could account for the observed Ni(6-Mes)($PPh_3$)(Ar)X (X= Br, O$^i$Pr) in the kinetic runs (Step G). Another example is step H (Scheme 5.58), where if the resulting interaction is a biomolecular oxidation, two Ni(II) species could form integrating into the Ni(II) cycle. Despite this, it is apparent **5.1** is a catalytically active species in this cycle regardless of which route HDH takes. As mentioned previously, the major factor deciding which route the HDH follows seems to be determined by the electronics of the aryl halide. Most of this study (especially the kinetics) has been investigated with 1-bromo-4-fluorobenzene and this cycle may differ if other substrates are used. Future work should focus on investigating other Ar-X substrates in both stoichiometric and kinetic studies in to establish if one of these cycles becomes dominant. Future work should also focus on the reactivity and isolation of the Ni(II) species **5.17**/**5.18**, and, potentially how they react with **5.19**. The reactivity of the low coordinate Ni(0) species **5.12** should also be investigated if it can be synthesised without going *via* **5.11**, as the additional $PPh_3$ may have perturbed what we observed.

Future work is also needed on the C-O bond forming reaction which leads to the side product **5.13**. Formation of such products of this type are limited in the literature. They could be useful to expand synthetic libraries. If a weaker C-X bond promotes this reaction (e.g. 4-bromobenzotrifluoride), then C-I or C-OTf bonds should be investigated to develop this reactivity.

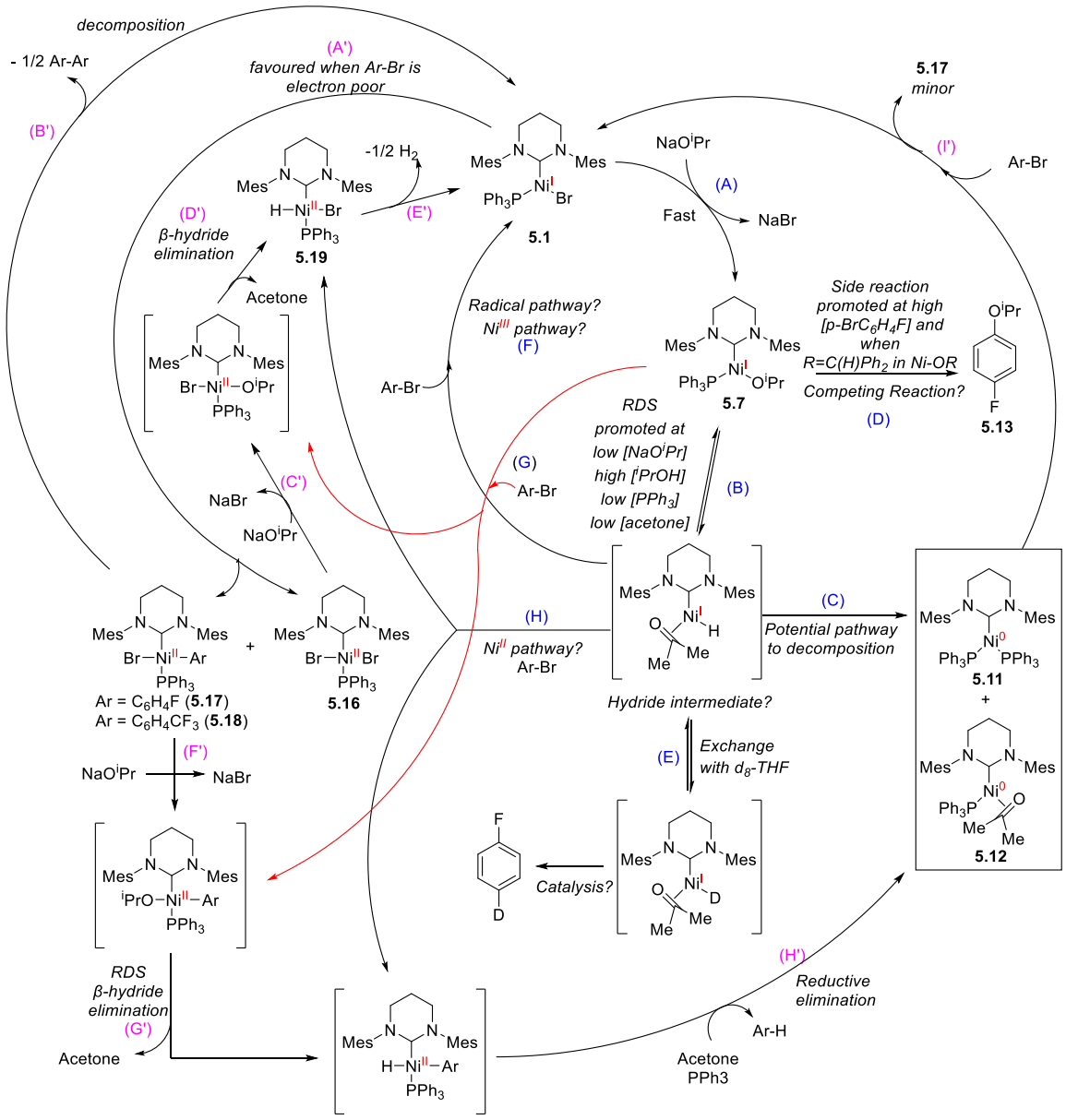


Scheme 5.58 – Overall scheme for Ni(RE-NHC) mediated catalytic hydrodehalogenation.

## 5.7 – References


1 F. Alonso, I. P. Beletskaya and M. Yus, *Chem. Rev.*, 2002, **102**, 4009–4091.

2 C. Desmarets, S. Kuhl, R. Schneider and Y. Fort, *Organometallics*, 2002, **21**, 1554–1559.

3 A. Leleu, Y. Fort and R. Schneider, *Adv. Synth. Catal.*, 2006, **348**, 1086–1092.

4 S. Kuhl, R. Schneider and Y. Fort, *Adv. Synth. Catal.*, 2003, **345**, 341–344.

5 R. A. Kelly, N. M. Scott, S. Diez, E. D. Stevens and S. P. Nolan, *Organometallics*, 2005, **24**, 3442–3447.

6 C. A. Rettenmeier, J. Wenz, H. Wadepohl and L. H. Gade, *Inorg. Chem.*, 2016, **55**, 8214–8224.

7 T. Inatomi, Y. Koga and K. Matsubara, *Molecules*, 2018, **23**, 140.

8 K. Matsubara, H. Yamamoto, S. Miyazaki, T. Inatomi, K. Nonaka, Y. Koga, Y. Yamada, L. F. Veiros and K. Kirchner, *Organometallics*, 2017, **36**, 255–265.

9 Z. Wang, X. Li, H. Sun, O. Fuhr and D. Fenske, *Organometallics*, 2018, **37**, 539–544.

10 C. J. E. Davies, M. J. Page, C. E. Ellul, M. F. Mahon and M. K. Whittlesey, *Chem. Commun.*, 2010, **46**, 5151–5153.

11 W. J. M. Blackaby, PhD Thesis, University of Bath, 2020.

12 R. C. Poulten, I. López, A. Llobet, M. F. Mahon and M. K. Whittlesey, *Inorg. Chem.*, 2014, **53**, 7160–7169.

13 R. C. Poulten, PhD Thesis, University of Bath, 2015.

14 M. J. Page, W. Y. Lu, R. C. Poulten, E. Carter, A. G. Algarra, B. M. Kariuki, S. A. Macgregor, M. F. Mahon, K. J. Cavell, D. M. Murphy and M. K. Whittlesey, *Chem. Eur. J.*, 2013, **19**, 2158–2167.

15 T. Inatomi, Y. Fukahori, Y. Yamada, R. Ishikawa, S. Kanegawa, Y. Koga and K. Matsubara, *Catal. Sci. Technol.*, 2019, **9**, 1784–1793.

16 N. P. van Leest, R. F. J. Epping, K. M. van Vliet, M. Lankelma, E. J. van den Heuvel, N. Heijtbrink, R. Broersen and B. de Bruin, *Single-Electron Elementary Steps in Homogeneous Organometallic Catalysis*, Elsevier: London, London, 2018, vol. 70.

17 C. Y. Lin and P. P. Power, *Chem. Soc. Rev.*, 2017, **46**, 5347–5399.

18 B. R. Dible, M. S. Sigman and A. M. Arif, *Inorg. Chem.*, 2005, **44**, 3774–3776.

19 M. I. Lipschutz and T. D. Tilley, *Organometallics*, 2014, **33**, 5566–5570.

20 L. M. Martínez-Prieto, P. Palma, E. Álvarez and J. Cámpora, *Inorg. Chem.*, 2017, **56**, 13086–13099.

21 W. J. M. Blackaby, S. Sabater, R. C. Poulten, M. J. Page, A. Folli, V. Krewald, M. F. Mahon, D. M. Murphy, E. Richards and M. K. Whittlesey, *Dalton. Trans.*, 2018, **47**, 769–782.

22 S. Sabater, M. J. Page, M. F. Mahon and M. K. Whittlesey, *Organometallics*, 2017, **36**, 1776–1783.

23 O. Blum and D. Milstein, *J. Am. Chem. Soc.*, 1995, **117**, 4582–4594.

24 T. Mutsumi, H. Iwata, K. Maruhashi, Y. Monguchi and H. Sajiki, *Tetrahedron*, 2011, **67**, 1158–1165.

25 V. I. Bakhmutov, F. Bozoglian, K. Gómez, G. González, V. V. Grushin, S. A. Macgregor, E. Martin, F. M. Miloserdov, M. A. Novikov, J. A. Panetier and L. V. Romashov, *Organometallics*, 2012, **31**, 1315–1328.

26 N. A. Eberhardt and H. Guan, *Chem. Rev.*, 2016, **116**, 8373–8426.

27 S. J. Tereniak, E. E. Marlier and C. C. Lu, *Dalton. Trans.*, 2012, **41**, 7862–7865.

28 A. L. J. Beckwith and A. A. Zavitsas, *J. Am. Chem. Soc.*, 1995, **117**, 607–614.

29 L. M. Martínez-Prieto and J. Cámpora, *Isr. J. Chem.*, 2020, **60**, 373–393.

30 S. Bertini and M. Albrecht, *Organometallics*, 2020, **39**, 3410–3424.

31 O. Blum and D. Milstein, *J. Organomet. Chem.*, 2000, **593**–**594**, 479–484.

32 N. A. Smythe, K. A. Grice, B. S. Williams and K. I. Goldberg, *Organometallics*, 2009, **28**, 277–288.

33 B. Martín-Matute, J. B. Åberg, M. Edin and J. E. Bäckvall, *Chem. Eur. J.*, 2007, **13**, 6063–6072.

34 J. C. M. Ritter and R. G. Bergman, *J. Am. Chem. Soc.*, 1998, **120**, 6826–6827.

35 N. M. Camasso and M. S. Sanford, *Science*, 2015, **347**, 1218–1220.

36 J. A. Terrett, J. D. Cuthbertson, V. W. Shurtleff and D. W. C. MacMillan, *Nature*, 2015, **524**, 330–334.

37 P. T. Matsunaga, G. L. Hillhouse and A. L. Rheingold, *J. Am. Chem. Soc.*, 1993, **115**,

2075–2077.

38 P. T. Matsunaga, J. C. Mavropoulos and G. L. Hillhouse, *Polyhedron*, 1995, **14**, 175–185.

39 R. A. Escobar and J. W. Johannes, *Chem. Eur. J.*, 2020, **26**, 5168–5173.

40 D. Wang and J. R. Gardinier, *Eur. J. Inorg. Chem*, 2020, 4425–4434.

41 J. B. Diccianni, J. Katigbak, C. Hu and T. Diao, *J. Am. Chem. Soc.*, 2019, **141**, 1788–1796.

42 S. Pelties, D. Herrmann, B. de Bruin, F. Hartl and R. Wolf, *Chem. Commun.*, 2014, **50**, 7014–7016.

43 U. Chakraborty, F. Urban, B. Mühldorf, C. Rebreyend, B. De Bruin, N. van Velzen, S. Harder and R. Wolf, *Organometallics*, 2016, **35**, 1624–1631.

44 B. C. Fullmer, H. Fan, M. Pink and K. G. Caulton, *Inorg. Chim. Acta*, 2011, **369**, 49–54.

45 A. M. Wright, H. T. Zaman, G. Wu and T. W. Hayton, *Inorg. Chem.*, 2013, **52**, 3207–3216.

46 D. Isrow and B. Captain, *Inorg. Chem.*, 2011, **50**, 5864–5866.

47 C. Rettenmeier, H. Wadepohl and L. H. Gade, *Chem. Eur. J.*, 2014, **20**, 9657–9665.

48 O. M. Gonzalez-James, X. Zhang, A. Datta, D. A. Hrovat, W. T. Borden and D. A. Singleton, *J. Am. Chem. Soc.*, 2010, **132**, 12548–12549.

49 H. Nishiyama, H. Hosoya, B. F. Parker, H. Tsurugi, J. Arnold and K. Mashima, *Chem. Commun.*, 2019, **55**, 7247–7250.

50 J. A. Przyojski, K. P. Veggeberg, H. D. Arman and Z. J. Tonzetich, *ACS Catal.*, 2015, **5**, 5938–5946.

51 A. C. Albéniz, P. Espinet, R. López-Fernández and A. Sen, *J. Am. Chem. Soc.*, 2002, **124**, 11278–11279.

52 J. Zhang, J. Xu, Y. Xu, H. Sun, Q. Shen and Y. Zhang, *Organometallics*, 2015, **34**, 5792–5800.

53 K. Matsubara, K. Ueno and Y. Shibata, *Organometallics*, 2006, **25**, 3422–3427.

54 E. E. Touney, R. Van Hoveln, C. T. Buttke, M. D. Freidberg, I. A. Guzei and J. M. Schomaker, *Organometallics*, 2016, **35**, 3436–3439.

55 J. Duczynski, A. N. Sobolev, S. A. Moggach, R. Dorta and S. G. Stewart, *Organometallics*, 2020, **39**, 105–115.

56 S. Miyazaki, Y. Koga, T. Matsumoto and K. Matsubara, *Chem. Commun.*, 2010, **46**, 1932–1934.

57 K. Zhang, M. Conda-Sheridan, S. R. Cooke and J. Louie, *Organometallics*, 2011, **30**, 2546–2552.

58 T. Schaub and U. Radius, *Chem. Eur. J.*, 2005, **11**, 5024–5030.

59 L. Kuehn, D. G. Jammal, K. Lubitz, T. B. Marder and U. Radius, *Chem. Eur. J.*, 2019, **25**, 9514–9521.

60 G. Lu, R. Li, Z. Shen, Q. Wu and H. Sun, *Appl. Organomet. Chem.*, 2020, **34**, e5741.

61 O. V. Ozerov, C. Guo, L. Fan and B. M. Foxman, *Organometallics*, 2004, **23**, 5573–5580.

62 K. Jonas and G. Wilke, *Angew. Chem. Int. Ed.*, 1969, **8**, 519–520.

63 A. L. Seligson, R. L. Cowan and W. C. Trogler, *Inorg. Chem.*, 1991, **30**, 3371–3381.

64 R. Beck, M. Shoshani, J. Krasinkiewicz, J. A. Hatnean and S. A. Johnson, *J. Chem. Soc. Dalton. Trans.*, 2013, **42**, 1461–1475.

65 J. A. Hatnean, R. Beck, J. D. Borrelli and S. A. Johnson, *Organometallics*, 2010, **29**, 6077–6091.

66 M. L. H. Green and T. Saito, *J. Chem. Soc. D Chem. Commun.*, 1969, 1969.

67 L. H. Green, *J. Chem. Soc. A*, 1971, 152–154.

68 Y. Tian, X. Guo, I. Krummenacher, Z. Wu, J. Nitsch, H. Braunschweig, U. Radius, T. Marder, *J. Am, Chem, Soc*., 2020, **142**, 18231-18242.

# Chapter 6

# Chapter 6 – Experimental

## 6.1 – General Methods and Instrumentation

All manipulations were carried out using standard Schlenk line or glovebox techniques under an atmosphere of argon unless stated otherwise. Solvents were purified (i) using an MBraun SPS solvent system (dichloromethane, diethyl ether, hexane, toluene), (ii) by refluxing/distillation under $N_2$ over sodium/benzophenone (benzene, tetrahydrofuran) or $Mg/I_2$ (*iso*-propanol, *tert*-butanol, MeOH), (iii) by stirring under Ar with Drierite™ followed by vacuum transfer (acetone) and, for dichloromethane, diethyl ether and tetrahydrofuran, storage over activated 4 Å molecular sieves ( and (v) by standing over a potassium mirror (benzene, hexane, toluene). Deuterated solvents were vacuum transferred from potassium ($C_6D_6$, *d*$_8$-toluene, *d*$_8$-THF) or calcium hydride ($CD_2Cl_2$, $CDCl_3$). $^1$H, $^{11}$B, $^{13}$C, $^{19}$F and $^{31}$P NMR spectra were recorded on Bruker Avance 300, 400 and 500 MHz or Agilent 500 MHz NMR spectrometers at 298 K unless stated otherwise. $^1$H and $^{13}$C NMR spectra are referenced internally to solvent resonances ($C_6D_6$ = 7.16 and 128.0 ppm; $CDCl_3$ = 7.26 and 77.2 ppm; $CD_2Cl_2$ = 5.32 and 54.0 ppm; *d*$_8$-THF = 3.58 and 67.2 ppm; *d*$_8$-toluene = 2.08 and 20.4 ppm).[1] $^{11}$B, $^{19}$F and $^{31}$P NMR spectra are referenced externally to δ = 0.00 ($^{11}$B = 15% $BF_3{\cdot}OEt_2$ in $CDCl_3$; $^{19}$F = $CFCl_3$; $^{31}$P = $H_3PO_4$). Assignments were confirmed as necessary with the use of selective decoupling and two-dimensional correlation experiments. Chemical shifts (δ) are quoted in ppm and coupling constants (*J*) in Hz. Elemental analyses were performed by Elemental Microanalysis Ltd., Okehampton, Devon, UK. High-resolution mass spectrometry was conducted with a MaXis HD quadrupole APCI time-of-flight (APCI-QTOF) mass spectrometer (Bruker) with analyses performed in APCI positive mode. A 8890 gas chromatography (GC, Agilent) system coupled with 5977B MSD (MS, Agilent) was used for the analysis. Split injections of 1 µL were performed, with a split ratio of 10:1 (split flow of 10 mL/min), using with a single taper, ultra-inert wool inlet liner (Agilent 5190-2293). The inlet was heated to 220°C with 3 mL/min septum purge flow. An Agilent HP-5MS (30 m, 0.25mm, 0.25µm) column was used with He (BOC, N5.5) as the carrier gas, at a constant flow of 1.0 mL/min. The column oven gradient started at 40°C, then ramped at 10°C/min to 120°C, then at 80°C/min to 320°C, with a total analysis time of 15 mins. The MSD transfer line was set at 280°C, MSD source at 230°C, and the MSD quad temperature was set to 150°C. After an initial solvent delay of 4 min the MSD detection

was performed using full scan mode, over the range of 50 – 350 m/z, with a scan speed of 1562 µs, and a gain factor of 15. Data analysis was performed in the Agilent Qualitative Analysis v.10.0 and used the NIST 17 library to identify and confirm compounds through spectral matching. A representative GC spectrum is shown in Appendix 4. The GC was calibrated by preparing a multiple point external standard calibration curve. Standard solutions were prepared covering the expected substrate concentration range. A linear response of the detector to substrate concentration was determined for the whole range.

## 6.2 – Literature Procedures and Starting Materials

[6-MesH]$BF_4$,[2] [7-MesH]$BF_4$,[2] [6-XylylH]$BF_4$,[2] [7-XylylH]$BF_4$,[2] [6-DippH]$BF_4$,[2] [7-DippH]$BF_4$,[2] [7-neoPentH]$BF_4$,[3] [8-MesH]$BF_4$,[4] (6-MesDAC)CuMes,[5] (6-Mes)CuMes,[5] (6-Mes)CuO$^t$Bu,[5] 6-Mes,[2] 7-Mes,[2] 6-*o*-Tolyl,[2] 6-Xylyl[2], 6-Dipp[2] and N,N'-dimesitylformimidamide[6] were made according to literature procedures. Ni(6-Mes)($PPh_3$)Br and [8-MesH]Br was prepared using a modified literature procedure described in 6.2.1 and 6.2.2 respectively.[4,7] $[CuMes]_n$, $Ni(PPh_3)_2Br_2$, $Ni(COD)_2$, KHMDS, $Pd(PPh_3)_2Cl_2$, Amberlite® IRA402 chloride, CuI, $(EtO)_3SiF$ and $Et_3N{\cdot}3HF$ were obtained from commercial sources.

### 6.2.1 – Synthesis of Ni(6-Mes)($PPh_3$)Br (**5.1**)

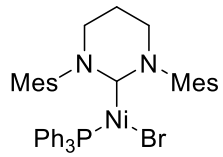


6-Mes (500 mg, 1.56 mmol), $Ni(PPh_3)_2Br_2$ (581 mg, 0.781 mmol) and $Ni(COD)_2$ (215 mg, 0.781 mmol) were placed in a J. Youngs resealable ampoule. THF (30 mL) was added and the mixture was stirred for 1 h at room temperature to give a yellow brown solution. The solution was concentrated *in vacuo* and hexane (30 mL) was added to precipitate a yellow solid. The solution was removed by cannula, the residue dried and extracted into $C_6H_6$ (30 mL) and filtered. The bright yellow $C_6H_6$ filtrate was concentrated *in vacuo* and $Et_2O$ (30 mL) added to precipitate a yellow solid. This was isolated, washed with $Et_2O$ (2 x 10 mL) and dried to yield a bright yellow powder (837 mg, yield 74%). NMR data are in agreement with published data.[7]

### 6.2.2 – Synthesis and characterisation of 8-MesH·Br

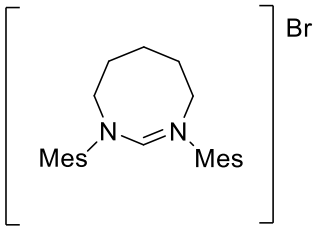


Into a 10-20 mL microwave vial was added 1,5-dibromopentane (486 uL, 3.57 mmol), N,N'-dimesitylformimidamide (1.00g, 3.57 mmol), $K_2CO_3$ (493 mg, 3.57 mmol) and MeCN (10 mL). The vial was sealed and heated in a microwave at 110 °C for 12 h. The suspension was then filtered, the residue washed with MeCN (2x 5 mL) and the filtrate and washings concentrated *in vacuo* to give an oil. To this was added $Et_2O$ (20 mL) and the solution was stirred vigorously to yield a white precipitate, which was isolated and then recrystallised from $CH_2Cl_2$/pentane to yield an off-white powder (843 mg, yield 55 %). $^1$H NMR (500 MHz, $CDCl_3$, 298 K) δ 7.38 (s, 1H, NC*H*N), 6.93 (s, 4H, $C_{Ar}H$), 4.85 (br s, 4H, NC$H_2$), 2.41 (s, 12H, $C_{Ar}CH_3$), 2.30 – 2.26 (m, 10H, $C_{Ar}CH_3$ + $NCH_2CH_2$), 2.15 – 2.10 (m, 2H, $NCH_2CH_2CH_2$). HRMS ES+: *m/z* 349.2643 $[M]^+$ corresponds to $C_{24}H_{33}N_2$ with a 0.03 ppm mass error. Spectroscopic data are in agreement with published literature.[4]

## 6.3 – Experimental Details and Characterisation for Chapter 2 : Copper Semihydrogenation

### 6.3.1 – Synthesis and Characterisation of (7-Mes)CuMes

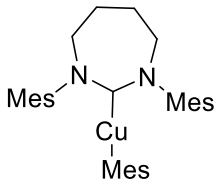


7-Mes (300 mg, 0.90 mmol) and $Cu(Mes)_n$ (163.9 mg, 0.90 mmol) were combined in benzene (30 mL) in a J. Youngs resealable ampoule and stirred for 1 h. The resulting solution was filtered, concentrated, and hexane (30 mL) was added to yield a near colourless precipitate of (7-Mes)CuMes. The solid was isolated by cannula filtration and dried *in vacuo* to yield (7-Mes)CuMes as an off-white solid (267 mg, yield 58%). Crystalline material was obtained from benzene/hexane. $^1$H NMR (500 MHz, $C_6D_6$, 298

K) δ 6.81 (s, 2H, $C_{Ar}H$), 6.74 (s, 4H, $C_{Ar}H$), 3.10 (m, 4H, $NCH_2$), 2.28 (s, 12H, $C_{Ar}CH_3$), 2.24 (s, 3H, $C_{Ar}CH_3$), 2.09 (s, 6H, $C_{Ar}CH_3$), 2.02 (s, 6H, $C_{Ar}CH_3$), 1.55 (quint, $^3J_{HH}$ = 2.8 Hz, 4H, $NCH_2CH_2$). $^{13}C\{^1H\}$ NMR (126 MHz, $C_6D_6$, 298 K) δ 214.8 (s, N*C*N), 163.5 (s), 147.2 (s), 137.4 (s), 134.7 (s), 132.1 (s), 130.2 (s), 129.4 (s), 124.3 (s), 52.7 (s), 28.4 (s), 25.6 (s), 21.6 (s), 20.9 (s), 18.9 (s).

## 6.3.2 – Synthesis and Characterisation of (6-*o*-Tolyl)CuMes

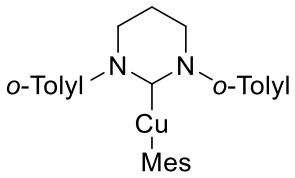


[6-*o*-TolylH]$BF_4$ (300 mg, 0.852 mmol) and KHMDS (171 mg, 0.860 mmol) were combined in THF (10 mL) in a J. Youngs resealable ampoule and stirred for 1 h. The volatiles were removed *in vacuo*, the product was extracted in $Et_2O$ (20 mL) and cannula filtered into a new J. Youngs resealable ampoule. The colourless solution was concentrated to dryness and $Cu(Mes)_n$ (140 mg, 0.767 mmol) was added, followed by benzene (20 mL). The brown suspension was stirred for 15 min and then the solution was cannula filtered into a new J. Youngs resealable ampoule, concentrated and the product precipitated upon the addition on hexane (20 mL). The solution was removed and the off-white precipitate was washed further with hexane (2 x 20 mL) to yield (6-*o*-Tolyl)CuMes as an off-white solid (213 mg, yield 62 %). Crystalline material was obtained from benzene/hexane. $^1H$ NMR (500 MHz, $C_6D_6$, 298 K) δ 7.02 (s, 8H, $C_{Ar}H$), 6.87 (s, 2H, $C_{Ar}H$), 2.59 (m, 4H, $NCH_2$) *‡, 2.28 (s, 3H, $C_{Ar}CH_3$), 2.19 (s, 6H, $C_{Ar}CH_3$), 2.00 (s, 6H, $C_{Ar}CH_3$), 1.34 (m, 2H, $NCH_2CH_2$). $^{13}C\{^1H\}$ NMR (126 MHz, $C_6D_6$, 298 K) δ 203.5 (s, N*C*N)* , 203.3 (s)‡ , 163.7 (s)* , 163.7 (s)‡ , 162.8 (s), 147.3 (s)‡ , 147.3 (s)* , 146.7 (s)‡ , 146.7 (s)* , 135.1 (s)* , 135.0 (s)‡ , 132.4 (s)‡ , 132.4 (s)* , 131.8 (s)‡ , 131.7 (s)* , 128.8 (s), 128.6 (s), 128.4 (s), 127.7 (s), 124.4 (s), 45.7 (s)* , 45.7 (s)‡ , 28.4 (s), 21.7 (s), 21.2 (s)* , 21.1 (s)‡ , 18.1 (s)‡ , 18.1 (s) *. A doubling up of some resonances was taken as evidence for conformers these are assigned above as major (‡) and minor (*) conformers (see appendix 7.1.1)

## 6.3.3 – Synthesis and Characterisation of (6-Xylyl)CuMes

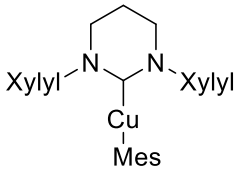


6-Xylyl (140 mg, 0.479 mmol) and $Cu(Mes)_n$ (87 mg, 0.479 mmol) were combined in benzene (10 mL) in a J. Youngs resealable ampoule and stirred for 1 h. The resulting precipitate was filtered, washed further with benzene (10 mL) and dried *in vacuo* to yield an off-white solid (159 mg, yield 70 %). Crystalline material suitable for X-ray diffraction was obtained from THF/hexane at -30 °C. $^{1}$H NMR (500 MHz, $d_8$-THF, 298 K) δ 7.10 (s, 6H, $C_{Ar}H$), 6.13 (s, 2H, $C_{Ar}H$), 3.39 (t, $^{3}J_{HH}$ = 5.9 Hz, 4H, $NCH_2$), 2.41 (s, 12H, $C_{Ar}CH_3$), 2.36 (quint, $^{3}J_{HH}$ = 5.9 Hz, 2H, $NCH_2CH_2$), 1.91 (s, 3H, $C_{Ar}CH_3$), 1.43 (s, 6H, $C_{Ar}CH_3$). $^{13}C\{^{1}H\}$ NMR (126 MHz, $d_8$-THF, 298 K) δ 204.6 (s), 146.9 (s), 145.8 (s), 136.1 (s), 131.3 (s), 129.6 (s), 128.4 (s), 128.4 (s), 127.4 (s), 123.4 (s), 45.1 (s), 28.0 (s), 21.9 (s), 21.1 (s), 18.2 (s).

## 6.3.4 – Synthesis and Characterisation of (6-Dipp)CuMes

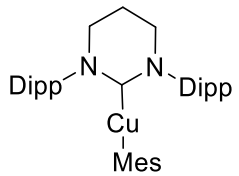


6-Dipp (150 mg, 0.371 mmol) and $Cu(Mes)_n$ (68 mg, 0.371 mmol) were combined in $C_6H_6$ (10 mL) in a J. Youngs resealable ampoule and stirred for 1 h. The resulting solution was filtered, concentrated, and hexane was added to yield a near colourless precipitate of (6-Dipp)CuMes. The solid was isolated by cannula filtration and dried *in vacuo* to yield (6-Dipp)CuMes as an off-white solid (98 mg, yield 45%). Crystalline material was obtained from $C_6H_6$/hexane. $^{1}$H NMR (500 MHz, $C_6D_6$, 298 K) δ 7.23 (t, $^{3}J_{HH}$ = 7.5 Hz, 2H, $C_{Ar}H$), 7.10 (d, $^{3}J_{HH}$ = 7.6 Hz, 4H, $C_{Ar}H$), 6.87 (s, 2H, $C_{Ar}H$), 3.09 (sept, $^{3}J_{HH}$ = 7.0 Hz, 4H, $CH(CH_3)_2$), 2.68 (t, $^{3}J_{HH}$ = 5.9 Hz, 4H, $NCH_2$), 2.28 (s, 3H, $C_{Ar}CH_3$), 1.67 (s, 6H, $C_{Ar}CH_3$), 1.47 (m, 2H, $NCH_2CH_2$), 1.43 (d, $^{3}J_{HH}$ = 6.9 Hz, 12H, $CH(CH_3)_2$), 1.21 (d, $^{3}J_{HH}$ = 6.9 Hz, 12H, $CH(CH_3)_2$). $^{13}C\{^{1}H\}$ NMR (126 MHz, $C_6D_6$, 298 K) δ 205.1 (s), 162.7 (s), 147.5 (s), 145.9 (s), 142.7 (s), 132.6 (s), 129.3 (s), 128.6 (s), 128.4 (s), 125.1 (s), 124.5 (s), 46.7 (s), 29.0 (s), 27.6 (s), 25.3 (s), 24.4 (s), 21.6 (s), 20.6 (s).

6.3.5 –Synthesis and Characterisation of (IPr)CuO$^t$Bu (**2.2**)

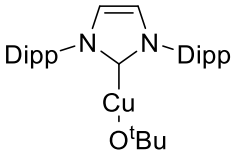


Compound **2.2** was prepared as for **2.4** by reaction of IPr (400 mg, 1.03 mmol) with Cu(Mes)$_n$ (188 mg, 1.03 mmol) in $C_6H_6$ (5 mL), followed by reaction with $^t$BuOH (1 mL) in $C_6H_6$ to give **2.2** as an off-white solid (268 mg, yield 49%). $^1$H NMR (500 MHz, $C_6D_6$, 298 K) δ 7.22 (t, $^3J_{HH}$ = 7.8 Hz, 2H, C$_{Ar}$*H*), 7.07 (d, $^3J_{HH}$ = 7.8 Hz, 4H, C$_{Ar}$*H*), 6.28 (s, 2H, NC*H*), 2.60 (sept, $^3J_{HH}$ = 6.9 Hz, 4H, C*H*(CH$_3$)$_2$), 1.41 (d, $^3J_{HH}$ = 6.9 Hz, 12H, CH(C*H*$_3$)$_2$), 1.28 (s, 9H, C(C*H*$_3$)$_3$), 1.07 (d, $^3J_{HH}$ = 6.9 Hz, 12H, CH(C*H*$_3$)$_2$). $^1$H NMR data matched those in the literature.[8]

6.3.6 – Synthesis and Characterisation of (6-Dipp)CuO$^t$Bu (**2.3**)

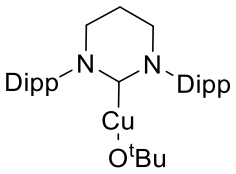


Compound **2.3** was prepared as for **2.4** by reaction of 6-Dipp (prepared in situ from [6-DippH]Br (300 mg, 0.62 mmol) and KHMDS (136 mg, 0.68 mmol)) with Cu(Mes)$_n$ (113 mg, 0.62 mmol) followed by reaction with $^t$BuOH (1 mL) to afford **2.3** as an off-white solid. Crystalline material was obtained from $C_6H_6$/hexane (110 mg, yield 33%). $^1$H NMR (500 MHz, $C_6D_6$, 298 K) δ 7.15 – 7.13 (m, 2H, C$_{Ar}$*H*), 7.06 – 7.04 (m, 4H, C$_{Ar}$*H*), 3.03 (sept, $^3J_{HH}$ = 6.9 Hz, 4H, C*H*(CH$_3$)$_2$), 2.71 (t, $^3J_{HH}$ = 5.9 Hz, 4H, NC*H*$_2$), 1.57 (d, $^3J_{HH}$ = 6.8 Hz, 12H, CH(C*H*$_3$)$_2$), 1.51 – 1.43 (m, 2H), 1.19 (d, $^3J_{HH}$ = 6.9 Hz, 12H, CH(C*H*$_3$)$_2$), 1.16 (s, 9H, C(C*H*$_3$)$_3$). NMR data matched those in the literature.[9]

## 6.3.7 – Synthesis and Characterisation of (7-Mes)CuO$^t$Bu (**2.4**)

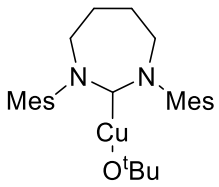


7-Mes (141 mg, 0.42 mmol) and Cu(Mes)$_n$ (77 mg, 0.42 mmol) were combined in $C_6H_6$ (5 mL) in a J. Youngs resealable ampoule and stirred for 1 h. The resulting solution was concentrated, and pentane was added to yield a near colourless precipitate of (7-Mes)CuMes. The solid was isolated by cannula filtration and dried under vacuum. It was then dissolved in $C_6H_6$ (5 mL), and $^t$BuOH (1 mL) was added. After being stirred for 2 h at room temperature, the solution was reduced to dryness, and the residue was redissolved in a minimum amount of $C_6H_6$ and then reprecipitated with hexane. This process was repeated twice more, after which the resulting precipitate was isolated as a colourless solid (163 mg, yield 93%). Crystalline material was obtained from $C_6H_6$/hexane. $^1$H NMR (500 MHz, $C_6D_6$, 298 K) δ 6.75 (s, 4H, $C_{Ar}H$), 3.05 (m, 4H, $NCH_2CH_2$), 2.24 (s, 12H, $C_{Ar}CH_3$), 2.10 (s, 6H, $C_{Ar}CH_3$), 1.49 (quint, $^3J_{HH}$ = 3.0 Hz, 4H, $NCH_2CH_2$), 1.18 (s, 9H, $C(CH_3)_3$). $^{13}C\{^1H\}$ NMR (126 MHz, $C_6D_6$) δ 213.3 (s), 145.3 (s), 137.4 (s), 134.3 (s), 130.3 (s), 68.3 (s), 52.0 (s), 37.0 (s), 25.5 (s), 21.0 (s), 18.7 (s). Elemental analysis calcd (%) for $C_{27}H_{39}N_2OCu$: C, 68.83; H, 8.34; N, 5.95; found: C, 68.96; H, 8.34; N, 5.84.

## 6.3.8 –Synthesis and Characterisation of (6-*o*-Tolyl)CuO$^t$Bu (**2.5**)

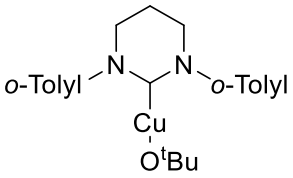


Compound **2.5** was prepared as for **2.4** by reaction of 6-*o*-tolyl (prepared in situ from [6-*o*-tolylH]$BF_4$ (500 mg, 1.42 mmol) and KHMDS (312 mg, 1.56 mmol)) with Cu(Mes)$_n$ (259 mg 1.42 mmol) followed by reaction with $^t$BuOH (1 mL) to yield **2.5** as an off-white solid (95 mg, yield 17%). Crystalline material was obtained from $C_6H_6$/hexane. $^1$H NMR (500 MHz, $C_6D_6$, 298 K) δ 7.16 – 6.94 (m, 8H, $C_{Ar}H$), 2.62 – 2.46 (m, 4H, $NCH_2$),‡* 2.13 (s, 6H, $CH_3$), 1.28 (m, 2H, $NCH_2CH_2$), 1.26 (s, 9H, $C(CH_3)_3$). $^{13}C\{^1H\}$ NMR (126 MHz, $C_6D_6$, 298 K) δ 201.9 (s), 146.9 (s), 134.7 (s)*, 134.6 (s)‡, 131.8 (s)‡, 131.7 (s)*, 128.6 (s), 128.4 (s), 128.3 (s), 128.2 (s), 127.7 (s), 68.6 (s),

45.4 (s)*, 45.3 (s)‡, 37.1 (s), 21.1 (s)*, 21.0 (s)‡, 18.0 (s)‡, 17.9 (s)*. More than one set of signals was apparent, which we assign to major (‡) and minor (*) conformers. See Appendix 1. Elemental analysis calcd (%) for $C_{22}H_{29}N_2OCu$: C, 65.89; H, 7.29; N, 6.99. Found: C, 65.85; H, 7.27; N, 6.68.

### 6.3.9 – Synthesis and Characterisation of (6-Xylyl)CuO$^t$Bu (**2.6**)

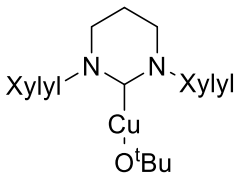


Compound **2.6** was prepared as for **2.4** by reaction of 6-Xylyl (prepared in situ from [6-XylylH]$BF_4$ (500 mg, 1.22 mmol) and KHMDS (269 mg, 1.34 mmol)) with $Cu(Mes)_n$ (223 mg, 1.22 mmol), followed by reaction with $^t$BuOH (1 mL). The product was recrystallized from THF/hexane to yield **2.6** as an off-white solid (122 mg, yield 23%). $^1$H NMR (500 MHz, $C_6D_6$, 298 K) δ 6.99 (t, $^3J_{HH}$ = 7.7 Hz, 2H, $C_{Ar}H$), 6.92 (d, $^3J_{HH}$ = 7.7 Hz, 4H, $C_{Ar}H$), 2.41 (m, 4H, $NCH_2$), 2.13 (s, 12H, $C_{Ar}CH_3$), 1.28 (m, 2H, $NCH_2CH_2$), 1.21 (s, 9H, $C(CH_3)_3$). $^{13}C\{^1H\}$ NMR (126 MHz, $C_6D_6$, 298 K) δ 202.7 (s), 145.2 (s), 135.1 (s), 129.4 (s), 68.4 (s), 43.6 (s), 37.0 (s), 20.7 (s), 18.1 (s). Anal. Calcd for $C_{24}H_{33}N_2OCu$: C, 67.18; H, 7.75; N, 6.53; Found: C, 66.78; H, 7.75; N, 6.55.

### 6.3.10 – Synthesis and Characterisation of (SIMes)CuO$^t$Bu (**2.7**)

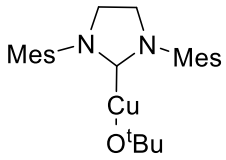


Compound **2.7** was prepared as for **2.4** by reaction of SIMes (made in situ from [SIMesH]Cl (563 mg, 1.64 mmol) and KHMDS (330 mg, 1.6 mmol)) with $Cu(Mes)_n$ (300 mg, 1.64 mmol) followed by reaction with $^t$BuOH (1 mL) to give **2.7** as an off-white solid (520 mg, yield 72%). Crystalline material was obtained from toluene/pentane at -30 °C. $^{13}C\{^1H\}$ NMR (126 MHz, $C_6D_6$, 298 K) δ 204.9 (s), 138.3 (s), 136.1 (s), 135.8 (s), 129.9 (s), 68.0 (s), 50.4 (s), 34.4 (s), 21.0 (s), 18.0 (s). The extreme air sensitivity of **2.7** precluded all attempts to measure CHN microanalysis data. $^1$H NMR data matched those in the literature.[10]

## 6.3.11 – Synthesis and Characterisation of (6-Mes)Cu(C(Ph)=C(H)Ph) (**2.8**)

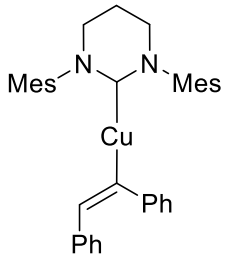


(6-Mes)CuO$^t$Bu (**2.1**) (100 mg, 0.21 mmol) and diphenylacetylene (37.4 mg, 0.21 mmol) were combined in $C_6H_6$ (5 mL) in a J. Youngs resealable ampoule. To this was added $Et_3SiH$ (34 uL, 0.42 mmol). After stirring for 48 h, the yellow precipitate formed was isolated by cannula filtration, washed with $C_6H_6$ (2 x 4 mL) and then dried under vacuum to yield the title compound as a yellow solid (67 mg, yield 57%). This was crystallized from THF/hexane. $^1$H NMR (500 MHz, $d_8$-THF, 298 K) δ 6.91 (s, 4H, $C_{Ar}H$), 6.74 (m, 4H, $C_{Ar}H$), 6.65 (t, $^3J_{HH}$ = 7.2 Hz, 1H, $C_{Ar}H$), 6.59 (d, $^3J_{HH}$ = 7.2 Hz, 3H, $C_{Ar}H$), 6.22 (d, $^3J_{HH}$ = 7.2 Hz, 2H, $C_{Ar}H$), 5.65 (s, 1H, C(*H*)Ph), 3.35 (t, $^3J_{HH}$ = 5.9 Hz, 4H, $NCH_2$), 2.29 – 2.26 (m, 20H, $CH_2$ + $CH_3$).

## 6.3.12 – General Method for Synthesis of Internal Alkynes.

To a Schlenk tube was added $Pd(PPh_3)_2Cl_2$ (16.1 mg, 0.023 mmol) and CuI (8.7 mg, 0.046 mmol). $Et_3N$ (6.6 mL, 0.048 mol), the appropriate aryl iodide (4.6 mmol) and terminal alkyne (5.5 mmol) were then added and the solution left to stir overnight. The solution was diluted with $Et_2O$ (100 mL) and then washed with water (3x 100 mL) followed by brine solution (100 mL). The aqueous layers were combined, washed with $Et_2O$ (200 mL) and the organic layer separated. The washings and initial organic extract were combined, dried over $MgSO_4$, filtered through Celite and dried in vacuo to yield oils. Vacuum distillation gave the pure alkynes.

## 6.3.13 – Characterisation of 1-(4-fluorophenyl)-1-phenylacetylene

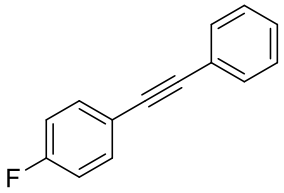


Prepared from 4-iodo-1-fluorobenzene (0.604 mL, 4.6 mmol) and PhC≡CH (0.604 mL, 5.5 mmol). Recrystallised from hot hexane to yield an off-white solid (0.53 g, yield 59 %). $^{1}$H NMR (500 MHz, $CDCl_3$, 298 K) δ 7.62 – 7.46 (m, 4H, Ar), 7.41 – 7.30 (m, 3H, Ar), 7.12 – 6.99 (m, 2H, Ar). $^{13}C\{^{1}H\}$ NMR (126 MHz, $CDCl_3$, 298 K) δ 162.5 (d, $J_{CF}$ = 249 Hz), 133.5 (d, $J_{CF}$ = 8 Hz), 131.6 (s), 128.4 (s), 128.2 (s), 123.4 (s), 119.6 (d, $J_{CF}$ = 3 Hz), 115.5 (d, $J_{CF}$ = 22 Hz), 89.5 (d, $J_{CF}$ = 1 Hz), 88.7 (s). $^{19}$F NMR (470 MHz, $CDCl_3$, 298 K) δ -110.77 (tt, $J_{HH}$ = 8.8, 5.6 Hz). $^{1}$H NMR (500 MHz, $C_6D_6$) δ 7.54 – 7.48 (m, 2H, Ar), 7.27 – 7.20 (m, 2H, Ar), 7.04 – 6.96 (m, 3H, Ar), 6.65 – 6.56 (m, 2H, Ar). HRMS APCI: Calcd for [M] + H: 196.0683, Found 196.0693. The NMR data are in agreement with published data.[11]

## 6.3.14 – Characterisation of 1-(4-fluorophenyl)-1-hexyne

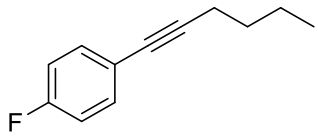


Prepared from 4-iodo-1-fluorobenzene (0.536 mL, 4.6 mmol) and 1-hexyne (0.632 mL, 5.5 mmol). Distilled at 0.1 bar/75 ºC to give the product as a clear colourless oil (0.397 g, yield 47 %). $^{1}$H NMR (500 MHz, $CDCl_3$, 298 K) δ 7.42 – 7.31 (m, 2H, $C_{Ar}H$), 7.02 – 6.92 (m, 2H, $C_{Ar}H$), 2.39 (t, $^{3}J_{HH}$ = 7.1 Hz, 2H, $CH_2$), 1.61 – 1.56 (m, 2H, $CH_2$), 1.50 – 1.46 (m, 2H, $CH_2$), 0.95 (t, $^{3}J_{HH}$ = 7.3 Hz, 2H, $CH_3$). $^{13}C\{^{1}H\}$ NMR (126 MHz, $CDCl_3$, 298 K) δ 162.2 (d, $J_{CF}$ = 248 Hz), 133.4 (d, $J_{CF}$ = 8 Hz), 120.3 (d, $J_{CF}$ = 4 Hz), 115.5 (d, $J_{CF}$ = 22 Hz), 90.2 (d, $J_{CF}$ = 2 Hz), 79.6 (s), 31.0 (s), 22.2 (s), 19.2 (s), 13.8 (s). $^{19}$F NMR (470 MHz, $CDCl_3$, 298 K) δ -112.32 (tt, $J_{HH}$ = 8.8, 5.4 Hz). $^{1}$H NMR (500 MHz, $C_6D_6$) δ 7.27 – 7.16 (m, 2H, Ar), 6.69 – 6.58 (m, 2H, Ar), 2.19 (t, $J$ = 6.9 Hz, 2H, $CH_2$), 1.44 – 1.40 (m, 2H, $CH_2$), 1.35 – 1.30 (m, 2H, $CH_2$), 0.81 (t, $^{3}J_{HH}$ = 7.3 Hz, 3H, $CH_3$). HRMS APCI: Calcd for [M]: 176.1006, Found 176.0996. The NMR data in agreement with published data.[11]

## 6.3.15 – Characterisation of 1-(4-fluorophenyl)-1-hexyne

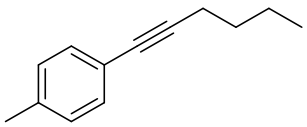

Prepared from 4-iodotoluene (1.00 g, 4.6 mmol) and 1-hexyne (0.632 mL, 5.5 mmol). Distilled at 0.1 bar/85 ºC to give the product as a clear colourless oil (0.745 g, yield 94 %). $^{1}$H NMR (500 MHz, $CDCl_3$, 298 K) δ 7.31 – 7.28 (m, 2H, $C_{Ar}H$), 7.11 – 7.07 (m, 2H, $C_{Ar}H$), 2.41 (t, $^{3}J_{HH}$ = 7.1 Hz, 2H, C≡C$H_2$CH$_2$), 2.33 (s, 3H, $C_{Ar}CH_3$), 1.64 – 1.56 (m, 2H, C$H_2$CH$_2$CH$_3$), 1.51 – 1.46 (m, 2H, CH$_2$C$H_2$CH$_3$), 0.96 (t, $^{3}J_{HH}$ = 7.3 Hz, 3H, CH$_2$CH$_2$C$H_3$). $^{13}$C{$^{1}$H} NMR (126 MHz, $CDCl_3$, 298 K) δ 137.5 (s), 131.5 (s), 129.1 (s), 121.2 (s), 89.7 (s), 80.7 (s), 31.1 (s), 22.2 (s), 21.5 (s), 19.3 (s), 13.8 (s). $^{1}$H NMR (500 MHz, $C_6D_6$, 298 K) δ 7.47 – 7.42 (m, 2H, $C_{Ar}H$), 6.86 – 6.82 (m, 2H, $C_{Ar}H$), 2.25 (t, $^{3}J_{HH}$ = 7.0 Hz, 2H, C≡C$H_2$CH$_2$), 2.00 (s, 3H, $C_{Ar}CH_3$), 1.47 – 1.44 (m, 2H, C$H_2$CH$_2$CH$_3$), 1.36 (m, 2H, CH$_2$C$H_2$CH$_3$), 0.81 (t, $^{3}J_{HH}$ = 7.3 Hz, 3H, CH$_2$CH$_2$C$H_3$). HRMS APCI: Calcd for [M] + H: 173.1325, Found 173.1334. The NMR data are in agreement with published data.[12]

## 6.3.16 – Characterisation of 1-(3-methylphenyl)-1-hexyne

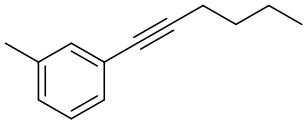

Prepared from 3-iodotoluene (0.59 mL, 4.6 mmol) and 1-hexyne (0.632 mL, 5.5 mmol). Distilled at 0.1 bar/85 ºC to give the product as a clear colourless oil (0.702 g, yield 89 %). $^{1}$H NMR (500 MHz, $CDCl_3$, 298 K) δ 7.23 – 7.18 (m, 2H, $C_{Ar}H$), 7.16 (t, $^{3}J_{HH}$ = 7.5 Hz, 1H, $C_{Ar}H$), 7.10 – 7.04 (m, 1H, $C_{Ar}H$), 2.40 (t, $^{3}J_{HH}$ = 7.1 Hz, 2H, C≡C$H_2$CH$_2$), 2.31 (s, 3H, $C_{Ar}CH_3$), 1.60 (m, 2H, C$H_2$CH$_2$CH$_3$), 1.48 (m, 2H, CH$_2$C$H_2$CH$_3$), 0.95 (t, $^{3}J_{HH}$ = 7.3 Hz, 3H, CH$_2$CH$_2$C$H_3$). $^{13}$C{$^{1}$H} NMR (126 MHz, $CDCl_3$, 298 K) δ 137.9 (s), 132.3 (s), 128.7 (s), 128.5 (s), 128.2 (s), 124.1 (s), 90.2 (s), 80.8 (s), 31.4 (s), 22.2 (s), 21.3 (s), 19.3 (s), 13.8 (s). $^{1}$H NMR (500 MHz, $C_6D_6$, 298 K) δ 7.40 – 7.33 (m, 2H, $C_{Ar}H$), 6.97 (t, $^{3}J_{HH}$ = 7.6 Hz, 1H, $C_{Ar}H$), 6.83 (d, $^{3}J_{HH}$ = 7.7 Hz, 1H, $C_{Ar}H$), 2.25 (t, $^{3}J_{HH}$ = 6.9 Hz, 2H, C≡C$H_2$CH$_2$), 1.99 (s, 3H, $C_{Ar}CH_3$), 1.40 (m, 4H, CH$_2$C$H_2$C$H_2$CH$_3$), 0.81 (t, $^{3}J_{HH}$ = 7.3 Hz, 3H, CH$_2$CH$_2$C$H_3$). HRMS APCI: Calcd for [M] + H: 173.1325, Found 173.1334. The NMR data are in agreement with published data.[12]

## 6.3.17 – Characterisation of 1-(2-methylphenyl)-1-hexyne

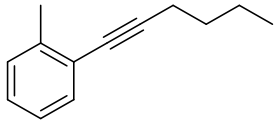

Prepared from 2-iodotoluene (0.584 mL, 4.6 mmol) and 1-hexyne (0.632 mL, 5.5 mmol). Distilled at 0.1 bar/75 ºC to give the product as a clear colourless oil (0.687 g, yield 87 %). $^{1}$H NMR (500 MHz, $CDCl_3$, 298 K) δ 7.36 (d, $^{3}J_{HH}$ = 7.4 Hz, 1H, $C_{Ar}H$), 7.19 – 7.06 (m, 3H, $C_{Ar}H$), 2.46 (t, $^{3}J_{HH}$ = 7.0 Hz, 2H, $C{\equiv}CH_2CH_2$), 2.42 (s, 3H, $C_{Ar}CH_3$), 1.62 (m, 2H, $CH_2CH_2CH_3$), 1.50 (m, 2H, $CH_2CH_2CH_3$), 0.96 (t, $^{3}J_{HH}$ = 7.3 Hz, 3H, $CH_2CH_2CH_3$). $^{13}C\{^{1}H\}$ NMR (126 MHz, $CDCl_3$, 298 K) δ 140.1 (s), 131.9 (s), 129.4 (s), 127.6 (s), 125.5 (s), 124.0 (s), 94.5 (s), 79.6 (s), 31.2 (s), 22.1 (s), 20.9 (s), 19.4 (s), 13.8 (s). $^{1}$H NMR (500 MHz, $C_6D_6$, 298 K) δ 7.48 (d, $^{3}J_{HH}$ = 7.5 Hz, 1H, Ar), 7.06 – 6.90 (m, 3H, Ar), 2.41 (s, 3H, $C_{Ar}CH_3$), 2.26 (t, $^{3}J_{HH}$ = 6.9 Hz, 2H, $C{\equiv}CH_2CH_2$), 1.40 (m, 4H, $CH_2CH_2CH_2CH_3$), 0.82 (t, $^{3}J_{HH}$ = 7.3 Hz, 3H, $CH_2CH_2CH_3$). HRMS APCI: Calcd for [M] + H: 173.1325, Found 173.1327. The NMR data are in agreement with published data.[12]

## 6.3.18 – Characterisation of 1-(4-acylphenyl)-1-hexyne

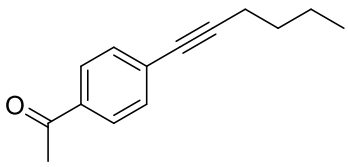


Prepared from 4-iodoacetophenone (0.863g, 3.5 mmol) and 1-hexyne (0.632 mL, 5.5 mmol). Distilled at 0.1 bar/120 ºC to give the product as a clear pale yellow oil (0.652 g, yield 93%). $^{1}$H NMR (500 MHz, $C_6D_6$) δ 7.66 – 7.62 (m, 2H), 7.40 – 7.36 (m, 2H), 2.20 (t, $^{3}J_{HH}$ = 7.0 Hz, 2H), 2.01 (s, 3H), 1.39 – 1.34 (m, 4H), 0.80 (t, $^{3}J_{HH}$ = 7.3 Hz, 3H). $^{1}$H NMR (500 MHz, $CDCl_3$) δ 7.87 (d, $^{3}J_{HH}$ = 8.0 Hz, 2H), 7.46 (d, $^{3}J_{HH}$ = 8.4 Hz, 2H), 2.58 (s, 3H), 2.44 (t, $^{3}J_{HH}$ = 7.1 Hz, 2H), 1.52 – 1.50 (m, 2H), 1.49 – 1.46 (m, 2H), 0.96 (t, $^{3}J_{HH}$ = 7.2, 3H). $^{13}C\{^{1}H\}$ NMR (126 MHz, $CDCl_3$) δ 197.5 (s), 135.8 (s), 131.8 (s), 129.3 (s), 128.3 (s), 94.5 (s), 80.2 (s), 30.8 (s), 26.7 (s), 22.2 (s), 19.4 (s), 13.8 (s). HRMS APCI: Calcd for [M] + H : 201.1274, Found 201.1300.

## 6.3.19 – Characterisation of (*Z*)-1-phenyl-1-propylene

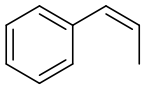

$^{1}$H NMR (500 MHz, $C_6D_6$, 298 K) δ 7.22 – 7.18 (m, 2H, Ar), 7.16 – 7.10 (m, 3H, Ar), 7.04 – 6.99 (m, 1H, Ar), 6.39 (dq, $^{3}J_{HH}$ = 11.5, $^{4}J_{HH}$ = 1.8 Hz, 1H, $C_{Ar}CH$), 5.61 (dq, $^{3}J_{HH}$ = 11.5, $^{3}J_{HH}$ = 7.2 Hz, 1H, $CHCH_3$), 1.67 (dd, $^{3}J_{HH}$ = 7.2, $^{4}J_{HH}$ = 1.9 Hz, 3H, $CHCH_3$). $^{13}C\{^{1}H\}$ NMR (126 MHz, $C_6D_6$, 298 K) δ 137.3 (s), 130.2 (s), 128.9 (s), 128.2 (s), 127.0 (s), 126.4 (s), 14.7 (s). GCMS-EI: RMM 118.1, Found: 118.1 g mol$^{-1}$. The NMR data are in agreement with published data.[13,14]

## 6.3.20 – Characterisation of (Z)-4-fluorostillbene

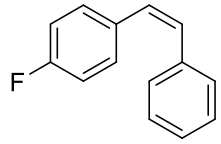


$^{1}$H NMR (500 MHz, $CDCl_3$, 298 K) δ 7.28 – 7.20 (m, 7H, Ar), 6.96 – 6.89 (m, 2H, Ar), 6.62 (d, $^{3}J_{HH}$ = 12.2 Hz, 1H, Ar), 6.57 (d, $^{3}J_{HH}$ = 12.2 Hz, 1H, Ar). $^{13}C\{^{1}H\}$ NMR (126 MHz, $CDCl_3$, 298 K) δ 162.0 (d, $J_{CF}$ = 247 Hz), 137.2 (s), 133.3 (d, $J_{CF}$ = 3 Hz), 130.7 (d, $J_{CF}$ = 8 Hz), 130.4 (d, $J_{CF}$ = 1 Hz), 129.2 (s), 129.0 (s), 128.4 (s), 127.3 (s), 115.3 (d, $J_{CF}$ = 21 Hz). $^{1}$H NMR (500 MHz, $C_6D_6$, 298 K) δ 7.16 – 7.14 (m, 2H, Ar), 7.05 – 6.91 (m, 5H, Ar), 6.66 – 6.58 (m, 2H, Ar), 6.40 (d, $J$ = 12.1 Hz, 1H, Ar), 6.29 (d, $J$ = 12.2 Hz, 1H, Ar). $^{19}$F NMR (470 MHz, $C_6D_6$, 298 K) δ -114.32 (tt, $J_{FC}$ = 8.7, 5.5 Hz). HRMS APCI: Calcd for [M] + H: 198.0839, Found 198.0849. The NMR data are in agreement with published data.[15]

## 6.3.21 – Characterisation of (Z)-1-(4-fluorophenyl)-1-hexene

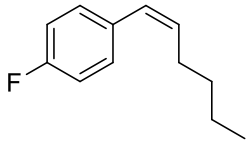


$^{1}$H NMR (500 MHz, $CDCl_3$, 298 K) δ 7.32 – 7.26 (m, 2H, Ar), 7.10 – 7.03 (m, 2H, Ar), 6.41 (dt, *J* = 11.6, 1.9 Hz, 1H, $C_{Ar}CH$), 5.70 (dt, $^{3}J_{HH}$ = 11.6, $^{3}J_{HH}$ = 7.3 Hz, 1H, $CHCH_2$), 2.35 (qd, $^{3}J_{HH}$ = 7.3, $^{3}J_{HH}$ =1.8 Hz, 2H, $CHCH_2$), 1.47 – 1.43 (m, 4H, $CH_2CH_2CH_2CH_3$), 0.96 (t, $^{3}J_{HH}$ = 7.3 Hz, 3H, $CH_2CH_2CH_3$). $^{13}C\{^{1}H\}$ NMR (126 MHz, $CDCl_3$, 298 K) δ 161.6 (d, $J_{CF}$ = 246 Hz), 134.0 (d, $J_{CF}$ = 3 Hz), 133.2 (d, $J_{CF}$ = 1 Hz), 130.4 (d, $J_{CF}$ = 8 Hz), 127.8 (s), 115.1 (d, $J_{CF}$ = 21 Hz), 32.3 (s), 28.4 (s), 22.6 (s), 14.1 (s). $^{1}$H NMR (500 MHz, $C_6D_6$, 298 K) δ 7.05 – 6.98 (m, 2H, Ar), 6.84 – 6.77 (m, 2H, Ar), 6.27 (dd, *J* = 11.6, 1.9 Hz, 1H, $C_{Ar}CH$), 5.52 (dt, $^{3}J_{HH}$ = 11.6, $^{3}J_{HH}$ = 7.2 Hz, 1H, $CHCH_2$), 2.16 (qd, $^{3}J_{HH}$ = 7.4, $^{3}J_{HH}$ = 1.9 Hz, 2H, $CH_2CH_2CH_2$), 1.26 – 1.20 (m, 4H, $CH_2CH_2CH_2CH_3$), 0.80 (t, $^{3}J_{HH}$ = 7.1 Hz, 3H, $CH_2CH_2CH_3$). $^{19}$F NMR (470 MHz, $CDCl_3$, 298 K) δ -116.0 (m). GCMS-EI: RMM 178.3, Found : 178.2 g mol$^{-1}$, m/z: 178.20 (29%), 146.10 (5%), 135.10 (100%), 122.10 (55%).

## 6.3.22 – Characterisation of (Z)-1-(4-tolyl)-1-hexene

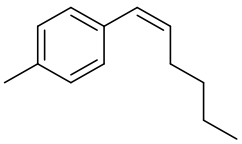

$^{1}$H NMR (500 MHz, $CDCl_3$, 298 K) δ 7.22 – 7.18 (m, 2H, Ar), 7.17 – 7.13 (m, 2H, Ar), 6.39 (dt, $^{3}J_{HH}$ = 11.7, $^{4}J_{HH}$ = 1.9 Hz, 1H, $C_{Ar}CH$), 5.63 (dt, $^{3}J_{HH}$ = 11.6, $^{3}J_{HH}$ = 7.2 Hz, 1H, $CHCH_2$), 2.36 – 2.36 (m, 5H, $C_{Ar}CH_3$ + $CHCH_2CH_2$), 1.43 – 1.39 (m, 4H, $CH_2CH_2CH_2CH_3$), 0.91 (t, *J* = 7.2 Hz, 3H, $CH_3$). $^{13}C\{^{1}H\}$ NMR (126 MHz, $CDCl_3$, 298 K) δ 136.2 (s), 135.1 (s), 132.7 (s), 128.9 (s), 128.8 (s), 128.7 (s), 32.4 (s), 28.5 (s), 22.6 (s), 14.1 (s). $^{1}$H NMR (500 MHz, $C_6D_6$, 298 K) δ 7.24 (d, $^{3}J_{HH}$ = 8.0 Hz, 2H, Ar), 7.02 (d, $^{3}J_{HH}$ = 7.9 Hz, 2H, Ar), 6.50 – 6.45 (m, 1H, $C_{Ar}CH$), 5.60 (dt, $^{3}J_{HH}$ = 11.6, $^{3}J_{HH}$ = 7.2 Hz, 1H, $CHCH_2$), 2.32 (qd, $^{3}J_{HH}$ = 7.3, $^{3}J_{HH}$ = 1.9 Hz, 2H, $CHCH_2CH_2$), 2.13 (s, 3H, $C_{Ar}CH_3$), 1.35 – 1.31 (m, 2H, $CH_2CH_2CH_3$), 1.28 – 1.22 (m, 2H, $CH_2CH_2CH_3$), 0.81 (t, $^{3}J_{HH}$ = 7.3 Hz, 3H, $CH_2CH_2CH_3$). GCMS-EI: RMM 174.3, Found 174.2 g mol$^{-1}$. The NMR data are in agreement with published data.[16]

## 6.3.23 – Characterisation of (Z)-1-(3-tolyl)-1-hexene

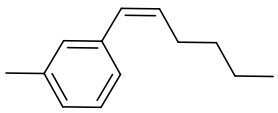

$^{1}$H NMR (500 MHz, $CDCl_3$, 298 K) δ 7.29 – 7.24 (m, 1H, Ar), 7.19 – 7.11 (m, 2H, Ar), 7.08 (d, *J* = 7.7 Hz, 1H, Ar), 6.46 – 6.40 (m, 1H, $C_{Ar}CH$), 5.70 (dt, $^{3}J_{HH}$ = 11.7, $^{3}J_{HH}$ = 7.3 Hz, 1H, $CHCH_2$), 2.42 – 2.35 (m, 5H, $C_{Ar}CH_3$ + $CHCH_2CH_2$), 1.38 – 1.34 (m, 4H, $CH_2CH_2CH_2CH_3$), 0.96 (t, $^{3}J_{HH}$ = 7.2 Hz, 3H, $CH_2CH_2CH_3$). $^{13}C\{^{1}H\}$ NMR (126 MHz, $CDCl_3$, 298 K) δ 137.9 (s), 137.7 (s), 133.2 (s), 129.7 (s) 128.9 (s), 128.1 (s), 127.3 (s), 125.9 (s), 32.3 (s), 28.5 (s), 22.6 (s), 21.6 (s), 14.1 (s). $^{1}$H NMR (500 MHz, $C_6D_6$, 298 K) δ 7.18 – 7.13 (m, 2H, Ar), 7.11 – 7.09 (m, 1H, CH), 6.93 – 6.89 (m, 1H, Ar), 6.46 (dt, *J* = 11.6, 1.9 Hz, 1H, $C_{Ar}CH$), 5.61 (dt, $^{3}J_{HH}$ = 11.6, $^{3}J_{HH}$ = 7.3 Hz, 1H, $CHCH_2$), 2.31 (qd, *J* = 7.3, 1.8 Hz, 2H, $CHCH_2CH_2$), 2.15 (s, 3H, $C_{Ar}CH_3$), 1.33 – 1.31 (m, 2H, $CH_2CH_2CH_3$), 1.25 – 1.21 (m, 2H, $CH_2CH_2CH_3$), 0.81 (t, $^{3}J_{HH}$ = 7.3 Hz, 3H, $CH_2CH_2CH_3$). GCMS-EI: RMM 174.3, Found 174.2 g mol$^{-1}$, m/z: 174.20 (45%), 145.18 (5%), 131.15 (100%), 118.10 (42%).

## 6.3.24 – Characterisation of (Z)-1-(2-tolyl)-1-hexene

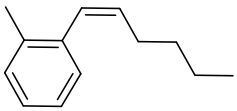

$^{1}$H NMR (500 MHz, $CDCl_3$, 298 K) δ 7.29 – 7.24 (m, 1H, Ar), 7.19 – 7.11 (m, 2H, Ar), 7.08 (d, $^{3}J_{HH}$ = 7.7 Hz, 1H, Ar), 6.46 – 6.40 (m, 1H, $C_{Ar}CH$), 5.70 (dt, $^{3}J_{HH}$ = 11.7, $^{3}J_{HH}$ =7.3 Hz, 1H, $CHCH_2$), 2.42 – 2.35 (m, 5H, $C_{Ar}CH_3$+ $CHCH_2CH_2$), 1.38 – 1.34 (m, 4H, $CH_2CH_2CH_2CH_3$), 0.96 (t, $^{3}J_{HH}$ =7.2 Hz, 3H, $CH_2CH_2CH_3$). $^{13}C\{^{1}H\}$ NMR (126 MHz, $CDCl_3$, 298 K) δ 137.9 (s), 137.7 (s), 133.2 (s), 129.7 (s) 128.9 (s), 128.1 (s), 127.3 (s), 125.9 (s), 32.3 (s), 28.5 (s), 22.6 (s), 21.6 (s), 14.1 (s). $^{1}$H NMR (500 MHz, $C_6D_6$, 298 K) δ 7.18 – 7.13 (m, 2H, Ar), 7.11 – 7.09 (m, 1H, CH), 6.93 – 6.89 (m, 1H, Ar), 6.46 (dt, *J* = 11.6, 1.9 Hz, 1H, $C_{Ar}CH$), 5.61 (dt, $^{3}J_{HH}$ = 11.6, $^{3}J_{HH}$ =7.3 Hz, 1H, $CHCH_2$), 2.31 (qd, *J* = 7.3, 1.8 Hz, 2H, $CHCH_2CH_2$), 2.15 (s, 3H, $C_{Ar}CH_3$), 1.33 (m, 2H, $CH_2CH_2CH_3$), 1.23 (m, 2H, $CH_2CH_2CH_3$), 0.81 (t, $^{3}J_{HH}$ = = 7.3 Hz, 3H, $CH_2CH_2CH_3$). GCMS-EI: RMM 174.3, Found 174.2, m/z: 174.20 (45%), 145.18 (5%), 131.15 (100%), 118.10 (42%).

## 6.3.25 – Characterisation of (Z)-1-(1-acylphenyl)-1-hexene

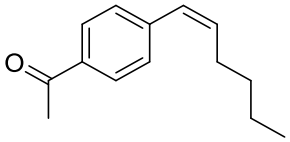

$^{1}$H NMR (500 MHz, $CDCl_3$) δ 7.94 – 7.90 (m, 2H, $C_{Ar}H$), 7.35 (d, $^{3}J_{HH}$ = 8.3 Hz, 2H, $C_{Ar}H$), 6.43 (d, $^{3}J_{HH}$ = 11.7 Hz, 1H, $C_{Ar}CH$), 5.79 (dt, $^{3}J_{HH}$ = 11.7, $^{3}J_{HH}$ = 7.4 Hz, 1H, $CHCH_2$), 2.60 (s, 3H, $CCH_3$), 2.34 (qd, $^{3}J_{HH}$ = 7.4, 1.9 Hz, 2H, $CHCH_2CH_2$), 1.42 – 1.38 (m, 4H, $CH_2CH_2CH_2CH_3$), 0.89 (t, $^{3}J_{HH}$ = 7.2 Hz, 3H, $CH_2CH_2CH_3$). $^{13}C\{^{1}H\}$ NMR (126 MHz, $CDCl_3$) δ 197.3 (s), 142.7 (s), 135.6 (s), 135.0 (s), 128.8 (s), 128.2 (s), 127.9 (s), 31.9 (s), 28.5 (s), 26.5 (s), 22.3 (s), 13.9 (s). $^{1}$H NMR (500 MHz, $C_6D_6$) δ 7.75 (d, $^{3}J_{HH}$ = 8.3 Hz, 2H, $C_{Ar}H$), 7.12 (m, 2H, $C_{Ar}H$), 6.28 (d, $^{3}J_{HH}$ = 11.7 Hz, 1H, $C_{Ar}CH$), 5.57 (dt, $^{3}J_{HH}$ = 11.7, $^{3}J_{HH}$ = 7.4 Hz, 1H, $CHCH_2$), 2.34 (q, $^{3}J_{HH}$ = 6.96 Hz, 2H, $CHCH_2CH_2$), 2.09 (s, 3H, $CCH_3$), 1.21 (m, 4H, $CH_2CH_2CH_2CH_3$), 0.76 (t, $^{3}J_{HH}$ = 7.2 Hz, 3H, $CH_2CH_2CH_3$). GCMS-EI: RMM 202.1, Found 202.2 g mol$^{-1}$, m/z: 202.2 (60%), 187.2 (100%), 131.1 (92%), 117.1 (50%). The NMR data are in agreement with published data.[17]

## 6.3.26 – Characterisation of (*Z*)-4-Octene

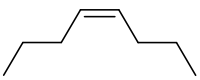

$^{1}$H NMR (500 MHz, $C_6D_6$, 298 K) δ 5.43 – 5.39 (m, 2H, $CHCH_2CH_2$), 1.99 (q, $^{3}J_{HH}$ = 5.8 Hz, 4H, $CH_2CH_2CH_3$), 1.33 (sext, $^{3}J_{HH}$ = 7.2 Hz, 4H, $CH_2CH_3$), 0.86 (t, $^{3}J_{HH}$ = 7.2 Hz, 6H, $CH_2CH_3$). $^{13}C\{^{1}H\}$ NMR (126 MHz, $C_6D_6$, 298 K) δ 130.1 (s), 29.7 (s), 23.3 (s), 14.0 (s). The NMR data are in agreement with published data.[18]

6.3.27 – Characterisation of (*Z*)-2-Hexene

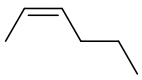

$^{1}$H NMR (500 MHz, $C_6D_6$, 298 K) δ 5.48 – 5.42 (m, 2H, C*H*=C*H*$CH_2$), 1.96 (q, $^{3}J_{HH}$ = 7.2 Hz, 2H, C$H_2$$CH_2CH_3$), 1.52 (d, $^{3}J_{HH}$ = 6.4 Hz, 3H, CHC$H_3$), 1.32 (quint, $^{3}J_{HH}$ = 7.4 Hz, 2H, $CH_2$C$H_2$$CH_3$), 0.86 (t, $^{3}J_{HH}$ = 7.4 Hz, 3H, $CH_2$C$H_3$). $^{13}$C{$^{1}$H} NMR (126 MHz, $C_6D_6$, 298 K) δ 130.8 (s), 124.1 (s), 29.3 (s), 23.1 (s), 13.9 (s), 12.9 (s). The NMR data are in agreement with published data.[19]

6.3.28 – Characterisation of (*Z*)-4,4,5,5-tetramethyl-2-(1-phenylprop-1-en-1-yl)-1,3,2-dioxaborolane

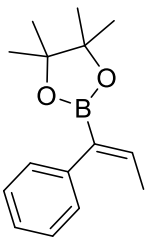


$^{1}$H NMR (500 MHz, $CDCl_3$, 298 K) δ 7.36 – 7.32 (m, 2H, $C_{Ar}$*H*), 7.26 – 7.22 (m, 3H, $C_{Ar}$*H*), 6.74 (q, $^{3}J_{HH}$ = 7.0 Hz, 1H, C*H*$CH_3$), 1.78 (d, $^{3}J_{HH}$ = 7.0 Hz, 3H, CHC$H_3$), 1.28 (s, 12H, C(C$H_3$)$_2$). $^{11}$B NMR (160 MHz, $CDCl_3$, 298 K) δ 30.1 (s). GCMS-EI: RMM 244.1, Found: 244.2 g mol$^{-1}$. The NMR data are in agreement with published data.[20]

6.3.29 – Characterisation of (*Z*)-4,4,5,5-tetramethyl-2-(1-phenylprop-1-en-2-yl)-1,3,2-dioxaborolane

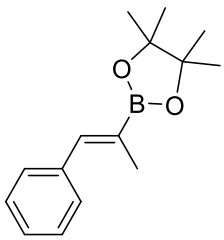


$^{1}$H NMR (500 MHz, $CDCl_3$, 298 K) δ 7.36 – 7.32 (m, 4H, $C_{Ar}$*H*), 7.26 – 7.22 (m, 2H, $C_{Ar}$*H* and $C_{Ar}$C*H*), 2.01 (s, 3H, C$H_3$), 1.32 (s, 12H, C(C$H_3$)$_2$). $^{11}$B NMR (160 MHz, $CDCl_3$, 298 K) δ 30.9 (s). GCMS-EI: RMM 244.1, Found: 244.2 g mol$^{-1}$. The NMR data are in agreement with published data.[20]

6.3.30 – Characterisation of (*Z*)-2-(1,2-diphenylvinyl)-4,4,5,5-tetramethyl-1,3,2-dioxaborolane

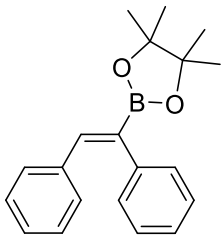

$^{1}$H NMR (500 MHz, $CDCl_3$, 298 K) δ 7.37 (s, 1H, $C_{Ar}CH$), 7.11 (m, 10H, $C_{Ar}H$), 1.30 (s, 12H, $C(CH_3)_2$). $^{11}$B NMR (160 MHz, $CDCl_3$, 298 K) δ 30.1 (br s). $^{13}C\{^{1}H\}$ NMR (126 MHz, $CDCl_3$, 298 K) δ 143.1 (s), 140.5 (s), 137.0 (s), 130.0 (s), 128.8 (s), 128.2 (s), 127.9 (s), 127.6 (s), 126.2 (s), 83.8 (s), 24.8 (s). The NMR data are in agreement with published data.[21]

6.3.31 – Characterisation of (*Z*)-2-(1-(4-fluorophenyl)-2-phenylvinyl)-4,4,5,5-tetramethyl-1,3,2-dioxaborolane

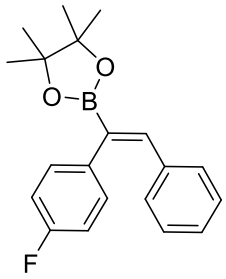

$^{1}$H NMR (500 MHz, $C_6D_6$, 298 K) δ 7.82 (s, 1H, $C_{Ar}CH$), 7.36 (d, $^{3}J_{HH}$ = 8.65 Hz, 2H, $C_{Ar}H$), 7.21 – 7.17 (m, 2H, $C_{Ar}H$), 7.22 – 7.18 (m, 2H, $C_{Ar}H$), 6.79 (t, $^{3}J_{HH}$ = 8.3Hz, 3H, $C_{Ar}H$), 0.41 (s, 12H, $C(CH_3)_2$). $^{19}$F NMR (470 MHz, $C_6D_6$, 298 K) δ -117.3 (m). $^{13}C\{^{1}H\}$ NMR (126 MHz, $CDCl_3$, 298 K) δ 161.7 (d, $J_{CF}$ = 245 Hz), 143.7 (s), 136.9 (s), 136.3 (d, $J_{CF}$ = 3 Hz), 130.6 (d, $J_{CF}$ = 8 Hz), 130.0 (s), 128.1 (s), 127.8 (s), 115.3 (d, $J_{CF}$ = 21 Hz), 84.0 (s), 24.9 (s). GCMS-ESI: RMM 324.17, Found 324.2, m/z: 324.2 (100%), 223.1 (28%), 208.2 (88%), 196.1 (22%)

6.3.32 – Characterisation of (Z)-2-(2-(4-fluorophenyl)-1-phenylvinyl)-4,4,5,5-tetramethyl-1,3,2-dioxaborolane

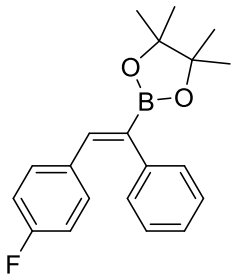


$^{1}$H NMR (500 MHz, $C_6D_6$, 298 K) δ 7.71 (s, 1H, $C_{Ar}CH$), 7.14 (d, 2H, partially obscured by solvent, $C_{Ar}H$), 6.96 – 6.92 (m, 2H, $C_{Ar}H$), 6.90 – 6.86 (m, 2H, $C_{Ar}H$), 6.50 (t, $^{3}J_{HH}$ = 8.62 Hz, 3H, $C_{Ar}H$), 1.08 (s, 12H, $C(CH_3)_2$). $^{19}$F NMR (470 MHz, $C_6D_6$, 298 K) δ -113.0 (m). $^{13}C\{^{1}H\}$ NMR (126 MHz, $CDCl_3$, 298 K) δ 162.1 (d, $J_{CF}$ = 248 Hz), 142.0 (s), 140.3 (s), 134.4 (br s), 133.2 (d, $J_{CF}$ = 3 Hz), 131.8 (d, $J_{CF}$ = 8 Hz), 128.9 (s), 128.5 (s), 126.5 (s), 115.0 (d, $J_{CF}$ = 21 Hz), 83.9 (s), 24.9 (s). GCMS-EI: RMM 324.17, Found 324.2, m/z: 324.2 (100%), 223.1 (28%), 208.2 (88%), 196.1 (22%).

6.3.33 – Characterisation of (Z)-trimethyl(2-phenyl-2-(4,4,5-trimethyl-1,3,2-dioxaborolan-2-yl)vinyl)silane

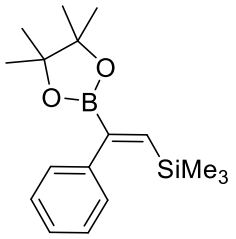


$^{1}$H NMR (500 MHz, $C_6D_6$, 298 K) δ 7.91 (s, 1H, $C_{Ar}CH$), 7.31 (m, 3H, $C_{Ar}H$), 7.22 (m, 2H, $C_{Ar}H$), 1.21 (s, 12H, $C(CH_3)_2$), -0.11 (s, (9H, $Si(CH_3)_3$). The NMR data are in agreement with published data.[21]

6.3.34 – Characterisation of (Z)-trimethyl(2-phenyl-1-(4,4,5,5-tetramethyl-1,3,2-dioxaborolan-2-yl)vinyl)silane

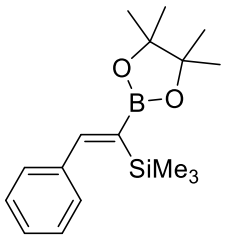


$^{1}$H NMR (500 MHz, $C_6D_6$, 298 K) δ 7.35 (br s, 1H, $C_{Ar}CH$), 7.35 (m, 4H, $C_{Ar}H$), 7.21 (m, 1H, $C_{Ar}H$), 1.17 (s, 12H, $C(CH_3)_2$), -0.23 (s, 9H, $Si(CH_3)_3$). The NMR data are in agreement with published data.[21]

6.3.35 – Characterisation of (Z)-2-(1-(4-fluorophenyl)hex-1-en-1-yl)-4,4,5,5-tetramethyl-1,3,2-dioxaborolane

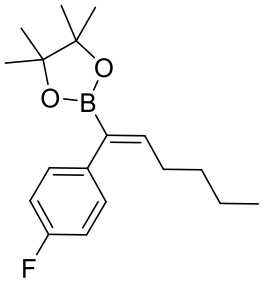


$^{1}$H NMR (500 MHz, $C_6D_6$, 298 K) δ 7.19 – 7.16 (m, 4H, $C_{Ar}H$), 6.94 (t, $^{3}J_{HH}$ = 7.2 Hz, 1H, $CHCH_2$), 2.12 (q, $^{3}J_{HH}$ = 7.2 Hz, 2H, $CHCH_2CH_2$), 1.25 (m, 2H, $CH_2CH_2CH_3$), 1.12 (m, 2H, $CH_2CH_2CH_3$), 1.06 (s, 12H, $C(CH_3)_2$), 0.70 (t, $^{3}J_{HH}$ = 7.2 Hz, 3H, $CH_2CH_2CH_3$). $^{1}$H NMR (500 MHz, $CDCl_3$) δ 7.09 (m, 2H, $C_{Ar}H$), 6.98 (m, 2H, $C_{Ar}H$), 6.58 (t, $^{3}J_{HH}$ = 7.3 Hz, 1H, $CHCH_2$), 2.12 (q, $^{3}J_{HH}$ = 7.4 Hz, 2H, $CHCH_2$), 1.37 (m, 2H, $CH_2CH_2CH_3$), 1.27 (m, 14H, $C(CH_3)_2$, $CH_2CH_2CH_3$), 0.83 (t, $^{3}J_{HH}$ = 7.3 Hz, 3H, $CH_2CH_2CH_3$). $^{13}C\{^{1}H\}$ NMR (126 MHz, $C_6D_6$, 298 K) δ 161.9 (d, $J_{CF}$ = 244 Hz), 149.4, 136.7 (d, $J_{CF}$ = 3 Hz), 133.7 (d, $J_{CF}$ = 8 Hz), 131.0 (d, $J_{CF}$ = 8 Hz), 114.9 (d, $J_{CF}$ = 21 Hz), 83.5 (s), 31.8 (s), 30.0 (s), 24.9 (s), 22.7 (s), 14.0 (s). $^{13}C\{^{1}H\}$ NMR (126 MHz, $CDCl_3$) δ 161.4 (d, $J_{CF}$ = 244 Hz), 149.0 (s), 136.2 (d, $J_{CF}$ = 3 Hz), 133.4 (d, $J_{CF}$ = 8 Hz), 130.5 (d, $J_{CF}$ = 8 Hz), 114.7 (d, $J_{CF}$ = 21 Hz), 83.6 (s), 31.6 (s), 29.7 (s), 24.9 (s), 22.6 (s), 14.0 (s). $^{19}$F NMR (470 MHz, $C_6D_6$, 298 K) δ -117.2 (m). GCMS-EI: RMM 304.2, Found 304.3, m/z: 304.3 (23%), 247.2 (76%), 148.1 (26%), 101.2 (100%).

### 6.3.36 – Catalytic Procedure for Semihydrogenation

Under an argon atmosphere of the glovebox, alkyne (0.22 mmol), PMHS (0.24 mmol), 1,3,5-$(MeO)_3C_6H_3$ (0.022 mmol, internal standard), and 500 μL of $2.2 \times 10^{-3}$ M $C_6D_6$ stock solution of copper catalyst were added to a flame-dried J. Youngs resealable NMR tube. Catalysis was initiated by addition of $^tBuOH$ (0.24 mmol) and reactions followed by $^1H$ NMR spectroscopy. After the desired reaction time, solutions were filtered through a silica plug (hexane as eluent), and the filtrate was reduced to dryness using a flow of $N_2$. The residue was dissolved in minimal $CHCl_3$ and washed through a silica plug with hexane to afford alkene products.

### 6.3.37 – Catalytic Procedure for Hydroboration of Alkynes

Under an argon atmosphere of the glovebox, alkyne (0.51 mmol), 1,3,5-$(MeO)_3C_6H_3$ (100 μL from a 0.2 M stock solution in $C_6D_6$, internal standard), and copper catalyst (400 μL from a $0.025 \times 10^{-3}$ M stock solution in $C_6D_6$) were added to a flame-dried J. Youngs resealable NMR tube. HBPin (81.2 μL, 0.560 mmol, 1.1 equiv) was added to initiate the reaction. The solution was shaken at room temperature for 3 h at which point the clear yellow solution was flushed through a silica plug with $CH_2Cl_2$. The resulting solution was reduced to dryness and analysed by GC.

## 6.4 – Experimental Details and Characterising Data for Chapter 3.

### 6.4.1 – Synthesis and Characterisation of [ITrH]$BF_4$

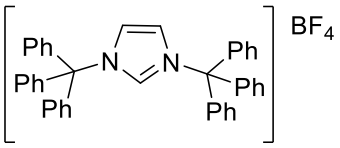


Tritylium tetrafluoroborate (532 mg, 1.61 mmol) and 1-(triphenylmethyl)imidazole (500 mg, 1.61 mmol) were placed into an ampoule fitted with a J. Youngs resealable valve and $C_6H_6$ (20 mL) added to form a suspension. After stirring vigourously for 20 h, the solid material was isolated by filtration, washed with additional $C_6H_6$ and then dissolved in minimal $CH_2Cl_2$. Addition of excess $Et_2O$ gave [ITrH]$BF_4$ as a white crystalline solid (830 mg, 80% yield). $^1H$ NMR (500 MHz, $CD_2Cl_2$, 298 K) δ 8.03 (t, $^4J_{HH}$ = 1.9 Hz, 1H, NC*H*N), 7.49 – 7.40 (m, 20H, $C_{Ar}H$ + NC*H*), 7.15 – 7.07 (m, 12H, $C_{Ar}H$). $^{13}C\{^1H\}$NMR (126 MHz, $CD_2Cl_2$, 298 K) δ 139.4 (s), 138.0 (s), 130.0 (s), 129.7 (s), 129.5 (s), 124.7

(s), 80.8 (s). Elemental analysis calcd (%) for $C_{41}H_{33}N_2BF_4$ (640.65): C, 76.88; H, 5.19; N, 4.37; found C, 76.87; H, 5.19; N, 4.59. HRMS ES+: m/z 555.2647 $[M\text{-}BF_4]^+$ corresponds to $C_{51}H_{33}N_2$ with a 0.5 ppm mass error.

## 6.4.2 – Synthesis and Characterisation of for [ITrDippH]$BF_4$

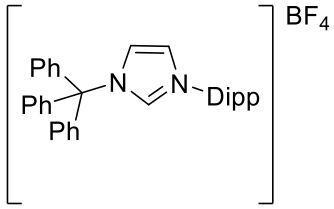


Tritylium tetrafluoroborate (910 mg, 2.60 mmol) and 1-(2,6-diisopropylphenyl)imidazole (600 mg, 2.60 mmol) were placed into an ampoule fitted with a J. Youngs resealable valve and $C_6H_6$ (20 mL) added to form a suspension. After stirring vigourously for 20 h, the solid material was isolated by cannula filtration, washed with $C_6H_6$ (10 mL) and then $Et_2O$ (2 x 10 mL). The product was obtained as an off-white powder (1.12 g, 77% yield). $^1$H NMR (400 MHz, $CD_2Cl_2$, 298 K) δ 8.11 (t, $^4J_{HH}$ = 1.8 Hz, 1H, NC*H*N), 7.72 (m, 1H, NC*H*), 7.63 (m, 1H, NC*H*), 7.59 (t, $^3J_{HH}$ = 7.8 Hz, 1H, $C_{Ar}H$), 7.55 – 7.44 (m, 9H, $C_{Ar}H$), 7.36 (d, $^3J_{HH}$ = 7.9 Hz, 2H, $C_{Ar}H$), 7.26 – 7.17 (m, 6H, $C_{Ar}H$), 2.29 (sept, $^3J_{HH}$ = 6.8 Hz, 2H, C*H*$(CH_3)_2$), 1.25 (d, $^3J_{HH}$ = 6.8 Hz, 6H, CH(C*H*$_3)_2$), 1.11 (d, $^3J_{HH}$ = 6.9 Hz, 6H, CH(C*H*$_3)_2$). $^{13}$C{$^1$H} NMR (101 MHz, $CDCl_3$, 298 K) δ 145.2 (s), 139.5 (s), 136.4 (s), 132.3 (s), 130.1 (s), 129.8 (s), 129.4 (s), 129.4 (s), 126.5 (s), 125.9 (s), 124.9 (s), 80.2 (s), 29.0 (s), 24.7 (s), 23.8 (s). HRMS ES+: m/z 471.2793 $[M\text{-}BF_4]^+$ corresponds to $C_{34}H_{35}N_2$ with a 1.5 ppm mass error.

## 6.4.3 – Synthesis and Characterisation of (ITr)CuMes

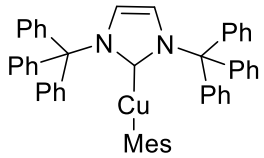


[ITrH]$BF_4$ (900 mg, 1.41 mmol) and KHMDS (275 mg, 1.38 mmol) were placed into an ampoule fitted with a J. Youngs resealable valve with THF (10 mL). The resulting suspension was stirred for 16 h at room temperature, reduced to dryness and the carbene extracted with THF (10 mL) into a new ampoule. The solution was again reduced to dryness and $Cu(Mes)_n$ (285 mg, 1.27 mmol) added, along with $C_6H_6$ (10 mL). After

stirring for 2 h, the solution was filtered by cannula, reduced in volume and hexane added to yield a colourless precipitate. The precipitate was washed further with hexane (2 x 5 mL) and recrystallised from $C_6H_6$/hexane to yield the product as an off-white powder (780 mg, 72% yield). $^1$H NMR (500 MHz, $C_6D_6$, 298 K) δ 7.25 – 7.20 (m, 12H, $C_{Ar}H$), 7.08 – 7.00 (m, 18H, $C_{Ar}H$), 6.79 (s, 2H, $C_{Ar}H$), 6.60 (s, 2H, NC*H*), 2.34 (s, 3H, C$H_3$), 1.72 (s, 6H, C$H_3$). $^{13}$C{$^1$H} NMR (126 MHz, $C_6D_6$, 298 K) δ 192.7 (s, NCN), 166.0 (s), 145.7 (s), 143.3 (s), 130.8 (s), 130.4 (s), 128.2 (s), 128.0 (s), 123.9 (s), 119.4 (s), 78.2 (s), 29.9 (s), 21.7 (s). Elemental analysis calcd (%) for $C_{50}H_{43}N_2Cu$ (735.41): C, 81.66; H, 5.89; N, 3.81; found C, 81.57; H, 5.85; N, 3.76.

## 6.4.4 – Synthesis and Characterisation of (ITrDipp)CuMes

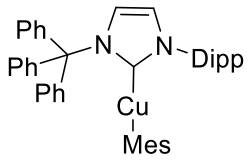


[ITrDippH]$BF_4$ (460 mg, 0.824 mmol) and KHMDS (275 mg, 0.832 mmol) were placed into an ampoule fitted with a J. Youngs resealable valve with THF (5 mL). The resulting suspension was stirred for 1 h at room temperature, reduced to dryness and the carbene extracted with $Et_2O$ (10 mL) into a new ampoule. The solution was again reduced to dryness and $Cu(Mes)_n$ (150 mg, 0.820 mmol) added, along with $C_6H_6$ (5 mL). After stirring for 16 h, the solution was filtered by cannula into a new ampoule. The residue was washed further with $C_6H_6$ (5 x 10 mL) and combined by filtration by cannula into the new ampoule. The solution was reduced in volume and hexane added to yield (ITrDipp)Cu(Mes) as a colourless precipitate (170 mg, 32%). $^1$H NMR (500 MHz, $C_6D_6$, 298 K) δ 7.41 – 7.36 (m, 6H, $C_{Ar}H$), 7.23 – 7.17 (m, 1H, $C_{Ar}H$), 7.10 – 7.03 (m, 8H, $C_{Ar}H$), 7.02 – 6.97 (m, 3H, $C_{Ar}H$), 6.84 (s, 2H, $C_{Ar}H$), 6.66 (d, $^3J_{HH}$ = 2.0 Hz, 1H, NC*H*), 6.17 (d, $^3J_{HH}$ = 1.9 Hz, 1H, NC*H*), 2.66 (sept, $^3J_{HH}$ = 6.5 Hz, 2H, C*H*($CH_3$)$_2$), 2.29 (s, 3H, $CH_3$), 1.99 (s, 6H, $CH_3$), 1.34 (d, $^3J_{HH}$ = 6.9 Hz, 6H, CH(C$H_3$)$_2$), 1.09 (d, $^3J_{HH}$ = 6.9 Hz, 6H, CH(C$H_3$)$_2$). $^{13}$C{$^1$H} NMR (126 MHz, $C_6D_6$, 298 K) δ 189.7 (s, NCN), 163.6 (s), 146.6 (s), 145.6 (s), 143.4 (s), 136.7 (s), 132.1 (s), 130.5 (s), 130.3 (s), 128.3 (s), 128.1 (s), 124.3 (s), 124.2 (s), 121.7 (s), 120.4 (s), 77.9 (s), 29.0 (s), 29.0 (s), 24.4 (s), 24.3 (s), 21.6 (s). Elemental analysis calcd (%) for $C_{43}H_{45}N_2Cu$ (653.35): C, 70.04; H, 6.94; N, 4.29; found C, 78.75; H, 6.95; N, 4.22.

## 6.4.5 – Synthesis and Characterisation of ($^{Menthyl}$CAAC)CuMes

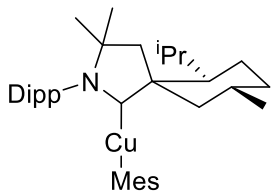


[$^{menthyl}$CAACH]$BF_4$ (500 mg, 1.07 mmol)1 and KHMDS (214 mg, 1.76 mmol) were placed into an ampoule fitted with a J. Youngs resealable valve and dissolved in a mixture of $Et_2O$ (3 mL) and pentane (10 ml). After stirring for 1 h at room temperature, the volatiles were removed in vacuo. The residue was redissoved in $Et_2O$, the solution filtered by cannula to a new ampoule and the solution reduced to dryness. $[CuMes]_n$ (194 mg, 1.07 mmol) and $C_6H_6$ (5 mL) were then added and the suspension stirred for 1 h at room temperature. After cannula filtration, the filtrate was reduced to dryness to yield a colourless solid. The solid was washed at -78 °C with minimal pentane to yield the product as an off-white powder (391 mg, yield 72%). $^1$H NMR (500 MHz, $C_6D_6$, 298 K) δ 7.22 – 7.12 (m, 1H, partially obscured by $C_6D_5H$, $C_{Ar}H$), 7.07 – 7.02 (m, 2H, $C_{Ar}H$), 7.00 (s, 2H, $C_{Ar}H$), 3.32 – 3.17 (m, 2H), 2.94 – 2.79 (m, 2H), 2.35 (s, 3H), 2.28 (s, 6H), 2.26 – 2.19 (m, 1H), 1.90 (d, $^3J_{HH}$ = 13.5 Hz, 1H), 1.87 – 1.80 (m, 2H), 1.78 – 1.72 (m, 1H), 1.39 (d, $^3J_{HH}$ = 6.7 Hz, 3H), 1.33 (d, $^3J_{HH}$ = 6.6 Hz, 3H), 1.27 (d, $^3J_{HH}$ = 13.6 Hz, 1H), 1.24 – 1.01 (m, 12H), 0.98 – 0.92 (m, 12H). $^{13}$C{$^1$H} NMR (126 MHz, $C_6D_6$, 298 K) δ 257.2 (s, NCC), 162.3 (s), 147.4 (s), 146.0 (s), 145.6 (s), 136.6 (s), 133.1 (s), 129.6 (s), 125.3 (s), 125.2 (s), 77.1 (s), 66.3 (s), 53.2 (s), 51.9 (s), 49.0 (s), 36.2 (s), 30.7 (s), 29.6 (s), 29.6 (s), 29.4 (s), 29.3 (s), 28.8 (s), 28.2 (s), 27.4 (s), 26.4 (s), 24.9 (s), 24.3 (s), 23.2 (s), 23.0 (s), 22.8 (s), 21.6 (s), 20.1 (s). Elemental analysis calcd (%) for $C_{36}H_{54}NCu$ (564.35): C, 76.61; H, 9.65; N, 2.48; found C, 76.73; H, 9.65; N, 2.58.

## 6.4.6 – Synthesis and Characterisation of (7-Mes)CuF (**3.1**)

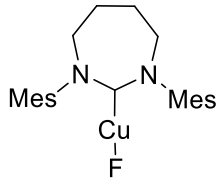


As for **3.2**, using (7-Mes)CuMes (260 mg, 0.5 mmol) and $Et_3N{\cdot}3HF$ (23.5 μL, 0.15 mmol) to yield **3.1** as an off-white solid (123 mg, yield 66%). $^1H$ NMR (500 MHz, $CDCl_3$, 298 K) δ 6.90 (s, 4H, $C_{Ar}H$), 3.85 (m, 4H, $NCH_2$), 2.35 (s, 12H, $CH_3$), 2.29 – 2.20 (m, 10H, $CH_3$ + $NCH_2CH_2$). $^{13}C\{^1H\}$ NMR (126 MHz, $CDCl_3$, 298 K) δ 211.4 (d, $^2J_{CF}$ = 36 Hz, NCN), 144.6 (s), 137.9 (s), 134.1 (s), 130.2 (s), 52.6 (s), 25.7 (s), 21.2 (s), 18.7 (s). $^{19}F$ NMR (470 MHz, $CDCl_3$, 298 K) δ -253.8 (s). $^{19}F$ NMR (470 MHz, $CD_2Cl_2$, 298 K) δ -246.0 (s). Anal. Calcd for $C_{23}H_{30}N_2FCu$ (417.02): C, 66.24; H, 7.25; N, 6.72, found: C, 65.98; H, 7.23; N, 6.71.

## 6.4.7 – Synthesis and Characterisation of (6-Mes)CuF (**3.2**)

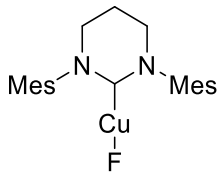


$Et_3N{\cdot}3HF$ (46.5 μL, 0.29 mmol) was added to a stirred $C_6H_6$ solution (5 mL) of (6-Mes)CuMes (495 mg, 0.99 mmol) to afford a colourless precipitate within 5 min. After stirring for a further 1 h, the precipitate was filtered, washed with $C_6H_6$ (2 × 3 mL), and dried in vacuo to yield **3.2** as an off-white powder (230 mg, yield 66%). Crystals suitable for X-ray diffraction were obtained from $CH_2Cl_2/Et_2O$. **3.2** could also be obtained upon reaction of (6-Mes)CuO$^t$Bu with $Et_3N{\cdot}3HF$. $^1H$ NMR (500 MHz, $CD_2Cl_2$, 298 K) δ 7.01 (s, 4H, $C_{Ar}H$), 3.35 (t, $^3J_{HH}$ = 5.9 Hz, 4H, $NCH_2$), 2.23 (m, 20H, $CH_3$ + $NCH_2CH_2$). $^{13}C\{^1H\}$ NMR (126 MHz, $CD_2Cl_2$, 298 K) δ 201.0 (s, N*C*N),* 142.6 (s), 138.1 (s), 134.8 (s), 129.7 (s), 44.3 (s), 20.9 (s), 20.8 (s), 17.8 (s). $^{19}F$ NMR (470 MHz, $CD_2Cl_2$) δ -244.6 (s). $^{19}F$ NMR (470 MHz, $CDCl_3$) δ -252.4 (s). Anal. Calcd for $C_{22}H_{28}N_2FCu$ (403.00): C, 65.56; H, 7.00; N, 6.95. Found: C, 65.22; H, 7.03; N, 6.88. *Seen by HMBC

## 6.4.8 – Synthesis and Characterisation of (ITr)CuF (**3.3**)

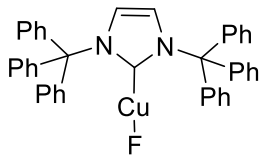


As for **3.2**, using (ITr)CuMes (648 mg, 0.881 mmol) and $Et_3N{\cdot}3HF$ (45 μL, 0.278 mmol) to yield **3.3** as an off-white solid (365 mg, yield 69%). $^1$H NMR (500 MHz, $CDCl_3$, 298 K) δ 7.32 – 7.27 (m, 18H, $C_{Ar}H$), 7.25 – 7.20 (m, 12H, $C_{Ar}H$), 6.96 (s, 2H, NC*H*). $^{13}C\{^1H\}$ NMR (126 MHz, $CDCl_3$, 298 K) δ 188.0 (d, $^2J_{CF}$ = 32 Hz, NCN), 142.4 (s), 130.1 (s), 128.2 (s), 128.1 (s), 120.2 (s), 78.1 (s). $^{19}$F NMR (470 MHz, $CDCl_3$, 298 K) δ −251.4 (s) $^{19}$F NMR (470 MHz, $CD_2Cl_2$, 298 K) δ -244.3 (s). Anal. Calcd for $C_{41}H_{32}N_2FCu{\cdot}2CH_2Cl_2$ (805.08): C, 64.15; H, 4.51; N, 3.48; found: C, 63.96; H, 4.53; N, 3.62.

## 6.4.9 – Synthesis and Characterisation of (ITrDIPP)CuF (**3.4**)

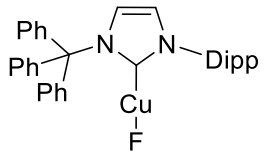


$Et_3N{\cdot}3HF$ (13 μL, 0.082 mmol) was added to a stirred $C_6H_6$ suspension (5 mL) of (ITrDipp)CuMes (170 mg, 0.26 mmol) to afford a yellow-brown solution. After stirring for 1 h, the solution was filtered, concentrated, and precipitated by addition of $Et_2O$ to give an off-white solid. Precipitation with $Et_2O$ from $C_6H_6$ was performed twice more to yield **3.4** as an off-white powder (112 mg, yield 82%). Analytically clean compound was obtained from $CH_2Cl_2$/pentane. $^1$H NMR (500 MHz, $CDCl_3$, 298 K) δ 7.41 – 7.31 (m, 16H, $C_{Ar}H$), 7.23 – 7.16 (m, 3H, $C_{Ar}H$ + NC*H*), 6.86 (d, $^3J_{HH}$ = 1.2 Hz, 1H, NC*H*), 2.41 (sept, $^3J_{HH}$ = 6.9 Hz, 2H, C*H*$(CH_3)_2$), 1.22 (d, $^3J_{HH}$ = 6.9 Hz, 6H, CH(C*H*$_3)_2$), 1.15 (d, $^3J_{HH}$ = 6.9 Hz, 6H, CH(C*H*$_3)_2$). $^{13}C\{^1H\}$ NMR (126 MHz, $CDCl_3$, 298 K) δ 184.3 (d, $^2J_{CF}$ = 33 Hz, NCN), 145.4 (s), 142.5 (s), 135.7 (s), 130.3 (s), 130.2 (s), 128.5 (s), 128.4 (s), 124.3 (s), 122.4 (s), 121.2 (s), 77.9 (s), 28.7 (s), 24.8 (s), 24.0 (s). $^{19}$F NMR (470 MHz, $CDCl_3$, 298 K) δ -250.4 (s). Anal. Calcd for $C_{34}H_{34}N_2FCu$ (553.18): C, 73.82; H, 6.20; N, 5.06. Found: C, 73.90; H, 6.08; N, 5.08.

## 6.4.10 – Synthesis and Characterisation of ($^{Menthyl}$CAAC)CuF (**3.5**)

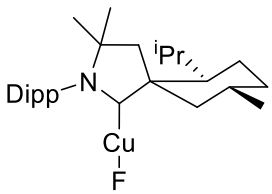


$Et_3N{\cdot}3HF$ (36 μL, 0.22 mmol) was added to a stirred $Et_2O$ (5 mL) solution of ($^{menthyl}$CAAC)CuMes (391 mg, 0.69 mmol) to give a colourless precipitate. After 1 h, the suspension was filtered and the precipitate washed with $Et_2O$ (2 × 10 mL) and dried in vacuo to yield **3.5** as an off-white powder (190 mg, yield 62%). $^1$H NMR (500 MHz, $CD_2Cl_2$) δ 7.44 (t, $^3J_{HH}$ = 7.7 Hz, 1H, $C_{Ar}H$), 7.33 – 7.28 (m, 2H, $C_{Ar}H$), 2.94 – 2.78 (m, 2H), 2.75 – 2.61 (m, 2H), 2.29 (d, $^3J_{HH}$ = 13.7 Hz, 1H), 2.14 – 2.06 (m, 1H), 1.98 – 1.81 (m, 3H), 1.77 (d, $^3J_{HH}$ = 13.7 Hz, 1H), 1.43 – 1.27 (m, 17H), 1.24 (d, $^3J_{HH}$ = 6.6 Hz, 3H, $CH(CH_3)_2$), 1.16 – 0.99 (m, 7H), 0.90 (d, $^3J_{HH}$ = 6.5 Hz, 3H, $CH(CH_3)_2$). $^{13}$C{$^1$H} NMR (126 MHz, $CD_2Cl_2$, 298 K) δ 250.9 (br s, NCC), 160.0 (s), 145.6 (s), 136.2 (s), 129.9 (s), 125.3 (s), 125.1 (s), 77.8 (s), 65.4 (s), 52.8 (s), 51.5 (s), 48.9 (s), 36.1 (s), 31.4 (s), 30.0 (s), 29.6 (s), 29.6 (s), 29.4 (s), 28.1 (s), 27.8 (s), 26.8 (s), 25.4 (s), 24.5 (s), 22.9 (s), 22.6 (s), 22.5 (s), 20.2 (s). $^{19}$F NMR (470 MHz, $CD_2Cl_2$, 298 K) δ -240.0 (s). $^{19}$F NMR (470 MHz, $CDCl_3$, 298 K) δ -245.1 (s). Anal. Calcd for $C_{27}H_{43}NFCu$ (463.27) C, 69.86; H, 9.34; N, 3.02. Found: C, 69.93; H, 9.27; N, 3.26.

## 6.4.11 – Synthesis and Characterisation of (6-MesDAC)CuF (**3.6**)

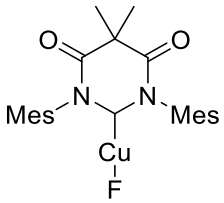


As for **3.2**, using (6-MesDAC)CuMes (370 mg, 0.697 mmol) and $Et_3N{\cdot}3HF$ (32.9 μL, 0.202 mmol) to yield **3.6** as yellow blocks after crystallisation from $CH_2Cl_2$/pentane (137 mg, yield 43%). $^1$H NMR (500 MHz, $CD_2Cl_2$, 298 K) δ 7.10 (s, 4H, $C_{Ar}H$), 2.38 (s, 6H, $C(CH_3)_2$), 2.19 (s, 12H, $CH_3$), 1.76 (s, 6H, $CH_3$). $^{13}$C{$^1$H} NMR (126 MHz, $CD_2Cl_2$) 171.6 (s, NCN), 140.8 (s), 136.0 (s), 134.7 (s), 130.5 (s), 52.0 (s), 25.0 (s), 21.3 (s), 18.4 (s). $^{19}$F NMR (470 MHz, $CD_2Cl_2$, 298 K) δ -239.5 (br s). Anal. Calcd for

$C_{24}H_{28}N_2FO_2Cu \cdot 0.5CH_2Cl_2$ (500.00) C, 58.68; H, 5.83; N, 5.59. Found: C, 58.78; H, 5.85; N, 5.57.

### 6.4.12 – Synthesis and Characterisation of (ITr)Cu($CH_2CHCH_2$) (**3.7**)

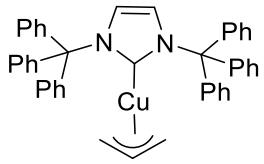


Trimethoxylallylsilane (31 μL, 0.18 mmol) was added to a stirred $C_6H_6$ solution (10 mL) of **3.3** (115 mg, 0.18 mmol) to afford a bright yellow solution. After 1 h, the solution was filtered and concentrated and pentane added to afford a colourless precipitate. This was collected, washed with cold pentane (2 × 5 mL), and dried under vacuum to give 3**.7** as an off-white powder (43 mg, yield 36%). Crystals suitable for X-ray diffraction were obtained from $Et_2O$/pentane at −30 °C. $^1$H NMR (500 MHz, $C_6D_5CD_3$, 298 K) δ 7.30 – 7.25 (m, 12H, $C_{Ar}H$), 7.11 − 7.06 (m, 14H, $C_{Ar}H$), 7.05−7.02 (m, 4H, $C_{Ar}H$), 6.54 (s, 2H, NC*H*), 5.83 (quint, $^3J_{HH}$ = 11.1 Hz, 1H, C*H*), 2.39 (d, $^3J_{HH}$ = 11.1 Hz, 4H, CHC$H_2$). $^{13}$C{$^1$H} NMR (126 MHz, $C_6D_5CD_3$, 298 K) δ 192.6 (s, NCN), 150.3 (s), 143.4 (s), 130.4 (s), 128.0 (s), 127.7 (s), 119.1 (s), 78.1 (s), 57.7 (br s). Efforts to determine an elemental analysis for $C_{44}H_{37}N_2Cu$ (657.30) gave consistently low %C (e.g., calcd C, 80.40; H, 5.67; N, 4.26: found C, 78.03; H, 5.45; N, 4.20).

### 6.4.13 – Synthesis and Characterisation of [{(6-Mes)Cu}$_2$(μ-OEt)][$SiF_5$] (**3.8**)

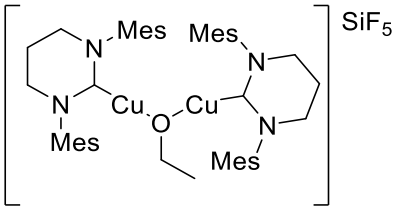


Triethoxyfluorosilane (176 μL, 0.947 mmol) was added to a stirred $C_6H_6$ suspension (10 mL) of **2.2** (150 mg, 0.316 mmol) to afford a colourless solution. After <5 min, the solution yielded a colourless precipitate, which was isolated by filtration, redissolved in $CH_2Cl_2$ (5 mL), and then reprecipitated via addition of pentane. After isolation by filtration, the solid was washed with pentane (2 × 5 mL) and dried in vacuo to yield an off-white powder (120 mg, yield 81%). Crystals suitable for X-ray diffraction were obtained from $CH_2Cl_2$/pentane. $^1$H NMR (400 MHz, $CD_2Cl_2$, 272 K) δ 6.89 (s, 8H, $C_{Ar}H$),

3.25 (t, $^{3}J_{HH}$ = 5.9 Hz, 8H, NC$H_2$), 2.37 (br q, 2H, OC$H_2$; 235 K: δ 2.33 (q, $^{3}J_{HH}$ = 6.9 Hz)), 2.28 (s, 12H, C$H_3$), 2.23 (q, $^{3}J_{HH}$ = 5.9 Hz, 4H, NCH$_2$C$H_2$), 2.12 (s, 24H, C$H_3$), 0.07 (br t, $^{3}J_{HH}$ = 7.1 Hz, 3H, OCH$_2$C$H_3$; 235 K: δ -0.04 (t, $^{3}J_{HH}$ = 6.9 Hz)). $^{19}$F (376 MHz, $CD_2Cl_2$, 235 K) δ -138.9 (s; $^{1}J_{FSi}$ = 147 Hz). $^{13}$C{$^{1}$H} NMR (101 MHz, $CD_2Cl_2$, 272 K) δ 199.1 (s, NCN), 142.3 (s), 138.2 (s), 134.8 (s), 129.7 (s), 63.6 (br s), 44.5 (s), 22.6 (br s), 21.1 (s), 20.9 (s), 18.0 (s). Anal. Calcd for $C_{46}H_{61}N_4OF_5SiCu_2 \cdot 0.75CH_2Cl_2$ (999.86; Based upon NMR): C, 56.15; H, 6.30; N, 5.60. Found: C, 56.09; H, 6.33; N, 5.67

6.4.14 – Synthesis and Characterisation of [{(ITr)Cu}$_2$(μ-OEt)][SiF$_5$] (**3.9**)

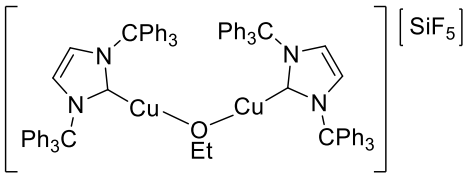


As for **3.8**, using (ITr)CuF (400 mg, 0.630 mmol) and (EtO)$_3$SiF (351 μL, 1.89 mmol) to yield **3.9** as colourless blocks after crystallisation from $CH_2Cl_2$/pentane. Yield is not given due to the unknown nature of the final product (see chapter 3), however 243 mg was collected.

6.4.15 – Synthesis and Characterisation of [{($^{Menthyl}$CAAC)Cu}$_2$(μ-OEt)][SiF$_5$] (**3.10**)

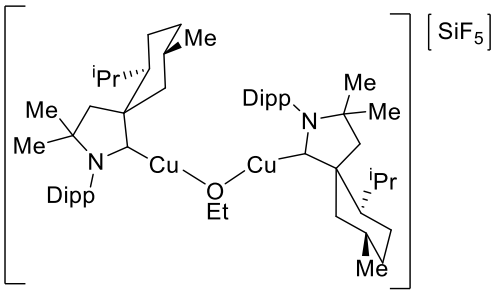


As for **3.8**, using ($^{Menthyl}$CAAC)CuF (100 mg, 0.215 mmol) and (EtO)$_3$SiF (120 μL, 0.646 mmol) to yield **3.10** as colourless blocks after crystallisation from $CH_2Cl_2$/pentane. Yield is not given due to the unknown nature of the final product (see chapter 3), however 63 mg was collected.

## 6.4.16 – Characterisation of 1-undecen-4-ol

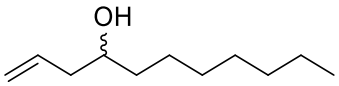


$^{1}$H NMR (500 MHz, $CDCl_3$, 298 K) δ 5.89 – 5.77 (m, 1H,), 5.17 – 5.10 (m, 2H), 3.74 – 3.58 (m, 1H), 2.37 – 2.26 (m, 1H), 2.21 – 2.06 (m, 1H), 1.61 – 1.53 (m, 1H), 1.49 – 1.23 (m, 12H), 0.88 (t, $^{3}J_{HH}$ = 6.8 Hz, 3H). $^{13}C\{^{1}H\}$ NMR (126 MHz, $CDCl_3$, 298 K) δ 135.1 (s), 118.2 (s), 70.9 (s), 42.1 (s), 37.0 (s), 32.0 (s), 29.8 (s), 29.4 (s), 25.8 (s), 22.8 (s), 14.3 (s). HRMS ES+: m/z 193.1578 $[M+Na]^+$ corresponds to $C_{11}H_{22}O$ with a 3.72 ppm mass error.

## 6.4.17 – Catalytic Procedure for Allylation of Octanal

*NMR-Scale Reactions*. To a $C_6D_6$ (1 mL) suspension of NHC-copper fluoride (1 mol %) and 1,3,5-$C_6H_3(OMe)_3$ reference (56 mg, 0.33 mmol) in a J. Youngs NMR tube was added octanal (156 μL, 1.0 mmol) followed by $(MeO)_3SiCH_2CH{=}CH_2$ (185 μL, 1.1 mmol, 1.1 equiv). The reaction mixture was shaken at room temperature and monitored by NMR spectroscopy.

*Preparative-Scale Reactions*. Under the argon atmosphere of a glovebox, to a $C_6H_6$ (3 mL) suspension of **3.1 – 3.5** (1 mol %) in an screw-cap vial equipped with a PTFE stirrer bar was added octanal (468 uL, 3.0 mmol) followed by $(MeO)_3SiCH_2CH{=}CH_2$ (185 uL, 3.3 mmol, 1.1 equiv). After they were stirred at room temperature for 24 h, the solutions were filtered through a silica plug in air. After the vial was washed with $CH_2Cl_2$ (3 × 1 mL), the filtrates were combined, reduced to dryness, and redissolved in MeOH (10 mL) and *p*TsOH (190 mg, 1.0 mmol, 0.33 equiv) was added. After the mixture was stirred for 24 h, a saturated aqueous solution of $KHCO_3$ was added to quench the reaction. Upon removal of solvent, the residue was extracted with EtOAc (3 × 10 mL), filtered, concentrated, and purified via column chromatography (5% EtOAc/ 95% pentane) to yield 1-undecen-4-ol as a colourless oil.

## 6.5 – Experimental Details and Characterising Data for Chapter 4

### 6.5.1 – General Synthesis for [NHCH]Cl from [NHCH]$BF_4$

Salt exchanges were carried out following a published procedure.[22] The loss of the $BF_4$ peak was used as an indicator the exchange had occurred. The [RE-NHCH]Cl salts in most cases are extremely hygroscopic. Amberlite® IRA402 chloride form contains water thus was dried before use via a rotary evaporator till the beads were falling fluidly. Excessive heat ca 140 $^oC$ of the Amberlite® IRA402 chloride yields a biproduct during the exchange hence the use of milder conditions involving the rotary evaporator. This did not completely dry the beads, however it allowed for the RE-NHC salt to be obtained with less difficulty.

### 6.5.2 – Characterisation of [6-MesH]Cl

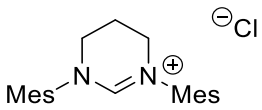


$^1$H NMR (500 MHz, $CDCl_3$, 298 K) δ 7.64 (s, 1H, NC*H*N), 6.90 (s, 4H, $C_{Ar}H$), 4.13 (t, $^3J_{HH}$ = 5.8 Hz, 4H, NC$H_2$), 2.61 (quint, $^3J_{HH}$ = 5.8 Hz, 2H, $NCH_2CH_2$), 2.30 (s, 12H, C$H_3$), 2.23 (s, 6H, C$H_3$). $^{13}C\{^1H\}$ NMR (75 MHz, $CDCl_3$, 298 K) δ 153.8 (s), 140.6 (s), 136.6 (s), 134.5 (s), 130.2 (s), 47.2 (s), 21.1 (s), 19.8 (s), 18.1 (s).

### 6.5.3 – Characterisation of [6-XylylH]Cl

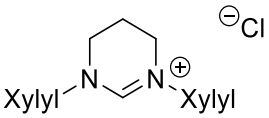


$^1$H NMR (300 MHz, $CDCl_3$, 298 K) δ 7.65 (s, 1H, NC*H*N), 7.29 – 7.24 (m, 2H, Obscured by $CHCl_3$ residual peak, $C_{Ar}H$), 7.17 – 7.15 (m, 4H, $C_{Ar}H$), 4.31 (t, $^3J_{HH}$ = 5.7 Hz, 4H, NC$H_2$), 2.67 (quint, $^3J_{HH}$ = 5.7 Hz, 2H, $NCH_2CH_2$), 2.43 (s, 12H, $CH_3$). $^{13}C\{^1H\}$ NMR (75 MHz, $CDCl_3$,298 K) δ 153.5 (s), 139.0 (s), 135.0 (s), 130.5 (s), 129.7 (s), 47.1 (s), 19.7 (s), 18.2 (s).

6.5.4 – Characterisation of [6-DippH]Cl

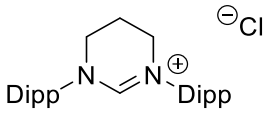


$^{1}$H NMR (300 MHz, $CDCl_3$, 298 K) δ 7.54 (s, 1H, NC*H*N), 7.43 (m, 2H, $C_{Ar}H$), 7.25 (d, *J* = 7.8 Hz, 4H + $CHCl_3$ peak, $C_{Ar}H$), 4.27 (t, $^{3}J_{HH}$ = 5.7 Hz, 4H, NC$H_2$), 3.05 (sept, $^{3}J_{HH}$ = 6.7 Hz, 4H, C*H*$(CH_3)_2$), 2.83 (quint, $^{3}J_{HH}$ = 5.7 Hz, 2H, $NCH_2CH_2$), 1.38 (d, $^{3}J_{HH}$ = 6.7 Hz, 12H, CH($CH_3$)$_2$), 1.23 (d, $^{3}J_{HH}$ = 6.8 Hz, CH($CH_3$)$_2$). $^{13}$C{$^{1}$H} NMR (75 MHz, $CDCl_3$, 298 K) δ 153.0 (s), 145.8 (s), 136.0 (s), 131.3 (s), 125.3 (s), 49.3 (s), 29.0 (s), 25.0 (s), 24.9 (s), 19.5 (s).

6.5.5 – Characterisation of [7-MesH]Cl

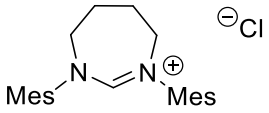


$^{1}$H NMR (500 MHz, $CDCl_3$, 298 K) δ 7.22 (s, 1H, NC*H*N), 6.94 (s, 4H, $C_{Ar}H$), 4.76 – 4.59 (m, 4H, NC$H_2$), 2.57 (quint, $^{3}J_{HH}$ = 2.8 Hz, 4H, $NCH_2CH_2$), 2.41 (s, 12H, C$H_3$), 2.27 (s, 6H, C$H_3$). $^{13}$C{$^{1}$H} NMR (75 MHz, $CDCl_3$, 298 K) δ 158.0 (s), 140.3 (s), 139.6 (s), 133.9 (s), 130.3 (s), 54.8 (s), 25.4 (s), 21.1 (s), 18.5 (s).

6.5.6 – Characterisation of [7-XylylH]Cl

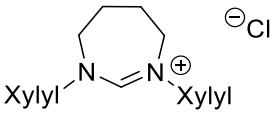


$^{1}$H NMR (500 MHz, $CDCl_3$, 298 K) δ 7.27 (s, 1H, NC*H*N), 7.22 (dd, $^{3}J_{HH}$ = 8.7, 6.3 Hz, 2H, $C_{Ar}H$), 7.17 – 7.11 (m, 4H, $C_{Ar}H$), 4.75 – 4.68 (m, 4H, NC$H_2$), 2.64 – 2.54 (m, 4H, $NCH_2CH_2$), 2.47 (s, 12H, $CH_3$). $^{13}$C{$^{1}$H} NMR (75 MHz, $CDCl_3$, 298 K) δ 157.8 (s), 141.8 (s), 134.3 (s), 130.3 (s), 129.8 (s), 54.8 (s), 25.5 (s), 18.6 (s).

6.5.7 – Characterisation of [7-DippH]Cl

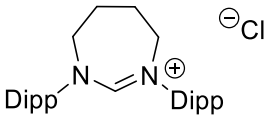


$^{1}$H NMR (300 MHz, $CDCl_3$, 298 K) δ 7.40 (dd, *J* = 8.4, 7.2 Hz, 2H, $C_{Ar}H$), 7.25 – 7.22 (m, 5H, $C_{Ar}H$ + NC*H*N), 4.83 – 4.65 (m, 4H, NC$H_2$), 3.25 (sept, $^{3}J_{HH}$ = 6.8 Hz, 4H, C*H*$(CH_3)_2$), 2.74 – 2.52 (m, 4H, $NCH_2CH_2$), 1.39 (d, $^{3}J_{HH}$ = 6.7 Hz, 12H, CH(C$H_3$)$_2$),

1.24 (d, $^{3}J_{HH}$ = 6.9 Hz, 12H, CH(C*H*$_3$)$_2$). $^{13}$C{$^{1}$H} NMR (75 MHz, $CDCl_3$, 298 K) δ 157.1 (s), 145.0 (s), 139.1 (s), 131.0 (s), 125.4 (s), 56.2 (s), 29.1 (s), 25.2 (s), 25.1 (s), 24.8 (s).

6.5.8 – Characterisation of [7-neoPentH]Cl

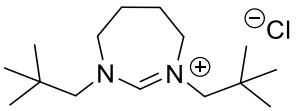


$^{1}$H NMR (500 MHz, $CDCl_3$, 298 K) δ 9.37 (s, 1H, NC*H*N), 3.77 – 3.71 (m, 4H, NC*H*$_2$CH$_2$), 3.65 (s, 4H, NC*H*$_2$C), 2.20 – 2.18 (m, 4H, NCH$_2$C*H*$_2$), 1.06 (s, 18H, C(C*H*$_3$)$_3$). $^{13}$C{$^{1}$H} NMR (126 MHz, $CDCl_3$, 298 K) 162.7 (s), 69.6 (s), 52.7 (s), 33.4 (s), 27.8 (s), 25.4 (s).

6.5.9 – Characterisation of [8-MesH]Cl

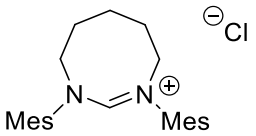


$^{1}$H NMR (300 MHz, $CDCl_3$, 298 K) δ 7.38 (s, 1H, NC*H*N), 6.93 (s, 4H, C$_{Ar}$*H*), 4.86 (br s, 4H, NC*H*$_2$), 2.41 (s, 12H, C*H*$_3$), 2.35 – 2.21 (s, 10H, CH3, NCH$_2$C*H*$_2$), 2.17 – 2.06 (m, 2H, NCH$_2$CH$_2$C*H*$_2$). $^{13}$C{$^{1}$H} NMR (75 MHz, $CDCl_3$, 298 K) δ 158.1 (s), 142.0 (s), 140.1 (s), 133.7 (s), 130.4 (s), 53.8 (s), 28.4 (s), 21.0 (s), 21.0 (s),* 18.8 (s). * two closely lying peaks.

6.5.10 – Characterisation of (6-Mes)CuCl (**4.1**)

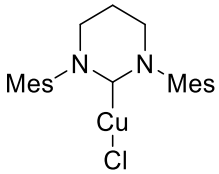


$^{1}$H NMR (500 MHz, $CD_2Cl_2$, 298 K) δ 7.00 (s, 4H, C$_{Ar}$H), 3.35 (t, $^{3}J_{HH}$ = 5.9 Hz, 6H), 2.32 – 2.29 (m, 20H, C*H*$_3$ + NCH$_2$C*H*$_2$). $^{1}$H NMR (500 MHz, $CDCl_3$, 298 K) δ 6.93 (s, 4H, C$_{Ar}$H), 3.39 – 3.32 (m, 4H, NC*H*$_2$), 2.34 – 2.29 (m, 2H, NCH$_2$C*H*$_2$), 2.29 – 2.26 (m, 18H, C*H*$_3$). $^{13}$C{$^{1}$H} NMR (126 MHz, $CDCl_3$, 298 K) δ 201.0 (s, N*C*N), 142.1 (s), 138.2 (s), 134.6 (s), 130.0 (s), 44.3 (s), 21.2 (s), 18.1 (s). Elemental analysis calcd (%) for $C_{22}H_{28}N_2ClCu$: C, 62.99; H, 6.73; N, 6.68; found C, 62.32; H, 6.69; N, 6.56. X-ray parameters matched those in literature.[23]

6.5.11 – Characterisation of (6-Mes)CuBr (**4.2**)

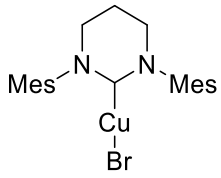


$^{1}$H NMR (500 MHz, $CD_2Cl_2$, 298 K) δ 6.99 (s, 4H, $C_{Ar}H$), 3.40 – 3.30 (m, 4H. NC*H*$_2$), 2.34 – 2.27 (m, 20H, C*H*$_3$ + $NCH_2CH_2$). $^{13}$C{$^{1}$H} NMR (126 MHz, $CD_2Cl_2$, 298 K) δ 201.6 (*via* HMBC, N*C*N), 142.5 (s), 138.6 (s), 135.2 (s), 130.0 (s), 44.7 (s), 21.2 (s), 21.2 (s), 18.2 (s). $^{1}$H NMR (500 MHz, $CDCl_3$, 298 K) δ 6.93 (s, 4H, $C_{Ar}H$), 3.36 (t, $^{3}J_{HH}$ = 5.9 Hz, 4H, NC*H*$_2$), 2.35 – 2.29 (m, 2H, $NCH_2CH_2$), 2.28 (s, 12H, C*H*$_3$), 2.27 (s, 6H, C*H*$_3$). $^{13}$C{$^{1}$H} NMR (126 MHz, $CDCl_3$, 298 K) δ 201.5 (s, N*C*N), 142.0 (s), 138.2 (s), 134.6 (s), 130.0 (s), 44.3 (s), 21.2 (s), 21.0 (s), 18.1 (s). Elemental analysis calcd (%) for $C_{22}H_{28}N_2BrCu$; C, 56.96; H, 6.08; N, 6.04; found: C, 57.09; H, 6.10; N, 5.96. Spectroscopic data matched those in literature.[24]

6.5.12 – Characterisation of (6-Mes)CuI (**4.3**)

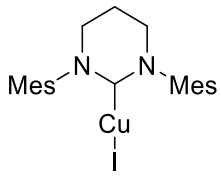


$^{1}$H NMR (500 MHz, $CDCl_3$, 298 K) δ 6.93 (s, 4H, $C_{Ar}H$), 3.36 (t, $^{3}J_{HH}$ = 5.9 Hz, 4H, NC*H*$_2$), 2.32 (quint, $^{3}J_{HH}$ = 6.1 Hz, 2H, $NCH_2CH_2$), 2.28 (s, 18H, C*H*$_3$). $^{13}$C{$^{1}$H} NMR (126 MHz, $CDCl_3$, 298 K) δ 202.9 (s, N*C*N), 141.7 (s), 138.3 (s), 134.7 (s), 129.9 (s), 44.4 (s), 21.2 (s), 21.0 (s), 18.2 (s). $^{1}$H NMR (500 MHz, $C_6D_6$, 298 K) δ 6.75 (s, 4H, $C_{Ar}H$), 2.50 – 2.46 (m, 4H, NC*H*$_2$), 2.12 (s, 12H, C*H*$_3$), 2.08 (s, 6H, C*H*$_3$), 1.38 – 1.27 (m, 2H, $NCH_2CH_2$). $^{13}$C{$^{1}$H} NMR (126 MHz, $C_6D_6$, 298 K) δ 203.6 (*via* HMBC, N*C*N), 142.1 (s), 138.2 (s), 134.7 (s), 130.1 (s), 43.8 (s), 21.1 (s), 20.6 (s), 18.1 (s). Elemental analysis calcd (%) for $C_{22}H_{28}N_2ICu$; C, 51.72; H, 5.52; N, 5.48; found C, 51.70; H, 5.52; N, 5.54. Spectroscopic data matched those in literature.[24]

## 6.5.13 –Synthesis and Characterisation of [6-MesH][$CuCl_2$] (**4.4**)

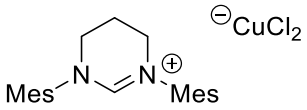


Under the argon atmosphere of the glovebox [6-MesH]Cl (100 mg, 0.281 mmol) and CuCl (30.6 mg, 0.309 mmol) were added to a vial with dry acetone (1 mL). After stirring for 1 h at room temperature, the suspension was filtered through Celite. The filtrate was dried to yield [6-MesH][$CuCl_2$] as a white powder (96 mg, yield 75 %). Crystalline material was grown from $CH_2Cl_2$/pentane. $^1$H NMR (500 MHz, $CDCl_3$, 298 K) δ 7.70 (s, 1H, NC*H*N), 6.98 (s, 4H, $C_{Ar}H$), 4.00 (t, $^3J_{HH}$ = 5.7 Hz, 4H, NC$H_2$), 2.64 (quint, $^3J_{HH}$ = 5.8 Hz, 2H, $NCH_2CH_2$), 2.34 (s, 12H, C$H_3$), 2.30 (s, 6H, C$H_3$). $^{13}C\{^1H\}$ NMR (126 MHz, $CDCl_3$, 298 K) δ 154.4 (s), 141.0 (s), 136.3 (s), 134.3 (s), 130.5 (s), 46.8 (s), 21.2 (s), 19.7 (s), 18.1 (s). Elemental analysis calcd (%) for $C_{22}H_{29}N_2Cl_2Cu$: C, 57.96; H, 6.41; N, 6.14; found: C, 57.52; H, 6.47; N, 6.14.

## 6.5.14 – Synthesis and Characterisation of [6-XylylH][$CuCl_2$] (**4.5**)

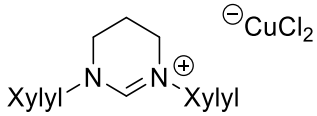


As for **4.4** starting from [6-XylylH]Cl (100 mg, 0.34 mmol) and CuCl (29.4 mg, 0.375 mmol). White powder (23 mg, yield 31%). $^1$H NMR (500 MHz, $CDCl_3$, 298 K) δ 7.80 (s, 1H, NC*H*N), 7.32 – 7.26 (m, 2H, $C_{Ar}H$), 7.19 (d, $^3J_{HH}$ = 7.7 Hz, 4H, $C_{Ar}H$), 4.05 (t, $^3J_{HH}$ = 5.7 Hz, 4H, NC$H_2$), 2.67 (quint, $^3J_{HH}$ = 5.8 Hz, 2H, $NCH_2CH_2$), 2.40 (s, 12H, $CH_3$). $^{13}C\{^1H\}$ NMR (126 MHz, $CDCl_3$, 298 K) δ 154.2 (s), 138.6 (s), 134.7 (s), 130.8 (s), 129.9 (s), 46.7 (s), 19.7 (s), 18.2 (s). Elemental analysis calcd (%) for $C_{20}H_{25}N_2Cl_2Cu$: C, 56.14; H, 5.89; N, 6.55; Found: C, 55.64; H, 5.89; N, 6.44.

6.5.15 – Synthesis and Characterisation of [7-MesH][$CuCl_2$] (**4.6**)

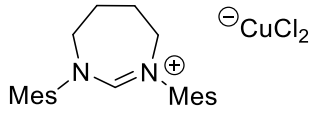


As for **4.4** starting from [7-MesH]Cl (100 mg, 0.27 mmol) and CuCl (29.4 mg, 0.297 mmol). White powder (93 mg, yield 74%). Crystalline material was grown from $CH_2Cl_2$/pentane. $^1$H NMR (500 MHz, $CDCl_3$, 298 K) δ 7.38 (s, 1H, NC*H*N), 6.97 (s, 4H, $C_{Ar}H$), 4.33 (br s, 4H, NC$H_2$), 2.58 (br s, 4H, $NCH_2CH_2$), 2.39 (s, 12H, C$H_3$), 2.28 (s, 6H, C$H_3$). $^{13}$C{$^1$H} NMR (126 MHz, $CDCl_3$, 298 K) δ 158.7 (s), 140.7 (s), 139.3 (s), 133.6 (s), 130.6 (s), 55.1 (s), 25.6 (s), 21.1 (s), 18.4 (s). Elemental analysis calcd (%) for $C_{23}H_{31}N_2Cl_2Cu$; C 58.78, H 6.65, N 5.96, Found: C 58.76, H 6.52, N 6.08

6.5.16 – Synthesis and Characterisation of [7-XylylH][$CuCl_2$] (**4.7**)

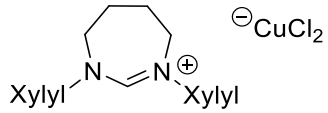


As for **4.4** starting from [7-XylylH]Cl (100 mg, 0.292 mmol) and CuCl (31.7 mg, 0.321 mmol). White powder (15 mg, yield 12%). Crystalline material was grown from $CH_2Cl_2$/pentane. $^1$H NMR (500 MHz, $CDCl_3$, 298 K) δ 7.43 (s, 1H, NC*H*N), 7.30 – 7.25 (m, 2H, $C_{Ar}H$), 7.18 (d, $^3J_{HH}$ = 7.7 Hz, 4H, $C_{Ar}H$), 4.44 – 4.35 (m, 4H, NC$H_2$), 2.65 – 2.57 (m, 4H, $NCH_2CH_2$), 2.46 (s, 12H, C$H_3$). $^{13}$C{$^1$H} NMR (126 MHz, $CDCl_3$, 298 K) δ 158.5 (s), 141.6 (s). 134.0 (s), 130.1 (s), 55.1 (s), 25.6 (s), 18.5 (s). Elemental analysis calcd (%) for $C_{20}H_{25}N_2Cl_2Cu \cdot 2/3\ H_2O$: C, 55.57; H, 6.29; N, 6.17; found: C, 55.33; H, 5.83; N, 6.07.

6.5.17 – Synthesis and Characterisation of [7-neoPentH][$CuCl_2$] (**4.8**)

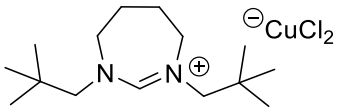


As for **4.4** starting from [7-neoPentH]Cl (100 mg, 0.365 mmol) and CuCl (39.7 mg, 0.401 mmol). White powder (123 mg, yield 91 %). Crystalline material was grown from $CH_2Cl_2$/pentane.$^1$H NMR (500 MHz, $CDCl_3$, 298 K) δ 7.85 (s, 1H, NC*H*N), 3.86 (m, 4H, NC$H_2CH_2$), 3.47 (s, 4H, NC$H_2$C), 2.24 (m, 4H, $NCH_2CH_2$), 1.03 (s, 18H, C(C$H_3$)$_3$) $^{13}$C{$^1$H} NMR (126 MHz, $CDCl_3$, 298 K) 160.6 (s), 70.6 (s), 53.1 (s), 33.5 (s), 27.8 (s),

25.2 (s). Elemental analysis calcd (%) for $C_{15}H_{31}N_2Cl_2Cu \cdot 2/3\ H_2O$: C, 46.69; H, 8.45; N, 7.26; found: C, 46.60; H, 7.91; N, 7.06.

6.5.18 –Characterisation of (6-Xylyl)CuCl (**4.9**)

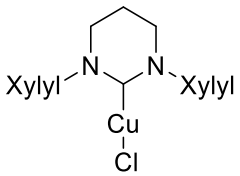


$^1$H NMR (500 MHz, $CD_2Cl_2$, 298 K) δ 7.24 (dd, $^3J_{HH}$ = 8.6, 6.3 Hz, 2H, $C_{Ar}H$), 7.19 (d, $^3J_{HH}$ = 7.4 Hz, 4H, $C_{Ar}H$), 3.40 (t, $^3J_{HH}$ = 5.9 Hz, 4H, $NCH_2$), 2.39 – 2.34 (m, 14H, $CH_3$ + $NCH_2CH_2$). $^{13}C\{^1H\}$ NMR (126 MHz, $CD_2Cl_2$, 298 K) δ 200.7 (s, N*C*N), 144.9 (s), 135.6 (s), 129.3 (s), 128.7 (s), 44.5 (s), 21.1 (s), 18.3 (s). Elemental analysis calcd (%) for $C_{20}H_{25}N_2ClCu$: C, 61.37; H, 6.18; N, 7.16; Found C, 61.48; H, 6.14; N, 7.27.

6.5.19 – Characterisation of (6-Dipp)CuCl (**4.10**)

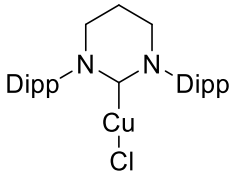


$^1$H NMR (500 MHz, $CDCl_3$, 298 K) δ 7.36 (t, $^3J_{HH}$ = 7.7 Hz, 2H, $C_{Ar}H$), 7.21 (d, $^3J_{HH}$ = 7.7 Hz, 4H, $C_{Ar}H$), 3.45 – 3.42 (m, 4H, $NCH_2$), 3.06 (sept, $^3J_{HH}$ = 6.9 Hz, 4H, $CH(CH_3)_2$), 2.42 – 2.33 (m, 2H, $NCH_2CH_2$), 1.35 (d, $^3J_{HH}$ = 6.9 Hz, 12H, $CH(CH_3)_2$), 1.31 (d, $^3J_{HH}$ = 6.9 Hz, 12H, $CH(CH_3)_2$). $^{13}C\{^1H\}$ NMR (126 MHz, $CDCl_3$, 298 K) δ 201.0 (s, N*C*N), 145.6 (s), 141.6 (s), 129.6 (s), 124.9 (s), 46.4 (s), 28.8 (s), 25.0 (s), 24.8 (s), 20.7 (s). spectroscopy data matched those in the literature.[9]

6.5.20 – Characterisation of (7-Mes)CuCl (**4.11**)

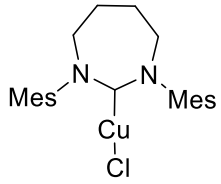


$^{1}$H NMR (500 MHz, $CD_2Cl_2$, 298 K) δ 6.98 (s, 4H, $C_{Ar}H$), 4.07 – 3.76 (m, 4H, $NCH_2$), 2.37 (s, 12H, $CH_3$), 2.32 – 2.26 (m, 10H, $CH_3$ + $NCH_2CH_2$). $^{13}$C{$^{1}$H} NMR (126 MHz, $CD_2Cl_2$, 298 K) δ 210.2 (via HMBC, N*C*N), 144.9 (s), 138.2 (s), 134.8 (s), 130.0 (s), 52.9 (s), 26.0 (s), 21.1 (s), 18.7 (s). Elemental analysis calcd (%) for $C_{23}H_{30}N_2ClCu$: C, 63.73; H, 6.98; N, 6.46; found: C, 63.65; H, 7.05; N, 6.55.

6.5.21 – Characterisation of (7-Xylyl)CuCl (**4.12**)

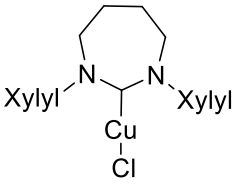


$^{1}$H NMR (500 MHz, $CD_2Cl_2$, 298 K) δ 7.25 – 7.12 (m, 6H, $C_{Ar}H$), 3.93 – 3.90 (m, 4H, $NCH_2$), 2.42 (s, 12H, $CH_3$). 2.34 – 2.30 (m, 4H, $NCH_2CH_2$) $^{13}$C{$^{1}$H} NMR (126 MHz, $CD_2Cl_2$, 298 K) δ 210.7 (s, N*C*N), 147.3 (s), 135.2 (s), 129.5 (s), 128.5 (s), 52.8 (s), 26.1 (s), 18.9 (s). Elemental analysis calcd (%) for $C_{21}H_{26}N_2ClCu$: C, 62.21; H, 6.46; N, 6.19; found: C, 62.02; H, 6.36; N, 6.87.

6.5.22 – Characterisation of (7-Dipp)CuCl (**4.13**)

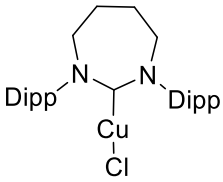


$^{1}$H NMR (500 MHz, $CD_2Cl_2$, 298 K) δ 7.37 (t, $^{3}J_{HH}$ = 7.7 Hz, 2H, $C_{Ar}H$), 7.24 (d, $^{3}J_{HH}$ = 7.7 Hz, 4H, $C_{Ar}H$), 4.04 – 3.95 (m, 4H, $NCH_2$), 3.30 (sept, $^{3}J_{HH}$ = 6.9 Hz, 4H, $CH(CH_3)_3$), 2.33 (quint, $^{3}J_{HH}$ = 2.7 Hz, 4H, $NCH_2CH_2$), 1.35 (d, $^{3}J_{HH}$ = 6.9 Hz, 12H, $CH(CH_3)_3$), 1.33 (d, $^{3}J_{HH}$ = 6.9 Hz, 12H, $CH(CH_3)_3$). $^{13}$C{$^{1}$H}NMR (126 MHz, $CD_2Cl$, 298 K) δ 210.3 (s, N*C*N), 145.6 (s), 144.6 (s), 129.2 (s), 125.1 (s), 54.4 (s), 29.2 (s), 25.6 (s), 24.9 (s), 24.7 (s). $^{1}$H NMR (500 MHz, $C_6D_6$, 298 K) δ 7.17 – 7.14 (m, obscured by $C_6D_6H$, $C_{Ar}H$), 7.05 (d, $^{3}J_{HH}$ = 7.8 Hz, 4H, $C_{Ar}H$), 3.29 – 3.24 (m, 4H, $NCH_2$), 3.18 (sept, $^{3}J_{HH}$ = 6.9 Hz, 4H,

C*H*($CH_3$)$_3$), 1.64 – 1.58 (m, 4H, $NCH_2CH_2$), 1.48 (d, $^3J_{HH}$ = 6.9 Hz, 12H, CH(C*H*$_3$)$_3$), 1.18 (d, $^3J_{HH}$ = 6.9 Hz, 12H, CH(C*H*$_3$)$_3$).

6.5.23 – Characterisation of (8-Mes)CuCl (**4.14**)

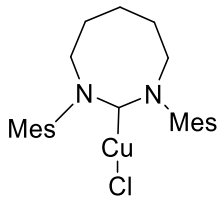


$^1$H NMR (500 MHz, $CD_2Cl_2$, 298 K) δ 6.96 (s, 4H, $C_{Ar}H$), 4.04 (t, $^3J_{HH}$ = 6.4 Hz, 4H, NC*H*$_2$), 2.37 (s, 12H, C*H*$_3$), 2.29 (s, 6H, C*H*$_3$), 2.12 – 1.96 (m, 6H). $^{13}$C{$^1$H} NMR (126 MHz, $CD_2Cl_2$, 298 K) δ 208.4 (*via* HMBC, N*C*N), 147.2 (s), 137.9 (s), 134.4 (s), 130.2 (s), 52.2 (s), 29.4 (s), 22.0 (s), 21.1 (s), 19.2 (s). Elemental analysis calcd (%) for $C_{15}H_{30}N_2ClCu$; C, 64.41; H, 7.42; N, 6.25; Found: C, 63.76; H, 7.21; N, 6.24.

6.5.24 – Characterisation of (7-neoPent)CuCl (**4.15**)

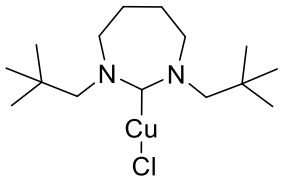


$^1$H NMR (500 MHz, $CD_2Cl_2$, 298 K) δ 3.75 (s, 4H, NC*H*$_2$C), 3.60 – 5.56 (m, 4H, NC*H*$_2$CH$_2$), 1.92 – 1.90 (m, 4H, $NCH_2CH_2$), 1.03 (s, 18H, C(C*H*$_3$)$_3$). $^{13}$C{$^1$H} NMR (126 MHz, $CD_2Cl_2$, 298 K) δ 212.6 (s, N*C*N), 75.3 (s), 54.2 (s), 33.0 (s), 28.0 (s), 25.1 (s). Elemental analysis calcd (%) for $C_{15}H_{30}N_2ClCu$: C, 53.40; H, 8.96; N, 8.30; found: C, 53.14; H, 8.73; H, 7.95.

## 6.5.25 –Characterisation of (6-Dipp)CuBr (**4.16**)

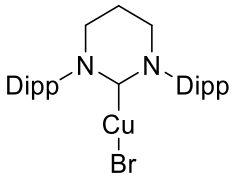


$^{1}$H NMR (500 MHz, $CD_2Cl_2$, 298 K) δ 7.41 (t, $^{3}J_{HH}$ = 7.7 Hz, 2H, $C_{Ar}H$), 7.25 (d, $^{3}J_{HH}$ = 7.8 Hz, 4H, $C_{Ar}H$), 3.45 – 3.40 (m, 4H, $NCH_2$), 3.08 (sept, $^{3}J_{HH}$ = 6.9 Hz, 4H, $CH(CH_3)_2$), 2.40 – 2.33 (m, 2H, $NCH_2CH_2$), 1.33 (d, $^{3}J_{HH}$ = 6.9 Hz, 12H, $CH(CH_3)_2$), 1.31 (d, $^{3}J_{HH}$ = 7.0 Hz, 12H, $CH(CH_3)_2$). $^{13}C\{^{1}H\}$ NMR (126 MHz, $CD_2Cl_2$, 298 K) δ 201.3 (s, NCN), 146.2 (s), 142.0 (s), 129.6 (s), 125.0 (s), 46.7 (s), 29.0 (s), 25.0 (s), 24.7 (s), 20.8 (s). Elemental analysis calcd (%) for $C_{28}H_{40}N_2BrCu \cdot CH_2Cl_2$: C, 55.03; H, 6.69; N, 4.43; found: C, 55.54; H, 6.74; N, 4.41.

## 6.5.26 –Characterisation of (7-Mes)CuI (**4.17**)

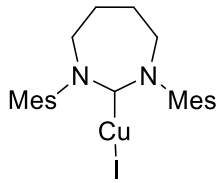


$^{1}$H NMR (500 MHz, $CDCl_3$, 298 K) δ 6.92 (s, 4H, $C_{Ar}H$), 3.90 – 3.85 (m, 4H, $NCH_2$), 2.35 (s, 12H, $CH_3$), 2.31- 2.28 (m, 4H, $NCH_2CH_2$), 2.27 (s, 6H, $CH_3$). $^{1}$H NMR (300 MHz, $C_6D_6$, 298 K) δ 6.78 (s, 4H, $C_{Ar}H$), 3.05 – 2.99 (m, 4H, $NCH_2$), 2.22 (s, 12H, $CH_3$), 2.11 (s, 6H, $CH_3$), 1.49 (quint, $^{3}J_{HH}$ = 2.9 Hz, 4H, $NCH_2CH_2$). Spectroscopic data matches those in literature.[24]

## 6.5.27 – Catalytic Procedure for [3+2] Cycloaddition of Azides and Alkynes.

Under the argon atmosphere of a glovebox was weighed the catalyst precursor (0.5 mol%) into a 4 mL screw cap vial. To this was added the alkyne (1 mmol) followed by the azide (1 mmol) to start the reaction. The vial was closed, removed from the glovebox and left sealed while stirring for the appropriate time, after which it was quenched with $CH_2Cl_2$ (3 mL) in air. The suspension was sonicated before a sample of 0.3 mL was taken and diluted further by $CH_2Cl_2$ (0.9 mL) for GC analysis.

## 6.6 – Experimental Details and Characterising Data for Chapter 5

### 6.6.1 –Synthesis and Characterisation of Ni(6-Mes)($PPh_3$)O$^i$Pr (**5.7**)

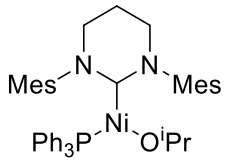


**5.1** (300 mg, 0.416 mmol) and KH (17 mg, 0.425 mmol) were placed in a J. Youngs resealable ampoule in $Et_2O$ (20 mL). $^i$PrOH (0.2 mL) was added at room temperature and the suspension was stirred for 5 min at -78 $^o$C to give an orange solution. The solution was cannula filtered into a new J. Youngs resealable ampoule containing pentane (20 mL) cooled to -78 °C. The orange solution was concentrated to dryness when removed from dry ice acetone bath. The solid was vigorously stirred with cold pentane (20 mL) which was removed *via* cannula filtration to leave **5.7** as an orange solid (154 mg, yield 56 %). Crystals suitable for X-ray diffraction were obtained by slow diffusion of pentane into a concentrated solution of **5.7** in $Et_2O$ at -30 °C. $^1$H NMR (500 MHz, $C_6D_6$, 298 K) δ 28.1 (br s), 16.9 (br s), 11.2 (br s), 8.5 (br s), 6.9 (br s), 6.94, 6.78, 3.21 (s), 3.2 (br s), 0.5 (br s), 0.0 (br s) -2.54 (br s), -16.3 (br s). Elemental analysis calcd (%) for $C_{43}H_{50}N_2OPNi.C_3H_8O$; C, 72.63; H, 7.68; N, 3.68; found C, 72.52; H, 7.12; N, 3.80; $\mu_{eff}$ (Evans method, THF, 298 K): 1.82 μB

### 6.6.2 – Synthesis and Characterisation of Ni(6-Mes)($PPh_3$)O$^t$Bu (**5.8**)

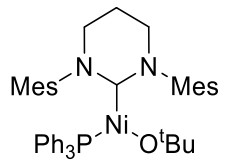


As for **5.7** but using **5.1** (100 mg, 0.139 mmol), KH (6 mg, 0.15 mmol) and $^t$BuOH (0.1 mL) to give **5.8** as an orange solid (48.5 mg, yield 49 %). Crystals suitable for X-ray diffraction were obtained by storing a filtered concentrated solution of **5.8** in $Et_2O$ at -30 $^o$C. $^1$H NMR (500 MHz, $C_6D_6$, 298 K) δ 10.7 (br s), 7.8 (br s), 7.0 (br s), 6.8 (br s) 3.1 (s), 2.3 (br s), 2.1 (br s) 0.8 (br s), -2.0 (br s), -17.5 (br s). Elemental analysis calcd (%) for $C_{44}H_{52}N_2OPNi\cdot C_4H_{10}O$: C, 73.10; H, 7.92; N, 3.55; found C, 72.75; H, 7.44; N, 3.84; $\mu_{eff}$ (Evans method, THF, 298 K): 2.08 μB

6.6.3 – Synthesis and Characterisation of Ni(6-Mes)($PPh_3$)OC(H)$Ph_2$ (**5.9**)

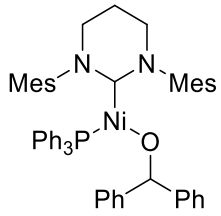


**5.1** (200 mg, 0.276 mmol), KH (13.2 mg, 0.332 mmol) and $Ph_2C(H)OH$ (56 mg, 0.304 mmol) were placed in a J. Youngs resealable ampoule. $Et_2O$ (10 mL) was added and the suspension was stirred for 5 min at room temperature to give an orange solution. The solution was diluted with $Et_2O$ (20 mL) and cannula filtered into a new J. Youngs resealable ampoule. The solvent was removed *in vacuo* and the residue was washed with cold pentane (5 mL) to give **5.9** as an orange-yellow solid (130 mg, yield 57 %). Crystals suitable for X-ray diffraction were obtained from a concentrated solution of **5.9** in hexane at room temperature. $^1$H NMR (500 MHz, $C_6D_6$, 298 K) δ 31.7 (br s), 17.5 (br s), 11.3 (br s) 9.3 (br s), 8.7 (br s), 7.7 (br s), 7.3 (br s), 6.8 (br s), 3.8 (br s), 3.5 (br s), 1.2 (br s), 0.3 (br s), -0.5 (br s), -2.5 (br s), -15.4 (br s). $^1$H NMR (500 MHz, *d*$_8$-THF, 298 K) δ 32.4 (br s, 2H), 18.5 (br s, 1H), 11.4 (br s, 9H), 8.8 (br s, 4H), 7.2 (br s, 18H), 3.9 (br s, 10H), 1.3 (br s, 4H), -0.2 (br s, 4H), -14.5 (br s, 2H). Elemental analysis calcd (%) for $C_{53}H_{54}N_2PNi$: C, 72.28; H, 6.81; N, 6.16; found C, 69.98; H, 6.75; N, 5.77; $\mu_{eff}$ (Evans method, THF, 298 K): 1.99 μB

6.6.4 – Synthesis and Characterisation of Ni(6-Mes)($PPh_3$)OMe (**5.10**)

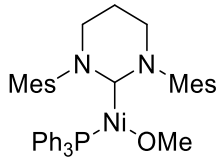


As for **5.7** but using **5.1** (51.4 mg, 0.07 mmol), KH (3 mg, 0.07 mmol) and MeOH (0.1 mL) to give **5.10** as an orange solid (25 mg, yield 53 %). Crystals suitable for X-ray diffraction were obtained by slow diffusion of pentane into a concentrated solution of **5.10** in THF at -30 °C. $^1$H NMR (500 MHz, $C_6D_6$, 298 K) δ 29.6 (br s), 16.9 (br s), 11.3 (br s), 8.5 (br s), 7.6 (br s), 7.0 (br s), 6.8 (br s), 6.6 (br s), 6.1 (br s), 5.6 (br s), 4.7 (br s), 4.6 (br s), 3.3 (s), 1.4 (br s), 0.5 (br s), -0.2 (br s), -16.1 (br s). Elemental analysis calcd (%) for $C_{41}H_{46}N_2OPNi \cdot C_2H_8O_2$: C, 70.11; H, 7.38; N, 3.80; found C, 70.34; H, 6.92; N, 3.86; $\mu_{eff}$ (Evans method, THF, 298 K): 1.82 μB

## 6.6.5 – Synthesis and Characterisation of 4-$FC_6H_4O^iPr$ (**5.13**)

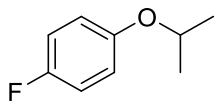


2-Bromopropane (1.66 mL, 0.0177 mol), 4-fluorophenol (1.00 g, 8.87 mmol), $K_2CO_3$ (2.46 g, 0.0177 mol) were placed in a 20 mL microwave vial in MeCN (12 mL) and sealed. The mixture was heated at 70 °C for 5 days, allowed to cool to room temperature, extracted into EtOAc (200 mL) and filtered. The organics were washed with water (3 x 200 mL). The aqueous layers were combined and extracted with EtOAc (2 x 200 mL). The organic layers were combined, concentrated, dried over $MgSO_4$ and then purified by column chromatography (5 % EtOAc/hexane) to provide 4-$FC_6H_4O^iPr$ as a colourless oil (819 mg, yield 60%). $^1$H NMR (500 MHz, $CDCl_3$, 298 K) δ 6.99 – 6.92 (m, 2H, $C_{Ar}H$), 6.87 – 6.79 (m, 2H, $C_{Ar}H$), 4.45 (sept, $^3J_{HH}$ = 6.1 Hz, 1H, $CH(CH_3)_2$), 1.32 (d, $^3J_{HH}$ = 6.1 Hz, 6H, $CH(CH_3)_2$). $^{13}C\{^1H\}$ NMR (126 MHz, $CDCl_3$) δ 157.3 (d, $J_{CF}$ = 238 Hz), 154.1 (d, $J_{CF}$ = 2 Hz), 117.4 (d, $J_{CF}$ = 8 Hz), 115.9 (d, $J_{CF}$ = 23 Hz), 71.0 (s), 22.2 (s). $^{19}$F NMR (376 MHz, $CDCl_3$) 124.0 (m).

## 6.6.6 – Synthesis and Characterisation of Ni(6-Mes)(κ$^2$-TEMPO)Br (**5.14**)

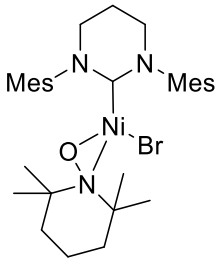


As for **5.15**, but using Ni(6-Mes)($PPh_3$)Br (**5.1**) (20 mg, 0.028 mmol), and TEMPO (4.33 mg, 0.028 mmol) to give **5.14** as a purple solid (12 mg, yield 68 %). X-ray suitable crystals were obtained from a concentrated THF solution layered with pentane. $^1$H NMR (500 MHz, $CD_2Cl_2$, 298 K) δ 7.08 (s, 4H), 3.22 (br s, 4H), 2.42 (br s, 6H), 2.37 (s, 6H), 2.12 (br s, 9H), 1.58 (s, 6H), 1.40 – 1.27 (m, 3H), 1.19 – 1.05 (m, 3H), 0.84 (s, 6H). $^{13}C\{^1H\}$ NMR (126 MHz, $CD_2Cl_2$, 298 K) δ 207.3 (s, N*C*N), 144.1 (s), 137.8 (s), 130.2 (s), 78.0 (s), 64.2 (s), 47.7 (s), 38.0 (s), 30.5 (s), 23.7 (s), 22.0 (s), 21.2 (s), 17.0 (s). Elemental analysis calcd (%) for $C_{31}H_{46}N_3BrONi$: C, 60.51; H, 7.54; N, 6.83; found C, 60.19; H, 7.15; N, 6.77.

6.6.7 –Synthesis and Characterisation of Ni(6-Mes)(κ$^2$-TEMPO)O$^i$Pr (**5.15**)

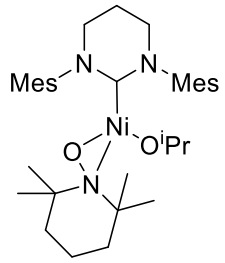


**5.7** (40 mg, 0.0571 mmol), TEMPO (8.9 mg, 0.0571 mmol) in THF (1 mL) were allowed to stir for 10 min to form a pink solution. The solution was filtered and layered with pentane (5 mL) to yield crystalline **5.15** as deep red blocks (23 mg, yield 68%). $^1$H NMR (500 MHz, $C_6D_6$, 298 K) δ 7.15 – 7.06 (m, 4H), 3.01 (sept, $^3J_{HH}$ = 5.9 Hz, 1H), 2.90 – 2.04 (br m, 8H), 2.69 (t, $^3J_{HH}$ = 5.9 Hz, 4H), 2.34 (s, 6H), 1.93 (s, 6H), 1.53 – 1.42 (m, 2H), 1.30 – 1.27 (m, 1H), 1.27 – 1.24 (m, 1H), 1.21 (d, $^3J_{HH}$ = 5.9 Hz, 6H), 1.00 (s, 6H), 0.99 – 0.93 (m, 2H). $^{13}$C{$^1$H} NMR (126 MHz, $C_6D_6$, 298 K) δ 207.9 (s, N*C*N), 145.1 (s), 137.1 (s), 129.9 (s), 72.7 (s), 61.2 (s), 46.4 (s), 39.2 (s), 32.3 (s), 29.0 (s), 22.8 (s), 21.9 (s), 21.3 (s), 17.2(s). Elemental analysis calcd (%) for $C_{34}H_{53}N_3O_2Ni$: C, 68.69; H, 8.99; N, 7.07; found C, 67.00; H, 58.85; N, 6.99.

6.6.8 –Synthesis and Characterisation of Ni(6-Mes)(PPh$_3$)Br$_2$ (**5.16**)

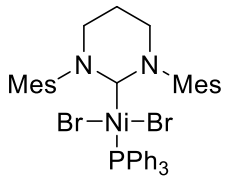


6-Mes (300 mg, 0.937 mmol) and Ni(PPh$_3$)$_2$Br$_2$ (697 mg, 0.937 mmol) were placed in a J. Youngs resealable ampoule in $C_6H_6$ (30 mL). The solution was allowed to stir for 1 h. The resulting deep purple solution was reduced in volume and hexane (30 mL) was added to precipitate a purple solid. The purple precipitate was collected via filtration in air and dissolved in minimal THF. To this solution was added $Et_2O$ (20 mL) to yield **5.16** as a purple solid (313 mg, yield 41%). Crystals suitable for X-ray diffraction were obtained by slow diffusion of pentane into a concentrated solution of **5.16** in THF at room temperature. $^1$H NMR (500 MHz, $C_6D_6$, 298 K) δ 7.63 – 7.54 (m, 6H), 7.14 – 6.89 (br s, *H), 7.04 – 6.99 (m, 10H), 3.00 – 2.00 (3 x br s, 22H), 1.38 (br s, 2H). $^{13}$C{$^1$H} NMR (126 MHz, $C_6D_6$, 298 K) δ 135.7 (d, $J_{CP}$ = 10 Hz), 133.7 (d, $J_{CP}$ = 41 Hz), 129.1 (d, $J_{CP}$ =

2 Hz), 127.4 (d, $J_{CP}$ = 10 Hz). $^{31}P\{^{1}H\}$ NMR (202 MHz, $C_6D_6$, 298 K) δ 15.1 (br s). $^{1}H$ NMR (400 MHz, $d_8$-THF, 235 K) δ 7.22 (t, $^{3}J_{HH}$ = 8.7 Hz, 9H), 7.16 – 7.09 (m, 6H), 3.42 (t, $J$ = 5.7 Hz, 4H), 2.52 (s, 6H), 2.44 (s, 12H), 2.16 (q, $J$ = 5.8 Hz, 2H). $^{13}C\{^{1}H\}$ NMR (101 MHz, $d_8$-THF, 235 K) δ 196.3 (d, $J_{CP}$ = 130 Hz, N*C*N), 143.2 (s), 138.7 (s), 137.9 (s), 136.1 (d, $J_{CP}$ = 9 Hz), 134.0 (d, $J_{CP}$ = 41 Hz), 130.3 (s), 129.7 (s), 127.8 (d, $J_{CP}$ = 9 Hz), 48.6 (s), 21.9 (s), 21.8 (s), 21.7 (s). $^{31}P\{^{1}H\}$ NMR (162 MHz, $d_8$-THF, 235 K) δ 13.5 (s) Elemental analysis calcd (%) for $C_{40}H_{43}N_2Br_2PNi$: C, 59.96; H, 5.41; N, 3.50; found C, 60.05; H, 5.37; N, 3.55. See appendix 7.1.2 for room temperature $^{1}H$ NMR and DEPT vs a low temperature NMR. DEPT only showed those peaks related to the $PPh_3$ ligand when at room temperature.

6.6.9 – Characterisation of Ni(6-Mes)($PPh_3$)($C_6H_4CF_3$)Br (**5.18**)

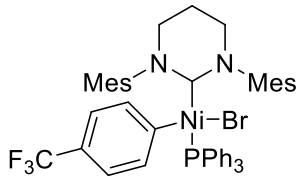


To a solution of **5.1** (38 mg, 0.0527 mmol) in $d_8$-THF (0.5 mL) in a J. Youngs resealable NMR tube was added 1-bromo-4-fluorobenzene (40 μL, 0.286 mmol). The tube was allowed to shake for 40 mins at room temperature before the volatiles were removed. The solids were redissolved in minimal $C_6H_6$ and layered with pentane to yield a mixture of crystals of **5.16** and **5.18**. The orange crystals of **5.18** were picked out for characterisation.

$^{1}H$ NMR (500 MHz, $d_8$-THF, 298 K) δ 7.38 (br s, 2H, $C_{Ar}H$), 7.16 (br t, $J_{HH}$ = 8.7 Hz, 9H, $PC_{Ar}H$), 7.03 (br t, $J_{HH}$ = 7.6 Hz, 6H, $PC_{Ar}H$), 6.97 (br s, 2H, $C_{Ar}H$), 6.38 (br d, $^{3}J_{HH}$ = 7.8 Hz, 2H, $C_{Ar}H$), 6.23 (br d, $^{3}J_{HH}$ = 7.8 Hz, 2H, $C_{Ar}H$), 3.46 – 3.37 (m, 2H, $NCH_2$), 3.36 – 3.29 (m, 2H, $NCH_2$), 2.72 (s, 6H, $CH_3$), 2.49 (s, 6H, $CH_3$), 2.35 (s, 1H, $NCH_2CH_2$), 2.14 – 2.04 (m, 1H, $NCH_2CH_2$). $CH_3$ hidden under $d_7$-THF see $^{1}H$ NMR 259 K. $^{19}F$ NMR (470 MHz, $d_8$-THF, 298 K) δ -64.2. $^{31}P\{^{1}H\}$ NMR (202 MHz, $d_8$-THF, 298 K) δ 26.2.

$^{1}H$ NMR (400 MHz, $d_8$-THF, 259 K) δ 7.41 (s, 2H, $C_{Ar}H$), 7.22 – 7.10 (m, 9H, $PC_{Ar}H$), 7.08 – 7.02 (m, 6H, $PC_{Ar}H$), 6.98 (s, 2H, $C_{Ar}H$), 6.35 (d, $J_{HH}$ = 7.8 Hz, 2H, $C_{Ar}H$), 6.22 (d, $J_{HH}$ = 7.8 Hz, 2H, $C_{Ar}H$), 3.44 (td, $J_{HH}$ = 11.8, 3.3 Hz, 2H, $NCH_2$), 3.34 – 3.26 (m, 2H, $NCH_2$), 2.71 (s, 6H, $CH_3$), 2.50 (s, 6H, $CH_3$), 2.40 – 2.28 (m, 1H, $NCH_2CH_2$), 2.13 – 2.05 (m, 1H, $NCH_2CH_2$), 1.71 (s, 6H, $CH_3$).$^{13}C\{^{1}H\}$ NMR (101 MHz, $d_8$-THF, 259 K) δ 208.5 (d, $J_{CP}$ = 99 Hz, N*C*N), 163.8 (d, $J_{CP}$ = 41 Hz, Ni$C_{Ar}$), 142.7 (s), 139.5 (d, $J_{CP}$ = 5 Hz),

139.0 (s), 138.1 (s), 137.8 (s), 135.2 (d, $J_{CP}$ = 10 Hz), 134.0 (d, $J_{CP}$ = 41 Hz), 133.1 (s), 130.7 (s), 130.0 (s), 129.2 (d, $J_{CP}$ = 2 Hz), 128.9 (s), 127.5 (d, $J_{CP}$ = 9 Hz), 120.1 (br s), 48.7 (s), 48.7 (s), 21.8 (s), 21.5 (s), 21.1 (s), 20.0 (s).* $^{31}P\{^{1}H\}$ NMR (162 MHz, *d*$_8$-THF, 259 K) δ 26.8 (s).

*quartet expected for $C_{Ar}CF_3$ not observed

## 6.6.10 – Synthesis of the Postulated Ni(6-Mes)($PPh_3$)(H)Br (**5.19**)

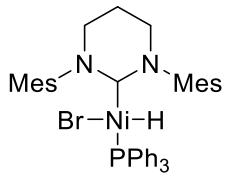


**5.16** (200 mg, 0.250 mmol) in THF (10 mL) was added to a pre-cooled solution (-78 °C) of $LiHBEt_3$ (250 μL, 1 M solution in THF, 0.250 mmol) in a J. Youngs resealable ampoule. The solution was allowed to warm to room temperature (the solution turned deep red) and allowed to stir for 20 mins. The red solution was concentrated to dryness, washed with pentane (10 mL), redissolved in benzene (10 mL) and filtered. The filtrate was reduced in volume and $Et_2O$ was added to precipitate the final product as a yellow solid (116 mg). The final solid contained a mix of **5.19** and **5.1** as discussed in Chapter 5.

$^{1}H$ NMR (400 MHz, $C_6D_6$, 298 K) δ 7.40 – 7.30 (m, 6H, $PC_{Ar}H$), 6.99 (br s, 11H, $PC_{Ar}H$ + $C_{Ar}H$), 6.61 (s, 2H, $C_{Ar}H$), 2.79 – 2.55 (m, 10H, $NCH_2$ + $C_{Ar}CH_3$), 2.18 (s, 6H, $C_{Ar}CH_3$), 2.15 (s, 6H, $C_{Ar}CH_3$), 1.63 – 1.50 (m, 1H, $NCH_2CH$), 1.37 – 1.25 (m, 1H, $NCH_2CH$), -20.8 (d, $J_{HP}$ = 84 Hz, 1H, Ni-H). $^{31}P$ NMR (162 MHz, $C_6D_6$, 298 K) δ 27.9 (d, $J_{PH}$ = 84 Hz, 1H, Ni-H). $^{1}H$ NMR (500 MHz, *d*$_8$-THF, 298 K) δ 7.20 (t, $J_{HH}$ = 7.2 Hz, 3H, $PC_{Ar}H$), 7.12 – 7.04 (m, 12H, $PC_{Ar}H$), 7.00 (s, 2H, $C_{Ar}H$), 6.64 (s, 2H, $C_{Ar}H$), 3.40 – 3.28 (m, 4H, $NCH_2$), 2.50 (s, 6H, $C_{Ar}CH_3$), 2.33 – 2.23 (br s + s, 7H, $C_{Ar}CH_3$ + $NCH_2CH$), 2.21 – 2.12 (br s + s, 7H, $C_{Ar}CH_3$ + $NCH_2CH$), -21.8 (d, $J_{HP}$ = 84 Hz, 1H, Ni-H). $^{31}P\{^{1}H\}$ NMR (202 MHz, *d*$_8$-THF, 298 K) δ 26.9 (s, 1H, Ni-H). $^{31}P$ NMR (202 MHz, *d*$_8$-THF, 298 K) δ 26.9 (d, $J_{PH}$ = 84 Hz, 1H, Ni-H).

## 6.6.11 – Catalytic Procedure for Hydrodehalogenation

Under an argon atmosphere of the glovebox, $NaO^iPr$ (12.1 mg, 0.147 mmol), Ar-X/Alk-X (0.134 mmol), $^iPrOH$ (5.12 μL, 0.0670 mmol) and dodecane reference (50 μL) were added to a screw cap vial with a stirrer bar with THF (800 μL). Catalysis was initiated by

addition of the Ni precursor (200 μL, from a 0.0302M stock in THF). After the desired time an aliquot (50 μL) was taken and diluted in THF (1 mL) in a vial for analysis by GC-MS.

An example run is as follows: Under an argon atmosphere of the glovebox, NaO$^{i}$Pr (12.1 mg, 0.147 mmol), 1-bromo-4-fluorobenzene (14.7 μL, 0.134 mmol), $^{i}$PrOH (5.12 μL, 0.0670 mmol) and 1,4-$C_6H_4F_2$ reference (13.8 μL, 0.134 mmol) were added to a J. Youngs resealable NMR tube containing THF (800 μL). Catalysis was initiated by addition the addition of the Ni precursor (200 μL, from a 0.0302M stock in THF) and monitored by $^{19}$F NMR spectroscopy.

### 6.6.12 – Kinetic Study Procedure for Hydrodehalogenation

Under an argon atmosphere of the glovebox, NaO$^{i}$Pr (12.1 mg, 0.147 mmol), Ar-X/Alk-X (0.134 mmol), $^{i}$PrOH (5.12 μL, 0.0670 mmol) and dodecane reference (50 μL) were added to a screw cap vial with a stirrer bar with THF (800 μL). Catalysis was initiated by addition of the Ni precursor (200 μL, from a 0.0302M stock in THF). After the desired time an aliquot (50 μL) was taken and diluted in THF (1 mL) in a vial for analysis by GC-MS.

## 6.7 – References for Chapter 6


1 G. R. Fulmer, A. J. M. Miller, N. H. Sherden, H. E. Gottlieb, A. Nudelman, B. M. Stoltz, J. E. Bercaw and K. I. Goldberg, *Organometallics*, 2010, **29**, 2176–2179.

2 M. Iglesias, L. Male, M. B. Hursthouse, A. Dervisi, I. A. Fallis, J. C. Knight, A. Stasch, L. Ooi, S. Coles, D. J. Beetstra and K. J. Cavell, *Organometallics*, 2008, **27**, 3279–3289.

3 J. J. Dunsford, D. S. Tromp, K. J. Cavell, C. J. Elsevier and B. M. Kariuki, *Dalton. Trans.*, 2013, **42**, 7318–7329.

4 W. Y. Lu, K. J. Cavell, J. S. Wixey and B. Kariuki, *Organometallics*, 2011, **30**, 5649–5655.

5 L. R. Collins, I. M. Riddlestone, M. F. Mahon and M. K. Whittlesey, *Chem. Eur. J.*, 2015, **21**, 14075–14084.

6 H. Kinuta, M. Tobisu and N. Chatani, *J. Am. Chem. Soc.*, 2015, 1593–1600.

7 C. J. E. Davies, M. J. Page, C. E. Ellul, M. F. Mahon and M. K. Whittlesey, *Chem. Commun.*, 2010, **46**, 5151–5153.

8 N. P. Mankad, D. S. Laitar and J. P. Sadighi, *Organometallics*, 2004, **23**, 3369–3371.

9 A. J. Jordan, C. M. Wyss, J. Bacsa and J. P. Sadighi, *Organometallics*, 2016, **35**, 613–616.

10 G. G. Dubinina, J. Ogikubo and D. A. Vicic, *Organometallics*, 2008, **27**, 6233–6235.

11 N. P. Bizier, J. W. Wackerly, E. D. Braunstein, M. Zhang, S. T. Nodder, S. M. Carlin and J. L. Katz, *J. Org. Chem.*, 2013, **78**, 5987–5998.

12 H.-J. Chen, Z.-Y. Lin, M.-Y. Li, R.-J. Lian, Q.-W. Xue, J.-L. Chung, S.-C. Chen and Y.-J. Chen, *Tetrahedron*, 2010, **66**, 7755–7761.

13 C. Rim and D. Y. Son, *Org. Lett.*, 2003, **5**, 3443–3445.

14 J. C. Colberg, A. Rane, J. Vaquer and J. A. Soderquist, *J. Am. Chem. Soc.*, 1993, **115**, 6065–6071.

15 M. Das and D. F. O'Shea, *Org. Lett.*, 2016, **18**, 336–339.

16 F. C. Tucci, A. Chieffi, J. V. Comasseto and J. P. Marino, *J. Org. Chem.*, 1996, **61**, 4975–4989.

17 M. Yan, T. Jin, Y. Ishikawa, T. Minato, T. Fujita, L. Y. Chen, M. Bao, N. Asao, M. W. Chen and Y. Yamamoto, *J. Am. Chem. Soc.*, 2012, **134**, 17536–17542.

18 J. Hori, K. Murata, T. Sugai, H. Shinohara, R. Noyori, N. Arai, N. Kurono and T. Ohkuma, *Adv. Synth. Catal.*, 2009, **351**, 3143–3149.

19 T. A. Perera, M. Masjedi and P. R. Sharp, *Inorg. Chem.*, 2014, **53**, 7608–7621.

20 Y. D. Bidal, F. Lazreg and C. S. J. Cazin, *ACS Catal.*, 2014, **4**, 1564–1569.

21 H. R. Kim and J. Yun, *Chem. Commun.*, 2011, **47**, 2943–2945.

22 Y. D. Bidal, M. Lesieur, M. Melaimi, D. B. Cordes, A. M. Z. Slawin, G. Bertrand and C. S. J. Cazin, *Chem. Commun.*, 2015, **51**, 4778–4781.

23 G. M. Pawar, B. Bantu, J. Weckesser, S. Blechert, K. Wurst and M. R. Buchmeiser, *Dalton. Trans.*, 2009, 9043–9051.

24 F. Sebest, J. J. Dunsford, M. Adams, J. Pivot, P. D. Newman and S. Díez-González, *ChemCatChem*, 2018, **10**, 2041–2045.

# Chapter 7 – Appendix

## 7.1 –Appendix 1 : NMR spectra

### 7.1.1 – NMR spectra of (6-*o*-Tolyl)CuO$^t$Bu (**2.3**)

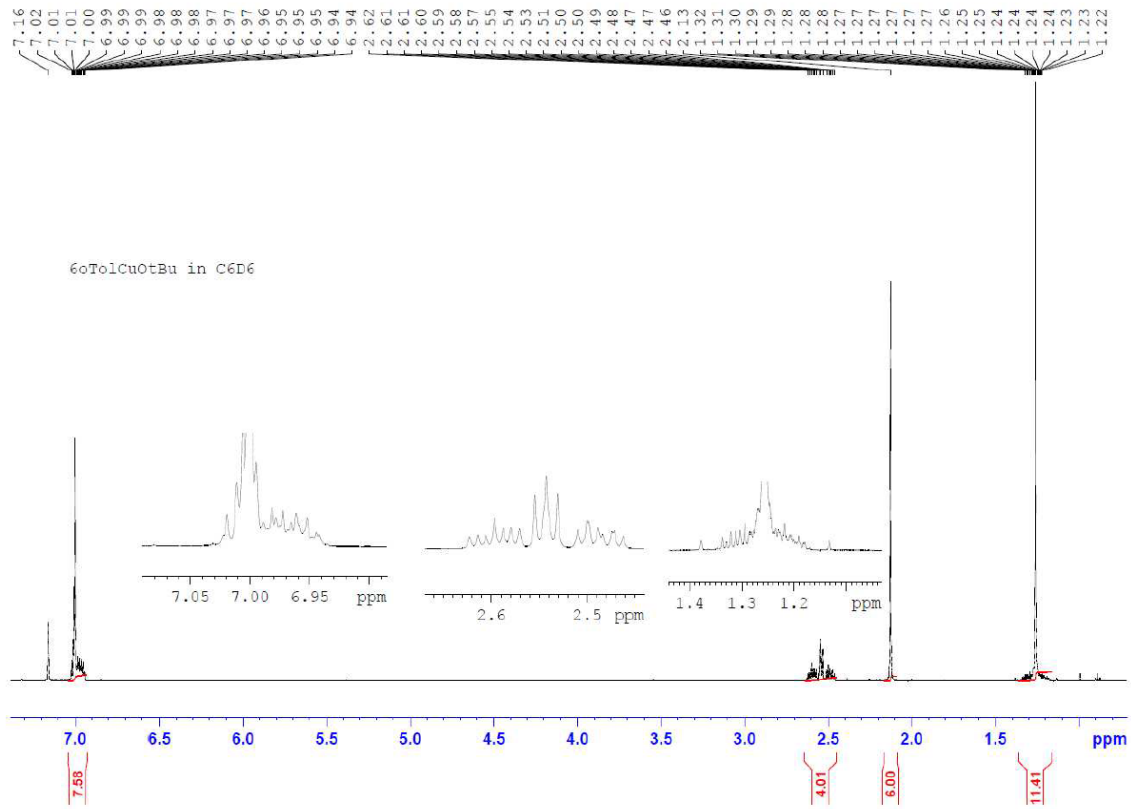


Figure 40 – $^1$H NMR spectrum (500 MHz, $C_6D_6$, 298 K) of (6-*o*-Tolyl)CuO$^t$Bu (**2.3**).

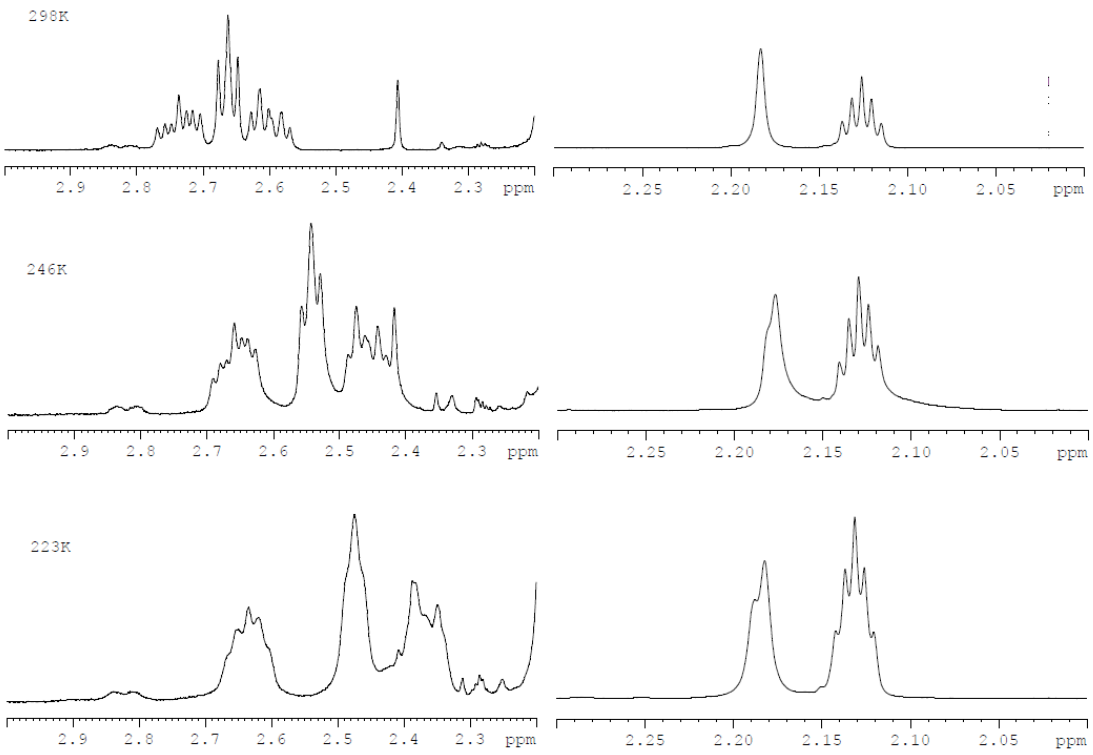


Figure 41 – Variable temperature $^{1}$H NMR spectra (400 MHz, $d_8$-toluene) of (6-*o*-Tolyl)CuO$^{t}$Bu (**2.3**).

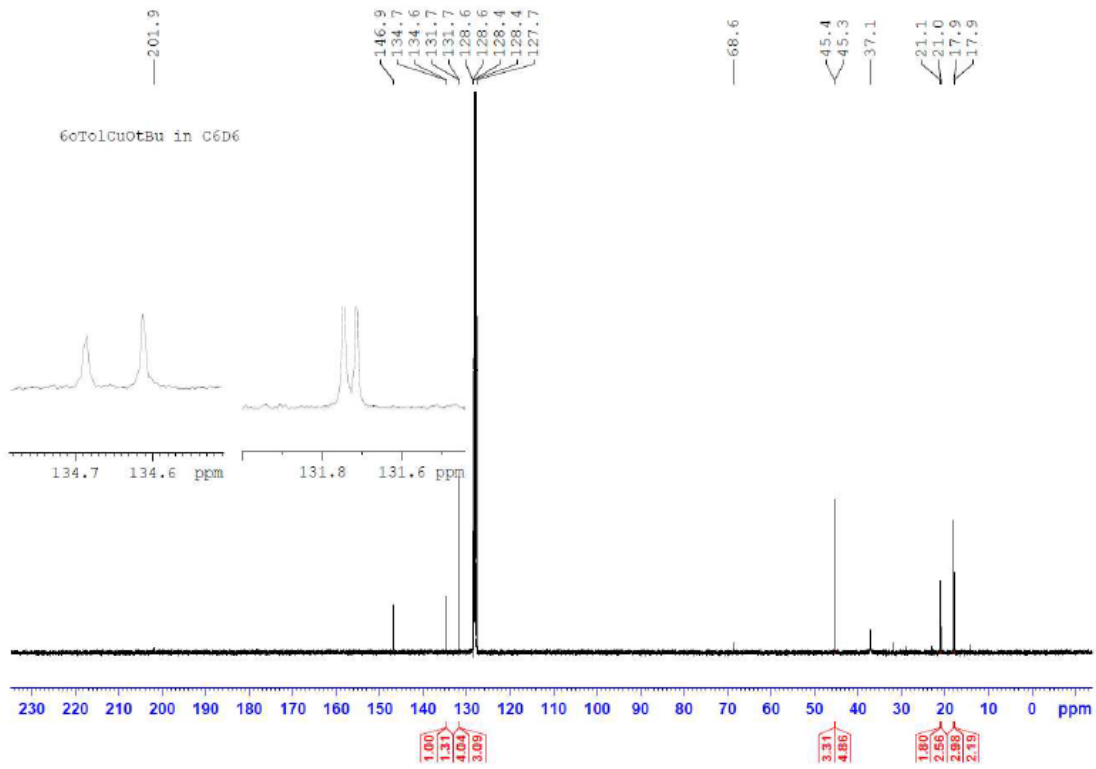


Figure 42 - $^{13}$C{$^{1}$H} NMR spectrum (126 MHz, $C_6D_6$, 298 K) of (6-*o*-Tol)CuO$^{t}$Bu (**2.3**).

## 7.1.2 – NMR spectra of Ni(6-Mes)$PPh_3Br_2$ (**5.16**)

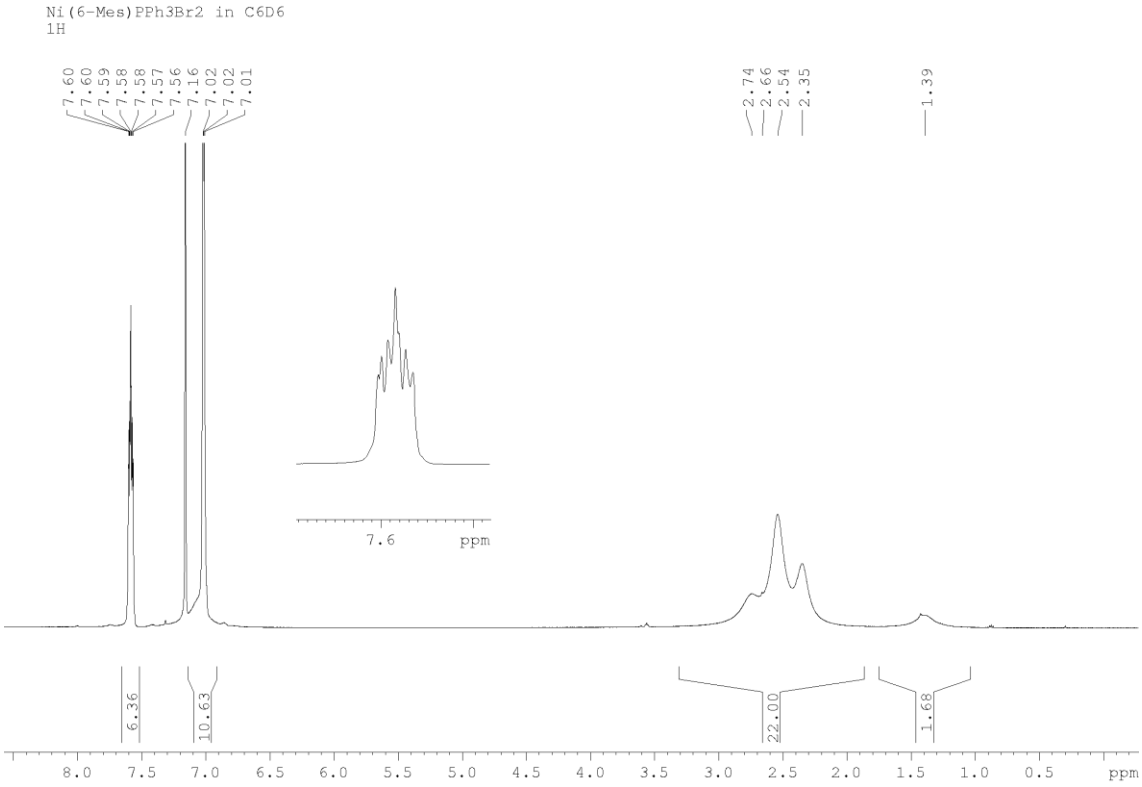


Figure 43 – $^{1}H$ NMR spectrum (500 MHz, $C_6D_6$, 298K) of **5.16**.

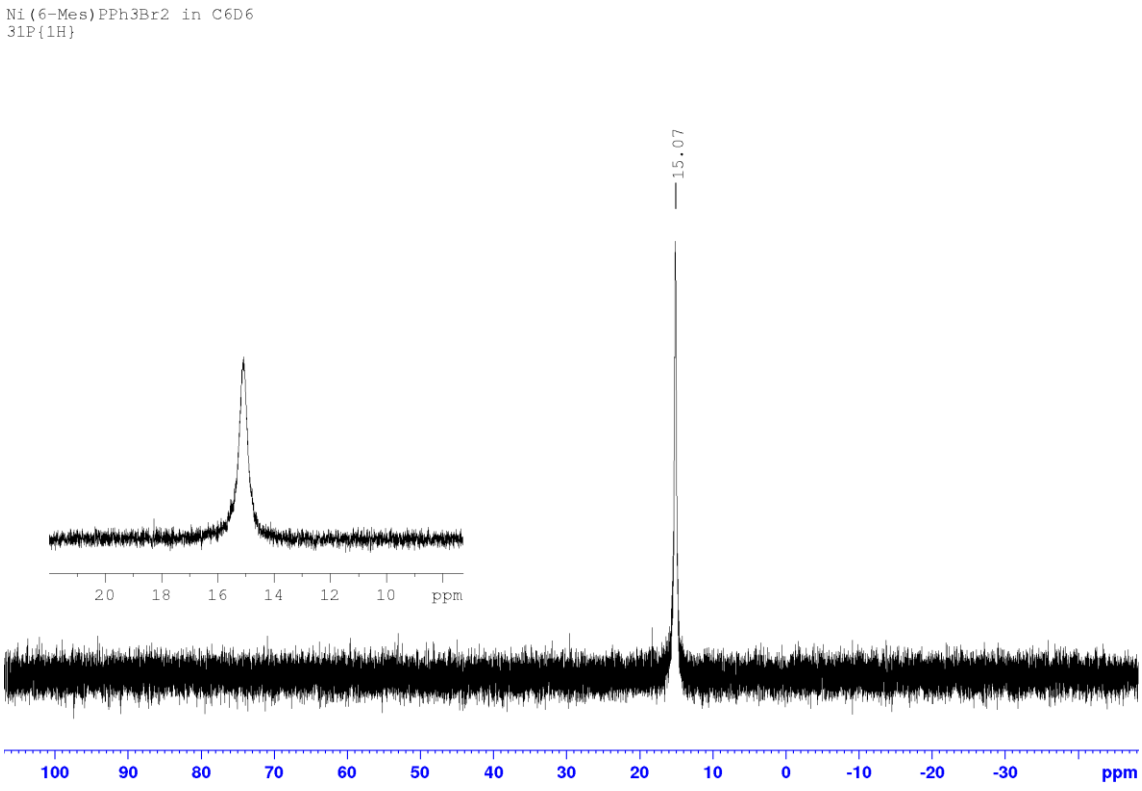


Figure 44 – $^{31}P\{^{1}H\}$ NMR spectra (202 MHz, $C_6D_6$, 298K) of **5.16**.

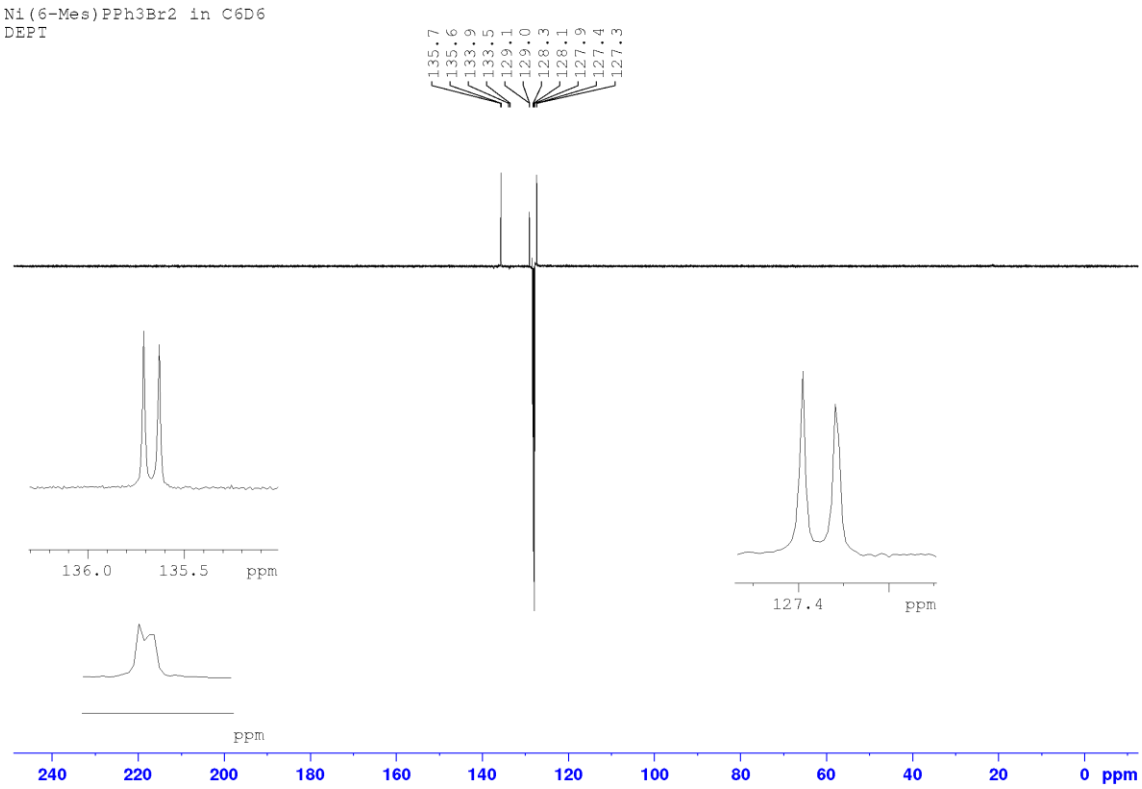


Figure 45 - DEPT NMR spectra (126 MHz, $C_6D_6$, 298K) of **5.16**.

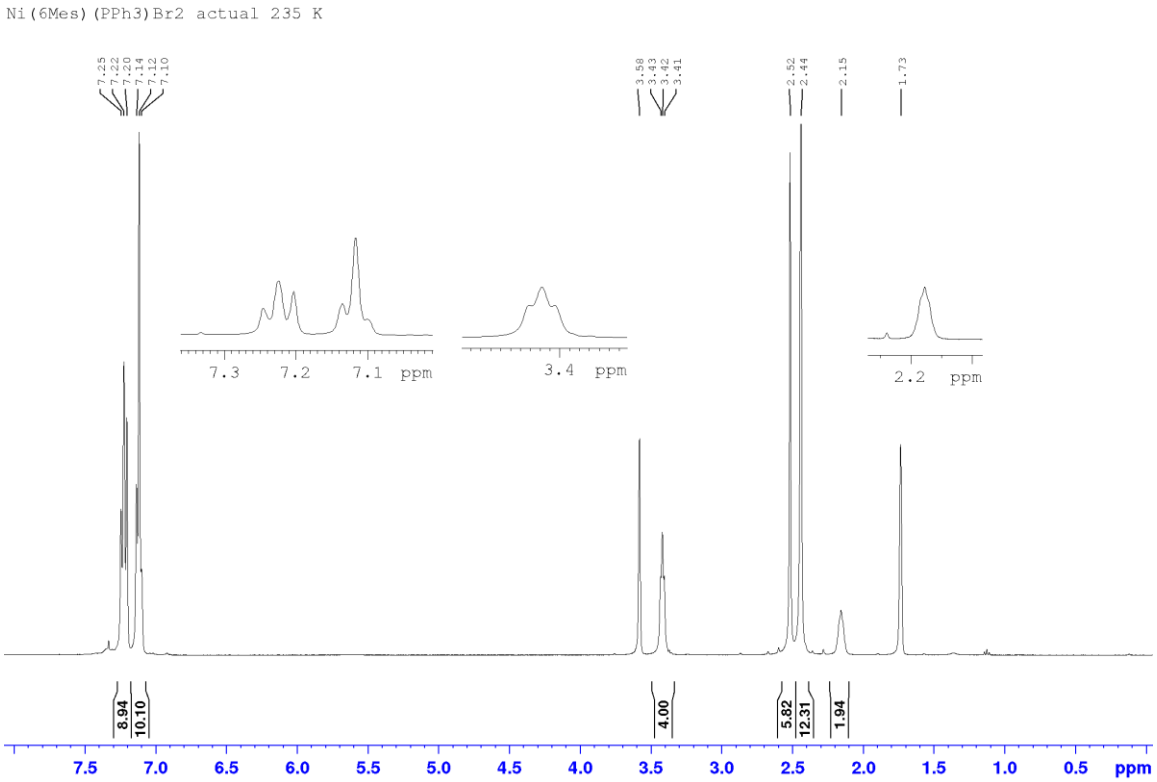


Figure 46 - $^{1}$H NMR spectrum (400 MHz, $d_8$-THF, 235K) of **5.16**.

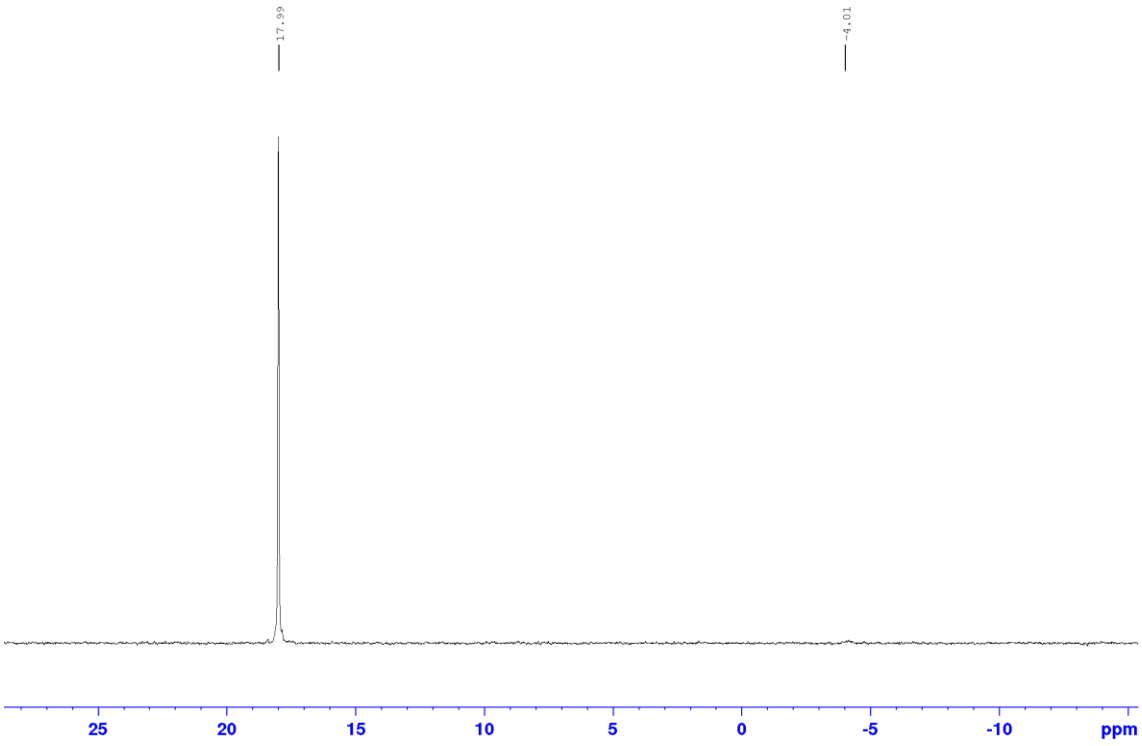


Figure 47 - $^{31}$P{$^{1}$H} NMR spectra (162 MHz, $d_8$-THF, 235K) of **5.16.**

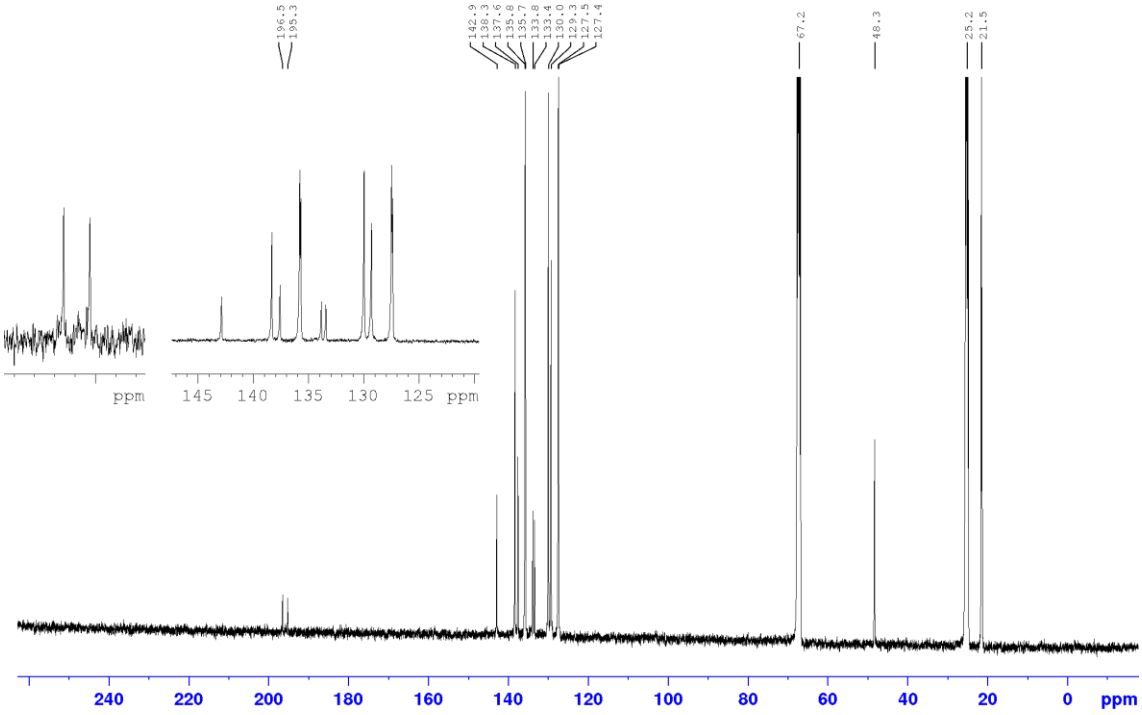


Figure 48 – $^{13}C\{^{1}H\}$ NMR spectra (101 MHz, $d_8$-THF, 235K) of **5.16**.

## 7.1.3 –NMR spectra of Ni(6-Mes)($\kappa^2$-TEMPO)O$^i$Pr **(5.15)**

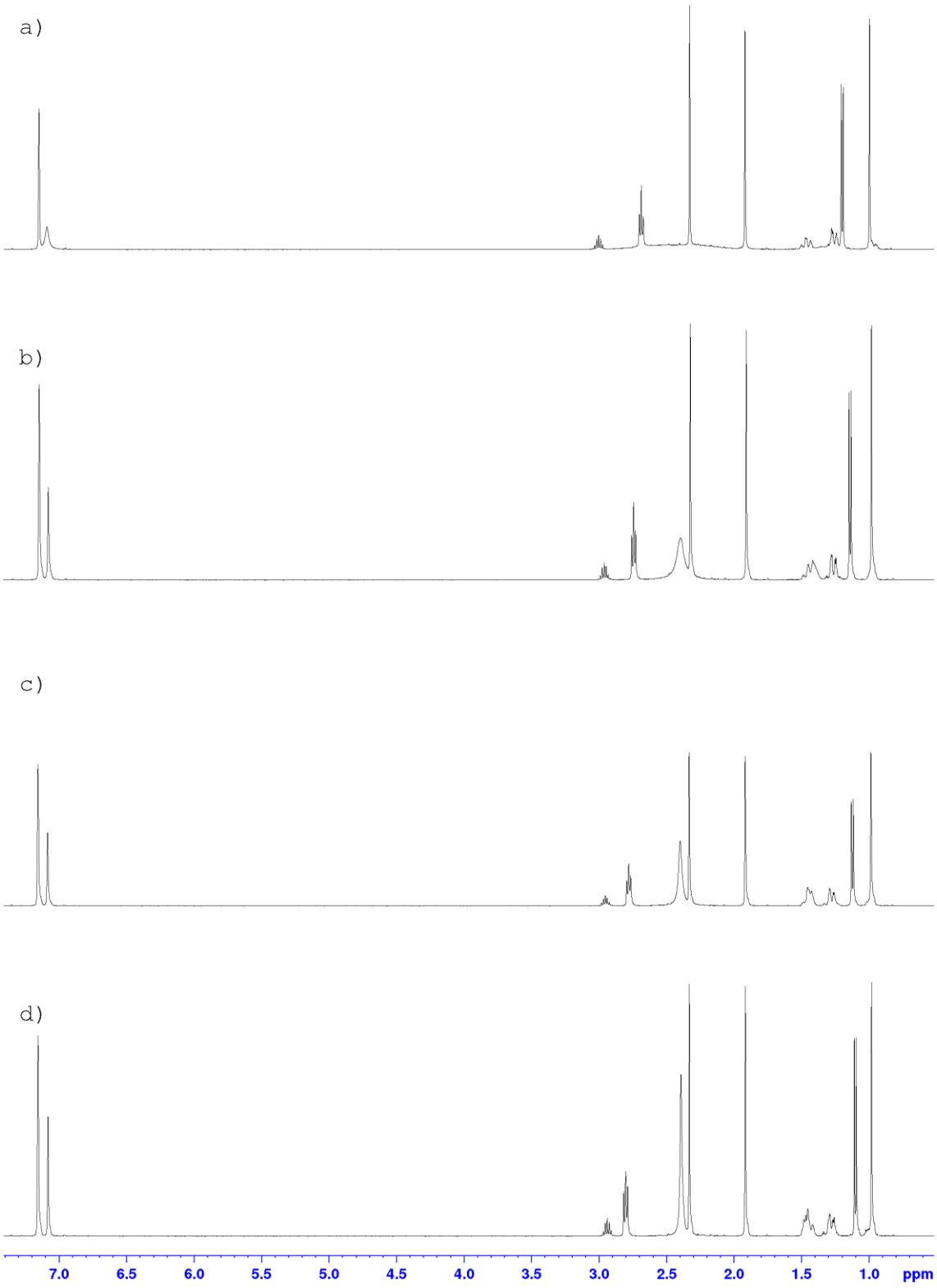


Figure 49 – $^1$H NMR (400 MHz, $C_6D_6$) spectra of **5.15** at a) 298 K, b) 318 K, c) 328 K and d) 338 K.

### 7.1.4 – NMR spectra of Ni(6-Mes)($PPh_3$)OC(H)$Ph_2$ **(5.9)**

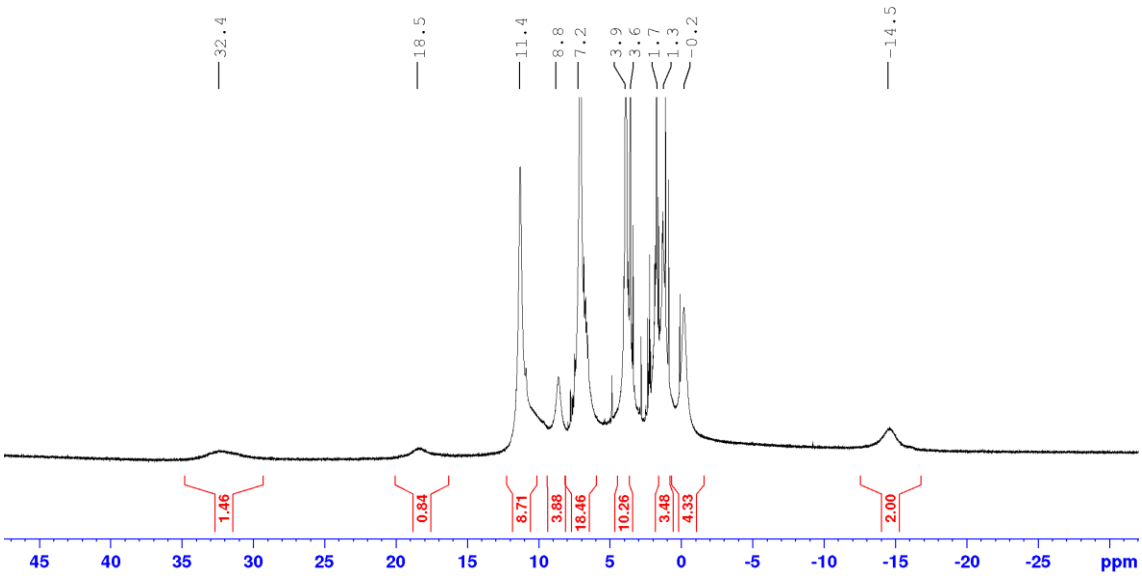


Figure 50 - $^1$H NMR spectrum (500 MHz, $d_8$-THF, 298K) of **5.9**.

## 7.2 – Appendix 2 : X-Ray Structures

### 7.2.1 – (7-Mes)CuMes

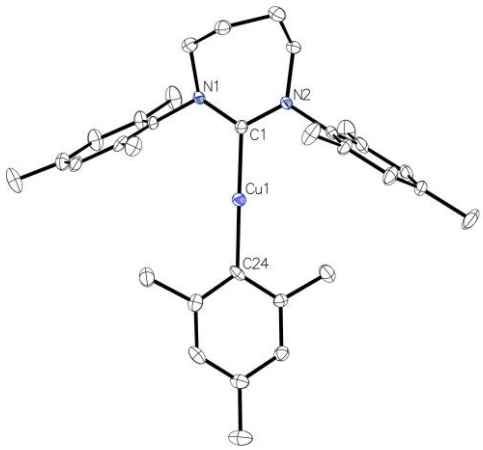


Figure 51 - Molecular structure of (7-Mes)CuMes. Hydrogen atoms have been omitted for clarity. Ellipsoids are represented at 30% probability. Selected bond lengths (Å) and angles (°): Cu1-C1 1.926(4), Cu1-C24 1.943(4), C1-Cu1-C24 177.1(4).

## 7.2.2 – (6-Xylyl)CuMes

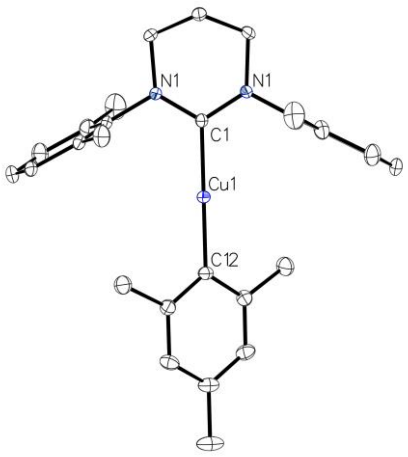


Figure 52 - Molecular structure of (6-Xylyl)CuMes. Hydrogen atoms have been omitted for clarity. Ellipsoids are represented at 30% probability. Selected bond lengths (Å) and angles (°): Cu1-C1 1.926(2), Cu1-C12 1.932(2), C1-Cu1-C12 180. C1-Cu1-C12 are coincident with a crystallographic 2-fold rotation axis.

## 7.2.3 – (6-Dipp)CuMes

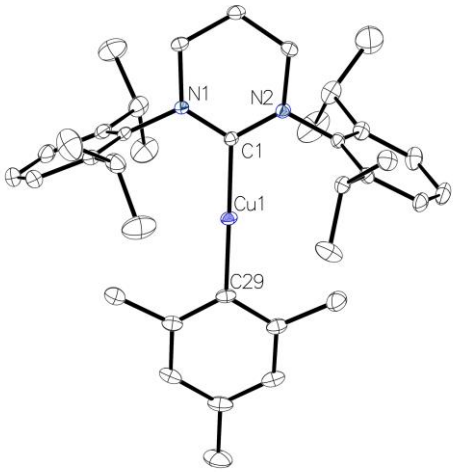


Figure 53 - Molecular structure of (6-Dipp)CuMes. Hydrogen atoms have been omitted for clarity. Ellipsoids are represented at 30% probability. Selected bond lengths (Å) and angles (°): Cu1-C1 1.923(17), Cu1-C29 1.9278(18), C1-Cu1-C29 177.78(7).

## 7.2.4 – ($^{Menthyl}$CAAC)CuMes

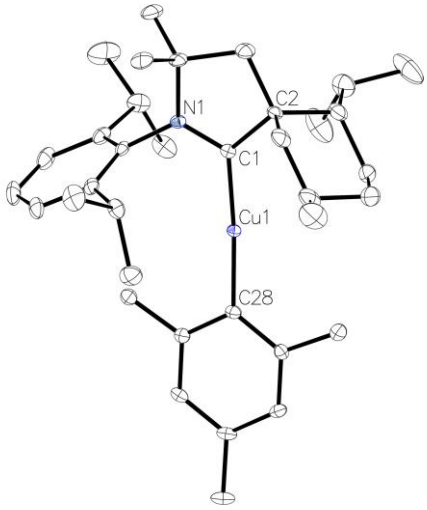


Figure 54 - Molecular structure of ($^{Menthyl}$CAAC)CuMes. Hydrogen atoms have been omitted for clarity. Ellipsoids are represented at 30% probability. Selected bond lengths (Å) and angles (°): Cu1-C1 1.928(3), Cu1-C29 1.943(3), C1-Cu1-C29 175.35(12).

## 7.3 – Appendix 3 : Crystallographic Data

| | (7-Mes)CuMes | (6-Xylyl)CuMes | (6-Dipp)CuMes |
|---|---|---|---|
| Identification code | e16mkw13 | e17mkw14 | e16mkw17 |
| Empirical formula | $C_{32}H_{41}CuN_2$ | $C_{29}H_{35}CuN_2$ | $C_{37}H_{51}CuN_2$ |
| Formula weight | 517.21 | 475.13 | 587.33 |
| Temperature/K | 150.1(2) | 150.00(10) | 150.00(10) |
| Crystal system | monoclinic | monoclinic | monoclinic |
| Space group | Cc | C2/c | $P2_1/n$ |
| a/Å | 11.0433(6) | 11.5008(5) | 20.6654(5) |
| b/Å | 17.9929(7) | 17.2285(4) | 16.1912(3) |
| c/Å | 14.4188(7) | 13.1306(5) | 21.4801(5) |
| α/° | 90 | 90 | 90 |
| β/° | 103.608(5) | 106.457(4) | 106.979(2) |
| γ/° | 90 | 90 | 90 |
| Volume/Å$^3$ | 2784.6(2) | 2495.12(16) | 6873.9(3) |
| Z | 4 | 4 | 8 |
| $\rho_{calc}$g/cm$^3$ | 1.234 | 1.265 | 1.135 |
| μ/mm$^{-1}$ | 0.806 | 0.894 | 0.661 |
| F(000) | 1104.0 | 1008.0 | 2528.0 |
| Crystal size/mm$^3$ | 0.578 × 0.237 × 0.068 | 0.44 × 0.296 × 0.283 | 0.665 × 0.37 × 0.195 |
| Radiation | MoKα (λ = 0.71073) | MoKα (λ = 0.71073) | MoKα (λ = 0.71073) |
| 2Θ range for data collection/° | 7.372 to 52.736 | 6.898 to 54.958 | 6.676 to 54.97 |
| Index ranges | $-13 \le h \le 13$, $-21 \le k \le 22$, $-17 \le l \le 18$ | $-14 \le h \le 10$, $-21 \le k \le 22$, $-16 \le l \le 16$ | $-26 \le h \le 26$, $-21 \le k \le 21$, $-27 \le l \le 27$ |
| Reflections collected | 10899 | 10278 | 77499 |
| Independent reflections | 5285 [$R_{int}$= 0.0273, $R_{sigma}$ = 0.0369] | 2832 [$R_{int}$ = 0.0249, $R_{sigma}$ = 0.0259] | 15707 [$R_{int}$=0.0409, $R_{sigma}$= 0.0357] |
| Data/restraints/parameters | 5285/2/326 | 2832/10/183 | 15707/6/763 |
| Goodness-of-fit on $F^2$ | 1.069 | 1.065 | 1.016 |
| Final R indexes [I>=2σ (I)] | $R_1$ = 0.0413, $wR_2$ = 0.1082 | $R_1$ = 0.0319, $wR_2$ = 0.0823 | $R_1$ = 0.0373, $wR_2$ = 0.0846 |
| Final R indexes [all data] | $R_1$ = 0.0441, $wR_2$ = 0.1110 | $R_1$ = 0.0358, $wR_2$ = 0.0843 | $R_1$ = 0.0554, $wR_2$ = 0.0933 |
| Largest diff. peak/hole / e Å$^{-3}$ | 0.66/-0.23 | 0.46/-0.34 | 0.39/-0.31 |

| | (7-Mes)CuO$^t$Bu (**2.2**) | (6-*o*-Tolyl)CuO$^t$Bu (**2.3**) | (6-Dipp)CuO$^t$Bu (**2.5**) |
|---|---|---|---|
| Identification code | s16mkw68 | s16mkw69 | s17mkw14 |
| Empirical formula | $C_{27}H_{39}CuN_2O$ | $C_{22}H_{29}CuN_2O$ | $C_{25.6}H_{39.2}Cu_{0.8}N_{1.6}O_{0.8}$ |
| Formula weight | 471.14 | 401.01 | 433.02 |
| Temperature/K | 210.00(10) | 210.01(10) | 150.00(10) |
| Crystal system | triclinic | monoclinic | monoclinic |
| Space group | P-1 | $P2_1/c$ | $P2_1/c$ |
| a/Å | 8.9869(3) | 13.790(2) | 15.6837(2) |
| b/Å | 10.3748(4) | 10.5958(16) | 19.8499(4) |
| c/Å | 15.1098(4) | 14.2117(13) | 20.4080(2) |
| α/° | 99.699(3) | 90 | 90 |
| β/° | 96.278(2) | 95.824(11) | 99.7600(10) |
| γ/° | 109.686(3) | 90 | 90 |
| Volume/Å$^3$ | 1286.38(8) | 2065.8(5) | 6261.46(16) |
| Z | 2 | 4 | 10 |
| $\rho_{calc}$g/cm$^3$ | 1.216 | 1.289 | 1.148 |
| μ/mm$^{-1}$ | 1.333 | 1.572 | 1.154 |
| F(000) | 504.0 | 848.0 | 2336.0 |
| Crystal size/mm$^3$ | 0.269 × 0.218 × 0.175 | 0.110 × 0.078 × 0.043 | 0.548 × 0.141 × 0.08 |
| Radiation | CuKα (λ = 1.54184) | CuKα (λ = 1.54184) | CuKα (λ = 1.54184) |
| 2Θ range for data collection/° | 6.032 to 146.804 | 10.434 to 140.11 | 5.718 to 146.714 |
| Index ranges | $-11 \le h \le 10$, $-9 \le k \le 12$, $-18 \le l \le 17$ | $-16 \le h \le 15$, $-12 \le k \le 12$, $-17 \le l \le 14$ | $-11 \le h \le 19$, $-24 \le k \le 24$, $-25 \le l \le 25$ |
| Reflections collected | 13089 | 15668 | 50537 |
| Independent reflections | 5146 [$R_{int}$ =0.0198,$R_{sigma}$ =0.0218] | 3917 [$R_{int}$ =0.1032,$R_{sigma}$ =0.0921] | 12467 [$R_{int}$=0.0448,$R_{sigma}$=0.0360] |
| Data/restraints/parameters | 5146/0/289 | 3917/1/250 | 12467/0/671 |
| Goodness-of-fit on $F^2$ | 1.048 | 1.052 | 1.128 |
| Final R indexes [I>=2σ (I)] | $R_1$ = 0.0290, $wR_2$ = 0.0811 | $R_1$ = 0.0741, $wR_2$ = 0.1518 | $R_1$ = 0.0624, $wR_2$ = 0.1469 |
| Final R indexes [all data] | $R_1$ = 0.0306, $wR_2$ = 0.0825 | $R_1$ = 0.1195, $wR_2$ = 0.1813 | $R_1$ = 0.0755, $wR_2$ = 0.1534 |
| Largest diff. peak/hole / e Å$^{-3}$ | 0.31/-0.27 | 0.69/-0.60 | 1.06/-0.88 |

| | (SIMes)CuO$^t$Bu (**2.6**) | (6-Mes)Cu(C(Ph)=C(H)Ph) (**2.8**) | ($^{Menthyl}$CAAC)CuMes |
|---|---|---|---|
| Identification code | e17mkw20 | e17mkw18 | e19mkw27 |
| Empirical formula | $C_{28}H_{38}CuN_2O$ | $C_{36}H_{39}CuN_2$ | $C_{36}H_{54}CuN$ |
| Formula weight | 482.14 | 563.23 | 564.34 |
| Temperature/K | 150.01(11) | 150.00(10) | 149.90(10) |
| Crystal system | triclinic | monoclinic | orthorhombic |
| Space group | P-1 | $P2_1/n$ | $P2_12_12_1$ |
| a/Å | 9.0267(7) | 12.0665(5) | 10.3195(3) |
| b/Å | 9.6520(12) | 15.8315(5) | 17.0308(4) |
| c/Å | 17.3314(11) | 15.9969(5) | 18.4421(5) |
| α/° | 101.919(8) | 90 | 90 |
| β/° | 91.617(6) | 91.795(3) | 90 |
| γ/° | 113.858(9) | 90 | 90 |
| Volume/Å$^3$ | 1340.6(2) | 3054.40(18) | 3241.19(15) |
| Z | 2 | 4 | 4 |
| $\rho_{calc}$g/cm$^3$ | 1.194 | 1.225 | 1.156 |
| μ/mm$^{-1}$ | 0.835 | 0.741 | 0.697 |
| F(000) | 514.0 | 1192.0 | 1224.0 |
| Crystal size/mm$^3$ | 0.325 × 0.274 × 0.162 | 0.561 × 0.505 × 0.315 | 0.533 × 0.355 × 0.214 |
| Radiation | MoKα (λ = 0.71073) | MoKα (λ = 0.71073) | MoKα (λ = 0.71073) |
| 2Θ range for data collection/° | 6.782 to 54.964 | 6.704 to 54.966 | 7.048 to 60.776 |
| Index ranges | $-11 \le h \le 8$, $-12 \le k \le 12$, $-22 \le l \le 22$ | $-15 \le h \le 13$, $-20 \le k \le 20$, $-15 \le l \le 20$ | $-13 \le h \le 14$, $-23 \le k \le 19$, $-25 \le l \le 23$ |
| Reflections collected | 6426 | 27234 | 30448 |
| Independent reflections | 6426 [$R_{int}$ = 0.0401, $R_{sigma}$ = 0.0954] | 6925 [$R_{int}$ = 0.0262, $R_{sigma}$ = 0.0290] | 8549 [$R_{int}$ = 0.0385, $R_{sigma}$ = 0.0453] |
| Data/restraints/parameters | 6426/0/299 | 6925/0/358 | 8549/0/355 |
| Goodness-of-fit on $F^2$ | 0.962 | 1.028 | 1.041 |
| Final R indexes [I>=2σ (I)] | $R_1$ = 0.0500, $wR_2$ = 0.1028 | $R_1$ = 0.0491, $wR_2$ = 0.1214 | $R_1$ = 0.0384, $wR_2$ = 0.0826 |
| Final R indexes [all data] | $R_1$ = 0.0814, $wR_2$ = 0.1114 | $R_1$ = 0.0655, $wR_2$ = 0.1329 | $R_1$ = 0.0479, $wR_2$ = 0.0876 |
| Largest diff. peak/hole / e Å$^{-3}$ | 0.54/-0.64 | 1.70/-0.82 | 0.48/-0.27 |

| | (7-Mes)CuF (**3.1**) | (6-Mes)CuF (**3.2**) | (ITr)CuF (**3.3**) |
|---|---|---|---|
| Identification code | e18mkw18 | s18mkw25 | e18mkw31 |
| Empirical formula | $C_{23}H_{30}CuFN_2$ | $C_{22}H_{28}N_2FCu$ | $C_{43}H_{36}Cl_4CuFN_2$ |
| Formula weight | 417.03 | 403.00 | 805.08 |
| Temperature/K | 150.1(4) | 150.00(10) | 150.00(10) |
| Crystal system | monoclinic | orthorhombic | orthorhombic |
| Space group | $P2_1/c$ | Pbca | Fdd2 |
| a/Å | 14.2192(2) | 17.08390(10) | 34.1390(9) |
| b/Å | 17.9966(3) | 16.01770(10) | 25.0699(9) |
| c/Å | 8.14380(10) | 29.6637(2) | 8.8076(2) |
| α/° | 90 | 90 | 90 |
| β/° | 91.815(2) | 90 | 90 |
| γ/° | 90 | 90 | 90 |
| Volume/Å$^3$ | 2082.93(5) | 8117.32(9) | 7538.1(4) |
| Z | 4 | 16 | 8 |
| $\rho_{calc}$g/cm$^3$ | 1.330 | 1.319 | 1.419 |
| μ/mm$^{-1}$ | 1.067 | 1.638 | 0.902 |
| F(000) | 880.0 | 3392.0 | 3312.0 |
| Crystal size/mm$^3$ | 0.231 × 0.173 × 0.149 | 0.341 × 0.176 × 0.121 | 0.356 × 0.206 × 0.151 |
| Radiation | MoKα (λ = 0.71073) | CuKα (λ = 1.54184) | MoKα (λ = 0.71073) |
| 2Θ range for data collection/° | 6.75 to 58.958 | 7.894 to 146.248 | 6.826 to 56.564 |
| Index ranges | $-17 \le h \le 19$, $-23 \le k \le 23$, $-10 \le l \le 10$ | $-20 \le h \le 21$, $-19 \le k \le 15$, $-36 \le l \le 36$ | $-44 \le h \le 45$, $-27 \le k \le 33$, $-11 \le l \le 9$ |
| Reflections collected | 17328 | 102057 | 15675 |
| Independent reflections | 5056 [$R_{int}$ = 0.0284, $R_{sigma}$ = 0.0367] | 8098 [$R_{int}$ = 0.0453, $R_{sigma}$ = 0.0175] | 4178 [$R_{int}$ = 0.0314, $R_{sigma}$ = 0.0337] |
| Data/restraints/parameters | 5056/0/250 | 8098/0/481 | 4178/15/250 |
| Goodness-of-fit on $F^2$ | 1.023 | 1.014 | 1.049 |
| Final R indexes [I>=2σ (I)] | $R_1$ = 0.0343, $wR_2$ = 0.0745 | $R_1$ = 0.0322, $wR_2$ = 0.0864 | $R_1$ = 0.0316, $wR_2$ = 0.0652 |
| Final R indexes [all data] | $R_1$ = 0.0493, $wR_2$ = 0.0801 | $R_1$ = 0.0346, $wR_2$ = 0.0883 | $R_1$ = 0.0360, $wR_2$ = 0.0673 |
| Largest diff. peak/hole / e Å$^{-3}$ | 0.40/-0.30 | 0.56/-0.56 | 0.31/-0.32 |

| | (ITrDipp)CuF (**3.4**) | ($^{Menthyl}$CAAC)CuF (**3.5**) | (ITr)Cu($CH_2CHCH_2$) (**3.7**) |
|---|---|---|---|
| Identification code | s18mkw26 | s19mkw42 | e19mkw28 |
| Empirical formula | $C_{34}H_{34}CuFN_2$ | $C_{27}H_{43}CuFN$ | $C_{44}H_{37}CuN_2$ |
| Formula weight | 553.17 | 464.16 | 657.29 |
| Temperature/K | 150.00(10) | 150.00(10) | 149.89(10) |
| Crystal system | orthorhombic | monoclinic | triclinic |
| Space group | Pbca | $P2_1$ | P-1 |
| a/Å | 16.1371(1) | 11.70553(15) | 10.3512(6) |
| b/Å | 16.5025(1) | 17.32454(19) | 11.5614(7) |
| c/Å | 21.1107(1) | 12.96239(18) | 15.7625(10) |
| α/° | 90 | 90 | 85.807(5) |
| β/° | 90 | 93.1866(12) | 72.002(5) |
| γ/° | 90 | 90 | 67.360(5) |
| Volume/Å$^3$ | 5621.83(6) | 2624.62(6) | 1653.56(19) |
| Z | 8 | 4 | 2 |
| $\rho_{calc}$g/cm$^3$ | 1.307 | 1.175 | 1.320 |
| μ/mm$^{-1}$ | 1.337 | 1.310 | 0.695 |
| F(000) | 2320.0 | 1000.0 | 688.0 |
| Crystal size/mm$^3$ | 0.355 × 0.184 × 0.165 | 0.229 × 0.17 × 0.035 | 0.685 × 0.452 × 0.314 |
| Radiation | CuKα (λ = 1.54184) | CuKα (λ = 1.54184) | MoKα (λ = 0.71073) |
| 2Θ range for data collection/° | 8.376 to 146.852 | 6.83 to 146.174 | 6.814 to 60.85 |
| Index ranges | $-20 \le h \le 19$, $-14 \le k \le 20$, $-25 \le l \le 26$ | $-14 \le h \le 14$, $-21 \le k \le 15$, $-16 \le l \le 15$ | $-14 \le h \le 12$, $-16 \le k \le 15$, $-18 \le l \le 21$ |
| Reflections collected | 79322 | 29519 | 16033 |
| Independent reflections | 5642 [$R_{int}$ = 0.0341, $R_{sigma}$ = 0.0123] | 8050 [$R_{int}$ = 0.0396, $R_{sigma}$ = 0.0379] | 8472 [$R_{int}$ = 0.0293, $R_{sigma}$ = 0.0571] |
| Data/restraints/parameters | 5642/0/347 | 8050/70/644 | 8472/5/444 |
| Goodness-of-fit on $F^2$ | 1.048 | 1.043 | 1.023 |
| Final R indexes [I>=2σ (I)] | $R_1$ = 0.0335, $wR_2$ = 0.0923 | $R_1$ = 0.0436, $wR_2$ = 0.1113 | $R_1$ = 0.0446, $wR_2$ = 0.0880 |
| Final R indexes [all data] | $R_1$ = 0.0350, $wR_2$ = 0.0936 | $R_1$ = 0.0454, $wR_2$ = 0.1132 | $R_1$ = 0.0621, $wR_2$ = 0.0959 |
| Largest diff. peak/hole / e Å$^{-3}$ | 0.26/-0.64 | 0.99/-0.69 | 0.37/-0.38 |

| | [{(6-Mes)Cu}$_2$(μ-OEt)][$SiF_5$] (**3.8**) | [{(ITr)Cu}$_2$(μ-OEt)][$SiF_5$] (**3.9**) | [{($^{Menthyl}$CAAC)Cu}$_2$(μ-OEt)][$SiF_5$] (**3.10**) |
|---|---|---|---|
| Identification code | e19mkw42 | e19mkw34 | s20mkw3 |
| Empirical formula | $C_{47}H_{63}Cl_2Cu_2F_5N_4OSi$ | $C_{85}H_{71}Cu_2F_5N_4OSiCl_2$ | $C_{57}H_{93}Cl_2Cu_2F_5N_2OSi$ |
| Formula weight | 1021.08 | 1485.52 | 1143.40 |
| Temperature/K | 150.00(10) | 150.01(10) | 150.00(10) |
| Crystal system | monoclinic | monoclinic | triclinic |
| Space group | C2/c | $P2_1/n$ | P1 |
| a/Å | 22.8096(3) | 14.5812(4) | 10.4668(5) |
| b/Å | 19.4559(3) | 24.6024(6) | 10.4689(4) |
| c/Å | 24.2915(4) | 20.0600(4) | 28.9962(9) |
| α/° | 90 | 90 | 88.319(3) |
| β/° | 110.405(2) | 94.771(2) | 87.919(3) |
| γ/° | 90 | 90 | 70.617(4) |
| Volume/Å$^3$ | 10103.7(3) | 7171.2(3) | 2994.7(2) |
| Z | 8 | 4 | 2 |
| $\rho_{calc}$g/cm$^3$ | 1.343 | 1.376 | 1.268 |
| μ/mm$^{-1}$ | 1.027 | 0.748 | 0.873 |
| F(000) | 4256.0 | 3072.0 | 1216.0 |
| Crystal size/mm$^3$ | 0.635 × 0.499 × 0.384 | 0.403 × 0.384 × 0.225 | 0.221 × 0.177 × 0.131 |
| Radiation | MoKα (λ = 0.71073) | Mo Kα (λ = 0.71073) | MoKα (λ = 0.71073) |
| 2Θ range for data collection/° | 6.81 to 60.886 | 6.684 to 56.64 | 5.442 to 60.882 |
| Index ranges | $-32 \le h \le 31$, $-27 \le k \le 25$, $-33 \le l \le 31$ | $-17 \le h \le 19$, $-32 \le k \le 32$, $-26 \le l \le 26$ | $-14 \le h \le 12$, $-14 \le k \le 14$, $-38 \le l \le 40$ |
| Reflections collected | 46581 | 75220 | 29106 |
| Independent reflections | 13338 [$R_{int}$ = 0.0231, $R_{sigma}$ = 0.0265] | 17661 [$R_{int}$ = 0.0345, $R_{sigma}$ = 0.0359] | 19849 [$R_{int}$ = 0.0240, $R_{sigma}$ = 0.0439] |
| Data/restraints/parameters | 13338/56/617 | 17661/174/938 | 19849/278/1492 |
| Goodness-of-fit on $F^2$ | 1.062 | 1.109 | 1.052 |
| Final R indexes [I>=2σ (I)] | $R_1$ = 0.0432, $wR_2$ = 0.1086 | $R_1$ = 0.0626, $wR_2$ = 0.1530 | $R_1$ = 0.0437, $wR_2$ = 0.1029 |
| Final R indexes [all data] | $R_1$ = 0.0637, $wR_2$ = 0.1239 | $R_1$ = 0.0776, $wR_2$ = 0.1598 | $R_1$ = 0.0496, $wR_2$ = 0.1080 |
| Largest diff. peak/hole / e Å$^{-3}$ | 1.21/-0.90 | 1.23/-0.71 | 0.54/-0.54 |

| | (6-Mes)CuBr (**4.2**) | (6-Mes)CuI (**4.3**) | [6-MesH][$CuCl_2$] (**4.4**) |
|---|---|---|---|
| Identification code | e19mkw33 | e19mkw54 | e19mkw6 |
| Empirical formula | $C_{22}H_{28}BrCuN_2$ | $C_{22}H_{28}CuIN_2$ | $C_{22}H_{29}Cl_2CuN_2$ |
| Formula weight | 463.91 | 510.90 | 455.91 |
| Temperature/K | 149.89(10) | 149.99(10) | 150.01(10) |
| Crystal system | orthorhombic | orthorhombic | orthorhombic |
| Space group | Pbcn | Pbca | $P2_12_12_1$ |
| a/Å | 30.4618(10) | 8.94008(14) | 9.8914(3) |
| b/Å | 8.8796(2) | 16.0949(2) | 13.5617(4) |
| c/Å | 15.8119(4) | 30.9208(5) | 16.6291(5) |
| α/° | 90 | 90 | 90 |
| β/° | 90 | 90 | 90 |
| γ/° | 90 | 90 | 90 |
| Volume/$Å^3$ | 4276.9(2) | 4449.18(12) | 2230.70(12) |
| Z | 8 | 8 | 4 |
| $\rho_{calc}g/cm^3$ | 1.441 | 1.525 | 1.358 |
| $\mu/mm^{-1}$ | 2.897 | 2.377 | 1.228 |
| F(000) | 1904.0 | 2048.0 | 952.0 |
| Crystal size/$mm^3$ | ? × ? × ? | 0.2 × 0.152 × 0.133 | 0.453 × 0.374 × 0.248 |
| Radiation | MoKα (λ = 0.71073) | Mo Kα (λ = 0.71073) | MoKα (λ = 0.71073) |
| 2Θ range for data collection/° | 7.03 to 61.024 | 6.938 to 56.608 | 7.072 to 59.022 |
| Index ranges | $-43 \leq h \leq 39$, $-12 \leq k \leq 9$, $-22 \leq l \leq 21$ | $-11 \leq h \leq 11$, $-21 \leq k \leq 21$, $-41 \leq l \leq 41$ | $-12 \leq h \leq 12$, $-17 \leq k \leq 17$, $-20 \leq l \leq 22$ |
| Reflections collected | 39305 | 39498 | 20908 |
| Independent reflections | 5934 [$R_{int}$ = 0.0422, $R_{sigma}$ = 0.0339] | 5502 [$R_{int}$ = 0.0309, $R_{sigma}$ = 0.0205] | 5369 [$R_{int}$ = 0.0341, $R_{sigma}$ = 0.0409] |
| Data/restraints/parameters | 5934/0/241 | 5502/0/241 | 5369/0/254 |
| Goodness-of-fit on $F^2$ | 1.054 | 1.200 | 1.024 |
| Final R indexes [I>=2σ (I)] | $R_1$ = 0.0650, $wR_2$ = 0.1781 | $R_1$ = 0.0331, $wR_2$ = 0.0663 | $R_1$ = 0.0336, $wR_2$ = 0.0643 |
| Final R indexes [all data] | $R_1$ = 0.0882, $wR_2$ = 0.1934 | $R_1$ = 0.0404, $wR_2$ = 0.0687 | $R_1$ = 0.0465, $wR_2$ = 0.0682 |
| Largest diff. peak/hole / e $Å^{-3}$ | 1.58/-2.19 | 0.51/-0.92 | 0.28/-0.27 |

| | [7-MesH][$CuCl_2$] (**4.6**) | [7-XylylH][$CuCl_2$] (**4.7**) | [7neoPent][$CuCl_2$] (**4.8**) |
|---|---|---|---|
| Identification code | e19mkw7 | e19mkw5 | e19mkw8 |
| Empirical formula | $C_{23}H_{31}Cl_2CuN_2$ | $C_{21}H_{27}Cl_2CuN_2$ | $C_{15}H_{31}Cl_2CuN_2$ |
| Formula weight | 469.94 | 441.88 | 373.86 |
| Temperature/K | 149.98(10) | 150.00(10) | 149.99(10) |
| Crystal system | orthorhombic | monoclinic | orthorhombic |
| Space group | $P2_12_12_1$ | I2/a | $P2_12_12_1$ |
| a/Å | 10.2791(3) | 14.9252(5) | 8.8039(3) |
| b/Å | 14.5586(5) | 11.8383(4) | 9.3553(3) |
| c/Å | 15.4499(4) | 24.5595(9) | 22.6631(7) |
| α/° | 90 | 90 | 90 |
| β/° | 90 | 107.040(4) | 90 |
| γ/° | 90 | 90 | 90 |
| Volume/$Å^3$ | 2312.07(12) | 4148.9(3) | 1866.60(10) |
| Z | 4 | 8 | 4 |
| $\rho_{calc}g/cm^3$ | 1.350 | 1.415 | 1.330 |
| $\mu/mm^{-1}$ | 1.187 | 1.318 | 1.450 |
| F(000) | 984.0 | 1840.0 | 792.0 |
| Crystal size/$mm^3$ | 0.451 × 0.229 × 0.223 | 0.455 × 0.303 × 0.172 | 0.551 × 0.176 × 0.148 |
| Radiation | MoKα (λ = 0.71073) | MoKα (λ = 0.71073) | MoKα (λ = 0.71073) |
| 2Θ range for data collection/° | 6.858 to 58.968 | 6.884 to 58.688 | 6.604 to 59.236 |
| Index ranges | $-12 \le h \le 13$, $-19 \le k \le 19$, $-21 \le l \le 18$ | $-20 \le h \le 18$, $-15 \le k \le 14$, $-33 \le l \le 33$ | $-11 \le h \le 9$, $-10 \le k \le 12$, $-30 \le l \le 31$ |
| Reflections collected | 21268 | 17958 | 17374 |
| Independent reflections | 5608 [$R_{int}$ = 0.0367, $R_{sigma}$ = 0.0394] | 5053 [$R_{int}$ = 0.0257, $R_{sigma}$ = 0.0284] | 4606 [$R_{int}$ = 0.0314, $R_{sigma}$ = 0.0372] |
| Data/restraints/parameters | 5608/13/300 | 5053/0/245 | 4606/0/191 |
| Goodness-of-fit on $F^2$ | 1.076 | 1.048 | 1.035 |
| Final R indexes [I>=2σ (I)] | $R_1$ = 0.0441, $wR_2$ = 0.0899 | $R_1$ = 0.0332, $wR_2$ = 0.0738 | $R_1$ = 0.0317, $wR_2$ = 0.0581 |
| Final R indexes [all data] | $R_1$ = 0.0602, $wR_2$ = 0.0969 | $R_1$ = 0.0455, $wR_2$ = 0.0791 | $R_1$ = 0.0408, $wR_2$ = 0.0611 |
| Largest diff. peak/hole / e $Å^{-3}$ | 0.64/-0.28 | 0.33/-0.30 | 0.30/-0.31 |

| | (6-Xylyl)CuCl (**4.9**) | (7-Mes)CuCl (**4.11**) | (7-Xylyl)CuCl (**4.12**) |
|---|---|---|---|
| Identification code | e19mkw29 | e18mkw22 | e19mkw9 |
| Empirical formula | $C_{20}H_{24}ClCuN_2$ | $C_{23}H_{30}ClCuN_2$ | $C_{21}H_{28}N_2ClCu$ |
| Formula weight | 391.40 | 433.48 | 407.44 |
| Temperature/K | 149.90(10) | 150.00(10) | 150.01(10) |
| Crystal system | monoclinic | monoclinic | orthorhombic |
| Space group | $P2_1/n$ | $P2_1/n$ | $Pna2_1$ |
| a/Å | 8.1773(3) | 8.8263(3) | 16.6355(5) |
| b/Å | 18.0576(6) | 16.1089(6) | 14.4550(4) |
| c/Å | 13.1571(5) | 30.6232(18) | 8.1709(3) |
| α/° | 90 | 90 | 90 |
| β/° | 98.147(3) | 92.255(4) | 90 |
| γ/° | 90 | 90 | 90 |
| Volume/Å$^3$ | 1923.20(12) | 4350.7(3) | 1964.82(11) |
| Z | 4 | 8 | 4 |
| $\rho_{calc}$g/cm$^3$ | 1.352 | 1.324 | 1.377 |
| μ/mm$^{-1}$ | 1.277 | 1.136 | 1.253 |
| F(000) | 816.0 | 1824.0 | 856.0 |
| Crystal size/mm$^3$ | 0.525 × 0.465 × 0.338 | 0.44 × 0.229 × 0.111 | 0.327 × 0.258 × 0.111 |
| Radiation | MoKα (λ = 0.71073) | MoKα (λ = 0.71073) | MoKα (λ = 0.71073) |
| 2Θ range for data collection/° | 6.76 to 60.712 | 6.5 to 56.656 | 6.99 to 59.002 |
| Index ranges | $-11 \le h \le 10$, $-23 \le k \le 25$, $-18 \le l \le 17$ | $-11 \le h \le 11$, $-21 \le k \le 21$, $-40 \le l \le 40$ | $-21 \le h \le 21$, $-19 \le k \le 19$, $-6 \le l \le 11$ |
| Reflections collected | 19078 | 11014 | 16121 |
| Independent reflections | 5168 [$R_{int}$ = 0.0356, $R_{sigma}$ = 0.0390] | 11014 [$R_{int}$ = 0.1104, $R_{sigma}$ = 0.0598] | 3730 [$R_{int}$ = 0.0307, $R_{sigma}$ = 0.0281] |
| Data/restraints/parameters | 5168/0/221 | 11014/0/500 | 3730/1/230 |
| Goodness-of-fit on $F^2$ | 1.037 | 1.122 | 1.029 |
| Final R indexes [I>=2σ (I)] | $R_1$ = 0.0368, $wR_2$ = 0.0805 | $R_1$ = 0.0779, $wR_2$ = 0.1851 | $R_1$ = 0.0273, $wR_2$ = 0.0613 |
| Final R indexes [all data] | $R_1$ = 0.0549, $wR_2$ = 0.0884 | $R_1$ = 0.0943, $wR_2$ = 0.1934 | $R_1$ = 0.0318, $wR_2$ = 0.0633 |
| Largest diff. peak/hole / e Å$^{-3}$ | 0.31/-0.39 | 0.83/-0.99 | 0.36/-0.26 |

| | (8-Mes)CuCl (**4.14**) | Ni(6-Mes)($PPh_3$)$Br_2$ (**5.16**) | Ni(6-Mes)($PPh_3$)($C_6H_4CF_3$)Br (**5.18**) |
|---|---|---|---|
| Identification code | e19mkw29 | p09mkw11 | e16mkw6 |
| Empirical formula | $C_{20}H_{24}ClCuN_2$ | $C_{40}H_{43}Br_2N_2NiP$ | $C_{47}H_{47}BrF_3N_2NiP$ |
| Formula weight | 391.40 | 801.26 | 866.45 |
| Temperature/K | 149.90(10) | 150(2) K | 150.02(19) |
| Crystal system | monoclinic | monoclinic | triclinic |
| Space group | $P2_1/n$ | C2/c | P-1 |
| a/Å | 8.1773(3) | 38.9620(14) | 10.6699(4) |
| b/Å | 18.0576(6) | 9.5046(2) | 10.8620(5) |
| c/Å | 13.1571(5) | 19.6660(4) | 19.7492(10) |
| α/° | 90 | 90 | 86.786(4) |
| β/° | 98.147(3) | 98.538(3) | 85.347(4) |
| γ/° | 90 | 90 | 63.009(4) |
| Volume/$Å^3$ | 1923.20(12) | 7202.0(3) | 2032.34(18) |
| Z | 4 | 8 | 2 |
| $\rho_{calc}g/cm^3$ | 1.352 | 1.478 | 1.416 |
| $\mu/mm^{-1}$ | 1.277 | 2.833 | 1.549 |
| F(000) | 816.0 | 3280 | 896.0 |
| Crystal size/$mm^3$ | 0.525 × 0.465 × 0.338 | 0.27 x 0.20 x 0.20 | 0.382 × 0.138 × 0.113 |
| Radiation | MoKα (λ = 0.71073) | MoKα (λ = 0.71073) | MoKα (λ = 0.71073) |
| 2Θ range for data collection/° | 6.76 to 60.712 | 2.95 to 27.48 | 7.246 to 54.964 |
| Index ranges | -11 ≤ h ≤ 10, -23 ≤ k ≤ 25, -18 ≤ l ≤ 17 | -47<=h<=50; -11<=k<=12; -25<=l<=25 | -13 ≤ h ≤ 13, -14 ≤ k ≤ 11, -25 ≤ l ≤ 15 |
| Reflections collected | 19078 | 28513 | 21437 |
| Independent reflections | 5168 [$R_{int}$ = 0.0356, $R_{sigma}$ = 0.0390] | 8247 [R(int) = 0.0218] | 9301 [$R_{int}$ = 0.0572, $R_{sigma}$ = 0.0923] |
| Data/restraints/parameters | 5168/0/221 | 8247 / 0 / 421 | 9301/6/502 |
| Goodness-of-fit on $F^2$ | 1.037 | 0.931 | 1.171 |
| Final R indexes [I>=2σ (I)] | $R_1$ = 0.0368, $wR_2$ = 0.0805 | R1 = 0.0218 *wR*2 = 0.0510 | $R_1$ = 0.0858, $wR_2$ = 0.1757 |
| Final R indexes [all data] | $R_1$ = 0.0549, $wR_2$ = 0.0884 | R1 = 0.0344 *wR*2 = 0.0521 | $R_1$ = 0.1237, $wR_2$ = 0.1924 |
| Largest diff. peak/hole / e $Å^{-3}$ | 0.31/-0.39 | 0.386 and -0.522 | 1.67/-0.95 |

| | Ni(6-Mes)($PPh_3$)O$^i$Pr (**5.7**) | Ni(6-Mes)($PPh_3$)O$^t$Bu (**5.8**) | Ni(6-Mes)($PPh_3$)OC(H)$Ph_2$ (**5.9**) |
|---|---|---|---|
| Identification code | e16mkw11 | s16mkw53 | s16mkw48 |
| Empirical formula | $C_{43}H_{50}N_2NiOP$ | $C_{44}H_{52}N_2NiOP$ | $C_{53}H_{54}N_2NiOP$ |
| Formula weight | 700.53 | 714.55 | 824.66 |
| Temperature/K | 150.0(2) | 150.00(10) | 150.00(10) |
| Crystal system | monoclinic | monoclinic | triclinic |
| Space group | C2/c | C2/c | P-1 |
| a/Å | 36.3831(11) | 37.0355(4) | 11.1082(3) |
| b/Å | 10.8223(3) | 10.69843(9) | 19.3547(5) |
| c/Å | 19.2527(7) | 19.51695(19) | 20.7393(6) |
| α/° | 90 | 90 | 86.843(2) |
| β/° | 93.173(3) | 92.5791(9) | 88.754(2) |
| γ/° | 90 | 90 | 86.929(2) |
| Volume/Å$^3$ | 7569.1(4) | 7725.21(13) | 4444.9(2) |
| Z | 8 | 8 | 4 |
| $\rho_{calc}$g/cm$^3$ | 1.229 | 1.229 | 1.232 |
| μ/mm$^{-1}$ | 0.589 | 1.375 | 1.268 |
| F(000) | 2984.0 | 3048.0 | 1748.0 |
| Crystal size/mm$^3$ | 0.52 × 0.338 × 0.191 | 0.224 × 0.187 × 0.075 | 0.444 × 0.117 × 0.055 |
| Radiation | MoKα (λ = 0.71073) | CuKα (λ = 1.54184) | CuKα (λ = 1.54184) |
| 2Θ range for data collection/° | 6.712 to 54.97 | 8.604 to 145.126 | 6.09 to 145.348 |
| Index ranges | -47 ≤ h ≤ 42, -13 ≤ k ≤ 14, -25 ≤ l ≤ 24 | -45 ≤ h ≤ 45, -13 ≤ k ≤ 13, -22 ≤ l ≤ 24 | -13 ≤ h ≤ 13, -23 ≤ k ≤ 21, -25 ≤ l ≤ 25 |
| Reflections collected | 31033 | 52745 | 56245 |
| Independent reflections | 8668 [$R_{int}$ = 0.0323, $R_{sigma}$ = 0.0342] | 7668 [$R_{int}$ = 0.0351, $R_{sigma}$ = 0.0193] | 17529 [$R_{int}$ = 0.0629, $R_{sigma}$ = 0.0521] |
| Data/restraints/parameters | 8668/0/441 | 7668/0/451 | 17529/0/1057 |
| Goodness-of-fit on $F^2$ | 1.030 | 1.038 | 1.031 |
| Final R indexes [I>=2σ (I)] | $R_1$ = 0.0402, $wR_2$ = 0.0940 | $R_1$ = 0.0337, $wR_2$ = 0.0904 | $R_1$ = 0.0559, $wR_2$ = 0.1432 |
| Final R indexes [all data] | $R_1$ = 0.0569, $wR_2$ = 0.1030 | $R_1$ = 0.0365, $wR_2$ = 0.0925 | $R_1$ = 0.0698, $wR_2$ = 0.1535 |
| Largest diff. peak/hole / e Å$^{-3}$ | 0.78/-0.31 | 0.31/-0.29 | 1.39/-0.54 |

| | Ni(6-Mes)($PPh_3$)OMe (**5.10**) | Ni(6-Mes)($PPh_3$)(TEMPO)Br (**5.14**) | Ni(6-Mes)(TEMPO)O$^i$Pr (**5.15**) |
|---|---|---|---|
| Identification code | s17mkw7 | | e20mkw2 |
| Empirical formula | $C_{41}H_{46}N_2NiOP$ | | $C_{34}H_{53}N_3NiO_2$ |
| Formula weight | 672.48 | | 594.50 |
| Temperature/K | 149.8(3) | | 149.99(10) |
| Crystal system | monoclinic | | triclinic |
| Space group | $P2_1/n$ | | P-1 |
| a/Å | 10.75659(7) | | 11.8630(13) |
| b/Å | 17.83505(12) | | 12.9897(8) |
| c/Å | 18.55588(15) | | 21.1239(19) |
| α/° | 90 | | 90.961(6) |
| β/° | 102.1982(7) | | 91.845(8) |
| γ/° | 90 | | 91.157(7) |
| Volume/Å$^3$ | 3479.47(4) | | 3252.3(5) |
| Z | 4 | | 4 |
| $\rho_{calc}$g/cm$^3$ | 1.284 | | 1.214 |
| μ/mm$^{-1}$ | 1.495 | | 0.629 |
| F(000) | 1428.0 | | 1288.0 |
| Crystal size/mm$^3$ | 0.349 × 0.258 × 0.078 | | 0.286 × 0.258 × 0.218 |
| Radiation | CuKα (λ = 1.54184) | | MoKα (λ = 0.71073) |
| 2Θ range for data collection/° | 6.952 to 146.856 | | 5.972 to 58.26 |
| Index ranges | $-13 \le h \le 11$, $-21 \le k \le 22$, $-22 \le l \le 23$ | | $-16 \le h \le 16$, $-17 \le k \le 17$, $-28 \le l \le 28$ |
| Reflections collected | 47050 | | 17915 |
| Independent reflections | 6989 [$R_{int}$ = 0.0286, $R_{sigma}$ = 0.0161] | | 17915 [$R_{int}$ = 0456, $R_{sigma}$ = 0.1262] |
| Data/restraints/parameters | 6989/6/425 | | 17915/8/755 |
| Goodness-of-fit on $F^2$ | 1.037 | | 0.803 |
| Final R indexes [I>=2σ (I)] | $R_1$ = 0.0387, $wR_2$ = 0.1019 | | $R_1$ = 0.0423, $wR_2$ = 0.0692 |
| Final R indexes [all data] | $R_1$ = 0.0410, $wR_2$ = 0.1038 | | $R_1$ = 0.0927, $wR_2$ = 0.0752 |
| Largest diff. peak/hole / e Å$^{-3}$ | 0.59/-0.71 | | 0.50/-0.44 |

# 7.4 – Appendix 4 : GC Chromatograms

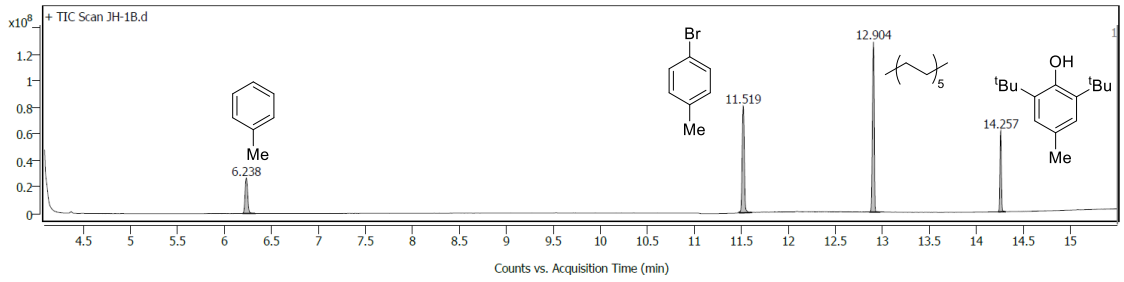


Figure 55 – Typical calibration GC chromatogram.

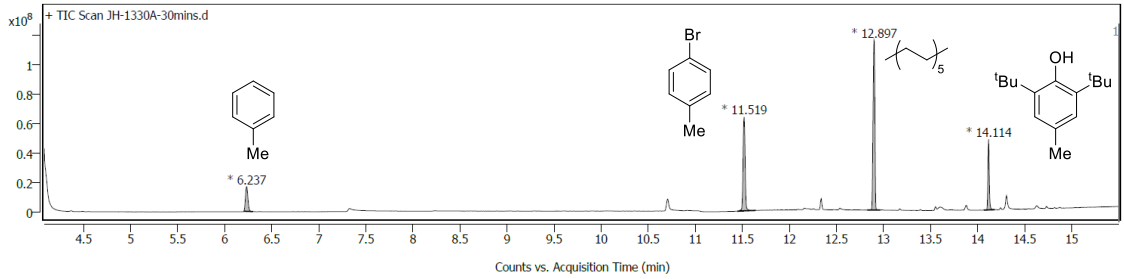


Figure 56 – Typical catalytic run GC chromatogram.

# 7.5 – Appendix 5 : Complexes

## 7.5.1 – Chapter 2

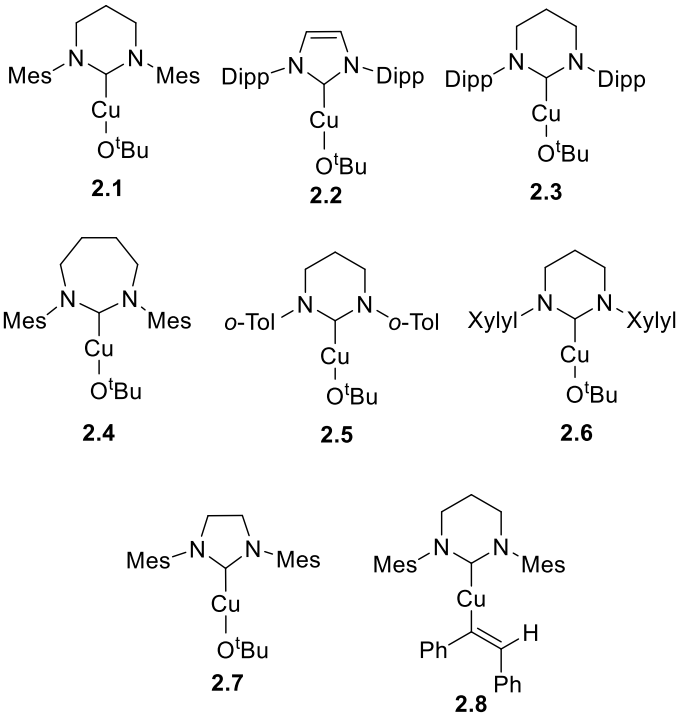

## 7.5.2 – Chapter 3

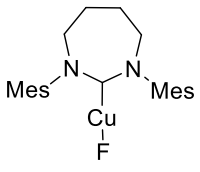


**3.1**

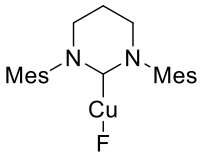


**3.2**

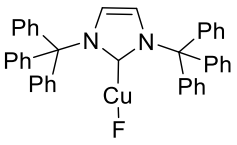


**3.3**

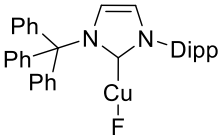


**3.4**

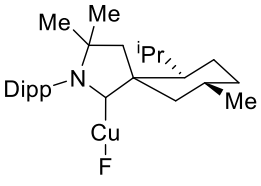


**3.5**

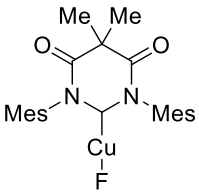


**3.6**

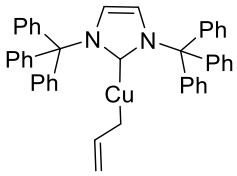


**3.7**

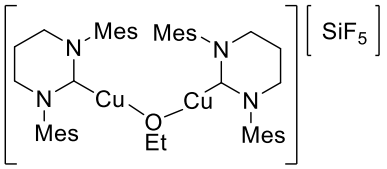


**3.8**

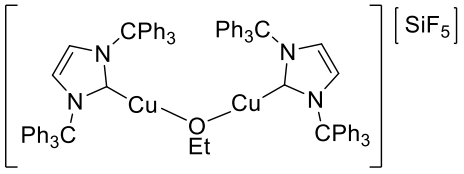


**3.9**

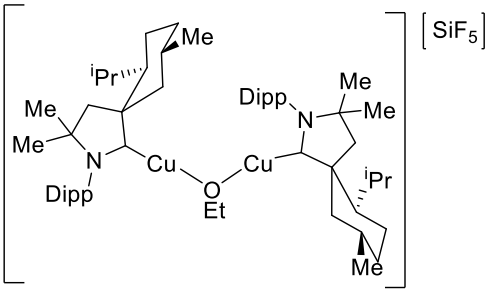


**3.10**

## 7.5.3 – Chapter 4

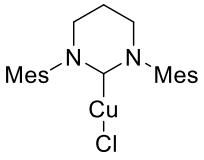


**4.1**

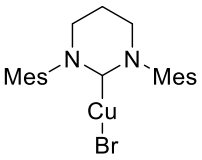


**4.2**

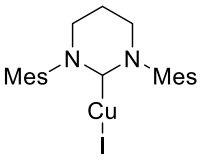


**4.3**

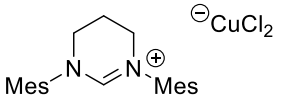


**4.4**

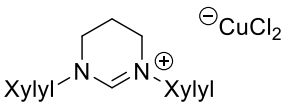


**4.5**

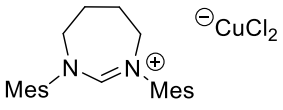


**4.6**

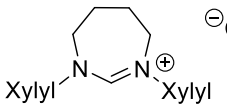


**4.7**

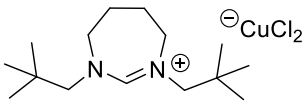


**4.8**

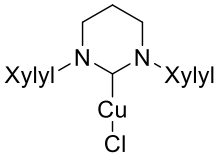


**4.9**

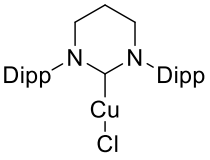


**4.10**

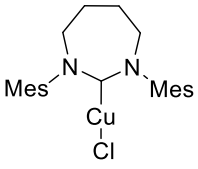


**4.11**

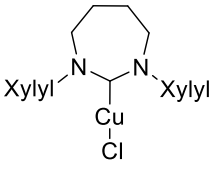


**4.12**

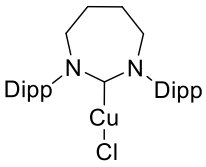


**4.13**

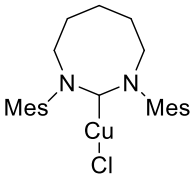


**4.14**

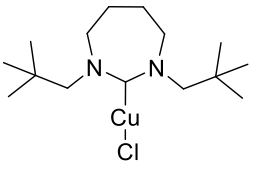


**4.15**

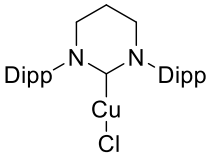


**4.16**

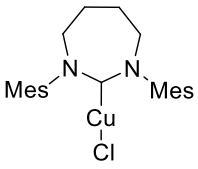


**4.17**

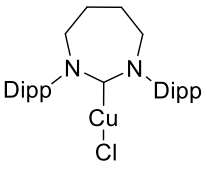


**4.18**

## 7.5.4 – Chapter 5

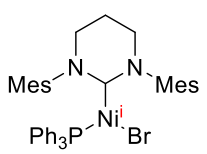

**5.1**

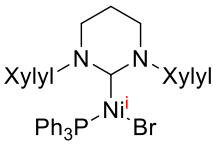

**5.2**

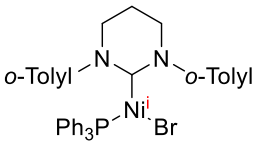

**5.3**

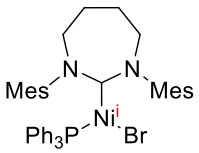

**5.4**

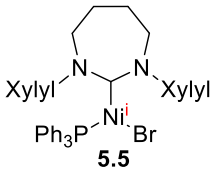

**5.5**

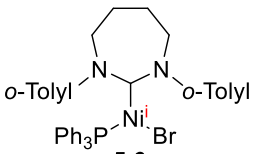

**5.6**

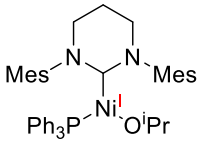

**5.7**

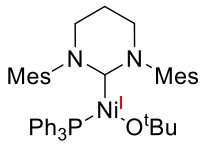

**5.8**

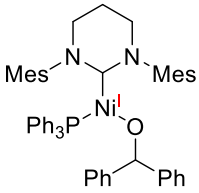

**5.9**

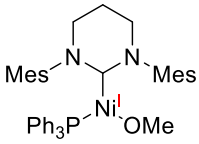

**5.10**

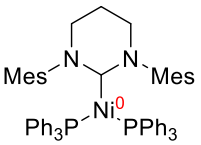

**5.11**

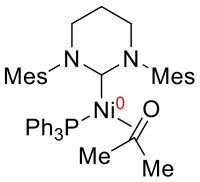

**5.12**

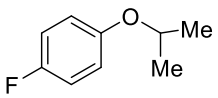

**5.13**

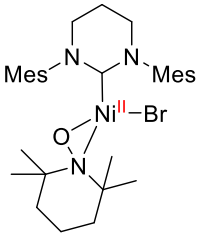

**5.14**

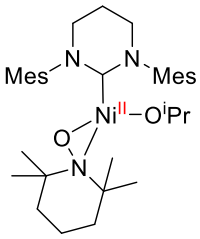

**5.15**

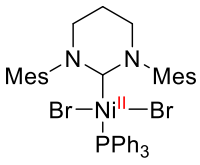

**5.16**

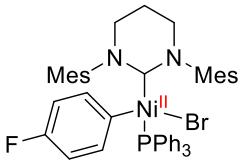

**5.17**

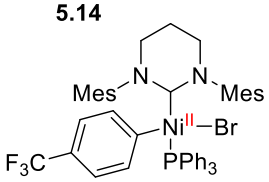

**5.18**

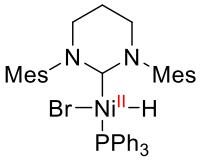

**5.19**

## 7.6 – Appendix 6 : Synthesis and Characterisation of (ITr)CuO$^{i}$Pr

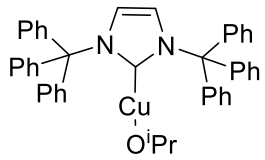


(ITr)CuMes (110 mg, 0.149 mmol) and $^{i}$PrOH (200 μL, 2.61 mmol) were combined in benzene (10 mL) in a J. Youngs resealable ampoule and stirred for 2 h at room temperature. The resulting solution concentrated to dryness, washed with hexane (2 x 10 mL) to yield an off-white precipitate of (ITr)CuO$^{i}$Pr (54.8 mg, yield 54%). Crystalline material was obtained from benzene/hexane. $^{1}$H NMR (500 MHz, $C_6D_6$, 298 K) δ 7.32 – 7.28 (m, 12H, $C_{Ar}H$), 7.12 – 7.02 (m, 18H, $C_{Ar}H$), 6.51 (s, 2H, NC*H*), 3.92 (hept, $^{3}J_{HH}$ = 5.9 Hz, 1H, C*H*$(CH_3)_2$), 0.94 (d, $^{3}J_{HH}$ = 5.9 Hz, 6H, CH(C*H*$_3)_2$). $^{13}$C{$^{1}$H} NMR (126 MHz, $C_6D_6$, 298 K) δ 191.7 (s), 143.3 (s), 130.5 (s), 128.2 (s), 128.0 (s), 119.3 (s), 78.2 (s), 66.6 (s), 31.7 (s).

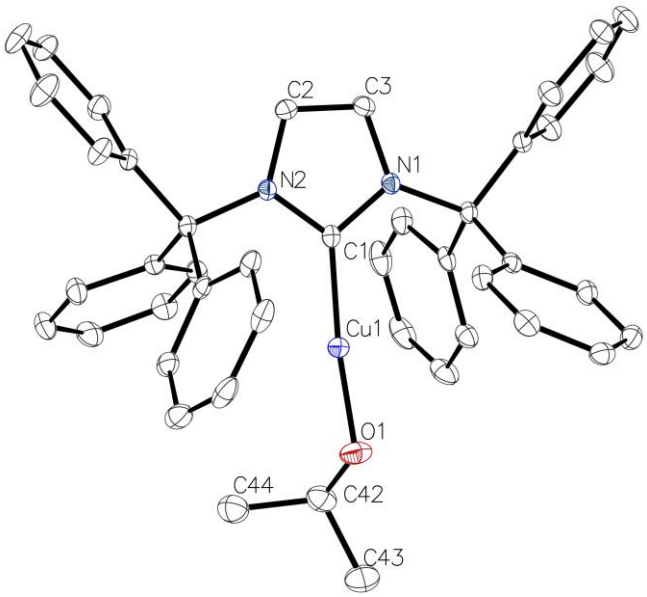


Figure 57 - Molecular structure of (ITr)CuO$^{i}$Pr. Ellipsoids shown at 30% probability. Hydrogen atoms are removed for clarity.

Table 7.1 - Crystal data and structure refinement for (ITr)CuO$^{i}$Pr.

| | |
|---|---|
| Identification code | e18mkw6 |
| Empirical formula | $C_{44}H_{39}CuN_2O$ |
| Formula weight | 675.31 |
| Temperature/K | 150.0(3) |
| Crystal system | monoclinic |
| Space group | $P2_1/n$ |
| a/Å | 18.3755(5) |
| b/Å | 10.3285(3) |
| c/Å | 19.2503(5) |
| α/° | 90 |
| β/° | 108.901(3) |
| γ/° | 90 |
| Volume/Å$^3$ | 3456.54(17) |
| Z | 4 |
| $\rho_{calc}$g/cm$^3$ | 1.298 |
| μ/mm$^{-1}$ | 0.669 |
| F(000) | 1416.0 |
| Crystal size/mm$^3$ | 0.596 × 0.553 × 0.475 |
| Radiation | MoKα (λ = 0.71073) |
| 2Θ range for data collection/° | 6.92 to 54.964 |
| Index ranges | $-23 \leq h \leq 23$, $-10 \leq k \leq 13$, $-24 \leq l \leq 24$ |
| Reflections collected | 30591 |
| Independent reflections | 7783 [$R_{int}$ = 0.0287, $R_{sigma}$ = 0.0327] |
| Data/restraints/parameters | 7783/0/435 |
| Goodness-of-fit on $F^2$ | 1.036 |
| Final R indexes [I>=2σ (I)] | $R_1$ = 0.0364, $wR_2$ = 0.0857 |
| Final R indexes [all data] | $R_1$ = 0.0519, $wR_2$ = 0.0929 |
| Largest diff. peak/hole / e Å$^{-3}$ | 0.36/-0.41 |

## 7.7 – Appendix 7 : Additional Plots for Chapter 5

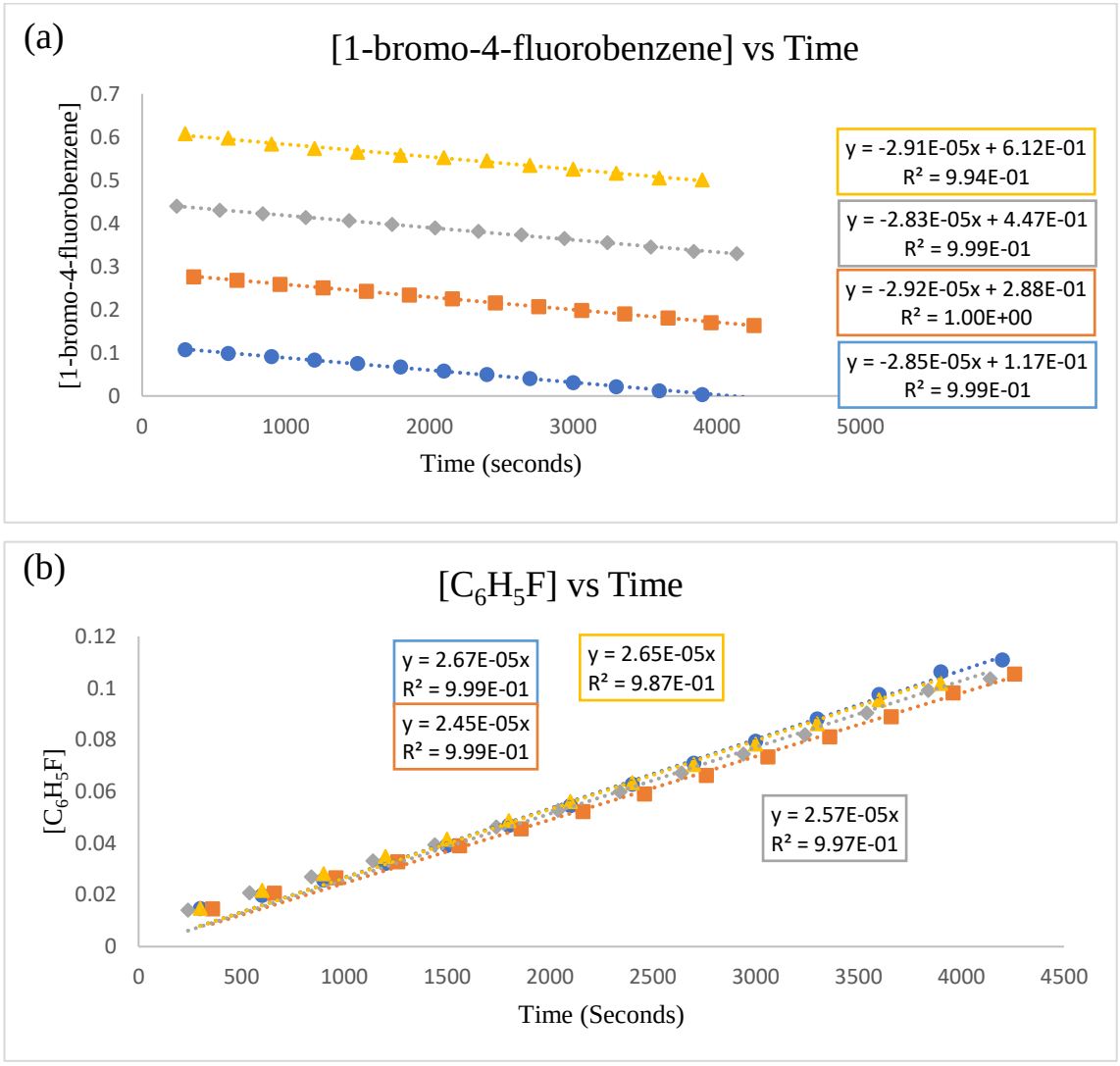


Figure 58 - (A) Same excess experiment using 4 mol% of complex **5.1.** Blue = 0.134M, Orange = 0.268 M, Grey = 0.402M, Yellow = 0.536 M, (B) Same experiment as A but showing the formation of $C_6H_5F$. Blue = 0.134M, Orange = 0.268 M, Grey = 0.402M, Yellow t= 0.536 M.